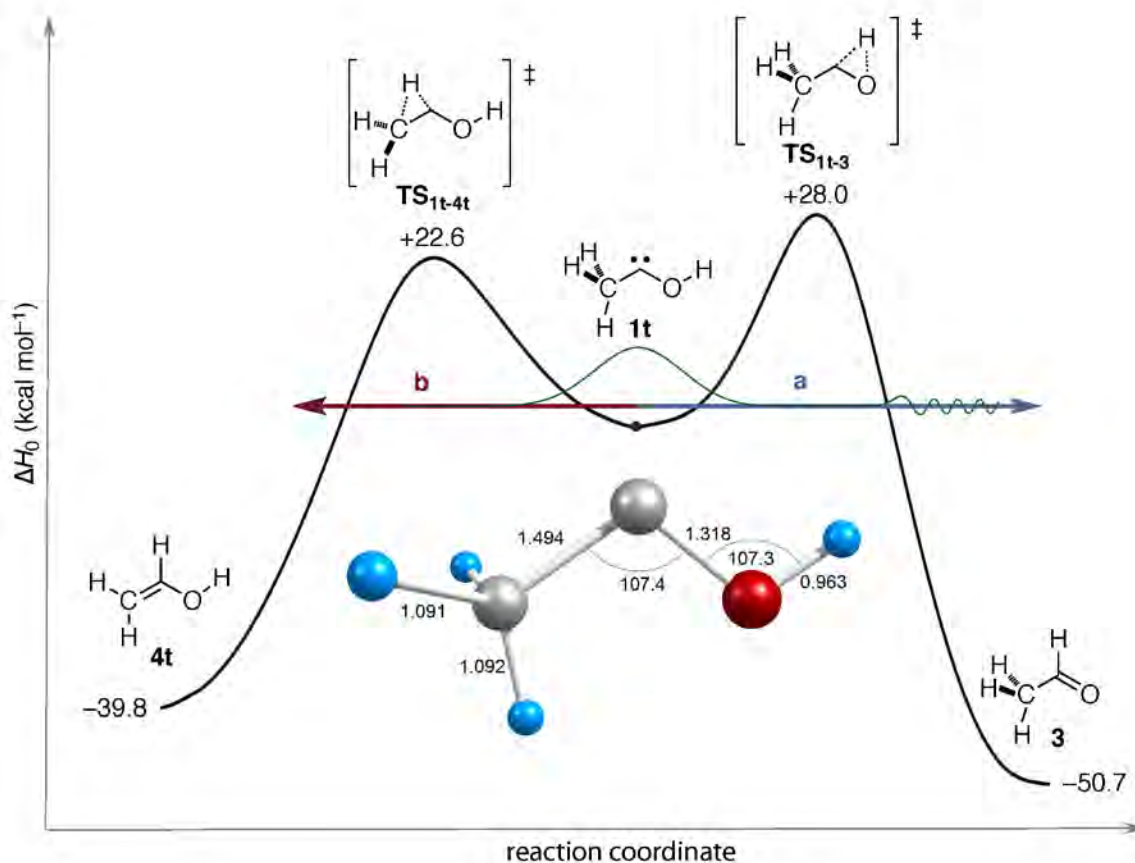


33rd Annual Combustion Research Meeting

Bolger Conference Center
Potomac, Maryland
May 29 – June 1, 2012



U.S. DEPARTMENT OF
ENERGY

Office of
Science

Office of Basic Energy Sciences
Chemical Sciences, Geosciences &
Biosciences Division

33rd Annual Combustion Research Meeting

DOE Principal Investigators'
Meeting Program and Abstracts

Bolger Conference Center
Potomac, MD
May 29 – June 1, 2012

Chemical Sciences, Geosciences, and Biosciences Division
Office of Basic Energy Sciences
Office of Science
U.S. Department of Energy

Cover Graphics:

Energetic profiles for [1,2]H-shift isomerizations of trans-methylhydroxycarbene (**1t**); relative energies (in kcal mol⁻¹) pinpointed from convergent focal-point analysis (FPA) computations. The bond lengths (Å) and angles (°) given for **1t** are ground-state optimum geometrical parameters given by AE-CCSD(T)/cc-pCVQZ theory. The curves are drawn quantitatively with the intrinsic reaction coordinate (IRC) in massweighted Cartesian space as the abscissa in order to reflect the proper barrier heights and widths for the two competing reactions. Simple visual inspection thus indicates a higher hydrogen tunneling probability for the more narrow energy profile of path **a**.

Wesley D. Allen, Chia-Hua Wu - University of Georgia

Peter R. Schreiner, Hans Peter Reisenauer, David Ley, Dennis Gerbig, - Justus-Liebig University

This document was produced under contract number DE-AC05-06OR23100 between the U.S. Department of Energy and Oak Ridge Associated Universities.

The research grants and contracts described in this document are supported by the U.S. DOE Office of Science, Office of Basic Energy Sciences, Chemical Sciences, Geosciences and Biosciences Division.

Foreword

This abstract booklet provides a record of the thirty-third U.S. Department of Energy principal investigators' meeting focused on gas-phase chemical physics. The reports appearing in this volume present work in progress in basic research contributing to the development of a predictive capability for combustion processes. The work reported herein is supported by the Department of Energy's Office of Basic Energy Sciences (BES) and, in large measure, by the chemical physics program. The long-term objective of this effort is the provision of theories, data, and procedures to enable the development of reliable computational models of combustion processes, systems, and devices.

The objective of this meeting is to provide a fruitful environment in which researchers with common interests will present and exchange information about their activities, build collaborations among research groups with mutually reinforcing strengths, identify needs of the research community, and uncover opportunities for future research directions. The agenda consists of an invited keynote talk, oral presentations by program PIs and invited poster presentations from junior level researchers in an effort to increase the awareness of the Gas Phase Chemical Physics program. Approximately one third of the PIs in the program speak each year in rotation. With ample time for discussion and interactions, we emphasize that this is an informal meeting for exchange of information and building of collaborations; it is not a review of researchers' achievements or a forum to define the future direction of the program.

We appreciate the privilege of serving in the management of this research program. In carrying out these tasks, we learn from the achievements and share the excitement of the research of the many sponsored scientists and students whose work is summarized in the abstracts published on the following pages.

We thank all of the researchers whose dedication and innovation have advanced DOE BES research and made this meeting possible and productive. We hope that this conference will help you will build on your successes and we look forward to our assembly in 2014 for our 34th annual meeting. *A DOE Combustion Research Meeting will not be held in 2013.*

We thank Diane Marceau of the Chemical Sciences, Geosciences and Biosciences Division, and Connie Lansdon and Tim Ledford of the Oak Ridge Institute for Science and Education for their important contributions to the technical and logistical features of this meeting.

Michael Casassa
Mark Pederson
Wade Sisk

Agenda

33rd Annual Combustion Research Meeting
U.S. Department of Energy
Office of Basic Energy Sciences

Agenda

Tuesday, May 29, 2012

3:00 pm *Registration*
5:00 pm *No-host Reception at the Pony Express Bar and Grill*
7:00 pm *Dinner*

Wednesday, June 1, 2012

7:00 am *Breakfast*

Session I

Josette Bellan, Chair & Meeting Co-Chair (Stained Glass Hall)

8:00 am Welcome and Introduction - Wade Sisk, DOE/BES
Introduction of Invited Poster Presenters and keynote speaker
– Wesley Allen, Meeting Co-Chair

8:30 am **Keynote Speaker** “Direct Dynamics Simulations of Chemical Reaction Dynamics,” William L. Hase, Texas Tech University..... 1

9:30 am “Gas-Phase Molecular Dynamics: High Resolution Spectroscopy and Collision Dynamics of Transient Species,”
Gregory E. Hall, Brookhaven National Laboratory109

10:00 am “Universal and State-Resolved Imaging Studies of Chemical Dynamics,”
Arthur G. Suits, Wayne State University.....295

10:30 am *Break*

Session II

Millard Alexander, Chair

11:00 am “Optical Probes of Atomic and Molecular Decay Processes,”
Stephen T. Pratt, Argonne National Laboratory.....261

11:30 am “Theoretical Studies of Elementary Hydrocarbon Species and Their Reactions,”
Wesley D. Allen and Henry F. Schaefer III, University of Georgia.....27

12:00 pm “Ultrafast Structural Dynamics in Combustion Relevant Model Systems,”
Peter M. Weber, Brown University.....319

12:30 pm *Lunch*

Session III
Guillaume Blanquart, Chair

3:30 pm “Theoretical Studies of Chemical Reactions Related to the Formation and
Growth of PAHs and Molecular Properties of Their Key Intermediates,”
Alexander M. Mebel, Florida International University.....193

4:00 pm “Developing a predictive model for the chemical composition of soot
nanoparticles: Integrating Model and Experiment,”
Angela Violi, University of Michigan.....311

4:30 pm Poster Session / Reception (Stained Glass Hall)

“Investigating Multiphase Combustion in an Evolving Fuel Environment using
Novel Numerical Methods,” Olivier Desjardins, Cornell University3

“Simulating Liquid Fuel Atomization,”
Marcus Herrmann, Arizona State University.....7

“Reduction and Computational Diagnostics of Detailed Chemical Kinetics for
Combustion Simulations,” Tianfeng Lu, University of Connecticut.....11

“Chemical Reaction Dynamics: State-to-State Photodissociation Studies of
Reactive Intermediates using Ion Imaging,”
Simon North, Texas A&M University.....15

“Fundamental Studies of Combustion Applied to Engines,”
David Rothamer, University of Wisconsin.....19

“Photoinitiated Dissociation Dynamics of Combustion Radicals,”
Jingsong Zhang, University of California.....21

6:00 pm *Dinner - Tribute to Dr. Terrill Cool, Cornell University*

7:00 pm “Flame Chemistry and Diagnostics,”
Nils Hansen, Sandia National Laboratories.....113

Thursday, June 2, 2011

7:00 am

Breakfast

Session IV

Laurie Butler, Chair

8:00 am

“Dynamics of Radical Reactions in Biodiesel Combustion,”
Theodore S. Dibble, SUNY – Environmental Science and Forestry79

8:30 am

“Probing the Reaction Dynamics of Hydrogen-Deficient Hydrocarbon
Molecules and Radical Intermediates via Crossed Molecular Beams,”
Ralf I. Kaiser, University of Hawaii145

9:00 am

“Theoretical Kinetics and Non-Born–Oppenheimer Chemistry,”
Ahren W. Jasper, Sandia National Laboratories141

9:30 am

“Photoinitiated Reactions of Radicals and Diradicals in Molecular Beams,”
Hanna Reisler, University of Southern California265

10:00 am

Break

Session V

David Osborn, Chair

10:30 am

“Spectroscopy and Kinetics of Combustion Gases at High Temperatures,”
Ronald K. Hanson and Craig T. Bowman, Stanford University117

11:00 am

“Theoretical Chemical Kinetics,”
Stephen J. Klippenstein, Argonne National Laboratory161

11:30 am

“Argonne-Sandia Consortium on High-Pressure Combustion Chemistry,”157

- “Project Overview,” Stephen J. Klippenstein, Argonne National Laboratory
- “Experimental Studies of the Oxidation Chemistry of Propane – a prototypical alkane fuel,” Leonid Sheps, Sandia National Laboratories
- “Development of a miniature high repetition rate shock tube (HRRST),” Robert Tranter, Argonne National Laboratory

12:30 pm

Lunch

Session VI

John Stanton, Chair

3:30 pm	“New Single- and Multi-Reference Coupled-Cluster Methods for High Accuracy Calculations of Ground and Excited States,” Piotr Piecuch, Michigan State University.....	249
4:00 pm	“Detection and Characterization of Free Radicals Relevant to Combustion Processes,” Terry A. Miller, The Ohio State University.....	205
4:30 pm	“Dynamical Analysis of Highly Excited Molecular Spectra,” Michael E. Kellman, University of Oregon.....	149
5:00 pm	<i>Break</i>	

Session VII

Robert Tranter, Chair

5:30 pm	“Mechanism and Detailed Modeling of Soot Formation,” Michael Frenklach, University of California Berkeley.....	99
6:00 pm	“Development of Kinetics for Soot Oxidation at High Pressures under Fuel-Lean Conditions,” JoAnn S. Lighty, University of Utah.....	181
6:30 pm	“Chemical Kinetics of Elementary Reactions,” Judit Zádor, Sandia National Laboratories.....	237
7:00 pm	<i>Dinner - Garden Patio</i>	

Friday, June 3, 2011

7:00 am	<i>Breakfast</i>	
----------------	------------------	--

Session VIII

Joel Bowman, Chair

8:00 am	“Theoretical Studies of Molecular Systems,” William A. Lester, Jr., Lawrence Berkeley National Laboratory	177
8:30 am	“Dissociation Pathways and Vibrational Dynamics in Excited Molecules and Complexes,” F.F. Crim, University of Wisconsin-Madison.....	67
9:00 am	“Breakthrough Design and Implementation of Electronic and Vibrational	

	Many-Body Theories,” So Hirata, University of Illinois at Urbana-Champaign.....	133
9:30 am	“Dynamics of Activated Molecules,” Amy S. Mullin, University of Maryland....	213
10:00 am	<i>Break</i>	
Session IX <i>Marshall Long, Chair</i>		
10:30 am	“Combustion Chemistry,” Nancy J. Brown, Lawrence Berkeley National Laboratory.....	47
11:00 am	“Quantitative Imaging Diagnostics for Reacting Flows,” Jonathan H. Frank, Sandia National Laboratories.....	95
11:30 am	“Reacting Flow Modeling with Detailed Chemical Kinetics,” Habib N. Najm, Sandia National Laboratories	217
12:00 pm	Closing Remarks	
12:15 pm	<i>Lunch</i>	

Table of Contents

Table of Contents

Foreword	iii
Agenda	v
Table of Contents	x
Abstracts	1
<u>Invited Presentations</u>	
William L. Hase - Direct Dynamics Simulations of Chemical Reaction Dynamics.....	1
Olivier Desjardins - Investigating Multiphase Combustion in an Evolving Fuel Environment using Novel Numerical Methods.....	3
Marcus Herrmann - Simulating Liquid Fuel Atomization.....	7
Tianfeng Lu - Reduction and Computational Diagnostics of Detailed Chemical Kinetics for Combustion Simulations.....	11
Simon W. North - Chemical Reaction Dynamics: State-to-State Photodissociation Studies of Reactive Intermediates using Ion Imaging.....	15
David A. Rothamer - Fundamental Studies of Combustion Applied to Engines.....	19
Jingsong Zhang - Photoinitiated Dissociation Dynamics of Combustion Radicals.....	21
<u>Principal Investigator Presentations</u>	
Millard H. Alexander - The relaxation of methylene in collisions with He	23
Wesley Allen and Henry F. Schaefer III - Theoretical Studies of Elementary Hydrocarbon Species and Their Reactions.....	27
Robert S. Barlow - Turbulence-Chemistry Interactions in Reacting Flows.....	31
Josette Bellan - Modeling Reactions in High-Pressure Turbulence in the Cold Ignition Regime.....	35
Guillaume Blanquart - Towards predictive simulations of soot formation: from surrogate to turbulence.....	39
Joel M. Bowman - Theoretical Studies of Combustion Dynamics	43
Nancy J. Brown - Combustion Chemistry.....	47
Laurie J. Butler - Dynamics of Product Branching in Elementary Combustion Reactions: OH + Alkenes and Nitrogen Chemistry.....	51
David W. Chandler - Collision Dynamics Studied in Crossed Molecular Beams and New High Resolution Spectrometer Demonstrated.....	55
Jacqueline H. Chen - Petascale Direct Numerical Simulation and Modeling of Turbulent Combustion.....	59
Robert E. Continetti - Dynamics and Energetics of Elementary Combustion Reactions and Transient Species.....	63
F.F. Crim - Dissociation Pathways and Vibrational Dynamics in Excited Molecules and Complexes.....	67

H. Floyd Davis - Bimolecular Dynamics of Combustion Reactions.....	71
Michael J. Davis - Exploration and validation of chemical-kinetic mechanisms.....	75
Theodore S. Dibble - Dynamics of Radical Reactions in Biodiesel Combustion.....	79
Kent M. Ervin - Hydrocarbon Radical Thermochemistry: Gas-Phase Ion Chemistry Techniques.....	83
Robert W. Field - Spectroscopic and Dynamical Studies of Highly Energized Small Polyatomic Molecules.....	87
George Flynn - Scanning Tunneling Microscopy Studies of Chemical Reactions on Surfaces.....	91
Jonathan H. Frank - Quantitative Imaging Diagnostics for Reacting Flows.....	95
Michael Frenklach - Mechanism and Detailed modeling of Soot Formation.....	99
William H. Green - Computer-Aided Construction of Chemical Kinetic Models.....	103
Hua Guo - Quantum Dynamics of Elementary Combustion Reactions.....	107
Gregory E. Hall - Gas-Phase Molecular Dynamics: High Resolution Spectroscopy and Collision Dynamics of Transient Species.....	109
Nils Hansen - Flame Chemistry and Diagnostics.....	113
Ronald K. Hanson and Craig T. Bowman - Spectroscopy and Kinetics of Combustion Gases at High Temperatures.....	117
Lawrence B. Harding - Theoretical Studies of Potential Energy Surfaces.....	121
Martin Head-Gordon - Chemical Accuracy from Ab-Initio Molecular Orbital Calculations.....	125
John F. Hershberger - Laser Studies of Combustion Chemistry.....	129
So Hirata - Breakthrough Design and Implementation of Electronic and Vibrational Many-Body Theories.....	133
Mark R. Hoffmann - Generalized Van Vleck Variant of Multireference Perturbation Theory...	137
Ahren W. Jasper - Theoretical Kinetics and Non-Born–Oppenheimer Molecular Dynamics...	141
Ralf I. Kaiser - Probing the Reaction Dynamics of Hydrogen-Deficient Hydrocarbon Molecules and Radical Intermediates via Crossed Molecular Beams.....	145
Michael E. Kellman - Dynamical Analysis of Highly Excited Molecular Spectra.....	149
Christopher J. Kliewer - Time-Resolved Diagnostics.....	153
Stephen J. Klippenstein and Craig A. Taatjes et. al - Argonne-Sandia Consortium on High- Pressure Combustion Chemistry.....	157
Stephen J. Klippenstein - Theoretical Chemical Kinetics.....	161
Anna I. Krylov - Theoretical Modeling of Spin-Forbidden Channels in Combustion Reactions.....	165
Stephen R. Leone - Synchrotron Studies of Combustion Radical Reactions and Aerosol Chemistry.....	169
Marsha I. Lester - Intermolecular Interactions of Hydroxyl Radicals on Reactive Potential Energy Surfaces.....	173
William A. Lester, Jr. - Theoretical Studies of Molecular Systems.....	177
Joanna Lighty.- Development of Kinetics for Soot Oxidation at High Pressures Under Fuel- Lean Conditions.....	181

Robert P. Lucht - Advanced Nonlinear Optical Methods for Quantitative Measurements in Flames	185
R. G. Macdonald - Time-Resolved Infrared Absorption Studies of Radical Reactions	189
Alexander M. Mebel - Theoretical Studies of Chemical Reactions Related to the Formation and Growth of PAHs and Molecular Properties of Their Key Intermediates	193
Joe V. Michael - Flash Photolysis-Shock Tube Studies	197
H. A. Michelsen - Particle Diagnostics Development	201
Terry A. Miller - Detection and Characterization of Free Radicals Relevant to Combustion Processes	205
William H. Miller - Reaction Dynamics in Polyatomic Molecular Systems	209
Amy S. Mullin - Dynamics of Activated Molecules	213
Habib N. Najm - Reacting Flow Modeling with Detailed Chemical Kinetics	217
David J. Nesbitt - Spectroscopy, Kinetics and Dynamics of Combustion Radicals	221
Daniel M. Neumark - Radical Photochemistry and Photophysics	225
C. Y. Ng - Determination of Accurate Energetic Database for Combustion Chemistry by High-Resolution Photoionization and Photoelectron Methods	229
Joseph C. Oefelein - Large Eddy Simulation of Turbulence-Chemistry Interactions in Reacting Multiphase Flows	233
David L. Osborn - Kinetics and Dynamics of combustion Chemistry	237
Carol A. Parish - Theoretical Studies of the Combustion Reactions of Asphaltene Model Compounds	241
David S. Perry - The Dynamics of Large-Amplitude Motion in Energized Molecules	245
Piotr Piecuch - New Single- and Multi-Reference Coupled-Cluster Methods for High Accuracy Calculations of Ground and Excited States	249
William J. Pitz and Charles K. Westbrook - Chemical Kinetic Modeling of Combustion Chemistry	253
Stephen B. Pope - Investigation of Non-Premixed Turbulent Combustion	257
Stephen T. Pratt - Optical Probes of Atomic and Molecular Decay Processes	261
Hanna Reisler - Photoinitiated Reactions of Radicals and Diradicals in Molecular Beams	265
Klaus Ruedenberg - Electronic Structure, Molecular Bonding and Potential Energy Surfaces	269
Branko Ruscic - Active Thermochemical Tables – Progress Report	271
Trevor Sears - Gas-Phase Molecular Dynamics: High Resolution Spectroscopy and Collision Dynamics of Transient Species	275
Ron Shepard - Theoretical Studies of Potential Energy Surfaces and Computational Methods	279
Raghu Sivaramakrishnan - Mechanisms and Models for Combustion Simulations	283
M. D. Smooke and M. B. Long - Computational and Experimental Study of Laminar Flames	287
John F. Stanton - Quantum Chemistry of Radicals and Reactive Intermediates	291
Arthur G. Suits - Universal and State-Resolved Imaging Studies of Chemical Dynamics	295

Craig A. Taatjes - Elementary Reaction Kinetics of Combustion Species.....	299
Robert S. Tranter - Elementary Reactions of PAH Formation.....	303
Donald G. Truhlar - Variational Transition State Theory.....	307
Angela Violi - Developing a predictive model for the chemical composition of soot nanoparticles: Integrating Model and Experiment.....	311
Albert Wagner - Pressure Dependence Of Combustion Reactions: Quantum Inelastic Dynamics On Automatically Generated Potential Energy Surfaces.....	315
Peter M. Weber - Ultrafast Structural Dynamics in Combustion Relevant Model Systems.....	319
Curt Wittig - Detailed Studies of Hydrocarbon Radicals:C ₂ H Dissociation Dynamics.....	323
Margaret S. Wooldridge - Experimental Ignition Studies of Oxygenated Hydrocarbons.....	327
David R. Yarkony - Theoretical Studies of the Reactions and Spectroscopy of Radical Species Relevant to Combustion Reactions and Diagnostics.....	331
Hua-Gen Yu - Gas-Phase Molecular Dynamics: Theoretical Studies in Spectroscopy and Chemical Dynamics.....	335
Judit Zádor - Chemical Kinetics of Elementary Reactions.....	339
Timothy S. Zwier - Isomer-specific Spectroscopy and Isomerization in Aromatic Fuels.....	343
Participant List	347

*Abstracts
of
Invited Presentations*

Direct Dynamics Simulations of Chemical Reaction Dynamics

William L. Hase
Department of Chemistry and Biochemistry
Texas Tech University
Lubbock, Texas

Classical trajectory direct dynamics simulations are a broadly applicable method for studying the atomistic details of chemical reactions.¹ The simulation results may be compared with experiment, and used to test and develop theoretical models for chemical reaction dynamics. Here we discuss work we have done to develop algorithms and software for direct dynamics simulations, and applications to different chemical problems. The accuracy of classical chemical dynamics is also considered. Selecting proper initial conditions for the trajectories is a critical component for the simulations, and algorithms for fixed energy Wigner sampling,² sampling a quantum mechanical microcanonical ensemble at a potential energy minimum or conical intersection are discussed.³ Enhancing the computational efficiency of the direct dynamics simulations is important and a Hessian-based predictor corrector algorithm⁴ and higher-accuracy schemes for approximating the Hessian from electronic structure calculations will be discussed.⁵

The applications of the direct dynamics simulations include studies of unimolecular and bimolecular reactions, and post-transition state dynamics. As will be discussed, the trajectories are overall accurate for classically allowed direct processes, but become inaccurate for long-lived indirect processes for which the unphysical flow of zero-point energy flow becomes a serious problem.⁶ Post-transition dynamics is an important approach for alleviating the latter problem.⁷ It may be used to study product energy partitioning and the branching between multiple reaction pathways after passing a rate controlling transition state (TS). With the use of QM/MM methods, direct dynamics simulations may also be performed in solution.

The chemical reactions and dynamical issues which will be discussed include: S_N2 nucleophilic substitution reactions, including the role of microsolvation;⁸ non-intrinsic reaction coordinate (IRC) reaction pathways;⁹ product energy partitioning in unimolecular reactions;⁷ the branching between multiple reaction pathways for enzyme catalysis,¹⁰ and the use of direct dynamics to obtain unimolecular Arrhenius parameters without traditional TS searching.¹¹ Also of interest is the possibility that a classical trajectory simulation of an initial quantum mechanical microcanonical ensemble will give an accurate anharmonic RRKM rate constant.¹²

1. L. Sun and W. L. Hase, *Rev. Comput. Chem.* **19**, 79 (2003).
2. L. Sun and W. L. Hase, *J. Chem. Phys.* **133**, 044313 (2010).
3. K. Park, J. Engelkemier, M. Persico, P. Manikandan, and W. L. Hase, *J. Phys. Chem. A* **115**, 6603 (2011).
4. U. Lourderaj, K. Song, T. L. Windus, Y. Zhuang, and W. L. Hase, *J. Chem. Phys.* **126**, 044105 (2007).

5. H. Wu, M. Rahman, J. Wang, U. Lourderaj, W. L. Hase, and Y. Zhuang, *J. Chem. Phys.* **133**, 074101 (2010).
6. W. L. Hase and D. G. Buckowski, *J. Comput. Chem.* **3**, 335 (1982).
7. U. Lourderaj, K. Park, and W. L. Hase, *Int. Rev. Phys. Chem.* **27**, 361 (2008).
8. P. Manikandan, J. Zhang, and W. L. Hase, *J. Phys. Chem. A* **116**, 3061 (2012).
9. L. Sun, K. Song, and W. L. Hase, *Science* **296**, 875 (2002).
10. M. R. Siebert, J. Zhang, S. V. Addepalli, D. J. Tantillo, and W. L. Hase, *J. Am. Chem. Soc.* **133**, 8335 (2011).
11. L. Yang, R. Sun, and W. L. Hase, *J. Chem. Theory and Comput.* **7**, 3478 (2011).
12. P. Manikandan and W. L. Hase, *J. Chem. Phys.*, submitted.

Investigating Multiphase Combustion in an Evolving Fuel Environment using Novel Numerical Methods

Olivier Desjardins

Sibley School of Mechanical & Aerospace Engineering, Cornell University

Ithaca, NY 14853-7501

olivier.desjardins@cornell.edu

I. Program Scope

Today, over 97% of worldwide energy needs for transportation are met with petroleum-based fuels, i.e., fuels that have been derived from crude oil [1]. In the near future, greener fuels are expected to progressively replace these conventional fuels, in an effort to reduce our dependence on crude oil and mitigate anthropological climate change associated with fossil fuel usage. Aggressive policies are being introduced to this end in several countries. As an illustration, in the United States, the DOE has a near-term goal of reducing gasoline usage by 20% by 2017, and a long term “30 × 30” goal to displace 30% of gasoline with biofuels by 2030. To make such audacious goals possible to reach, the necessary industrial effort needs to be supported by new fundamental research focused towards understanding the differences in physical and chemical characteristics of petroleum-based and bio-derived fuels, and the effects that blending both types of fuels will have on the combustion process.

In this context of evolving fuels, our ability to predict combustion processes is critical. While the combustion characteristics of alternative fuels exhibit strong similarities with that of the fuel they aim to replace, significant differences remain. Research on biofuel combustion has been intensifying in the recent years, and significant advancements have been reported. In particular, our understanding of the chemical kinetics of many important bio-derived fuel components is rapidly progressing. For example, Westbrook’s research group at LLNL proposed recently a new detailed mechanism for biodiesel surrogates, based on the combination of detailed mechanisms for the oxidation of *n*-heptane, methyl-decanoate, and methyl-9-decenoate [2]. In parallel to the progress in understanding chemical kinetics, researchers are developing novel strategies for predicting the impact that the new components will have on the combustion process, such as the effect of oxygenated additives on the sooting propensities of hydrocarbon fuels [3, 4].

Virtually all the current research on this topic aims at unravelling the effect of blending hydrocarbon fuels with bio-derived fuels on the gaseous combustion process. However, it is paramount to realize that these fuels are always stored in liquid form, and therefore need to be atomized and evaporated before they can burn. As a result, one can fully comprehend the impact of replacing petroleum-based fuels by biofuels only by accounting for (1) how liquid fuel atomization changes in the presence of biofuels, (2) how evaporation is affected by the use of blending, and (3) how the combustion process itself reacts to the change in kinetics. The first two points have thus far been virtually ignored, and all the focus has been set on the third issue. Yet, the combustion process is tightly coupled to the spray generation and evaporation processes, and should be studied as such.

II. Recent Progress

Detailed studies of the interaction between spray dynamics and combustion have remained limited thus far [5–8]. Desjardins and Pitsch [7] and Luo *et al.* [5] showed through direct numerical simulation (DNS) that spray flames exhibit both premixed and diffusion flame regions, whose spatial distribution is strongly linked to the nature of spray and flow dynamics. In the case of the swirl-stabilized spray flame showed in Fig. 1, it was found that the central recirculation region generates

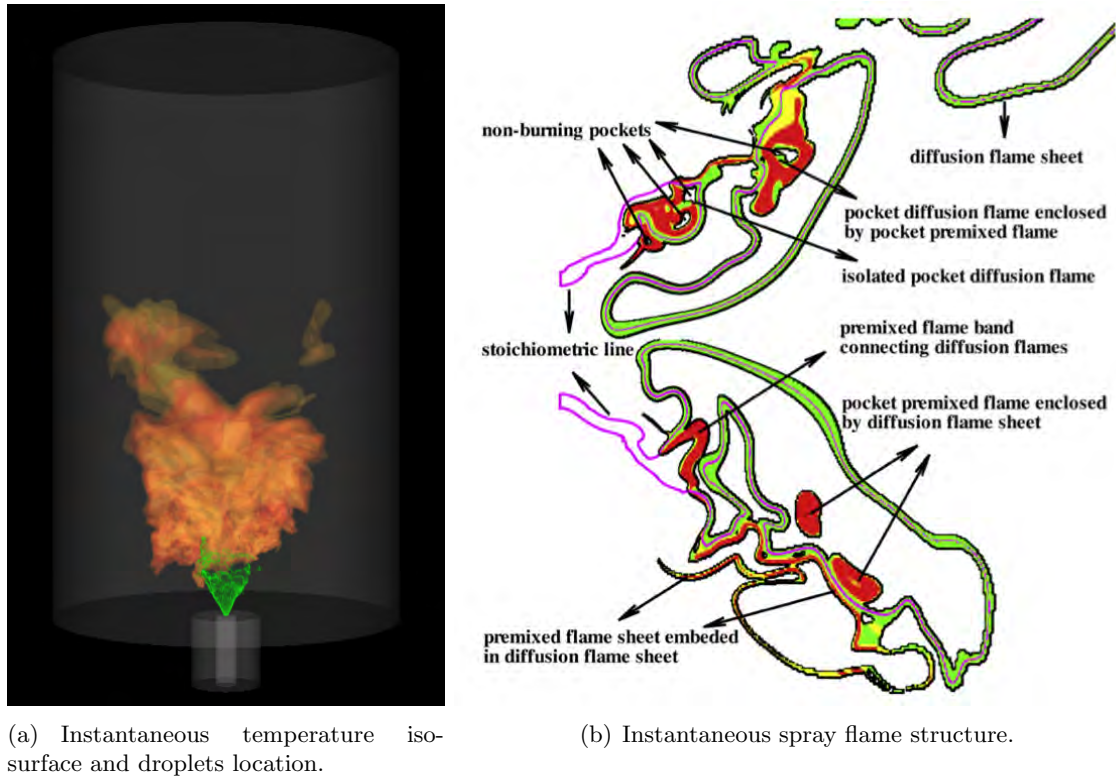


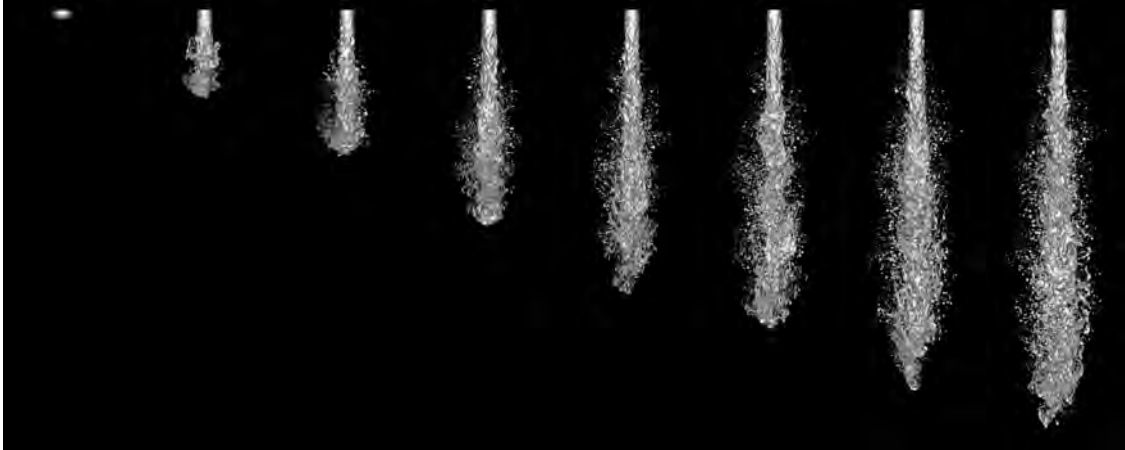
Figure 1: Simulation of a model spray combustor [5].

a zone of premixed combustion that is driving the evaporation of the liquid fuel, while the outer flame region is diffusion-limited. The premixed flame was found to contribute up to 70% of the total heat release rate, and to be critical to flame stabilization. These two studies also highlighted the importance of accounting for evaporation when modeling combustion, since evaporation was found to modify significantly the scalar dissipation rate as well as the probability density function of mixture fraction, two quantities often used in the formulation of combustion models.

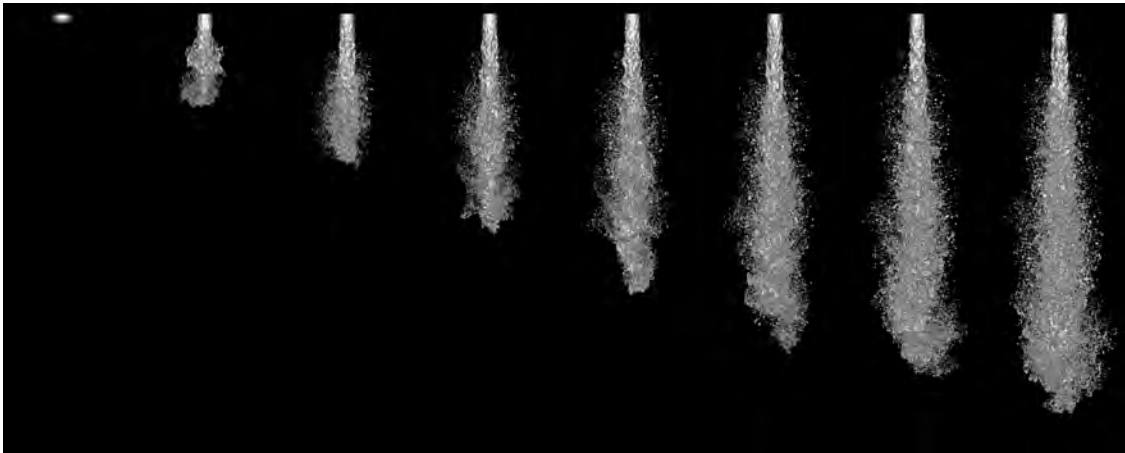
The transition to biofuels is also expected to impact fuel atomization directly. Alternative fuels exhibit significant differences with current fuels, a major one being their material properties. For instance, biomass-derived oils have been shown to have a surface tension coefficient two to three times larger than that of standard Diesel fuel. Desjardins and Pitsch [9] showed that such a difference in surface tension changes drastically the nature of the liquid break-up process, leading for example to much larger droplets, as illustrated in Fig. 2. This will have direct consequences on the evaporation rate of the fuel, its spatial distribution, and ultimately on the combustion process.

III. Future Work

We have argued that predicting the atomization and evaporation of a multi-component fuel is a critical step in building a predictive combustion model. Hence, future work will include detailed investigation, through direct numerical simulations, of the combustion of atomizing and evaporating multi-component liquid fuels, and the development of large-eddy simulation models that enable predictive simulations of turbulent combustion in realistic propulsion devices in an evolving fuel



(a) $Re = 5000$, $We = 2000$



(b) $Re = 5000$, $We = 5000$

Figure 2: Temporal evolution of two liquid jets with different Weber number issued from a pressurized injector. Turbulent atomization simulations conducted on 402 million cells using the NGA code (manuscript in preparation).

environment.

Discretizing the discontinuous equations that commonly arise in multiphase flow problems onto a fixed mesh has proven to be an remarkably difficult task. Despite the vast amount of research devoted to the development of computational methodologies capable of handling discontinuities in PDEs, no gold standard has emerged at this point. Instead, numerous algorithms have been proposed, each displaying specific strengths but also severe limitations. The lack of a systematic discretization methodology explains in part the somewhat limited role that detailed simulations have played so far in multiphase flow research. We propose a paradigm shift for solving fluid-solid or gas-liquid flows, thanks to a novel systematic finite volume discretization strategy that is sharp, robust, conservative, and accurate, while remaining straightforward to implement.

The starting point for the proposed formalism is a conservative immersed boundary scheme recently developed in Desjardins' group [10]. This algorithm combines all the properties listed

above, in particular it has been shown to be second order accurate using the method of manufactured solutions. The first task will be to extend this algorithm to moving interfaces without sacrificing conservation nor accuracy. Then, the extension to liquid-gas flows will be considered, for which the Navier-Stokes equations with discontinuous variables need to be solved. In that case, the proposed formalism shares similarities with a finite volume ghost fluid method. All developments will be implemented and tested in the computational platform NGA, an arbitrarily high-order, fully conservative flow solver that has been shown to be ideally suited for the accurate computation of turbulent multiphase flows [11]. This novel discretization strategy will allow to conduct robust and accurate simulations of liquid-gas problems with phase change and chemistry.

IV. References

- [1] D. Sandalow. *Freedom from oil: How the next president can end the United States oil addiction*. McGraw Hill, 2008.
- [2] O. Herbinet, W. J. Pitz, and C. K. Westbrook. Detailed chemical kinetic mechanism for the oxidation of biodiesel fuels blend surrogate. *Combust. Flame*, 157:893–908, 2010.
- [3] P. Pepiot and H. Pitsch. Structural group analysis for soot reduction tendency of oxygenated fuels. *Combust. Flame*, 154:191–205, 2008.
- [4] C. K. Westbrook, W. J. Pitz, and H. J. Curran. Chemical kinetic modeling study of the effects of oxygenated hydrocarbons on soot emissions from diesel engines. *J. Phys. Chem. A*, 110:6912–6922, 2006.
- [5] K. Luo, H. Pitsch, M. G. Pai, and O. Desjardins. Direct numerical simulations and analysis of three-dimensional n-heptane spray flames in a model swirl combustor. *Proceedings of the Combustion Institute*, page in press, 2010.
- [6] J. Reveillon and L. Vervisch. Analysis of weakly turbulent dilute-spray flames and spray combustion regimes. *J. Fluid Mech.*, 537:317–347, 2005.
- [7] O. Desjardins and H. Pitsch. Modeling effect of spray evaporation on turbulent combustion. *10th International Congress on Liquid Atomization and Spray Systems, Kyoto, Japan, 2006*, 2006.
- [8] Y. Baba and R. Kurose. Analysis and flamelet modelling for spray combustion. *J Fluid Mech.*, 612:45 – 79, 2008.
- [9] O. Desjardins and H. Pitsch. Detailed numerical investigation of turbulent atomization of liquid jets. *Atom. Spray*, 20:311–336, 2010.
- [10] P. Pepiot and O. Desjardins. Direct numerical simulation of dense particle-laden flows using a conservative immersed boundary technique. In *Proceedings of the 2010 Summer Program*. Center for Turbulence Research, Stanford, CA, 2010.
- [11] O. Desjardins, G. Blanquart, G. Balarac, and H. Pitsch. High order conservative finite difference scheme for variable density low Mach number turbulent flows. *J. Comput. Phys.*, 227(15):7125–7159, 2008.

Simulating Liquid Fuel Atomization

M. Herrmann

School for Engineering of Matter, Transport and Energy
Arizona State University, Tempe, AZ 85287
marcus.herrmann@asu.edu

Energy conversion by combustion for transportation purposes almost exclusively relies on fuel in liquid form and oxidizer in the gaseous phase. For chemical combustion reactions to occur, the liquid fuel must be vaporized and mixed with the oxidizer. Since evaporation of the liquid fuel in itself is a slow process, but available residence time in combustion devices is typically small, the evaporation rate must be enhanced by increasing the available liquid surface area for evaporation. This is achieved by atomizing the injected liquid fuel into a large number of small scale drops, thus providing drastically increased total surface area for fast evaporation. Once evaporated, the fuel vapor has to mix with the oxidizer before combustion reactions can occur. In modern reciprocal engines, such as common-rail Diesel engines or direct injection gasoline engines, the turbulence needed to obtain an optimal gaseous fuel/air mixture is largely generated by the injected liquid fuel and the dynamics of the immiscible liquid/gas phase interface. Engine performance, efficiency, and pollutant production strongly depend on the quality of this gaseous fuel/air mix prior to combustion. The details of the liquid fuel atomization process are thus of paramount importance, yet as of this day, they remain poorly understood.

Commonly, liquid fuel atomization is thought to occur in two consecutive steps: the initial primary atomization of the injected liquid into large and small scale structures, followed by a secondary atomization of these structures into ever smaller drops. While a number of established models exist for the latter process, supported by numerous experimental studies of single drops or small numbers of drops, the lack of understanding of the former process is mostly due to the fact that experimental observations in the primary atomization region are often times not possible. Some progress has been made in recent years in visualizing the phase interface during the initial phase of atomization using X-ray phase contrast imaging [1] and ballistic imaging [2], however the data available from these techniques is not yet sufficient to study the dynamics during primary atomization in detail under relevant operating conditions.

Detailed numerical simulations, on the other hand, can help study the fundamental mechanisms of the initial breakup in regions, where experimental access and analysis is virtually impossible. However, simulating atomization accurately is a tremendous numerical challenge since time and length scales vary over several orders of magnitude, the phase interface is a material discontinuity, and surface tension forces that dominate the final stages of topology change events are singular.

To address these issues, the motion of the phase interface during atomization needs to be tracked or captured. This is achieved by employing a level set approach using the Refined Level Set Grid (RLSG) method [3]. It introduces a separate, equidistant Cartesian grid,

using a dual-narrow band methodology for efficiency, on which all level set related equations are solved. This RLSG grid is overlaid onto the flow solver grid on which the Navier-Stokes equations are solved. The RLSG grid can be independently refined, providing high resolution of the phase interface geometry in an efficient way. To account for the phase interface being a material discontinuity with singular surface tension forces, a balanced force finite volume approach is employed solving the low Mach number limit Navier-Stokes equations on fully unstructured flow solver meshes using volume fractions and phase interface curvatures calculated on the fine RLSG grid. Since atomization in combustion devices occurs in a non-isothermal environment, effects of temperature variations on the surface tension can be taken into account by incorporating temperature dependent surface tension coefficients and Marangoni forces into the formulation [4].

In order to couple detailed simulations of the primary atomization region to simulations of the secondary atomization region using Lagrangian spray models including evaporation, mixing and potentially combustion, a multi-scale Eulerian/Lagrangian coupling procedure is employed [5]. It identifies broken-off, nearly spherical liquid structures in the fully resolved level set RLSG representation and transfers them into a Lagrangian point particle description that is typically used for spray models. Evaporation of the liquid fuel then predominantly occurs in the Lagrangian description, although modifications to the level set formulation are possible to account for phase transition during the primary atomization process. Figure 1

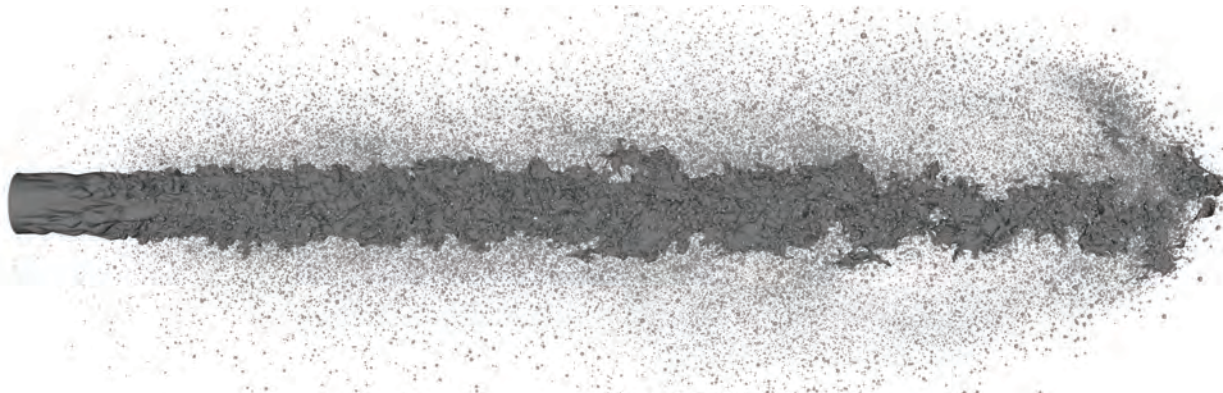


Figure 1: Atomization of a turbulent liquid jet $20\mu\text{s}$ after start of injection: level set liquid core (shaded surface) and Lagrangian tracked spray drops [6].

shows as an example the result of a detailed simulation of the initial breakup of a turbulent liquid jet ($\text{Re} = 5000$, $\text{We} = 17,000$) injected into stagnant compressed air, using the method outlined above.

Although use of the multi-scale Eulerian/Lagrangian coupling procedure provides for a significant reduction of the computational cost of simulating liquid fuel atomization, predictive modeling approaches that do not require the resolution of all length and time scales during primary atomization are still desirable to reduce computational cost even further. A modeling approach in the spirit of a Large Eddy Simulation (LES) would be desirable, since the mixing processes of evaporated fuel vapors with the gaseous oxidizer are generally better predicted by LES models than Reynolds averaged approaches. Introducing spatial fil-

tering into the governing equations, results in several additional unclosed terms that require modeling, as compared to a single phase formulation. Closing them, using a standard LES approach would necessitate the existence of a cascade process, in order to infer the dynamics of the sub-filter scales from the dynamics of the resolved scales. The presence of such a cascade process for primary atomization processes is, however, questionable, since detailed simulations have indicated that the generation of smallest scale drops can occur directly from the largest scale injected continuous liquid structures [6].

Instead, the use of the RLSG method allows for an alternative, dual-scale Sub-Grid Surface Dynamics (SGSD) model. On the RLSG grid, a fully resolved realization of the phase interface geometry is maintained. Then, all previously unclosed terms in the filtered Navier-Stokes equations related to the phase interface can be closed exactly by explicitly filtering the resolved RLSG realization. However, to maintain a fully resolved realization of the phase interface, a fully resolved realization of the advection velocity of the phase interface must be reconstructed from the filtered velocity field. This is achieved by solving a model equation for the subgrid velocity component on the RLSG mesh that contains contributions to account for subgrid surface tension forces, subgrid viscous effects, subgrid turbulent eddies, and subgrid shear [7]. Figure 2 shows the result of an example simulation

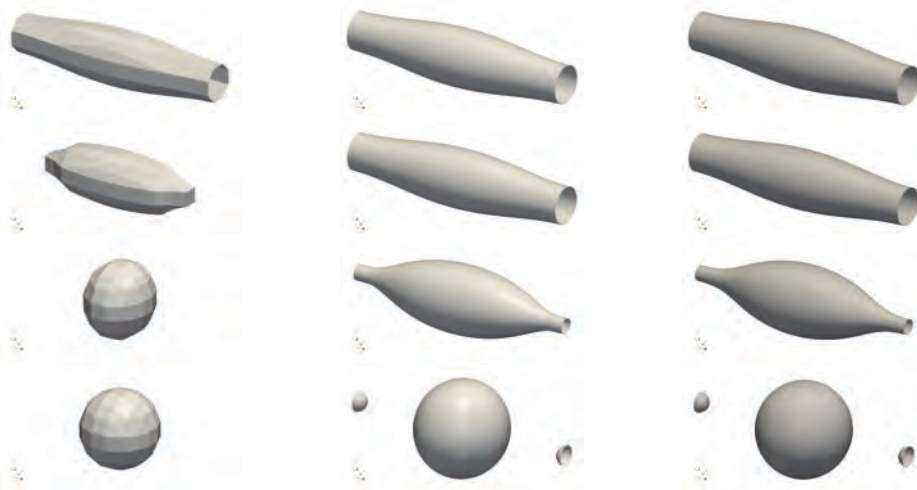


Figure 2: Breakup of a liquid viscous column simulated using 3.2 flow solver mesh points per column diameter. Left: no RLSG-SGSD model; center: RLSG-SGSD model; right: reference DNS simulation.

of the breakup of a liquid viscous column due to capillary forces. On the left, results are shown obtained solving only the Navier-Stokes equations on a mesh resolving the column diameter by 3.2 mesh points. While breakup due to capillary forces does occur, only a single drop is generated. In the center of the figure results with the same flow solver resolution of 3.2 mesh points per column diameter but using the RLSG-SGSD model are compared to a reference DNS simulation shown on the right. As in the reference simulation, the column not only breaks into a main drop, but also a small satellite drop is generated. It is important to capture these small scale satellite drops, since they may provide a sufficient evaporated

fuel source close to the injector for flame stabilization.

Finally, it should be pointed out that both the RLSG approach and the dual scale SGSD model are in principle not only applicable to immiscible interfaces, but can also be applied to the modeling of turbulent premixed combustion using the level set flamelet approach. In that case, a fully resolved realization of the premixed flame front geometry is maintained on the RLSG mesh that moves due to a local laminar burning velocity and a reconstructed turbulent velocity field.

Acknowledgments

This work was supported in part by the National Science Foundation under grants CBET-0853627/CBET-1054272, and CASCADE Technologies Inc. under NavAir SBIR N07-046.

References

- [1] Yujie Wang, Xin Liu, Kyoung-Su Im, Wah-Keat Lee, Jin Wang, Kamel Fezzaa, David L. S. Hung, and James R. Winkelman. Ultrafast X-ray study of dense-liquid-jet flow dynamics using structure-tracking velocimetry. *Nat Phys*, 4(4):305–309, 2008.
- [2] Mark Linne, Megan Paciaroni, Tyler Hall, and Terry Parker. Ballistic imaging of the near field in a diesel spray. *Experiments in Fluids*, 40(6):836–846, 2006.
- [3] M. Herrmann. A balanced force refined level set grid method for two-phase flows on unstructured flow solver grids. *J. Comput. Phys.*, 227(4):2674–2706, 2008.
- [4] P. T. Brady, M. Herrmann, and J. M. Lopez. Confined thermocapillary motion of a three-dimensional deformable drop. *Physics of Fluids*, 23(2):022101–11, 02 2011. URL <http://link.aip.org/link/?PHF/23/022101/1>.
- [5] M. Herrmann. A parallel Eulerian interface tracking/Lagrangian point particle multi-scale coupling procedure. *J. Comput. Phys.*, 229:745–759, 2010.
- [6] M. Herrmann. On simulating primary atomization using the refined level set grid method. *Atom. Sprays*, 21(4), 2011.
- [7] M. Herrmann and M. Gorokhovski. A large eddy simulation subgrid model for turbulent phase interface dynamics. In *ICLASS 2009, 11th Triennial International Annual Conference on Liquid Atomization and Spray Systems*, number ICLASS2009-205, Vail, CO, 2009.
- [8] M. Herrmann. Refined level set grid method for tracking interfaces. In *Annual Research Briefs-2005*, pages 3–18. Center for Turbulence Research, 2005.

Reduction and Computational Diagnostics of Detailed Chemical Kinetics for Combustion Simulations

Tianfeng Lu

Department of Mechanical Engineering, University of Connecticut
Storrs, CT 06269-3139
tlu@engr.uconn.edu

I. Program Scope

Detailed chemical kinetics can be computationally expensive for combustion simulations and may induce complex flame behaviors, particularly at near-limit flame conditions. We study two important topics in combustion simulations with detailed chemistry of practical fuels: a) systematic mechanism reduction to enable efficient large scale flame simulations with detailed chemical kinetics, and b) computational flame diagnostics to systematically extract salient information from massive flame simulation data and to identify chemical kinetic processes controlling critical flame features such as ignition, extinction and flame propagation.

II. Recent Progress

A. Systematic reduction of detailed chemical kinetics

A suit of algorithms were developed to derive reduced mechanisms that are amenable for large scale combustion simulations, including state of the art 3-D large eddy simulations (LES) and direct numerical simulations (DNS) with detailed chemical kinetics (Lu&Law 2009, Lu 2011). The reduction starts from the method of directed relation graph (DRG), which maps species couplings to a digraph. Important species and reactions were then identified through a recursive graph search starting from a few important species. The DRG method features the highest computational efficiency and is suitable to reduce extremely large mechanisms that may consist of hundreds or thousands of species. DRG was further extended to exploit expert knowledge (DRGX) and sensitivity analysis (DRGASA). DRGX allows species specific error control to obtain high-fidelity mechanisms that are needed in chemical kinetics research, while DRGASA generates skeletal mechanisms that are minimal in size for given accuracy requirements for system parameters of interest. Second, quasi steady state (QSS) species in the skeletal mechanisms obtained using the DRG-based methods are identified using an algorithm based on computational singular perturbation. The algebraic equations for the QSS species are solved analytically. Third, molecular diffusion based on the mixture averaged model was simplified using binary integer programming, such that it is no longer computational expensive to evaluate molecular diffusion in laminar flame simulations and DNS. In the end, chemical stiffness is removed on-the-fly by dynamically tracking exhausted fast chemical processes. As a result, explicit integration can be adopted in DNS with affordable time step sizes that are limited by the flow time, i.e. the Courant–Friedrichs–Lewy condition. The cost of DNS using dynamic stiffness removal was shown to be linearly proportional to the number of species in contrast to the quadratic or cubic dependence in most previous flame simulations that require implicit solvers. A variety of reduced mechanisms have been developed using these algorithms for small gaseous fuels, e.g. methane and ethylene, to transportation fuels with large molecular structures, e.g. gasoline, diesel and biodiesel surrogates. In particular, a 58-species reduced mechanism for n-heptane (Yoo et al, 2011a) was derived from a 561-species detailed mechanism by Lawrence Livermore National Laboratory (LLNL), and a 73-species reduced mechanism for biodiesel (Lu, 2011) was obtained from a 3299-species LLNL mechanism. The reduced mechanisms are in general as accurate and comprehensive as the detailed mechanisms, thus not only significantly reduce computation cost for flame simulations but also are much easier for mechanism validation with flame data and the subsequent reaction parameter update. The accuracy of reduced mechanisms is demonstrated in Fig. 1, which shows the high fidelity of the 58-species reduced mechanism for n-heptane for both ignition and extinction applications.

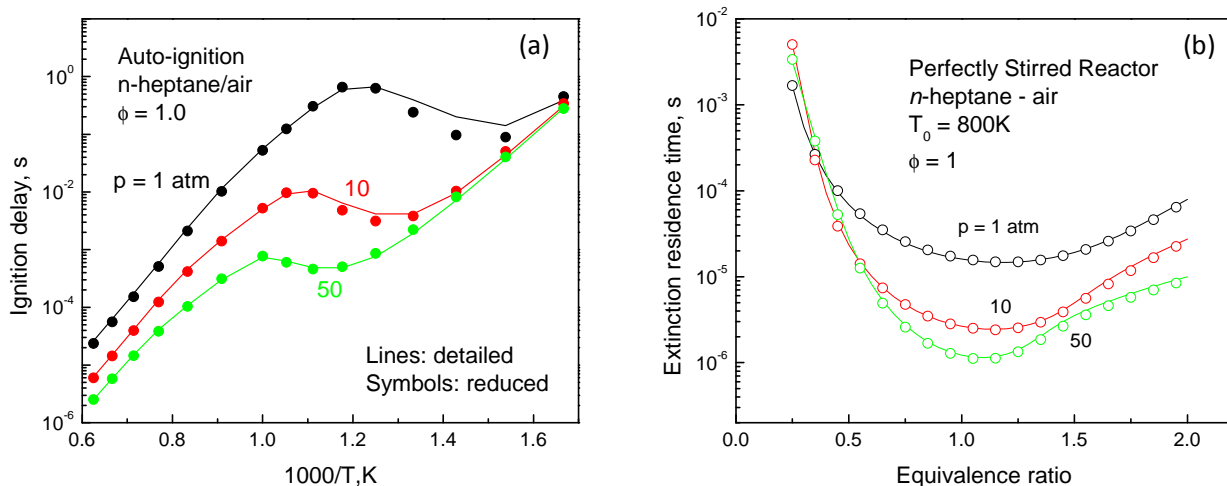


Figure 1. (a) Ignition delays for constant-pressure auto-ignition, and (b) extinction residence time in perfectly stirred reactors, calculated with reduced (58 species) and detailed (561 species) *n*-heptane mechanisms, respectively (Yoo et al, 2011a).

The reduced mechanisms have been widely adopted in combustion simulations including practical turbulent flame simulations using Reynolds Averaged Navier Stokes equations (RANS), e.g. the internal engine simulations at Argonne National Laboratory (S. Som) and Engine Combustion Network (<http://www.sandia.gov/ecn/>), and the state of the art DNS at Sandia national Laboratories (J.H. Chen). Figure 2 shows selected flame simulations at Argonne and Sandia using our reduced mechanisms.

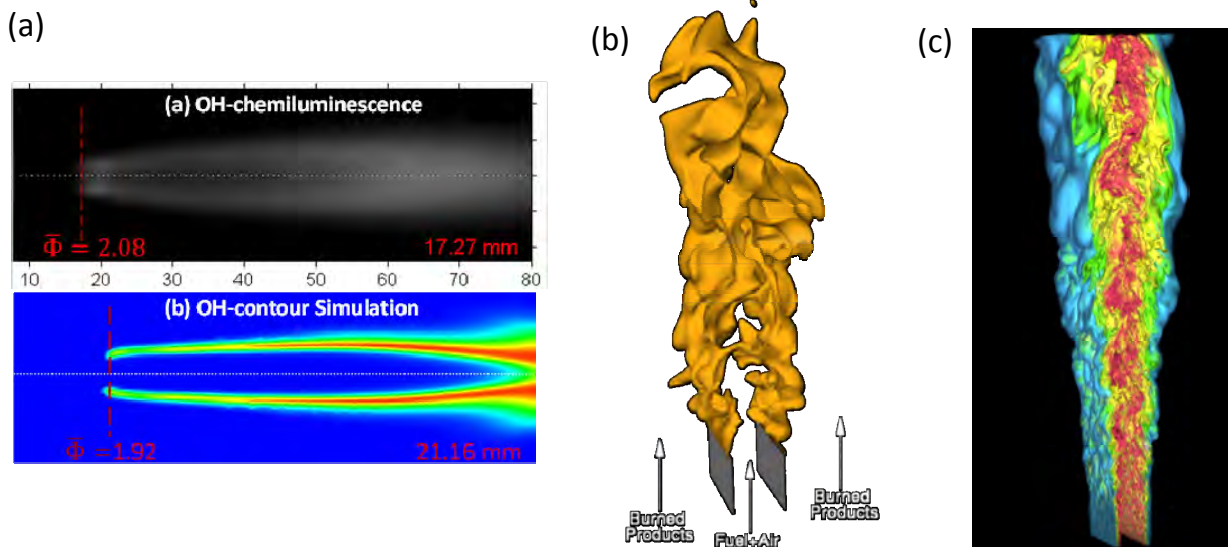


Figure 2. (a) OH concentration of an auto-igniting biodiesel jet in air coflow at 1000K, simulated at Argonne National Laboratory using 3-D RANS and a 123-species skeletal mechanism derived from a 3299-species detailed LLNL mechanism (Luo et al, 2012a), compared with Sandia's experimental results (top panel); (b) an instantaneous flame surface in a weakly turbulent premixed Bunsen flame of methane-air, 3-D DNS at Sandia using a 13-species reduced mechanism (Sankaran et al, 2007); (c) mixture fraction of a turbulent lifted ethylene jet flame into heated coflowing air, a landmark DNS simulated at Sandia using a 22-species reduced mechanism (Yoo et al, 2011b; Luo et al, 2012b), volume rendering by H. Yu;

B. Computational diagnostics for flame simulations with detailed chemical kinetics

While large scale flame simulations are routinely performed today with reduced mechanisms, new challenges emerge because of the massive datasets generated from these large simulations. For example, Sandia's DNS of the lifted ethylene jet flame in Fig. 2c generated 240TB data, which defies

almost any currently available methods for DNS data mining (Yoo et al, 2011b). The challenge will be worsened if transportation fuels with large molecules are involved. Second, the couplings of detailed chemical kinetics and transport processes can result in highly complex flame behaviors that are not well understood (Lu 2011; Shan&Lu 2012). Third, it is difficult to quantify the effects of uncertainties in different reaction pathways on flame behaviors in multi-dimensional flows, which is however important in for the update of reaction pathways in chemical kinetics studies. To respond to these challenges, we developed methods for computational flame diagnostics to extract salient information from both elementary flame results complicated by detailed chemistry and the massive datasets from multi-dimensional flame simulations.

A method of chemical explosive mode analysis (CEMA) was developed to systematically detect important flame features, including ignition, extinction, premixed flame fronts and diffusion flame kernels, from large flame simulations (Lu et al, 2010, Luo et al, 2012b, Lu, 2011). CEMA is based on eigenanalysis of the chemical Jacobian. It was found that zero-crossover of the eigenvalues are strongly correlated with limit phenomena of flames. CEMA is efficient and reliable to perform compared with conventional methods that are based on individual scalars such as temperature and a species concentration. Figure 3 shows the structure of the lifted ethylene jet flame in Fig. 2c identified by CEMA (Luo et al, 2012). In Fig. 3a, the pre- and post-ignition mixtures are shown in red and blue colors, respectively, on the plot of the timescale of the chemical explosive mode (CEM). The sharp transition between red and blue zones pinpoints the premixed flame fronts, which are shown difficult to detect in the temperature plot in Fig. 3b. The auto-ignition layers and diffusion flame kernels were shown in red and blue, respectively, in Fig. 3c, based on a Damköhler number defined on the timescale of CEM and the scalar dissipation rate. The controlling species in different flame zones identified with CEMA are shown in Fig. 3d.

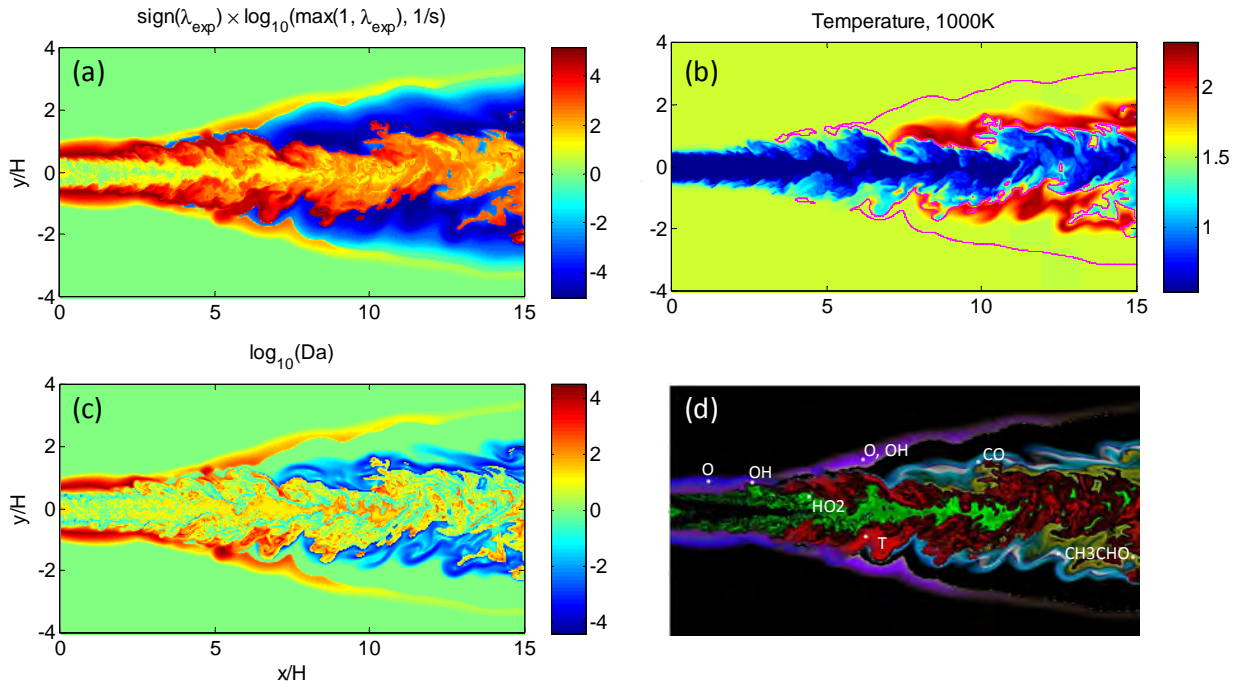


Figure 3: Structure of a lifted ethylene jet flame in heated coflowing air: (a) timescale of CEM, red color indicates pre-ignition mixture ($\lambda_{\text{exp}} > 0$) and blue indicates post-ignition mixture ($\lambda_{\text{exp}} < 0$); (b) isocontour of temperature, the magenta isoline indicates premixed flame fronts detected by CEMA; (c) Damköhler number defined on CEM timescale and scalar dissipation rate, red color indicates auto-ignition zones, blue indicates the diffusion flame kernel; (d) controlling species at different flame zones identified with CEMA.

For diagnostics of steady state combustion characterized by “S”-curves, a bifurcation analysis was developed based on Full Jacobian of the system, which involves both chemical reactions and mixing

processes (Lu, 2011, Shan&Lu, 2012). The bifurcation points are important states that determine flame ignition, extinction and stability. The results from the rigorous bifurcation analysis were accurately replicated by the substantially simpler and more efficient CEMA method, as demonstrated in Fig. 4 for a steady state perfectly stirred reactor with n-heptane/air. The bifurcation points on the “S”-curve, i.e. the transition between red and blue segments, including both turning points and Hopf bifurcation, were accurately captured with CEMA, indicating that CEM is most important in determining ignition and extinction states in steady state combustion. Controlling reactions for each bifurcation points were then identified at each bifurcation point. Such information is important to understand limit flame phenomena and to guide the refinement of the detailed chemistry to accurately predict such flame behaviors as ignition and blow-out.

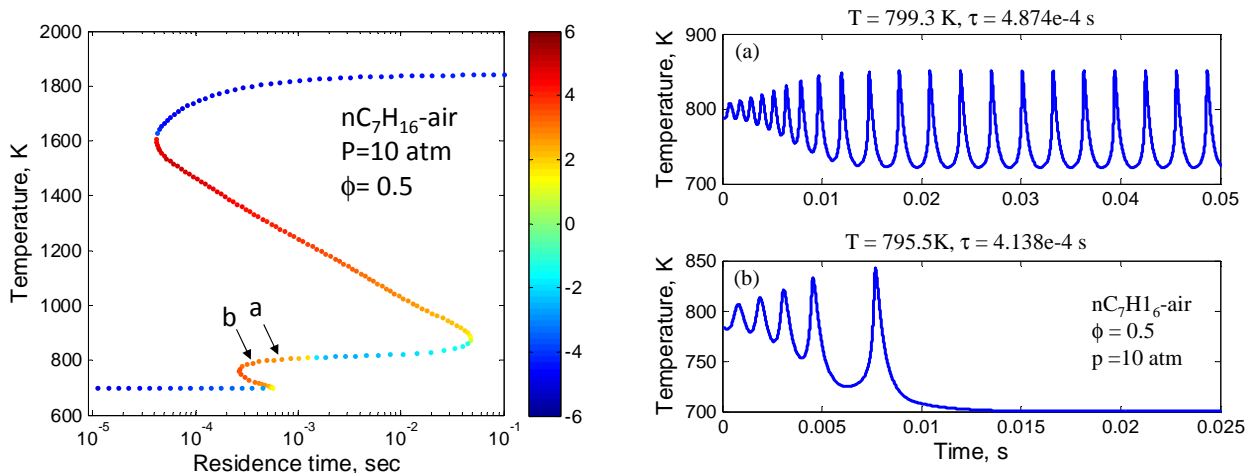


Figure 4: Stable (red) and unstable (blue) branches identified using CEMA for n-heptane/air in steady state perfectly stirred reactors (Lu, 2011; Shan&Lu 2012). Right panels show that flame instabilities, including limit cycle oscillation and extinction, occur at points *a* and *b*, respectively, on the cool flame branch of the “S”-curve.

III. Future Work

Efforts will be devoted in the future for several immediate extensions of the above work. First, the combination of mechanism reduction methods and the bifurcation analysis makes it possible to derive highly reduced chemical kinetics for large transportation fuels by identifying only a few dominate reactions that determines flame ignition and extinction. Such highly reduced chemistry, say with 20~30 species, can enable high-fidelity device-scale flame simulations using realistic chemistry. Second, CEMA will be extended to visualize and track critical flame features in complex flame fields to understand the interactions between flames, turbulence and pollutant emissions, and to guide turbulent combustion modeling. Third, the results from mechanism reduction and computational flame diagnostics will be combined with detailed chemical kinetics development to obtain compact and high-fidelity reaction mechanisms that can efficiently and accurately predict limit flame behaviors.

IV. References

- i. Lu T.F., Law C. K., *Prog. Energy Combust. Sci.*, **2009**, 35, 192.
- ii. Lu T.F., Yoo C.S., Chen J.H., Law C.K., *J. Fluid Mech.*, **2010**, 652, 45.
- iii. Lu T.F., Plenary Talk in the Fall Technical Meeting of the ESSCI, **2011**.
- iv. Luo Z., Plomer M., Lu T.F., Som S., and Longman D.E., *Combust. Theory Model.*, **2012a**, 16, 369.
- v. Luo Z., Yoo C.S., Richardson E., Chen J.H., Law C.K., Lu T.F., *Combust. Flame*, **2012b**, 159, 265.
- vi. Sankaran R., Hawkes E.R., Chen J.H., Lu T.F., Law C.K., *Proc. Combust. Inst.*, **2007**, 31, 1291.
- vii. Shan R., Lu T.F., *Combust. Flame*, **2012**, 159, 2069.
- viii. Yoo C.S., Lu T.F., Chen J.H., Law C.K., *Combust. Flame*, **2011a**, 158, 1727.
- ix. Yoo C.S., Richardson E.S., Sankaran R., Chen J.H., *Proc. Combust. Inst.*, **2011b**, 33, 1619.

Chemical Reaction Dynamics: State-to-State Photodissociation Studies of Reactive Intermediates using Ion Imaging

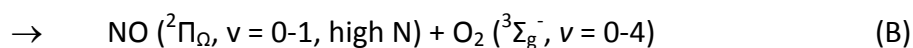
Simon W. North¹

Program Overview

Our research involves the identification of factors that influence the rates, energy disposal and final products of chemical reactions. We are particularly interested in understanding photo-initiated processes involving reactive intermediates. Our approach combines novel high intensity radical beam sources with velocity map ion imaging. Recent efforts include the development of methods for extracting speed-dependent vector correlations from ion images.¹

Imaging Studies of NO₃ Photodissociation

The importance of the NO₃ → NO + O₂ photolysis channel to atmospheric ozone destruction cycles is well known but until very recently the mechanism by which this reaction proceeds has long been a mystery. Although the pathway to NO and O₂ products was originally assumed to arise from the barrier of a concerted 3-center transition state, no such transition state at an accessible energy has been identified. Several measurements of the photofragment energy distributions arising from this channel have revealed the formation of energetically excited O₂ products.² Our ion imaging studies (figure 1) uncovered the presence of two distinct pathways for the formation of NO + O₂:³



Pathway A is associated with vibrationally excited O₂ fragments (v = 5-10) in coincidence with rotationally cold NO fragments, while pathway B is associated with rotationally excited but vibrationally cold fragments. It was noted that the vibrational population inversion of the O₂

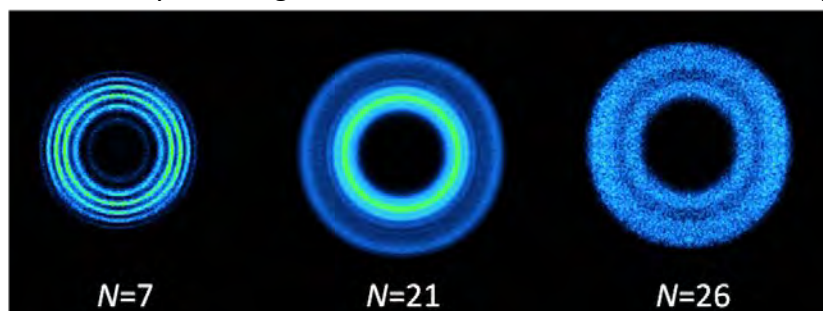


Figure 1. Ion images of NO (²Π, v = 0, N) fragments arising from the dissociation of NO₃ at 588 nm.

fragment originating from the dominant pathway A is similar to the internal energy distributions of products resulting from the roaming mechanism in other systems, such as formaldehyde and acetaldehyde.⁴ Additionally, the excited O₂ vibrational distribution is consistent with

the distribution obtained from the O + NO₂ → NO + O₂ intermolecular abstraction reaction, a

¹ Department of Chemistry, Texas A&M University, College Station, TX 77842

recognized signature of roaming, which has been classified as an *intramolecular* abstraction, and has been shown in the formaldehyde case to yield equivalent product distributions to the corresponding bi-molecular abstraction reaction.

Multistate Roaming

Theoretical calculations by Morokuma and co-workers identified the origins of the two observed pathways.⁵ Multiple potential energy surfaces were explored systematically at the five state-averaged CASSCF (11e,8o)/6-31G level by the global reaction route mapping (GRRM) method. The calculations identified roaming-like ONO-O transition states on the ground and first excited (and optically dark) electronic states. The authors speculated that oxygen atom roaming occurs on the first excited electronic state, but a conical intersection with the ground state along the roaming trajectory results in dissociation on both the ground and excited state potentials. The different O-O bond lengths of the roaming transition state on each potential surface were expected to lead to qualitatively similar O₂ vibrational distributions to the experimental observations, and suggested that *both* reaction pathways may be due to the roaming mechanism, on separate potential energy surfaces. This was the first reported system where roaming accesses multiple electronic potentials, and a system with no experimentally observed competing tight transition state pathway. Klippenstein, Harding, and co-workers have noted that roaming reactions can be classified by the dominance of long-range orientational dynamics and do not require the presence of an alternative tight transition state.⁶

Recently, we measured relative Λ doublet propensities of NO molecules originating from both pathways and determined opposite propensities for fragments arising from the two pathways, consistent with *ab initio* calculations of the orbital occupancy associated with the two electronic states in the exit channel (figure 2).⁷ These studies provided a direct confirmation of the two-state dissociation model with the NO originating from pathway B possessing a strong $^2\Pi$ (A'') propensity, as expected from planar dissociation on the dark state potential. NO originating from pathway A was observed to possess a strong $^2\Pi$ (A') propensity, consistent with both in plane dissociation on the ground state potential.

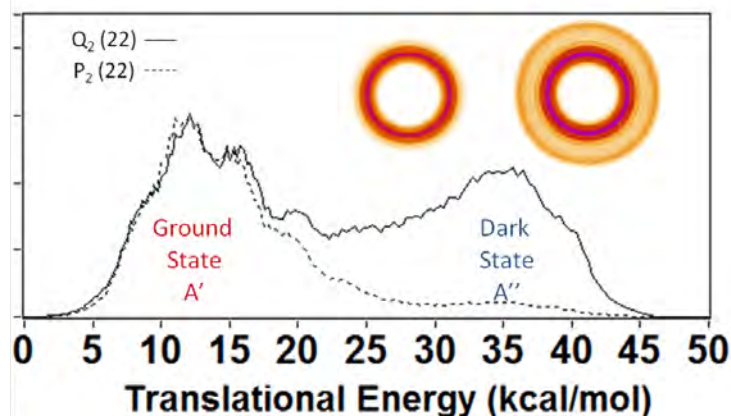


Figure 2. Total translational energy distribution obtained from ion images of the NO ($^2\Pi_{3/2}$, $v=0$, $N=22$) probing the P₂₂ (22) (dashed) and Q₂₂ (22) (solid) transitions.

intriguing that no other system exhibiting roaming behavior has shown any evidence of excited state dynamics. The majority of roaming molecules identified, however, have been close-shell.

The question arises of whether roaming reactions are more or less prone to non-adiabatic surface crossing in the exit channel than conventional dissociation dynamics. Roaming-type mechanisms sample a large area of the potential energy surface in the flat asymptotic region of the surface where the electronic potentials converge, and thus may often involve multistate dynamics. It is therefore

Open-shell molecules such as NO₃ possess many low-lying excited states approaching the same product asymptotes, and multi-state roaming should be more likely for radical molecules. We are currently exploring systems which may exhibit multistate roaming.

Stereodynamics in Roaming

In our studies of NO₃ photodissociation we observed strong vector correlations implying directed torques in the roaming dynamics dispelling previous speculation about unconstrained abstraction as a signature of the roaming mechanism.⁸ No **v-j** correlations have been observed in prior roaming systems. Vector correlations are not unexpected, however, as roaming dynamics are analogous to the corresponding bimolecular reaction, which may or may not possess geometrical constraints and strongly directed torques. Based on our measurements, we would predict similar stereodynamics in NO₂ + O → NO + O₂ reactive scattering. It should be noted that the photodissociation of a low **J** parent molecule via roaming is analogous to a helicity-restricted subset of bimolecular abstraction trajectories. Comparison to trajectory calculations will be extremely insightful in this regard. We are interested in pursuing additional studies aimed at determining the vector correlations in previously reported roaming systems where strong **v-j** correlations are anticipated. Our recent method of extracting *speed-dependent bipolar moment parameters* from DC sliced images should provide an unprecedented view into the dynamics of roaming dynamics.

References

- ¹ M. P. Grubb, M. L. Warter, C. D. Freeman, N. A. West, K. M. Usakoski, K. M. Johnson, J. A. Bartz and S. W. North, *J. Chem. Phys.*, 2011, **135**.
- ² H. F. Davis, B. S. Kim, H. S. Johnston and Y. T. Lee, *J. Phys. Chem.*, 1993, **97**, 2172-2180; K. Mikhaylichenko, C. Riehn, L. Valachovic, A. Sanov and C. Wittig, *J. Chem. Phys.*, 1996, **105**, 6807-6817.
- ³ M. P. Grubb, M. L. Warter, A. G. Suits and S. W. North, *J Phys Chem Lett*, 2010, **1**, 2455-2458; M. P. Grubb, M. L. Warter, K. M. Johnson and S. W. North, *J. Phys. Chem. A*, 2011, **115**, 3218-3226
- ⁴ D. Townsend, S. A. Lahankar, S. K. Lee, S. D. Chambreau, A. G. Suits, X. Zhang, J. Rheinecker, L. B. Harding and J. M. Bowman, *Science*, 2004, **306**, 1158-1161; P. L. Houston and S. H. Kable, *Proc. Natl. Acad. Sci. U.S.A.*, 2006, **103**, 16079-16082.
- ⁵ H. Y. Xiao, S. Maeda and K. Morokuma, *J Phys Chem Lett*, 2011, **2**, 934-938.
- ⁶ L. B. Harding and S. J. Klippenstein, *J Phys Chem Lett*, 2010, **1**, 3016-3020; S. J. Klippenstein, Y. Georgievskii and L. B. Harding, *J. Phys. Chem. A*, 2011, **115**, 14370-14381.
- ⁷ M. P. Grubb, M. L. Warter, H. Y. Xiao, S. Maeda, K. Morokuma and S. W. North, *Science*, 2012, **335**, 1075-1078.
- ⁸ J. M. Bowman and B. C. Shepler, *Annu Rev Phys Chem*, 2011, **62**, 531-553.

Fundamental Studies of Combustion Applied to Engines

David A. Rothamer

Department of Mechanical Engineering, University of Wisconsin-Madison

Madison, WI 53706

rothamer@wisc.edu

I. Program Scope

Internal combustion engines represent a major application of combustion research with significant economic and social importance. Operation of such devices is limited by the regulation of pollutant emissions and fuel economy requirements. Increasingly strict emissions regulations combined with requirements to increase fuel economy necessitate detailed understanding of the combustion process to enable optimization of the in-cylinder energy conversion process in terms of efficiency and emissions.

Work in the principal investigator's laboratory at the University of Wisconsin-Madison Engine Research Center utilizes a broad range of tools to improve understanding of combustion fundamentals applicable to IC engine combustion. These include: development and refinement of laser-based imaging diagnostic techniques, study of laboratory flames to understand the impact of fuel chemistry on the combustion process, application of optical diagnostics to study the in-cylinder combustion process in optically accessible engines, and the use of instrumented single-cylinder metal engines to study combustion under engine relevant in-cylinder conditions.

II. Recent Progress

A. Developments in temperature imaging using thermographic phosphors

Thermographic phosphors have seen widespread use for numerous temperature measurement applications including surface temperature, droplet temperature, and more recently gas-phase temperature measurements. Measurements of the gas phase temperature involve aerosolizing micron sized phosphor particles into the gas of interest to act as tracer particles enabling measurement of the local gas temperature. Phosphors consist of a host material doped with an active ion dopant with well-known spectroscopic transitions. Oxide-based host materials, such as yttrium oxide (Y_2O_3), yttrium stabilized zirconia (YSZ), and yttrium aluminum garnet ($Y_3Al_5O_{12}$, YAG), have melting points in excess of 2200 K, potentially enabling measurements at combustion temperatures. To date, gas-phase measurements using thermographic phosphors have been limited to maximum temperatures of approximately 1100 K in combustion environments due to low signal-levels and signal interference from chemiluminescence [1, 2].

The current work is focused on extending gas phase measurements to higher temperatures in combustion environments. As part of this work a new ion dopant host material combination, trivalent praseodymium doped into YAG (Pr:YAG), has been identified as a phosphor with potential to improve and extend measurement capabilities. The praseodymium ion has unique spectroscopic properties. In particular, it has a 4f-4f transition from $^3P_0 \rightarrow ^3H_4$ which is spin allowed resulting in a high emission rate ($\approx 10^5 \text{ s}^{-1}$) compared to other 4f transitions in rare earth ions.

Non-radiative relaxation processes including: direct multi-phonon relaxation, cross relaxation, and relaxation through a charge transfer state, limit signal levels at elevated temperatures and influence the time decay and relative signal levels impacting the measurement of temperatures. To study these processes a series of time-resolved measurements have been performed as a function of temperature using phosphors with Pr^{3+} doping levels varying from 0.5 to 4.0%. These data have been used to develop a rate based model describing the decay of the luminescence signal.

The time resolved data have also been used to optimize the temperature measurement technique using the phosphor. The signals were used in an optimization process which allowed the optimal camera integration durations and timing to be determined. This allowed for the development of a novel detection technique combining both time-decay measurements and spectral ratio-based measurements to determine temperature.

B. Comparison of the sooting propensity of real fuels and there commonly used surrogates

Applied computational fluid dynamics modeling of internal combustion engines has historically viewed the in-cylinder measured pressure trace and the calculated heat release rate as the primary parameters for model validation. Increasingly stringent emissions regulations, particularly with regards to soot mass and soot particle number, have place increased emphasis on also obtaining accurate, predictive, information on the formation of soot in-cylinder. Due to computational time limitations models using detailed chemistry generally utilize reduced mechanisms of surrogate fuels to simulate the chemistry of the real fuels (gasoline, jet, or diesel fuel) [3]. Therefore, it is of utmost importance that, to at least first order, the sooting propensity of the real fuel and its surrogate are matched under the conditions of interest.

To aid in understanding whether a surrogate mixture replicates the sooting behavior of a real fuel with sufficient fidelity an experimental study was undertaken. Measurements were performed using a methane laminar co-flow diffusion flame seeded with 2000 ppm of the surrogate and real fuels of interest. The spatial distribution of soot volume fraction within the flames was measured using a combination of line-of-sight extinction and planar laser-induced incandescence measurements. The impact of the seeded fuels on soot morphology was also quantified using TEM imaging of thermophoretically sampled soot.

A large range of real fuels were tested including gasoline, #2 diesel, jet-A, and an iso-paraffinic kerosene (IPK) jet fuel. Results of the soot volume fraction measurements indicate that matching aromatics concentration in the surrogate with the real fuel being simulated is a key first step to matching diffusive sooting propensity of the surrogate fuels. Additionally, taking into account the sulfur content of the fuel appears to be of importance when comparing non-sulfur containing surrogate mixtures with sulfur containing real fuels. Morphology of the sooting was generally closely matched between the real and surrogate mixtures when soot volume fraction was also matched.

C. Study of the ignition characteristics of jet fuels in a diesel engine

Ignition delay plays a key role in the operation and performance of diesel engines and other practical combustion devices. To understand the impact of fuel volatility and autoignition properties on ignition at conditions relevant for diesel engines, ignition delay measurements were performed over a wide range of in-cylinder conditions for five fuels: jet-A, three blends of Sasol IPK and jet-A, and a #2 diesel fuel, were performed in a 2.44 L heavy-duty single-cylinder diesel engine. A single injection of fuel was used at 5 crank angle degrees before top-dead center (TDC). The in-cylinder conditions at the start of injection were systematically varied over a range of in-cylinder densities from 15 to 40 kg/m³ in 5 kg/m³ increments. For each density, average in-cylinder temperature was varied over as large of a range as possible by heating the intake air. The range of obtainable temperatures was density dependent, but for each density the temperature was varied from approximately 900 to 1100 K. In-cylinder pressure measurements were performed allowing for ID determination. Methods for in-cylinder temperature determination and ID measurement criteria were tested and compared. The results indicate that the fuel volatility and properties influencing spray breakup have minimal impact on the ignition process. Ignition delay results show good agreement with previous measurements by other investigators performed in a constant volume combustion vessel.

III. References

1. Takada, N., et al., Two-Dimensional Temperature Measurements in Diesel Piston Bowl Using Phosphor Thermometry. SAE Technical Paper, 2009. **2009-24-0033**.
2. Hasegawa, R., et al., Two-dimensional gas-phase temperature measurements using phosphor thermometry. Applied Physics B-Lasers and Optics, 2007. **88**(2): p. 291-296.
3. Ra, Y. and R.D. Reitz, A combustion model for IC engine combustion simulations with multi component fuels. Combustion and Flame, 2011. **158**(1): p. 69-90.

Photoinitiated Dissociation Dynamics of Combustion Radicals

Jingsong Zhang
Department of Chemistry
University of California at Riverside
Riverside, CA 92521
Email: jingsong.zhang@ucr.edu

Our research program focuses on spectroscopy and photochemistry of free radicals important in combustion and atmospheric chemistry. The photodissociation dynamics studies probe potential energy surfaces and their influences on chemical reactivity, and provide basic understanding of free radical electronic structures, excited states, and decomposition mechanisms. Our group exploits a high-sensitivity, high-resolution high- n Rydberg-atom time-of-flight (HRTOF) technique to obtain photoproduct translational energy and angular distributions, the key information for probing photodissociation mechanisms. The free radicals that have been investigated include diatomic (OH, SH/SD), alkyl (methyl, ethyl, propyl, butyl), unsaturated aliphatic (vinyl, propargyl, allyl), aromatic (phenyl, benzyl), and oxygen- and sulfur-containing radicals (formyl, vinoxy, thiomethoxy).¹⁻¹⁰

This presentation focuses on the ultraviolet (UV) photodissociation dynamics of a series of prototypical alkyl radicals (methyl, ethyl, propyl, and butyl) using the HRTOF technique. The UV photodissociation dynamics of the methyl (CH_3) radical via its $3s$ Rydberg state at 216.3 nm has been examined. The $\text{H} + \text{CH}_2$ product translational energy

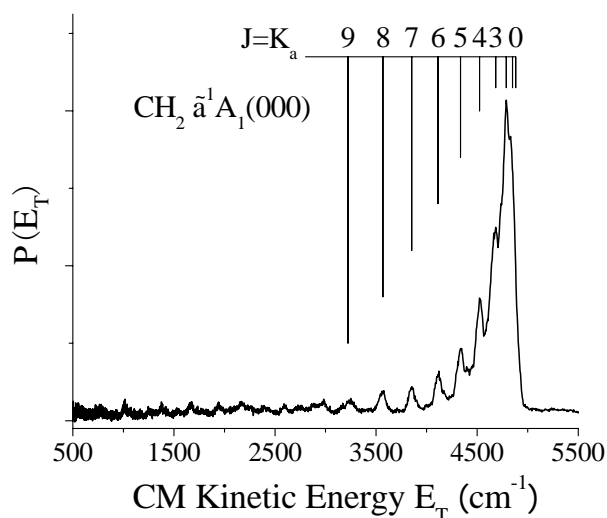


Fig. 1. CM product translational energy distribution $P(E_T)$ of the $\text{H} + \text{CH}_2$ product channel from CH_3 photodissociation at 216.3 nm. CH_2 is produced predominantly in the ground vibrational level of the $\tilde{a}^1\text{A}_1$.

distribution indicates that CH₂ is produced predominantly in the ground vibrational level of the \tilde{a}^1A_1 state, with small rotational excitation (Figure 1). A negative anisotropy parameter is observed, consistent with the perpendicular $B^2A_1' \leftarrow X^2A_2''$ transition (excitation of $2p_z$ electron to $3s$ Rydberg orbital) at 216.3 nm and a fast dissociation by tunneling. The rotational structure of the CH₂ ($\tilde{a}^1A_1, v = 0$) product is resolved for the first time, indicating that CH₂ rotates preferentially around its a axis (with $J = K_a$) and H atom departs slightly off the plane of the parent CH₃. State-resolved tunneling dynamics in CH₃ is revealed. The bond dissociation energy $D_0(\text{CH}_2\text{-H}) = 38188 \pm 30 \text{ cm}^{-1}$ is deduced from the product translational energy distribution.

Upon excitation to the $\tilde{A}^2A_1(3s)$ state at 245-nm, ethyl dissociates into H atom and ethylene. Bimodal profile in the product translational energy distribution and energy-dependent product angular distribution indicate two different dissociation pathways that are influenced by conical intersection. A slow and isotropic component corresponds to unimolecular dissociation of the hot radical after internal conversion from the \tilde{A} state to the ground state. A fast and anisotropic component corresponds to a direct, rapid H-atom scission via a nonclassical H-bridged transition state from the $3s$ state to yield H + C₂H₄. The dissociate rate of the H-atom elimination channel of ethyl is reinvestigated.

Upon excitation to the $3p$ state in the region of 237 nm, n -propyl radical and iso -propyl radical dissociate into the H atom and propene products. The product translational energy release of both n -propyl and iso -propyl radicals also have bimodal distributions. The H-atom product angular distribution in n -propyl is anisotropic (with $\beta \sim 0.5$), while that in iso -propyl is isotropic. The bimodal translational energy distributions also indicate two dissociation pathways, a unimolecular dissociation pathway from the ground-state propyl after internal conversion from the $3p$ state and a repulsive pathway directly connected with the excited state of the propyl radical. Isotope labeling experiments are also carried out.

References

- (1) K. Xu and J. Zhang, *J. Chem. Phys.* **111**, 3783 (1999).
- (2) G. Amaral, K. Xu and J. Zhang, *J. Chem. Phys.* **114**, 5164 (2001).
- (3) W. Zhou, Y. Yuan, and J. Zhang, *J. Chem. Phys.* **119**, 9989 (2003).
- (4) J. Zhang, "Photodissociation Dynamics of Free Radicals," in *Modern Trends in Chemical Reaction Dynamics Part II, Advanced Series in Physical Chemistry, Vol. 14*, ed. Xueming Yang and Kopin Liu, World Scientific, Singapore, 2004, pp. 465.
- (5) W. Zhou, Y. Yuan, S. Chen, and J. Zhang, *J. Chem. Phys.* **123**, 054330 (2005).
- (6) S. Chen, W. Zhou, and J. Zhang, *Chem. Phys. Lett.* **418**, 328 (2006).
- (7) X. Zheng, Y. Song, J. Wu, and J. Zhang, *Chem. Phys. Lett.* **467**, 46 (2008).
- (8) X. Zheng, Y. Song, and J. Zhang, *J. Phys. Chem. A* **113**, 4604 (2009).
- (9) X. Zheng, J. Wu, Y. Song, and J. Zhang, *Phys. Chem. Chem. Phys.* **11**, 4761 (2009).
- (10) Y. Song, X. Zheng, M. Lucas, and J. Zhang, *Phys. Chem. Chem. Phys.*, **13**, 8296 (2011).
- (11) Y. Song, M. Lucas, M. Alcaraz, J. Zhang, and C. Brazier, *J. Chem. Phys.* **136**, 044308 (2012).

*Abstracts
of
Principal Investigator
Presentations*

The relaxation of methylene in collisions with He

Millard H. Alexander (mha@umd.edu),¹ LiFang Ma,[†] Jacek Klos[‡]

Department of Chemistry and Biochemistry, University of Maryland, College Park, MD 20742-2021

Paul J. Dagdigian[§] and Qianli Ma[†]

Department of Chemistry, The Johns Hopkins University, Baltimore, MD 21218-2685

I. Program Scope

Our group studies inelastic and reactive collisions of small molecules, focusing on radicals important in combustion environments. Our goal is the better understanding of kinetic processes which may be difficult to access experimentally. An essential component is the accurate determination of potential energy surfaces (PES's). After fitting the *ab initio* points to obtain global PESs, we treat the dynamics using time-independent (close-coupling) methods.

II. Recent Progress

Inelastic collisions of the methylene radical (CH₂) are currently under experimental study at Brookhaven.¹⁻³ Since inception of our DOE-funded program (fall, 2009) we focused on the study of collisions of He with methylene in its \tilde{a}^1A_1 state and, more recently, in its \tilde{X}^3B_1 ground state, as well with the methyl radical (CH₃) in its \tilde{X}^2A_2'' ground electronic state. Our work is among the first detailed simulations of state-to-state relaxation of asymmetric and symmetric top molecules.

Our quantum simulations of the collision dynamics are based on highly-accurate CCSD(T) determinations of the interaction potentials, with correlation-consistent basis sets, extrapolated to the complete basis set limit. The calculations are carried out on a large grid of CH_n-He orientations and separation distances. These *ab initio* points are then fitted⁴ by expansions in spherical harmonics.

In the case of CH₂ the expansion is in the appropriate inertial frame, in which the *z* axis lies perpendicular to the C₂ axis, but along the *a* inertial axis (Fig. 1). In the \tilde{X} state, the out-of-plane 2*p_y* orbital is singly occupied, thus the electronic anisotropy of the state is reduced, compared to that in the \tilde{a} state, where this orbital is unoccupied. Thus CH₂(\tilde{a}) behaves as an amphoteric Lewis acid/base. When, as shown in Fig. 2, He approaches perpendicular to the molecular plane, the interaction is substantially less repulsive than when He approaches in the molecular plane. This electronic anisotropy is substantially reduced in the interaction of He with CH₂(X).



Fig. 1. Geometry of the CH₂-He system, with the *z* axis aligned along the *a* inertial axis, perpendicular to the C₂ axis.

Fig. 2. Dependence of PES for motion of the He atom in the *xy*-plane for three CH₂-He distances. Left panel: X state; right panel: \tilde{a} state.

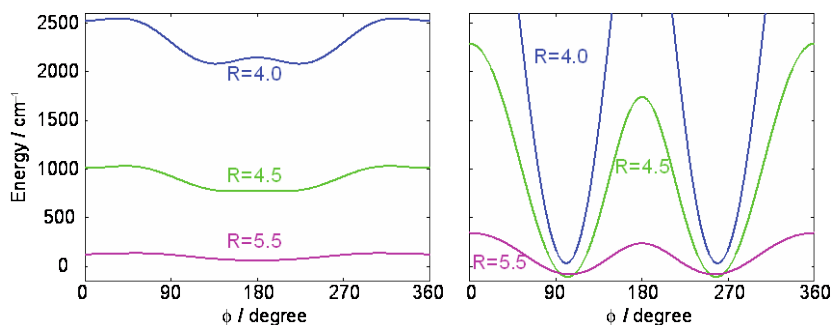


Figure 3 shows the relative spacing and dependence on the HCH angle θ of the potentials of the isolated CH₂ molecule for the X and \tilde{a} states. Since the barrier to linearity lies below the higher bending levels in the X state, the molecule samples a wide range of bending angles. We calculated

¹ Principal investigator; [†] Graduate student; [‡] Research Assistant Professor; [§] Senior collaborator.

the $\text{CH}_2(X)\text{-He}$ potential at a number of bending angles, then averaged over the square of individual bending vibrational wavefunction.

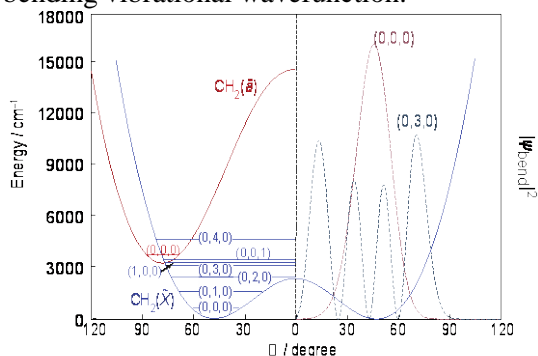


Fig. 3. (Left-hand panel) The dependence on the bending angle of the energies of the \tilde{a} (red curve) and the X (blue curve) states of CH_2 . In both cases the bond lengths are frozen at their equilibrium values. The horizontal lines indicate the positions of the lower vibrational levels. (Right-hand panel) The dependence of the bending probability (the square of the bending wavefunction) on the bending angle for the $(0,0,0)$ vibrational level of the \tilde{a} state (red) and the $(0,3,0)$ level of the X state (blue).

Cross sections and rate constants for collisions of He with CH_2 and CH_3 were determined with our Hibridon program suite.⁵ Figure 4 compares representative inelastic cross sections. We observe

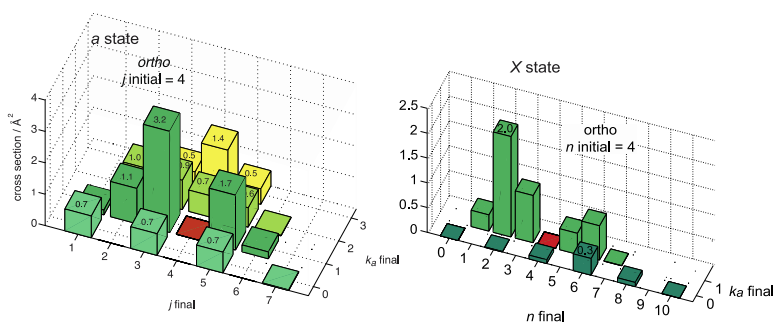


Fig. 4. Bar plot of the cross sections for rotationally inelastic scattering of *ortho* CH_2 in the $k_a=1$ state in the \tilde{a} $(0,0,0)$ state (left) and X $(0,3,0)$ state (right) in collisions with He at a collision energy of 300 cm^{-1} . The red square denotes the initial level.

first that the magnitude of the cross section for scattering of CH_2 in the a state is roughly a factor of two larger than for scattering of the molecule in its ground electronic state. This reflects the much larger anisotropy of the PES in the excited state due to the hole in the out-of-plane $2p_y$ orbital on the C atom.

Because of the lower barrier to linearity in the X state, the k stacks are more widely separated. Consequently, as is seen in Fig. 4, the scattering of the X state is much less inelastic in the projection quantum number k_a . As the degree of bending vibrational excitation decreases, and the average degree of bending increases, the k stacks become more closely spaced and the degree of inelasticity in k increases.

As seen in Table I, both these effects are manifest in total rotationally inelastic cross sections and the average change in the rotational and projection quantum numbers for scattering out of the $n=4$ rotational level of *ortho*- CH_2 in several bending vibrational levels of the a state and X states.

Quantity	$a(0,0,0)$	X			
		$(0,0,0)$	$(0,1,0)$	$(0,2,0)$	$(0,3,0)$
σ_R (\AA^2)	14.2	7.7	7.5	6.1	4.9
$\langle \Delta n \rangle$	1.1	1.32	1.59	1.80	1.79
$\langle \Delta k \rangle$	0.71	0.65	0.54	0.31	0.10

Table I. Overall inelastic cross sections, and averaged changes in the rotational and projection quantum numbers for collisions of *ortho*- CH_2 with He at a collision energy of 300 cm^{-1} .

In collisions of the planar methyl radical with He, the PES is dominated by the strong anisotropy arising from the equilateral arrangement of the three H atoms in the molecular plane. We found a strong propensity for transitions that involve $\Delta k = \pm 3$ transitions. This propensity results from the large magnitude of the v_{33} term in the angular expansion of the PES, reflecting the strength and symmetry of the repulsion between the hydrogen atoms in the CH_3 radical and the He collision partner.

III. Comparison with Experiment

Figure 5 compares the rate constants for collisional removal (summed over all final states) for the $k_a=1$ levels of *ortho*-CH₂(\tilde{X} , \tilde{a}) with experimental results from Brookhaven.³ The experiments monitor the rate of infilling of an initially depleted rotational level. This rate can be shown to be equivalent to the rate of collisional removal for the same level.⁶

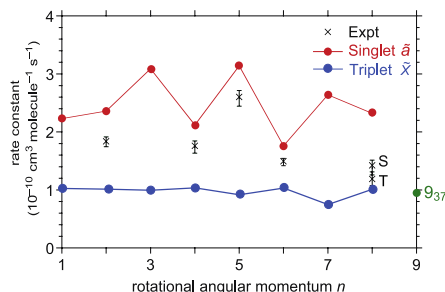


Fig. 5. Rate constants for collisional removal by rotational transitions for *ortho* $k_a = 1$ levels of CH₂(\tilde{a} , 0,0,0) (red) and CH₂(\tilde{X} , 0,3,0) in collisions with helium. Our theoretical values are compared with the experimental results of Hall, Sears, and their co-workers (Ref. 3). The $j = 8$ level of the manifold is known to be strongly perturbed by a vibration-rotation level of the \tilde{X}^3B_1 state (Ref. 7). The labels “S” and “T” denote the experimentally observed rate constants for the two perturbed levels of predominantly singlet and triplet character, respectively. Also shown is the calculated relaxation rate of the $n=9$, $k_a=3$ level of the (0,2,0) manifold. One spin component of this \tilde{X} level is mixed with the $j=8$, $k_a=1$ level of the (0,0,0) manifold of the \tilde{a} state.

We see that rotational relaxation of the \tilde{X} state will be substantially slower. Figures 4 and 5 demonstrate that the overall efficiency and the detailed state-to-state pathways of rotational relaxation are very dependent on the electronic state. The extent of this difference is larger than one might anticipate from a consideration of the relaxation of a diatomic molecule, where the anisotropy of the electronic charge distribution in the allowable valence states is very similar. In the case of CH₂, the difference is due to a remarkable, but easily understandable, variation in the anisotropy of the charge distribution. More generally, one should expect similar variations in other open-shell triatomic (and polyatomic) molecules. Thus, in modeling the kinetics of different excited states of these molecules, one should not uncritically adopt a single set of parameters which are independent of electronic state.

IV. Kinetic modeling

In joint work with Hall at Brookhaven we presented a pedagogical, mathematical study of the so-called master equation which describes the approach of initial rotational distribution to a Boltzmann equilibrium population. In particular, we show, in an approachable way, how the time change in population can be analyzed in terms of a set of “normal modes” of the relaxation, which evolve independently in time. We also use techniques from linear algebra to prove that all of these normal modes relax to zero except the lowest mode, which is the Boltzmann distribution.

V. Future Work

a. Electronic-rotational relaxation involving the \tilde{X} state of methylene

Up to now we have not investigated collisional energy transfer between the mixed \tilde{a} and \tilde{X} state levels. Experimentally, facile energy transfer has been observed.^{8,9} We will model this process by the “gateway” mechanism of Gelbart and Freed,¹⁰ whereby singlet-triplet energy transfer occurs through discrete vibration-rotation levels of the \tilde{a} and \tilde{X} states with the same total angular momentum and parity, which are coincidentally nearly degenerate and hence strongly-mixed by the weak spin-orbit coupling. The consequence of this electronic mixing is seen in Fig. 5 in the experimental $j=8$ points marked “S” and “T”. Cross sections (and, subsequently, rate constants) can be obtained by taking linear combinations of the S -matrix elements for scattering of the CH₂ molecule in either one or the other of these two states.

b. Vibrational relaxation in methylene and methyl

Having determined the CH₂(\tilde{X})-He and CH₃(\tilde{X})-He potential energy surface as a function of the methylene bending angle, we will modify our Hibridon⁵ inelastic scattering code to allow the determination of cross sections for (bending) vibrationally-inelastic processes. Our goal is to obtain an estimate of the relative efficiency of these processes to aid, eventually, in developing more accurate kinetic models for simulations of combustion environments involving methylene, methyl and similar

polyatomic species. Because the calculated PES depends little on the bending angle, we anticipate that vibrational relaxation will be relatively inefficient in CH₂.

c. Depolarization in the CN radical

We have been involved in studies, with McKendrick's group in Edinburgh (UK) of depolarization in collisions of the CN radical.¹¹ Similar experimental work is underway in Hall and Sears' group at Brookhaven. We will use our quantum scattering studies to interpret and compare these experiments.

VI. Publications and submitted journal articles supported by this project to date

1. L. Ma, M. H. Alexander, and P. J. Dagdigian, "Theoretical investigation of rotationally-inelastic collisions of CH₂(\tilde{a}) with helium," J. Chem. Phys. **134**, 154307 (2011)
2. M. H. Alexander, G. Hall, and P. J. Dagdigian, "The Approach to Equilibrium: Detailed Balance and the Master Equation," J. Chem. Educ. **88**, 1538 (2011).
3. L. Ma, M. H. Alexander, and P. J. Dagdigian, "Theoretical investigation of rotationally-inelastic collisions of CH₂(\tilde{X}) with helium," J. Chem. Phys. (submitted).
4. P. J. Dagdigian and M. H. Alexander, "Theoretical investigation of rotationally inelastic collisions of the methyl radical with helium", J. Chem. Phys. **135**, 064306 (2011).

VII. References

1. Y. Kim, A. V. Komissarov, G. E. Hall, and T. J. Sears, "Observation of the c^1A_1 state of methylene by optical-optical double resonance," J. Chem. Phys. **123**, 24306 (2005).
2. Z. Wang, Y. Kim, G. E. Hall, and T. J. Sears, "State mixing and predissociation in the c^2a band system of singlet methylene studied by optical-optical double resonance," J. Phys. Chem. A **112**, 9248-9254 (2008).
3. S. K. Lee, Y. Kim, T. J. Sears, and G. E. Hall, private communication.
4. P. J. Dagdigian and M. Alexander, "Depolarization in H₂O-He collisions," Mol. Phys. **108**, 1159-1169 (2010).
5. HIBRIDON is a package of programs for the time-independent quantum treatment of inelastic collisions and photodissociation written by M. H. Alexander, D. E. Manolopoulos, H.-J. Werner and others. More information and/or a copy of the code can be obtained from the website <http://www2.chem.umd.edu/groups/alexander/hibridon/hib43>.
6. M. H. Alexander, G. Hall, and P. J. Dagdigian, "The Approach to Equilibrium: Detailed Balance and the Master Equation," J. Chem. Educ. **88**, 1538-1543 (2011).
7. U. Bley and F. Temps, "Collision-induced intersystem crossing of CH₂ from a^1A_1 to X^3B_1 : A case-study of the mixed-state model," J. Chem. Phys. **98**, 1058-1072 (1993).
8. A. V. Komissarov, A. Lin, T. J. Sears, and G. E. Hall, "State-resolved thermalization of singlet and mixed singlet-triplet states of CH₂," J. Chem. Phys. **125**, 084308 (084305 pages) (2006).
9. D. Patel-Misra and P. J. Dagdigian, "State-resolved electronic quenching of NH($a^1\Delta$) by Xe and CO," J. Chem. Phys. **97**, 4871-4880 (1992).
10. W. M. Gelbart and K. F. Freed, "Intramolecular perturbations and quenching of luminescence in small molecules," Chem. Phys. Lett. **18**, 470-475 (1973).
11. S. J. McGurk, K. G. McKendrick, M. L. Costen, D. I. G. Bennett, J. Klos, M. H. Alexander, and P. J. Dagdigian, "Depolarization of rotational angular momentum in CN($A^2\Pi$, $v = 4$) + Ar collisions," J. Chem. Phys. **136**, 00000 (2012).

Theoretical Studies of Elementary Hydrocarbon Species and Their Reactions

Wesley D. Allen and Henry F. Schaefer III
Center for Computational Chemistry and Department of Chemistry
University of Georgia, Athens, GA 30602-2525
E-mail: wdallen@uga.edu and sch@uga.edu; Phone: (706) 542-7729

Methylhydroxycarbene: Tunneling Control of a Chemical Reaction

In joint theoretical and experimental work published in *Science* within the last year,³⁰ methylhydroxycarbene (**1**, Me-C-OH) was generated for the first time by high vacuum flash pyrolysis (HVFP) of pyruvic acid (at 900 °C) and spectroscopically (IR, UV/Vis) characterized via immediate matrix isolation in solid Ar at 11 K. The identity of **1** was unequivocally confirmed by precise agreement between observed IR bands and theoretical anharmonic vibrational frequencies computed from an all-electron (AE) CCSD(T)/cc-pCVTZ complete quartic force field. The UV/Vis spectrum of **1** displays a broad band with maximum absorption at 393 nm (3.2 eV) that extends to around 460 nm (2.7 eV), in full accord with our aug-cc-pVTZ multireference coupled cluster [Mk-MRCCSD(T)] computations that gave a gas-phase vertical (adiabatic) excitation energy of 3.4 (2.7) eV. Surprisingly, we observed rapid disappearance **1** after cryogenic trapping. Upon standing in Ar at 11 K in the dark, the IR peaks of **1** decayed gradually via first-order kinetics with a half-life of $t_{1/2} = 66 (\pm 5)$ min. In stark contrast, the bands of the deuterium isotopologue Me-C-OD (**d-1**) did not change under identical conditions for extended periods of time (at least 16 h). The kinetic experiments thus revealed that **1** isolated in its ground vibrational and electronic state exhibits facile [1,2]-hydrogen tunneling and that two conspicuous phenomena occur simultaneously: efficient penetration of a formidable 28.0 kcal mol⁻¹ barrier to yield acetaldehyde (**3**), and complete obstruction of the formation of vinyl alcohol (**4**) despite a much lower 22.6 kcal mol⁻¹ barrier.

We established the theoretical basis for the remarkable behavior of methylhydroxycarbene by computing pure tunneling rates for both **1** → **3** and **1** → **4**. The AE-CCSD(T)/cc-pCVTZ method was employed to precisely map out the associated intrinsic reaction paths (IRPs) descending from transition states **TS_{1t-3}** and **TS_{1t-4t}** (Fig. 1) and to determine zero-point vibrational energies (ZPVEs) along these steepest-descent routes. Final potential energy curves for the isomerization paths were then constructed from high-quality AE-CCSD(T)/cc-pCVQZ energy points appended with the ZPVEs. Tunneling probabilities for our high-accuracy IRPs were computed by exact numerical methods and also by WKB theory. This theoretical analysis yielded a tunneling half-life of 71 min for **1** → **3**, in close agreement with the observed rate of decay. Moreover, the computed half-life for **1** → **4** was 190 days, nicely explaining why vinyl alcohol is not the preferred product of methylhydroxycarbene isomerization, despite the lower barrier for formation of **4**.

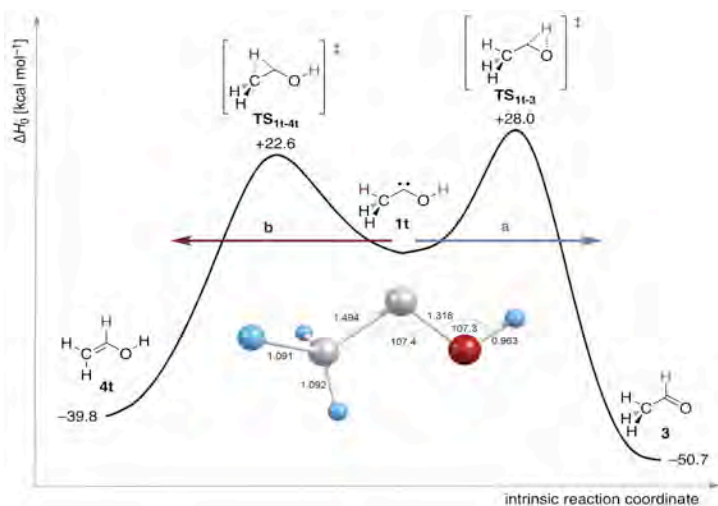


Figure 1. Energetic profiles for [1,2]H-shift isomerizations of *trans*-methylhydroxycarbene (**1t**); relative energies (in kcal mol⁻¹) pinpointed from convergent focal-point analysis (FPA) computations. The bond lengths (Å) and angles (°) given for **1t** are ground-state optimum geometrical parameters given by AE-CCSD(T)/cc-pCVQZ theory. The curves are drawn quantitatively with the intrinsic reaction coordinate (IRC) in mass-weighted Cartesian space as the abscissa in order to reflect the proper barrier heights and widths for the two competing reactions. Simple visual inspection thus indicates a higher hydrogen tunneling probability for the more narrow energy profile of path **a**.

Methylhydroxycarbene highlights the possibility of reactions in which the observed product is neither the one requiring the lowest activation barrier nor the one with the lowest free energy but rather the one most readily reached by quantum mechanical tunneling. It is worth emphasizing that the remarkable tunneling behavior of

methylhydroxycarbene is not an isolated occurrence, as our earlier research demonstrated that both hydroxymethylene [*Nature* **453**, 906–909 (2008)] and phenylhydroxycarbene¹⁹ spontaneously isomerize to their respective aldehydes via H-tunneling under large barriers near 30 kcal mol⁻¹.

Explicitly Correlated R12 Methods for Radicals

The Coulomb singularities in the electronic Hamiltonian require the exact wave function to display a cusp and corresponding depletion of electron density (Coulomb hole) when any interelectronic distance (r_{12}) approaches zero. Unlike conventional electronic structure methods, approaches using wave functions that depend explicitly on r_{12} can effectively treat the cusp region without the need for large orbital basis sets. While closed-shell and spin-orbital explicitly correlated (R12) methodologies for coupled-cluster theory have been well developed, open-shell, spin-restricted R12 methods are lacking, which is problematic for the free-radical chemistry predominant in combustion applications. An ideal starting point for open-shell R12 methods is the symmetric exchange or Z-averaged approach. By introducing a symmetric exchange operator for α and β electrons, the number of wave function parameters is drastically reduced. This formalism has negligible spin contamination compared to unrestricted methods, and the imposed spin constraints do not introduce size-consistency errors as in many other spin-adapted schemes. Building on our previous work on ZAPT2-R12 perturbation theory for open-shell systems,⁸ we have now developed capabilities for the more complicated and robust ZA-CCSD-R12 method.²² We have demonstrated the excellent basis set convergence of our ZA-CCSD-R12 method for a series of atomization energies. Specifically, with only a triple- ζ (TZ) quality basis, ZA-CCSD-R12 surpasses the accuracy of conventional computations with augmented sextuple- ζ (aV6Z) basis sets.

The Propyl + O₂ Reaction System

Reactions of alkyl radicals (R·) with O₂ are ubiquitous in combustion, atmospheric chemistry, and biological processes. As the size of the alkyl radical grows, R + O₂ reactions rapidly become more complex, and isomerizations to hydroperoxyalkyl radicals (QOOH) can increase in importance relative to concerted elimination of HO₂. The need for definitive *ab initio* theoretical research on propyl + O₂ is demonstrated by the disparity between the reaction energetics from the best existing electronic structure computations and parameters derived from master equation kinetic models that best reproduce the available body of experimental measurements. In a herculean investigation, we have fully optimized geometries at the CCSD(T)/cc-pVTZ level of theory for all chemically relevant minima and transition states of the *n*-propyl and *i*-propyl + O₂ systems (Fig. 2). Final energetics for combustion models were derived from explicit computations with basis sets as large as cc-pV5Z and correlation treatments as extensive as coupled cluster through full triples with perturbative inclusion of quadruple excitations [CCSDT(Q)]. Focal point analyses (FPA) targeting the complete basis set (CBS) limit of CCSDT(Q) theory were executed with inclusion of auxiliary corrections for core correlation and relativistic effects. For the *n*-propyl + O₂ system, the critical transition state (TS1) for concerted elimination of HO₂ lies 3.4 kcal mol⁻¹ below the reactants and 2.6 kcal mol⁻¹ lower than the key isomerization transition state (TS2) for CH₃CHCH₂OOH radical formation. Even the robust CCSD(T)/cc-pVQZ method yields a concerted elimination barrier that is 1.8 kcal mol⁻¹ too high, a striking result because such shifts of barrier heights in R + O₂ reactions can change branching fractions by an order of magnitude.

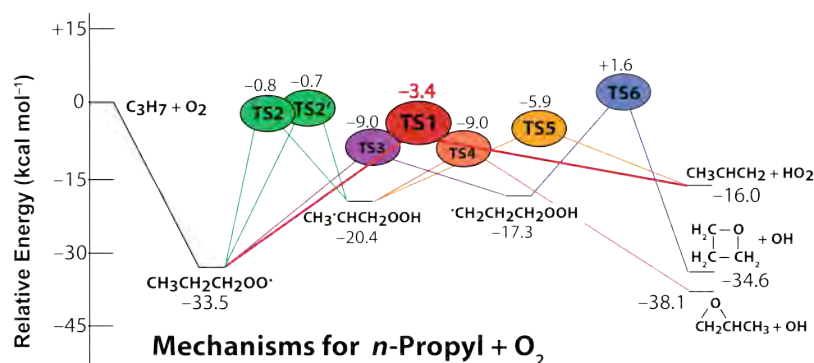


Figure 2. Energetic results from rigorous focal-point analyses (FPA) of the potential energy surfaces for the reactions of *n*-propyl radicals with molecular oxygen.

A new discovery is that two distinct, nearly isoenergetic transition states (Fig. 3; TS2, -0.84 kcal mol⁻¹; TS2', -0.71 kcal mol⁻¹) exist for producing the CH₃CHCH₂OOH radical by hydrogen transfer from the peroxypropyl intermediate. Earlier master equation kinetic models did not include the TS2' path, resulting in an empirically-

adjusted barrier height for $\text{CH}_3\text{CHCH}_2\text{OOH}$ formation that is too low. Our definitive energetics for propyl + O_2 provide benchmarks for critical assessment and improvement of current kinetic models.

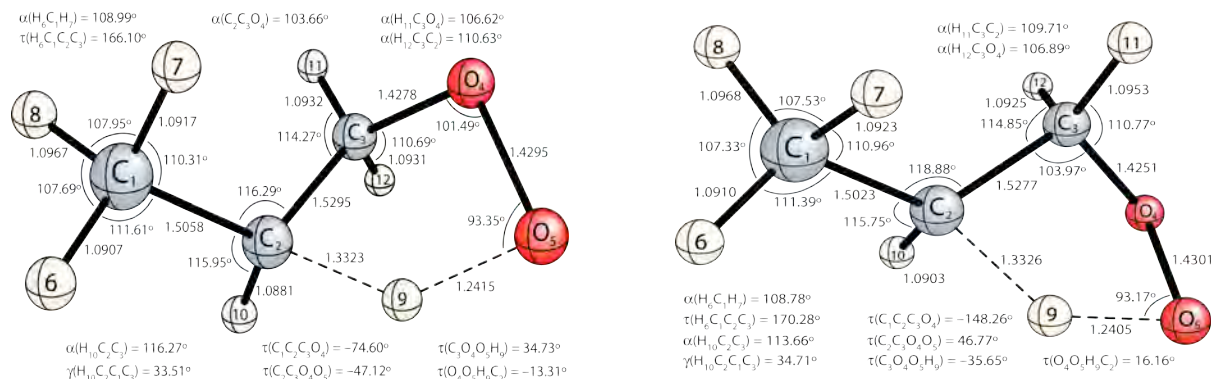


Figure 3. Competing CCSD(T)/cc-pVTZ transition states (TS2, left; TS2', right) for formation of hydroperoxypropyl QOOH radicals from peroxypropyl intermediates.

Vibrational Anharmonicity in Combustion Kinetics; Radical-Radical Abstraction Reactions

Collaborations with Stephen Klippenstein and Larry Harding at Argonne have been undertaken with two primary objectives: (1) Exploration of the effects of vibrational anharmonicity in combustion kinetics by rigorous investigation of the $\text{H} + \text{H}_2\text{O}_2 \rightarrow \text{H}_2\text{O} + \text{OH}$ and $\text{H} + \text{H}_2\text{O}_2 \rightarrow \text{H}_2 + \text{HO}_2$ reactions at the highest possible levels of electronic structure theory. Full quartic force fields and vibrational anharmonicity constants (x_{ij}) were computed for the reactants and transition states of these two reactions at the coupled-cluster CCSD(T)/aug-cc-pVQZ level of theory. Anharmonic vibrational state counts were employed with various options for computation of rate coefficients. (2) Examination of paradigmatic potential energy surfaces for radical-radical abstractions, a general class of reactions in combustion chemistry. Our multireference coupled cluster methods (Mk-MRCC) were applied to the $\text{CH}_3 + \text{C}_2\text{H}_5 \rightarrow \text{CH}_4 + \text{C}_2\text{H}_4$ hydrogen-abstraction reaction path, as well as the $\text{CH}_3 + \text{CH}_3 \rightarrow \text{C}_2\text{H}_6$ recombination curve. These rigorous results provide important benchmarks for validating more approximate electronic structure methods for studying radical-radical abstraction and recombination.

Publications Supported by DOE: 2009-2012

1. S. E. Wheeler, K. N. Houk, P. v. R. Schleyer, and W. D. Allen, "A Hierarchy of Homodesmotic Reactions," *J. Am. Chem. Soc.* **131**, 2547 (2009).
2. P. R. Schreiner, H. P. Reisenauer, E. Mátyus, A. G. Császár, A. Siddiqi, A. C. Simmonett, and W. D. Allen, "Infrared Signatures of the NCCO Radical," *Phys. Chem. Chem. Phys.* **11**, 10385 (2009).
3. A. C. Simmonett, H. F. Schaefer, and W. D. Allen, "The Enthalpy of Formation and Anharmonic Force Field of Diacetylene," *J. Chem. Phys.* **130**, 044301 (2009).
4. A. C. Simmonett, N. J. Stibrich, B. N. Papas, H. F. Schaefer, and W. D. Allen, "The Barrier to Linearity and Anharmonic Force Field of the Ketenyl Radical," *J. Phys. Chem. A* **113**, 11643 (2009).
5. S. E. Wheeler and H. F. Schaefer, "Thermochemistry of the HOSO Radical, a Key Intermediate in Fossil Fuel Combustion," *J. Phys. Chem. A* **113**, 6779 (2009).
6. Q. Hao, A. C. Simmonett, Y. Yamaguchi, D.-C. Fang, and H. F. Schaefer, "Structures and Energetics of H_6^+ Clusters," *J. Phys. Chem. A* **113**, 13608 (2009).
7. Q. Cheng, F. A. Evangelista, A. C. Simmonett, Y. Yamaguchi, and H. F. Schaefer, "The Water Dimer Radical Cation: Structures, Vibrational Frequencies, and Energetics," *J. Phys. Chem. A* **113**, 13779 (2009).
8. J. J. Wilke and H. F. Schaefer, "The Subtleties of Explicitly Correlated Z-Averaged Perturbation Theory: Choosing an R12 Method for High-Spin Open-Shell Molecules," *J. Chem. Phys.* **131**, 244116 (2009).
9. J. C. Hargis, H. F. Schaefer, K. N. Houk, and S. E. Wheeler, "Non-Covalent Interactions of a Benzo[a]pyrene Diol Epoxide with DNA Base Pairs: Insight into the DNA Intercalation of (+) - BaP DE-2," *J. Phys. Chem. A* **114**, 2038 (2010).
10. J. A. Miller, S. J. Klippenstein, Y. Georgievskii, L. B. Harding, W. D. Allen, and A. C. Simmonett, "Reactions between Resonance-Stabilized Radicals: Propargyl + Allyl," *J. Phys. Chem. A* **114**, 4881 (2010).

11. T. Lu, Q. Hao, A. C. Simmonett, F. A. Evangelista, Y. Yamaguchi, D.-C. Fang, and H. F. Schaefer, "Low-Lying Triplet States of Diphosphene and Diphosphinylidene," *J. Phys. Chem. A* **114**, 9617 (2010).
12. Q. Wu, A. C. Simmonett, Y. Yamaguchi, Q. Li, and H. F. Schaefer, "Silacyclopropenylidene and its Most Important SiC₂H₂ Isomers," *Barbara J. Garrison Special Issue, J. Phys. Chem. C* **114**, 5447 (2010).
13. E. Mátyus, C. Fábri, T. Szidarovszky, G. Czakó, W. D. Allen, and A. G. Császár, "Assigning Quantum Labels to Variationally Computed Rotational-Vibrational Eigenstates of Polyatomic Molecules," *J. Chem. Phys.* **133**, 034113 (2010).
14. Q. Wu, Q. Cheng, Y. Yamaguchi, Q. Li, and H. F. Schaefer, "Triplet States of Cyclopropenylidene and its Isomers," *J. Chem. Phys.* **132**, 044308 (2010).
15. U. Bozkaya, J. M. Turney, Y. Yamaguchi, and H. F. Schaefer, "The Barrier Height, Unimolecular Rate Constant, and Lifetime for the Decomposition of HN₂," *J. Chem. Phys.* **132**, 064308 (2010).
16. H. Feng and W. D. Allen, "The Problematic F₂ + C₂H₄ Reaction Barrier," *J. Chem. Phys.* **132**, 094304 (2010).
17. Q. Cheng, A. C. Simmonett, F. A. Evangelista, Y. Yamaguchi, and H. F. Schaefer, "Characterization of the BNNO Radical," *J. Chem. Theory Comput.* **6**, 1915 (2010).
18. Q. Wu, Q. Hao, J. J. Wilke, A. C. Simmonett, Y. Yamaguchi, Q. Li, D.-C. Fang, and H. F. Schaefer, "Anharmonic Vibrational Analysis for the Propadienylidene Molecule (H₂C=C=C)," *J. Chem. Theory Comput.* **6**, 3122 (2010).
19. D. Gerbig, H. P. Reisenauer, C.-H. Wu, D. Ley, W. D. Allen, and P. R. Schreiner, "Phenylhydroxycarbene," *J. Am. Chem. Soc.* **132**, 7273 (2010).
20. Y. Yamaguchi and H. F. Schaefer, "Analytic Derivative Methods in Molecular Electronic Structure Theory and its Applications to Spectroscopy," in *Handbook of High Resolution Spectroscopy*, Editors M. Quack and F. Merkt (Wiley, Chichester, 2011).
21. D. S. Hollman, A. C. Simmonett, and H. F. Schaefer, "The Benzene + OH Potential Energy Surface: Intermediates and Transition States," *Phys. Chem. Chem. Phys.* **13**, 2214 (2011).
22. J. J. Wilke and H. F. Schaefer, "Spin-Restricted Explicitly Correlated Coupled Cluster for High-Spin Open-Shell Molecules. The Z-Averaged CCSD-R12 Approach," *J. Chem. Theory Comput.* **7**, 2416 (2011).
23. P. N. Ascik, J. J. Wilke, A. C. Simmonett, Y. Yamaguchi, and H. F. Schaefer, "The Beryllium Tetramer: Profiling an Elusive Molecule," *J. Chem. Phys.* **134**, 074110 (2011).
24. J. C. Hargis, E. Vöhringer-Martinez, H. L. Woodcock, A. Toro-Labbe, and H. F. Schaefer, "Characterizing the Mechanism of the Double Proton Transfer in the Formamide Dimer," *J. Phys. Chem. A* **115**, 2650 (2011).
25. H. Feng, W. Sun, Y. Xie, and H. F. Schaefer, "Structures and Energetics of the *t*-Butyl Cation: The Final Answer or a Never-Ending Story," *Chem. Eur. J.* **17**, 10551 (2011).
26. H. M. Jaeger, H. F. Schaefer, E. G. Hohenstein, and C. D. Sherrill, "Protonated Benzene Dimer: Demystifying Intermolecular Interactions of Complex Systems," *Computational and Theoretical Chemistry* **973**, 47 (2011).
27. J. M. Turney, A. C. Simmonett, R. M. Parrish, E. G. Hohenstein, F. Evangelista, J. T. Fermann, B. J. Mintz, L. A. Burns, J. J. Wilke, M. L. Abrams, N. J. Russ, M. L. Leininger, C. L. Janssen, E. T. Seidl, W. D. Allen, H. F. Schaefer, R. A. King, E. F. Valeev, C. D. Sherrill, and T. D. Crawford, "Psi4: An Open-Source *Ab Initio* Electronic Structure Program," *Wiley Interdisciplinary Reviews: Computational Molecular Science*, doi: 10.1002/wcms.93, published online, October 31, 2011.
28. J. Agarwal, J. M. Turney, and H. F. Schaefer, "Reaction Energetics for the Abstraction Process C₂H₃ + H₂ → C₂H₄ + H," *J. Phys. Chem. Lett.* **2**, 2587 (2011).
29. G. Koleva, B. Galabov, J. Kong, H. F. Schaefer, and P. R. Schleyer, "Electrophilic Aromatic Sulfonation with SO₃: Concerted or Classical S_EAr Mechanism," *J. Am. Chem. Soc.* **133**, 19094 (2011).
30. P. R. Schreiner, H. P. Reisenauer, D. Ley, D. Gerbig, C.-H. Wu, and W. D. Allen, "Methylhydroxycarbene: Tunneling Control of a Chemical Reaction," *Science* **332**, 1300 (2011).
31. H. Feng, W. Sun, Y. Xie, and H. F. Schaefer, "Is There an Entrance Complex for the F + NH₃ Reaction?" *Chem. Asian J.* **6**, 3152 (2011).
32. B. S. Narendrapurapu, A. C. Simmonett, H. F. Schaefer, J. A. Miller, and S. J. Klippenstein, "Combustion Chemistry: Important Features of the C₃H₅ Potential Energy Surface, Including Allyl Radical, Propargyl + H₂, Allene + H, and Eight Transition States," *J. Phys. Chem. A* **115**, 14209 (2011).
33. D. S. Hollman and H. F. Schaefer, "In Search of the Next Holy Grail of Polyoxide Chemistry: Explicitly Correlated *Ab Initio* Full Quartic Force Fields for HOOH, HOOOH, HOOOOH, and Their Isotopologues," *J. Chem. Phys.* **136**, 084302 (2012).

Turbulence-Chemistry Interactions in Reacting Flows

Robert S. Barlow
Combustion Research Facility
Sandia National Laboratories, MS 9051
Livermore, California 94550
barlow@sandia.gov

Program Scope

This program is directed toward achieving a more complete understanding of turbulence-chemistry interactions in flames and providing detailed measurements for validation of combustion models. In the Turbulent Combustion Laboratory (TCL) simultaneous line imaging of spontaneous Raman scattering, Rayleigh scattering, and two-photon laser-induced fluorescence (LIF) of CO is applied to obtain spatially and temporally resolved measurements of temperature, the concentrations of all major species, mixture fraction, and reaction progress, as well as gradients in these quantities in hydrocarbon flames. The instantaneous three-dimensional orientation of the turbulent reaction zone is also measured by imaging of OH LIF or Rayleigh scattering at 355 nm in two crossed planes, which intersect along the laser axis for the multiscale measurements. These combined data characterize both the thermo-chemical state and the instantaneous flame structure, such that the influence of turbulent mixing on flame chemistry may be quantified. Our experimental work is closely coupled with international collaborative efforts to develop and validate predictive models for turbulent combustion. This is accomplished through our visitor program and through the TNF Workshop series. Although the past emphasis has been on nonpremixed and partially premixed combustion, the workshop and this program have expanded their scope in recent years to address a broad range of combustion modes, including premixed and stratified flames. We are also working to extend our quantitative multiscale diagnostics to more complex hydrocarbon fuels. Entry into these new research areas has prompted developments in both hardware and methods of data analysis to achieve unprecedented spatial resolution and precision of multiscale measurements. Within the CRF we collaborate with Jonathan Frank, who applies advanced imaging diagnostics to turbulent flames, and with Joe Oefelein, who performs high fidelity large-eddy simulations (LES) of our experimental flames in order to gain greater fundamental understanding of the dynamics of multi-scale flow-chemistry interactions.

Recent Progress

Preferential Transport Effects in Turbulent Premixed Flames

Multiscale measurements in bluff-body stabilized turbulent premixed CH₄/air flames have revealed strong effects of preferential species transport, which cause significant changes in atom balances and the measured equivalence ratio going from reactants to product across a thin flame brush [Barlow et al. CNF 2011]. Briefly, H₂ and H₂O are preferentially transported toward the reactant side of the flame and then convectively carried downstream, while excess CO₂ is retained within the compact recirculation zone. During the past year, we have completed additional experiments and analysis to better understand this newly observed phenomenon. This work included premixed flame series with equivalence ratio, $\phi = 0.62, 0.77, 1.0, \text{ and } 1.23$, as

well as a broader range in reactant flow velocity [Dunn & Barlow, ProCI 2012], with maximum velocity over 50 times the laminar flame speed. Results confirm a strong influence of preferential transport on the scalar structure of bluff-body flames at all equivalence ratios considered. It was also observed that the effect reaches a limiting condition at high reactant velocity, as can be seen in Fig. 1, which shows results from a series of 9 flames with $\phi = 1.0$. Here the conditional mean results for C/H are essentially the same for the four highest velocity cases. The physical mechanisms causing this saturation effect are not yet clear.

Results from the $\phi = 1.23$ flame series show indications of high strain in that trajectories of major species mass fractions vs. temperature are nearly linear. However, whereas compressive strain reduces flame thickness, the measured turbulent flame profiles in this shear flow configuration are always significantly thicker than obtained from Chemkin for an unstrained, freely propagating flame.

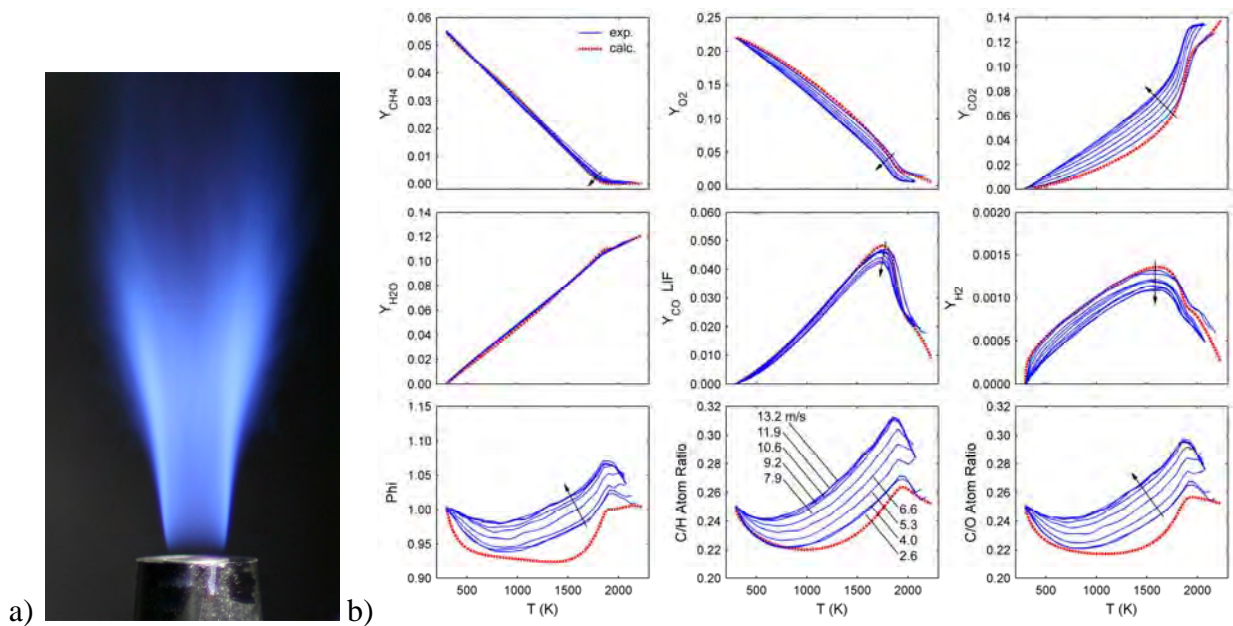


Figure 1. a) Premixed CH_4 -air flame stabilized on an annular bluff-body burner. b) Conditional mean species mass fractions, equivalence ratio ϕ , and atom ratios C/H and C/O plotted against temperature. The measurements (blue) reveal a clear trend of increasing deviation of the from an unstrained laminar flame calculation (red) as the velocity of the annular reactant flow is increased. Bulk reactant velocities are labeled in the C/H plot, and the direction of increasing velocity is indicated by arrows in the other plots.

Stratified Swirl Flames

In collaboration with Mark Sweeney and Simone Hochgreb at Cambridge University, we have continued analysis and publication of results from our experimental campaign on the effects of stratification and swirl on the structure of turbulent premixed flames. Major conclusions from this work are the following:

- Stratification elevates levels of H_2 and CO relative to homogeneously premixed flames when data are conditioned on local equivalence ratio and temperature. Figure 2a shows conditional mean mass fractions vs. temperature, where the stratified flame data are further conditioned to be within 2.5% of the mean equivalence ratio measured in the premixed turbulent flame at

the same temperature. This elevation of H₂ and CO is attributed to the “back supported” flame structure, in which the instantaneous flame burns from higher toward lower equivalence ratio. These results have important implications for the use of premixed laminar flamelets or tabulated chemistry in the modeling of turbulent stratified flames.

- Surface density function and scalar dissipation rate (both derived from measurements of gradients in reaction progress variable) show little dependence on stratification.
- Curvature pdfs (Fig. 2b) show only slight effects of stratification where flame crosses mixing layer. This contrasts with results from low turbulence flames and indicates that the influence of stratification on flame curvature is quickly overcome when turbulence levels increase.
- High swirl causes the recirculation zone behind the bluff body to open, and this prevents amplification of the preferential diffusion effect, which are associated with trapping of excess CO₂ within a compact recirculation zone in the non-swirling and moderately swirling cases.
- Addition of swirl produces higher gradients in equivalence ratio at the intersection of flame brush and mixing layer than observed in corresponding non-swirling flames.

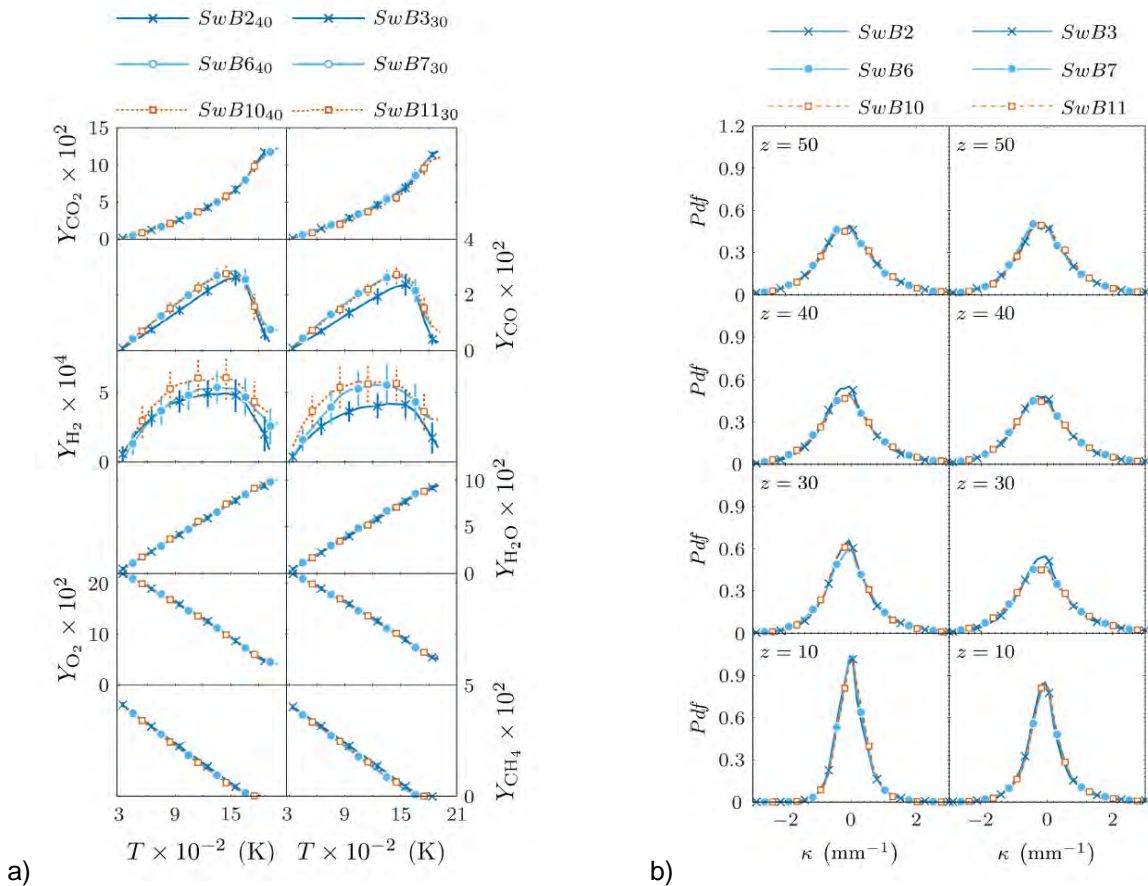


Figure 2. a) Mean of major species in temperature space, where stratified flame data are conditioned on equivalence ratio to be within $\pm 2.5\%$ of the mean value from the premixed flame within the same temperature bin. Vertical bars denote \pm one standard deviation. b) Curvature pdfs obtained from planar LIF imaging of OH. Legends refer to swirl burner (SwB) case numbers for moderate swirl (2, 6 and 10) and high swirl (3, 7 and 11) with stratification ratio equal to 1.0 for cases 2 and 3, 2.0 for cases 6 and 7, and 3.0 for cases 10 and 11. The subscripts in a) refer to the downstream distance in mm where the flame brush crosses the center of the mixing layer in stratified cases.

Future Plans

Experimental priorities for the next year include further developments on data acquisition/analysis methods for extension of spontaneous Raman scattering to achieve quantitative measurements in turbulent DME flames, including direct measurement of some stable intermediates (collaboration with TU Darmstadt, UT Austin, and Ohio State) and completion of experiments on a series of piloted partially premixed DME/air jet flames (collaboration Jonathan Frank and with Jeff Sutton and Frederik Fuest, Ohio State University).

BES Supported Publications (2010 - present)

M.J. Dunn, A.R. Masri, R.W. Bilger, R.S. Barlow. "Finite Rate Chemistry Effects in Highly Sheared Turbulent Premixed Flames," *Flow. Turb. Combust.* **85**, 621-648 (2010).

J. Cai, C. Tong, R.S. Barlow, A.N. Karpetis, "Noise Correction and Length Scale Estimation for Scalar Dissipation Rate Measurements in Turbulent Partially Premixed Flames," *Flow. Turb. Combust.* **85**, 309-332 (2010).

F. Fuest, R.S. Barlow, D. Geyer, F. Seffrin, A. Dreizler, "A Hybrid Method for Evaluation of 1D Raman Spectroscopy," *Proc. Combust. Inst.* **33**, 815–822 (2011).

J. Cai, C. Tong, R.S. Barlow, A.N. Karpetis, "Conditionally filtered diffusion of mixture fraction and temperature in turbulent partially premixed flames," *Proc. Combust. Inst.*, **33**, 1505-1513 (2011).

M.S. Sweeney, S. Hochgreb, R.S. Barlow, "The structure of premixed and stratified low turbulence flames," *Combust. Flame* **158**, 935–948. (2011).

M.S. Sweeney, S. Hochgreb, M.J. Dunn, R.S. Barlow, "A comparative analysis of flame surface density metrics in premixed and stratified flames," *Proc. Combust. Inst.* **33**, 1419–1427 (2011).

R.S. Barlow, M.J. Dunn, M.S. Sweeney, S. Hochgreb, "Effects of preferential transport in turbulent bluff-body-stabilized lean premixed CH₄/air flames," *Combust. Flame.* (in press) doi:10.1016/j.combustflame.2011.11.013.

M.S. Sweeney, S. Hochgreb, M.J. Dunn, R.S. Barlow, "The structure of turbulent stratified and premixed methane/air flames I: Non-swirling flows," *Combust. Flame.* (accepted).

M.S. Sweeney, S. Hochgreb, M.J. Dunn, R.S. Barlow, "The structure of turbulent stratified and premixed methane/air flames II: Swirling flows," *Combust. Flame.* (accepted).

A. Sevault, M.J. Dunn, R.S. Barlow and Mario Ditaranto, "On the structure of the near field of oxy-fuel jet flames using Raman/Rayleigh laser diagnostics," *Combust. Flame.* (accepted).

M.J. Dunn, R.S. Barlow, "Effects of preferential transport and strain in bluff body stabilized lean and rich premixed CH₄/air flames," *Proc. Combust. Inst.* **34** (accepted).

TNF Workshop Information: <http://www.sandia.gov/TNF>

Modeling Reactions in High-Pressure Turbulence in the Cold Ignition Regime

Josette Bellan

Mechanical and Civil Engineering Department, California Institute of Technology
Pasadena, CA 91125

Josette.Bellan@jpl.nasa.gov

DOE Award Number: **DE-FG02-09ER16107**

STRIPES award number of **SC0002679**

I. Program Scope

This study addresses issues highlighted in the Basic Energy Needs for Clean and Efficient Combustion of 21st Century Transportation Fuels (DOE BES, 2006) under the topic of Combustion under Extreme Pressure. It is there noted that “the most basic concepts of thermal autoignition” are “based on experience and theory at near atmospheric pressures” and that “as pressure increases significantly..., many of these conceptual pictures begin to change or disappear”. It is also stated “A better description of the coupling and interaction of high pressure flow and molecular transport processes with chemistry is also necessary”, particularly because “Ignition and flame propagation of alternative and renewable fuels, as well as of the changing feed stocks of conventional fossil-based fuels, are very likely to be much different at very high pressures than under the more familiar, lower pressure conditions of current engines.” Recognizing that “Under such (*increasing pressure*) conditions distinctions between gas and liquid phases become moot, new equations of state must be used...”, it is immediately apparent that there must be “a re-examination of the basic assumptions that govern the physics and chemistry related to combustion; and the need for this type of re-examination increases as the combustion pressure increases.” This recognition is also stated under the topic of Multiscale Modeling since due to the new equations of state “The combination of unexplored thermodynamic environments and new physical and chemical fuel properties results in complex interactions among multiphase (*according to the above, the multiphase distinction becomes moot with increasing pressure*) fluid dynamics, thermodynamic properties, heat transfer, and chemical kinetics that are not understood even at a fundamental level.” From the theoretical viewpoint for “systems at high pressure, fluid dynamic time scales can be comparable to chemical time scales.” and therefore “completely diffusion-controlled reactions ... can become important”.

Thus, the objective of this study is the investigation of the coupling among thermodynamics, transport properties, intrinsic kinetics and turbulence under the high-pressure and the relatively (with respect to combustion) low-temperature conditions typical of the auto-ignition regime, with particular emphasis on the manifestation of this coupling on the effective kinetic rate. As planned, we established collaboration with Dr. Joseph Oefelein of the Combustion Research Facility at Sandia Livermore to work together towards implementing the models developed in this research into the high-pressure Large Eddy Simulation code under development by him at Sandia.

II. Recent Progress

This study was initiated in September 2009 and began in earnest with the arrival of the Post Doc at the end of July 2010. This report contains results obtained during the last year of study.

The focus of this year was on multi-species mixing as a preamble to conducting reactive flow simulations. Considering the importance of molecular diffusion in the low-temperature and high-pressure environment of pre-ignition, we have first performed DNS of 5 species mixing (*n*-heptane, nitrogen, oxygen, carbon dioxide and water vapor) under supercritical-pressure conditions using the Peng-Robinson equation of state [i] and accurate transport properties. The goal of this study was two-fold: First, we wanted to show that it is possible to compute multi-species multi-dimensional mixing using accurate transport properties, including a full mass-diffusion matrix. Second, since it is planned to conduct reactive-flow simulations using a reaction mechanism which is of the reduced-kinetics type, we wanted to explore the range of occurring equivalence ratios (ERs) so as to ensure that the chosen reduced kinetics has been validated for a significant range of ERs present in this flow field. A single DNS realization has been first performed where all transport properties are spatially and temporally varying. This DNS is based on computational transport properties that have been scaled so that despite the necessary scaling of the viscosity to enable DNS, the physical values of the Prandtl number and of the many Schmidt numbers are maintained. The thermal conductivity and viscosity are computed using mixing rules [ii]. The binary diffusion coefficients are computed according to [iii], and they, together with the EOS, form the building blocks for computing the (5×5) mass diffusion coefficient matrix according to [iv]. The thermal diffusion factors are also computed according to [iv]. The mixing rules derived in [iv] originate from Grad’s 13-moment theory, meaning that they are valid for high-pressure conditions. The DNS realization reached a state having turbulent characteristics, and the analysis was performed on this particular state. Figure 1 illustrates transport properties in the mixing region at this transitional state and shows their very large spatial variation: more than a factor of 10 for the diffusivity and more than a factor

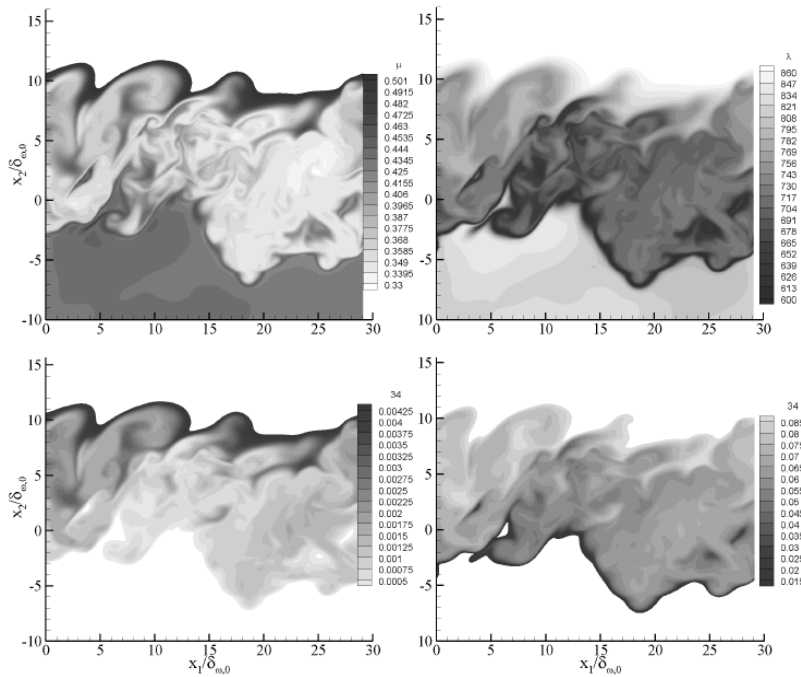


Figure 1. Scaled transport-property variation in a streamwise -- cross-stream plane at transition. Viscosity in Pa·s (top left), thermal conductivity in W/(m·K) (top right), mass-diffusion coefficient D_{34} (3 labels oxygen, 4 labels *n*-heptane) in m^2/s (bottom left), and ρD_{34} in $kg/(m \cdot s)$ (bottom right).

initially having *n*-heptane (with traces of carbon dioxide and water vapor) while much larger ER values exist elsewhere in the lower stream (not illustrated). Thus, on this single example it

of six for the generally considered constant product ρD where ρ is the density and D is a mass diffusivity coefficient. Substantial subgrid-scale (SGS) activity can be seen in the viscosity, thermal conductivity and mass diffusivities. The results depicted in Fig. 2 (left) show that the stoichiometric region is thin, located in the upper stream originally having air (with traces of carbon dioxide and water vapor) and that, for example, the region $0.1 < ER < 5$ forms a thin band around the stoichiometric region. Islands of $1 < ER < 5$ also occur in the lower stream

is clear that most reduced-kinetics mechanisms would be inappropriate to use for describing reaction since they are typically derived and tested in the $0.5 < ER < 2$ regime. This study indicates that we should select for LES the [v,vi] reduced mechanism because of its demonstrated success in the $0.25 < ER < 4$ regime, and even for ER as small as 1/8 and as large as 8. Figure 2 (right) shows that mixing is very vigorous particularly in the rich region and that the stoichiometric region is in the initially lean region.

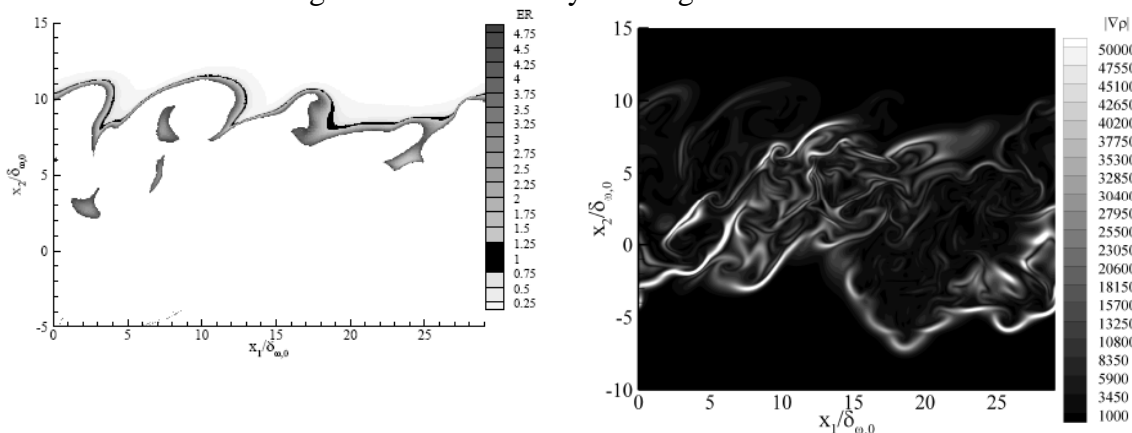


Figure 2. Equivalence ratio (left) and density gradient in kg/m^4 (right) in a streamwise/cross-stream plane at turbulence transition.

Since ultimately one wishes to derive conclusions based on statistics rather than on a single simulation, we have enlarged the DNS study to several realizations obtained by changing one parameter at the time: either increasing the initial Reynolds number or the pressure. Each realization has achieved transition. This created database is so rich in scientific information that its analysis is still in progress. Of particular interest are two aspects: (1) In [vii] we found that for binary-species mixing under supercritical pressure, new SGS significant terms appear in the momentum and energy equations. These SGS terms were modeled [viii, ix] and it was shown that the LES solution including these terms is considerably more accurate than that devoid of them. For binary-species mixing [vii], no new SGS terms were found in the species equations. However, visual inspection of Fig. 1 reveals substantially higher SGS diffusivity activity than for binary species, and thus the database is being tested to inquire whether for 5-species mixing there will be new SGS terms in the species equation; if so, we will develop one or several models for these terms. (2) In preparation for reactive flow simulations where we will inquire whether the flamelet concept of Williams [x] is applicable to the modeling of hydrocarbon auto-ignition in diesel engines, and if so, whether the flamelet model of Peters [xi] is feasible, we are now analyzing the 5-species-mixing database for possibilities of constructing a conserved scalar of Peters'-model type, having boldly assumed here that for the future reactive flows the reaction rates could be eliminated (by additions/subtractions) from the equations. Arguing for the applicability of the flamelet model is the thin stoichiometric region seen in Fig. 2 (left), although the contribution to combustion from the rich and lean regions closely surrounding it must be first ascertained in the future and compared to that of the stoichiometric region when we will analyze next year the reactive-flow database. Arguing against the applicability of Peters' flamelet model is the fact that the Soret effect will most likely prevent the finding of a conserved scalar [1], and that it is quite clear that the mass-diffusion matrix will not be diagonalizable with the same eigenvalues in the entire domain. Finding an equation for conserved chemical elements rather than species [xii] may be also problematic due to the complex variation of the diffusion coefficients. These arguments are only indications and a full analysis is necessary before making a definite pronouncement.

We have initiated the reactive-flow DNS studies; we used a single, global reaction for *n*-heptane oxidation with the reaction rate of [xiii], scaled so that there is coupling between chemistry and turbulence. The code has been debugged and a preliminary test of the DNS code with such a rate has been successful in that turbulence transition has been obtained. Full attention to the reactive-flow DNS will be given next year.

The PI has continued the collaboration established with Dr. Oefelein by providing additionally to the new SGS models developed in [viii, ix] transmitted last year, the SGS scalar variance model of [1].

III. Future Plans

The following activities are planned for the next year:

- Finalize the manuscript describing the database and analysis of 5-species mixing under supercritical pressure and submit it to a refereed journal for publication.
- Create a database of reacting-flow simulations by conducting a series of DNS.
- Analyze *a priori* the reacting-flow database and propose subgrid-scale models for the turbulent reaction terms.

IV. References

- i. Harstad, K.; Miller, R. S.; Bellan, J. *A.I.Ch.E. J.* **1997**, *43*(6), 1605
- ii. Reid, R. C.; Prausnitz, J. M.; Poling, B. E. *The Properties of Gases and Liquids*, 4th edition, McGraw-Hill, NY, **1987**
- iii. Harstad, K.; Bellan, J. *Journal of Chemical Physics* **2004a**, *120*(12), 5664
- iv. Harstad, K.; Bellan, J. *Ind. & Eng. Chem. Res.* **2004b**, *43*(2), 645
- v. Harstad, K.; Bellan, J. *Combustion and Flame* **2010a**, *157*, 1594
- vi. Harstad, K.; Bellan, J. *Combustion and Flame* **2010b**, *157*, 2184
- vii. Selle, L. C.; Okong'o, N. A.; Bellan, J.; Harstad, K. G. *J. Fluid Mech.* **2007**, *593*, 57
- viii. Taşkinoglu, E. S.; Bellan, J. *J. Fluid Mech.* **2010**, *645*, 211
- ix. Taşkinoglu, E. S.; Bellan, J. *J. Fluid Mech.* **2011**, *679*, 156
- x. Williams, F. A. *Recent advances in the theoretical descriptions of turbulent diffusion flames* (ed. S. Murthy), Plenum, N. Y., **1975**, 189
- xi. Peters, N., *Turbulent Combustion*, Cambridge University Press, **2000**
- xii. Sutherland, J. S.; Smith, P. J.; Chen, J. H. *Combust. Theory Model.*, **2005**, *9*(2), 365
- xiii. Westbrook, C. K.; Dryer, F. L. *Comb. Sci. Techn.* **1981**, *27*, 31

V. Publications, presentations and submitted articles supported by this project September 2009-April 2012

- [1] Masi, E.; Bellan J. The subgrid-scale scalar variance under supercritical pressure conditions, *Phys. Fluids*, *23*(8), doi:085101 (22 pages), 2011
- [2] Masi, E.; Bellan J. The subgrid scalar variance equation under supercritical pressure conditions, paper 1C04 presented at the 7th US National Combustion meeting, Atlanta, GA., March 21-23, 2011
- [3] Masi, E.; Bellan, J; Harstad, K. Direct Numerical Simulation of High-Pressure Multispecies Turbulent Mixing in the Cold Ignition Regime, paper AIAA 2012-0351, presented at the 50th Aerospace Sciences Meeting, Nashville, TN, January 9-12, 2012
- [4] Masi, E.; Bellan, J; Harstad, K. Modeling and Direct Numerical Simulation of High-Pressure Multispecies Turbulent Mixing in the Cold Ignition Regime, submitted to the 34th International Symposium on Combustion, 2011

Towards predictive simulations of soot formation: from surrogate to turbulence

Guillaume Blanquart
Department of Mechanical Engineering
California Institute of Technology
1200 E. California Blvd., Pasadena, CA 91125

Objectives

The combustion of hydrocarbon fuels, including kerosene, gasoline, and diesel, leads to the formation of soot particles which are known to be the source of several health problems and environmental issues.

The objective of the proposed work is to reduce the gap in the present understanding and modeling of soot formation both in laminar and turbulent flames. This effort spans several length scales from the molecular level to large scale turbulent transport. More precisely, the objectives are three fold: 1) develop a *single combined chemical and soot model* validated for all relevant components usually found in real fuel surrogates; 2) develop a framework able to *explain the complete evolution of soot particles* from cluster of PAHs to oxidation of large fractal aggregates; 3) *understand and model the interplay* between unsteady chemistry, differential diffusion, and turbulent transport.

Recent progress

Detailed chemical model

In order to describe adequately the combustion of transportation fuels (kerosene, gasoline, and diesel), whose complete chemical compositions remain unknown, surrogates should be formulated with *well-defined chemical kinetics*. In a previous work, a detailed chemical mechanism was developed for the high temperature combustion of hydrocarbons with an emphasis on soot precursors (24). Later, this chemical model was extended to include the oxidation of substituted aromatic fuels such as toluene ($C_6H_5CH_3$), xylene ($C_6H_5(CH_3)_2$), ethyl-benzene ($C_6H_5C_2H_5$), and methyl-naphthalene ($C_{10}H_7CH_3$) (29).

Over the past year, the base mechanism has been extended to include additional heavy molecules of importance to surrogates such as *n*-dodecane. The chemistry of *n*-dodecane is taken from the recent detailed chemical mechanism of Westbrook et al. (3). This chemical mechanism is too large to be integrated into the base mechanism in its present form and it is therefore reduced following a multi-

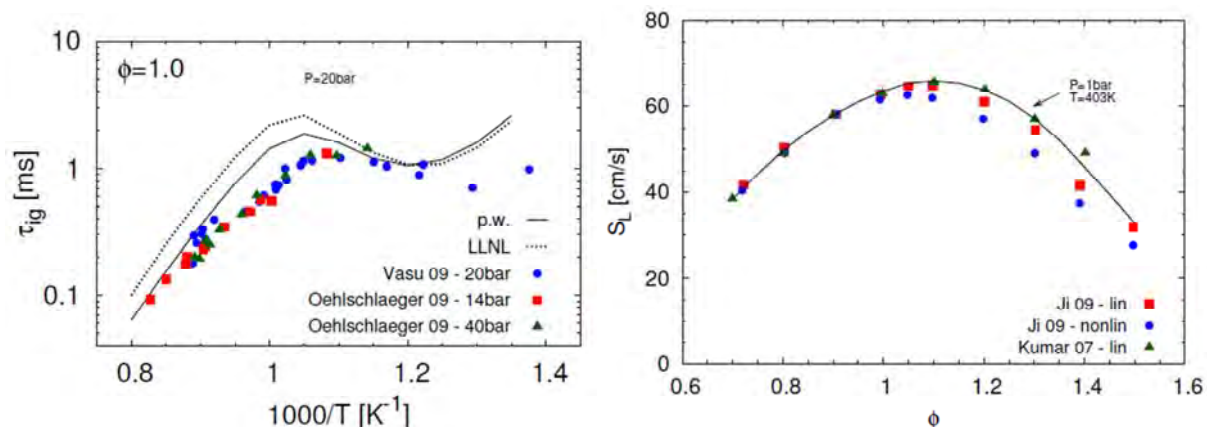


Figure 1. Ignition delay times of *n*-dodecane in air (left) and laminar burning velocities for *n*-dodecane in air (right).

step approach. A similar approach has been used successfully for the reduction of the *n*-heptane and iso-octane chemistry during the development of the base mechanism (4). The resulting final mechanism consists of 181 species and 1885 reactions, forward and backward reactions being counted separately, of which 15 species and 96 reactions come from the *n*-alkanes LLNL mechanism.

Laminar burning velocities and ignition delay times were chosen as targets for the validation of the presented chemical mechanism. The combination of these data provides a good test for the developed mechanism. These two cases also represent possible modes of combustion often found in engines: flame front propagation and local thermal ignition. The quality of the chemical mechanism is assessed first for single component fuels such as shown in Figure 1.

The overall comparison of ignition delay times between predictions with the current chemical model and the experiments is reasonably good. In fact, the current model performs better than the detailed model on which it is based. The predictions of laminar flame speeds with the current chemical model compare extremely well with all sets of experimental data for lean mixtures. For rich mixtures, where the scatter among the experimental data appear greater, the current mechanism seems to predict laminar flame speeds between the two sets of experimental data.

Surrogate formulation

The combustion of JP-8 fuel is analyzed by considering a surrogate composed of 77% of *n*-dodecane and 23% of *m*-xylene (by volume). This surrogate has been used in the past in several studies. Once again, ignition delay times, laminar flame speeds, and a laminar premixed flame have been considered as test cases for the validation of the surrogate formulation (Figure 2).

The overall agreement between the predictions and the measurements is very good for most equivalence ratios. Given the fact that the surrogate formulation is a weighted average of pure *n*-dodecane and pure *m*-xylene, the flame speeds were observed to fall between the values for the pure fuels. The same behavior was observed in the experiments.

The final validation case corresponds to the laminar rich premixed flame of kerosene/air. Molecular oxygen and the main products of combustion are predicted accurately by the chemical model and the yields of soot precursors are also well reproduced. Given the uncertainties in the imposed temperature profile, the overall agreement of the mole fractions of the different species with experimental data remains very satisfactory.

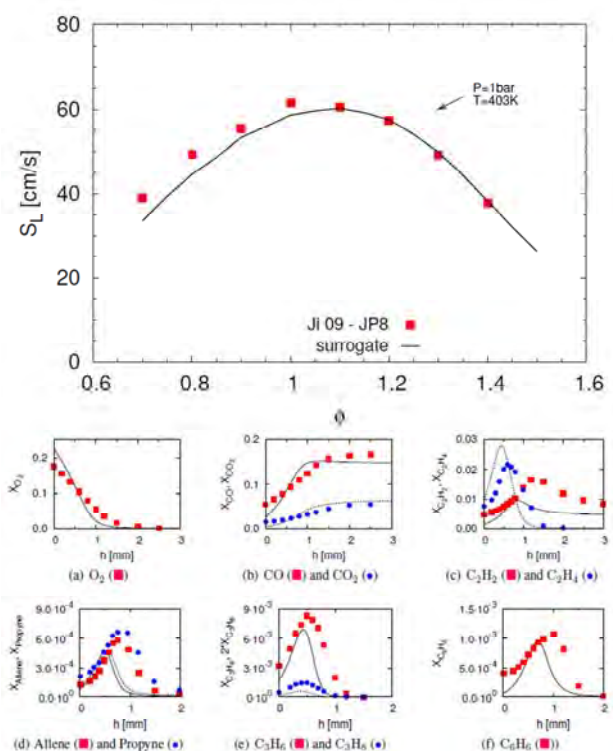


Figure 2. Laminar burning velocities for JP-8 in air (top) and species profiles in a laminar premixed flame (bottom).

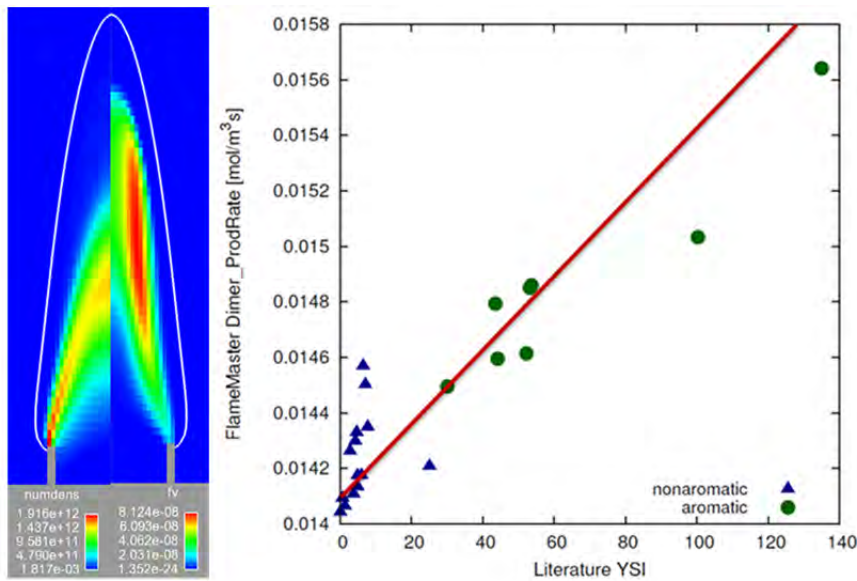


Figure 3. Number density and soot volume fraction for the 2D coflow diffusion flame (left). Preliminary results from the 2D simulations with tabulated chemistry show a linear relationship between overall soot yield and nucleation rate (right).

Predicting sooting tendencies

Sooting tendencies of common hydrocarbon compounds have been investigated extensively by McEnally & Pfefferle in an axisymmetric coflow diffusion flame (5; 6). In the present work, we propose an approach to investigate sooting tendencies together by reproducing this experimental setup.

The burner consists of two concentric tubes, with the fuel flows in the inner tube and air flows in the region between the inner and outer tube. For a faster integration of chemistry and fluid dynamics, all chemical properties are tabulated with respect to the mixture fraction, scalar dissipation rate, and total enthalpy. The later quantity is necessary to capture the effects of radiation heat losses on the flame structure. State of the art soot models are integrated into the numerical framework (7; 8). Preliminary results from the 2D simulations with tabulated chemistry show a linear relationship between overall soot yield and nucleation rate for most species. Based on these results, we propose a new modeling approach to compute the sooting tendencies directly from the chemical model without the need for the full 2D fluids dynamics simulations (Figure 3). In addition, these results highlight deficiencies in 1) the chemical pathways leading to PAH formation and 2) the soot nucleation model. Both of these issues are currently being investigated.

Current and future work

Soot nucleation model

The first element currently under consideration is the soot nucleation model and its integration in the fluid dynamics simulations. Current work focuses on two elements: 1) predicting soot inception from PAH only in the vicinity of the flame front, and 2) capturing the soot inception time-scale in the chemistry tabulation.

Direct Numerical Simulations of turbulent sooting flames

Simultaneously to the development of the chemistry and soot models, we have started setting up the

Direct Numerical Simulations of soot formation. The first configuration to be analyzed is a diffusion mixing layer. Currently, the focus is placed on two elements: 1) developing an accurate and robust numerical scheme for the transport of soot quantities in a highly turbulent flow field, and 2) identifying the most relevant initial conditions to study the inception of soot in a turbulent flow field.

Bibliography

1. *Chemical mechanism for high temperature combustion of engine relevant fuels with emphasis on soot precursors*. **Blanquart, G., Pepiot-Desjardins, P. and Pitsch, H.** 2009, Comb. Flame, Vol. 156, pp. 588-607.
2. *A consistent chemical mechanism for oxidation of substituted aromatic species*. **Narayanaswamy, K., Blanquart, G. and Pitsch, H.** 2010, Comb. Flame, Vol. 157, pp. 1879-1898.
3. *A Detailed Chemical Kinetic Reaction Mechanism for n-Alkane Hydrocarbons from n-Octane to n-Hexadecane*. **Westbrook, C. K., Pitz, W. J., Herbinet, O., Curran, H. J. and Silke, E. J.** 2009, Comb. Flame, Vol. 156, pp. 181-199.
4. *An efficient error-propagation-based reduction method for large chemical kinetic mechanisms*. **Pepiot-Desjardins, P. and Pitsch, H.** 2008, Comb. Flame, Vol. 154, pp. 67-81.
5. *Improved sooting tendency measurements for aromatic hydrocarbons and their implications for naphthalene formation pathways*. **McEnally, C.S. and Pfefferle, L.D.** 2007, Comb. Flame, Vol. 148, pp. 210-222.
6. *Sooting tendencies of non-volatile aromatic hydrocarbons*. **McEnally, C.S. and Pfefferle, L.D.** 2009, Proc. Comb. Inst., Vol. 32, pp. 673-679.
7. **Blanquart, G. and Pitsch, H.** A joint Volume-Surface-Hydrogen multi-variate model for soot formation. [book auth.] H. Bockhorn, A. D'Anna, A. F. Sarofim and H. Wang. *Combustion Generated Fine Carbonaceous Particles*. 2008.
8. *Analyzing the Effects of Temperature on Soot Formation with a Joint Volume-Surface-Hydrogen Model*. **Blanquart, G. and Pitsch, H.** 2009, Comb. Flame, Vol. 156, pp. 1614-1626.
9. *On the formation and early evolution of soot in turbulent nonpremixed flames*. **Bisetti, F., Blanquart, G., Mueller, M.E. and Pitsch, H.** 2010, Comb. Flame, p. (submitted).

Theoretical Studies of Combustion Dynamics (DE-FG02-97ER14782)

Joel M. Bowman

Cherry L. Emerson Center for Scientific Computation and Department of Chemistry,
Emory University Atlanta, GA 30322, jmbowma@emory.edu

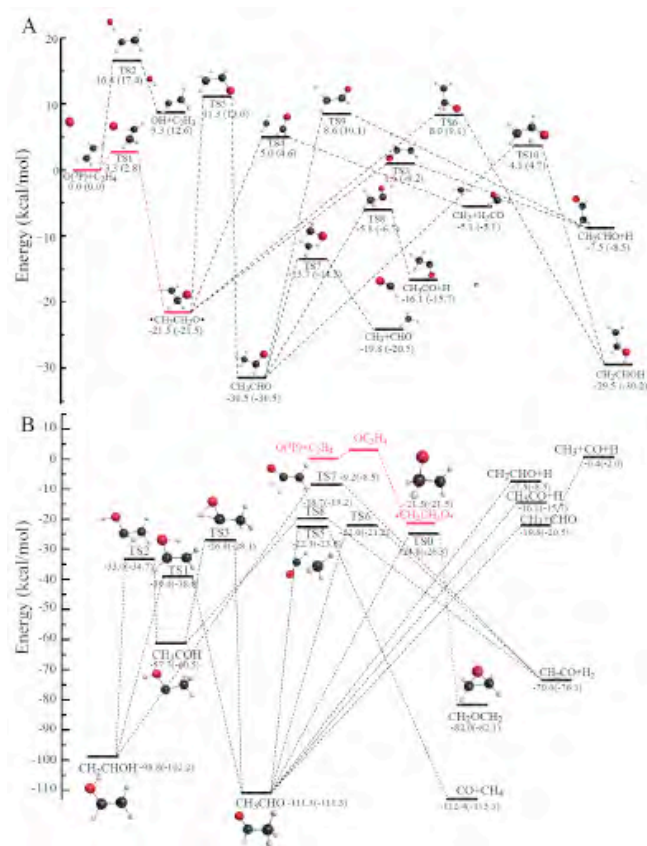
Program Scope. The research supported by this Department of Energy grant focuses on the development of rigorous computational methods to model and predict the basic chemical and physical processes of importance in gas-phase combustion reaction dynamics. This includes the development of full-dimensional, global, *ab initio*-based potential energy surfaces (PESs) that describe complex unimolecular and bimolecular reactions. Dynamics on these potentials, which may contain multiple minima and saddle points, are done mainly using classical trajectories, for long times and can reveal new pathways and mechanisms of chemical reactions. Large amplitude motion, including isomerization, "roaming", energy transfer in collisions with atoms and molecules can be studied with these potentials. The choice of reaction system to study is generally motivated by experiments that challenge and ultimately advance basic understanding of combustion reaction dynamics.

Recent Progress: Multi-state Dynamics of the $O(^3P)+C_2H_4$ reaction and CH_3CHO Photodissociation. A global PES for the first triplet state (T_1) and a semi-global PES for S_1 have been developed and together with the existing PES for S_0 have been used in two types of multi-state (spin-orbit) coupled dynamics.

There are many new interesting results from these calculations; however, we highlight a few that bear directly on recent experiments of both processes. First, we show at the left the usual schematics of the T_1^{P33} and S_0^{P15} PESs. (The numbers in parentheses are the CCSD(T)/aug-cc-pVTZ energies). The full dimensional PESs contain all of these stationary points and reactant/product channels indicated. As seen, both PESs are quite complex and thus are major challenges to represent in full dimensionality. However, using techniques have reported numerous times to this community we were able to do this.

For the reaction $O(^3P) + C_2H_4$, tens of thousands of quasiclassical trajectories were run at several collision energies, E_c , corresponding to crossed molecular beam experiments done by Cassavechia and co-

workers.¹ Results at $E_c=8.4$ kcal/mol have just been reported in a joint publication with Cassavechia group.^{P36} The calculated and measured branching ratios to measured products (the interesting CH_4+CO channel is unfortunately hidden in the experiments) are given in the table below. As seen, there is very good agreement



between theory and experiment and, perhaps more importantly, both find substantial intersystem crossing to S_0 and in fact the major products come from S_0 .

Product channel <i>i</i>	Theory	Experiment
$\text{CH}_3 + \text{CHO}$ (from S_0)	0.49	0.34 ± 0.09
$\text{CH}_2\text{CHO} + \text{H}$ (from T_1)	0.28	0.30 ± 0.06
$\text{H}_2\text{CO} + \text{CH}_2$ (from T_1)	0.08	0.20 ± 0.05
$\text{CH}_3\text{CO} + \text{H}$ (from S_0)	0.10	0.03 ± 0.01
$\text{CH}_2\text{CO} + \text{H}_2$ (from S_0)	0.05	0.13 ± 0.04

(An isomerization barrier on T_1 blocks the pathway to these radical products from T_1 .) This crossing occurs mainly in biradical region of the S_0 and T_1 PESs in accord with electronic structure

calculations^{2,3} and also low-level direct dynamics surface hopping calculations.⁴ Very good agreement between theory and experiment is also found for angular and translational energy distributions for the two major channels, shown to the left. As seen, these distributions are quite different for these channels, indicating substantial differences in the exit channel dynamics. These are discussed in detail in the forthcoming publication.^{ref}

CH_3CHO photodissociation reveal quite different multi-state dynamics owing to the very different preparation of the system. Space does not permit a detailed presentation of results, however a schematic of the dissociation, which originates on S_1 at a configuration very different from the bimolecular reaction. We have calculated the dependence of the $T_1:S_0$ branching ratio to the major products CH_3+HCO vs photolysis energy and find it rises rapidly once the T_1 barrier is surmounted. It is interesting that this energy is below the energy of the bimolecular reaction, where these products are blocked from emanating from T_1 , as noted already.

Potential Energy Surfaces for F, Cl, and $\text{O}(^3\text{P})+\text{CH}_4$ reactions. We developed full-dimensional, *ab initio*-based PESs for the title reactions,^{P2,P20,P29,P35} based on fitting roughly 20 000 highly accurate composite electronic energies. These PESs are the most accurate one available and has been used by us in dynamics calculations of detailed reaction dynamics, motivated by experiments by Lui and co-workers.⁵⁻⁷

Future Plans. In addition to further studies of intersystem crossing in reactions of $\text{O}(^3\text{P})$ with hydrocarbons we hope to initiate new studies of energy transfer and recombination using many of the PESs we have developed for complex unimolecular dynamics. With additional potentials describing the interactions with inert collision partners, we plan to study collision induced isomerization, energy transfer, dissociation and recombination.

References

1. Dynamics of the $\text{O}(^3\text{P}) + \text{C}_2\text{H}_4$ Reaction:..., P. Cassavechia, G. Capozza, E. Segoloni, F. Leonori, N. Balucani, G. G. Volpi, J. Phys. Chem. A **109**, 3527 (2005) and references therein.
2. Potential energy surfaces, product distributions and thermal rate coefficients of the reaction of $\text{O}(^3\text{P})$ with $\text{C}_2\text{H}_4(X^1\text{A}_g)$: a comprehensive theoretical study, T.J. Nguyen, L. Vereecken, X.J. Hou, et al, J. Phys. Chem. A **109**, 7489 (2005).
3. $\text{O} + \text{C}_2\text{H}_4$ potential energy surface: excited states and biradicals at the multireference level, A. C. West, J. D. Lynch, B. Sellner, H. Lischka, W. L. Hase, T. L. Windus, Theo. Chem. Acc. **131**, 1123 (2012).
4. Trajectory surface hopping studies of the $\text{O}(^3\text{P})+\text{ethylene}$ reaction dynamics, W. Hu, G. Lendvay, B. Maiti, G.C. Schatz, J. Phys. Chem. A **112**, 2093 (2008).
5. CH Stretching Excitation in the Early Barrier $\text{F} + \text{CHD}_3$ Reaction Inhibits CH Bond Cleavage, W. Zhang, H. Kawamata, and K. Liu, Science **325**, 303 (2009).
6. Steric Control of the Reaction of CH Stretch-Excited CHD_3 with Chlorine Atom, F. Wang, J.-S. Lin, and K. Liu, Science **331**, 900 (2011).
7. Enlarging the reactive cone of acceptance by exciting the C–H bond in the $\text{O}(^3\text{P}) + \text{CHD}_3$ reaction, F. Wang F, K. Liu, Chem. Sci. **1**, 126 (2010).

PUBLICATIONS SUPPORTED BY THE DOE (2009-present)

1. Three Reaction Pathways in the $\text{H} + \text{HCO} \rightarrow \text{H}_2 + \text{CO}$ reaction, K. M. Christoffel and J. M. Bowman, Three reaction pathways in the $\text{H} + \text{HCO} \rightarrow \text{H}_2 + \text{CO}$ reaction, K. Christoffel and J. M. Bowman, *Phys. Chem. A*, **113**, 4138 (2009).
2. Accurate ab initio potential energy surface, dynamics, and thermochemistry of the $\text{F} + \text{CH}_4 \rightarrow \text{HF} + \text{CH}_3$ reaction, G. Czako, B. C. Shepler, B. J. Braams, and J. M. Bowman, *J. Chem. Phys.* **130** 084301 (2009).
3. Quasiclassical Trajectory Calculations of the $\text{HO}_2 + \text{NO}$ Reaction on a Global Potential Surface, C. Chen, B. C. Shepler, B. J. Braams and J. M. Bowman, *Phys. Chem. Chem. Phys.* **11**, 4722 (2009).
4. Production of vibrationally excited H_2O from charge exchange of H_3O^+ with cesium, J. E. Mann, Z. Xie, J. D. Savee, J. M. Bowman, and R. Continetti, *J. Chem. Phys.* **130**, 041102 (2009).
5. Full-dimensional *ab initio* potential energy surface and vibrational configuration interaction calculations for vinyl. A. R. Sharma, B. J. Braams, S. Carter, B. C. Shepler, and J. M. Bowman, *J. Chem. Phys.* **130**, 174301 (2009).
6. CH stretching excitation steers the F atom to the CD bond in the $\text{F} + \text{CHD}_3$ reaction, G. Czako and J. M. Bowman, *J. Am. Chem. Soc.* **131**, 17534 (2009).
7. Roaming dynamics in formaldehyde- d_2 dissociation, V. Goncharov, S. A. Lahankar, J. D. Farnum, J. M. Bowman, and A. G. Suits, *J. Phys. Chem. A* **113** (52), 15315 (2009).
8. Permutationally invariant potential energy surfaces in high dimensionality, B. J. Braams and J. M. Bowman, *Int. Rev. Phys. Chem.* **28**, 577 (2009).
9. Permutationally invariant polynomial basis for molecular energy surface fitting via monomial symmetrization, Z. Xie and J. M. Bowman, *J. Chem. Theo Comp.* **6**, 26 (2010).
10. Seven-degree-of-freedom, quantum scattering dynamics study of the $\text{H}_2\text{D}^+ + \text{H}_2$ reaction, D. Y. Wang, Z. Xie, and J. M. Bowman, *J. Chem. Phys.* **132** (8) (2010).
11. Communications: Classical trajectory study of the postquenching dynamics of $\text{OH A } ^2\Sigma^+$ by H_2 initiated at conical intersections, E. Kamarchik, B. N. Fu, and J. M. Bowman, *J. Chem. Phys.* **132** (9) (2010).
12. Depression of reactivity by the collision energy in the single barrier $\text{H} + \text{CD}_4 \rightarrow \text{HD} + \text{CD}_3$ reaction, W. Q. Zhang, Y. Zhou, G. R. Wu, et al., *Proc Nat Acad Sci* **107**, 12782-12785 (2010).
13. Evidence for Vinylidene Production in the Photodissociation of the Allyl Radical, C. Chen, B. Braams, D. Y. Lee, J. M. Bowman, P. L. Houston, and D. Stranges, *J. Phys. Chem. Lett.* **1**, 1875-1880 (2010).
14. Invited Perspective: Ab-Initio-Based Potential Energy Surfaces for Complex Molecules and Molecular Complexes, J. M. Bowman, B. J. Braams, S. Carter, C. Chen, G. Czako, B. Fu, X. Huang, E. Kamarchik, A. R. Sharma, B. C. Shepler, Y. Wang, and Z. Xie, *J. Phys. Chem. Lett.* **1**, 1866-1874 (2010).
15. Dynamics of the Reaction of Methane with Chlorine Atom on an Accurate Potential Energy Surface, G. Czako and J. M. Bowman, *Science* **334**, 343 (2011).
16. Quasiclassical Trajectory Calculations of the Dissociation Dynamics of CH_3CHO at High Energy Yield Many Products Y-C Han, B. C. Shepler, and J. M. Bowman *J. Phys. Chem. Lett.* **2**, 1715 (2011).
17. Communication: Probing the Entrance Channels of the $\text{X} + \text{CH}_4 \rightarrow \text{HX} + \text{CH}_3$ ($\text{X} = \text{F}, \text{Cl}, \text{Br}, \text{I}$) Reactions via Photodetachment of $\text{X}^- - \text{CH}_4$, M. Cheng, Y. Feng, Y. Du, Q. Zhu, W. Zheng, G. Czako, and J. M. Bowman, *J. Chem. Phys.* **134**, 191102 (2011).
18. The Dynamics of Allyl Radical Dissociation, C. Chen, B. Braams, D. Y. Lee, J. M. Bowman, P. L. Houston, and D. Stranges, *J. Phys. Chem. A* **115**, 6797 (2011).
19. Three-State Trajectory Surface Hopping Studies of the Photodissociation Dynamics of Formaldehyde...”, B. Fu, B. C. Shepler, and J. M. Bowman, *J. Am. Chem. Soc.* **133**, 7957 (2011).

20. Are Roaming and Conventional Saddle Points for H₂C=O and CH₃C=O Dissociation to Molecular Products Isolated from Each Other? B. C. Shepler, Y. Han, and J. M. Bowman, *J. Phys. Chem. Lett.* **2**, 834 (2011).
21. An *ab initio* spin-orbit-corrected potential energy surface and dynamics for the F + CH₄ and F + CHD₃ reactions, G. Czako and J. M. Bowman, *Phys. Chem. Chem. Phys.* **13**, 8306-8312 (2011).
22. Invited Perspective: High-dimensional *ab initio* potential energy surfaces for reaction dynamics calculations, J. M. Bowman, G. Czako, and B. Fu, *Phys. Chem. Chem. Phys.* **13**, 8094-8111 (2011).
23. Roaming Radicals, J. M. Bowman and B. C. Shepler, *Annu. Rev. Phys. Chem.* **62**, 531 (2011).
24. Quasiclassical trajectory study of the postquenching dynamics of OH(A)²Σ⁺ by H₂/D₂ on a global potential energy surface, B. Fu, E. Kamarchik, and J. M. Bowman *J. Chem. Phys.* **133**, 164306 (2010).
25. Collisional quenching of OD (A)²Σ⁺ by H₂: Experimental and theoretical studies of the state-resolved OD X²Π product distribution and branching fraction, J. H. Lehman, L. P. Dempsey, M. I. Lester, B. Fu, E. Kamarchik, and J. M. Bowman, *J. Chem. Phys.* **133**, 164307 (2010).
26. Global potential energy surfaces for O(³P)+H₂O(1A₁) collisions, P. F. Conforti, M. Braunstein, B. J. Braams, and J. M. Bowman *J. Chem. Phys.* **133**, 164312 (2010).
27. Communication: Experimental and theoretical investigations of the effects of the reactant bending excitations in the F+CHD₃ reaction, G. Czako, Q. Shuai, and K. Liu, *J. Chem. Phys.* **133**, 131101 (2010).
28. Roaming Pathway Leading to Unexpected Water + Vinyl Products in C₂H₄OH Dissociation, E. Kamarchik, L. Koziol, H. Reisler, J. M. Bowman, and A. I. Krylov, *J. Phys. Chem. Lett.* **1**, 3058 (2010).
29. Roaming reactions: The third way, J. M. Bowman and A. G. Suits, *Phys. Today* **64**, 33 (2011).
30. Accurate *ab initio* potential energy surface, thermochemistry, and dynamics of the Cl(²P, ²P_{3/2}) + CH₄ → HCl + CH₃ and H + CH₃Cl reactions, G. Czako and J. M. Bowman, *J. Chem. Phys.* **136**, 044307 (2012).
31. Communication: A chemically accurate global potential energy surface for the HO + CO → H + CO₂ reaction, J. Li, Y. Wang, B. Jiang, J. Ma, R. Dawes, D. Xie, J. M. Bowman, and H. Guo, *J. Chem. Phys.* **136**, 041103 (2012).
32. Large-amplitude dynamics in vinyl radical: The role of quantum tunneling as an isomerization mechanism, A. R. Sharma, J. M. Bowman, and D. J. Nesbitt, *J. Chem. Phys.* **136**, 034305 (2012).
33. Overtone-induced dissociation and isomerization dynamics of the hydroxymethyl radical (CH₂OH and CD₂OH). I. A theoretical study, E. Kamarchik, C. Rodrigo, J. M. Bowman, H. Reisler, and A. I. Krylov. *J. Chem. Phys.* **136**, 084304 (2012)
34. Three-state surface hopping calculations of acetaldehyde photodissociation to CH₃+HCO on *ab initio* potential surfaces, B. Fu, Y.-C. Han, and J. M. Bowman, *Faraday Disc.* DOI:10.1039/C2FD20010D.
35. MULTIMODE Calculations of Rovibrational Energies of C₂H₄ and C₂D₄, S. Carter, J. M. Bowman, and N. C. Handy, *Mol. Phys.* DOI: 10.1080/00268976.2012.669504
36. Dynamics of the O(³P) + CHD₃(*v*_{CH}=0,1) reactions on an accurate *ab initio* potential energy surface, G. Czako and J. M. Bowman, *Proc. Natl. Acad. Sci., USA*, in press.
37. Intersystem crossing and dynamics in O(³P)+C₂H₄ multichannel reaction: Experiment validates theory, B. Fu, Y.-C. Han, J. M. Bowman, L. Angelucci, N. Balucani, F. Leonori, P. Casavecchia, *Proc. Nat. Acad. Sci., USA*, in press.

COMBUSTION CHEMISTRY
Principal Investigator: Nancy J. Brown
Environmental Energy Technologies Division
Lawrence Berkeley National Laboratory
Berkeley, California, 94720
510-486-4241 NJBrown@lbl.gov

PROJECT SCOPE

Combustion processes are governed by chemical kinetics, energy transfer, transport, fluid mechanics, and their complex interactions. Understanding the fundamental chemical processes offers the possibility of optimizing combustion processes. The objective of our research is to address fundamental issues of chemical reactivity and molecular transport in combustion systems. Our long-term research objective is to contribute to the development of reliable combustion models that can be used to understand and characterize the formation and destruction of combustion-generated pollutants. We emphasize studying chemistry at both the microscopic and macroscopic levels. Our current work is concerned with improving the calculation of transport properties for combustion modeling.

RECENT PROGRESS

We have recently investigated thermal diffusion to determine a methodology for computing more accurate thermal diffusion factors (TDFs) that are suitable for combustion modeling. Mason et al. [1] provide an excellent phenomenological description of thermal diffusion as: “Thermal diffusion is the relative motion of the components of a mixture arising from a temperature gradient. It is also known as the Soret effect, named after one of its discoverers. The resulting composition gradients in the mixture lead to ordinary diffusion, which tends to eliminate gradients. A steady state is reached when the separating effect of thermal diffusions is balanced by the remaining effects of ordinary diffusion. As a result of this steady state, the components of a mixture will be partially separated. The heavier component is usually concentrated in the colder region, and when this occurs, the thermal diffusion coefficient is positive.” TDFs are slowly varying functions of composition and are independent of pressure.

Thermal diffusion is important in combustion for both H₂/Air flames and hydrocarbon flames, and especially for light species such as hydrogen radical and molecular hydrogen. Bongers and de Goey [2] found that the inclusion of the Soret effect reduced the flame speed in H₂+Air flames and that the effect was greater for rich flames. Ern and Giovangigli [3] also found that the flame velocity was decreased in Bunsen flames of H₂+Air. In contrast, Grcar et al. [4] have indicated that including the Soret effect in modeling calculations of a freely propagating lean premixed H₂+Air flames affects a number of flame properties. Inclusion of the Soret effect increased flame speed and the frequency of cell divisions or extinctions, and that the diffusive focusing delivers more fuel to the flame cells.

Obtaining the TDF requires one to solve an infinite set of equations; consequently there are a number of approximations for computing thermal diffusion factors. Various approximations involve estimates of the solution of the infinite set, namely by treating it as a finite set of equations like the Chapman-Cowling[5] solution, or by neglecting higher order derivatives of collision integrals like the Kihara[6] approximation. Hirschfelder [7] provides an approximation for the TDF of binary mixtures derived from the Chapman-Enskog theory based upon thermal conductivities and ratios of collision integrals. Multicomponent diffusion coefficients, thermal conductivities, and thermal diffusion coefficients are computed from the solution of a $3K \times 3K$ system of equations, where K is the number of species in TRANLIB[8,9]. It involves computing the L-matrix whose components are experimental or calculable quantities such as heat capacities, masses, pure species viscosities, and binary diffusion coefficients.

Each TDF approximation involves collision integrals, gas composition, and temperature. We investigate the various approaches using 7 different intermolecular potentials, and analyze the results statistically by comparing them with experimental values. We recently collected experimental data on eight binary mixtures to investigate the efficacy of seven intermolecular potentials and five approximations for computing TDFS to ascertain which of these might be suitable to use for combustion modeling. All the potentials except one have the attractive part expressed as $(1/r^6)$. We evaluated the approximate schemes of Chapman and Cowling, Kihara and Hirschfelder et al., and the TRANLIB mixture and multi-component approximations.

We evaluated the suitability of three Lennard-Jones potentials and four modified Buckingham Exp α -6 potentials ($\alpha = 12-15$) to describe molecular interactions between non-polar species with sufficient accuracy to calculate thermal diffusion factors. The LJ 28-7 model, as expected, produced poor results and is not suitable for such gases. The other potentials have the attractive part expressed as $(1/r^6)$, allowing us to focus on the importance of the repulsive term. TDFs were found to be sensitive to the potential shape function (exponential branch or inverse power term). Despite considerable theoretical and experimental evidence that suggested the repulsive energy is described better by an exponential form, the Exp α -6 potentials are not widely applicable to non-polar species and are overall too repulsive when α is greater than 12. The Lennard-Jones 12-6 potential, used extensively in computer simulations of transport properties for non-polar species, is too repulsive for mono- and diatomic neutral species. The LJ 9-6 that has a softer repulsive branch is preferable.

Four TDF approximations are investigated to determine their suitability for calculating TDFs for binary mixtures. When applied to a LJ 9-6 potential, the four methods are quite accurate and give very similar results: on average, deviations are approximately 10 % and do not differ from each other by more than 3 % as shown in the Table below. TRANLIB uses a LJ 12-6 potential for non-polar molecules, and using the TRANLIB multicomponent expression with this potential leads to a mean deviation of 12 %. The

TRANLIB method could benefit from the use of a LJ 9-6 potential, but there are more important changes to consider where significant uncertainties could be reduced like those associated with radical species. While TRANLIB includes the effects of internal degrees of freedom for polyatomic species, no improvement over the original Chapman and Cowling's method has been observed. The TRANLIB mixture-averaged approximation is not correct for the application indicated in the manual. Instead, this should only be used for isotopic binary mixtures as recommended by Hirschfelder. It gives poor results for most binary mixtures.

Mean deviations (in %) as a function of potential model and TDF approximation.

	LJ 9-6	LJ 12-6	LJ 28-7	Exp 12-6	Exp 13-6	Exp 14-6	Exp 15-6
Chapman	9.4	10.1	34.8	11.5	12.8	15.8	19.4
Kihara	9.1	19.5	52.0	13.7	19.5	24.9	30.1
Hirschfelder	11.3	7.5	32.2	12.1	11.2	13.2	16.3
TRANLIB Multicomponent	8.9	11.9	38.9	11.2	13.6	17.3	21.3

Greater accuracy may be attained by the use of higher approximations or more detailed potentials. Greater improvements could be achieved if more experimental data were available for polar molecules or radical species. We demonstrated that the uncertainty of experimental thermal diffusion data is often underestimated. When the potential is adequate, the accuracy of the four approximations is similar, while great variations between approximations are observed when the potential gives an unfaithful description of molecular interactions. This suggests that the potential model is more important than the choice of the TDF approach for binary mixtures. All expressions reviewed here are second-order approximations, and they are adequate for combustion modeling where the largest uncertainty appears to be in the supporting data required for transport property calculations.

A sensitivity analysis of the TDF to the intermolecular potential would give more information regarding additional items that could be improved to achieve more accurate TDFs. This study is limited to binary neutral mixtures and should be extended to both polar molecules and multicomponent mixtures. Two programs are used to compute multicomponent transport properties: the TRANLIB and EGLIB libraries. Further evaluation of these libraries should be conducted when new experimental data for polar gases and for ternary (or more complex) mixtures are available.

Publications supported by DOE for last two years:

Bastien, L.A.J., Price, P.N. and Brown, N.J. "Intermolecular Potential Parameters and Combining Rules Determined from Viscosity Data," *International Journal of Chemical Kinetics* 42, DOI 10.1002/kin.20521, pp 713-723 (2010).

Brown, N.J., Bastien, L.A.J., and Price, P.N. "Transport Properties for Combustion Modeling." *Progress in Energy and Combustion Science* doi.org/10.1016/j.pecs.2010.12.001 (2010) .

Ling Jin, Nancy Brown, Robert A. Harley, Jian-Wen Bao, Sarah Michelson, James M. Wilzak, Seasonal versus Episodic Performance Evaluation for an Eulerian Photochemical Model, *Journal Geophysical Research Atmospheres* 115 DO9302,doi:10.1029/2009JDO12680, 2010.

Jin, L., Harley, R.A., Brown, N.J., "Meteorology-induced Variations in the Spatial Behavior of Summer Ozone Pollution in Central California" *Atmospheric Environment* 45 pp4704-4718 (2011).

Shearer, S.M., Harley, R.A., Jin L., and Brown, N.J., "Evaluation of the Condensed SAPRC07 Chemical Mechanism: Predictions of Photochemical Air Pollution in Central California," *Atmospheric Environment* 46 (2012) pp205-216.

E.C. McDonald-Buller, D.T. Allen, N. J. Brown, D.J. Jacobs, D. Jaffe, C.E. Kolb, A.S. Lafohn, S. Oltmans, D.D. Parrish, G. Yarwood, and Lin Zhang."Establishing Policy Relevant Background (PRB) Ozone Concentrations in the United States," *Env. Sci. Tech.* 2011, 45 pp9484-9497.

References

[1] Mason, E.A., Munn, R.J. and Smith, F.J. Thermal Diffusion in Gases. *Advances in Atomic and Molecular Physics*, 1966, 2, 33-91.

[2] Bongers, H. and Goey, L.P.H.D. The effect of simplified transport modeling on the burning velocity of laminar premixed flames. *Combustion Science and Technology*, 2003, 175(10), 1915-1928.

[3] Ern, A. and Giovangigli, V. Thermal diffusion effects in hydrogen-air and methane-air flames. *Combustion Theory and Modelling*, 1998, 2(4), 349-372.

[4] Grcar, J.F., Bell, J.B. and Day, M.S. The Soret effect in naturally propagating, premixed, lean, hydrogen-air flames. *Proceedings of the Combustion Institute*, 2009, 32(1), 1173-1180.

[5] Chapman, S. and Cowling, T.G. *The Mathematical Theory of Non-uniform Gases*. (Cambridge University Press, Cambridge, 1952)

[6] Kihara, T. *Imperfect Gases*. (Asakura Bookstore, Tokyo, 1949). Originally published in Japanese and translated into English by the US Office of Air Research, Wright-Patterson.

[7] Hirschfelder, J.O., Curtis, C.F. and Bird, R.B. *Molecular Theory of Gases and Liquids*. (John Wiley and Sons, New York, 1954)

[8] Kee, R.J. and Warnatz, J.M., Miller, J.A. *A Fortran computer code package for the evaluation of gas-phase viscosities, conductivities, and diffusion coefficients*. Sandia National Laboratories Report: SAND83-8209, 1983.

[9] Kee, R.J., Dixon-Lewis, G., Warnatz, J., Coltrin, M.E. and Miller, J.A. *A Fortran Computer Package for the Evaluation of Gas-Phase Multicomponent Transport Properties*. Sandia National Laboratory Report: SAND86-8246, 1986.

Dynamics of Product Branching in Elementary Combustion Reactions: OH + Alkenes and Nitrogen Chemistry

Laurie J. Butler

The University of Chicago, The James Franck Institute

5640 South Ellis Avenue, Chicago, IL 60637

L-Butler@uchicago.edu

I. Program Scope

The elementary reactions that determine the performance of a combustion system range from direct H-atom abstraction reactions to complex reactions involving competing addition/elimination mechanisms. While the total rate constant for many elementary reactions is well-characterized, understanding the product branching in complex reactions presents a formidable challenge. To study such reactions, our experiments directly probe the dynamics of the product channels that arise from long-lived radical intermediates along the bimolecular reaction coordinates. The work uses the methodology developed in my group in the last ten years, using both imaging and scattering apparatuses. The experiments generate a particular isomeric form of an unstable radical intermediate along a bimolecular reaction coordinate and investigate the branching between the ensuing product channels of the energized radical as a function of its internal energy under collision-less conditions.

The experiments¹⁻⁷ use a combination of: 1) measurement of product velocity and angular distributions in a crossed laser-molecular beam apparatus, with electron bombardment detection in my lab and with tunable vacuum ultraviolet photoionization detection at Taiwan's National Synchrotron Radiation Research Center (NSRRC), and 2) velocity map imaging using state-selective REMPI ionization and single photon VUV ionization of radical intermediates and reaction products. Our publications this year^{6,7} focused on imaging and scattering studies on a partially deuterated radical intermediate to understand the product branching from the addition mechanism for the OH + ethene reaction, starting from the 2-hydroxyethyl radical. We have also studied a photolytic precursor to two radical intermediates important in the reaction of OH with propene. Finally, we took preliminary data on the C₂H₄CHO combustion intermediate that results in ethene + HCO products. We plan to use it to definitively determine the absolute photoionization cross section of HCO in comparison to the ethene standard. The paragraphs below detail each of these efforts. Overall, our results develop insight on product channel branching in reactions that proceed via an addition/elimination mechanism and benchmark theoretical predictions of polyatomic reactions that proceed through unstable radical intermediates.

II. Recent Progress

A. Angular Momentum Effects on the Product Channel Branching in OH + Ethene

The total rate constant OH + ethene reaction has been well characterized since the 1980s. The reaction was understood as an H atom abstraction competing with an addition mechanism (some of the best work was published by Frank Tully in Chem. Phys. Lett. 96, 14 (1983) and 143, 510 (1988)). Studies of the product branching from the CH₂CH₂OH radical intermediate formed in the addition mechanism were incomplete, though ethenol + H had been definitively identified as a product channel by Taatjes and coworkers, confirming the assignment of this channel in flame studies by Cool et al., J. Chem. Phys. 119, 8356 (2003). In 2011 we published⁵ the first definitive measurements of product branching to all energetically allowed channels from the CH₂CH₂OH radical intermediate of the OH + ethene reaction. Using tunable VUV photoionization in the scattering apparatus at the NSRRC, the

data showed the radicals dissociate to three major product channels, H + ethenol (2.6%), CH₃ + formaldehyde (6.3%), vinyl + H₂O (14.5%) as well as to the OH + ethene reactant asymptote (76.5%) when the radicals are produced photolytically with an internal energy distribution characterized in Pub. 1 below. The most surprising result was the substantial branching to the H₂O + vinyl channel (RRKM calculations had only considered the possibility of branching to this channel from the OH + ethene reactants, not from the CH₂CH₂OH addition intermediate, since the tight transition state from the radical intermediate is high in energy). The vinyl signal evidenced the forward/backward symmetric scattering expected for the dissociation of a rotationally and vibrationally excited CH₂CH₂OH radical. We proposed that the CH₂CH₂OH radical intermediate might begin to dissociate to the OH + ethene reactant asymptote but return to instead abstract an H atom. We learned that Bowman and co-workers had, before my inquiry, identified such trajectories (subsequently reported in *J. Phys. Chem. Lett.* **1**, 3058 (2010)) on the global potential energy surface calculated by A. Krylov.

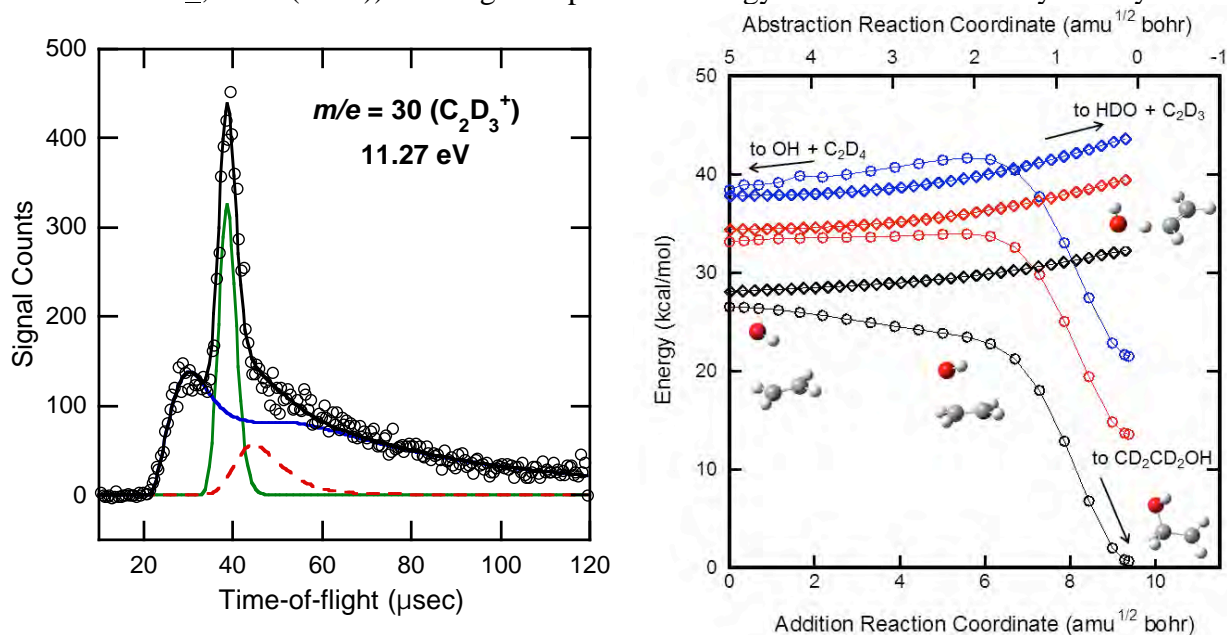


Fig. 1. Vinyl products (blue) from the CD₂CD₂OH (left) and centrifugal corrections (right).

This year, we investigated the product channels from the CD₂CD₂OH radical intermediate to assess the importance of tunneling and centrifugal effects in the frustrated dissociation to OH + ethene that results in water + vinyl products. (The quasiclassical trajectory studies had reported only a couple percent branching to this channel.) Our calculated transition state (Fig. 1) involves primarily D atom motion (with a reduced mass of near 2 amu for motion across the transition state), but our data showed that branching to the water+vinyl channel was not decreased in the deuterated system. This result motivated us to consider centrifugal effects on the branching between the OH + ethene and the water+vinyl channels. Fig. 1 shows the highly rotationally excited radicals formed in our experiments encounter a centrifugal barrier en route to the OH + ethene products, but the moment of inertia at the water+vinyl transition state is large, so the centrifugal correction to that barrier is smaller. The right panel of Fig. 1 shows a centrifugal correction to the energy along the reaction coordinate for these two product channels. The blue curve shows that CD₂CD₂OH radicals produced with higher rotational energies (from the gauche photolytic precursor) see an abstraction barrier that is only 2 kcal/mol higher than the centrifugally corrected barrier to

dissociate to OH + ethene (when the uncorrected barrier difference is 6 kcal/mol). This may well explain why our experimental branching to this channel was higher than predicted in the quasiclassical trajectories, as the trajectories were done for rotationally cold radicals.

B. Radical Intermediates in OH + Propene

This year we have also studied the photolytic generation of two radical intermediates of importance in the reaction of OH with propene. Two theory/modeling groups in the combustion program (Zador et al. *Phys. Chem. Chem. Phys.* **11**, 11040 (2009) and Truong and coworkers, *J. Phys. Chem. A* **113**, 3177 (2009)) have published high quality electronic structure calculations of the transition states en route to products on the global C₃H₇O potential energy surface. Our experiments, in preparation for publication, photodissociate at 193 nm a molecular beam of 30% 2-bromo-1-propanol and 70% 1-bromo-2-propanol seeded in helium. In our imaging apparatus, we use REMPI detection of the Br atom co-fragments, measuring the velocity distributions of the Br atoms in each spin-orbit state to determine the internal energy distributions of the momentum-matched C₃H₇OH radicals. One isomer corresponds to the radical intermediate formed when OH adds to the center C atom of propene while the other corresponds to addition at an end C atom. The data show that C-Br photofission partitions from 20 to 50 kcal/mol to recoil kinetic energy, so the C₃H₇OH radicals are formed with internal energies that span the theoretically predicted transition states to several important products, including alkenols, aldehydes, and acetone. We are also interested in the possibility that a frustrated dissociation to OH + propene might result in an allyl radical + H₂O product channel (in analogy with our results on OH + ethene). In our first paper, we present the characterization of the internal energy distribution of the nascent C₃H₇OH radicals along with a prediction as to what fraction of each would be energetically stable to the OH + propene product asymptote. We also analyze the time-of-flight spectrum of the propene product from the dissociation of the unstable radical intermediates. The conformer of the photolytic precursor strongly affects the partitioning of the internal energy of the nascent radicals between vibration and rotation.

C. Determining the Absolute Photoionization Cross Section of HCO

Because HCO is an important combustion intermediate, its detection using photoionization has received much attention. The photoionization spectrum of HCO was reported in Ref. 2 below, a study of the product channels from a radical intermediate the O + allyl reaction that included scattering experiments with tunable VUV ionization at the NSRRC in Taiwan. Measuring the relative signal levels from HCO and ethene produced in a 1:1 ratio allowed us to determine, using the literature photoionization cross section of ethene, the absolute photoionization cross section of HCO from 9 to 11.3 eV. The photoionization spectrum has a relatively low resolution and may include a contribution from the dissociative ionization of CH₃O products in the same experiment. Nevertheless, our determination agrees with the HCO photoionization cross section at 10.3 eV measured by Steve Pratt (*J. Phys. Chem. A* **114**, 11238 (2010)). That study produced the HCO from acetaldehyde photodissociation and measured the HCO photoionization signal relative to that of the methyl radical co-fragment. This work has its own uncertainties, as some of the HCO may be subject to secondary dissociation, the HCO is likely to have much higher vibrational energies than in a thermal system, and the methyl radical reference is not as well determined as ethene. We thus initiated experiments to identify a better photolytic precursor for this measurement.

Our work this year optimized the synthesis of the ClCH₂CH₂CHO photolytic precursor for the CH₂CH₂CHO radical. Our hope was that when this precursor was photodissociated at 193 nm that substantial energy would be partitioned to relative kinetic energy so the HCO radicals would span the barrier to C₂H₄ + HCO and produce HCO with low internal energies.

Surprisingly, the distribution of relative kinetic energies upon C-Cl bond fission peaked near 2 kcal/mol. While this gives a wonderfully narrow range of internal energies for studying the competing product channels from the $\text{CH}_2\text{CH}_2\text{CHO}$ radical, it is not ideal for measuring the photoionization cross section of HCO. We plan to investigate 157 nm photodissociation of the precursor, as it should produce lower internal energy radicals. (This might be at first counter-intuitive, but C-Cl bond photofission occurs on a repulsive excited state upon excitation at 157 nm, so the larger partitioning of energy to relative kinetic energy should more than offset the higher photon energy.)

III. Ongoing Work

We have just begun collaborating with Kamarchik and Bowman on quasiclassical trajectories on the product channels of the $\text{CH}_2\text{CH}_2\text{OH}$ and the $\text{CD}_2\text{CD}_2\text{OH}$ radical intermediates. We wish to investigate the effect of rotational energy on the product channel branching, particularly the unexpectedly large branching to the water + vinyl channel. Our model for the rotational angular momenta imparted upon C-Br fission in 2-bromoethanol at 193 nm generates appropriate initial conditions for the new trajectory calculations. We anticipate completing the tunable VUV photoionization source this spring, so plan the experiments to establish the absolute photoionization cross section of HCO at 10.7 eV this summer. We have also initiated a collaboration with Terry Miller's group to characterize for them the primary photodissociation channels of their photolytic precursor for the $\text{CH}_2\text{CH}_2\text{ONO}$ radical.

IV. Publications Acknowledging DE-FG02-92ER14305 (2010 or later)

1. Modeling the Rovibrationally Excited $\text{C}_2\text{H}_4\text{OH}$ Radicals from the Photodissociation of 2-Bromoethanol at 193 nm, B. J. Ratliff, C. C. Womack, X. N. Tang, W. M. Landau, L. J. Butler, and D. E. Szpunar, *J. Phys. Chem. A* **114**, 4934-4945 (2010).
2. Primary Photodissociation Pathways of Epichlorohydrin and Analysis of the C-C Bond Fission Channels from an $\text{O}(^3\text{P})$ + Allyl Radical Intermediate, B. L. FitzPatrick, B. W. Alligood, L. J. Butler, S. -H. Lee, and J. J. Lin, *J. Chem. Phys.* **133**, 094306 (2010).
3. Assessing an Impulsive Model for Rotational Energy Partitioning to Acetyl Radicals from the Photodissociation of Acetyl Chloride at 235 nm, C. C. Womack, W. H. Fang, D. B. Straus, and L. J. Butler, *J. Phys. Chem. A* **114**, 13005-10 (2010).
4. Theoretical Study of Isomerization and Dissociation Transition States of $\text{C}_3\text{H}_5\text{O}$ Radical Isomers: Ab Initio Characterization of the Critical Points and Statistical Transition-State Theory Modeling of the Dynamics, B. L. FitzPatrick, *J. Phys. Chem. A* **115**, 1701 (2011). (Work completed as a Ph.D. student with L. J. Butler.)
5. Product Branching from the $\text{CH}_2\text{CH}_2\text{OH}$ Radical Intermediate of the OH + Ethene Reaction, B. J. Ratliff, B. W. Alligood, L. J. Butler, S. -H. Lee, and J. J. Lin, *J. Phys. Chem. A* **115**, 9097-110 (2011).
6. Characterizing the ro-vibrational distribution of $\text{CD}_2\text{CD}_2\text{OH}$ radicals produced via the photodissociation of 2-bromoethanol- d_4 , C. C. Womack, R. S. Booth, M. D. Brynteson, L. J. Butler, and D. E. Szpunar, *J. Phys. Chem. A* **115**, 14559-14569 (2011).
7. Photoproduct channels from $\text{BrCD}_2\text{CD}_2\text{OH}$ at 193 nm and the HDO + vinyl products from the $\text{CD}_2\text{CD}_2\text{OH}$ radical intermediate, C. C. Womack, B. J. Ratliff, L. J. Butler, S. -H. Lee, and J. J. Lin, *J. Phys. Chem. A*, DOI 10.1021/jp21217t (2012).

Collision Dynamics Studied in Crossed Molecular Beams and New High Resolution Spectrometer Demonstrated

David W. Chandler
Combustion Research Facility
Sandia National Laboratory
Livermore, CA 94551-0969
Email: chand@sandia.gov

Program Scope:

My research focuses on the chemical dynamics and optical diagnostics for gas phase molecular species. Chemical dynamics is the detailed study of the motion of molecules and atoms on potential energy surfaces in order to learn about the details of the surface as well as the dynamics of their interactions. We have begun study of the collision dynamics of molecules in vibrationally and electronically excited states. We excite a molecule entrained in a molecular beam at the crossing (or just before the crossing) of another atomic or molecular beam in order to prepare an electronically or vibrationally excited state molecule. Collisions transfer energy into the excited molecule producing molecules in new quantum states. The details of that transfer are monitored state selectively. New experiments are focusing on very vibrationally excited polyatomic molecules. In another set of experiments, a new concept for time-resolved Fourier transform spectroscopy has been demonstrated. This spectrometer is based on the interference between two transient frequency combs and has many potential uses including time-resolved, broad-band spectroscopy with a nanosecond time scale and high-resolution spectroscopy.

Progress Report:

Scattering of Electronically Excited State Molecules.

By exciting a molecule into an electronically excited state while it is at the crossing point of a second atomic or molecular beam, scattering of the electronically excited state molecules can be studied if the lifetime of the electronic state is longer than ~200 ns. NO(A, j=0) state has a lifetime of 200 ns, and we excited it with near-UV light around 226 nm at the crossing of a 5%NO/He beam and a neat beam of He, Ne or Ar atoms. A 400-ns delay between the excitation and performing state-selective REMPI of the NO(A) state molecules is sufficient time to allow for collisions in the crossed molecular / atomic beams. During this delay ~90% of the NO(A) state molecules have decayed back to the ground state and of those remaining in the excited state approximately 1% have a collision. Those collisions cause rotational energy transfer to about 20 possible quantum states. Quantum-state resolved ionization detection of the collision products reveals both the differential cross section and the alignment of the angular momentum vector of the product molecule. Ionization is accomplished by selectively ionizing the NO (A, N) molecules by (1 + 1) REMPI through the NO(E) state at ~620 nm, and those ions are velocity-mapped Ion Imaged. In Fig 1 are images of NO(A, N=4,5,7,9) from such an experiment where the NO(A) collision partner is Ne. The two image columns on the left side of the figure were taken with different polarizations of the 620-nm light in order to observe the alignment of the product molecules. This work is being done in collaboration with the groups of Ken McKendrick and Matt Costen (Harriott-Watt Univeristy) and Millard Alexander and Jacek Klos (University of Maryland).

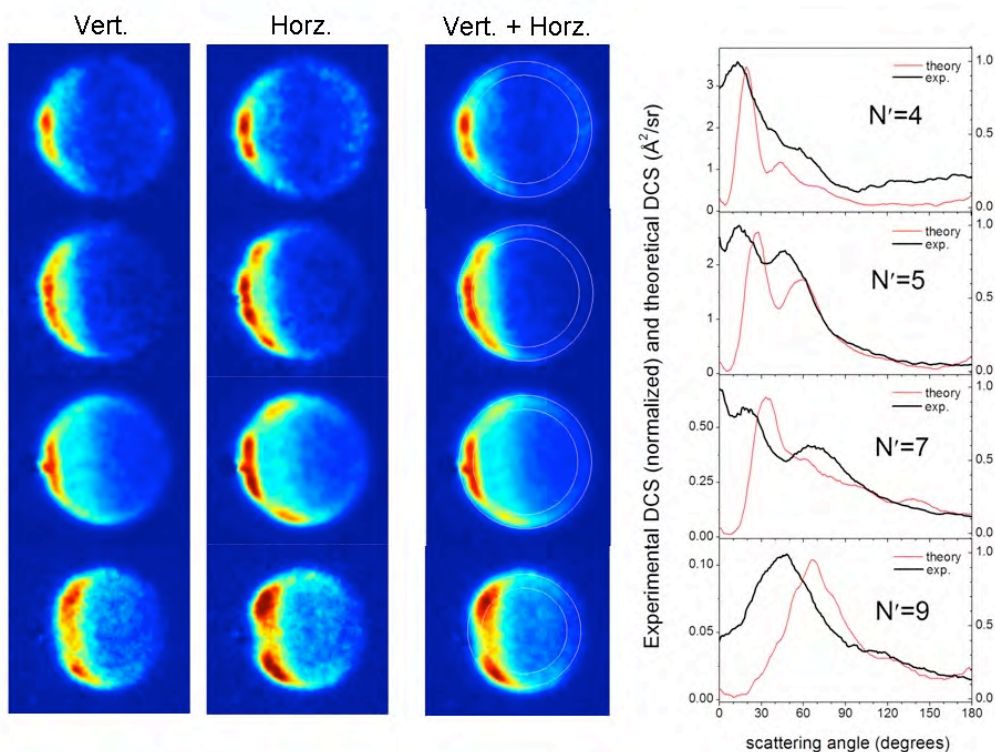


Figure 1: Angular momentum alignment and differential cross section (DCS) measurements for the process of $\text{NO } A(N=0) + \text{Ne} \rightarrow \text{NO } A(N=4,5,7,9) + \text{Ne}$. The measured DCS is shown in black, theory in red in far right panel.

Dual Etalon Frequency COMB (DEFKOM) Spectroscopy

The first demonstration of a new type of Fourier-transform (FT) based spectrometer has recently been completed. The Dual Etalon Frequency Comb (DEFKOM) spectrometer utilizes two independent etalons to generate two frequency combs. The bandwidth of the combs is set by the bandwidth of the laser beam used to excite the etalons. The etalon lengths are set such that the free spectral ranges ($\sim 300\text{MHz}$) of the two etalons are slightly different, approximately 250 kHz apart in our initial demonstration. An atom or molecule placed inside of one or both of the etalons possessing an optical transition resonant with some of the frequencies present within the etalons will absorb some of the light associated with some of the frequency-comb teeth. In order to quantitatively determine the intensity of each of the frequency comb teeth, the outputs of the etalons are combined onto a single photo detector. At the detector the outputs interfere producing a transient interferogram. Figure 2 is a schematic of the spectrometer showing the signals coming from each individual etalon as well as the signal coming from the combined outputs of the etalons. The spectrum is retrieved by Fourier transforming the interference pattern. As the light “rings down” from the etalons for over 100 microseconds, and every segment of the interferogram contains the entire spectrum, one may obtain sequential spectra with a time resolution that one chooses by selectively Fourier transforming segments of the interferogram. Here we Fourier transform 5 microseconds time segments sequentially for approximately 100 microseconds. This is illustrated in figure 3. In the first demonstration the (1,1,3) overtone spectrum of H_2O and the R(7) line of the weak gamma band of O_2 were recorded. This is shown in figure 4. A single laser pulse provided a 3GHz spectrum across a transition with a frequency

resolution of 300 MHz (0.01 cm^{-1}). This spectrometer can be thought of as a FT spectrometer where instead of moving a mirror in an interferometer the light is moved back and forth between the mirrors of the etalon.

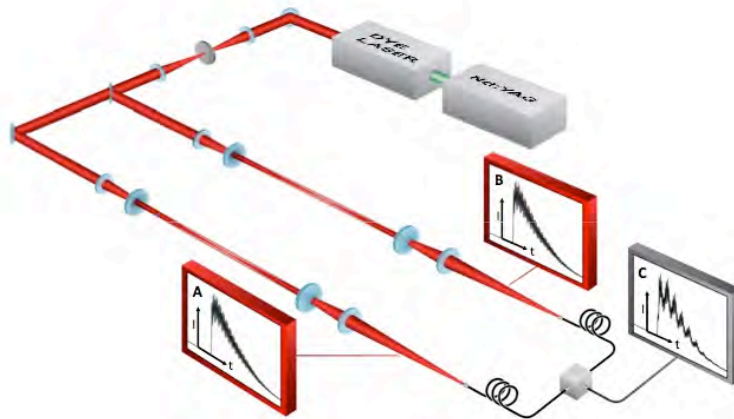


Figure 2 Schematic of the DEFCOM spectrometer. A beam of broadband laser light is spatially filtered, and a beam splitter separates the light into two beams that are coupled into two arms of the spectrometer. The outputs of the two arms are combined using single-mode fiber optics, and the intensity of the combined signal is monitored by a fast photomultiplier tube or if there is sufficient light intensity a photodiode. The current from the detector is recorded using a digitizing scope and Fourier transformed to recover the spectrum.

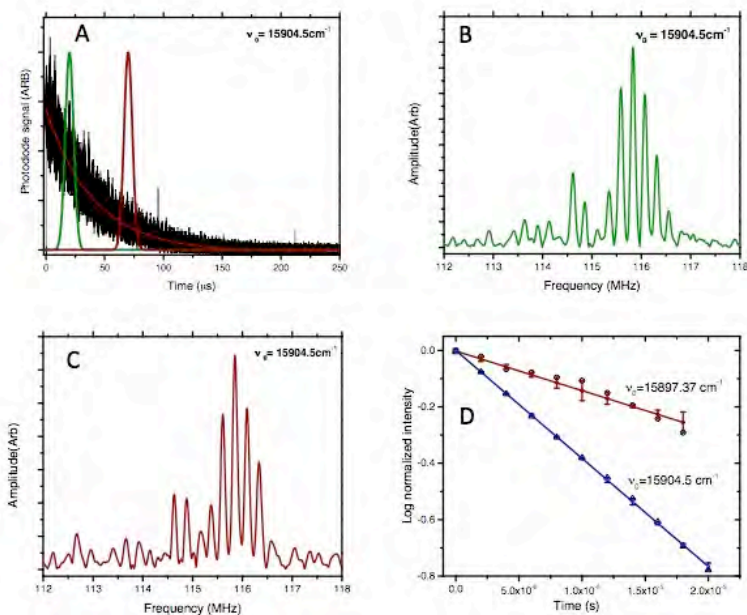


Figure 3. Panel A is the interferogram obtained from a single laser shot of the DEFCOM spectrometer with two 5 microsecond Gaussian functions superimposed. Panels B and C are portions of the Fourier transformed interferogram associated with the two Gaussian windows of panel A. Panel D is a plot of the intensity of two different modes at two different laser frequencies, the slope giving the absorption coefficient at those particular frequencies.

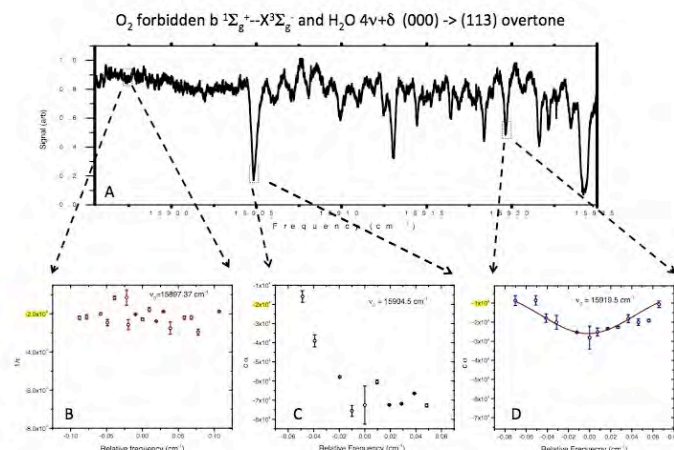


Figure 4. Panel A is a CRD spectrum of water saturated air around 628 nm. The laser is scanned to three different frequencies: (B) a background, (C) the (1,1,3) water transition and (D) the O₂ transition. At each laser setting an interferogram is recorded and high resolution spectra are obtained.

In the present spectrometer each comb tooth has a bandwidth of approximately 10 KHz. The absolute frequency of each tooth can be determined to approximately 10 MHz.

Future Plans: A new set of scattering experiments to measure the entire collisional energy transfer function, $P(E, E')$, of a very vibrationally excited molecule are beginning. We will accomplish this by excitation of a molecule just below its dissociation energy followed by collision induced dissociation and velocity map Ion Imaging of the collision product fragments. NO₂ is the first molecule we will study. This study will provide both a direct measure of the entire $P(E, E')$ excitation curve of a dissociating molecule and provide information on a process that is the microscopic reverse of a three-body recombination process.

A second generation of DEFCON spectrometer is being built that will use one monolithic body containing both etalons. The etalons will be optically locked and electronically scanned for signal averaging and the recording of high-resolution spectra and time-dependent, multi-frequency spectra.

Publications 2010-2012:

- 1) Dual-Etalon Frequency-Comb Cavity-Ring-Down Spectrometer: D. W. Chandler and K. E. Strecker: J. Chem. Phys. 136,154201 (2012).
- 2) Collisions of electronically excited molecules: differential cross-sections for rotationally inelastic scattering of NO(A²Σ⁺) with Ar and He.: J. J. Kay, J. D. Steill, J. Klos, G. Paterson, M. L. Costen, K. E. Strecker, K. G. McKendrick, M. H. Alexander & D. W. Chandler, Molecular Physics DOI 10.1080/00268976.2012.670283. (2012)
- 3) Atom-Molecule Interactions Beyond billiard ball collisions: D. W. Chandler Source: Nature Chemistry, Vol. 3(8) 574-575 (2011).
- 4) Direct Angle Resolved Measurements of collision dynamics with electronically excited state molecules: NO(A²S⁺)+Ar, Kay J.J., Paterson G., Costgen M.L., Strecker K.E., McKendrick K.G., Chandler D.W., J Chem. Phys. 134,091101 (2011)
- 5) Cold and ultracold molecules: Spotlight on orbiting resonances, Chandler DW, J Chem. Phys. Vol.132 110901 (2010).
- 6) Cold atoms by kinematic cooling, Kay, JJ; Klos, J; Alexander, MH, Strecker KE, Chandler DW, Phys. Rev. A Vol.82(3) 032709 (2010)

Petascale Direct Numerical Simulation and Modeling of Turbulent Combustion

Jacqueline H. Chen (PI)

Sandia National Laboratories, Livermore, California 94551-0969

Email: jhchen@sandia.gov

Program Scope

In this research program we have developed and applied massively parallel three-dimensional direct numerical simulation (DNS) of building-block, laboratory scale flows that reveal fundamental turbulence-chemistry interactions in combustion. The simulation benchmarks are designed to expose and emphasize the role of particular phenomena in turbulent combustion. The simulations address fundamental issues associated with chemistry-turbulence interactions at atmospheric pressure that underly practical combustion devices: extinction and reignition, premixed and stratified flame propagation and structure, flame stabilization in autoignitive coflowing jet flames and reactive jets in crossflow, and flame propagation in boundary layers. In addition to the new understanding provided by these simulations, the resultant DNS data are used to develop and validate predictive mixing and combustion models required in engineering Reynolds-Averaged Navier Stokes (RANS) and large-eddy (LES) simulations.

Recent Progress

In the past year, computer allocations from a DOE Innovative and Novel Computational Impact on Theory and Experiment (INCITE) grant have enabled us to perform several petascale three-dimensional DNS of turbulent flames with detailed chemistry. These studies focused on understanding: 1) Premixed flame boundary layer flashback in turbulent channel flow [1], 2) Coupling between turbulence and flame structure in transverse jets analyzed in jet-trajectory based coordinates [2], and 3) a posteriori comparison of large eddy simulation and DNS of a lifted ethylene jet flame using a dynamic nonequilibrium model for subfilter scalar variance and dissipation rate [3]. The DNS data were also used to assess mixing and combustion models for RANS and LES [3-6]. Highlights of our accomplishments in the past year are summarized below, followed by a summary of future research directions.

Direct numerical simulation of premixed flame boundary layer flashback in turbulent channel flow

Direct numerical simulations were performed to investigate the transient upstream propagation (flashback) of premixed hydrogen-air flames in the boundary layer of a fully developed turbulent channel flow. Results show that the well-known near-wall velocity fluctuations pattern found in turbulent boundary layers triggers wrinkling of the initially flat flame sheet as it starts propagating against the main flow direction, and that the structure of the turbulent boundary layer characteristic streaks ultimately has an important impact on the resulting flame shape and on its propagation mechanism. It is observed that the leading edges of the upstream-propagating premixed flame are always located in the near-wall region of the channel and assume the shape of several smooth, curved bulges propagating upstream side by side in the spanwise direction and convex towards the reactants' side of the flame. These leading-edge flame bulges are separated by thin regions of spiky flame cusps pointing towards the products' side at the trailing edges of the flame. Analysis of the instantaneous velocity fields clearly reveals the existence, on the reactants' side of the flame sheet, of back flow pockets that extend well above the wall-quenching distance (see Figure 1), and are spatially correlated with leading edge convex flame bulges. Likewise, high-speed streaks of fast flowing fluid are found to be always co-located with the spiky flame cusps pointing towards the products' side of the flame. The DNS indicate that the origin of the formation of the back flow pockets, along with the subsequent mutual feedback mechanism, is due to the interaction of the approaching streaky turbulent flow pattern with the Darrieus-Landau hydrodynamic instability and pressure fluctuations triggered by the flame sheet. Moreover, the presence of the back flow pockets, coupled to the associated hydrodynamic instability and pressure-flow field interaction, greatly facilitate flame propagation in turbulent boundary layers, and ultimately results in high flashback velocities that increase proportionately with pressure.

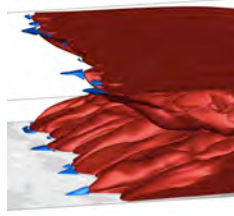


Figure 1. Spatial correlation of premixed flame (progress variable of 0.7 (red isosurface) with back flow regions (blue) from DNS of H_2 /air premixed flame boundary layer flashback in a turbulent channel flow.

DNS of turbulence and flame structure in transverse jets analyzed in jet-trajectory based coordinates

A H_2/N_2 jet in a cross-flow of air is studied using three-dimensional DNS with and without chemical reaction in order to investigate the role of the complex JICF turbulent flow field in promoting fuel-oxidant mixing and enabling aerodynamic flame stabilization in the near field of the jet nozzle. The primary focus is on delineating the flow/mixing/chemistry conditions that are necessary and/or sufficient to achieve flame anchoring that ultimately enables the formulation of guidelines for design of fuel injection nozzles. We describe a new jet parametrization technique used to describe the jet trajectory based on solution of Laplace's equation upon, and then within, an opportune scalar surface anchored by Dirichlet boundary conditions at the jet nozzle and plume exit from the domain provides a smoothly varying field along the jet path. The surface is selected to describe the scalar mixing and reaction associated with a transverse jet. The derived field is used as a condition to mark the position along the natural jet trajectory when analyzing the variation of relevant flow, mixing and reaction quantities in the present DNS datasets. Results indicate the presence of a correlation between the flame base location in parameter space and a region of low velocity magnitude, high enstrophy, high mixing rate and high equivalence ratio (flame root region). Instantaneously, a variety of vortical structures, well known from the literature as important contributors to fuel oxidant mixing, are observed in both inert and reactive cases with a wide span in length and time scales. Moreover, instantaneous plots from reactive cases illustrate that the most upstream flame tongues propagate close to the trailing edge of the fuel jet potential core near the jet shear layer vortices.

LES of a lifted ethylene jet flame DNS using a dynamic nonequilibrium model for subfilter scalar variance and dissipation rate

Accurate prediction of nonpremixed turbulent combustion using large eddy simulation (LES) requires detailed modeling of the mixing between fuel and oxidizer at scales finer than the LES filter resolution. In conserved scalar combustion models, the small scale mixing process is quantified by two parameters, the subfilter scalar variance and the subfilter scalar dissipation rate. The most commonly used models for these quantities assume a local equilibrium exists between production and dissipation of variance. Such an assumption has limited validity in realistic, technically relevant flow configurations. However, nonequilibrium models for variance and dissipation rate typically contain a model coefficient whose optimal value is unknown a priori for a given simulation. Furthermore, conventional dynamic procedures are not useful for estimating the value of this coefficient. In this work, an alternative dynamic procedure based on the transport equation for subfilter scalar variance is presented. This dynamic nonequilibrium modeling approach is used in the simulation of a turbulent lifted ethylene flame, previously studied using DNS by Yoo *et al.* (Proc. Combust. Inst., 2011). The predictions of the new model are compared to those of a static nonequilibrium modeling approach using an assumed model coefficient, as well as those of the equilibrium modeling approach. The equilibrium models systematically underpredicted both subfilter scalar variance and dissipation rate. Use of the dynamic procedure increases the accuracy of the nonequilibrium modeling approach. However, numerical errors that arise as a consequence of grid-based implicit filtering appear to degrade the accuracy of all three modeling options. Therefore, while these results confirm the utility of the new dynamic model, they also suggest that the quality of subfilter model predictions depends on factors external to the subfilter model itself.

Future Work:

DNS of Turbulent Syngas Jet Flames in Crossflow

We plan to systematically examine the effect of fuel composition (namely, varying volume fractions of CO in syngas) on flame stabilization in a lifted turbulent jet flame in a cross-flow of heated air relevant to fuel injection in hydrogen-enriched fuels for stationary gas turbine combustors. The coupling of shear-induced turbulent mixing with different autoignition and flame propagation characteristics of these fuels provides a unique data set for evaluating mixing and combustion models in mixed regimes of combustion for practical engineering modeling and, at the same time, for gaining detailed insight into the physical mechanisms of flame stabilization and blowout for novel fuels. By systematically varying the amount of hydrogen in the fuel stream, the effects of preferential diffusion of hydrogen on entrainment, mixing, and ignition and burning rates will be studied in detail. Preferential diffusion of hydrogen containing species is amplified in the presence of turbulence induced curvature stretch which may lead to locally rich pockets of hydrogen. Small variations in chemically crucial species such as hydrogen can lead to enhanced kinetic branching rates, which can alter the chemistry-turbulence interactions responsible for flame stabilization and blowout. In addition to gaining fundamental insights, the data will be used to evaluate multi-scalar mixing and combustion models that account for preferential diffusion of species.

DNS and Experiments of Non-premixed and Partially-Premixed Unsteady Laminar and Highly Turbulent Opposed Jet Flames

In collaboration with Jonathan Frank and Bruno Coriton of Sandia we propose to perform a joint experimental/computational study of highly turbulent non-premixed and partially-premixed flames in intense turbulent opposed jet hydrogen/air flames. The combined approach and cross-validation will provide insights into finite-rate phenomena including extinction/reignition and the effect of mixture stratification (e.g. enrichment of radicals and enthalpy in back supported partially-premixed flames) on flame structure and burning rates. In a laminar unsteady opposed jet flame joint experiment/computation we plan to investigate the effect of unsteady strain rate on extinction/reignition in di-methyl ether flames.

References:

1. A. Gruber, J. H. Chen, D. Valiev, and C. K. Law, "Direct numerical simulation of premixed flame boundary layer flashback in turbulent channel flow," submitted to *J. Fluid Mech.* 2012.
2. R. W. Grout, A. Gruber, H. Kolla, P.-T. Bremer, J. C. Bennett, A. Gyulassy and J. H. Chen, "A direct numerical simulation study of turbulence and flame structure in transverse jets analysed in jet-trajectory based coordinates," submitted to *J. Fluid Mech.* 2012.
3. C. M. Kaul, V. Raman, E. Knudsen, E. S. Richardson, J. H. Chen, "Large eddy simulation of a lifted ethylene flame using a dynamic nonequilibrium model for subfilter scalar variance and dissipation rate," submitted to *Proc. Comb. Inst.* 34 (2012).
4. E. Knudsen, E. S. Richardson, E. M. Doran, H. Pitsch, and J. H. Chen, "Modeling scalar dissipation and scalar variance In LES: algebraic and transport equation closures," in press *Phys. Fluids* 2012.
5. E. S. Richardson and J. H. Chen, "Probability density function modelling of molecular mixing in flames with differential diffusion," doi:10.1016/j.combustflame.2012.02.026.
6. Y. Yang, H. Wang, S. B. Pope, J. H. Chen, "Large-eddy simulation/probability density function modeling of a non-premixed CO/H₂ temporally evolving jet flame," in press *Proc. Comb. Inst.* 34 (2012).

BES Publications (2010-2012):

1. C. S. Yoo, R. Sankaran, and J. H. Chen "3D Direct Numerical Simulation of a Turbulent Lifted Hydrogen/Air Jet Flame in Heated Coflow: Stabilization and Structure," *J. Fluid Mech.* **460**:453-481 (2010).
2. T. Lu, C. S. Yoo, J. H. Chen, and C. K. Law, "3D Direct Numerical Simulation of a Turbulent Lifted Hydrogen/Air Jet Flame in Heated Coflow: Explosive Mode Analysis," *J. Fluid Mech.* **652** (2010) 45-64.
3. A. Gruber, R. Sankaran, E. R. Hawkes and J. H. Chen, "A Flame-Wall Interaction: A DNS Study," *J. Fluid Mech.* (2010), vol. **658**, pp. 5-32.

4. U. Lee, C. S. Yoo, J. H. Chen, J. H. Frank, "Effect of NO on Extinction and Reignition of Vortex-Perturbed Hydrogen Flames," *Combust. Flame* **157**(2): 217-229 (2010).
5. E. S. Richardson, R. Sankaran, R. W. Grout, and J. H. Chen, "Numerical Analysis of Reaction-Diffusion Effects in Turbulent Premixed Methane-Air Combustion," *Combust. Flame* **157**:506-515 (2010).
6. E. S. Richardson, V. E. Granet, A. Eyssartier, and J. H. Chen, "Effects of Equivalence Ratio Variation on Lean, Stratified Methane-Air Laminar Counterflow Flames," *Combust. Theory and Modeling* (2010) **14**:6, 775 – 792.
7. O. Chatakonda, E. R. Hawkes, M. J. Brear, J.H. Chen, E. Knudsen, and H. Pitsch, *Proceedings of the Summer Program 2010*, Center for Turbulence Research, Stanford University, Stanford, USA.
8. R. W. Grout, A. Gruber, J. H. Chen and C. S. Yoo, "Direct Numerical Simulation of Flame Stabilization Downstream of a Transverse Fuel Jet in Cross-Flow," *Proc. Combust. Inst.* **33** (2011), 1629-1637.
9. C. S. Yoo, E. S. Richardson, R. Sankaran, and J. H. Chen, "A DNS Study of the Stabilization Mechanism of a Turbulent Lifted Ethylene Jet Flame in Highly-Heated Coflow," *Proc. Combust. Inst.* **33** (2011)1619-1627.
10. L. Wang, E. R. Hawkes, and J. H. Chen, "Flame Edge Statistics in Turbulent Combustion," *Proc. Combust. Inst.* **33** (2011) 1439-1446.
11. E. R. Hawkes, R. Sankaran, and J. H. Chen, "Estimates of the Three-Dimensional Flame Surface Density and All Terms in its Transport Equation from Two-Dimensional Measurements," *Proc. Combust. Inst.* **33** (2011) 1447-1454.
12. N. Punati, J. C. Sutherland, A. R. Kerstein, E. R. Hawkes, and J. H. Chen, "An Evaluation of the One-Dimensional Turbulence Model: Comparison with Direct Numerical Simulations of CO/H₂ Jets with Extinction and Reignition," *Proc. Combust. Inst.* **33** (2011)1515-1522.
13. J. H. Chen, *Plenary Paper* "Petascale Direct Numerical Simulation of Turbulent Combustion – Fundamental Insights Towards Predictive Models," *Proc. Combust. Inst.* **33** (2011) 99-123.
14. D. Lignell and J. H. Chen, and H. Schmutz "Effects of Damköhler number on flame extinction and reignition in turbulent non-premixed flames using DNS," *Combust. Flame* **158** (2011) 949-963.
15. C. S. Yoo, T. Lu, J. H. Chen, and C.K. Law, "Direct numerical simulations of ignition of a lean n-heptane/air mixture with temperature inhomogeneities at constant volume: parametric study," in press *Combust. Flame* **158** (2011), 1727-1741.
16. Z. Luo, C. S. Yoo, E. Richardson, J. H. Chen, C. K. Law, T. Lu, "Chemical explosive mode analysis for a turbulent lifted ethylene jet flame in highly-heated coflow," *Combust. Flame*, (2011) doi:10.1016/j.combustflame.2011.05.023.
17. E. R. Hawkes, O. Chatakonda, H. N. Kolla, and J. H. Chen, "A Petascale DNS Study of the Modelling of Flame Wrinkling for Large-Eddy Simulations in Intense Turbulence," *Combust. Flame* (2012), doi:10.1016/j.combustflame.2011.11.020.
18. E. S. Richardson and J. H. Chen, "Probability Density Function Modelling of Molecular Mixing in Flames with Differential Diffusion," *Combust. Flame* (2012) doi:10.1016/j.combustflame.2012.02.026.
19. H. Kolla, R. Grout, A. Gruber, J. H. Chen, "Mechanisms of flame stabilization and blowout in a reacting turbulent hydrogen jet in cross-flow," *Combust. Flame* (2012) doi:10.1016/j.combustflame.2012.01.012.
20. A. Gruber, J. H. Chen, D. Valiev, and C. K. Law, "Direct numerical simulation of premixed flame boundary layer flashback in turbulent channel flow," submitted to *J. Fluid Mech.* 2012.
21. R. W. Grout, A. Gruber, H. Kolla, P.-T. Bremer, J. C. Bennett, A. Gyulassy and J. H. Chen, "A direct numerical simulation study of turbulence and flame structure in transverse jets analysed in jet-trajectory based coordinates," submitted to *J. Fluid Mech.* 2012.
22. E. Knudsen, E. S. Richardson, E. M. Doran, H. Pitsch, and J. H. Chen, "Modeling Scalar Dissipation And Scalar Variance In LES: Algebraic And Transport Equation Closures," in press *Phys. Fluids* 2012.
23. E. Knudsen, E. S. Richardson, J. H. Chen and H. Pitsch, "LES Of An Auto-Igniting C₂H₄ Flame DNS," *Center for Turbulence Research Annual Research Briefs*, 237-248, 2011.
24. Y. Yang, H. Wang, S. B. Pope, J. H. Chen, "Large-eddy simulation/probability density function modeling of a non-premixed CO/H₂ temporally evolving jet flame," in press *Proc. Comb. Inst.* 34 (2012).
25. N. Chakraborty, H. Kolla, R. Sankaran, E. R. Hawkes, J. H. Chen, and N. Swaminathan, "Determination of three-dimensional quantities related to scalar dissipation rate and its transport from two dimensional measurements: Direct Numerical Simulation based validation," in press *Proc. Comb. Inst.* 34 (2012).
26. C. M. Kaul, V. Raman, E. Knudsen, E. S. Richardson, J. H. Chen, "Large eddy simulation of a lifted ethylene flame using a dynamic nonequilibrium model for subfilter scalar variance and dissipation rate," in press *Proc. Comb. Inst.* 34 (2012).

Dynamics and Energetics of Elementary Combustion Reactions and Transient Species

Grant DE-FG03-98ER14879

Robert E. Continetti (rcontinetti@ucsd.edu)

Department of Chemistry and Biochemistry, University of California San Diego
9500 Gilman Drive, La Jolla, CA 92093-0340

I. Program Scope

The focus of this research program is on experimental studies of the energetics and dynamics of transient neutral species relevant to combustion phenomena. Measurements of the photodetachment and dissociative photodetachment (DPD) of negative ion precursors are made using photoelectron-photofragment coincidence (PPC) spectroscopy, yielding information on the stability and dynamics of internal-energy resolved intermediates. This technique has been considerably improved by the installation of a cryogenic electrostatic ion beam trap (CEIBT) that provides much colder anion precursors than previous single-pass experiments. (DOE pubs. 1 and 4) In the past year we published new results using the CEIBT to experimentally characterize the decomposition of HOCO/DOCOC to H/D + CO₂ via tunneling including experimental extraction of the barrier to CO₂ production. (DOE pub. 3) We also measured high-resolution photoelectron spectra for HOCO⁻ and DOCOC⁻ at a number of wavelengths, providing accurate electron affinities and a number of new gas-phase vibrational frequencies with the support of theoretical calculations by Stanton, and determining that $\geq 95\%$ of the anions are the more stable *cis* isomer. (DOE pub. 5) The implications of these studies on dissociation to the OH + CO channel will be discussed below, along with new results on the predissociation of the formylxyl radical, HCO₂/DCO₂ and the isomers of the tert-butoxy radical (CH₃)₃CO. These experiments are laying the groundwork for optical preparation of vibrationally excited anion precursors in the coming year, allowing examination of the effect of vibrational excitation on radical isomerization and dissociation processes.

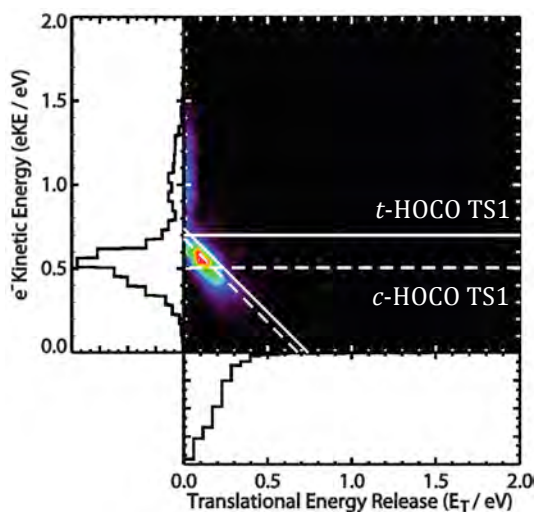


Figure 1. PPC spectrum for the OH + CO + e⁻ channel at a photon energy of 3.20 eV. Diagonal lines indicate total available energy (KE_{max}) for DPD of *trans*- (solid) and *cis*-HOCO⁻ anions (dashed). Barrier heights to formation of OH + CO on the neutral HOCO PES are shown by the horizontal lines for the isomers.

II. Recent Progress

A. Dissociation dynamics and branching fractions for the OH + CO channel

In these experiments, precursor anions are photodetached and the electron kinetic energy (eKE) is recorded in coincidence with either a stable neutral or dissociation products. In the latter case of DPD, the translational energy release, E_T, between the products is measured. In the case of DPD, the PPC spectrum shows the correlation of eKE and E_T, and a lower eKE corresponds to higher internal energy in the nascent neutral. Figure 1 shows the observed dynamics in the OH + CO channel for the DPD of HOCO⁻, providing quantitative information about the energetics of the HOCO potential energy surface. The spectrum shows that no vibration is present in either fragment - analysis of the single diagonal band shows a FWHM of 0.08 eV in the total kinetic energy spectrum (eKE + E_T, not shown), setting an upper limit to the internal energy of the anions, or conversely to the internal energy of the OH and

CO products. This feature can be fit to a two-component Boltzmann rotational distribution, assuming equipartition of energy between the OH and CO fragments to find an upper limit of 250 K for the internal temperature of the products, an upper limit since there are contributions from the experimental resolution and ion internal temperature. The diagonal feature is peaked very close to zero E_T , implying that in the Franck-Condon region of the anion, the neutral potential energy surface is very flat. This is not surprising, as the anionic central OC bond length is 0.2 Å longer than the neutral, with OH and CO equilibrium bond lengths close to those of asymptotic products.

Most of the dissociation to OH + CO observed occurs from photodetachment producing HOCO with internal energy below the barrier from *cis*-HOCO to OH + CO but above that of *trans*-HOCO, as shown by the horizontal lines in Figure 1. The energy resolved branching fractions for HOCO and DOCO at 3.20 eV are shown in Figure 2. Since the ions are primarily *cis*-HOCO⁻, two possible explanations arise: dissociation to OH + CO in this

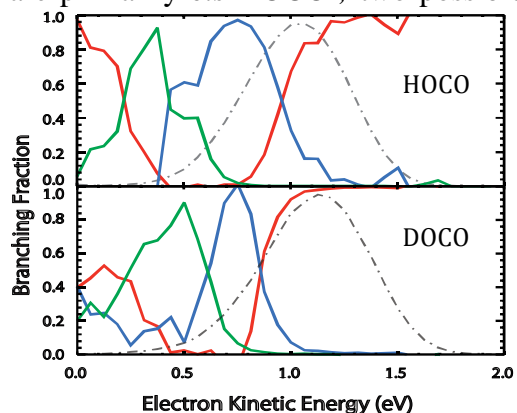


Figure 2. Branching fractions for the DPD of HOCO⁻ and DOCO⁻ at $h\nu = 3.20$ eV. Dot-dashed lines: total photoelectron spectrum; red line: stable HOCO/DOCO radicals; blue line: H/D + CO₂; green lines: OH/OD + CO.

internal energy range proceeds exclusively from the small percentage of *trans*-HOCO⁻ anions, or photoneutrals that are initially *cis* first isomerize to *trans*-HOCO prior to dissociation. However, even with unity efficiency of the reaction the DPD of *trans*-HOCO⁻ to OH + CO + e⁻, the yield of OH + CO products in this energy range is too large for this to be the sole mechanism. Figure 2 shows that below the *cis*-HOCO → OH + CO barrier there is competition between the OH + CO and H + CO₂ channels, leading to roughly equal amounts of each product at eKE ~ 0.5 eV. Above the barrier from *cis*-HOCO to OH + CO, the only product is OH + CO, implying that, when energetically allowed, this dissociation is significantly faster than dissociation to H + CO₂. The region of strong competition ~ 0.5 eV is consistent with an isomerization mechanism, with the process of isomerization from *cis*- to *trans*-HOCO occurring at a similar rate as dissociation to H + CO₂, and dissociation of *trans*-HOCO to OH + CO occurring promptly. This argument is further reinforced by the observation that this region of competition is not present in DOCO shown in the lower frame of Figure 2, where essentially all events in this energy range lead to dissociation to OD + CO. In this case, the isomerization and OD + CO barriers and asymptotic energetics all shift to lower energy due to the reduction in zero-point energy upon deuteration, while the barrier to D + CO₂ remains essentially constant since the OD stretch is the reaction coordinate. This shift in relative energies is more than sufficient to explain the loss of the competition feature, as the lifetimes for D + CO₂ production are significantly longer and thus the isomerization to *trans*-DOCO is favored prior to dissociation to OD + CO. Contributions from other mechanisms cannot be conclusively ruled out, and there will be some contribution to this channel from the small fraction of *trans*-HOCO⁻. Quantum dynamics studies of the isomerization from *cis*- to *trans*-HOCO and dissociation to OH + CO products would be of considerable interest.

B. Dissociative photodetachment of the (CH₃)₂COHCH₂⁻ carbanion

The decomposition pathways of oxygenated organic radical species continue to be of interest, and in the present year we have completed a study of the photodetachment of tert-butoxide, (CH₃)₃CO⁻, and the dissociative photodetachment of the isomeric carbanion, (CH₃)₂COHCH₂⁻. Both deuterated and non-deuterated tert-butanol precursors were used in

the pulsed-discharge ion source, and upon photodetachment both stable radicals and dissociative products, corresponding to the loss of CH_3/CD_3 , were observed. The vibronic structure observed in the non-dissociative photoelectron spectra are consistent with previous work on the photodetachment of tert-butoxide¹ and are not shown here.

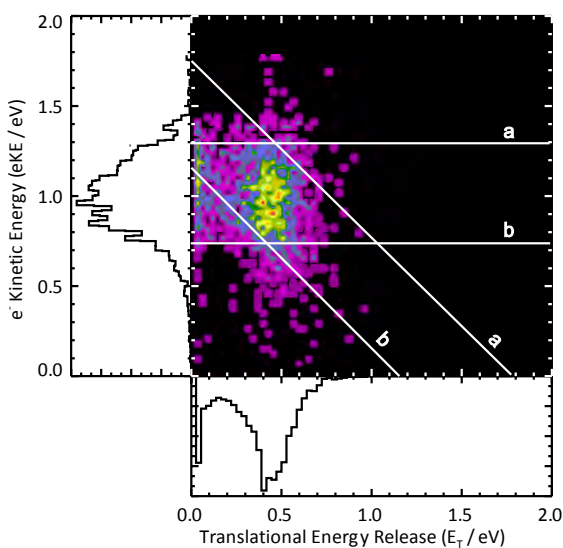


Figure 3. PPC spectrum at 388 nm of $(\text{CH}_3)_2\text{COHCH}_2^-$. The horizontal lines, at 1.30 eV and 0.72 eV for pathways (a) $(\text{CH}_3)_2\text{COHCH}_2^- + h\nu \rightarrow \text{CH}_3 + \text{CH}_3\text{COHCH}_2$ and (b) $(\text{CH}_3)_3\text{COH}^- + h\nu \rightarrow \text{CH}_3 + (\text{CH}_3)_2\text{CO}$ respectively, represent theoretical barrier heights for dissociation. Diagonal lines at 1.77 eV (a) and 1.16 eV (b) denote their respective KE_{max} .

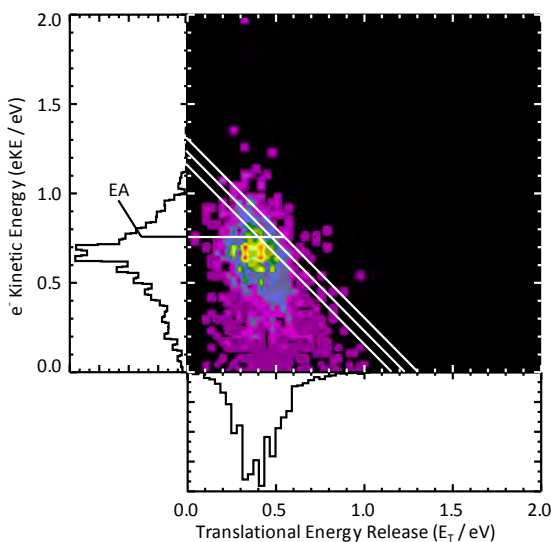


Figure 4. PPC spectrum of $\text{DCO}_2^- + h\nu \rightarrow \text{D} + \text{CO}_2 + e^-$ at 290 nm. The horizontal line indicates the EA.⁴ The upper diagonal line corresponds to KE_{max} , with ground-state products. The lower diagonal lines denote $v = 1, 2$ in the CO_2 product bend.

Excitation of the OCO bending mode of the transient formylxyl neutral is coupled to the bending excitation observed in the state-resolved translational energy distribution for the CO_2 product. Each vibrational state of the nascent neutral can predissociate to several CO_2 product

PPC spectra were recorded for the dissociative channel, and measurements on both the non-deuterated and deuterated species confirmed that fragmentation involved the loss of CH_3/CD_3 . There are two possible DPD reaction pathways resulting in methyl radical loss: from the carbanion isomer, (a) $(\text{CH}_3)_2\text{COHCH}_2^- + h\nu \rightarrow \text{CH}_3 + \text{CH}_3\text{COHCH}_2$ or from tert-butoxide, (b) $(\text{CH}_3)_3\text{CO}^- + h\nu \rightarrow \text{CH}_3 + (\text{CH}_3)_2\text{CO}$ (acetone). The PPC spectrum shown in Figure 3 compares the experimental results with theoretically calculated energetics using CBS-Q level theory for the barriers and product energetics for each dissociative pathway. The horizontal lines indicate the maximum eKE expected for dissociation above the barrier for formation of the products (a) or (b). The diagonal lines indicate the maximum kinetic energies available assuming ground state products using the theoretically calculated reaction enthalpies. These energetics indicate that pathway (b) is not viable as a result of not only the barrier height but the conservation of energy as shown by the diagonal line (b), under the assumption that the parent anions are not vibrationally excited.

To summarize, the dissociation of the tert-butoxy radical through the methyl radical elimination pathway (b) was not observed, and the PPC spectra are assigned to the decomposition of $\text{CH}_3\text{COHCH}_2$ radical, which has also been observed in the combustion of tert-butanol.²

C. State-resolved predissociation dynamics of the formylxyl radical

Extending earlier work done in our lab,³ the DPD dynamics of the $\text{DCO}_2^- + h\nu \rightarrow \text{D} + \text{CO}_2 + e^-$ reaction were studied at 290 nm. Photodetachment accesses three low-lying electronic states (2A_1 , 2B_2 , and 2A_2) of the formylxyl radical with the resulting vibrational features dominated by the OCO bending mode.^{3,4,5}

states leading to the observation of vibrational predissociation sequence bands seen in the correlation of the resolved features in the eKE and E_T spectra in Figure 4.

While the signal-to-noise and resolution is limited, evidence is seen for a series of state-resolved correlated features that constitute predissociation sequence bands. In this case, each peak corresponds to a specific partitioning of energy in the initial DCO₂ and final D + CO₂ products, with preferential excitation of the CO₂ product bending mode. One immediate observation from the extent of the photoelectron spectrum to higher eKE than the EA is that we are observing vibrational hot bands in this experiment as well. Neumark and co-workers assigned the vibrational hot bands in this system to the totally symmetric ν_3 mode of the anion, expected to have an extremely long radiative lifetime. No evidence for radiative decay of the hot bands was observed on a 500 ms time-scale in these measurements.

III. Ongoing and future work

The PPC spectrometer has important new capabilities with the implementation of the CEIBT. Both the sensitivity of the apparatus with the CEIBT installed and the eKE resolution of the photoelectron spectrometer are higher than the old single-pass configuration of the spectrometer. A key advantage of the new configuration of the apparatus is that *high* duty cycle coincidence experiments can be carried out in conjunction with *low* duty cycle ion sources. One of the primary goals in the coming year will be to use a new 10 Hz tunable infrared OPO system to selectively excite vibrational modes in precursor anions prior to injection into the trap and examine in a controlled fashion the influence of vibrational excitation on the branching ratios in radical dissociation and isomerization processes in HOCO and other systems.

IV. Publications and submitted journal articles supported by this project 2010-2012

1. C.J. Johnson, R.E. Continetti, *Dissociative photodetachment of cold HOCO⁻ and below-barrier dissociation to H + CO₂*, J. Phys Chem. Lett. **1**, 1895-1899 (2010).
2. B.L.J. Poad, C.J. Johnson, R.E. Continetti, *Photoelectron-photofragment coincidence studies of NO⁻-X clusters (X = H₂O, CD₄)*, Discussions of the Faraday Society **150**, 481-492 (2011).
3. C.J. Johnson, B.L.J. Poad, B.B. Shen, R.E. Continetti, *Communication: New insight into the barrier governing CO₂ formation from OH + CO*, J. Chem. Phys. **134**, 171106-1-4 (2011).
4. C.J. Johnson, B.B. Shen, B.L.J. Poad, R.E. Continetti, *Photoelectron-photofragment coincidence spectroscopy in a cryogenically cooled electrostatic ion beam trap*, Rev. Sci. Instrum. **82**, 105105-1-9 (2011).
5. C.J. Johnson, M.E. Harding, B.L.J. Poad, J.F. Stanton, R.E. Continetti, *Communication: The electron affinities, well depths and vibrational spectroscopy of cis- and trans-HOCO*, J. Am. Chem. Soc. **133**, 19606-19609 (2011).

V. References

-
1. T.M. Ramond, G.E. Davico, R.L. Schwartz and W.C. Lineberger, J. Chem. Phys. **112**, 1158 (2000).
 2. R. Grana, A. Frassoldati, T. Faravelli, U. Niemann, E. Ranzi, R. Seiser, R. Cattolica and K. Seshadri, Comb. and Flame **157**, 2137 (2010).
 3. T.G. Clements and R.E. Continetti, J. Chem. Phys. **115**, 5345 (2001).
 4. E. Garand, K. Klein, J.F. Stanton, J. Zhou, T.I. Yacovitch and D.M. Neumark, J. Phys. Chem. A **114**, 1374 (2010).
 5. K. Klein, E. Garand, T. Ichino, D.M. Neumark, J. Gauss and J.F. Stanton, Theor. Chem. Acc. **129**, 527 (2011).

Dissociation Pathways and Vibrational Dynamics in Excited Molecules and Complexes

F.F. Crim
Department of Chemistry
University of Wisconsin–Madison
Madison, Wisconsin 53706
ffcrim@chem.wisc.edu

Our research investigates the chemistry of vibrationally excited molecules. The properties and reactivity of vibrationally energized molecules are central to processes occurring in environments as diverse as combustion, atmospheric reactions, and plasmas and are at the heart of many chemical reactions. The goal of our work is to unravel the behavior of vibrationally excited molecules and to exploit the resulting understanding to determine molecular properties and to control chemical processes. A unifying theme is the preparation of a molecule in a specific vibrational state using one of several excitation techniques and the subsequent photodissociation of that prepared molecule. Because the initial vibrational excitation often alters the photodissociation process, we refer to our double-resonance photodissociation scheme as *vibrationally mediated photodissociation*. In the first step, fundamental or overtone excitation prepares a vibrationally excited molecule, and then a second photon, the photolysis photon, excites the molecule to an electronically excited state from which it dissociates. Vibrationally mediated photodissociation provides new vibrational spectroscopy, measures bond strengths with high accuracy, alters dissociation dynamics, and reveals the properties of and couplings among electronically excited states.

Our recent experiments have used ion imaging to follow the adiabatic and nonadiabatic dissociation pathways in ammonia, to study the influence of vibrational excitation on the dynamics at conical intersections in phenol, and to obtain new vibrational spectroscopy on the formic acid dimer. These studies have set the stage for our newest measurements on the spectroscopy and vibrational predissociation dynamics of ammonia dimers and trimers. Our goal is to understand and prepare vibrations in the ground electronic state, to study the vibrational structure of the electronically excited molecule, and to probe and control the dissociation dynamics of the excited state in clusters.

Spectroscopy of Ammonia Oligomers

The detailed insights that have come from our experiments on the influence of vibrational excitation on the excited state dynamics of ammonia suggest that the vibrationally mediated photodissociation of ammonia dimers and of complexes of ammonia with other small molecules could reveal novel behavior. Our two central concerns are the influence of complexation on the dynamics at the conical intersection and the changes that complexation produces in the vibrationally mediated photodissociation of ammonia. There are detailed studies of the photodissociation of bare ammonia molecules that provide a starting point for our work. We have studied the vibrational predissociation of ammonia dimers and trimers as a prelude to experiments that add electronic excitation.

A supersonic expansion of ammonia in He produces the oligomers we study. Exciting the N-H stretching vibration in an oligomer produces vibrationally and rotationally excited ammonia fragments that we detect by (2+1) REMPI through the \tilde{B} state, as illustrated on the left-hand side of Figure 1. The right-hand side of the figure shows the infrared action spectrum obtained by observing NH_3 fragments with one quantum of excitation in the umbrella bending vibration (ν_2). As the lower trace in the figure shows, these features are consistent with the transitions observed in He droplets (Slipchenko *et al.*, J. Phys. Chem. A

111, 7460 (2007)) and show that excitation of either the symmetric N-H stretch or the antisymmetric N-H stretch initiates vibrational predissociation.

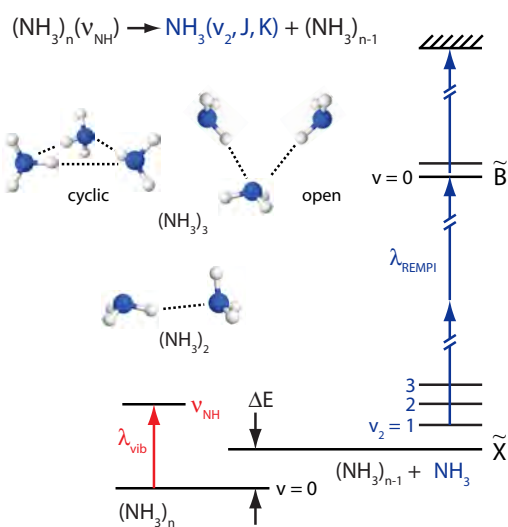
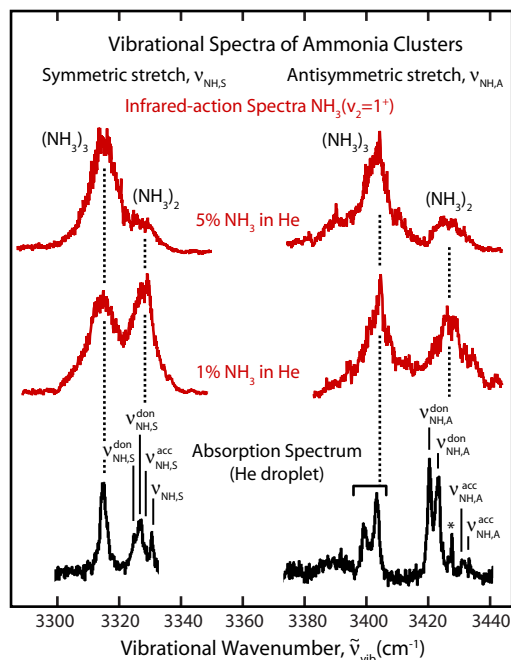


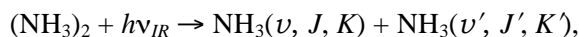
Figure 1



The key to obtaining these action spectra and to the analysis of the predissociation dynamics described below is the ability to interrogate individual vibrational rotational states (v, J, K) of the ammonia products using REMPI detection. A collaboration with Dr. Collin Western at the University of Bristol has been critical to simulating and assigning the spectra. Along the way, we have been able to identify new transitions and refine some spectroscopic constants.

Dissociation Energy and Dynamics of Ammonia Dimers

Velocity-map ion-imaging detection of fragments $\text{NH}_3(v, J, K)$ directly provides the distribution of recoil speeds of the undetected partner fragment $\text{NH}_3(v', J', K')$ formed in the vibrational predissociation of the dimer,



where J and K are the quantum numbers for the total angular momentum and its projection on the symmetry axis, respectively. Because the distribution of recoil energies mirrors the distribution of internal energies $E'_{\text{int}}(\text{NH}_3)$ of the undetected fragment, analysis of the recoil distributions yields the binding energy of the dimer.

Even though there are many available states, clear patterns of state population are apparent in the distribution of recoil speeds. For example, Figure 2 shows the distribution extracted from the ion image of the product, $\text{NH}_3(v_2=2^+, J=6, K=6)$. As the vertical lines indicate, the maxima in the distribution align with recoil speeds corresponding to the formation of the undetected product in various J' states with $K'=0$. The identification of the features marked in the figure comes from using conservation of energy

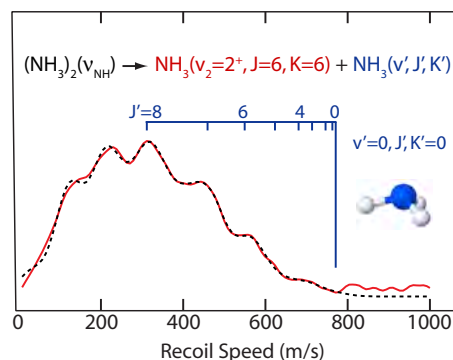


Figure 2

and a dissociation energy of 658 cm^{-1} . Introducing all of the possible values of K' in the analysis produces the simulation of the recoil speed distribution shown as the dashed line in the figure. Performing this same analysis self-consistently for a total of 17 different detected rovibrational states (ν, J, K) produces comparably good fits to all of the data and gives a dissociation energy for the dimer of $D_0 = 660 \pm 20 \text{ cm}^{-1}$. This value is much more precise than previous experimental estimates and is consistent with recent calculations. Calculating the dissociation energy is challenging because of the large contribution of zero-point energy (about 40% of the well depth D_e) in this loosely bound complex

The analysis of the images also shows that most of the available energy appears as vibrational excitation, with there being at least two quanta of umbrella bending excitation distributed between the fragments. Producing $\text{NH}_3(\nu_2=3^+)$ requires almost all of the available energy and leaves the undetected partner with no vibrational energy. In many cases, $\text{NH}_3(\nu_2=2^+)$ appears in partnership with $\text{NH}_3(\nu'=0)$ although there are cases where it is possible to make $\text{NH}_3(\nu_2'=1)$. In cases where the detected product is $\text{NH}_3(\nu_2=1^+)$, the distributions suggest that the partner is born with a quantum of umbrella bending excitation as well, reflecting the transfer of vibrational energy between the two moieties during dissociation. Although the antisymmetric umbrella bending vibration (ν_4) is energetically accessible, we see no evidence of its formation, perhaps reflecting a dynamical bias in the vibrational predissociation.

Dissociation Energy of Ammonia Trimers

Features corresponding to higher-order clusters appear in the infrared-action spectra in the regions of the intramolecular symmetric N-H stretching vibration ($\nu_{NH,S}$) and the intramolecular antisymmetric N-H stretching vibration ($\nu_{NH,A}$) shown in Figure 1. The spectra illustrate the influence of expansion conditions on the relative intensities of the features in the spectrum. The top trace is for an expansion containing 5% NH_3 in He and the middle trace is for one containing only 1% NH_3 . The spectra in both the symmetric and antisymmetric stretching regions differ markedly for the two different expansion conditions, with the lower energy feature being more prominent in the expansions containing more NH_3 . Because these larger seed ratios should favor the formation of larger clusters, the changes between the spectra suggest that the lower energy feature comes from the trimer and that the higher energy feature comes from the dimer, in agreement with the assignments from the He droplet spectra.

Removing an NH_3 fragment from the cyclic trimer requires breaking two hydrogen bonds, and, thus, the dissociation into monomer and dimer fragments,



consumes more energy than cleaving the single hydrogen bond of the dimer. Indeed, as the left hand side of Fig. 3 shows, the trimer feature is prominent in the infrared-action spectrum for detection of $\text{NH}_3(\nu_2 = 1^+, J = 1, K = 0)$ but is essentially absent for detection of $\text{NH}_3(\nu_2 = 3^+, J = 3, K = 0)$. The relative intensities of the dimer and trimer features in the infrared-action spectra depend on the amount of energy available for breaking the hydrogen bonds in the cluster, a quantity that depends on the energy content of the detected fragment. Infrared-action spectra for ammonia fragments with large amounts of internal energy have almost no trimer component because there is not enough energy available to break two bonds in the cyclic trimer. By contrast, infrared-action spectra for fragments with low amounts of internal energy have a substantial trimer component. The right-hand side of the figure shows a quantitative analysis of the trimer contribution compared to that of the dimer in the action spectra. The growth in the trimer signal suggests that fragmentation of the trimer into a monomer and dimer requires an energy of 1700 to 1800 cm^{-1} , a range that is consistent with several theoretical estimates.

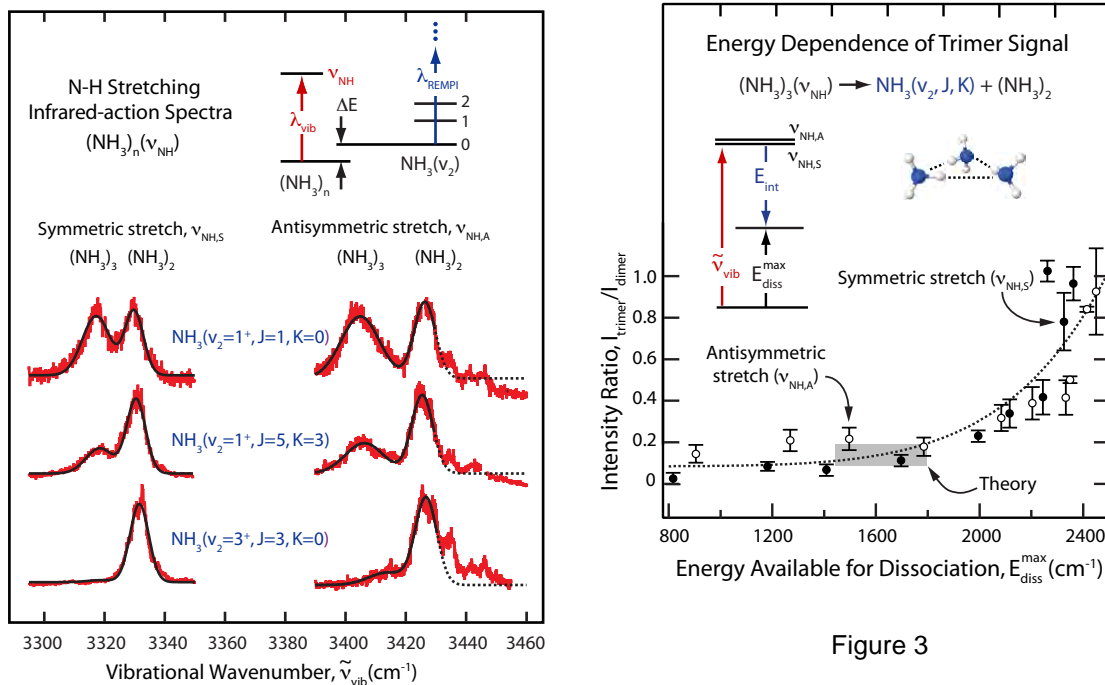


Figure 3

Future Directions

We are beginning our first vibrationally mediated photodissociation experiments on the ammonia dimer cluster. Our goal is to study complexes with ammonia as well as other bare and complexed molecules where we can use vibrational excitation to influence the passage through conical intersections. The variety of complexes available, including ones with different bonding motifs, offers a rich array of possibilities in which to study the influence of an adduct and initial vibrational excitation.

PUBLICATIONS SINCE 2010 SUPPORTED BY DOE

Reactive Scattering: Quantum-State-Resolved Chemistry, F. Fleming Crim, in *Tutorials in Molecular Reaction Dynamics*, Eds. Mark Brouard and Claire Vallance (Royal Society of Chemistry, London, 2010).

A. S. Case, C. G. Heid, S. H. Kable, and F. F. Crim, *Dissociation energy and vibrational predissociation dynamics of the ammonia dimer*, *J. Chem. Phys.* **135**, 084312 (2011).

A. S. Case, C. G. Heid, C. M. Western, and F. F. Crim, *Determining the dissociation threshold of ammonia trimers from action spectroscopy of small clusters*, *J. Chem. Phys.* **136**, 124310 (2012).

Bimolecular Dynamics of Combustion Reactions

H. Floyd Davis

Department of Chemistry and Chemical Biology
Baker Laboratory, Cornell University, Ithaca NY 14853-1301
hfd1@Cornell.edu

I. Program Scope:

The aim of this research program is to better understand the mechanisms and product energy disposal in elementary bimolecular reactions fundamental to combustion chemistry. Using the crossed molecular beams method, a molecular beam containing highly reactive free radicals is crossed with a second molecular beam. The angular and velocity distributions of the neutral products from single reactive collisions are measured using “universal” mass spectrometry with single photon pulsed vacuum ultraviolet (VUV) photoionization, or for reactions leading to H, D, or O products, by Rydberg tagging time-of-flight (TOF) methods.

II. Recent Progress:

During the past year, we have further developed four-wave mixing of collimated (*i.e.*, unfocussed)¹ nanosecond laser pulses on both crossed molecular beams machines in our laboratory. In our rotatable source crossed beams apparatus, universal photoionization, typically using 9.9 eV (125 nm) light, is used. During the past year, we have expanded our studies of the reactions of C₆H₅ to include reactions with O₂, C₃H₆ (propene) and C₄H₈ (butene isomers) at various collision energies. On our rotatable detector apparatus, O atom Rydberg time-of-flight (ORTOF) spectroscopy has been applied to several reactions producing O(³P₁), including C₆H₅ + O₂ → C₆H₅O + O and C₂H₃ + O₂ → C₂H₃O + O. As described in section iv) below, we have introduced a new approach for generation of extreme ultraviolet (XUV) radiation at wavelengths shorter than the LiF cutoff (104 nm) that promises significantly greater intensities than have been possible using previous methods.

i. Crossed Beams Study of Phenyl Oxidation: the C₆H₅ + O₂ Reaction

Phenyl radicals (C₆H₅) react with oxygen molecules (O₂) to form phenylperoxy radicals (C₆H₅OO), which may decompose by a variety of pathways.² In 2010, we published an account of our first study of this reaction at a mean collision energy of 64 kJ/mol using the crossed molecular beams technique, employing detection via pulsed single photon ionization at 9.9 eV.³ In that work, we monitored the formation of phenoxy radicals (C₆H₅O) from the C₆H₅O + O channel, providing insight into the lifetimes of the C₆H₅OO intermediates. The measured distributions implied that the C₆H₅OO lifetimes (τ) are at least comparable to their rotational timescales, *i.e.* τ ≥ 1 ps. Our lower limit for τ was at least 100 times longer than an upper limit inferred from a previous crossed beams experiment at a higher collision energy.⁴ Even when the different collision energies were taken into account, our results seemed inconsistent with the occurrence of direct reaction dynamics inferred from experiments employing a phenyl radical beam produced by pyrolysis of nitrosobenzene.⁴

Very recent work at collision energies *lower* than in our work confirms our conclusion that the reaction is complex-mediated.⁵ However, according to the Hawaii group, the dynamics at high collision energies are direct, implying that RRKM theory cannot be applied to this benchmark system.

In recent studies at Cornell, we have been unable to observe any evidence for a transition to direct dynamics even at elevated collision energies. In an effort to understand the apparent discrepancy between our studies and those in refs. 4 and 5, we recently employed photionization spectroscopy with TOF mass analysis to characterize the phenyl radical beams produced by photolysis of chlorobenzene and by pyrolysis of nitrosobenzene. These studies clearly indicate significant levels of phenoxy radical impurities in phenyl radical beams produced using pyrolysis of nitrosobenzene. Furthermore, the peak densities of phenyl radicals produced in the pyrolytic source are significantly smaller than using photolysis of chlorobenzene. Consequently, we have found that phenoxy signals from inelastic scattering of phenoxy radical impurities in pyrolytic phenyl beams are typically greater than the phenoxy signals from the true $C_6H_5 + O_2 \rightarrow C_6H_5O + O$ reaction.

ii. Competing Pathways in the Reaction $C_6H_5 + C_3H_6$ (Propene) and $C_6H_5 + C_4H_8$ (2-butene)⁶

We have studied the phenyl + propene reaction at collision energies of 80 and 110 kJ/mol. As in previous work⁷ carried out at higher collision energies, we observed the H atom elimination channel, corresponding to production of C_9H_{10} . However, we also observed strong signal at $m/e = 104$, corresponding to C_8H_8 from methyl radical elimination, *i.e.*, $C_6H_5 + CH_2CHCH_3 \rightarrow C_6H_5CHCH_2 + CH_3$. Evidence for this channel has also been obtained recently using electron impact ionization.⁸ We conclude from our studies that the CH_3 elimination channel is actually *dominant*, consistent with calculations showing this channel to be thermodynamically most favorable with a relatively low elimination barrier.⁹ In our complementary studies of the reaction with 2-butene, we also observe CH_3 elimination but find no evidence for H atom loss, further confirming that the barriers to H atom elimination are higher than for CH_3 loss in these systems.

iii. Progress Towards Studies of $H + O_2 \rightarrow OH (^2\Pi) + O (^3P_1)$ using ORTOF Detection.

The $H + O_2 \rightarrow OH (^2\Pi) + O (^3P_1)$ reaction is generally considered to be among the most important in combustion.¹⁰ It is well-known that the OH is preferentially formed in high-N levels in $v = 0$ and 1. Using our high-intensity VUV pulsed laser system, we have finally been able to achieve sensitivity levels sufficient to study this reaction. As indicated in the recent literature, a particularly interesting feature of this system is that while complex-forming dynamics play an important role, there is strong evidence for nonstatistical behavior, particularly at higher collision energies. This reaction will therefore be one focus of experimental studies during the upcoming months.

iv. Coherent pulsed XUV using Noncollinear Phasematching in Laser Ablated Metal Vapors.

Synchrotron light sources facilitate production of VUV and XUV radiation tunable in the 6-20 eV range. However, tabletop light sources employing nonlinear mixing of pulsed lasers provide a number of advantages, the most notable being higher spectral resolution and lower cost. Since the 1970's, four wave mixing in static cells containing noble gases or metal vapors have allowed production of short wavelength VUV at wavelengths down to the LiF cutoff (104 nm). Since there exists no window materials capable of transmitting light at $\lambda < 104\text{nm}$, differentially pumped capillary tubes or pulsed jets have been employed.¹¹ Typically a grating, with efficiencies of only ~10% is then employed to disperse the XUV from the unconverted UV and visible beams. Such methods lead to up to $\sim 10^{10}$ photons/pulse in the XUV.

In *noncollinear* phasematching, the two input laser beams are crossed at a small angle in the nonlinear medium. The resulting short wavelength radiation (typically from four-wave mixing) *emerges at a different angle* from the unconverted fundamental beams, eliminating the need for

inefficient gratings. Ubachs and coworkers have employed this method for generation of tunable XUV in a Kr jet.¹² Peet *et al.* have shown that noncollinear phasematching in a static cell produces intensities comparable to those produced using the more conventional collinear approach.¹³

At Cornell, we have explored a method that promises much higher XUV intensities than is possible using other methods. We employ doubly resonance-enhanced four wave mixing of tunable dye lasers in metal vapor produced by *laser vaporization*. Because of the low vapor pressure of metals at room temperature, this approach is very well-suited to windowless operation. As a proof of principle, we have employed noncollinear phasematching of focused 312 nm and 625 nm laser beams in Hg vapor produced by pulsed vaporization (532 nm, 2 mJ/pulse) of Hg held at 2 °C. The VUV intensities are within a factor of 5 of those generated in our laboratory using unfocussed beams in 1m long static Hg cells. The high nonlinearity of Hg, and the ability to achieve spatial separation of the VUV from unconverted input beams by noncollinear phasematching (with no optical elements) lead to much higher intensities than is possible using other methods. We believe this approach holds tremendous promise, as it should substantially increase our detection sensitivity using nonresonant photoionization of molecules with ionization energies above 10 eV.

v. Transfer of Endstation 1 (Universal Crossed Beams Machine) from LBNL to Cornell

A universal crossed molecular beams apparatus (Endstation 1), originally commissioned at the Advanced Light Source (ALS) at LBNL, has been in storage since around 2005. With a shift in research focus at the ALS, there are no plans to return it to use there. In August 2011, final DOE approval was granted, and the apparatus was moved to Cornell. We plan to dedicate it specifically to our DOE-supported project, thereby freeing-up a similar Cornell apparatus for unrelated NSF-supported research on transition metal reactivity. This apparatus is especially well-suited to universal photoionization detection using tabletop pulsed VUV and XUV light sources.

III. Future Plans:

During the upcoming year, we plan to continue our studies of the $R + O_2 \rightarrow RO + O$ reactions ($R = H, CH_3$) using ORTOF. The tunable high brightness pulsed VUV source (8-11eV) will be used to study oxidation reactions of other hydrocarbon free radicals ($C_2H_3, C_2H_5, C_3H_7, C_4H_9, etc.$). In order to better understand the competing reaction channels producing enols in combustion, bimolecular reactions of OH with ethene and propene will be studied using universal photoionization of reaction products.

IV. Publications citing DOE Support for 2010-Present:

1. Daniel R. Albert and H. Floyd Davis, "Collision Complex Lifetimes in the Reaction $C_6H_5 + O_2 \rightarrow C_6H_5O + O$ ", *J. Phys. Chem. Lett.* 1, 1107 (2010).
2. David L. Proctor, Daniel R. Albert and H. Floyd Davis, "Improved piezoelectric actuators for use in high-speed pulsed valves", *Rev. Sci. Instrum.* 81, 023106 (2010).

V. References:

-
1. A.V. Smith and W.J. Alford, *J. Opt. Soc. Am. B.* 4, 1765 (1987).

-
2. Tokmakov, I.V.; Kim, G.S.; Kislov, V.V.; Mebel, A.M.; Lin, M.C. *J. Phys. Chem. A*, **109**, 6114 (2005).
 3. Albert, D.R.; Davis, H.F. *J. Phys. Chem. Lett.* **1**, 1107 (2010).
 4. Gu, X.; Zhang, F.; Kaiser, R.I. *Chem. Phys. Lett.* **448**, 7 (2007).
 5. Parker, D.S.N.; Zhang, F.; Kaiser, R.I., *J. Phys. Chem. A* **115**, 11515 (2011).
 6. Albert, D.R.; Todt, M.; Davis, H.F. to be submitted to *J. Phys. Chem. A*.
 7. Zhang, F.; Gu, X.; Guo, Y.; Kaiser, R.I.; *J. Phys. Chem. A* **112**, 3284 (2006).
 8. R.I. Kaiser, D.S.N. Parker, M. Goswami, F. Zhang, V.V. Kislov, A.M. Mebel, J. Aguilera-Iparraguirre and W.H. Green, *Phys. Chem. Chem. Phys.* **14**, 720 (2012).
 9. Park, J, Nam, G.J.; Takmakov, I.V.; Lin, M.C., *J. Phys. Chem. A* **110**, 8729 (2006).
 10. Z. Sun, D.H. Zhang, C. Xu, S. Zhou, D. Xie, G. Lendvay, H. Guo; *J.Am.Chem.Soc.* **130**, 14962 (2008).
 11. C.-Y. Ng, *Ann. Rev. Phys. Chem.* **53**, 101 (2002), and references therein.
 12. S. Hannemann, U. Hollenstein, E.-J. van Duijn, and W. Ubachs, *Opt. Lett.* **30**, 1494 (2005).
 13. V.E. Peet, and R.V. Tsubin, *Opt. Comm.* **214**, 381 (2002).

Exploration and validation of chemical-kinetic mechanisms

Michael J. Davis

Chemical Sciences and Engineering Division
Argonne National Laboratory
Argonne, IL 60439
Email: davis@tcg.anl.gov

The main focus of the work is on the exploration and theoretical validation of chemical-kinetic mechanisms, which combines global sensitivity analysis with the exploration of the characteristics of the sensitivity analysis over the physical and chemical parameters. The tools used for generating these sensitivity maps can be applied to other types of fitting and optimization problems. We have implemented a bi-fidelity fitting and optimization method based on these techniques.

Recent Progress

Bi-fidelity Fitting and Optimization

In collaboration with Miller (CNM-ANL), Harding, and Gray (CNM-ANL), we adopted a procedure originally developed in the statistics literature [r1] that allows different levels of computation to be used in a correlated fashion for fitting and optimization, referred to as co-kriging. An example of the procedure as it is used for fitting of potential surfaces is shown in Fig. 1. In the example, a small portion of the H + HCO surface relevant to the roaming pathway is shown. The H and HCO fragments are restricted to a plane and the distance between the roaming H-atom and the midpoint of the CO bond is fixed at 4.5 au, with χ , the H atom-CO midpoint-C atom angle. Two different levels of electronic structure calculations are shown in the top panel.

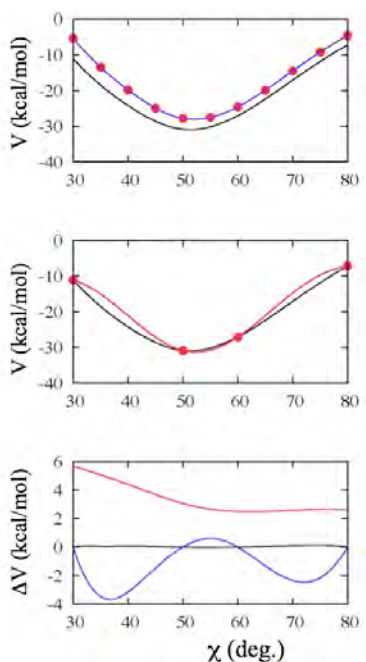


Fig.1 Bi-fidelity fitting example.

The upper curve with the dots was generated from a low-fidelity CASSCF calculation and the lower curve from a more accurate, high-fidelity CASPT2 calculation [p6]. The top curve in the bottom panel shows the difference between these two curves. The middle panel of Fig. 1 repeats the CASPT2 surface, but also includes a wavy curve, which is a single-fidelity fit using the CASPT2 calculation at the four points plotted on the curve. The fitting procedure is interpolative, and thus goes through the points, but is inaccurate away from the points. The error is shown as the oscillating curve in the bottom panel of Fig. 1.

Although the four high-fidelity points in the middle panel lead to an inaccurate fit, the co-kriging procedure correlates the 11 low-fidelity points from the top panel with the 4 high-fidelity points to give a much more accurate fit. The nearly flat curve in the bottom panel of Fig. 1 shows the error between the bi-fidelity fit and the CASPT2 surface, with the largest error being 0.11 kcal/mole. Because the ratio of effort between the two calculations is 35:1, the effort used to generate the bi-fidelity potential fit is equivalent to running less than a single extra CASPT2 point.

In collaboration with Zhou and Skodje (Boulder), our work on global sensitivity analysis [p1-p3] has been applied to large mechanisms and the study of speciation. We have investigated the ignition of butanol using the mechanism of Ref. 2 and have based our speciation studies on the experiments and modeling in Ref. 3. The sensitivities of the relative amounts of the species are studied as the rate coefficients are varied based on their assumed uncertainties. The goal of this work is improvement of the reaction mechanism [p1-p2]. The speciation studies point to key reactions that are important for accurate modeling and broaden our previous work, which used ignition delay time as the target for the global sensitivity analysis.

Figures 2a and 2b show results for two of the species studied in Ref. 3. We examined constant-volume auto-ignition using the same set of initial conditions used in the modeling efforts in Ref. 3 (Figs. 12 – 20).

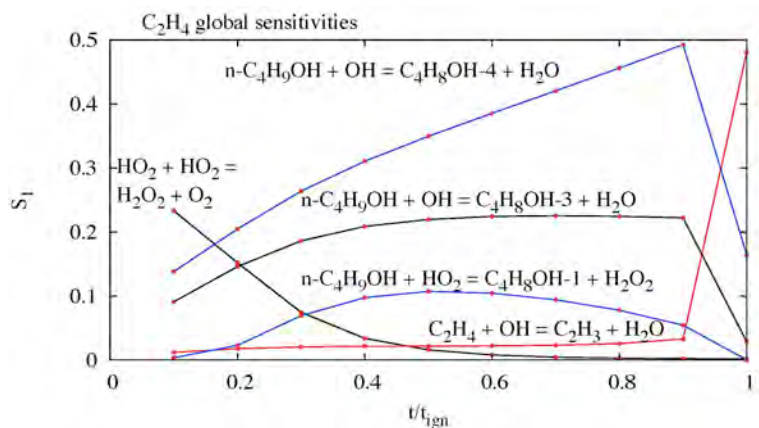


Fig. 2a. Global Sensitivities for C_2H_4 .

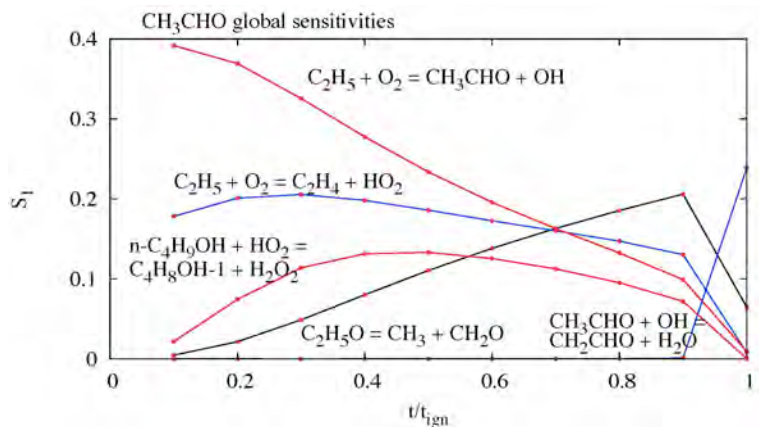


Fig. 2b. Global Sensitivities for CH_3CHO .

The sensitivities of the relative amounts of ethylene in the reacting mixture as a function of individual reaction rates are plotted in Fig. 2a. The plot shows these sensitivities as a function of time to ignition. Figure 2a shows all five reactions that contribute at least 10% of the variance in the amount of ethylene leading up to ignition. Figure 2b shows the same type of results for acetaldehyde.

The global sensitivity analysis can be compared to the modeling efforts in Ref. 3. Figure 2a indicates that a change in the rate coefficients for the reactions of OH and butanol can have a significant impact on the relative amount of ethylene in the reacting mixture over the complete time history, while a change in the rate coefficients for these same

reactions have a modest impact on the relative amount of acetaldehyde, except near the ignition time. This is borne out in the modeling study in Ref. 3, where updated rate coefficients for these reactions were included in a second set of modeling studies (see Fig. 12 there).

The global sensitivity analysis can also be compared to reaction pathway analysis (Figs. 16 and 19 in Ref. 3). Our experience with the ignition-time target is that there is a difference between reaction path analysis and global sensitivity analysis. Comparison of Fig. 2 with Ref. 3 demonstrates that this is true for speciation sensitivities, also. For example, a reaction pathway analysis indicates that the primary pathways to formation of ethylene start with the abstraction of

an H-atom from butanol by OH, consistent with the sensitivity analysis in Fig. 2a. However, the reaction path analysis indicates that the main abstraction routes are abstraction of the α - and δ -hydrogens, while the global sensitivity analysis indicates that the relative amount of ethylene depends most on abstraction of the γ - and δ -hydrogens.

Reaction Sensitivities under Turbulent Spray-Combustion Conditions and in Engine Simulations

A collaboration has been initiated between the chemical dynamics group (Sivaramakrishnan, Davis, and a postdoc, W. Liu) and the Engine and Emissions group at Argonne (Som and Longman). We developed a model of a biodiesel surrogate, a blend of methylbutanoate and n-heptane. This model was analyzed with global and local sensitivity analysis and several rate coefficients were calculated based on this analysis. In collaboration with Lu (U. Conn.) the model was reduced using a directed relation graph with expert knowledge (DRG-X). The model was then used in simulations of 3-D turbulent spray combustion and in

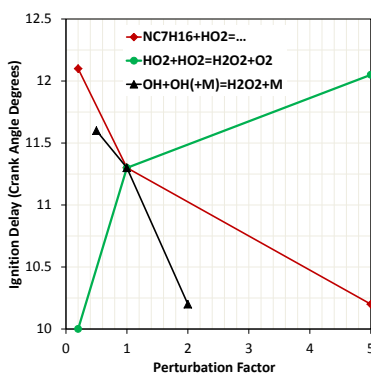


Fig. 3. Ignition delays for an engine Model vs. the uncertainty factor f .

engine simulations. As part of this study we examined the sensitivity of the ignition delay time in the engine model to a few select reactions, which were chosen based on the global sensitivity analysis of homogeneous ignition. Figure 3 shows the results of this analysis. Three sets of reactions were studied for three values of the rate coefficient, depending on the uncertainty factors. Figure 3 demonstrates that the ignition delay time is sensitive to all these rate coefficients, particularly the reaction $\text{HO}_2 + \text{HO}_2 = \text{H}_2\text{O}_2 + \text{O}_2$, with the difference in crank angle for this reaction (> 0.2 ms) large enough that misfiring may occur.

New Rate Coefficient for $\text{HO}_2 + \text{HO}_2 = \text{H}_2\text{O}_2 + \text{O}_2$

In collaboration with Zhou and Skodje (Boulder), Harding, and Han and Zhang (Dalian), a new rate coefficient was calculated based on statistical rate theory using high level *ab initio* electronic structure calculations. Figure 4 demonstrates that at high temperature the new rate coefficient is lower by a factor of 2 or 3, than the previously used rate coefficient, derived from experiments.

The statistical formulation used to derive the new rate coefficient relied on vibrationally adiabatic modeling of the torsion and the associated inclusion of the tunneling through the transition state ridge, both novel formulations. Because this reaction is important in the engine modeling described above, this indicates that a detailed understanding of molecular motion is crucial for the accurate modeling of the ignition characteristics of realistic devices.

Future Plans

There are a number of extensions of the work that are planned, and two of them are discussed. The butanol work showed the lack of correlation between standard methods of reaction path analysis and global sensitivity analysis. A new reaction path analysis tool based on stochastic simulations of complex chemical kinetics will be developed with Zhou and Skodje. It

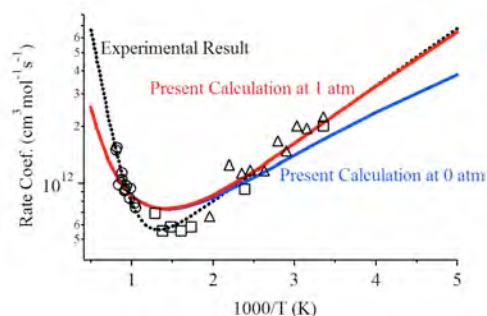


Fig. 4. Rate coefficient for $\text{HO}_2 + \text{HO}_2$

will permit the attribution of an observed global sensitivity to a specific sub-mechanism (or pathway) in the overall model, in which the sensitive reaction may be a rate-limiting step.

Until now we have implemented global sensitivity analysis using Monte Carlo simulations. Although we have implemented this procedure for mechanisms with up to 3000 reactions [p8, p9], the largest calculations take a few processor weeks of computation for simple 0-D simulations. In order to extend global sensitivity to larger mechanisms and to engine simulations we intend on developing methods that require far few simulations, such as the method in Ref. 4, which uses the Gaussian Process model for representing the response of a system to the uncertainties in its parameters. We will also investigate statistical techniques that are used for high-dimensional, low-sample size data for addressing this problem. [r5]

References

1. A. Forrester, A. Sobester, A. Keane, *Engineering Design via Surrogate Modeling: A Practical Guide* (John Wiley and Sons, Hoboken, 2008).
2. G. Black, H.J. Curran, S. Pichon, and J.M. Simmie, *Combustion and Flame* **157**, 363 (2010).
3. D. Karwat, S. Wagnon, P. D. Teini, and M. S. Wooldridge, *J. Phy. Chem.* **115**, 4909 (2011).
4. A. Marrel, B. Iooss, B. Laurent, and O. Roustant, *Reliab Eng Syst Saf* **94**, 742-751 (2009).
5. P. Hall, J. S. Marron, and A. Neeman, *J. R. Statist. Soc. B* **67**, 427–444 (2005); T. Hastie, R. Tibshirani, and J. Friedman, *Elements of Statistical Learning: Data Mining, Inference, and Prediction*, Second Edition (2009), Chapter 18.

Publications

1. R. T. Skodje, A. S. Tomlin, S. J. Klippenstein, L. B. Harding, and M. J. Davis, “Theoretical validation of chemical-kinetic mechanisms: Combustion of methanol”, *J. Phys. Chem. A* **114**, 8286-8301 (2010).
2. S. J. Klippenstein, L. B. Harding, M. J. Davis, R. T. Skodje, and A. S. Tomlin, “Uncertainty driven theoretical kinetics studies of CH₃OH ignition: HO₂ + CH₃OH and O₂ + CH₃OH”, *Proc. Combust. Inst.* **33**, 351-357 (2011).
3. M. J. Davis, R. T. Skodje, and A. S. Tomlin, “Global sensitivity analysis of chemical-kinetic reaction mechanisms: Construction and deconstruction of the probability density function”, *J. Phys. Chem A* **115**, 1556–1578 (2011).
4. R. Sivaramakrishnan, D. Y. Zhou, R. T. Skodje, and M. J. Davis, “A comprehensive mechanism for ethanol combustion”, *Proceedings of the 7th US National Technical Meeting of the Combustion Institute, Georgia Institute of Technology, Atlanta, GA* (2011).
5. R. Sivaramakrishnan, W. Liu, M. J. Davis, S. Som, and D. E. Longman, “A high temperature model for the combustion of methylbutanoate”, *East. States Section of the Comb. Instit.* (2011).
6. R. L. Miller, L. B. Harding, M. J. Davis, and S. K. Gray, “Bi-fidelity fitting and optimization”, *J. Chem. Phys.* **136**, 074102-1 – 074102-11 (2012).
7. D. D. Y. Zhou, K. Han, P. Zhang, L. B. Harding, M. J. Davis, and R. T. Skodje, “Theoretical Determination of the Rate Coefficient for the HO₂ + HO₂ → H₂O₂+O₂ Reaction: Adiabatic Treatment of Anharmonic Torsional Effects”, *J. Phys. Chem.* **116**, 2089-2100 (2012).
8. W. Liu, R. Sivaramakrishnan, M. J. Davis, S. Som, and D. E. Longman, “Development of a Reduced Biodiesel Surrogate Model for Compression Ignition Engine Modeling”, *Central States Section of the Combustion Institute* (2012).
9. W. Liu, R. Sivaramakrishnan, M. J. Davis, S. Som, D. E. Longman, and T. F. Lu, “Development of a Reduced Biodiesel Surrogate Model for Compression Ignition Engine Modeling”, *Proceedings of the Combustion Institute, submitted* (2012).

PROJECT NARRATIVE

Dynamics of Radical Reactions in Biodiesel Combustion

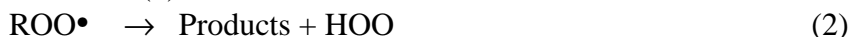
Theodore S. Dibble
Chemistry Department
SUNY-Environmental Science and Forestry
Syracuse, NY 13210
tsdibble@esf.edu

PROJECT SCOPE

The ignition of diesel fuel depends on isomerization of peroxy radicals (ROO•) via a hydrogen shift reaction:



Production of multiple OH radicals (chain branching) following reaction (1) leads to autoignition. Processes such as reaction (2):



compete with chain branching. Experimentalists face several difficulties in gaining an understanding of this chemistry, and no QOOH species has ever been detected by experiment! This has inspired many computational studies of these processes.

Biodiesel fuel is increasingly being used worldwide. Although we have a fair understanding of the molecular details of the chemistry of peroxy radicals derived from alkanes, biodiesel fuels contain ester and olefin groups which significantly impact the thermodynamics and kinetics of biodiesel ignition.¹ The broader goal of this research is to carry out systematic computational studies of the elementary kinetics of peroxy radical chemistry from compounds that are models for biodiesel ignition. This includes not only reactions (1) and (2), but also reactions leading to chain branching. In addition, the research will:

- include rigorous treatments of tunneling effects
- quantify the effect of chemically activated processes
- synthesize the results into structure-activity relations (SARs)

RECENT PROGRESS

Cis-trans Isomerization of Allylic Radicals.

Biodiesel fuel is composed largely of fatty acid methyl esters. The fatty acids are composed of long hydrocarbon chains, which are usually unsaturated. These double bonds are almost exclusively in cis configurations. By contrast, gaseous alkenes studied in combustion are mostly trans. Bounaceur, et al,² argued that the thermal cis-trans isomerization was unimportant, but did not actually calculate rate constants. At temperatures of 700 K and higher, the thermal rate constant for isomerization should out-compete addition of O₂ to these radicals.

At lower temperatures, chemically activated isomerization can be extensive. The potential energy profile for production of the 2-butenyl radical (CH₃CHCHCH₂) from OH + 2-butene is shown below in Figure 1. RRKM-Master Equation calculations were carried out with the MultiWell program³ to determine the fate of chemically activated 2-butenyl radical formed

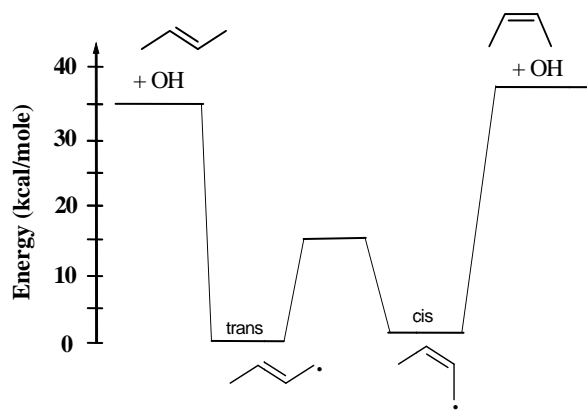


Figure 1. Potential energy profile for 2-butene + OH at M05-2X/6-311+G(2df,2p).

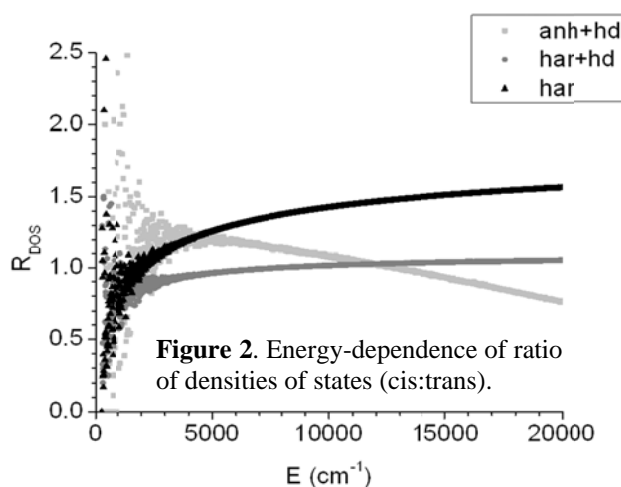
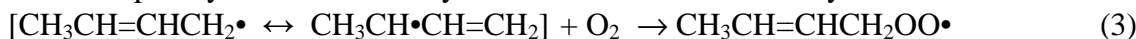


Figure 2. Energy-dependence of ratio of densities of states (cis:trans).

just above the barrier to isomerization (~ 15 kcal/mol or $\sim 5,500$ cm^{-1}) is reflected in the cis:trans ratio of quenched radicals. For the quantum chemical method used in Figure 2, the cis:trans ratio decreases in the order $\text{har} \gtrsim \text{anh+hd} > \text{har+hd}$.

Unimolecular Reactions of the Allylic Four-Carbon Peroxy Radical

We have carried out M05-2X and CBS-QB3 calculations on the reactions of the *cis*- and *trans*-but-2-en-1-peroxy radical formed by O_2 addition to C_1 of 2-butenyl radical:



This is a larger analog of allyl radical. Allyl radical adds O_2 but the resulting peroxy radical back-dissociates rather than reacting further. Only the *cis* isomer of the product of this reaction has the potential to undergo an H-shift reaction:



that could propagate radical chemistry and lead to autoignition of diesel fuel. The results above indicate that one should expect the *cis* isomer to be formed, even starting from *trans* alkenes. The quantum chemical results indicate that loss of O_2 (reaction -3) is ~ 3 kcal/mol favored over

from OH + *trans*-2-butene. In simulations at a range of pressures and temperatures, the *cis* isomer was quite abundant, if not dominant, over the *trans* isomer.

This result is counterintuitive, because it shows that the isomer which is thermodynamically less stable (at low temperature) is preferred. However, in this case, the key factor is the ratio, $R_{DOS}(E)$, of the density of states, $\rho(E)$, of the two isomers at a range of energies above the isomerization barrier at which the isomerization rate constant becomes smaller than quenching. This density of states generally favors the *cis* isomer.

The shape of $R_{DOS}(E)$ varies with the quantum chemical method used and the extent to which the harmonic oscillator approximation is invoked. The results at M06-2X/6-311+G(2df,2p) are shown at left, starting with highly energized radicals formed in N_2 bath gas at 300 K. Different symbols indicate different methods of calculating densities of states: har = all modes treated as harmonic oscillators; har+hd = as har but methyl torsion treated as hindered rotor; anh+hd = anharmonic treatment except methyl torsion.

The method dependence of R_{DOS} at energies

reaction (4). Given that reaction (-3) has a higher Arrhenius pre-exponential term than reaction (4), loss of O₂ will be favored under all conditions.

Autoignition Mechanism of Methyl Butanoate (MB)

Methyl butanoate (MB) is composed of a methyl ester group and a short alkyl group (see Figure 3). MB oxidation mechanism has been studied as the starting point for understanding biodiesel combustion for a decade.⁴ The CBS-QB3 composite method is used to determine reaction energies and activation barriers to reactions of peroxy radicals and the corresponding QOOH species. We include all four peroxy radicals formed subsequent to H-atom abstraction from MB (sites 1-3 and 5 in Figure 3). Reactions treated include H-shift and HO₂ elimination of ROO•, and decomposition of QOOH by C-C, C-O, and O-O scission.

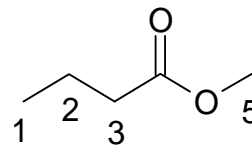
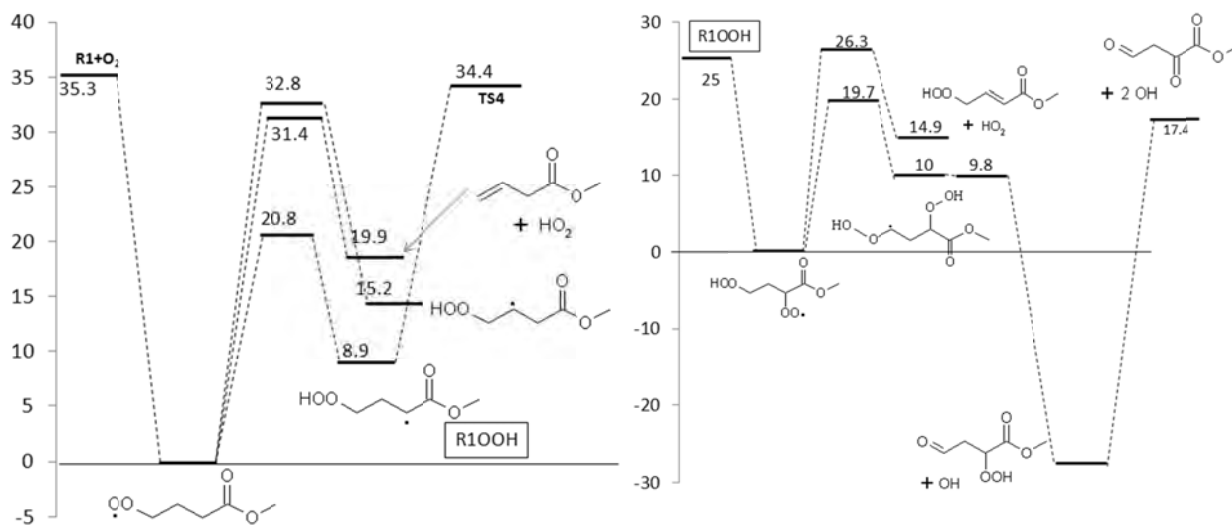


Figure 3. Methyl butanoate

Potential energy profiles have been obtained for all four peroxy radicals. Where one of these peroxy radicals isomerizes to form a carbon-centered radical, the chemistry of the second-generation peroxy radical has been investigated. Results are shown in Figure 4 for a single case.



Clearly, for this case, the most favorable reaction for the initially-formed peroxy radical is to isomerize to the structure labeled R1OOH, which cannot undergo further unimolecular reactions. Addition of O₂ to R1OOH leads to a second generation peroxy radical. This species has the potential to isomerize, followed by prompt loss of OH and generation of a highly oxidized stable organic molecule. A hydrogen-bonded complex between OH and the terminal carbonyl group complicates the potential energy profile. High-pressure limiting rate constants have been calculated for unimolecular reactions relevant to the fate of all four primary peroxy radicals and any second generation peroxy radicals. Investigations of reactions of chemically activated radicals are ongoing.

Tunneling in the 1,5 H-shift of the a Model Second-Generation Peroxy Radical

Consider the 1,5 H-shift reaction in propylperoxy radical (reaction 5) and in the peroxy radical formed subsequent to its isomerization (reaction 7):



The species $\text{HOOCH}_2\text{CH}_2\text{CH}\cdot\text{OOH}$ may or may not be a minimum on the potential energy surface, but even if it is, it likely lives for picoseconds or less.⁵ Reaction (7) and analogous reactions are very exothermic on account of the loss of OH radical and formation of a carbonyl compound. Tunneling calculations in such cases commonly invoke the asymmetric Eckart formula and use this large exothermicity as a parameter which influences the extent of tunneling. Quantum chemical calculations have been carried out for this system.

FUTURE PLANS

Rigorous semi-classical tunneling calculations will be started soon on reaction 7; these calculations will employ the POLYRATE program.⁶ We plan to compare the results to those obtained with Eckart approach.

RRKM/Master Equation simulations will be carried out on the peroxy radicals from methylbutanoate (MB). Phenomenological rate constants will be determined for a wide range of pressures and temperatures for use in kinetic modeling.

PUBLICATIONS ACKNOWLEDGING BES SUPPORT 2009-PRESENT

- T. S. Dibble, Y. Sha, W. F. Thornton, and F. Zhang. Cis-trans isomerization of chemically activated 1-methylallyl radical and fate of the resulting 2-buten-1-peroxy radical, *J. Phys. Chem. A.* **2012**, submitted.
- F. Zhang and T. S. Dibble. Impact of Tunneling on hydrogen-migration of n-propylperoxy radical. *Phys. Chem. Chem. Phys.*, **2011**, *13*, 17969-77.
- F. Zhang and T. S. Dibble, Effects of ester and olefin functional groups on kinetics of unimolecular reactions of peroxy radicals, *J. Phys. Chem. A.* **2011**, *115*, 655-663.
- T. S. Dibble and Yue Zeng, Potential energy profiles for the N + HOCO reaction and products of the chemically activated reactions N + HOCO and H + HOCO. *Chem. Phys. Letts.*, **2010**, *495*, 170-174.

REFERENCES

- [1] R. Sumathi and W. H. Green, *Phys. Chem. Chem. Phys.*, **2003**, *5*, 3402-17.
- [2] R. Bounaceur, V. Warth, B. Sirjean, P.A. Glaude, R. Fournet, and F. Battin-Leclerc, *F. Proc. Combust. Inst.*, **2009**, *32*, 387.
- [3] MultiWell-2011, Jan 2011, designed and maintained by J.R. Barker with contributors, University of Michigan, Ann Arbor, MI; <http://aoss.engin.umich.edu/multiwell/>.
- [4] S. Dooley, H. J. Curran, and J. M. Simmie, *Combustion and Flame* **2008**, *153*, 2-32.
- [5] A. Andersen and E. A. Carter, *J. Phys. Chem. A*, **2006**, *110*, 1393-1407.
- [6] J. Zheng, et al., POLYRATE-version 2010-A, University of Minnesota, Minneapolis.

Hydrocarbon Radical Thermochemistry: Gas-Phase Ion Chemistry Techniques

Kent M. Ervin
Department of Chemistry and Chemical Physics Program
University of Nevada, Reno
Reno, NV 89557-0216
ervin@unr.edu

I. Program Scope

Gas-phase ion chemistry and mass spectrometry techniques are employed to determine energetics of hydrocarbon radicals that are important in combustion processes and to investigate the dynamics of ion–molecule reactions. Tandem mass spectrometry is used to measure the activation of endoergic ion-molecule reactions as a function of kinetic energy. Modeling the measured reaction cross sections using statistical rate theory or empirical reaction models allows extraction of reaction threshold energies.¹ These threshold energies yield relative gas-phase acidities, proton affinities, or hydrogen atom affinities, which may then be used to derive neutral R–H bond dissociation enthalpies using thermochemical cycles involving established electron affinities or ionization energies.² The reactive systems employed in these studies include endoergic bimolecular proton transfer reactions, hydrogen-atom transfer reactions, and collision-induced dissociation of heterodimer complex anions and cations. Electronic structure calculations are used to evaluate the possibility of potential energy barriers or dynamical constrictions along the reaction path, and as input for RRKM and phase space theory calculations.

II. Recent Progress

A. Energy-Resolved Collision-Induced Dissociation

We have measured the oxygen–oxygen bond dissociation energy of the peroxyformate anion (HCO_3^-) using energy-resolved collision-induced dissociation with a guided ion beam tandem mass spectrometer.³ As shown in Figure 1, this bond dissociation energy connects the negative-ion thermochemical cycle for formic acid, HCO_2H , for which the enthalpy of formation is well established, to the thermochemical cycle for peroxyformic acid, HCO_3H , for which the enthalpy of formation had not been previously measured. We can also derive the enthalpy of formation of peroxyformyl radical, HCO_3 , which is of combustion interest as an intermediate in the oxidation of HCO .

The cross sections for the dissociation of HCO_3^- as a function of the collision energy with xenon are shown in Figure 2. We observe three dissociative product channels: $\text{HCO}_2^- + \text{O}$, $\text{HO}^- + \text{CO}_2$, and $\text{HOO}^- + \text{CO}$. The threshold energy for the $\text{HCO}_2^- (^1\text{A}')$ channel is consistent with formation of the ground state $\text{HCO}_2^- (^1\text{A}_2) + \text{O} (^3\text{P})$ products on the triplet surface, rather than the $\text{HCO}_2^- (^1\text{A}_2) + \text{O} (^1\text{D})$ products on the singlet surface. That is, the

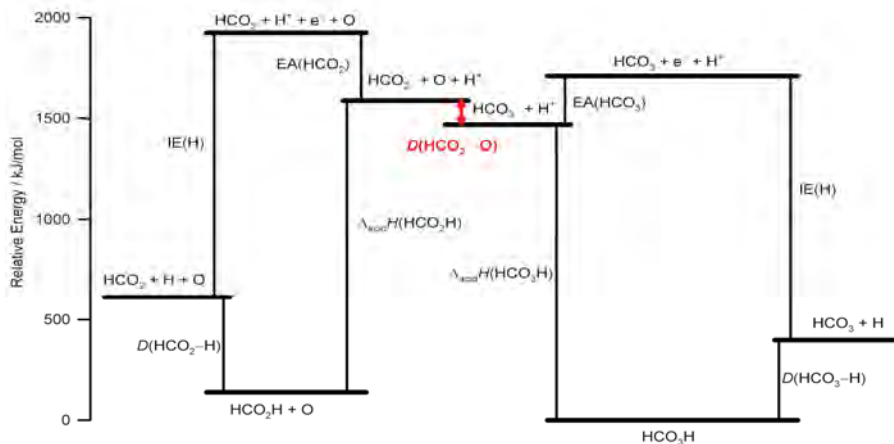


Figure 1

dissociation process requires a singlet-triplet conversion along the reaction path. Density functional theory calculations were used to show that there is indeed a crossing point along this path at energies below the asymptotic singlet product energies. The threshold energies for the OH^- product channel is about equal to that the $\text{HCO}_2^- + \text{O}$ products, even though formation of $\text{HO}^- + \text{CO}_2$ is strongly exothermic. That implies there is an energy barrier along that dissociation coordinate. The schematic potential energy surface in Figure 3, based on density functional theory calculations, confirms that there is a barrier associated with the necessary molecular rearrangement to form these products. The transition state to an intermediate HOCOO^- structure is shared by the $\text{HO}^- + \text{CO}_2$ and $\text{HOO}^- + \text{CO}$ reaction paths. To elucidate the overall dissociation processes, we developed an RRKM model of the competing paths with transition state switching to account for the multiple transition states to analyze the overall dissociation processes. This model is shown as solid lines in Figure 2. Based on the threshold energy obtained with this model, the measured oxygen–oxygen bond dissociation energy is $D_0(\text{HCO}_2^- - \text{O}) = 1.30 \pm 0.13$ eV (126 ± 12 kJ/mol). This threshold energy measurement is used in thermochemical cycles to derive the enthalpies of formation for peroxyformic acid, $\Delta_f H_{298}(\text{HCO}_3\text{H}) = -287 \pm 19$, kJ/mol, and peroxyformyl radical,

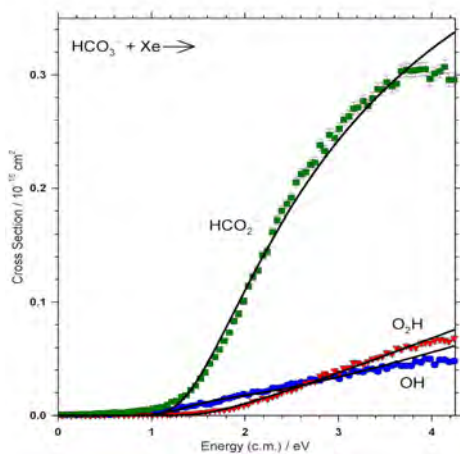


Figure 2

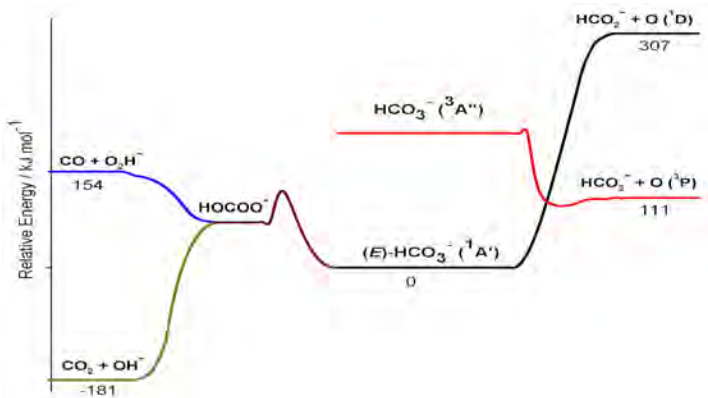


Figure 3

$\Delta_f H_{298}(\text{HCO}_3\cdot) = -98 \pm 12 \text{ kJ/mol}$. These values are in good agreement with computational energies

Preliminary experiments have been conducted for the analogous peroxyacetic acid system via collision-induced dissociation of the peroxyacetate anion, CH_3CO_3^- . Unfortunately, the production of $\text{CH}_3\text{CO}_2^- + \text{O}$ is only a minor channel, presumably because the energy barrier for molecular rearrangements is not as high relative to the oxygen atom loss channel as it is in the peroxyformate system. This result will likely prevent the determination of the enthalpy of formation for peroxyformic acid and the peroxyformyl radical by this method. We are looking into possible reference acids HX that could be used to measure the gas phase acidity via competitive CID of $\text{CH}_3\text{CO}_3^-(\text{HX})$ proton-bound complexes.

B. Instrumental Development

We are developing a quadrupole ion trap/time-of-flight tandem mass spectrometer to complement our guided ion beam tandem mass spectrometer used for the collision-induced dissociation work. Recent accomplishments include a novel optimization of the quadrupole ion trap for use as an ion source for the time-of-flight mass spectrometer.⁴ We have shown that replacing the conventional Paul ion trap with hyperbolic electrodes with a cylindrical trap with flat parallel electrodes can greatly improve the time-of-flight mass resolution by avoiding curvature in the electric field used to extract the ion cloud into the time-of-flight tube. At the same time, the radio-frequency trapping characteristics of the trap can be largely maintained.

C. Franck-Condon Analysis of Photoelectron and Photoionization Spectra

Determination of hydrocarbon R-H bond dissociation energies from our measured gas phase acidities require accurate electron affinities, which can be measured using negative ion photoelectron spectroscopy. For that reason, we have also been involved in collaborations involving photoelectron spectroscopy. Recent work on modeling the negative ion photoelectron spectra of dihalomethyl anions, in collaboration with Lineberger and coworkers, has been published.⁵ Our PESCAL software for simulating the Franck-Condon profiles for photoelectron spectra and photoionization threshold experiments has enjoyed increasing use in the community, including since 2010 in references 5–20.

III. Future Work

Experimental work will continue on the ion thermochemistry experiments detailed above and related work involving proton affinities in cationic systems. In the near term, we plan to delve more deeply into the relative gas-phase acidities of oxygen-containing hydrocarbons, in particular various isomers of alkyl and alkenyl alcohols.

IV. References

- (1) Armentrout, P. B.; Ervin, K. M.; Rodgers, M. T. *J. Phys. Chem. A* **2008**, *112*, 10071.
- (2) Ervin, K. M. *Chem. Rev.* **2001**, *101*, 391.
- (3) Nickel, A. A.; Lanorio, J. G.; Ervin, K. M. *J. Phys. Chem. A* **2012**, (in press, DOI: 10.1021/jp302089q).
- (4) Dangi, B. B.; Ervin, K. M. *J. Mass Spectrom.* **2012**, *47*, 41.
- (5) Vogelhuber, K. M.; Wren, S. W.; McCoy, A. B.; Ervin, K. M.; Lineberger, W. C. *J. Chem. Phys.* **2011**, *134*, 184306.

- (6) Adams, C. L.; Knurr, B. J.; Weber, J. M. *J. Chem. Phys.* **2012**, *136*, 064307.
- (7) Vogelhuber, K. M.; Wren, S. W.; Shaffer, C. J.; McMahon, R. J.; McCoy, A. B.; Lineberger, W. C. *J. Chem. Phys.* **2011**, *135*, 204307.
- (8) Mann, J. E.; Waller, S.E.; Rothgeb, D.W.; Jarrold, C. C. *J. Chem. Phys.* **2011**, *135*, 104317.
- (9) Wu, X. Xie, H.; Qin, Z. B.; Tan, K.; Tang, Z. C. Lu, X. *J. Phys. Chem. A* **2011**, *115*, 6321.
- (10) Goulay, F.; Soorkia, S.; Meloni, G.; Osborn, D. L.; Taatjes, C. A.; Leone, S. R. *Phys. Chem. Chem. Phys.* **2011**, *13*, 20820.
- (11) Kim, J. B.; Yacovitch, T. I.; Hock, C.; Neumark, D. M. *Phys. Chem. Chem. Phys.* **2011**, *13*, 17378.
- (12) Adams, C. L.; Weber, J. M. *J. Chem. Phys.* **2011**, *134*, 244301.
- (13) Yacovitch, T. I.; Kim, J. B.; Garand, E.; van der Poll, D. G.; Neumark, D. M. *J. Chem. Phys.* **2011**, *134*, 134307.
- (14) Ichino, T.; Villano, S. M.; Gianola, A. J.; Goebbert, D. J.; Velarde, L.; Sanov, A.; Blanksby, S. J.; Zhou, Hrovat, D. A.; Bordern, W. T.; Lineberger, W. C. *J. Phys. Chem. A* **2011**, *115*, 1634.
- (15) Vogelhuber, K. M.; Wren, S. W.; Sheps, L.; Lineberger, W. C. *J. Chem. Phys.* **2011**, *134*, 064302.
- (16) Wu, X.; Qin, Z.; Xie, H.; Cong, R.; Wu, X.; Tang, Z.; Fan, H. *J. Chem. Phys.* **2010**, *133*, 044303.
- (17) Zhou, J.; Takahashi, L. K.; Wilson, K. R.; Leone, S. R.; Ahmed, M. *Anal. Chem.* **2010**, *82*, 3905.
- (18) Yacovitch, T. I.; Garand, E.; Neumark, D. M. *J. Phys. Chem. A* **2010**, *114*, 11091.
- (19) Yen, T. A.; Garane, E.; Shreve, A. T.; Neumark, D. M. *J. Phys. Chem. A* **2010**, *114*, 3215.
- (20) Soorkia, S.; Trevitt, A. J.; Selby, T. M.; Osborn, D. L.; Taatjes, C. A.; Wilson, K. R.; Leone, S. R. *J. Phys. Chem. A* **2010**, *114*, 3340.

V. Publications supported by this project 2010-2012

1. Dangi, B. B.; Sassin, N. A.; Ervin, K. M. "Pulsed ion extraction diagnostics in a quadrupole ion trap linear time-of-flight mass spectrometer", *Rev. Sci. Instrum.* **2010**, *81*, 063302/1-10.
2. K. M. Ervin, PESCAL, Fortran program for Franck-Condon simulation of photoelectron spectra, <http://wolfweb.unr.edu/~ervin/pes/> (revised 2010).
3. Vogelhuber, K. M.; Wren, S. W.; McCoy, A. B.; Ervin, K. M.; Lineberger, W. C. "Photoelectron spectra of dihalomethyl anions: Testing the limits of normal mode analysis", *J. Chem. Phys.* **2011**, *134*, 184306/1-13.
4. Dangi, B. B.; Ervin, K. M. "Optimization of a quadrupole ion storage trap as a source for time-of-flight mass spectrometry", *J. Mass Spectrom.* **2012**, *47*, 41-48.
5. Nickel, A. A.; Lanorio, J. G.; Ervin, K. M. "Energy-resolved collision-induced dissociation of peroxyformate anion: Enthalpies of formation of peroxyformic acid and peroxyformyl radical", *J. Phys. Chem. A* **2012**, DOI: 10.1021/jp302089q (in press).

Spectroscopic and Dynamical Studies of Highly Energized Small Polyatomic Molecules

Robert W. Field
Massachusetts Institute of Technology
Cambridge, MA 02139
rwfield@mit.edu

I. Program Scope

The fundamental goal of this program is to develop the experimental techniques, diagnostics, interpretive concepts, spectrum-assignment strategies, and pattern-recognition schemes needed to reveal and understand how large-amplitude motions are encoded in the vibration-rotation energy level structure of small, gas-phase, combustion-relevant polyatomic molecules. We are focusing our efforts on unimolecular isomerization in several prototypical systems, including the $\text{HNC} \leftrightarrow \text{HCN}$ and $\text{HCCH} \leftrightarrow \text{CCH}_2$ isomerization systems. We are developing chirped-pulse millimeter wave (CPmmW) spectroscopy as a technique that can be used in conjunction with Stimulated Emission Pumping (SEP) and the Stark effect to populate and identify molecular states with high excitation in *local* large-amplitude vibrational modes, which are of key importance in understanding isomerization processes. In addition, we are attempting to demonstrate the capability of CPmmW spectroscopy to determine reaction mechanisms and the structures of molecular fragmentation transition states by measurement of fragment species/vibrational level populations.

II. Recent Progress

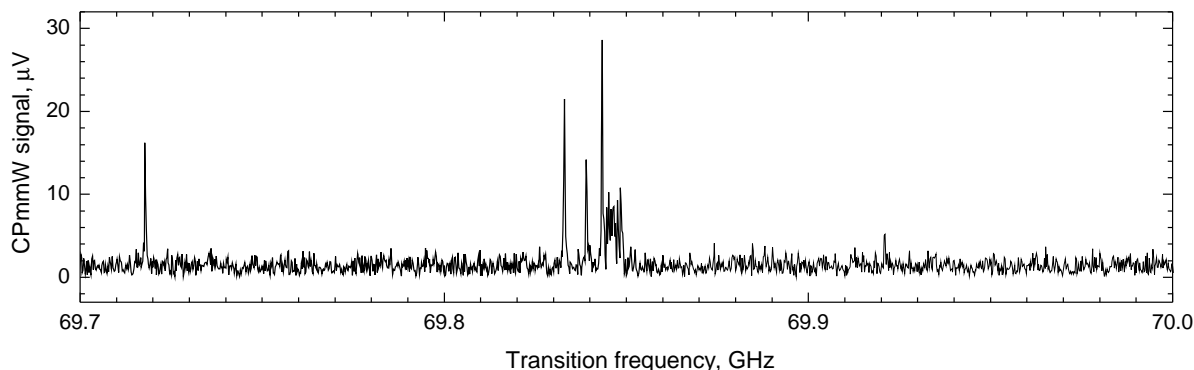


Figure 1: The first microwave spectrum of vinylidene? A slit-jet beam of vinyl cyanide (VCN) is photolyzed by 193 nm radiation. The line near 69.72 GHz is VCN. The 69.83-69.85 GHz cluster of lines is a one-photon photodissociation product, tentatively assigned as $J=1-0$ of S_0 vinylidene and local-bender levels of acetylene.

A. CPmmW Spectroscopy

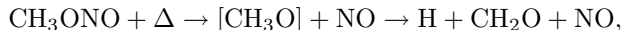
1. Chirped Pulse/Slit jet spectrometer

Chirped-Pulse Millimeter-Wave (CPmmW) spectroscopy is the first truly broadband and high resolution technique for spectroscopy in the millimeter wave region. We designed the technique in collaboration with the Brooks Pate research group at the University of Virginia, based on their pioneering Chirped-Pulse Fourier-Transform Microwave (CP-FTMW) spectrometer, which operates at frequencies up to 20 GHz. We have built and tested a CPmmW spectrometer that operates in the 70–102 GHz frequency range. The spectrometer can acquire up to 12 GHz of spectral bandwidth at better than 100 kHz resolution in a single shot. As part of our search for mm-wave transitions in vinylidene and highly excited local bender acetylene we have expanded the lower-frequency limit of our CPmmW spectrometer to 58 GHz and implemented a slit-jet

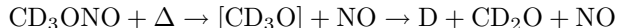
source. The slit-jet apparatus has increased the sensitivity of our CPmmW experiments by a factor of 10, due to increased number of molecules in the interaction region and reduced Doppler profile. The collisional region of the slit-jet supersonic expansion extends to up to 2 cm from the slit-jet source, allowing for precise control over the number of cooling collisions that the photolysis products experience in the expansion. This could be crucial in minimizing collisional relaxation of highly excited local-bender states of acetylene during the expansion. Improvements of the CPmmW detection electronics (mmW switches and low noise amplifiers) are expected to yield an additional factor of 10 in S:N. The CPmmW / slit-jet spectrometer is now fully operational and we have observed several mm-wave transitions around 69.84 GHz that we tentatively assign to vinylidene / acetylene local-bender levels proximal to the isomerization transition state (Fig. 1).

2. Pyrolysis

In the last two years we have implemented CPmmW spectroscopy of pyrolysis reaction products using the Peter Chen pyrolysis nozzle, in collaboration with the Ellison group at the University of Colorado. In this experiment, molecules entrained in a carrier gas are expanded into vacuum through a SiC tube, which is heated to 800–1800 °C, and the products of thermal decomposition are observed by CPmmW. It was previously assumed that unimolecular decomposition or unimolecular isomerization were the primary mechanisms by which pyrolysis reaction products are formed. Very recently we have realized that bimolecular reactions in a hot pyrolysis tube are crucial for an understanding of the reaction mechanisms, and can lead to new chemistry. Of particular interest are the free H-atom mediated reactions, which are our current focus in pyrolysis experiments. As demonstrated previously, methyl nitrite thermally decomposes as



which produces large amounts of hydrogen atoms in the pyrolysis tube. We have found that these free hydrogen (or deuterium) atoms can attack and break other molecules co-expanding in the hot tube. When fully deuterated methyl nitrite is mixed with acetaldehyde, the following reactions are observed:



In addition to HDCO, we observe the CPmmW spectrum of HDO, which is indicative of another reaction channel:



Bimolecular decomposition of acetaldehyde in reaction (1) is likely to proceed through addition of D atoms to the carbon in the carbonyl group. The decomposition reaction (2) may indicate the possibility of D atoms adding to the oxygen and forming an intermediate vinyl alcohol. These mechanisms could be potentially important to the understanding and catalysis of thermal biomass decomposition processes. We plan to study the generality of these bi-molecular mechanisms with other aldehydes and ketones.

B. High- and low-barrier unimolecular isomerization in S_0 and S_1 HCCH

The goal of our studies of the acetylene \leftrightarrow vinylidene system is to observe barrier-proximal vibrational states. Many studies have demonstrated that the vibrational eigenstates of acetylene and similar molecules undergo a normal-to-local transition in which the normal modes appropriate to describe small displacements from the equilibrium geometry evolve into local modes in which the excitation is isolated in a single large-amplitude C-H bond stretch or $\angle\text{CCH}$ bend. The evolution of vibrational character is of particular interest in the acetylene bending system, because the local-bending vibration bears a strong resemblance to the reaction coordinate for isomerization from acetylene to vinylidene, where one hydrogen moves a large distance off of the C-C bond axis while the other hydrogen remains nearly stationary. In the first singlet excited state of acetylene, we find ourselves in the unique situation of being close to characterizing the complete rovibronic level structure up to the transition state energy in a system exhibiting conformational change.

1. Observation and theoretical treatment of vibrational levels of S_1 *cis* acetylene

The S_1 state also presents the possibility of characterizing low-barrier isomerization from its *trans*-geometry minimum to a local minimum at the *cis*-bent geometry. This isomerization has been the focus of many theoretical studies, but it has been difficult to study experimentally because, though the *trans* minimum has been exhaustively characterized, the transition from the ground electronic state to the S_1 *cis* geometry is electronically forbidden and no transitions to this conformer have previously been observed. In the course of characterizing the S_1 surface, several vibrational levels were observed which could not be ascribed to S_1 -*trans* or other electronic states. These initially discovered levels have now definitively been identified as belonging to S_1 -*cis*, and surprisingly, were observed below the energy of the calculated barrier to *trans-cis* isomerization, and must therefore owe their observed intensity to mixing via tunneling with *trans*-geometry-localized states.

New IR-UV double resonance experiments via ν_3'' have revealed additional *cis* levels, providing valuable information on this elusive conformer's harmonic frequencies, vibrational anharmonicities, and some unusual features in its rotational structure, such as staggering of its K levels due to tunneling. Such information has led directly to the discovery of yet more *cis* levels, enabling the characterization of the *cis* side of the isomerization barrier.

As part of our search for the levels of the *cis* well, we have now collected enough information to completely determine experimentally the anharmonic force field for the *trans* conformer, i.e. all of the ω_i and x_{ij} (aside from x_{11} and x_{55}), a unique achievement in an electronically excited state of a polyatomic molecule. We recently completed the analysis of the 45800-46500 cm^{-1} region, containing the $1^1B^1, 2^1B^3, B^5, 3^3B^1, 3^15^1, 2^13^2B^1$ and 3^2B^3 ungerade polyads, which determined the x_{1B} parameters, but more importantly led to the development of a strategy for extrapolating parameters for yet higher energy polyads. Furthermore, the vibrational constants have been incorporated into a preliminary model that allows for the fitting of the $J = K = 0$ level positions of all of the known *trans* vibrational levels. Based on this new knowledge of both *trans* and *cis* minima on the excited state, we have begun a detailed analysis of the congested and complex spectrum in the region of the expected transition state energy.

An important component of our continued progress towards the successful analysis of the high energy regions in S_1 acetylene will involve a new effort to implement a detection scheme that overcomes the problem of predissociation, which sets in approximately 1000 cm^{-1} below the transition state energy. We have constructed and begun optimizing a simple, robust ion-detector that should allow us to record the first high resolution H-atom action spectra of S_1 acetylene. The combination of two distinct complementary data channels (LIF and H-atom action) will not only advance the spectroscopy of the \tilde{A} state, but also provide valuable information about the mode- and conformer-specific influence of vibrations on the predissociation mechanism.

Our comprehensive examination of the *cis-trans* isomerization in S_1 acetylene has led to the development of a universal model-independent spectroscopic diagnostic of transition state energies in systems exhibiting conformational change. We believe that it is possible to extend the concept of effective frequency as an indicator of qualitative dynamical changes, previously used for dissociation in diatomics (Birge-Sponer, LeRoy-Bernstein) and the bent-linear transition in quasilinear triatomics ("Dixon dip"), to determine the isomerization barrier height in asymmetric double minimum potentials. The results of such an analysis for S_1 *trans* acetylene are shown in Fig. 2, showing that the current upper range of vibrational assignments is close to the transition state energy.

III. Future Work

We expect to achieve a >100-fold improvement of the signal:background ratio of our CPmmW spectrometer by taking advantage of new millimeter-wave technology and by use of a custom designed slit-jet molecular beam chamber. These enhancements will enable us to measure the populations of vibrationally-excited photolysis and pyrolysis products and locate additional acetylene local-bender vibrational states. The combination of our S_1 results with the high resolution/survey capability of CPmmW/DF spectra will guide us towards conclusive SEP experiments that sample levels proximal to the acetylene-vinylidene isomerization barrier. We plan to record Stark effect spectra of the S_0 highly vibrationally excited levels, in order to measure the large predicted vibrationally-averaged dipole moments of the local-bender states and to use these measured dipole moments as a measure of progress along the large amplitude local-bender isomerization coordinate. CPmmW measurements of product state distributions will allow us to extract information about the structures of transition states for fragmentation and photodissociation.

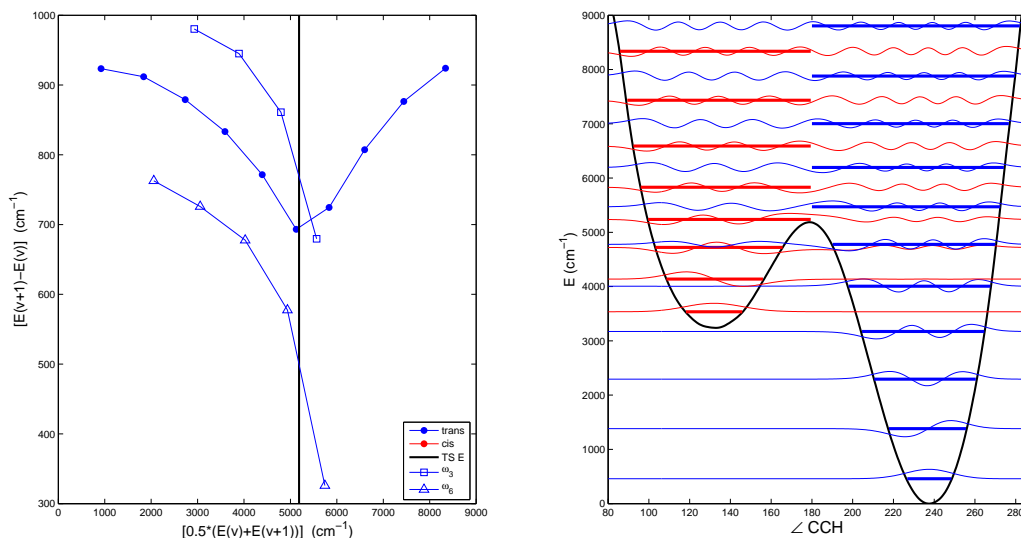


Figure 2: Determination of transition state energy from the pattern of vibrational level spacings. Demonstrated here by a simple one dimensional minimum energy isomerization path (MEIP) calculation, the minimum in the pattern of vibrational level spacings reveals, in a model-independent way, the transition state energy for any asymmetric double minimum potential. Experimental values for the vibrational level spacings in the $3^n B^2$ series are overlaid on the *ab initio* results in the left plot, showing remarkable agreement between the average of the experimental ω_3^{eff} and ω_6^{eff} normal mode spacings and those found in the 1D MEIP local Bender calculation. The highest energy points in the experimental traces are based on preliminary, unpublished assignments.

Publications supported by this project 2010–2012

- [1] G. Barratt Park, Adam H. Steeves, Kirill Kuyanov-Prozument, Justin L. Neill, and Robert W. Field. Design and evaluation of a pulsed-jet chirped-pulse millimeter-wave spectrometer for the 70–102 GHz region. *The Journal of Chemical Physics*, 135(2):024202, 2011.
- [2] J. H. Baraban, A. R. Beck, A. H. Steeves, J. F. Stanton, and R. W. Field. Reduced dimension discrete variable representation study of *cis*–*trans* isomerization in the S_1 state of C_2H_2 . *The Journal of Chemical Physics*, 134(24):244311, 2011.
- [3] Anthony J. Merer, Adam H. Steeves, Joshua H. Baraban, Hans A. Bechtel, and Robert W. Field. *cis*–*trans* isomerization in the S_1 state of acetylene: Identification of *cis*-well vibrational levels. *The Journal of Chemical Physics*, 134(24):244310, 2011.
- [4] Joshua H. Baraban, Anthony J. Merer, John F. Stanton, and Robert W. Field. Full dimensional Anharmonic Force Fields for *cis* and *trans* S_1 C_2H_2 . *Molecular Physics*, 2012, in preparation.
- [5] Joshua H. Baraban, P. Bryan Changala, Anthony J. Merer, Adam H. Steeves, Hans A. Bechtel, and Robert W. Field. The \tilde{A}^1A_u state of acetylene: *ungerade* vibrational levels in the region 45800–46500 cm^{-1} . *Molecular Physics*, 2012, in preparation.
- [6] Joshua H. Baraban, P. Bryan Changala, Anthony J. Merer, John F. Stanton, and Robert W. Field. *cis*–*trans* isomerization in the S_1 state of acetylene: *cis*-well rovibrational level structure. *Journal of Chemical Physics*, in preparation.
- [7] Anthony J. Merer, Joshua H. Baraban, P. Bryan Changala, and Robert W. Field. Perturbations in the 3^36^1 level of \tilde{A}^1A_u state of acetylene, C_2H_2 . *Journal of Chemical Physics*, in preparation.

Scanning Tunneling Microscopy Studies of Chemical Reactions on Surfaces

George Flynn, Department of Chemistry, Columbia University
Mail Stop 3109, 3000 Broadway, New York, New York 10027
gwf1@columbia.edu

Introduction:

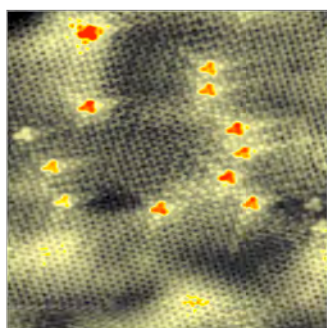
Our work is focused on fundamental chemical events taking place on carbon surfaces with the intent of shedding light on their role in mediating the formation of polycyclic aromatic hydrocarbons (PAHs) from small molecular precursors. For the past three years this effort has been focused on the chemical behavior of graphene (a single graphite carbon sheet).

Scanning tunneling microscopy (STM) is the main experimental probe technique that we use to study the interfacial structure and chemistry of graphene mainly because of its ability to investigate surface structure and dynamics with atomic resolution. Scanning tunneling spectroscopy (STS), which measures the local density of quantum states over a single atom, provides information about the electronic structure of graphene and graphite.

Results: Scanning Tunneling Microscopy Studies of Graphene Chemistry on Copper Substrates: Nitrogen substitution in the Graphene Lattice

The availability of a Chemical Vapor Deposition (CVD) method for preparing graphene has opened up the possibility of inserting atoms such as nitrogen or oxygen into the graphene lattice during sample preparation. Using STM we have studied the electronic structure and morphology of graphene films grown on a copper foil substrate in which N atoms substitute for a few carbon atoms in the 2-D graphene lattice.

The nitrogen substituted graphene films investigated in these experiments were fabricated using CVD on a copper foil substrate in a quartz tube furnace. The foil substrate was pre-cleaned with a flow of 10 sccm of H_2 and 200 sccm of Ar at a pressure of ~ 1.6 torr and a temperature of $1000^\circ C$ for 20 min. The nitrogen substituted graphene film was then grown using a mixture of 170 sccm of CH_4 , 10 sccm of H_2 and 5 sccm of NH_3 at a total pressure of 1.9 torr and a temperature of $1000^\circ C$ for 18 min. The graphene-coated copper foils were transferred soon after growth to our UHV low-temperature, high resolution STM. The treated copper substrates were degassed in UHV at a temperature of $350^\circ C$ for several hours before STM experiments were performed. While many areas of the copper foil display a rough topography due to poly-crystallinity, several large areas were found where atomically flat terraces were observed. Detailed STM measurements were performed on these terraces. The amount of nitrogen



substitution in the graphene lattice can be controlled by varying the NH_3 pressure during deposition.

Figure 1. STM image of N atom substituted graphene grown on copper foil. 14 dopants are found over an $8.5 \times 8.5 nm^2$ area, corresponding to an N concentration of 3/1000. ($8.5 \times 8.5 nm^2$; 0.8 V, 0.8 nA, 77 K) The red end of the height scale is $+0.8 \text{ \AA}$ above the mean indicating that the apparent height of the atoms around the N insert is 0.8 \AA .

Figure 1 shows a large area STM scan with sparsely distributed “defect” features scattered throughout an imaged area consisting mostly of the

graphene honeycomb structure. Copper foils not treated with NH_3 show no such “defects”.

The approximate concentration of N atoms is 3 per 1000 carbon atoms for this particular sample. A high-resolution image of a single “defect” site shows the triangular symmetry of the insertion point (see Figure 2). Theoretical calculations indicate that the center of the triangular feature contains a single N atom substituting for a C atom.

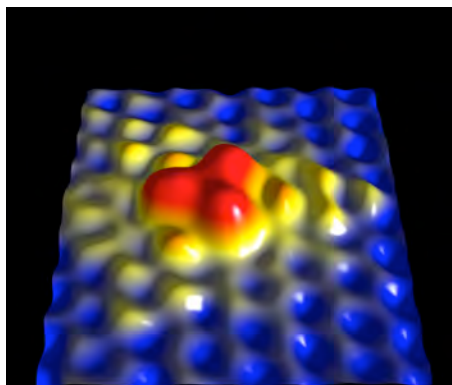


Figure 2. “3D” (Stereographic) STM topography of a single N atom substitution site in a graphene lattice. Note the 3-fold symmetry at the substitution point. Graphene honeycomb structure (blue atoms) re-establishes itself several lattice constants away from the insertion point of the N atom. ($1.6 \times 2.0 \text{ nm}^2$; 0.8V, 0.8 nA, 77 K)

The 3 C atoms (red bumps in Figure 2) adjacent to the nitrogen have their electronic structure most heavily perturbed by the N substitution and hence appear to be elevated by 0.8 \AA . This apparent elevation is likely not a protrusion of the nuclei, but rather represents an increase in the density of states over these atoms adjacent to the N atom. Note that next nearest neighbors (yellow bumps) are also perturbed, but the disturbed electronic structure quickly decays spatially (within a few lattice constants) back to a normal graphene structure (blue atoms). XPS spectra taken on samples cut from the same piece of treated Cu foil confirm the presence of graphitic nitrogen (single site N atom substitution into the graphene lattice). A very small number of substitution sites ($< 1/10$) observed in the STM images are not triangular, and these can be assigned to multiple N atom insertion at the same site.

Using Scanning Tunneling Spectroscopy (STS) it is possible to locate the Dirac point relative to the Fermi level in graphene. In neutral graphene these two features come at the same energy; however in nitrogen substituted graphene grown on a copper foil, inserted N atoms contribute “excess” electrons to the graphene lattice, thereby pushing the Dirac point below the Fermi level. (Electrons go into the unoccupied levels above the Dirac point.) Based on the assumption that the graphene π molecular orbitals are essentially unchanged by dilute N atom substitution, the shift of the Dirac point relative to the Fermi level for N substitution sites indicates that each N atom contributes approximately 0.4 electrons to the graphene lattice.

Summary

CVD grown graphene on copper has been a very fruitful system to study. We summarize here the salient features of the results we have obtained so far:

- ❖ Nitrogen impregnated graphene on Cu foil exhibits a triangular structure with an “apparent” slight elevation of $\sim 0.8 \text{ \AA}$ at N atom substitution sites;
- ❖ Nitrogen substitution results in ~ 0.4 electrons per N atom donated to the graphene lattice (graphene is reduced, or electron rich);
- ❖ Typical N impregnation of graphene on Cu foil shows mostly single site Carbon atom displacement ($\sim 3\text{N}/1000\text{C}$);

❖ Some multi-site C atom displacement is observed (<10% of single site events).

Future Work

In an effort designed to unravel aspects of the mechanisms for chemistry on graphene surfaces, STM and STS will be employed to investigate: (1) the oxidation pathway for single “pristine” graphene sheets grown in an ultra-high vacuum chamber on a copper surface using chemical vapor deposition techniques; (2) the effect of added water on this oxidation process; (3) the changes in oxidation brought about by the controlled introduction of nitrogen atom defects into the graphene sample sheets; (4) the chemistry of graphene flakes grown on cobalt metal surfaces with special emphasis on the size and shape dependence of reactivity; (5) the role of sample edge type (zig-zag or armchair) in determining reactivity; and (6) the mechanism for assembly of graphene flakes from smaller Polycyclic Aromatic Hydrocarbons such as hexabenzocoronene on cobalt, on copper (111), and on copper (100) surfaces.

DOE Publications: (2008-2011)

1. Elena Stolyarova, Daniil Stolyarov, Li Liu, Kwang T. Rim, Yuanbo Zhang, Melinda Han, Mark Hybertsen, Philip Kim and George Flynn, “STM Studies of Ultrathin Graphitic (Graphene) Films on an Insulating Substrate under Ambient Conditions”, *J. Phys. Chem. C*, 112, 6681-6688 (2008)
2. Li Liu, Kwang Taeg Rim, Daejin Eom, Tony Heinz, and George W. Flynn “Direct Observation of Atomic Scale Graphitic Layer Growth,” *Nanoletters*, 8, 1872-1878 (2008)
3. Li Liu, Sunmin Ryu, Michelle R. Tomasik, Elena Stolyarova, Naeyoung Jung, Mark S. Hybertsen, Michael L. Steigerwald, Louis E. Brus, George W. Flynn, “Graphene Oxidation: Thickness-Dependent Etching and Strong Chemical Doping”, *Nanoletters*, 8, 1965-1970 (2008)
4. Boaz Ilan, Gina M. Florio, Mark S. Hybertsen, Bruce J. Berne and George W. Flynn, “Scanning Tunneling Microscopy Images of Alkane Derivatives on Graphite: Role of Electronic Effects”, *Nanoletters*, 8, 3160-3165 (2008)
5. E. Stolyarova, D. Stolyarov, K. Bolotin, S. Ryu, L. Liu, M. Klima, M. Hybertsen, I. Pogorelsky, I. Pavlishin, K. Kusche, J. Hone, P. Kim, L. Brus, H. L. Stormer, V. Yakimenko, G. Flynn, “Observation of Graphene Bubbles and Effective Mass Transport Under Graphene Films”, *Nanoletters*, 9, 332-337 (2009)
6. Daejin Eom, Deborah Prezzi, Kwang T. Rim, Hui Zhou, Michael Lefenfeld, Colin Nuckolls, Mark S. Hybertsen, Tony F. Heinz, and George W. Flynn, “Structure and Electronic Properties of Epitaxial Graphene on Co(0001)”, *Nanoletters*, 9, 2844-2848 (2009)
7. Kwang Taeg Rim, Daejin Eom, Li Liu, Elena Stolyarova, Joan Marie Raitano, Siu-Wei Chan, Maria Flytzani-Stephanopoulos, and George W. Flynn, “Charging and Chemical Reactivity of Gold Nanoparticles and Adatoms on the (111) Surface of Single Crystal Magnetite: A Scanning Tunneling Microscopy/Spectroscopy Study”, *J. Phys. Chem. C*, 113, 10198-10205 (2009)
8. Chun Hung Lui, Li Liu, Kin Fai Mak, George W. Flynn, and Tony F. Heinz, “Ultraflat Graphene”, *Nature*, 462, 339-342 (2009)

9. Sunmin Ryu, Li Liu, Stephane Berciaud, Young-Jun Yu, Haitao Liu, Philip Kim, George W. Flynn and Louis E. Brus, "Atmospheric Oxygen Binding and Hole Doping in Deformed Graphene on a SiO₂ Substrate", *Nano Letters* 10, 4944-4951 (2010)
10. E. Stolyarova, K. Rim, K. Douglass, D. Eom, R. Opila, T. Heinz, A. V. Teplyakov, G. W. Flynn, "STM and XPS Studies of Graphene Films Prepared by Sonication-Assisted Dispersion", *ACS Nano*, 5, 6102-6108 (2011)
11. Liuyan Zhao, Kwang Taeg Rim, Hui Zhou, Rui He, Tony F. Heinz, Aron Pinczuk, George W. Flynn, Abhay N. Pasupathy, "Influence of Copper Crystal Surface on the CVD Growth of Large Area Monolayer Graphene", *Solid State Communications*, 151, 509-513 (2011)
12. George W. Flynn, "The Dawning of the Age of Graphene", *J. Chem. Phys.* 135, 050901-1-8 (2011)
13. L. Zhao, R. He, K. T. Rim, K. S. Kim, H. Zhou, C. Gutiérrez, S. Chockalingam, C. Arguello, T. Palova, T. Schiros, D. Nordlund, M.S. Hybertsen, D. R. Reichman, T. F. Heinz, P. Kim, A. Pinczuk, G. W. Flynn, A. N. Pasupathy, "Visualizing Individual Nitrogen Dopants in Monolayer Graphene", *Science* 333, 999-1003 (2011)
14. Li Liu, Zheyuan Chen, Lei Wang, James Hone, Louis E. Brus, George W. Flynn, "Slow Gold Add-atom Diffusion on Graphene: Effect of Silicon Dioxide and Boron Nitride Substrates", **in preparation**
15. Kwang Taeg Rim, Daejin Eom, Siu-Wai Chan, Maria Flytzani-Stephanopoulos, and George W. Flynn, "Scanning Tunneling Microscopy Study of Water Adsorption on the Reduced Surface of a Natural Single Hematite α -Fe₂O₃ Crystal", **in preparation**
16. Daejin Eom, Deborah Prezzi, Kwang T. Rim, Hui Zhou, Michael Lefenfeld, Shengxiong Xiao, Colin Nuckolls, Mark S. Hybertsen, Tony F. Heinz, and George W. Flynn, "Structure, Stability and Electronic Properties of the Edges of Graphene Nanoislands on Co(0001)", **in preparation.**

Quantitative Imaging Diagnostics for Reacting Flows

Jonathan H. Frank
Combustion Research Facility
Sandia National Laboratories
Livermore, CA 94551-0969
jhfrank@sandia.gov

Program Scope

The primary objective of this project is the development and application of quantitative laser-based imaging diagnostics for studying the interactions of fluid dynamics and chemical reactions in reacting flows. Imaging diagnostics provide temporally and spatially resolved measurements of species, temperature, and velocity distributions over a wide range of length scales. Multi-dimensional measurements are necessary to determine spatial correlations, scalar and velocity gradients, flame orientation, curvature, and connectivity. Current efforts in the Advanced Imaging Laboratory focus on studying the detailed structure of both isolated flow-flame interactions and turbulent flames. The investigation of flow-flame interactions is of fundamental importance in understanding the coupling between transport and chemistry in turbulent flames. These studies require the development of imaging diagnostic techniques to measure key species in the hydrocarbon-chemistry mechanism as well as mixture fraction, rates of reaction and dissipation. Recent studies on flow-flame interactions have focused on localized extinction and re-ignition as well as effects of stratification. Diagnostic development efforts are focused on techniques that are applicable to a broader range of combustion conditions, including combustion of more complex fuels. We are also in the process of developing diagnostic capabilities for probing the temporal evolution of turbulent flames using high-repetition rate imaging techniques.

Recent Progress

Effects of reactant-product stratification in turbulent premixed combustion

The effects of stratification between reactant and product equivalence ratios in turbulent premixed combustion are not well understood, despite their relevance to practical combustion systems, where stratification can be produced by intense turbulent mixing and gas recirculation. The effects of reactant-product stratification on the perturbation of local reaction rates of $\text{CO}+\text{OH}$ and $\text{CH}_2\text{O}+\text{OH}$ in turbulent premixed counterflow flames were studied in collaboration with Alessandro Gomez (Yale Univ.) and Bruno Coriton (Sandia Postdoc). These effects depend on the particular reactant and product mixtures as well as the proximity between the turbulent flame front and the stream of combustion products. Figure 1a shows the burner configuration and illustrates the measurements of the interaction distances that were performed using OH-LIF signals. The degree of interaction undergoes large fluctuations and depends on the distance Δ_f between the instantaneous flame front and the interface between the lower stream of combustion products and the products that are formed in the vicinity of the turbulent flame front. Reaction rate imaging uses simultaneous laser-induced fluorescence measurements of two species to probe the relative reaction rates along the turbulent premixed flame front as well as the interaction distance Δ_f .

In Fig. 1b, the conditional probability density functions (PDFs) for peak reaction rate of CO+OH show the effects of reactant-product stratification for interaction distances greater than and less than 1.75 mm, which was identified as a critical interaction length for the flames considered in this study. For all three reactant equivalence ratios ($\phi_u = 0.6, 0.8$ and 1.0), the effect of varying the product stream equivalence ratio from $\phi_b = 1$ to $\phi_b = 0.7$ was minimal as long as the interaction length was greater than 1.75 mm. In contrast, all of the reaction rate PDFs are shifted to lower values for shorter interaction lengths ($\Delta_f < 1.75$ mm), indicating the reduction of these reaction rates by interaction with the lean product stream. These studies provide insight into the conditions for which product stratification perturbs the local flame front. Results have implications for the length scales that must be considered when modeling turbulent stratified premixed combustion.

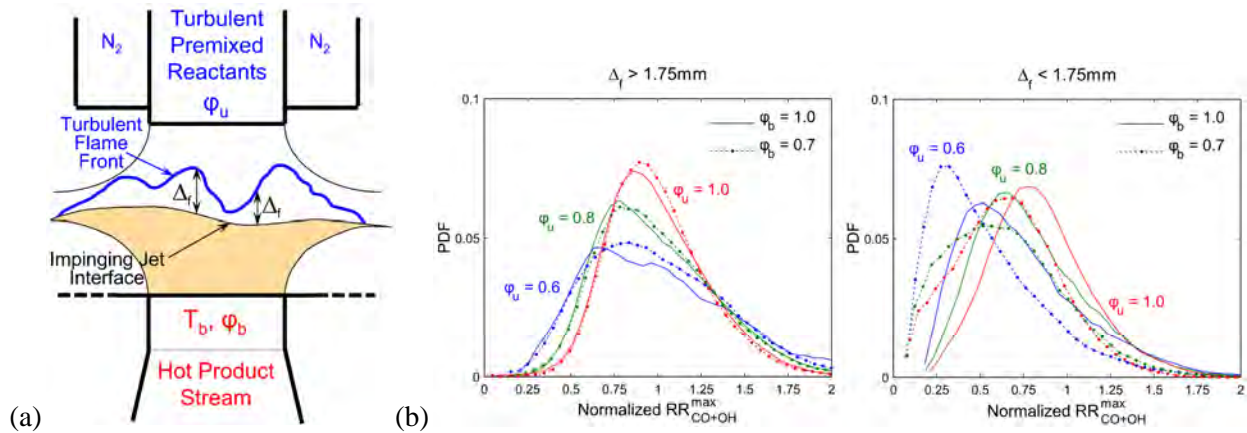


Figure 1: (a) Schematic diagram of a turbulent premixed counterflow flame with a reactant mixture of equivalence ratio ϕ_u and a stream of combustion products at equivalence ratio ϕ_b and temperature T_b . The degree of interaction between the turbulent flame front and the stream of combustion products depends on the interaction distance Δ_f between the instantaneous flame front and the interface between the lower stream of combustion products and the products formed in the vicinity of the turbulent flame front. (b) Effect of interaction distance on probability density functions of the normalized CO+OH reaction rate (RR_{CO+OH}) for different reactant-product stream stratification.

Soft x-ray absorption spectroscopy of flames

Soft x-ray imaging techniques for combustion could provide in situ measurements of key quantities for flame studies, such as mixture fraction, under conditions that are not amenable to traditional diagnostic techniques. X-rays promise several advantages over UV radiation, which is commonly used to probe flame species using valence spectroscopy. First, x-ray absorption is not subject to temperature-dependent variations in Boltzmann fraction populations. Second, core-level spectroscopy probes all carbon containing molecules, providing a spatial map of carbon concentration. We recently initiated experimental studies of soft x-ray absorption spectroscopy in flames at the Molecular Science Beamline of the Advanced Light Source (ALS) synchrotron of LBNL. Previously, in situ x-ray measurements in flames focused on studies of particle/soot detection using hard x-rays. Our new diagnostic technique, soft x-ray absorption tomography, will enable imaging of flame structure and mixture fraction in the gas phase.

We have demonstrated the promise of soft x-ray absorption measurements in flames in a proof-of-concept experiment that was performed in collaboration with David Osborn (Sandia), Hendrik Bluhm (LBNL), and Andrey Shavorskiy (LBNL). Measurements were performed in the carbon K-edge region of the absorption spectrum in both a low-pressure cell of pure non-reacting gases and a laminar axisymmetric non-premixed methane flame with helium dilution, shown in Fig 1. The non-reacting gas experiments established a set of reference spectra that serve as basis functions for determining concentrations of CO, CH₄, and CO₂ in a flame. A preliminary example of fitting the near-edge spectral features from an absorption spectrum in the flame is shown in Fig. 1. This spectrum was measured along a beam path that traversed the reaction zone of the flame and the unreacted fuel stream near the jet exit. The near-edge spectral features in the flame are fit to a linear superposition of the basis functions, demonstrating that near-edge features could be used to determine species concentrations. The far-edge region, which is less sensitive to differences between species, may be useful for mixture fraction measurements.

Results from this experiment show promise for quantitative absorption tomography and spectroscopy in flames. Development of this new diagnostic capability would enable key measurements of flow-flame interactions that cannot be accomplished with existing techniques. Plans for developing this capability involve a progression from diagnostic technique development in steady low-pressure methane flames to detailed studies of transient flow-flame interactions with increasingly complex fuels. Experimental results will be closely coupled with Habib Najm's (Sandia) numerical simulations and uncertainty quantification techniques to develop computations that accurately capture the coupling between transport and combustion chemistry.

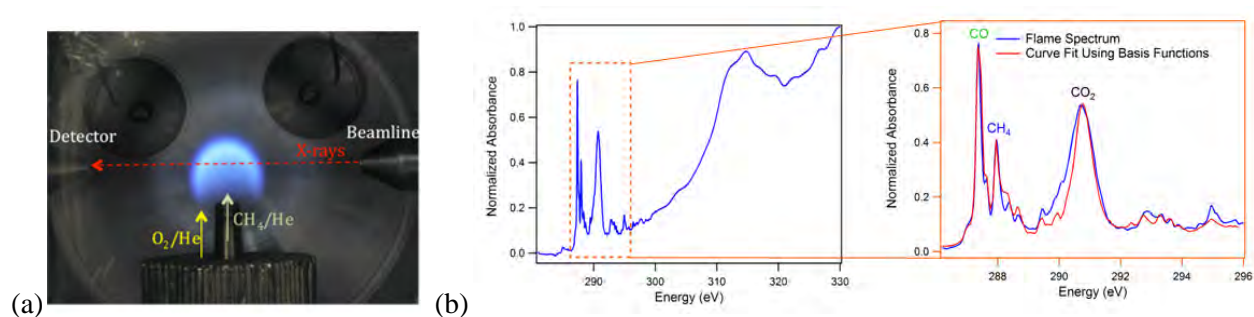


Figure 2: (a) Photograph of the low-pressure non-premixed methane jet flame during a proof-of-principle experiment at the ALS Molecular Science Beamline. (b) Preliminary absorption spectrum recorded along a path through the flame that included combustion products, intermediate species, and unburned fuel near the burner centerline. A linear superposition of measured basis functions for CO, CH₄, and CO₂ are fit to the near-edge spectral features.

Future Plans

The development of a high-repetition rate imaging facility with simultaneous scalar and velocity measurements remains a high priority in our research plan. As new capabilities are added, we will use them to study the dynamics of flow-flame interactions in turbulent premixed, non-premixed, and stratified modes of combustion. Our efforts to build this capability at Sandia continue to be enhanced through collaborations with other laboratories that have invested in high-repetition rate imaging equipment. Ongoing collaborations focus on studies of flame propagation dynamics in turbulent jet flows.

We plan to expand our ability to use a noble gas as a chemically inert tracer for mixing studies to a broad range of combustion environments. Most previous mixture fraction imaging techniques have used combined measurements of chemically reactive species and temperature to construct a conserved scalar. The advantage of this new approach is that the tracer gas remains chemically inert in a wide range of conditions. We plan to refine this diagnostic technique for a broader range of flame conditions and fuel mixtures.

We plan to continue companion experimental and computational studies of the coupling between transport and chemistry in isolated flow-flame interactions in collaboration with Jackie Chen (Sandia). We are investigating the ability of different chemical mechanisms and transport models to capture the wide range of thermochemical states involved in extinction and re-ignition. Ongoing studies focus on oxygenated fuels, such as dimethyl ether.

We are planning a detailed series of studies on turbulent jet flames with varying amounts of localized extinction and different fuel mixtures. The first phase of this effort will focus on a series of piloted partially premixed dimethyl ether/air jet flames that we have identified as target flames for the TNF Workshop. Experiments will be closely coupled with Joe Oefelein's (Sandia) efforts to develop high-fidelity large eddy simulations (LES) for turbulent combustion. This project will expand our ongoing collaboration in coupling imaging measurements with LES to advance numerical simulation capabilities and to develop new methods for comparing simulations and experiments.

BES-supported publications and submitted journal articles (2010-present)

- U.D. Lee, C.S. Yoo, J.H. Chen, J.H. Frank, "Effect of NO on extinction and re-ignition of vortex-perturbed hydrogen flames," *Combust. Flame* **157**, 217-229 (2010).
- J.H. Frank and S.A. Kaiser, "High-resolution imaging of turbulence structures in jet flames and non-reacting jets with laser Rayleigh scattering," *Exp. Fluids* **49**, 823-837 (2010).
- J.H. Frank, S.A. Kaiser, J.C. Oefelein, "Analysis of scalar mixing dynamics in LES using high-resolution imaging of laser Rayleigh scattering in turbulent non-reacting jets and non-premixed jet flames," *Proc. Combust. Inst.* **33**, 1373-1381 (2011).
- A.G. Hsu, V. Narayanaswamy, N.T. Clemens, J.H. Frank, "Mixture fraction imaging in turbulent non-premixed flames with two-photon LIF of krypton," *Proc. Combust. Inst.* **33**, 759-766 (2011).
- B. Böhm, J.H. Frank, A. Dreizler, "Temperature and mixing field measurements in stratified lean premixed turbulent flames," *Proc. Combust. Inst.* **33**, 1583-1590 (2011).
- A.M. Steinberg, I. Boxx, C.M. Arndt, J.H. Frank, W. Meier, "Experimental study of flame-hole re-ignition mechanism in a turbulent non-premixed jet flame using sustained multi-kHz PIV and crossed-plane OH PLIF," *Proc. Combust. Inst.* **33**, 1663-1672 (2011).
- B. Coriton, J.H. Frank, A.G. Hsu, M.D. Smooke, A. Gomez, "Effect of quenching of the oxidation layer in highly turbulent counterflow premixed flames," *Proc. Combust. Inst.* **33**, 1647-1654 (2011).
- S.A. Kaiser and J.H. Frank, "The effects of laser-sheet thickness on dissipation measurements in turbulent non-reacting jets and jet flames," *Meas. Sci. Technol.*, **22**, 045403 (2011).
- B. Coriton, J.H. Frank, A. Gomez, "Interaction of turbulent premixed flames with non-adiabatic counterflowing combustion products," *Proc. Combust. Inst.* **34**, submitted.

MECHANISM AND DETAILED MODELING OF SOOT FORMATION

Principal Investigator: Michael Frenklach
Department of Mechanical Engineering
The University of California
Berkeley, CA 94720-1740
Phone: (510) 643-1676; E-mail: myf@me.berkeley.edu

Project Scope: Soot formation is one of the key environmental problems associated with the operation of practical combustion devices. Mechanistic understanding of the phenomenon has advanced significantly in recent years, shifting the focus of discussion from conceptual possibilities to specifics of the reaction kinetics. However, along with the success of initial models comes the realization of their shortcomings. This project focuses on fundamental aspects of physical and chemical phenomena critical to the development of predictive models of soot formation in the combustion of hydrocarbon fuels, as well as on computational techniques for the development of predictive reaction models and their economical application to CFD simulations. This work includes theoretical and numerical studies of gas-phase chemistry of gaseous soot particle precursors, soot particle surface processes, particle aggregation into fractal objects, development of economical numerical approaches to reaction kinetics, and construction of a framework for predictive models and modeling.

Recent Progress:

Thermal Decomposition of Graphene Zigzag and Armchair Oxyradicals (with D. E. Edwards, X. You, D. Yu. Zubarev, and W. A. Lester, Jr.)

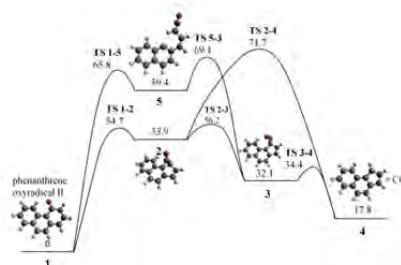
Chemical evolution of graphene edges is one of the key processes in the formation, growth, and oxidation of soot and its aromatic precursors. Assuming that the soot particle surface is comprised of molecular aromatic sites (i.e., graphene edges) and invoking chemical similarity, it was postulated earlier that soot surface reactions can be thought of as chemically analogous reactions of polycyclic aromatic hydrocarbons (PAHs). Growth reactions, those increasing PAH size by reactions with gaseous species, primarily acetylene, received immediate and continuing attention. However, it was also recognized that the chemical analogy was not sufficient to describe reactions taking place at the surface and steric effects, neighboring sites, and substrate size must also be considered. The latter realization increased substantially the number of possible elementary reactions; for instance, the latest detailed graphene-edge growth mechanism is composed of 42 elementary reactions (Refs 1,4,6 in Publications).

The oxidation of PAHs and soot surfaces has received lesser attention. The initial detailed models of soot oxidation invoked two principal steps: an elementary reaction of a surface radical with O_2 and an atomistically-unresolved attack of OH on a generic surface site. Both reactions were assumed to remove one C atom per O atom of the gaseous reactant and both assumed to form a “pristine” surface site ($C_{\text{surface}}-H$ or $C_{\text{surface}}\bullet$) as the substrate product of oxidation. The former reaction was modeled following the postulate of chemical similarity by phenyl + O_2 . The oxidation by OH was described using the collision efficiency determined in flame studies. This oxidation model, with varying values of the rate coefficients, has been widely adopted in modeling studies.

Considering the knowledge gained with growth reactions, where the reaction chemistry of larger aromatic edges turned out to be much richer than that of the analogous small aromatic species, there is clearly a need for similar exploration of possible pathways for oxidation. We began this process with the examination of the thermodynamic stability of the key intermediates, graphene-edge oxyradicals,

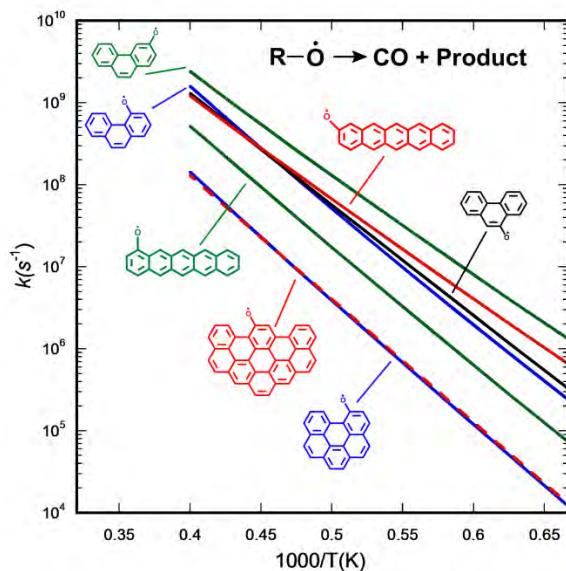
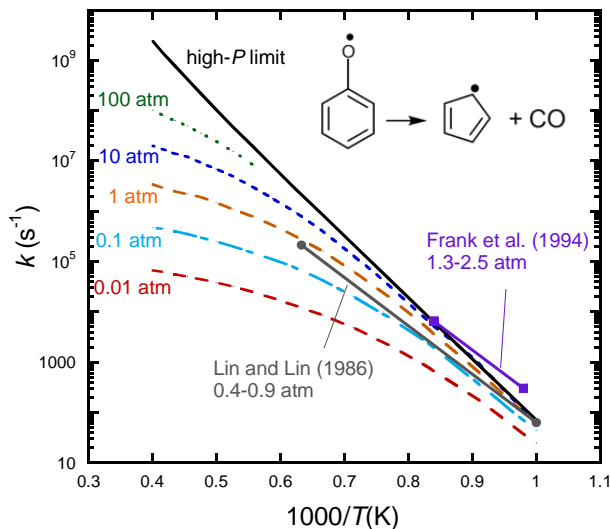
located at both zigzag and armchair sites (Refs 2,3,7,11 in Publications). It turns out that thermodynamic stability varies substantially at different chemisorbed O sites, and this variability can be explained and correlated with substrate aromaticity. We then turned to our next objective, the kinetics of graphene oxyradical decomposition. In a just-completed study (Ref 8 in Publications), we examined the decomposition of oxyradicals on a *zigzag* edge of graphene. In the past year, we initiated and completed the analysis of decomposition rates of graphene oxyradicals whose oxygen atom is located at *armchair* sites and compared these rates to those at zigzag sites (Ref 12 in Publications). The results indicated that the rate of decomposition varies with the location of the chemisorbed O site on the graphene edge.

Density functional theory (DFT) was employed to calculate potential energy surfaces of all stable species and transition states for the oxyradical systems. Geometry optimization and vibrational frequency calculations were performed to identify all stationary points on the reaction pathways using the B3LYP hybrid functional and a 6-311G(d,p) basis set. A typical potential-energy diagram is shown on the right.



The rate coefficients of the thermally-activated reaction systems were computed with the MultiWell suite of codes using the DFT results. All internal rotors were treated as 1-D hindered rotors. Reaction rates were computed at temperatures ranging from 1500 to 2500 K and pressures from 0.01 to 10 atm. For each set of initial conditions, the number of stochastic trials was varied from 10^4 to 10^9 to keep statistical error below 5 %. The thermal decomposition rate coefficients were derived from the exponential decay of the reactant molecule after a period of initial relaxation.

For the zigzag sites, we examined decomposition of pentacene oxyradicals, with the oxygen atom chemisorbed at four different positions. To study the decomposition of armchair edge oxyradicals, five molecules were selected, those shown in the right figure below. For comparison with literature, we also included decomposition of phenoxy, whose kinetics has been studied both experimentally and theoretically in the past, and our computed results are within the uncertainty ranges of the measured values (left figure below). The latter agreement can serve as validation of the present method and procedures.



In all cases studied, the computed decomposition rates are both temperature and pressure dependent. The extent of the pressure dependence, especially at higher temperatures, turned out to be substantial even for the largest molecular substrate studied, an eleven-ring PAH. Also noteworthy is the influence of substrate size on computed rates; the effect was clearly pronounced in going from three- to six-ring aromatics, yet seemed to level off for larger systems as found for six- to eleven-ring aromatics.

The computed values of the decomposition rate coefficients showed a clear dependence on the location of the oxyradical on the graphene edge. Applying the concept of “free edges” for polycyclic aromatics (Ref 8 in Publications), the trends obtained for the computed decomposition rates with substrate molecular structure could be rationalized as follows. Oxyradicals with the same number of free edges decompose at similar rates. Oxyradicals with two free edges decompose at a faster rate than those with one free edge.

The kinetic stability of graphene-edge oxyradicals, both zigzag and armchair, was shown to be correlated with change in aromaticity during the initial, typically rate-controlling, step of oxyradical decomposition. This correlation, together with the established similar scaling for thermodynamic stability, could lead to practical rules for predicting oxidation rate coefficients for arbitrary size and shape aromatics, thereby supplementing and enhancing models of soot oxidation.

The analysis showed that the corner zigzag and armchair site oxyradicals decompose the fastest. This implies that for an arbitrary shaped PAH, oxidation should predominantly remove armchair and corner-zigzag sites, leaving resistant-to-oxidation inner zigzag sites essentially intact. Considering that the growth of both armchair and zigzag edges proceed at effectively the same rate, we expect to find proliferation of zigzag-edge surfaces on soot particles formed in flame environments.

Process informatics tools for predictive modeling: Hydrogen combustion (with X. You and A. Packard)

To develop reliably predictive reaction models for complex reaction systems requires integration of large amounts of theoretical, computational, and experimental data collected by numerous researchers and often from different disciplines. The integration entails assessment of the consistency of the data, validation of models, and quantification of uncertainties for model predictions. The problem complexity and the volume and heterogeneity of the data call for a system approach, which we call Process Informatics Model (PrIME). The objective is not just to automate a single computation, but to automate the entire process from new data availability to improved predictions and accuracy, to identification of which experiments to perform next.

During the past year, we completed the developments that demonstrate the above for the hydrogen combustion system. Modeling and analysis tools were built to bridge the PrIME Data infrastructure with DataCollaboration, a framework designed to make inferences from experimental observations in the context of an underlying model. The developed tools were integrated with the PrIME Workflow Application, which allows users to create and run drag-and-drop applications on the fly. Organizing the data, linking the data to scientific methods, and automating the analysis not only speed up the analysis but, more importantly, offer new venues of scientific inquiry, such as evaluating consistency of heterogeneous data records, making uncertainty-quantified predictions, quantifying the contribution of newly obtained or even hypothetical data to the question of interest, or testing similar “what-if” scenarios. The developed system is currently operational for the chemical kinetics of hydrogen combustion. (Ref 10 in Publications).

Future Plans

Graphene Layer Growth and Oxidation Chemistry: We will continue exploration of reactions on graphene edges. One of the immediate goals is to investigate oxidation of PAH edge sites by OH, the principal oxidant of soot particles. The work will be performed in collaboration with William Lester's group, performing DFT analysis of the reaction systems and then QMC analysis of the most critical reaction steps identified in the prior DFT studies. For every reaction system, a complete set of rate coefficients will be calculated using master-equation modeling.

Graphene Layer Evolution: We will continue exploration of the evolution of graphene sheets through our detailed kinetic Monte-Carlo (KMC) approach. Now that we have established the thermodynamic stability of oxyradicals and the kinetics of their decomposition, we will start adding oxidation reaction steps to the growth mechanism and performing KMC simulations to examine the influence of the oxidation steps on the patterns of graphene-edge evolution.

Methodology of Predictive Models and Modeling: One of the immediate objectives is to undertake a rigorous comparison between our deterministic approach to uncertainty quantification, DataCollaboration, with the fully-resolved Bayesian method. We will continue collaborative studies with Phillip Westmoreland's group and his colleagues on the development and automation of the UQ-based framework of ALS data analysis. We will continue the efforts on extending further the PrIME framework for predictive modeling.

DOE-BES Supported Publications (2010-2012)

1. "Detailed kinetic Monte-Carlo simulations of graphene-edge growth," R. Whitesides and M. Frenklach, *J. Phys. Chem. A* **114**, 689-703 (2010), Feature Article.
2. "Polyaromatic hydrocarbon oxyradical stability," D. Yu. Zubarev, N. Robertson, D. Domin, J. McClean, J. H. Wang, W. A. Lester, Jr., R. Whitesides, X. You, M. Frenklach, *J. At. Mol. Sci.* **1**, 48-53 (2010).
3. "Local electronic structure and stability of pentacene oxyradicals," D. Y. Zubarev, N. Robertson, D. Domin, J. McClean, J. Wang, W.A. Lester, Jr., R. Whitesides, X. You, and M. Frenklach, *J. Phys. Chem. C* **114**, 5429 (2010).
4. "Extended simulations of graphene growth with updated rate coefficients," R. Whitesides, X. You, and M. Frenklach, Spring Technical Meeting, Western States Section of the Combustion Institute, Boulder, CO, March 22-23, 2010, Paper No. 10S-22.
5. "A diffusion Monte Carlo study of the O-H bond dissociation of phenol," J. Wang, D. Domin, B. Austin, D. Zubarev, J. McClean, M. Frenklach, T. Cui, and W. A. Lester, Jr., *J. Phys. Chem. A* **114**, 9832-9835 (2010).
6. "Bay-capping reactions: Kinetics and influence on graphene-edge growth," X. You, R. Whitesides, D. Zubarev, W. A. Lester, Jr., and M. Frenklach, *Proc. Combust. Inst.* **33**, 685-692 (2011).
7. "Patterns of local aromaticity in graphene oxyradicals," D. Yu. Zubarev, X. You, J. McClean, W. A. Lester, Jr., and M. Frenklach, *J. Mater. Chem.* **21**, 3404-3409 (2011).
8. "Thermal decomposition of pentacene oxyradicals," X. You, D. Yu. Zubarev, W. A. Lester, Jr., and M. Frenklach, *J. Phys. Chem. A* **115**, 14184-14190 (2011).
9. "Uncertainty-quantified analysis of complex experimental data," D. R. Yeates, W. Li, P. R. Westmoreland, T. Russi, A. Packard, and M. Frenklach, *Proceedings of the 7th U.S. National Combustion Meeting*, Atlanta, GA, 2011, Paper No. 2D01.
10. "Process informatics tools for predictive modeling: Hydrogen combustion," X. You, A. Packard, and M. Frenklach, *Int. J. Chem. Kinet.* **44**, 101-116 (2012).
11. "Delocalization effects in pristine and oxidized graphene substrates," D. Yu. Zubarev, X. You, M. Frenklach, and W. A. Lester, Jr., in *Advances in the Theory of Quantum Systems in Chemistry and Physics* (P. E. Hoggan, E. J. Brändas, J. Maruani, P. Piecuch, and G. Delgado-Barrio, Eds.), Progress in Theoretical Chemistry and Physics, Vol. 22, Springer, Dordrecht, 2012, Chapter 29, pp. 553-569.
12. "Thermal decomposition of graphene armchair oxyradical," D. E. Edwards, X. You, D. Yu. Zubarev, W. A. Lester, Jr., and M. Frenklach, accepted to the 34th Symp. (Int.) Combust., 2012.

Computer-Aided Construction of Chemical Kinetic Models

William H. Green
Department of Chemical Engineering, M.I.T.
Cambridge, MA 02139
whgreen@mit.edu

I. Program Scope

The combustion chemistry of even simple fuels can be extremely complex, involving hundreds or thousands of kinetically significant species. The most reasonable way to deal with this complexity is to use a computer not only to numerically solve the kinetic model, but also to construct the kinetic model in the first place. Because these large models contain so many numerical parameters (e.g. rate coefficients, thermochemistry) one never has sufficient data to uniquely determine them all experimentally. Instead one must work in “predictive” mode, using theoretical values for many of the numbers in the model, and as appropriate refining the most sensitive numbers through experiments. Predictive chemical kinetics is exactly what is needed for computer-aided design of combustion systems based on proposed alternative fuels, particularly for early assessment of the value and viability of proposed new fuels. Our research effort is aimed at making accurate predictive chemical kinetics practical; this is a challenging goal which necessarily includes a range of science advances. Our research spans a wide range from quantum chemical calculations on individual molecules and elementary-step reactions, through the development of improved rate/thermo estimation procedures, the creation of algorithms and software for constructing and solving the simulations, the invention of methods for model-reduction while maintaining error control, through comparisons with experiment. Many of the parameters in the models are derived from quantum chemistry, and the models are compared with experimental data measured in our lab or in collaboration with others.

II. Recent Progress

A. Methodology for Computer-Aided Kinetic Modeling

The main focus of this research project continues to be the development of methodology for constructing, reducing, and solving combustion simulations, and increasing the range of systems which can be automatically modeled. During the past year we have published a paper comparing different methods for computing $k(T,P)$ from the master equations, to select a suitable method for generating large mechanisms automatically.[8] We are now routinely computing thousands of chemically-activated reactions as we construct kinetic models for alternative fuels using the Reaction Mechanism Generator (RMG).

We continue to distribute the mechanism construction software to many research groups, and to train and support the new users. In the past year researchers from Sandia CRF, LLNL, NJIT, Belgium, Brazil, Canada, France, Sweden, and Turkey have visited our group for training in how to use the RMG software. We are currently arranging visits by researchers from UCSD and Germany. We are also collaborating with researchers at Oak Ridge to parallelize the mechanism generation software.

We also continuously add new chemistry to RMG (more on this below). One important advance this year was the inclusion of organosulfur reactions and functional groups (previously RMG was limited to $C_xH_yO_z$ molecules). We are currently adding nitrogen.

RMG applications funded separately

The work described above which is funded by this grant is heavily leveraged by larger application-oriented projects funded separately, which often provide test cases for improvements to RMG, and occasionally add some features to RMG.

The largest and most important of these related projects is the DOE Combustion Energy Frontier Research Center, which funded development of models for all four isomers of butanol (and many

experimental tests of the predictions of these models by other researchers, and many quantum chemistry calculations by our collaborators or by us which have been incorporated into the RMG database).[i] That project has provided excellent comprehensive test cases of the capabilities and accuracy of RMG, and has also led to the identification and correction of flaws in some of RMG's rate and thermochemistry estimates.

We also have a smaller separate DOE-funded collaboration with Craig Taatjes and researchers at Aachen, building kinetic models for the chemistry of methylated pentanones (proposed alternative fuels synthesized from biomass by some fungi), and testing the RMG-built model against a variety of experiments.

With separate industrial funding, the new capability of RMG to handle sulfur chemistry was tested by building models for fuel desulfurization in supercritical water, and comparisons with experimental data on those systems.

One RMG feature which was added largely with separate funding was the ability to model liquid phase oxidation using RMG (that industrial sponsor's interest was an industrial application to diesel injector fouling). We are about to submit a manuscript describing the method by which RMG automatically estimates solvent effects on both the thermochemistry and the rate coefficients, and demonstrating applications to liquid-phase autoxidation.

Another important feature added largely with outside funding was the ability to estimate the 3-d structure of fused-ring molecules, and use these as the initial guess geometries in automatically-spawned thermochemistry calculations. We have just submitted the manuscript describing this new capability.[11] This has allowed us to model the pyrolysis and combustion of the synthetic jet fuel JP-10 with much more fidelity than would be possible using Benson-type estimates of the thermochemistry.[ii]

With separate funding we improved the numerical solvers to make it practical to work with and test the very large chemistry models we construct. We have developed a strained flame solver which can handle much larger reaction mechanisms than the CHEMKIN solvers PREMIX and OPPDIFF. With separate funding we have also implemented error-controlled adaptive chemistry model-reduction into the engine simulator KIVA, using GPUs to accelerate the numerics.[iii,iv]

B. Quantum Calculations of Reaction Rates

In collaboration with A.M. Dean and H.-H. Carstensen, we have performed calculations on substituted allylic radicals plus O₂, considering dozens of isomerization – dissociation channels for the initially-formed unsaturated peroxy radicals. The barriers for intramolecular H abstraction across the double bond were lower than literature expectations, but at combustion-relevant temperatures even these low-barrier isomerizations were computed to be unimportant relative to the very fast reverse reaction back to an allylic radical + O₂. We are now completing this manuscript.

In collaboration with Alexander Mebel, we computed the rates for C₆H₅ + C₃H₆. Some of this forms allyl directly, but much of it reacts via an adduct. We have computed the subsequent chemically-activated isomerizations and dissociations, and compared them with Ralf Kaiser's experimental data in a jointly authored manuscript.[9,10]

In collaboration with Piotr Piecuch (whose work was funded by the BES Chemical Physics program), and leveraging separate funding from the Navy and Aerodyne to MIT, we performed high level calculations on the intramolecular disproportionation reactions of the biradicals formed by unimolecular ring-opening. Most conventional methods say these reactions have significant barriers (e.g. 7 kcal/mole barrier is reported in the literature for disproportionation of the biradical derived from JP-10), but our high level calculations show that these reactions are actually barrierless.[ii] Based on these results we have significantly revised the rate estimation rules for all intramolecular disproportionations used by RMG.

III. Future Work

A. Methodology and Rate Estimation

Most of the difficulty in predictive kinetics has to do with estimating the thousands of rate coefficients involved. We are developing more robust group-additivity methods for making initial estimates on new systems, and extensively revising and improving the estimates for reactions of aromatics and of NO_x / RNO_x species.

In the course of the numeric work reported above we invented a balanced operator splitting method with significant advantages over the conventional Strang Splitting [v] used to solve the partial differential equations encountered in flame simulations. We are about to submit a manuscript co-authored by Strang proving the accuracy and numerical stability of our new Balanced and Rebalanced Splitting.[vi]

We continue to make progress in automated mechanism reduction, to facilitate the use of detailed fuel chemistry models in reacting flow simulations. Our current model reduction work supported by this program is focused on clarifying the mathematical relationships between competing model-reduction methods, providing an equal basis for comparisons; we have found that many ostensibly different methods have identical mathematical form, and we have written this up for submission to *Combustion & Flame*. [vii] Additional manuscripts in preparation prove bounds on the errors associated with mechanism reduction.

As we push to higher molecular weight fuels, we are running into the limits of our current serial model-construction algorithm. We will parallelize the model construction process, and also develop new methods that naturally apply tighter tolerances to the sensitive chain-branching reactions than to the ordinary propagation reactions. We also are developing improved tools for handling the very large kinetic models produced, and to simplify the process of comparing their predictions with large experimental data sets measured e.g. at the advanced light source.

B. Individual Reactions: Quantum Chemistry

We are continually studying new species and reactions important for the fuel systems we are studying. In addition to the systems mentioned above, we are putting particular effort into understanding low temperature ignition chemistry at conditions relevant to the octane and cetane tests, and to HCCI engine knock. We have discovered several new reaction channels for hydroperoxides which explain some of the unexpected species observed in jet-stirred reactor experiments, and which also affect the ignition delay. As we get the CHO ignition chemistry firmly under control, we will explore the effects of nitrogen species such as NO_x and the cetane improver RONO₂ on ignition.

In the course of developing large kinetic models this year, we have identified more than 100 rate coefficients in the literature which significantly differ from the current estimates in RMG, indicating that either the RMG estimate or the literature values (or both) are incorrect. We have also encountered several cases where there are large discrepancies in the thermochemistry. In many cases the discrepancies can be resolved by a high-accuracy quantum chemistry calculation, and we have resolved about two dozen of these so far. We are writing up these cases for the archival literature as quickly as we can, and also making the corrections in the RMG database.

We have recently run into several cases where the conventional hindered rotor treatment gives partition functions off by an order of magnitude or more. Truhlar has recently invented a method for handling these cases which is very accurate and effective for systems with 3 or 4 coupled rotors [viii], but which does not scale well for transition states with a large number of coupled rotors. We will explore methods to reduce the cost of the calculations for these multirotor cases without losing accuracy.

IV. References

- i. N. Hansen, M.R. Harper, and W.H. Green, "High-Temperature Oxidation Chemistry of n-butanol: Experiments in Low-Pressure Pre-Mixed Flames and Detailed Modeling", *Phys. Chem. Chem. Phys.* **13**, 20262 - 20274 (2011).

- ii. Greg Magoon, Jorge Aguilera-Iparraguirre, William H. Green, Jesse J. Lutz, Piotr Piecuch, Hsi-Wu Wong, and O.O. Oluwole, "Detailed Chemical Kinetic Modeling of JP-10 (exo-tetrahydrodicyclopentadiene) High Temperature Oxidation: Exploring the Role of Biradical Species in Initial Decomposition Steps", *International Journal of Chemical Kinetics* **44**, 179-193 (2012).
- iii. Y. Shi, W.H. Green, H.-W. Wong, and O.O. Oluwole, "Accelerating multi-dimensional combustion simulations using GPU and hybrid explicit/implicit ODE integration", *Combust. Flame* (2012 submitted).
- iv. O.O. Oluwole, Yu Shi, Hsi-Wu Wong, and William H. Green, "An Exact-Steady-state Adaptive Chemistry method for combustion simulations: combining the efficiency of reduced models and the accuracy of the full model", *Combustion & Flame* (2012 accepted)
- v. G. Strang, *SIAM J. Numer. Anal.* **5**, 506-517 (1968).
- vi. R. Speth, W.H. Green, S. MacNamara, and G. Strang, "Balanced Splitting and Rebalanced Splitting", to be submitted to *SIAM Journal on Numerical Analysis*
- vii. G.M. Oxberry, P.I. Barton, and W.H. Green, "Three Representations of Projection-Based Model Reduction in Combustion", to be submitted to *Combustion & Flame*.
- viii. X. Xu, E. Papajak, J. Zheng, and D. G. Truhlar, *Phys. Chem. Chem. Phys.* **14**, 4204-4216 (2012).

V. Publications and submitted journal articles supported by this project 2010-2012

1. Amrit Jalan, Robert Ashcraft, Richard H. West, and William H. Green, "Predicting Solvation Energies for Kinetic Modeling", *Ann. Rep. Progress of Chemistry, Section C*, **106**, 1-49 (2010).
2. Sandeep Sharma, Michael R. Harper, and William H. Green, "Modeling of 1,3-hexadiene, 2,4-hexadiene and 1,4-hexadiene doped methane flames: Flame modeling, Benzene and Styrene formation", *Combustion & Flame* **157**, 1331-1345 (2010).
3. Sandeep Sharma, Sumathy Raman, and William H. Green, "Intramolecular Hydrogen Migration in Alkylperoxy and Hydroperoxyalkylperoxy Radicals: Accurate Treatment of Hindered Rotors", *J. Phys. Chem. A* **114**, 5689-5701 (2010).
4. G.R. Magoon, W.H. Green, O.O. Oluwole, H.-W. Wong, S.E. Albo and D.K. Lewis, "Updating Our Understanding of JP-10 Decomposition Chemistry: A Detailed JP-10 Combustion Mechanism Constructed Using RMG – an Automatic Reaction Mechanism Generator", 46th AIAA/ASME/SAE/ASEE Joint Propulsion Conference (2010); *AIAA* 2010-6825
5. C.F. Goldsmith, S.J. Klippenstein, and W.H. Green, "Theoretical rate coefficients for allyl + HO₂ and allyloxy decomposition", *Proc. Combust. Inst.* **33**(1), 273-282 (2011).
6. J.D. Mo, E. Kosovich, H.-H. Carstensen, W.H. Green, A.M. Dean, "Thermodynamic properties and kinetic parameters of reactions involving O₂ + substituted allylic radicals", *7th US Mtg. Combust. Inst.*, paper 1A05 (2011).
7. R.H. West, C.F. Goldsmith, M.R. Harper, W.H. Green, L. Catoire, and N. Chaumeix, "Kinetic Modeling of Methyl Formate Oxidation", *7th US Mtg. Combust. Inst.*, paper 1A06 (2011).
8. J.W. Allen, C.F. Goldsmith, and W.H. Green, "Automatic Estimation of Pressure-Dependent Rate Coefficients", *Physical Chemistry Chemical Physics* **14**, 1131 - 1155 (2012).
9. R. Kaiser, M. Goswami, F. Zhang, D. Parker, V.V. Kislov, A.M. Mebel, J. Aguilera-Iparraguirre, W.H. Green. "Crossed Beam Reaction of Phenyl and D5-Phenyl Radicals with Propene and Deuterated Counterparts – Competing Atomic Hydrogen and Methyl Loss Pathways", *Physical Chemistry Chemical Physics* **14**, 720–729 (2012).
10. V. Kislov, A. Mebel, J. Aguilera-Iparraguirre, W.H. Green, "Reaction of Phenyl Radical with Propylene as a Possible Source of Indene and Other Polycyclic Aromatic Hydrocarbons: An Ab Initio/RRKM-ME Study", *Journal of Physical Chemistry A* (submitted).
11. G.R. Magoon, W.H. Green, "Design and implementation of a next-generation software system for on-the-fly quantum and force field calculations in automated reaction mechanism generation", *Comp. Chem. Eng.* (submitted).

Quantum Dynamics of Elementary Combustion Reactions

Hua Guo (hguo@unm.edu)

Department of Chemistry and Chemical Biology, University of New Mexico

During the past year, we have continued to develop quantum dynamical methods for investigating reaction dynamics in small molecular systems. Specifically, we have finished an efficient quantum dynamical code for studying non-adiabatic photodissociation of triatomic systems.¹⁻² Our code is capable of calculating not only scalar properties such as total and partial cross sections, but also vector ones such as differential cross sections. We have used the code to compute the B-state photodissociation of H₂O on a new set of ab initio potential energy surfaces. As shown in Fig. 1, the agreement with the latest experimental data³ was quite satisfactory. Our study has further advanced understanding of non-Born-Oppenheimer dynamics in reactive systems.

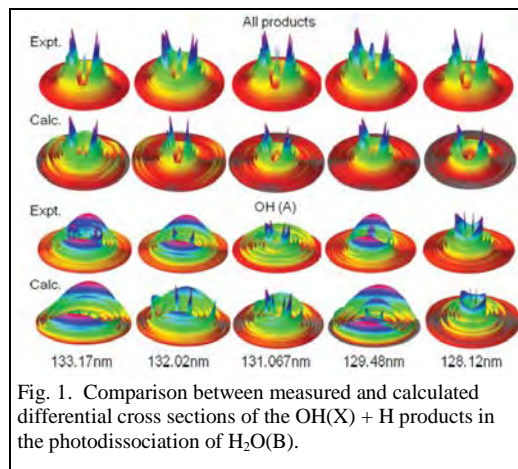


Fig. 1. Comparison between measured and calculated differential cross sections of the OH(X) + H products in the photodissociation of H₂O(B).

We have also made advances in understanding dynamics of complex-forming reactions. For example, we have investigated the state-to-state scattering of the $\text{H} + \text{O}_2(a^1\Delta) \rightarrow \text{O} + \text{OH}$ reaction⁴ on an ab initio PES of HO₂(A²A').⁵ Like its counterpart on HO₂(X²A''), this reaction also proceeds via a complex-forming mechanism, but significant deviations from the statistical limit have been identified. It was shown that the non-statistical rotational state distribution of the OH product can be traced to a unique feature in the asymptotic PES, which exerts a torque on the departing OH product. In addition, our results suggested that the excited state O₂ does indeed contribute significantly to the H + O₂ reaction at high temperatures.

More recently, we have collaborated with the Prof. D. Xie (Nanjing U, China) to map out an accurate global potential energy surface for the lowest triplet state of the HON/HNO system,⁶ and carried out state-to-state quantum dynamics calculations for the $\text{N} + \text{OH} \rightarrow \text{H} + \text{NO}$ reaction,⁷ which is involved in the combustion of nitrogen containing fuels. Comparison with available experiment on the product state distribution⁸ was satisfactory. Our calculated rate constant at low temperatures is shown in Fig. 2 to agree with the latest experimental data,⁹ which shed light on this important astrochemical reaction.

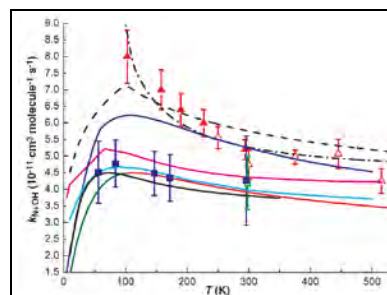


Fig. 2 Comparison of measured and calculated rate constant for the N + OH reaction.

One of key problems in many complex-forming reactions is the accurate description of the potential energy surface in the asymptotic region, because such reactions are often controlled by potential bottlenecks for the formation of the reaction intermediate. We have recently shown that care must be taken in electronic structure calculations in these regions. In collaboration with Prof. R. Dawes (MST), we have demonstrated that a “well-known” feature in the ozone formation potential, namely the so-called “submerged reef” structure, is an artifact, due apparently to the insufficient inclusion of excited states in the ab initio calculations.¹⁰ When a dynamical weighted multi-reference configuration interaction (DW-MRCI) scheme was used,¹¹ it was shown that this feature disappears. With this new potential, the observed negative temperature dependence for the $\text{O} + \text{O}_2$ exchange reaction can now be reproduced theoretically.

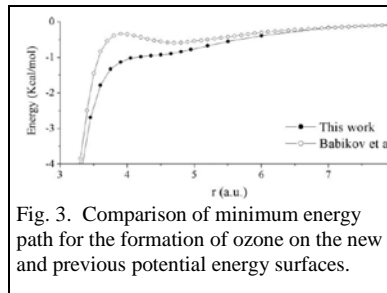


Fig. 3. Comparison of minimum energy path for the formation of ozone on the new and previous potential energy surfaces.

More recently, we have shifted our attention to more complex systems. In a recent publication,¹² we have investigated the photodetachment of the HCO_2^- anion using an existing potential energy surface of HOCO. Our results indicated that the potential is inaccurate. In collaboration with several groups (Dawes, and Xie, and Bowman,), we have developed a chemically accurate potential energy surface for the $\text{HO} + \text{CO} \rightarrow \text{H} + \text{CO}_2$ reaction.¹³ Our publication, which significantly improved the description of the reaction pathways in this important combustion reaction, was well received as one of top 20 most read articles on J. Chem. Phys. in January 2012. Preliminary quasi-classical trajectory (QCT) calculations showed good agreement with experimental thermal rate constants. We are in the process of extracting state-to-state reaction dynamics information from large scale QCT and quantum calculations.

In addition to reaction dynamics, we have also been interested in spectroscopy. For example, we have used a path integral Monte Carlo method to simulate the rotational dynamics of CO_2 and N_2O in superfluid ^4He clusters.¹² More recently, we have computed the bending vibrational overtones in deuterated acetylene, DCCD.¹⁴ To our surprise, the onset of localization of the cis and trans-bends of this molecule occurs much earlier than its hydrogen counterpart (HCCH).¹⁵⁻¹⁶

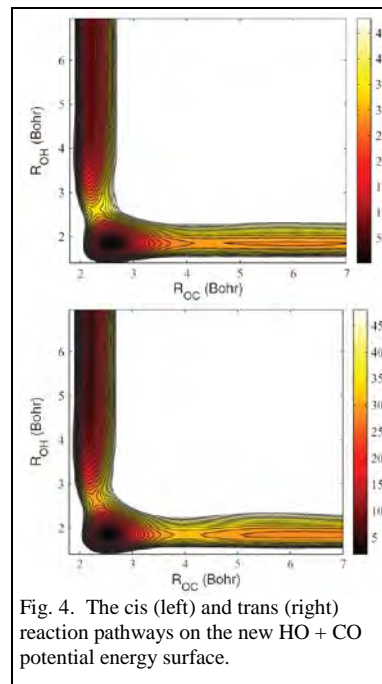


Fig. 4. The cis (left) and trans (right) reaction pathways on the new HO + CO potential energy surface.

We anticipate a productive year ahead. Much of our focus will be placed on a better understanding of the HOCO system, including the bimolecular reactions $\text{HO} + \text{CO} \leftrightarrow \text{H} + \text{CO}_2$, and the photodetachment of both HOCO^- and HCO_2^- .

References (* indicates DOE funded work in the past year):

- *1 B. Jiang, D. Xie and H. Guo, J. Chem. Phys. **134**, 231103 (2011).
- *2 B. Jiang, D. Xie and H. Guo, J. Chem. Phys. **136**, 034302 (2012).
- 3 Y. Cheng, K. Yuan, L. Cheng, Q. Guo, D. Dai and X. Yang, J. Chem. Phys. **134**, 064301 (2011).
- *4 J. Ma, H. Guo, A. Li, C. Xie and D. Xie, Phys. Chem. Chem. Phys. **13**, 8407 (2011).
- 5 A. Li, D. Xie, R. Dawes, A. W. Jasper, J. Ma and H. Guo, J. Chem. Phys. **133**, 144306 (2010).
- *6 A. Li, C. Xie, D. Xie and H. Guo, J. Chem. Phys. **134**, 194309 (2011).
- *7 C. Xie, A. Li, D. Xie and H. Guo, J. Chem. Phys. **135**, 164312 (2011).
- 8 I. W. M. Smith, R. P. Tuckett and C. J. Whitham, J. Chem. Phys. **98**, 6267 (1993).
- *9 J. Daranlot, M. Jorfi, C. Xie, A. Bergeat, M. Costes, P. Caubet, D. Xie, H. Guo, P. Honvault and K. M. Hickson, Science **334**, 1538 (2011).
- *10 R. Dawes, P. Lolur, J. Ma and H. Guo, J. Chem. Phys. **135**, 081102 (2011).
- 11 M. P. Deskevich, D. J. Nesbitt and H.-J. Werner, J. Chem. Phys. **120**, 7281 (2004).
- *12 J. Ma and H. Guo, Chem. Phys. Lett. **511**, 193 (2011).
- *13 J. Li, Y. Wang, B. Jiang, J. Ma, R. Dawes, D. Xie, J. M. Bowman and H. Guo, J. Chem. Phys. **136**, 041103 (2012).
- *14 J. Ma, D. Xu, H. Guo, V. Tyng and M. E. Kellman, J. Chem. Phys. **136**, 014304 (2012).
- 15 M. P. Jacobson and R. W. Field, J. Phys. Chem. A **104**, 3073 (2000).
- 16 D. Xu, R. Chen and H. Guo, J. Chem. Phys. **118**, 7273 (2003).

Gas-Phase Molecular Dynamics: High Resolution Spectroscopy and Collision Dynamics of Transient Species

Gregory E. Hall and Vasily Goncharov
Chemistry Department, Brookhaven National Laboratory
Upton, NY 11973-5000
gehall@bnl.gov

Program Scope

This research is carried out as part of the Gas-Phase Molecular Dynamics program in the Chemistry Department at Brookhaven National Laboratory. Chemical intermediates in the elementary gas-phase reactions involved in combustion chemistry are investigated by high resolution spectroscopic tools. Production, reaction, and energy transfer processes are investigated by transient, double resonance, polarization and saturation spectroscopies, with an emphasis on technique development and connection with theory, as well as specific molecular properties.

Recent Progress

A. Dual-beam FTIR spectroscopy with a mode-locked fiber laser source

We have been exploring methods to combine fiber laser frequency comb sources with commercial FTIR instrumentation to provide sensitive and accurate measurements of weak absorption features, for example, in attenuated reflection spectroscopy of surface species. We have developed a general dual-beam method, compatible with most common FTIR instrumentation that combines strong suppression of source noise with continuous correction for background drift. The use of a coherent broadband source enables

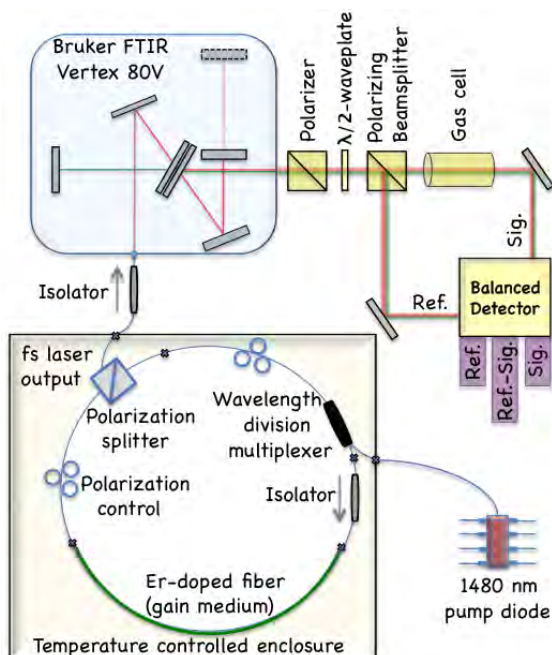


Figure 1. Optical layout for dual-beam FTIR spectroscopy with a mode-locked fiber laser.

additional signal enhancement through multi-pass geometries. Figure 1 illustrates a polarization additive-pulse mode-locked Er fiber ring laser, centered at 1560 nm, replacing the conventional lamp source in a commercial Bruker FTIR spectrometer. The modulated output beam is split into matched signal and reference beam paths and viewed with balanced InGaAs photodiode detectors. In order to correct for intensity noise in the source, the interferometer digitizes two channels simultaneously: Ref and Ref-Sig. This arrangement takes advantage of common mode noise suppression and increases the effective dynamic range of the acquired interferogram, while accounting for possible drift in the spectral power of the light source.

The noise suppression is demonstrated in Figure 2. The upper panel shows the baseline noise, obtained as the log of the ratio of an empty cell blank spectrum and a (nominally identical)

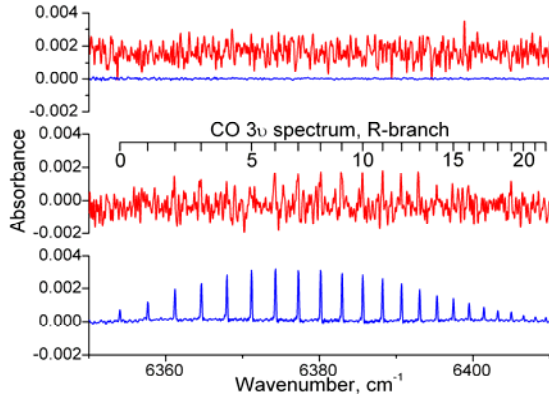


Figure 2. Baseline stability and small signal sensitivity comparison of single-beam conventional lamp FTIR (red) vs. dual beam laser FTIR spectra (blue). The spectrum in the lower comparison is the second overtone of CO, measured in a single scan, using simultaneously recorded interferograms from reference and (reference – signal) channels.

between the two paths but not the source noise or spectral fluctuations. The difference of two successive dual-beam blank spectra is plotted in the top panel of Figure 2, and demonstrates excellent baseline stability. Adding 160 Torr of CO to a 10 cm gas cell in the sample arm provides a weak test absorption in the second vibrational overtone. The rovibrational spectrum is barely detectable with a single scan (40 kHz, 0.2 cm^{-1} resolution) with the less intense lamp source, filtered to a comparable optical bandwidth, (center panel of Figure 2) but recorded with the dual-beam laser scheme at close to shot-noise limited sensitivity under otherwise identical conditions (bottom panel of Figure 2).

This demonstration uses only the oscillator of the Er fiber laser. Applications using other spectral regions in the 1000-1700 nm region are in progress, using a fiber amplifier and a highly nonlinear fiber to generate supercontinuum. Tests of this dual beam scheme with a much higher resolution FT interferometer are planned for the near future in the laboratory of Peter Bernath (Old Dominion Univ). None of the applications rely on active stabilization of carrier phase or repetition rate characteristic of frequency combs, and the short pulse structure is only required for generating the supercontinuum. Designs for a multipass internal reflection prism for studies of surface species by attenuated internal reflection are in progress.

B. Sub-Doppler saturation spectroscopy

Additional frequency stabilization has been implemented for our cw Ti:sapphire laser, locking a tunable sideband to a single-frequency HeNe-stabilized Fabry-Perot cavity. This improves the long-term frequency stability, as the scan offset from a stable reference frequency is controlled by a radio frequency synthesizer, rather than reliance on a passively stabilized, piezo-scanned reference cavity. As a first project using the new system, we have measured sub-Doppler saturation spectra in the (1–0) band of N_2 $B^3\Pi_g - A^3\Sigma_u^+$ near $11\,300 \text{ cm}^{-1}$. The high-resolution scans across the central portion of selected rovibrational transitions resolve the hyperfine structure. Two ^{14}N nuclear spins combine to a composite value of $I = 0$, or 2 for *ortho* states, 1 for *para* states, and the rovibronic levels are correspondingly split

repeated scan. With single-beam interferograms and an incandescent lamp source, uncompensated drift in the lamp intensity produces random baseline offsets, and higher frequency source noise is responsible for the spectral noise in the baseline. To implement the dual-beam laser variation, a (Ref-Sig) difference interferogram is algebraically subtracted from the simultaneously recorded Ref interferogram, and then inverse Fourier transformed to give a spectrum similar to a single-channel (empty cell) Signal spectrum, but computed with its broad-band background contribution derived primarily from the Reference channel. Dividing this synthetic signal spectrum by the inverse transform spectrum of the Reference interferogram, and taking the negative logarithm gives a dual-beam blank spectrum that depends primarily on small optical miss-match

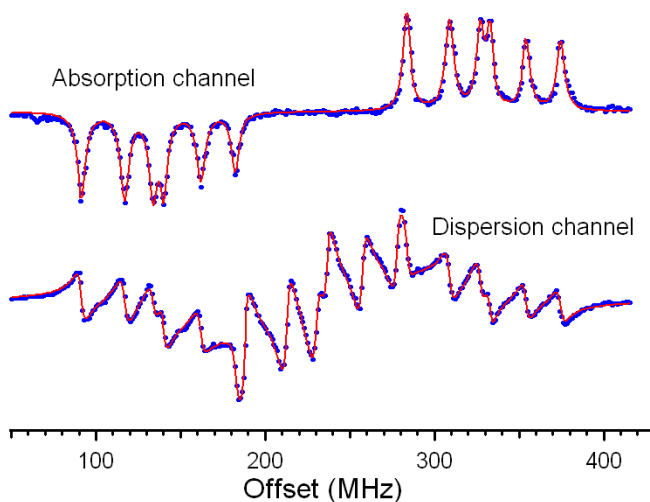


Figure 3. FM-detected sub-Doppler saturation spectrum of N_2 : hyperfine structure in the $R_{33}(10)$ rotational line of the (1-0) band of $B^3\Pi_g - A^3\Sigma_u^+$ near 11331cm^{-1} . The solid (red) line is a simultaneous fit to observed (blue points) absorption and dispersion features

amplification, the saturation spectra were finally processed with lock-in detection at the 1 kHz frequency of the sample discharge. Figure 3 shows a typical saturation spectrum, in this case the FM-detected saturation in the $R_{33}(10)$ line. The pattern of six hyperfine transitions is sampled twice in the absorption-phase signal: once each for the red and blue sidebands, appearing with opposite signs. The dispersion shows an additional feature when the carrier frequency of the laser scans through the sub-Doppler resonance. The fits to the hyperfine patterns in multiple rovibronic transitions give a heavily overdetermined set of hyperfine splittings, which in turn determine six hyperfine constants in the B state ($v=1$) and three in the A state ($v=0$). Previous high resolution LIF measurements[1] in a molecular beam of metastable N_2 had determined hyperfine splittings and constants for a selection of higher vibrational bands, accessible with a red cw dye laser. The hyperfine constants directly determined here for the $v=1$ level of the B state confirm the theoretical model used previously, and provide a slight improvement over values extrapolated from higher vibrational levels. The improved frequency stability of this scheme will enable future spectroscopic studies on C_3 and sub-Doppler saturation recovery kinetic studies on CN . (with Trevor Sears and Research Associate Damien Forthomme)

C. Saturation recovery kinetics

A general method for measuring rate coefficients for rotational energy transfer and elastic depolarization in ground state radicals has been developed based on high dynamic-range frequency modulation (FM) spectroscopy. Resonant, tunable pulsed laser radiation optically removes a polarized ensemble of molecules to an excited state, and a continuous probe laser can monitor the pulsed depletion and recovery due to rotationally inelastic collisions. The alignment or orientation of the depletion can also be monitored by comparing transient signals in different pump/probe polarizations. With Millard Alexander and Paul Dagdigian, we have analyzed master equation models for the time evolution of the perturbed Boltzmann distributions, and can analytically show that the “hole” kinetics provide identical information to what would be observed in an idealized experiment starting with a single rotational state populated in an otherwise empty manifold, generally a challenging proposition for ground state molecules. Depolarization kinetics differ, however, in the depletion recovery mode, where the confounding

into 6 (*ortho*) or 3 (*para*) hyperfine levels, separated by tens of MHz, primarily through the electron spin–nuclear spin magnetic dipole interaction. The metastable nitrogen spectra have been observed in an AC discharge, using three stages of modulation. A weak probe beam was frequency modulated at 192 MHz and detected with a photodiode, RF amplifier, and I&Q demodulator after passing through the nitrogen discharge. The I- and Q-phased signals separately monitor absorption and dispersion in the sample. A counter-propagating bleach beam from the same laser was amplitude-modulated at 490 kHz, and the bleach-laser-dependent absorption and dispersion saturation signals were isolated with additional mixers referenced to the bleach modulation frequency. After further filtering and

influence of returning partially polarized population is crucial in the analysis of single-state population relaxation studies, but can be well approximated as completely unpolarized in the saturation recovery analysis.

Future Work

A. Collision dynamics in CN radicals

Our move to a new temporary laboratory is now complete, and work has resumed on double resonance kinetic studies of ground-state energy and polarization transfer in CN. The frequency stabilization described above will allow more accurate signal averaging of sub-Doppler saturation recovery kinetics, keeping the probe laser from drifting relative to the very sharp hyperfine-resolved saturation peaks, as illustrated in Fig 3. The saturation recovery kinetics following rapid switching off of a sub-Doppler bleach laser can have contributions due to velocity-changing elastic collisions, as well as rotationally inelastic collisions, in both upper and lower levels of the saturated transition. The pressure-dependent recovery rates so derived can be compared to rotationally inelastic rates measured by other techniques, or in our own laboratory, from depletion recovery kinetics following broad-band (ns) saturation. Preliminary measurements reveal surprisingly small relative contributions from velocity-changing collisions (compared to rotationally inelastic collisions) for the case of CN(X) interacting with our photolytic precursor, CH₃COCN, a highly polar molecule. With better frequency stability and sensitivity now in hand, we expect to be able to characterize the elastic velocity-changing collisions with rare gases compared to rotationally inelastic and depolarizing collisions. Such studies will provide a microscopic view of the kinds of collisions that contribute to pressure broadening and allow comparison to quantum scattering calculations on realistic potentials.

Cited References

[1] H. Geisen, D. Neuschäfer, and C. Ottinger, *Z. Phys. D.* **4**, 263 (1987); **17**, 137 (1990).

Publications supported by this project since 2010

- Spectroscopic constants of the known electronic states of lead monofluoride. C. P. McRaven, P. Sivakumar, N. E. Shafer-Ray, G. E. Hall and T. J. Sears. *J. Mol. Spectrosc.* **262**, 89 (2010).
- Pseudo-continuous resonance-enhanced multiphoton ionization: application to the determination of the hyperfine constants of ²⁰⁸Pb¹⁹F. P. Sivakumar, C. P. McRaven, P. M. Rupasinghe, T. Zh. Yang, N. E. Shafer-Ray, G. E. Hall and T. J. Sears, *Mol. Phys.* **108**, 927 (2010).
- Frequency modulated circular dichroism spectroscopy: application to ICN photolysis. G. Hancock, G. Richmond, G.A.D. Ritchie, S. Taylor, M. L. Costen and G. E. Hall, *Mol. Phys.* **108**, 1083-1095 (2010).
- Sub-Doppler spectroscopy of mixed state levels in CH₂. C.-H. Chang, G. E. Hall, T. J. Sears, *J. Chem. Phys.* **133**, 144310 (2010).
- Transient laser absorption spectroscopy of CH₂ near 780 nm. C.-H. Chang, Z. Wang, G. E. Hall, T. J. Sears and J. Xin, *J. Molec. Spectrosc.* **267**, 50-57 (2011)
- CH₂ band origin at 1.20 μ. C.-H. Chang, J. Xin, T. Latsha, E. Otruba, Z. Wang, G. E. Hall, T. J. Sears and B.-C. Chang, *J. Phys. Chem. A*, **115**, 9440-9446 (2011)
- The Approach to Equilibrium: Detailed Balance and the Master Equation. M. H. Alexander, G. E. Hall and P. J. Dagdigian, *J. Chem. Educ.* **88**, 1538-1543 (2011)
- What is the best DFT function for vibronic calculations? A comparison of the calculated vibronic structure of the S₁ – S₀ transition of phenylacetylene with accurate experimental band intensities, G. V. Lopez, C.-H. Chang, P. M. Johnson, G. E. Hall, T. J. Sears, B. Markiewicz, M. Milan and A. Teslja, (submitted, 2012).
- Broadband laser-enhanced dual-beam interferometry. V. V. Goncharov and G. E. Hall (submitted 2012).

Flame Chemistry and Diagnostics

Nils Hansen

Combustion Research Facility, Sandia National Laboratories, Livermore, CA 94551-0969

Email: nhansen@sandia.gov

SCOPE OF THE PROGRAM

The goal of this program is to provide a rigorous basis for the elucidation of chemical mechanisms of combustion, combining experimental measurements employing state of the art combustion diagnostics with detailed kinetic modeling. The experimental program concentrates on the development and application of combustion diagnostics for measurements of key chemical species concentrations. These measurements are carried out in low-pressure, one-dimensional laminar flames and are designed to serve as benchmarks for the validation of combustion chemistry models. Comparison of experimental data to models employing detailed chemical kinetics is critical to determining important chemical pathways in combustion and in pollutant formation in combustion systems. As turbulent combustion models become increasingly sophisticated, accurate chemical mechanisms will play a larger role in computations of realistic combustion systems. Verification of detailed chemistry models against a range of precise measurements under thoroughly characterized steady conditions is necessary before such flame models can be applied with confidence in turbulent combustion calculations.

PROGRESS REPORT

The Chemical Structure of Low-Pressure Premixed Methylcyclohexane Flames as Benchmarks for the Development of a Predictive Combustion Chemistry Model: Together with W. J. Pitz (LLNL) and A. W. Jasper (Sandia), we investigated the chemical compositions of three low-pressure premixed flames of methylcyclohexane (MCH). The emphasis was put on the chemistry of MCH decomposition and the formation of aromatic species, including benzene and toluene. For this study, the MCH flames were stabilized on a flat-flame (McKenna type) burner at equivalence ratios of $\phi = 1.0, 1.75,$ and 1.9 and at low pressures between 15 Torr and 30 Torr. The complex chemistry of MCH consumption is illustrated in the experimental identification of several C_7H_{12} , C_7H_{10} , C_6H_{12} , and C_6H_{10} isomers and their distinct mole fraction profiles as a function of distance from the burner. Three initiation steps for MCH consumption were discussed: Ring opening to heptenes and methyl-hexenes (isomerization), methyl radical loss yielding the cyclohexyl radical (dissociation), and H abstraction from MCH. Mole fraction profiles as a function of distance from the burner for the C_7 species supplemented by theoretical calculations (by A. W. Jasper, Sandia) were presented, indicating that flame structures resulting in steeper temperature gradients and/or greater peak temperatures can lead to a relative increase in MCH consumption through the dissociation and isomerization channels. Trends observed among the stable C_6 species as well as 1,3-

pentadiene and isoprene also supported this conclusion. Relatively large amounts of toluene and benzene were observed in the experiments illustrating the importance of sequential H-abstraction steps from MCH to toluene and from cyclohexyl to benzene. Modeled results using the detailed chemical model of Pitz *et al.* (*Proc. Comb. Inst.* **2007**, 31, 267-275) were provided to illustrate the use of these data as a benchmark for the improvement or future development of a MCH mechanism.

Studies of Laminar Opposed-Flow Diffusion Flames of Acetylene at Low Pressures with Photoionization Mass Spectrometry: In collaboration with H. A. Michelsen (Sandia) and A. Violi (Michigan), we have designed an opposed-flow flame system to investigate the chemical composition of non-premixed flames using *in situ* flame-sampling molecular-beam mass spectrometry with synchrotron-generated tunable vacuum-ultraviolet light as an ionization source. To test the system, we have investigated the chemical composition of three low-pressure (30-50 Torr), non-premixed, opposed-flow acetylene(Ar)/O₂(Ar) flames. We measured quantitative mole-fraction profiles as a function of the distance from the fuel outlet for the major species and several intermediates, including the methyl and propargyl radicals. We determined the temperature profiles of these flames by normalizing a sampling-instrument function to thermocouple measurements near the fuel outlet. A comparison of the experimental temperature and major species profiles with modeling results provided by J. A. Miller (Argonne) indicates that flame perturbations caused by the sampling probe are minimal. The observed agreement between experimental and modeled results, apparent for most combustion species, was found to be similar to corresponding studies of premixed flames.

Near-Threshold Photoionization Mass Spectra of Combustion-Generated High-Molecular-Weight Soot Precursors: In the soot formation process, the transition from gas-phase species to particulate matter (i.e., nucleation) is not well understood. A better understanding of soot nucleation will require more specific chemical information on the large organic species involved. In collaboration with H. A. Michelsen (Sandia), A. Violi (Michigan), and K. R. Wilson (Berkeley), we recorded the aerosol mass spectra of organic species having mass-to-charge ratios between 15 and 900 sampled from near-atmospheric pressure, non-premixed, opposed-flow flames of acetylene, ethylene, and propane using an aerosol mass spectrometer with flash vaporization. Near-threshold photoionization was achieved by synchrotron-generated tunable-vacuum-ultraviolet (VUV) light. We observed variation among the three flames of the different fuels in the shape and mass progression of the spectra and the isomeric content identifiable in photoionization-efficiency curves. For example, one interesting feature appeared at $m/z = 116$ (C₉H₈), normally interpreted as signal arising from indene. In our data, however, the measured PIE curve could best be reproduced including contributions from phenylallene, 1-phenyl-1-propyne, and 3-phenyl-1-propyne. Based on our results, we concluded that the widely accepted HACA mechanism

cannot explain all observed features of the mass spectra, suggesting that different pathways are likely to contribute to molecular growth. The significance of these mechanisms and the isomeric content of the soot precursor species are likely to depend on the fuel structure and/or flame conditions. Considering that the formation of the first aromatic ring is widely regarded as a critical step in the soot formation process for non-aromatic fuels, this finding augments our earlier results that the fuel structure influences the significance of different benzene formation pathways.

OUTLOOK

Experimental Studies on the Molecular-Growth Chemistry of Soot Precursors in Combustion

Environments: With the chemistry of benzene/phenyl formation in flames well understood, now is the time to shift the emphasis to a fundamental chemical understanding of the molecular-growth mechanisms that are responsible for the formation of the large PAH's. Recognizing this opportunity, the goal of our research will be to create experimental benchmarks and a database for flames structures through application of advanced diagnostics methods. It will be the goal of our studies to directly address the molecular-growth chemistry from small combustion intermediates to larger and larger PAH's. We will study this complex combustion chemistry with an unprecedented level of detail by determining the chemical structures of species sampled from soot-producing laboratory-based model flames using state-of-the-art analytical tools, including flame-sampling mass spectrometry, laser spectroscopy, and gas chromatography. A worldwide-unique combination of these essential experimental facilities is available in Prof. Kohse-Höinghaus' laboratories at Bielefeld University, and funds from the Alexander von Humboldt-Foundation have been secured to pursue research in her laboratories for several month.

Investigating the Chemical Composition of Combustion-Generated Soot Nanoparticles: We will study the chemical composition of combustion-generated soot nanoparticles in flames fueled by acetylene (C_2H_2), the C_3H_4 isomers allene and propyne, propene (C_3H_6), and 1,3-butadiene (1,3- C_4H_6). It is of particular interest to study the chemical composition of the soot particles formed in these flames for several reasons: In acetylene flames, the molecular-weight growth should be dominated by the so-called HACA (hydrogen-abstraction- C_2H_2 -addition) mechanism and an accurate determination of the chemical structure of soot nanoparticles of acetylene flames will provide a unique test case for combustion chemistry models that include the HACA sub-mechanism. Flames fueled by allene, propyne, propene, and 1,3-butadiene are of special interest, because these molecules are potential precursors for the resonance-stabilized propargyl, allyl, and *i*- C_4H_5 radicals. Contributions towards molecular-weight growth and eventually particle formation via resonantly stabilized free radicals should be enhanced in these flames, thus making them a perfect test case for further development of soot-formation models with chemical details.

PUBLICATIONS ACKNOWLEDGING BES SUPPORT 2010-PRESENT

1. J. Wang, B. Yang, T. A. Cool, N. Hansen, "Absolute Cross-Sections for Dissociative Photoionization of Some Small Esters", *Int. J. Mass Spectrom.*, **292**, 14-22 (2010).
2. K. Kohse-Höinghaus, P. Oßwald, T. A. Cool, T. Kasper, N. Hansen, F. Qi, C. K. Westbrook, P. R. Westmoreland, "Biofuel Combustion Chemistry: From Ethanol to Biodiesel", *Angew. Chem. Int. Ed.*, **49**, 3472-3597 (2010).
3. U. Sruckmeier, A. Lucassen, N. Hansen, T. Wada, N. Peters, K. Kohse-Höinghaus, "Demonstration of a Burner for the Investigation of Partially Premixed Low-Temperature Flames", *Combust. Flame*, **157**, 1966-1975 (2010).
4. N. Hansen, W. Li, M. E. Law, T. Kasper, P. R. Westmoreland, B. Yang, T. A. Cool, A. Lucassen, "The Importance of Fuel Dissociation and Propargyl + Allyl Association for the Formation of Benzene in Fuel-Rich 1-Hexene Flame", *Phys. Chem. Chem. Phys.*, **12**, 12112-12122 (2010).
5. N. Hansen, T. Kasper, B. Yang, T. A. Cool, W. Li, P. R. Westmoreland, P. Oßwald, K. Kohse-Höinghaus, "Fuel-Structure Dependence of Benzene Formation Processes in Premixed Flames Fueled by C₆H₁₂ Isomers", *Proc. Combust. Inst.*, **33**, 585-592 (2011).
6. S. Dooley, F. L. Dryer, B. Yang, J. Wang, T. A. Cool, T. Kasper, N. Hansen, "An Experimental and Kinetic Modeling Study of Methyl Formate Low-Pressure Flames", *Combust. Flame*, **158**, 732-741 (2011).
7. B. Yang, T. A. Cool, C. K. Westbrook, N. Hansen, K. Kohse-Höinghaus, "Fuel-Specific Influences on the Composition of Reaction Intermediates in Premixed Flames of Three C₅H₁₀O₂ Ester Isomers", *Phys. Chem. Chem. Phys.*, **13**, 7205-7217 (2011).
8. W. Li, M. E. Law, P. R. Westmoreland, T. Kasper, N. Hansen, K. Kohse-Höinghaus, "Multiple Benzene-Formation Paths in a Fuel-Rich Cyclohexane Flame", *Combust. Flame*, **158**, 2077-2089 (2011).
9. N. Hansen, M. R. Harper, W. H. Green, "High-Temperature Oxidation Chemistry of n-Butanol – Experiments in Low-Pressure Premixed Flames and Detailed Kinetic Modeling", *Phys. Chem. Chem. Phys.*, **13**, 20262-20274 (2011).
10. B. Yang, C. K. Westbrook, T. A. Cool, N. Hansen, K. Kohse-Höinghaus, "The Effect of Carbon-Carbon Double Bonds on the Combustion Chemistry of Small Fatty Acid Esters", *Z. Phys. Chem.*, **225**, 1293-1314 (2011).
11. T. Kasper, A. Lucassen, A. W. Jasper, W. Li, P. R. Westmoreland, K. Kohse-Höinghaus, B. Yang, J. Wang, T. A. Cool, N. Hansen, "Identification of Tetrahydrofuran Reaction Pathways in Premixed Flames", *Z. Phys. Chem.*, **225**, 1237-1270 (2011).
12. S. A. Skeen, B. Yang, A. W. Jasper, W. J. Pitz, N. Hansen, "Chemical Structures of Low-Pressure Premixed Methylcyclohexane Flames as Benchmarks for the Development of a Predictive Combustion Chemistry Model", *Energy Fuels*, **25**, 5611-5625 (2011).
13. B. Yang, J. Wang, T. A. Cool, N. Hansen, S. Skeen, D. L. Osborn, "Absolute Photoionization Cross-Sections of Some Combustion Intermediates", *Int. J. Mass Spectrom.*, **309**, 118-128 (2012).
14. F. Zhang, R. I. Kaiser, A. Golan, M. Ahmed, N. Hansen, "A VUV Photoionization Study of the Combustion-Relevant Reaction of the Phenyl Radical (C₆H₅) with Propylene (C₃H₆) in a High-Temperature Chemical Reactor", *J. Phys. Chem. A*, accepted for publication (2012).
15. N. Hansen, J. A. Miller, S. J. Klippenstein, P. R. Westmoreland, K. Kohse-Höinghaus, "Exploring Formation Pathways of Aromatic Compounds in Laboratory-Based Model Flames of Aliphatic Fuels", *Combust. Expl. Shock Waves*, accepted for publication (2012).
16. C. K. Westbrook, B. Yang, T. A. Cool, N. Hansen, K. Kohse-Höinghaus, "Photoionization Mass Spectrometry and Modeling Study of Premixed Flames of Three Unsaturated C₅H₈O₂ Esters", *Proc. Combust. Inst.*, accepted for presentation (2012).
17. A. W. Jasper and N. Hansen, "Hydrogen-Assisted Isomerizations of Fulvene to Benzene and of Larger Cyclic Aromatic Hydrocarbons", *Proc. Combust. Inst.*, accepted for presentation (2012).
18. S. A. Skeen, B. Yang, H. A. Michelsen, J. A. Miller, A. Violi, N. Hansen, "Studies of Laminar Opposed-Flow Diffusion Flames of Acetylene at Low Pressures with Photoionization Mass Spectrometry", *Proc. Combust. Inst.*, accepted for presentation (2012).
19. N. J. Labbe, V. Seshadri, T. Kasper, N. Hansen, P. Oßwald, K. Kohse-Höinghaus, P. R. Westmoreland, "Flame Chemistry of Tetrahydropyran as a Model Heteroatomic Biofuel", *Proc. Combust. Inst.*, accepted for presentation (2012).

Spectroscopy and Kinetics of Combustion Gases at High Temperatures

R. K. Hanson and C. T. Bowman

Mechanical Engineering Department, Stanford University
Stanford, CA 94305-3032

rkhanson@stanford.edu, ctbowman@stanford.edu

I. Program Scope

This program involves two complementary activities: (1) development and application of cw laser absorption methods for the measurement of concentration time-histories and fundamental spectroscopic parameters for species of interest in combustion; and (2) shock tube studies of reaction kinetics relevant to combustion.

Species being investigated in the spectroscopic portion of the research include carbon monoxide (CO) in the IR (near 4.6 μm), formaldehyde (CH_2O) and acetaldehyde (CH_3CHO) in the UV (near 305 nm) and in the IR (near 3.4 μm), and ketones in the UV (near 305 nm). Tunable laser absorption is also used to acquire species time-histories of CH_3 (216 nm), OH (306 nm), H_2O (2.5 μm), CO_2 (2.7 μm), CH_4 (3.4 μm), and C_2H_4 (10.5 μm) in support of the accompanying kinetics studies.

In parallel with these spectroscopic studies, kinetics research has advanced on several fronts. The OH diagnostic has been used to measure the rate constants for the reaction of OH with 1-butanol and iso-butanol (2-methyl-1-propanol). The CO, C_2H_4 and UV ketone diagnostics have been used to provide improved measurements of the decomposition rate constants for acetone and 2-butanone and to provide a comprehensive database of species time-histories for ketone reaction mechanism validation.

II. Recent Progress: Spectroscopy

Formaldehyde Detection using 305 nm UV and 3.4 micron IR Laser Absorption

Formaldehyde can be detected in both the IR and the UV. The IR spectrum is discrete but densely populated near 3.5 μm , and overlapping lines provide an opportunity for stronger absorption and more sensitivity than with fully isolated lines. This wavelength range is also away from the dominant absorption feature of many fuel-relevant alkanes such as n-heptane. We are currently investigating several possible target wavelengths (in the wavelength region between 2826 and 2885 cm^{-1}) that can provide ~ 40 ppm minimum detectivity for formaldehyde (15 cm path, 1 atm, 1000 K, 1 MHz bandwidth, $\text{SNR} = 1$ for 0.1% absorption) with only limited interference from other hydrocarbons.

Formaldehyde also can be detected in the UV near 305 nm and in the VUV near 174 nm. Strong absorption by O_2 molecular bands in the VUV limits the usefulness of this deep UV CH_2O diagnostic for oxidative systems. However, this complication does not arise near 305 nm and we are able to access this wavelength region using the same laser technology we currently use to monitor OH (at 306.5 nm). Similar absorption structures have been seen for acetaldehyde in the IR and UV and we are currently investigating the possibility of measuring both species using a multiple-wavelength strategy.

Carbon Monoxide Detection using 4.6 micron IR Laser Absorption

A fixed-wavelength direct-absorption strategy using a tunable quantum cascade laser (QCL) operating in cw mode is being developed to measure CO concentration. The R(13) transition line at 2193.359 cm^{-1} in the CO fundamental rovibrational band at 4.56 μm appears to be optimal for kinetics studies because of the large sensitivity of this transition (at high temperatures) and the minimal interference absorption from H_2O and CO_2 . As compared to previous CO diagnostics near 1.5 and 2.3 μm , this new diagnostic scheme offers orders-of-magnitude greater sensitivity, resulting in ppm-level CO detectivity in shock tube measurements.

II. Recent Progress: Chemical Kinetics

Rate Constant Measurement: OH + 1-Butanol → Products

The rate constant for the overall reaction $\text{OH} + 1\text{-Butanol} \rightarrow \text{Products}$ was measured in experiments behind reflected shock waves at temperatures from 900 to 1200 K using tertbutylhydroperoxide (TBHP) as a fast source of OH radicals with 1-butanol in excess (Pang et al. 2012a). Narrow-linewidth laser absorption was employed for quantitative OH concentration measurement. A detailed mechanism with 1-butanol and TBHP kinetics was constructed to facilitate the rate constant determination and account for secondary chemistry influences on the pseudo-first order OH concentration decays. Representative OH time-history data are shown in Fig. 1. The current work extends the temperature range of high-temperature measurements of the rate constant in the literature to 900 to 1200 K. Over the temperature range studied, the overall rate constant can be expressed in Arrhenius form as $3.24 \times 10^{10} \exp(-2505/T[\text{K}]) \text{ cm}^3 \text{ molecule}^{-1} \text{ s}^{-1}$. A detailed uncertainty analysis was performed yielding an overall uncertainty in the measured rate constant of $\pm 20\%$ at 1197 K and $\pm 23\%$ at 925 K. The results were compared with previous experimental and theoretical studies and reasonable agreement was found.

Rate Constant Measurement: OH + iso-Butanol → Products

The first direct experimental study of the rate constant for the reaction of OH with iso-butanol (2-methyl-1-propanol) at elevated temperatures (907 to 1147 K) and near-atmospheric pressures was performed (Pang et al. 2012b). As in the OH+1-butanol study, OH time-histories were measured behind reflected shock waves using a narrow-linewidth laser absorption method during reactions of dilute mixtures of tert-butyl hydroperoxide with iso-butanol in excess. The overall rate constant, k_{overall} , ($\text{OH} + \text{iso-butanol} \rightarrow \text{all products}$) minus the rate constant for the β -radical-producing channel, k_{β} , ($\text{OH} + \text{iso-butanol} \rightarrow \beta\text{-iso-C}_4\text{H}_8\text{OH radical} + \text{H}_2\text{O}$) was determined from the pseudo-first-order rate of OH decay. The strategy for this approach is shown in Fig. 2. A two-parameter Arrhenius fit of the experimentally determined rate constant in the current temperature range yields the expression $(k_{\text{overall}} - k_{\beta}) = 1.84 \times 10^{-10} \exp(-2350/T [\text{K}]) \text{ cm}^3 \text{ molecule}^{-1} \text{ s}^{-1}$. Using this measurement, and theoretical estimates for k_{β} , a recommendation for the overall rate constant was made. Comparisons of the results to rate constant recommendations from the literature are shown in Fig. 3.

Multi-Species Time-History Measurements during Acetone and 2-Butanone Pyrolysis

High-temperature acetone and 2-butanone pyrolysis studies were conducted behind reflected shock waves using five species time-history measurements (ketone, CO, CH₃, CH₄ and C₂H) (Lam et al. 2011). Experimental conditions covered temperatures of 1100-1600 K at 1.6 atm, for mixtures of 0.25% to 1.5% ketone in argon. During acetone pyrolysis, the CO concentration time-history was found to be strongly sensitive to the acetone dissociation rate constant k_1 ($\text{CH}_3\text{COCH}_3 \rightarrow \text{CH}_3 + \text{CH}_3\text{CO}$), and this could be directly determined from the CO time-histories, yielding $k_1(1.6 \text{ atm}) = 2.46 \times 10^{14} \exp(-69.3 [\text{kcal/mol}]/\text{RT}) \text{ s}^{-1}$ with an uncertainty of $\pm 25\%$. This rate constant differs significantly from that of previous shock tube studies at temperatures below 1250 K. Using this revised k_1 value with the recent mechanism of Pichon et al. 2009, the simulated profiles during acetone pyrolysis show excellent agreement with all five species time-history measurements. Similarly, the overall 2-butanone decomposition rate constant k_{tot} was inferred from measured 2-butanone time-histories, yielding $k_{\text{tot}}(1.5 \text{ atm}) = 6.08 \times 10^{13} \exp(-63.1 [\text{kcal/mol}]/\text{RT}) \text{ s}^{-1}$ with an uncertainty of $\pm 35\%$. This rate constant is approximately 30% faster than that proposed by Serinyel et al. 2010 at 1119 K, and approximately 100% faster at 1412 K. Using the measured 2-butanone and CO time-histories and an O-atom balance analysis, a missing removal pathway for methyl ketene was identified. Representative data showing species time-histories are shown in Fig. 4. Using the revised k_{tot} value and adding a methyl ketene decomposition reaction to the Serinyel et al. mechanism, the simulated profiles during 2-butanone pyrolysis show good agreement with the measurements for all five species.

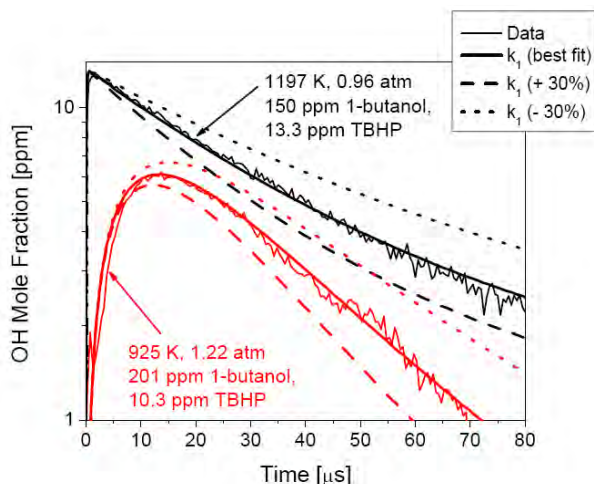


Fig. 1. Representative OH time-history measurements for the determination of the overall reaction rate constant for OH + 1-butanol.

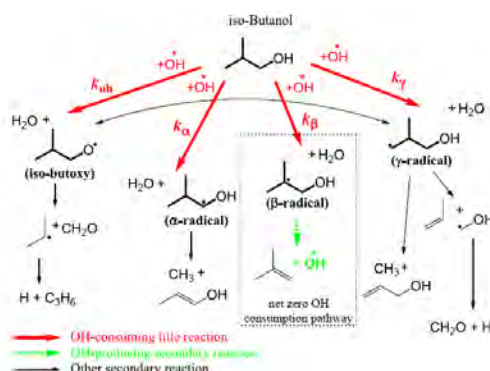


Fig. 2. Schematic of the product channels for the reaction of OH + iso-butanol. The β -radical channel has a zero net OH consumption.

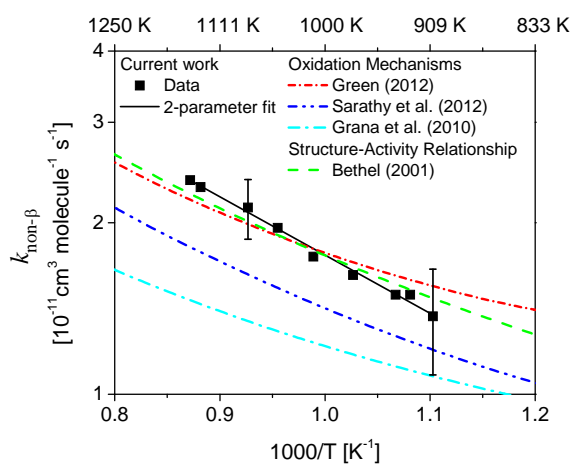


Fig. 3. Arrhenius plot of the reaction OH + iso-butanol \rightarrow all products and several current proposed rate constants.

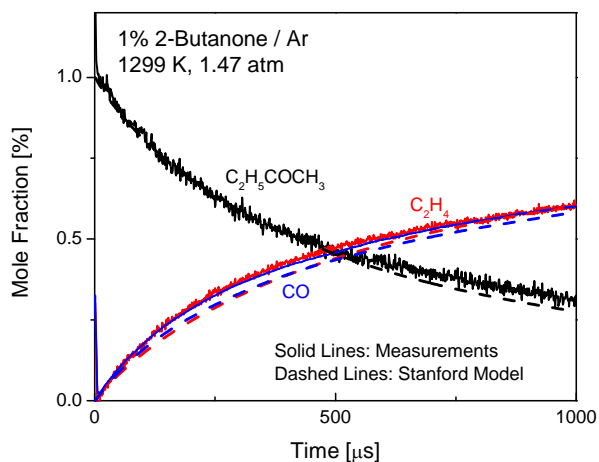


Fig. 4. Species time-histories during the pyrolysis of 2-butanone behind a reflected shock wave. The measured CO profile has a very high signal-to-noise ratio.

Future Work

Work is continuing to refine shock tube/laser absorption diagnostic capability for CO and aldehydes and ketones. These diagnostics will assist in achieving closure for the measurement of oxygen balance during oxygenate fuel pyrolysis and oxidation. Further rate constant measurements of oxidation reactions of the form OH+ketones and OH+methyl esters are also in progress. Lastly, a systematic investigation of species time-histories during the pyrolysis and oxidation of different classes of oxygenate species has been initiated, including work on ketones (3-pentanone) and ethers (dimethyl ether).

III. Publications and submitted journal articles supported by this project 2010-2012

G. A. Pang, R. K. Hanson, D. M. Golden, C. T. Bowman, "High-Temperature Rate Constant Determination for the Reaction of OH with iso-Butanol," submitted to Journal of Physical Chemistry A, March 2012a.

K.-Y. Lam, W. Ren, S. H. Pyun, A. Farooq, D. F. Davidson, R. K. Hanson, "Multi-Species Time-History Measurements during High-Temperature Acetone & 2-Butanone Pyrolysis," submitted to the Proceedings of the Combustion Institute, December 2011.

G. A. Pang, R. K. Hanson, D. M. Golden, C. T. Bowman, "Rate Constant Measurements for the Overall Reaction of OH+ 1-Butanol \rightarrow Products from 900 to 1200K," Journal of Physical Chemistry A116 (2012b) 2475-2483.

G. A. Pang, R. K. Hanson, D. M. Golden, C. T. Bowman, "High-Temperature Measurements of the Rate Constants for Reactions of OH with a Series of Large Normal Alkanes: n-Pentane, n-Heptane, and n-Nonane," Z. Phys. Chem. 225 (2011) 1157-1178.

S. S. Vasu, L. K. Huynh, D.F. Davidson, R. K. Hanson, D. M. Golden, "Reactions of OH with Butene Isomers: Measurements of the Overall Rates and a Theoretical Study," Journal of Physical Chemistry A115 (2011) 2549-2556.

S. S. Vasu, D. F. Davidson, R. K. Hanson, "A Shock Tube Study of Syngas Ignition in Rich CO₂ Mixtures and Determination of the Ratio of the Rate of H+O₂+CO₂ \rightarrow HO₂+CO₂, Energy and Fuels 25 (2011) 990-997.

S. Li, W. Ren, D. F. Davidson, R. K. Hanson, "Boundary Layer Effects Behind Incident and Reflected Shock Waves in a Shock Tube," Paper 2792, Proceedings of the International Symposium on Shock Waves 28 (2011).

K.-Y. Lam, Z. Hong, D. F. Davidson, R. K. Hanson, "Shock Tube Ignition Delay Time Measurements in Propane/O₂/Argon Mixtures at Near-Constant-Volume Conditions," Proceeding of the Combustion Institute. 33 (2011) 251-258.

Z. Hong, D. F. Davidson, R. K. Hanson, "An Improved H₂/O₂ Mechanism Based on Recent Shock Tube/Laser Absorption Measurements," Combustion and Flame 158 (2011) 633-644.

W. Ren, D. F. Davidson, R. K. Hanson, Shock Tube Measurements of Ethylene Concentration Time-histories during Ethylene, n-Heptane and methylcyclohexane Pyrolysis," 7th U.S. National Combustion Meeting, Atlanta, March 2011.

K.-Y. Lam, Z. Hong, S. W. Durrstein, D. F. Davidson, R. K. Hanson, C. Schulz, "Shock Tube Ignition Delay Times and OH and H₂O Species Time-histories in 3-pentanone/O₂/Ar Mixtures" 7th Intl. Conf. on Chemical Kinetics, MIT, July 2011.

S. S. Vasu, Z. Hong, D. F. Davidson, R. K. Hanson, D. M. Golden, "Shock Tube/Laser Absorption Measurements of the Reaction Rates of OH with Ethylene and Propene," J. Phys. Chem. A114 (2010) 11529-11537.

S. S. Vasu, J. Zador, D. F. Davidson, R. K. Hanson, D. M. Golden, J. A. Miller, "High-Temperature Measurements and a Theoretical Study of the Reaction of OH with 1,3-Butadiene," J. Phys. Chem. A114 (2010) 8312-8318.

Z. Hong, S. S. Vasu, D.F. Davidson, R. K. Hanson, "Experimental Study of the Ratio of OH+HO₂ \rightarrow H₂O+O₂ at High Temperatures using the Reverse Reaction," J. Phys. Chem. A 114 (2010) 5520-5525.

D. F. Davidson, S. C. Ranganath, K.-Y. Lam, M. Liaw, Z. Hong, R. K. Hanson, "Ignition Delay Time Measurements of Normal Alkanes and Simple Oxygenates," J. Prop. Power 26 (2010) 280-287.

S. S. Vasu, J. Zador, D. F. Davidson, R. K. Hanson, D. M. Golden, J. A. Miller, "High-temperature Measurement and a Theoretical Study of the Reaction of OH with 1-3 Butadiene," J. Chem. Phys. A 114 (2010) 8312-8318.

Theoretical Studies of Potential Energy Surfaces*

Lawrence B. Harding
Chemical Sciences and Engineering Division
Argonne National Laboratory, Argonne, IL 60439
harding@anl.gov

Program Scope

The goal of this program is to calculate accurate potential energy surfaces for both reactive and non-reactive systems. Our approach is to use state-of-the-art electronic structure methods (CASPT2, MR-CI, CCSD(T), etc.) to characterize multi-dimensional potential energy surfaces. Depending on the nature of the problem, the calculations may focus on local regions of a potential surface (for example, the vicinity of a minimum or saddle point), or may cover the surface globally. A second aspect of this program is the development of techniques to fit multi-dimensional potential surfaces to convenient, global, analytic functions that can then be used in dynamics calculations.

Recent Progress

HO₂+HO₂ → H₂O₂+O₂: The self reaction of HO₂ is consistently among the reactions with highest global sensitivity for the autoignition of hydrogen, methanol and butanol. This year in collaboration with Skodje and Davis, we completed a high level, theoretical determination of the rate for this reaction. The theoretical treatment of this reaction is complicated not only by the need to use multi-reference electronic structure methods (CASPT2 in this case) but also by the

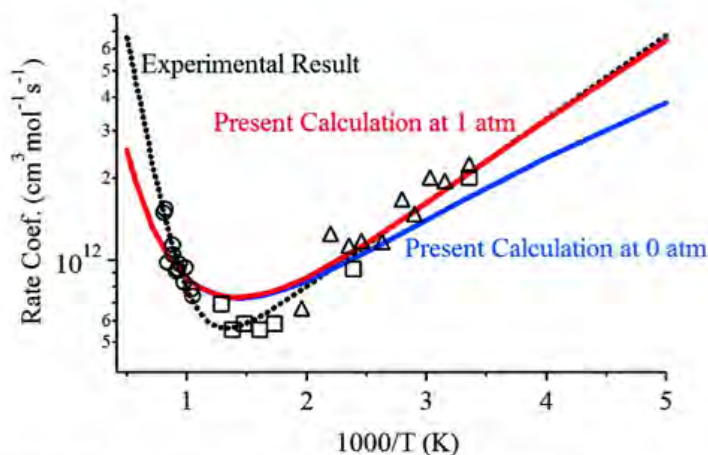


Figure 1

need to develop an adiabatic treatment of the torsional motion in the transition state. The latter was accomplished by characterizing a torsional ridge line for the transition state. In Figure 1 we show a comparison of our calculated rates to experimental results from Patrick and Pilling¹, Lightfoot et al², and Kappel et al³ (dotted line and symbols). The results agree well at low temperatures but do not rise as rapidly as the experimental results at higher temperatures.

Roaming Radical Mechanisms: Much of our work on roaming radical mechanisms this year focused on the question of the separability of roaming mechanisms from parallel mechanisms associated with tight transition states, i.e. when can one treat these two kinds of mechanisms separately and obtain a total rate by simply summing the separate contributions and when must one treat them in a more unified manner? In a collaboration with Klippenstein and Jasper, we started with the simplest example we know of having competing roaming and tight mechanisms connecting the same reactants and products, the dissociation of MgH₂ → Mg + H₂. Examination of

the global potential surface for this reaction reveals both a tight saddle point and a roaming saddle point lying on a common ridge, separated by a second order saddle point. We conclude that the second-order saddle point represents a rigorous energetic criterion for determining the separability of the two mechanisms. At energies below that of the second order saddle point the two mechanisms are clearly distinct. We were able to develop a global, transition state, dividing surface including both the tight and roaming saddle points and the second order saddle point between them. Analysis then of the differential contribution to the number of available states on this transition state, dividing surface at various energies reveals a distinct minimum at lower energies in the vicinity of the second order saddle point. This minimum becomes less pronounced as the energy increases. Somewhat surprisingly however, this minimum persists to energies well above that of the second order saddle point. We conclude that the existence of this minimum in the differential contribution to the state count points to a second, dynamical criterion for determining the separability of the two mechanisms.

With this new insight we have re-examined the formaldehyde potential surface focusing on the common ridge containing both the roaming and tight saddle points for molecular dissociation.

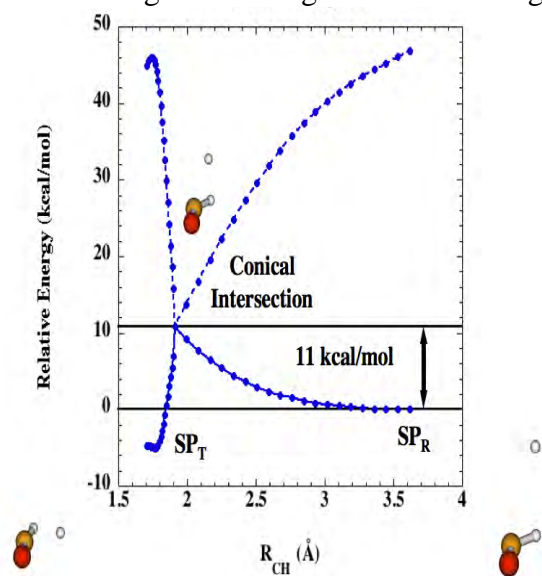


Figure 2

In this case we find the potential surface feature that separates the two first order saddle points is a conical intersection, one recently reported by Araujo et al⁴. The minimum energy point on this conical intersection (an analogue to a second-order saddle point) lies ~11 kcal/mol above the H+HCO asymptote suggesting that the two mechanisms are indeed distinct. A plot showing the geometries and energies of the two saddle points and the conical intersection is shown in Figure 2. The blue lines are the energies of the ground and first excited state along linearly interpolated paths connecting the two saddle points to the conical intersection. A similar conical intersection was found in the acetaldehyde potential surface.

This year we also looked at the possibility of a roaming component to the decomposition of $\text{HNNOH} \rightarrow \text{N}_2 + \text{H}_2\text{O}$, a key step in the thermal de- NO_x process. Here we find no evidence for a roaming saddle point, however when we follow the ridge from the tight saddle point to large HNN-OH separations we find a shoulder on the ridge starting at ~3 Å, lying ~5 kcal/mol below the radical asymptote. Examination of differential contributions to the number of states along this ridge, shows a clear dynamical separation between the tight saddle point region and this roaming shoulder even though there is no separate roaming saddle point. These results suggest that the roaming contribution will start to be significant at temperatures above ~600 K.

Finally we have continued our experimental/theoretical collaboration with Michael and Sivaramakrishnan concerning roaming in alkanes, recently reporting evidence for roaming in isobutane and neopentane.

Future Plans

We plan to continue studies begun a few years ago on multi-state effects in OH abstraction reactions including the reaction $\text{OH} + \text{HO}_2 \rightarrow \text{H}_2\text{O} + \text{O}_2$. Combustion mechanisms have shown a high sensitivity to this reaction but there is considerable uncertainty in the rate of this reaction. We also plan to continue our studies of roaming radical pathways in hydrocarbons, ethers and peroxides.

Acknowledgement: This work was performed under the auspices of the Office of Basic Energy Sciences, Division of Chemical Sciences, Geosciences and Biosciences, U.S. Department of Energy, under Contract DE-AC02-06CH11357.

References:

- (1) R. Patrick, Pilling, M. J. *Chem. Phys. Lett.* **91**, 343 (1982)
- (2) P. D. Lightfoot, B. Veyret, R. Lesclaux *Chem. Phys. Lett.* **150**, 120 (1988)
- (3) C. Kappel, K. Luther, J. Troe *Phys. Chem. Chem. Phys.* **4**, 4392 (2002)
- (4) M. Araujo, B. Basorne, M. J. Bearpark, M. A. Robb *J. Phys. Chem. A* **112**, 7489 (2008)

PUBLICATIONS (2010 - Present):

Roaming Radical Kinetics in the Decomposition of Acetaldehyde

L. B. Harding, Y. Georgievskii and S.J. Klippenstein, *J. Phys. Chem. A* **114**, 765-777 (2010)

Reactions Between Resonance Stabilized Radicals: Propargyl+Allyl

J. A. Miller, S. J. Klippenstein, L. B. Harding, Y. Georgievskii, W. D. Allen, and A. C. Simmonett *J. Phys. Chem. A* **114**, 4881-4890 (2010)

The Effect of Spin-Orbit Splitting on the Association Kinetics of Barrierless Halogen Atom-Hydrocarbon Radical Reactions

A. W. Jasper, S. J. Klippenstein and L. B. Harding, *J. Phys. Chem. A* **114**, 5759-5768 (2010)

Experimental and Theoretical Investigation of the Self-Reaction of Phenyl Radicals

R. S. Tranter, S. J. Klippenstein, L. B. Harding, B. R. Giri, X. Yang and J. H. Kiefer *J. Phys. Chem. A* **114**, 8240-8261 (2010)

Theoretical Validation of Chemical Kinetic Mechanisms: Combustion of Methanol

R. T. Skodje, A. S. Tomlin, S. J. Klippenstein, L. B. Harding and M. J. Davis *J. Phys. Chem. A* **114**, 8286-8301 (2010)

Rate Constants for the Thermal Decomposition of Ethanol and its Bimolecular Reaction with OH and D: Reflected Shock Tube and Theoretical Studies

R. Sivaramakrishnan, M.-C. Su, J. V. Michael, S. J. Klippenstein, L. B. Harding and B. Ruscic *J. Phys. Chem. A* **114**, 9425-9439 (2010)

Roaming Radical Pathways in the Decomposition of Alkanes

L. B. Harding and S. J. Klippenstein, *J. Phys. Chem. Letters* **1**, 3016-3020 (2010)

Uncertainty Driven Theoretical Kinetics Studies for CH₃OH Ignition: HO₂+CH₃OH and O₂+CH₃OH

S. J. Klippenstein, L. B. Harding, M. J. Davis, A. S. Tomlin, R. T. Skodje
33rd Symposium (International) on Combustion, **33**, 351-357 (2011)

The Role of NNH in NO Formation and Control

S. J. Klippenstein, L. B. Harding, P. Glarborg, J. A. Miller
Combustion and Flame, **158**, 774-489 (2011)

Roaming Radicals in the Thermal Decomposition of Dimethyl Ether: Experiment and Theory

R. Sivaramakrishnan, J. V. Michael, A. F. Wagner, R. Dawes, A. W. Jasper, L. B. Harding, Y. Georgievskii, S. J. Klippenstein, Combustion and Flame, **158**, 618-632 (2011)

Shock Tube and Theoretical Studies on the Thermal Decomposition of Propane: Evidence for a Roaming Radical Channel

R. Sivaramakrishnan, M.-C. Su, J. V. Michael, L. B. Harding, S. J. Klippenstein
J. Phys. Chem. A **115**, 3366-3379 (2011)

Near-threshold H/D Exchange in CD₃CHO Photodissociation

B. R. Heazlewood, A. T. Maccarone, D. U. Andrews, D. L. Osborn, L. B. Harding, S. J. Klippenstein, M. J. T. Jordan, and S. H. Kable, Nature Chemistry **3**, 443-448 (2011)

A Statistical Theory for the Kinetics and Dynamics of Roaming Reactions

S. J. Klippenstein, Y. Georgievskii and L. B. Harding
J. Phys. Chem. A **115**, 14370-14381(2011)

Bi-fidelity Fitting and Optimization

R. L. Miller, L. B. Harding, M. J. Davis, and S. K. Gray
J. Chem. Phys. **136**, 074102(2012)

Theoretical Determination of the Rate Coefficient for the HO₂+HO₂→ H₂O₂+O₂ Reaction: Adiabatic Treatment of Anharmonic Torsional Effects

D. D. Y. Zhou, K. Han, P. Zhang, L. B. Harding, M. J. Davis and R. T. Skodje
J. Phys. Chem. A **116**, 2089-2100 (2012)

Shock Tube Explorations of Roaming Radical Mechanisms: The Decomposition of Isobutane and Neopentane

R. Sivaramakrishnan, J. V. Michael, L. B. Harding and S. J. Klippenstein
J. Phys. Chem. A (in press)

A Quantitative Explanation for the Apparent Anomalous Temperature Dependence of OH + HO₂ → H₂O + O₂ through Multi-Scale Modeling

M. P. Burke, S. J. Klippenstein, L. B. Harding, Proc. Comb. Inst. (in press)

CHEMICAL ACCURACY FROM AB INITIO MOLECULAR ORBITAL CALCULATIONS

Martin Head-Gordon
Department of Chemistry, University of California, Berkeley, and,
Chemical Sciences Division, Lawrence Berkeley National Laboratory,
Berkeley, CA 94720.
mhg@cchem.berkeley.edu

1. Scope of Project.

Short-lived reactive radicals and intermediate reaction complexes play central roles in combustion, interstellar and atmospheric chemistry. Due to their transient nature, such molecules are challenging to study experimentally, and our knowledge of their structure, properties and reactivity is consequently quite limited. To expand this knowledge, we develop new theoretical methods for reliable computer-based prediction of the properties of such species. We apply our methods, as well as existing theoretical approaches, to study prototype radical reactions, often in collaboration with experimental efforts. These studies help to deepen understanding of the role of reactive intermediates in diverse areas of chemistry. They also sometimes reveal frontiers where new theoretical developments are needed in order to permit better calculations in the future.

2. Summary of Recent Major Accomplishments.

2.1 *Improved density functionals.*

Self-interaction errors in density functional theory can be as large as 50 kcal/mol for as simple a molecule as H_2^+ , treated by the widely used B3LYP functional. We have been interested in the use of range-separation to reduce self-interaction, and have developed the ω B97 family of functionals, that yield a reduction of roughly 2/3 in self-interaction errors, relative to e.g B3LYP. A recent comprehensive set of benchmarks has further established the good performance of these functionals for both ground and excited state properties that involve significant self-interaction effects [18], as well as cation radicals [15]. The analytical gradient has been implemented for excited state calculations involving these functionals [10]. Like all density functionals, there are still significant limitations and thus potentially significant scope for further improvements. The most clear-cut failures are for problems that involve strong electron correlations, which are partially addressed by the separate developments described in 2.3 and 2.4 below. Another example is charge transfer between Li and polycyclic aromatic hydrocarbons [6].

2.2 *Approximate Brueckner Orbital Methods.*

It is most common to perform correlation treatments such as second order Moller-Plesset (MP2) theory or coupled cluster theory using reference mean field orbitals from e.g. Hartree-Fock calculations. However, in a well-defined sense, the best orbitals are those that minimize the energy in absence of single excitations, which are termed Brueckner orbitals. For high levels of correlation (e.g. CCSDT), it doesn't matter greatly whether or not single excitations are included versus finding the Brueckner orbitals. But for more

approximate methods like MP2, it can make a very large difference. This is illustrated by our recent study of the soliton defect in polyene radicals [22], where use of Brueckner orbitals is essential to obtain realistic estimates of the size of the radical defect, as well reasonable values of $\langle S^2 \rangle$. For example, for the ground doublet state of C₄₁H₄₃, $\langle S^2 \rangle = 6.8$ for MP2 versus 0.78 for a Brueckner orbital based MP2 method (the O2 approach). The same effect also turns out to be important in fullerenes such as C₃₆ and C₆₀ [19]. We have also demonstrated the value of optimized orbitals using approximate spin-projection methods [16], as well as valence active space problems [1].

2.3 *Pairing methods for strong electron correlations.*

Strong electron correlations may be defined as effects which cause significant deviations in orbital occupations from the Pauli Principle. To treat large molecules with strong correlations (e.g. singlet biradicaloids), we have been developing generalized valence bond coupled cluster methods, which systematically approximate the valence space Schrodinger equation (CASSCF). Perfect pairing is the starting point: exact for one pair, and extensive. The next well-defined level is the perfect quadruples (PQ) model which is exact for two pairs (matches CASSCF) and extensive. This is followed by the perfect hexuples (PH) model, which is exact for 3 pairs of electrons, and scales computationally with only the 5th power of molecule size [3]. PH seems to be an excellent approximation to CASSCF for computational organic chemistry. It is a truncation of CCSDTQ56 in the valence active space, retaining only terms that entangle no more than 3 pairs of electrons, which accounts for its remarkably low computational scaling. However, the complexity of the model means that an automatic computer-generated implementation, which exploits sparsity, is essential [2]. We have begun to explore dynamical correlation corrections to the PQ and PH models [7,14], and have also made progress on the challenging problem of orbital optimization for these active space methods [16].

2.4 *Valence bond methods for strong electron correlations.*

Instead of approximating the CASSCF limit for treating strong correlations, another, relatively unexplored possibility is to approximate the spin-coupled valence bond (SCVB) wavefunction, which takes a simple product of n non-orthogonal spatial orbitals and spin-couples those orbitals together in all possible ways (the number grows exponentially with n). We have shown that it is possible to exactly reproduce the SCVB limit for fully broken bonds with only quadratic degrees of freedom (provided that the final state is describable by spin-projected unrestricted Hartree-Fock). Taking this limit as a model defines what we call the coupled cluster valence bond (CCVB) method [17]. We have now completed an implementation of CCVB which permits the method to be explored for realistic systems, and intend to more fully characterize its strengths and weaknesses. It appears to be very well-suited to describing strong spin correlations such as those associated with the antiferromagnetic coupling of high spin electrons at two different centers. Bond dissociations and some types of metal complexes are in this class.

2.5 *New algorithms.*

A variety of interesting novel algorithms for electronic structure calculations have been explored. First, we have reported possibly the most efficient implementation to date of the problem of computing the Cholesky decomposition and inversion associated with the

overlap matrix [12]. This is essential for large-scale DFT calculations. Second, we have explored a very interesting operator identity that permits the two-electron integrals of quantum chemistry to be replaced by products of overlap and kinetic energy integrals [13]. Third, we have investigated the use of the so-called higher order singular value decomposition to compact the tensors associated with electron correlation [9].

2.6 Fundamental studies of chemical bonding.

In addition to studies of hydrocarbon polyene radicals [22] to explore the soliton defect, we have also explored the interaction of PAH's with Li [6], and investigated electron correlations in the fullerenes, comparing C₃₆ and C₆₀ [19]. Other applications to biradicaloid [11] and tetradicaloid [4] molecules have recently been completed, including the tetradicaloid states associated with the singlet fission process in polycyclic aromatic hydrocarbons such as pentacene [20].

3. Summary of Research Plans.

- Improved density functionals: We are interested in further reducing self-interaction errors as well as improving the treatment of long-range correlations associated with van der Waals interactions.
- Extensions of the CC-VB model: The CCVB model can possibly be simplified for increased computational efficiency, and can possibly also be generalized to permit correct treatment of problems that lie beyond the present projected UHF limit.
- Efficient large-scale implementation of the PQ and PH models: A substantial barrier to routine use of methods such as PH is that fact that our present code does not perform at anywhere near peak machine speeds. We are attempting to address this limitation.
- Combining CC-VB ideas and coupled cluster theory. We believe that it may be possible to combine some of the best features of our new CCVB model (spin-pure bond-breaking) with some of the best features of coupled cluster theory.
- New studies of the properties of reactive radicals and radical reactions. New collaborations are planned in collaboration with experimental groups in the program.

4. Publications from DOE Sponsored Work, 2010-present.

- [1] "Orbitals that are unrestricted in active pairs for generalized valence bond coupled cluster methods", K.V. Lawler, D.W. Small and M. Head-Gordon *J. Phys. Chem. A* 114, 2930-2938 (2010).
- [2] "A Sparse Framework for the Derivation and Implementation of Fermion Algebra", J.A. Parkhill and M. Head-Gordon, *Mol. Phys.* 108, 513-522 (2010).
- [3] "A tractable and accurate model for static electron correlations: The perfect hexuples model", J.A. Parkhill, and M. Head-Gordon, *J. Chem. Phys.* 133, 024103 (2010) (10 pages).
- [4] "Theoretical study of substituted PBPB dimers: Structural analysis, tetradical character and excited states", F. Bell, D. Casanova and M. Head-Gordon, *J. Am. Chem. Soc.* 132, 11314-11322 (2010)
- [5] "An Additive Long-range Potential to Correct for the Charge-transfer Failure of Time-dependent Density Functional Theory", A. Dreuw, J. Plotner, M. Wormit, M. Head-Gordon, and A.D. Dutoi, *Z. Phys. Chem.* 224, 311-324 (2010)
- [6] "Modeling the charge transfer between alkali metals and polycyclic aromatic hydrocarbons using electronic structure methods", T. Baker and M. Head-Gordon, *J. Phys. Chem. A* 114, 10326-10333 (2010).

- [7] “A truncation hierarchy of coupled cluster models of strongly-correlated systems based on perfect-pairing references: the single plus doubles models”, J.A. Parkhill and M. Head-Gordon, *J. Chem. Phys.* 133, 124102 (2010)
- [8] “Ab initio molecular dynamics with dual-basis methods”, R.P. Steele, M. Head-Gordon and J.C. Tully, *J. Phys. Chem.* 114, 11853-11860 (2010)
- [9] “The higher-order singular value decomposition in quantum chemistry”, F. Bell, D.S. Lambrecht and M. Head-Gordon, *Mol. Phys.* 108, 2759-2774 (2010).
- [10] “A parallel implementation of the analytic nuclear gradient for time-dependent density functional theory within the Tamm-Dancoff approximation”, F.-L. Liu, Z. Gan, Y. Shao, C.-P. Hsu, A. Dreuw, M. Head-Gordon, B.T. Miller, B.R. Brooks, J.-G. Yu, T.R. Furlani and J. Kong, *Mol. Phys.* 108, 2791-2800 (2010).
- [11] “Intermediate-Valence Tautomerism in Decamethylterbocene Complexes of Methyl-Substituted Bipyridines”, C. Booth, D. Kazhdan, E. Werkema, M. Walter, W. Lukens, E. Bauer, Y.-J. Hu, L. Maron, O. Eisenstein, M. Head-Gordon, R. Andersen, *J. Am. Chem. Soc.* 132, 17537-17549 (2010).
- [12] “Fast Sparse Cholesky Decomposition and Inversion using Nested Dissection Matrix Reordering”, K. Brandhorst and M. Head-Gordon, *J. Chem. Theor. Comput.* 7, 351-368 (2011).
- [13] “A new fitting metric for resolution of the identity second-order Møller-Plesset perturbation theory”, D.S. Lambrecht, K. Brandhorst, W.H. Miller, and M. Head-Gordon *J. Phys. Chem. A* 115, 2794-2801 (2011).
- [14] “The formulation and performance of a perturbative correction to the Perfect Quadruples model”, J.A. Parkhill, J. Azar, and M. Head-Gordon, *J. Chem. Phys.* 134, 154112 (2011).
- [15] “Ground Electronic State of Peptide Cation Radicals: A Delocalized Unpaired Electron?” A.I. Gilson, G. van der Rest, J. Chamot-Rooke, W. Kurlancheek, M. Head-Gordon, D. Jacquemin, and G. Frison, *J. Phys. Chem. Lett.* 2, 1426-1431 (2011).
- [16] “Approximate spin-projected broken symmetry energies from optimized orbitals that are unrestricted in active pairs”, A.M. Mak, K.V. Lawler, and M. Head-Gordon, *Chem. Phys. Lett.* 515, 173-178 (2011).
- [17] “Post-modern valence bond theory for strongly correlated electron spins”, D.W. Small and M. Head-Gordon, *Phys. Chem. Chem. Phys.* 13, 19285-19297 (2011).
- [18] “How well do post-GGA density functionals perform on molecular problems where self-interaction effects are significant?” N. Mardirossian, J.A. Parkhill and M. Head-Gordon, *Phys. Chem. Chem. Phys.* 13, 19325-19337 (2011).
- [19] “On the Nature of Correlation in C₆₀”, D. Stück, T. Baker, P. Zimmerman, W. Kurlancheek, and M. Head-Gordon, *J. Chem. Phys.* 135, 194306 (2011) (5 pages).
- [20] “Mechanism for Singlet Fission in Pentacene and Tetracene: From Single Exciton to Two Triplets”, P.M. Zimmerman, F. Bell, D. Casanova, and M. Head-Gordon, *J. Am. Chem. Soc.* 133, 19944-19952 (2011).
- [21] “An energy decomposition analysis for intermolecular interactions from an absolutely localized molecular orbital reference at the coupled-cluster singles and doubles level”, R.J. Azar and M. Head-Gordon, *J. Chem. Phys.* **136**, 024103 (2012)
- [22] “Exploring the competition between localization and delocalization of the neutral soliton defect in polyenyl chains with the orbital optimized second order opposite spin method”, W. Kurlancheek, R. Lochan, K.V. Lawler, and M. Head-Gordon, *J. Chem. Phys.* 136, 054113 (2012) (11 pages).
- [23] “A computational and experimental study of the mechanism of hydrogen generation from water by a molecular molybdenum-oxo pentapyridine catalyst”, E.J. Sundstrom, X. Yang, V.S. Thoi, H.I. Karunadasa, C.J. Chang, J.R. Long and M. Head-Gordon, *J. Am. Chem. Soc.* 134, 5233-5242 (2012).

Laser Studies of Combustion Chemistry

John F. Hershberger

Department of Chemistry and Biochemistry
North Dakota State University
NDSU Dept. 2735, PO Box 6050
Fargo, ND 58108-6050
john.hershberger@ndsu.edu

Time-resolved infrared diode laser absorption and laser-induced fluorescence spectroscopy are used in our laboratory to study the kinetics and product channel dynamics of chemical reactions of importance in the gas-phase combustion chemistry of nitrogen-containing species. This program is aimed at improving the kinetic database of reactions crucial to modeling of combustion processes, with emphasis on NO_x chemistry. When feasible, we perform quantitative measurement of both total rate constants and product branching ratios.

NCCO Kinetics

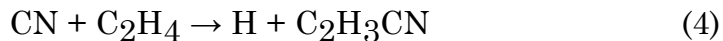
We have complete studies of the kinetics of NCCO radicals reacting with several molecules. As described in last year's report, the NCCO+O₂ and NCCO + NO reactions are slow at low pressure, but have pressure-dependent rate constants consistent with formation of a collisionally-stabilized adduct. The NCCO+NO₂ reaction, in contrast, is fast at low pressures. Possible product channels include:



We measured a total rate constant of $(2.1 \pm 0.1) \times 10^{-11} \text{ cm}^3 \text{ molecule}^{-1} \text{ s}^{-1}$ at 298 K and ~1.0 Torr total pressure, substantially faster than NCCO+NO or NCCO + O₂. Ab initio calculations suggest a complicated potential energy surfaces, with many loosely-bound intermediate structures, but channel (5a) appears to be the most likely product channel. Experimentally, we detected and quantified CO, CO₂, NO, and N₂O products by infrared spectroscopy. One complication is that the photolysis precursor forms CN radicals as well as NCCO, and the CN+NO₂ reaction produces some of the same products:



In order to suppress secondary chemistry of CN radicals, we added C₂H₄ reagent to the reaction mixture. NCCO does not react with C₂H₄, but CN does:



We find that upon addition of C₂H₄ reagents, the N₂O yield drops to near zero. The experimental data along with kinetic modeling simulations clearly indicate that N₂O was primarily formed by secondary chemistry, not channel (1c). The CO₂ yield, however, only drops by a moderate amount when C₂H₄ reagent is added, indicating a substantial yield of channels (1a) and/or (1d). The CO yield is small, indicating that channel (1a) dominates. We can also detect the NO yield, but numerous secondary reactions contribute to NO formation, and they are not suppressed by C₂H₄ reagents because the resulting H atoms from channel (4) react with NO₂ to produce NO.

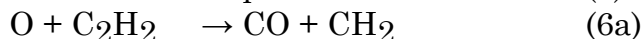
In summary, both experimental and computational evidence indicates that channel (1a) is the dominant product channel of this reaction. We estimate that channels (1b), (1c), and (1d) contribute at most a 0.05 branching fraction.

O + ICN Kinetics

In last year's DOE report, we stated that CN does not react with SO₂, with an upper limit of $k < 3.1 \times 10^{-14} \text{ cm}^3 \text{ molecule}^{-1} \text{ s}^{-1}$ at 298 K. This result was in disagreement with the one previous reported value¹ of $4.40 \times 10^{-12} \text{ cm}^3 \text{ molecule}^{-1} \text{ s}^{-1}$. Our study was performed by time-resolved detection of CN decay rates upon 266-nm photolysis of ICN/SO₂/buffer gas mixtures; i.e. a very standard flash photolysis experiment under pseudo-first order conditions. One possible concern was that oxygen atoms (perhaps produced by CN reacting with trace O₂, or by SO₂ multiphoton photolysis) might react with the ICN precursor molecules, possibly re-forming CN radicals. If this reaction is fast enough, the regeneration of CN would cause the signal to decay more slowly than expected, resulting in an erroneously small rate constant measurement. Although this possibility seemed rather unlikely, we felt it would be wise to investigate this reaction. No direct measurement of the rate of this reaction exists in the literature, although an early study² suggested the possibility of this reaction. Possible product channels include:



We have investigated this reaction using a relative rate technique. Several different approaches were attempted; the method found to be cleanest was to photolyze an SO₂/ICN/C₂H₂/NO/buffer gas mixture at 193 nm. SO₂ absorbs most strongly under these conditions, leading to SO + O(³P). The ICN and C₂H₂ then compete for oxygen atoms in the following reactions:



The CO product yield from (6a) then depends on the competition between reactions (5) and (6). Kinetic analysis shows that 1/[CO] is expected to increase linearly with [ICN], and the slope and intercept of this line can be used to obtain the desired rate constant k_5 . Possible complications include subsequent secondary chemistry of the CH₂ and HCCO radicals produced in (6). If these were to react with ICN, also producing CO, the result would be distorted. By including NO in the mixture, we remove these radicals:

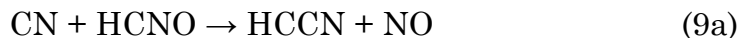


Although reaction (7b) results in additional CO formation, the CO yield is still governed by the competition between reactions (5) and (6). Another complication is that ICN photolysis at 193 nm produces CN radicals, which may react with trace O₂ or other species to ultimately produce CO; this CO yield would increase with [ICN]. We suppressed this by using isotopically labeled ¹³C₂H₂ reagents, and detecting ¹³CO products. Any CO produced from CN radicals from ICN photolysis would be formed in the ¹²CO isotope. We found this isotopic substitution made a small but measurable effect on our results.

Analysis of the experimental data yields a rate constant of $k_5 = (3.72 \pm 1.0 - 26.2 \pm 1.5) \times 10^{-14} \text{ cm}^3 \text{ molecule}^{-1} \text{ s}^{-1}$ over the total pressure range of 1.5 - 9.5 Torr. Two comments are in order: At low pressure, the rate constant is too slow to be a major problem in experiments such as the CN+SO₂ study described above; in other words, ICN may still be considered a quite clean photolysis precursor for CN radicals. Another comment is that the observed pressure dependence suggests that adduct formation, channel (5c), not (5a) or (5b), dominates this reaction. This is in agreement with ab initio calculations we have performed, which indicate a substantial barrier to (5b), and that (5a) is in fact a highly endothermic channel.

CN + HCNO

We have previously published a paper on the CN + HCNO reaction,³ reporting that the major product channel is (9a):



That conclusion was based on a measurement of [¹⁸O¹²C¹⁸O]/[¹⁶O¹²C¹⁸O] ratios upon inclusion of N¹⁸O reagent in the reaction mixture, and consideration of likely secondary chemistry. Our result disagrees with an ab initio study,⁴ which predicted that (9b) dominates, although the differences in barrier heights to the two channels are quite small. We are re-investigating this reaction by measuring the [NO] yield directly produced in (9a), while quenching any NCO formation (and subsequent NCO secondary chemistry) with N¹⁸O. Preliminary results appear to confirm our earlier experimental measurement.

References

1. T.A. Titarchuk and J.B. Halpern, Chem. Phys. Lett. 232, 192 (1995).
2. Q.J.F. Grady, C.G. Freeman, and I.F. Phillips, J. Phys. Chem. 72, 743 (1968).
3. W. Feng and J.F. Hershberger, J. Phys. Chem A 110, 12184 (2006).
4. J.-L. Pang, H.-B. Xie, S.-W. Zhang, Y.-H. Ding, and A.-Q. Tang, J. Phys. Chem. A 112, 5251 (2008).

Publications acknowledging DOE support (2010-present)

1. "Infrared Diode Laser Study of the Kinetics of the NCCO + O₂ Reaction", W. Feng and J.F. Hershberger, Chem. Phys. Lett. 488, 140 (2010).
2. "Kinetics and Mechanism of the NCCO + NO Reaction", W. Feng and J.F. Hershberger, J. Phys. Chem. A 114, 6843 (2010).
3. "Kinetics of the CN + CS₂ and CN + SO₂ Reactions", W. Feng and J.F. Hershberger, J. Phys. Chem. A 115, 286 (2011).
4. "Kinetics of the NCCO + NO₂ Reaction", W. Feng and J.F. Hershberger, J. Phys. Chem. A 115, 12173 (2011).
5. "Kinetics of the O + ICN Reaction", W. Feng and J.F. Hershberger, J. Phys. Chem. A (submitted).

Breakthrough Design and Implementation of Electronic and Vibrational Many-Body Theories

So Hirata (principal investigator: DE-FG02-11ER16211; formerly DE-FG02-04ER15621)

Department of Chemistry, University of Illinois at Urbana-Champaign,

600 South Mathews Avenue, Urbana, IL 61801

sohirata@illinois.edu

Program Scope

Predictive chemical computing requires hierarchical many-body methods of increasing accuracy for both electrons and vibrations. Such hierarchies are established, at least conceptually, as configuration-interaction (CI), many-body perturbation (MP), and coupled-cluster (CC) methods, which all converge at the exact limit with increasing rank of a hierarchical series. These methods can generate results of which the convergence with respect to various parameters of calculations can be demonstrated and which can thus be predictive in the absence of experimental information.

The wide use of the hierarchical electronic and vibrational many-body methods has, however, been hindered (1) by the immense cost of *executing* the calculations with these methods and, furthermore, the nonphysical rapid increase of the cost with increasing molecular size, (2) by the complexity and cost of *developing* some of the high-rank members of these methods, and (3) by the slow convergence of electronic energies and wave functions with respect to one-electron basis set sizes, which further drives up the cost of execution. For applications to large molecules and solids, the additional difficulties arise by the lack of (4) size consistency in some methods (whose energies and other observables scale non-physically with size) and of (5) efficient methods that work for strong correlation.

The overarching goal of our research is to address all three difficulties for electrons and vibrations in small molecules in the gas phase and all five for solids and molecules in condensed phases. We have eradicated the second difficulty (the complexity of equations and cost of implementations) for electrons by developing a computerized symbolic algebra system that completely automates the mathematical derivations of electron-correlation methods and their implementation. For vibrations, an assortment of vibrational many-body methods has been implemented in the general-order algorithm that allows us to include anharmonicity and vibrational mode-mode couplings to any desired extent. We have also addressed the third difficulty (the slow convergence with respect to basis set) by departing from the conventional Gaussian basis sets and introduce a new hierarchy of converging electron-correlation methods with completely flexible but rational (e.g., satisfying asymptotic decay and cusp conditions) basis functions such as numerical basis functions on interlocking multicenter quadrature grids and explicit r_{12} (inter-electronic distance) dependent basis functions.

Our current research focus is to address the first (the cost of execution) and fourth (the size consistency) difficulties to make the hierarchical electronic and vibrational methods applicable to solids.

Recent Progress

We have made important advances to the fundamental theories and algorithms of electronic and vibrational many-body methods of molecules and solids. Some of these are published, while others are still in various stages of investigation. We have obtained an easily understandable and pedagogical, if not completely rigorous, proof of extensivity of energy in metallic and non-metallic crystals by analyzing the distance decay of chemical interactions. On this basis, we have shown that the conventional definitions of the Fock and two-electron integrals need to be revised. This does not alter the Hartree–Fock (HF) orbitals, energies, electron-correlation energies, or excitation energies, but it does alter the orbital energies and indeed accelerate the convergence of their lattice sums. We have also proposed a number of theorems pertaining to the size consistency of electronic and vibrational methods. We have extended diagrammatic size-extensive vibrational self-consistent field (XVSCF) method to anharmonic geometry corrections.

Since the 32nd Annual Combustion Research Meeting, 6 peer-reviewed papers⁵⁻¹⁰ and one book chapter¹ in *Annual Reviews of Physical Chemistry* have been published and two more papers^{20,21} are currently under review. In total, 21 publications¹⁻²¹ (including two submitted) have resulted from this grant in 2010–2012. During the same period, the PI was an invited speaker at 14 international and domestic conferences and gave 11 invited talks at universities and national laboratories including the Moskowitz Memorial Lecture at The University of Minnesota. The PI received a Scialog Award from the Research Corporation for Science Advancement. The PI served as a member of the editorial boards of *Physical Chemistry Chemical Physics*, *Theoretical Chemistry Accounts*, *The Journal of Chemical Physics*, and *International Journal of Quantum Chemistry*. The PI was a guest editor of the 50th Year Anniversary Issue (with the regular editors, Christopher Cramer and Donald Truhlar as well as five other guest editors) of *Theoretical Chemistry Accounts* and of the Special Issue (with Gregory Beran) on Fragment and Local Orbital Methods in Electronic Structure Theory in *Physical Chemistry Chemical Physics*.

Thermodynamic limit of the energy density in a crystal (Hirata and Ohnishi).^{1,5,10} A thermodynamic observable of a chemical system is said to be either extensive or intensive. Extensive quantities include energy (E), entropy, mass, and so forth. They increase asymptotically linearly as we increase the volume (V) of the system while maintaining the particle density and composition unchanged. Intensive quantities such as temperature, chemical potential, and pressure are asymptotically independent of V . The assumption that E is extensive or, equivalently, E/V converges at a finite value in the thermodynamic (infinite- V) limit is one of the foundations of chemical thermodynamics. Yet, proving this (“the stability of matter of the second kind”) mathematically turns out to be extremely difficult, taking the finest mathematicians forty years to accomplish. The proof for electrically neutral matter consisting of mobile electrons and nuclei was obtained by Lebowitz and Lieb. The proof for electrically neutral perfect crystals was presented by Fefferman. Only in 2009 was the proof completed by Hainzl *et al.*, who reported those for perfect crystals and crystals with defects. We have presented a pedagogical, semi-rigorous proof of the existence of the thermodynamic limit of E/V in an electrically neutral perfect crystal, which is an alternative to that of Fefferman’s. Our shorter, simpler proof consists in showing the existence of thermodynamic limits for individual components of exact E/V in the spirit of Harris, of Lieb and Simon, of Catto *et al.*, and of Pisani *et al.*, who considered the Hartree or HF energy components. Our work is concerned with the whole, exact energy of an electrically neutral metallic or nonmetallic crystal. We have also addressed the issue of divergences of correlation energies in metals obtained by a perturbation theory in relation to the validity of this proof for such systems.

Charge-consistent redefinition of Fock and two-electron integrals (Ohnishi and Hirata).⁶ The Fock and two-electron integrals as defined and used by chemists involve the lattice sums of electron-electron repulsion that are not compensated by the corresponding lattice sums of nucleus-nucleus repulsion and electron-nucleus attraction. Consequently, some of them diverge in the thermodynamic limit. Solid-state physicists’ definitions of these quantities are different, carefully balancing the repulsive and attractive interactions. We thus redefine the Fock and two-electron integrals such that they contain the lattice sums of the electrostatic interactions between the net neutral charge densities by subtracting appropriate portion of the nuclear charge density in the unit cell from the electronic orbital pair density. These charge-consistent definitions are necessary to maintain the consistent size dependence of these integrals. We show that (1) the diagonal Fock integrals in the new definition converge more rapidly than the conventional Fock integrals as the former contain no charge-multipole interactions (see **Figure**); (2) the new and conventional definitions of the Fock integrals in the canonical HF orbital basis differ only in the diagonal elements merely by a constant and, hence,

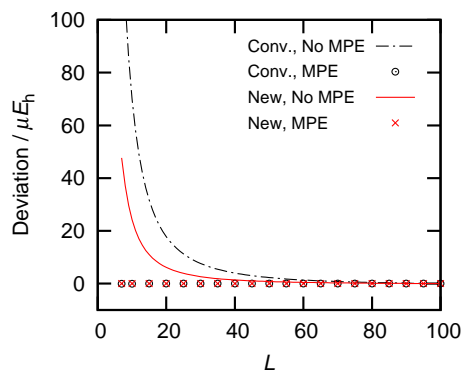


Fig. Convergence of orbital energies as a function of the number (L) of unit cells included in the lattice sums. MPE stands for multipole expansion corrections.

the HF energy, orbitals, correlation energies, etc. are not altered by the redefinition; and (3) the multipole expansion (MPE) corrections to the lattice sums of the charge-consistent Fock integrals are derived and shown to be simpler than the conventional counterparts because some of the multipole–multipole interactions are no longer there in the charge-consistent definition of the Fock integrals.

Size-consistency theorems (Hirata).^{1,10} On the basis of the above analysis of extensivity, I have derived some theorems pertaining to size consistency of electronic and vibrational methods. For example, the *normalization theorem* states that the excitation amplitudes of an extensive operator are subject to intermediate normalization and scale as $V^{1-n/2}$ where V is the volume and n is the number of edges of the corresponding vertex, whereas the amplitudes of an intensive operator are normalized and scale as $V^{1/2-n/2}$. The *intensive diagram theorem* (which complements the extensive diagram theorem of Goldstone) states that the equations defining an intensive quantity of a size-consistent method consist of connected diagrams with two intensive vertexes. The equations that determine the intensive amplitudes do not need to be connected or linked insofar as they have a prescribed number of intensive vertexes. I have also introduced the *extensive-intensive consistency theorem* which characterizes the methods that are size consistent for extensive and intensive quantities simultaneously.

Size-extensive vibrational self-consistent field method with anharmonic geometry corrections (Hermes, Keçeli, and Hirata).²¹ In the XVSCF method introduced earlier [M. Keçeli and S. Hirata, *J. Chem. Phys.* **135**, 134108 (2011)] in support of this grant, only a small subset of even-order force constants that can form connected diagrams has been used to compute extensive total energies and intensive transition frequencies. The mean-field potentials of XVSCF formed with these force constants have been shown to be effectively harmonic, in accordance with Makri’s theorem, making basis functions, quadrature, or matrix diagonalization in the conventional VSCF method unnecessary. We introduce two size-consistent VSCF methods, XVSCF(n) and XVSCF[n], for vibrationally averaged geometries in addition to energies and frequencies including anharmonic effects caused by up to the n th-order force constants. The methods are based on our observations that a small number of odd-order force constants of certain types can form open, connected diagrams isomorphic to the diagram of the mean-field potential gradients and that these nonzero gradients shift the potential minima by intensive amounts, which are interpreted as anharmonic geometry corrections. XVSCF(n) evaluates these mean-field gradients and force constants at the equilibrium geometry and estimates this shift accurately, but approximately, neglecting the coupling between these two quantities. XVSCF[n] solves the coupled equations for geometry corrections and frequencies with an iterative algorithm, giving results that should be identical to those of VSCF when applied to an infinite system. We present the diagrammatic and algebraic definitions, algorithms, and initial implementations as well as numerical results of these two methods. The results show that XVSCF(n) and XVSCF[n] reproduce the vibrationally averaged geometries of VSCF for naphthalene and anthracene in their ground and excited vibrational states accurately at fractions of the computational cost.

Future Plans

For the electronic structure theory, we will explore the following ideas: (1) the finite-temperature extension of the second- and higher-order MP for molecules and polymers; (2) the use of Monte Carlo integrations with the Metropolis sampling scheme for second- and higher-order MP for molecules and polymers; (3) the use of Wannier functions for MP2 and CCSD for polymers.

For the vibrational structure theory, we pursue (3) the extension of XVSCF(n) and XVSCF[n] for one-dimensional solids and the calculation of anharmonic phonon dispersion curves of polymers; (4) the vibrational Dyson equation at the second order perturbation level for molecules and one-dimensional solids; (5) the anharmonic vibrational theory for thermal expansions.

Publications of DOE Sponsored Research (2010–Present)

Book chapters

1. S. Hirata, M. Keçeli, Y.-Y. Ohnishi, O. Sode, and K. Yagi, "Extensivity of energy and size-consistent electronic and vibrational structure methods for crystals," *Annual Reviews of Physical Chemistry* **63**, 131-153 (2012).
2. S. Hirata, O. Sode, M. Keçeli, and T. Shimazaki, "Electron correlation in solids: Delocalized and localized orbital approaches," a chapter in *Accurate Condensed-Phase Quantum Chemistry* edited by F. Manby, p.129–161 (CRC Press, Boca Raton, 2010).
3. S. Hirata, T. Shiozaki, E. F. Valeev, and M. Nooijen, "Eclectic electron-correlation methods," a chapter in *Recent Progress in Coupled-Cluster Methods: Theory and Application* edited by P. Carsky, J. Paldus, and J. Pittner, p.191–217 (Springer, Dordrecht, 2010).
4. S. Hirata, P.-D. Fan, M. Head-Gordon, M. Kamiya, M. Keçeli, T. J. Lee, T. Shiozaki, J. Szczepanski, M. Vala, E. F. Valeev, and K. Yagi, "Computational interstellar chemistry," a chapter in *Recent Advances in Spectroscopy: Astrophysical, Theoretical and Experimental Perspective* edited by R. K. Chaudhuri, R. K. Mekkaden, M. V. Raveendran, A. S. Narayanan, p.21–30 (Springer-Verlag, Berlin, 2010).

Refereed articles (reviews, perspectives, and editorials in bold letters)

5. S. Hirata and Y.-Y. Ohnishi, *Physical Chemistry Chemical Physics* [Special Issue on "Fragment and Local Orbital Methods in Electronic Structure Theory"] (in press, 2012), "Thermodynamic limit of the energy density in a crystal."
6. Y.-Y. Ohnishi and S. Hirata, *Chemical Physics* [Debashis Mukherjee Special Issue] (in press, 2012), "Charge-consistent redefinition of Fock integrals."
7. **S. Hirata, *Theoretical Chemistry Accounts* [an introductory article in the 50th Anniversary Issue] **131**, 1071 (2012) (4 pages), "Electronic structure theory: Present and future challenges."**
8. M. Keçeli and S. Hirata, *The Journal of Chemical Physics* **135**, 134108 (2011) (11 pages), "Size-extensive vibrational self-consistent field method."
9. Y.-Y. Ohnishi and S. Hirata, *The Journal of Chemical Physics* **135**, 094108 (2011) (10 pages), "Hybrid coupled-cluster and perturbation method for extended systems of one-dimensional periodicity."
10. **S. Hirata, *Theoretical Chemistry Accounts* [an invited Feature Article] **129**, 727-746 (2011), "Thermodynamic limit and size-consistent design."**
11. D. G. Patel, Y.-Y. Ohnishi, Y. Yang, S.-H. Eom, R. T. Farley, K. R. Graham, J. Xue, S. Hirata, K. S. Schanze, and J. R. Reynolds, *Journal of Polymer Science Part B: Polymer Physics* **49** 557-565 (2011), "Conjugated polymers for pure UV light emission: Poly(*meta*-phenylenes)."
12. I. Grabowski, V. Lotrich, and S. Hirata, *Molecular Physics* [QTP Special Issue] **108**, 3313-3322 (2010), "Ab initio DFT--the seamless connection between WFT and DFT."
13. **S. Hirata, *Molecular Physics* [QTP Special Issue] **108**, 3113–3124 (2010), "Bridging quantum chemistry and solid-state physics."**
14. M. Keçeli and S. Hirata, *Physical Review B* **82**, 115107 (2010) (6 pages), "Fast coupled-cluster singles and doubles for extended systems: Application to the anharmonic vibrational frequencies of polyethylene in the Γ approximation."
15. O. Sode and S. Hirata, *The Journal of Physical Chemistry A* [Klaus Ruedenberg Special Issue] **114**, 8873–8877 (2010), "Second-order many-body perturbation study of solid hydrogen fluoride."
16. M. Keçeli, S. Hirata, and K. Yagi, *The Journal of Chemical Physics* **133**, 034110 (2010) (6 pages), "First-principles calculations on anharmonic vibrational frequencies of polyethylene and polyacetylene in the Γ approximation."
17. S. Hirata, M. Keçeli, and K. Yagi, *The Journal of Chemical Physics* **133**, 034109 (2010) (14 pages), "First-principles theories for anharmonic lattice vibrations."
18. Y.-Y. Ohnishi and S. Hirata, *The Journal of Chemical Physics* **133**, 034106 (2010) (8 pages), "Logarithm second-order many-body perturbation method for extended systems."
19. T. Shiozaki and S. Hirata, *The Journal of Chemical Physics (Communications)* **132**, 151101 (2010) (4 pages), "Explicitly correlated second-order Møller–Plesset perturbation method for extended systems."

Submitted articles

20. R. D. Thomas, I. Kashperka, E. Vigren, W. Geppert, M. Hamberg, M. Larsson, M. af Ugglas, V. Zhaunerchyk, N. Indriolo, K. Yagi, S. Hirata, and B. J. McCall, *Astrophysical Journal* (submitted, 2012), "Dissociative recombination of vibrationally cold CH_3^+ and interstellar implications."
21. M. R. Hermes, M. Keçeli, and S. Hirata, *The Journal of Chemical Physics* (submitted, 2012), "Size-extensive vibrational self-consistent field method with anharmonic geometry corrections."

Generalized Van Vleck Variant of Multireference Perturbation Theory

Mark R. Hoffmann
University of North Dakota
Chemistry Department
Grand Forks, ND 58202-9024
Email: mhoffmann@chem.und.edu

I. Project Scope

There is a continuing need to develop new, cutting edge theoretical and computational electronic structure methods to support the study of complex potential energy surfaces (PESs). While standard methods of computational chemistry are usually adequate for studying the ground electronic states of molecular species near their equilibrium geometries, reaction intermediates, transition states and excited states generally require advanced methods that take into account their multiconfigurational nature. Multireference (MRPT) and quasidegenerate (QDPT) perturbation theories have been demonstrated to be efficient and effective for the description of electron correlation in essentially arbitrarily complex molecules. Recent work demonstrated that the mathematically robust and physically correct structures in our MRPT, called Generalized van Vleck Perturbation Theory (GVVPT), are amenable to highly efficient algorithms. Specifically, second- and third-order approximations of GVVPT (i.e., GVVPT2 and GVVPT3) utilize routines in common with our efficient macroconfiguration-based, configuration-driven MRCISD¹. Consequently, theoretical and computational development can proceed by first addressing the structurally simpler equivalent CI problem. Chemical problems that are not addressed readily by other theoretical methods become accessible to MRPT or QDPT: problems such as the descriptions of large regions of excited electronic state PESs of polyatomics, especially when the characters of the excited states are doubly excited relative to the ground state, and the characterizations of multiple PESs of the same symmetry in close proximity. Within the scope of this grant, we apply these theoretical techniques primarily to combustion-relevant Group 15 and 16 oxides, and to develop their descriptions of derivative and spin-orbit nonadiabatic couplings.

II. Recent Progress

A.1. GVVPT2 Molecular Derivatives and Nonadiabatic Coupling Terms. The fully variational Lagrangian functional formalism, first introduced into quantum chemistry by Helgaker and Jørgensen,² provided the framework to construct analytical formulas for GVVPT2^{LoP7} and MRCISD^{LoP4} molecular gradients and nonadiabatic coupling terms. Computer programs for the gradients have been realized, and demonstrated to be correct even for difficult problems such as exemplified by one of the conical intersection seams of ozone (*vide infra*). Under this approach, a Lagrangian is formed from the constraint functions $\mathbf{e}(\mathbf{x}, \boldsymbol{\lambda}(\mathbf{x}))$, which determine the nonvariational electronic structure parameters $\boldsymbol{\lambda}(\mathbf{x})$ that influence the electronic energy, and a suitable function $g(\mathbf{x})$ which has a geometry gradient that corresponds to either the GVVPT2 (or MRCISD) molecular gradient or the GVVPT2 (or MRCISD) nonadiabatic coupling terms

$$\mathcal{L}(\mathbf{x}, \boldsymbol{\lambda}(\mathbf{x}), \boldsymbol{\eta}(\mathbf{x})) = g(\mathbf{x}, \boldsymbol{\lambda}(\mathbf{x})) + \langle \boldsymbol{\eta}(\mathbf{x}) | \mathbf{e}(\mathbf{x}, \boldsymbol{\eta}(\mathbf{x})) \rangle \quad (1)$$

In our completed work^{LoP4,LoP7}, it was shown that the nonredundant (or variational) rotation parameters for orthogonalized molecular orbitals (OMOs), the redundant rotation parameters for OMOs (i.e., to ensure quasicanonical orbitals), and the CI coefficients in the MCSCF space provided an appropriate set of $\boldsymbol{\lambda}(\mathbf{x})$ parameters. The corresponding constraint equations, $\mathbf{e}(\mathbf{x}, \boldsymbol{\eta}(\mathbf{x}))$, constitute a nonsingular set of simultaneous linear equations. While true, efforts to scale-up beyond transformation-based approaches, to iterative techniques, were faced with puzzling convergence issues that manifested themselves in the need to use unfeasibly large Lanczos or Arnoldi subspaces. Ultimately, it was realized that the source of the instability was the commonly used parameterization of the CI vectors in the MCSCF space and the affiliated constraint equation,

$$e_{ml}^c = \left\langle \tilde{F}_m \left| e^{-\Lambda(\mathbf{x})} H(\mathbf{x}) e^{\Lambda(\mathbf{x})} - E_I^{MC}(\mathbf{x}) \right| \tilde{\mathbf{F}}_M \right\rangle \mathbf{C}_{MI}(\mathbf{x}) + C_{ml}(\mathbf{x}) \left[1 - \sum_{n \in L_M} C_{nl}^2(\mathbf{x}) \right] \quad (2)$$

Specifically, since the eigenpair constraint needed to be combined with the normalization constraint, because of the requirement of a one-to-one correspondence between parameters and constraint equations, it became possible for the errors in the eigenpair part to offset the errors in the normalization part and additional (in fact, an infinite number of) non-physical solutions exist. Reparameterization in terms of state rotation operators,

$$|\tilde{\Phi}_P^{MC}(\mathbf{x})\rangle = e^{\hat{\Lambda}(\mathbf{x})} |\tilde{\Phi}_M^0(\mathbf{x})\rangle [e^{\mathbf{R}(\mathbf{x})}]_{MP}, \quad (3)$$

where

$$[e^{\mathbf{R}(\mathbf{x})}]_{MP} = \langle \tilde{\Phi}_M^0(\mathbf{x}) | e^{\hat{R}(\mathbf{x})} | \tilde{\Phi}_M^0(\mathbf{x}) \rangle, \quad (4)$$

and

$$\hat{R}(\mathbf{x}) = \sum_J \sum_{I(>J)}^{(P)(P+S)} R_{IJ}(\mathbf{x}) [|\tilde{\Phi}_I^0(\mathbf{x})\rangle \langle \tilde{\Phi}_J^0(\mathbf{x})| - |\tilde{\Phi}_J^0(\mathbf{x})\rangle \langle \tilde{\Phi}_I^0(\mathbf{x})|], \quad (5)$$

not only obviates separate conditions for eigenpairs and normalization, as expected, but allows continued use of the other, OMO-defined, orbital constraints. However, the elements of the response matrix are more complicated than those with the earlier, simpler parameterization. Development of concrete equations and modifications of the relevant sections of the computer programs is in progress.

A.2. Relativistic Effects. Two types of relativistic effects are considered within the scope of this project. One is the scalar (or spin-free) contribution and the other is spin-orbit coupling. In earlier work in this project, the spin-orbit terms were considered at the level of effective one-electron Breit-Pauli terms, and were included in the unperturbed model space Hamiltonian and as modifications to the nonrelativistic correction to the wave function. Scalar relativistic effects were considered at the level of second-order Douglas-Kroll-Hess (DKH). But, finite-order DKH approximations are being increasingly viewed as limited compared to the treatment of kinematic effects in exact transformations, such as in the exact two-component (X2C) approach.⁴ However, up to now there has not been a spin-free formulation of X2C that would preserve the useful spin-free plus Breit-Pauli paradigm, which preserves use of high performance computational chemistry codes for dynamic electron correlation. A spin-free X2C has been formulated and is being incorporated into relativistic GVVPT2 calculations.

Replacing the DKH approximation for the kinematic effects by a spin-free X2C variant has introduced an additional consideration. Specifically, the use of contracted basis functions in relativistic calculations can be problematic, because of requirements for restricted kinetic balance between large and small components of the wave function, and there is no *a priori* reason to expect that contractions that proved to be practically effective in DKH schemes will necessarily be useful in the context of calculating spin-free X2C. This in turn requires calculation of the so-called pVp-type integrals,

$$(\mathbf{a} | pVp | \mathbf{b}) = \int d\mathbf{r} \nabla \varphi(\mathbf{r}; \xi_a, \mathbf{a}, \mathbf{A}) \cdot \frac{1}{|\mathbf{r} - \mathbf{C}|} \nabla \varphi(\mathbf{r}; \xi_b, \mathbf{b}, \mathbf{B}) \quad (6)$$

in an uncontracted basis set, followed by a transformation which involves conventional overlap, kinetic energy and potential energy integrals. Contraction of the atomic basis integrals, critical for efficient calculation of molecular electronic structure, can proceed only then.

B. Ozone. While O₃ has been extensively studied both experimentally and theoretically, and there are many interesting resolved and unresolved questions to be addressed, we have specifically chosen one aspect as a model problem on which to assess the new GVVPT2 gradient code. Specifically, we

obtained^{LoP4} the position of the (near-)C_{2v} minimum of the conical intersection seam between the two lowest ¹A₁ states^{5,6} (cf. Figure), using a reasonable, but far from definitive, one-electron basis set (i.e. aug(sp)-cc-pVDZ). The GVVPT2 results were compared to MRCISD results using exactly the same basis set and active space, and to MRCISD literature results^{6,7}. A (12:7)-CAS reference model space was used to define the model and external CSFs. Preliminary GVVPT2 energy calculations were run using a (18:12)-CAS (composed of all the valence orbitals and valence electrons of O₃) and indicated that the (12:7)-CAS accounts for all of the dominant CSFs that are needed for each of the two lowest ¹A₁ electronic state. The (12:7)-CAS also does not include the CSFs that are needed to describe the two lowest ¹B₂ states. An active space with unbalanced number of b₂ and a₁ orbitals, as is the case in our study, cannot be expected to describe accurately distortions that could mix these orbitals, but this was not a major concern for present purposes. The molecular orbitals that were formed from the three 2s orbitals were restricted to be doubly occupied during the MCSCF orbital optimizations but were correlated during the GVVPT2 and MRCISD energy and gradient calculations.

The results of those calculations are displayed in the Table. They show that the GVVPT2 geometries closely agree with the MRCISD results and corroborate the observation that the GVVPT2 method is capable of providing an accurate description of potential energy surface for systems that are known to be require MRCISD or better to describe accurately. In their recent work, Han et al.⁷ performed line searches in the vicinity of the minimum energy point of the conical intersection seam of the two lowest ¹A₁ states. At a C_{2v} constrained geometry, with a fixed bond angle of 84.6°, they report bond lengths of 1.367 Å. They also show that, with the geometry constraint lifted, two bonds, of 1.386 Å and 1.396 Å, are obtained. Our results, which also optimized the bond angle (to 85.2°, GVVPT2, and 85.4°, MRCISD), are in very good agreement with their results. It is interesting to observe that for MRCISD an optimization that started with C_{2v} symmetry did not break C_{2v} symmetry, while our GVVPT2 results did (albeit by a very small amount, 0.002 Å), as was the case (by 0.010 Å) in the earlier study. Considering deficiencies in both the one-electron basis set, and the active space (and, in particular, balance of b₂ and a₁ orbitals) our results are far from definitive. Nonetheless, they demonstrate that GVVPT2 can be used to explore features on potential energy surfaces usually requiring a MRCISD study.

Fig. Sections of ozone PESs in vicinity of a conical intersection (from Fig. 2 of Ref. 6).

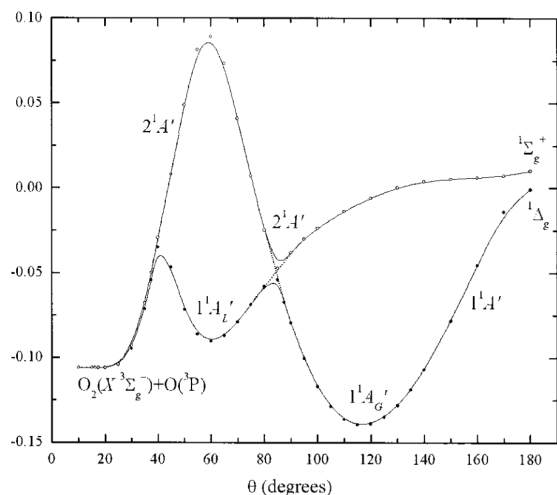


Table. Comparison of GVVPT2 results for minimum crossing point on ozone conical intersection seam with other methods.

	R ₁ (Å)	R ₂	∠
GVVPT2 (C _{2v}) ^a	1.382		85.2
GVVPT2 ^a	1.383	1.382	85.2
MRCISD ^a	1.391	1.391	85.4
MRCISD (C _{2v}) ^b	1.367		84.6 ^c
MRCISD ^b	1.396	1.386	85.0

^a LoP 7. ^b Ref. 7. ^c fixed value

III. Future Work

We expect continued progress in both the advancement of nuclear derivative and relativistic effects for GVVPT2 and MRCISD in applications to primarily Group 15 and 16 oxides. The highest priority vis-à-

vis GVVPT2 is to resolve the scale-up issue for gradients, which should be straightforward once the reparametrization of the state space rotations is complete. We then expect to make quick progress on scale-up of the GVVPT2 nonadiabatic coupling, since the response matrix is identical between GVVPT2 gradients and nonadiabatic coupling. With use of the in-house configuration-driven UGA code, effective one-electron Breit-Pauli spin-orbit coupling matrix elements, and now spin-free X2C treatment of kinematic effects, robust relativistic MRCISD and GVVPT2 computer programs, appropriate for much of the periodic table, should be operational before too long. As production computer codes become available, we intend to study the Se_mO_n potential energy surfaces in greater detail, with the eventual goal of understanding better the dynamics of $\text{Se}_m\text{O}_n + \text{Se}_m\text{O}_n$ reactions, with inclusion of nuclear derivative and spin-orbit nonadiabatic coupling. As the O_3 surfaces are related, but much is already known about them, we will also further investigate ozone, both for the purpose of validating new methodology and to provide insight into less understood features of the surfaces and reaction characteristics.

IV. References

- ¹ W. Jiang, Y. G. Khait, and M. R. Hoffmann, *J. Phys. Chem. A* **113**, 4374 (2009).
- ² T. Helgaker and P. Jørgensen, *Adv. Quantum Chem.* **19**, 183 (1988); *Theor. Chim. Acta* **75**, 111 (1989).
- ³ Y. G. Khait, D. P. Theis, and M. R. Hoffmann, *Mol. Phys.* **108**, 2703 (2010).
- ⁴ W. Liu, *Mol. Phys.* **108**, 1679 (2010).
- ⁵ J. Ivanic, G. J. Atchity, and K. Ruedenberg, *J. Chem. Phys.* **107**, 4307 (1997).
- ⁶ A. Kalemios and A. Mavridis, *J. Chem. Phys.* **129**, 054312 (2008).
- ⁷ H. Han, B. Suo, D. Xie, Y. Lei, Y. Wang, and Z. Wen, *Phys. Chem. Chem. Phys.* **13**, 2723 (2011).

V. Publications and Submitted Journal Articles Supported by this Project 2009-2012

- ¹ M. R. Hoffmann, D. Datta, S. Das, D. Mukherjee, A. Szabados, Z. Rolik, and P. R. Surjan, Comparative study of multireference perturbation theories for ground and excited states, *J. Chem. Phys.* **131**, 204104 (2009).
- ² E. S. Olson, A. Azenkeng, J. D. Laumb, R. R. Jensen, S. A. Benson, and M. R. Hoffmann, New Developments in the theory and modeling of mercury oxidation and binding on activated carbons in flue gas, *Fuel. Process. Technol.* **90**, 1360-1363 (2009).
- ³ D. P. Theis, Y. G. Khait, S. Pal, and M. R. Hoffmann, Molecular dipole moments using the GVVPT2 variant of multireference perturbation theory, *Chem. Phys. Lett.* **487**, 116 (2010).
- ⁴ Y. G. Khait, D. Theis, and M. R. Hoffmann, Lagrangian approach for geometrical derivatives and nonadiabatic coupling terms in MRCISD, *Mol. Phys.* **108**, 2703-2716 (2010).
- ⁵ Y. E. Bongfen Mbote, Y. G. Khait, C. Hardel, and M. R. Hoffmann, Multireference Generalized Van Vleck Perturbation Theory (GVVPT2) Study of the NCO + HCNO Reaction: Insight into Intermediates, *J. Phys. Chem. A* **114**, 8831-8836 (2010).
- ⁶ R. M. Mokambe, Y. G. Khait, and M. R. Hoffmann, Ground and Low-Lying Excited Electronic States of [3,3'] Bidiazirinylidene (C₂N₄), *J. Phys. Chem. A* **114**, 8119-8125 (2010).
- ⁷ D. Theis, Y. G. Khait, M. R. Hoffmann, GVVPT2 energy gradient using a Lagrangian formulation, *J. Chem. Phys.* **135**, 044117/1-14 (2011).
- ⁸ T. J. Dudley, J. J. Howard, and M. R. Hoffmann, Generalized Van Vleck Perturbation Theory Study of Chlorine Monoxide, *AIP Conference Proceedings* (in press).

Theoretical Kinetics and Non-Born–Oppenheimer Chemistry

Ahren W. Jasper
Combustion Research Facility, Sandia National Laboratories
Livermore, CA 94551-0969
ajasper@sandia.gov

I. Program Scope

Theoretical predictions of chemical kinetics are increasingly being used alongside experimental rate determinations. Under favorable circumstances and thanks to significant recent and ongoing developments of a variety of theoretical methods (quantum chemistry, transition state theory, master equation, molecular dynamics, etc.), as well as advances in high performance computing, theoretical kinetics calculations are now fairly broadly applicable and reliable, with accuracies that can rival those of experimental measurements. The goal of this project is the continued development and application of these predictive kinetics strategies, as well as the development of new theoretical methods to broaden their range of applicability. In particular, we have recently focused on the development of predictive methods for treating non-Born–Oppenheimer (electronically nonadiabatic) processes and pressure-dependent reactions.

II. Recent Progress

II.A. Theoretical Kinetics

The kinetics of *n*-alkyl (ethyl, propyl, and butyl) radicals R reacting with HO₂ was studied using variable reaction coordinate transition state theory and high-level quantum chemistry calculations. These reactions are relevant to both low-temperature and high-pressure chemistry, where HO₂ can be formed in significant amounts. These calculations showed that near room temperature the R + HO₂ addition (capture) rate coefficient is independent of the size of R, whereas at higher temperatures the rate coefficients differ by as much as a factor of three for different R. In every case, the major products are predicted to be RO + OH and RH + ³O₂, the former via capture and an ROOH* intermediate and the latter via direct abstraction on the triplet surface.

In collaboration with CRF experimentalist Hansen, dissociation thresholds and ionization energies were calculated for species relevant to the chemistry of tetrahydrofuran and methylcyclohexane flames. These joint theoretical/experimental studies revealed the presence of competing cyclic and ring-opening pathways for fuel decomposition and oxidation. We also characterized the H-assisted isomerization kinetics of fulvene → benzene in detail and discussed the importance of similar processes for the so-called “second-ring” isomers of naphthalene. If sufficiently fast, such processes may promote thermodynamic equilibria among some isomeric PAHs, thus simplifying the development of detailed reaction mechanisms for PAH growth.

In collaboration with Argonne experimentalists (Michael, Sivaramakrishnan) and theorists (Klippenstein, Harding, Wagner), the importance of roaming to molecular products in the thermal decomposition of dimethyl ether was studied. A strategy for obtaining analytic six-dimensional interaction potentials for studying roaming radical dynamics was developed and applied in reduced dimensional trajectory calculations. Roaming was identified as a minor channel both theoretically and experimentally, although the theory underpredicted the measured molecular branching fractions. The conditions under which the tight and roaming processes may be accurately treated as dynamically separable were analyzed, and a formal foundation for understanding this separability was developed.

New trajectory-based methods for parametrizing energy transfer models for use in master equation calculations were developed. The predictive accuracy of direct evaluations of the full dimensional potential energy surface was quantified, and these results were used to test commonly employed approximate potential energy surfaces. For simple interaction potentials (e.g., CH₄ + He),

the separable pairwise approach with Buckingham pair potentials parameterized to ab initio calculations was shown to be very accurate. For more complicated interaction potentials, this approximation was found to introduce errors of up to 40% in the predicted energy transfer averages. A universal hydrocarbon parameterization scheme for atomic and diatomic baths alongside an efficient semiempirical model for the intramolecular hydrocarbon potential energy surface was tested against full-dimensional direct dynamics for $C_2H_x + He$ ($x=3,5,6$), where it was shown to reproduce the higher-level energy transfer averages to within 20% with a computational speedup of a factor of 10^6 . An efficient scheme for calculating energy transfer parameters for multiple temperatures simultaneously was developed, further improving the efficiency of these calculations.

Our joint experimental/theoretical studies of unimolecular decomposition kinetics with Tranter were continued. Dioxane decomposition was studied theoretically using a combination of single reference and multireference quantum chemistry calculations. Four low-energy ring-opening pathways were found, and three of these involved a concerted H-atom transfer across the ring as it opens. For each of the concerted pathways, related stepwise pathways were found with weakly-bound diradical intermediates. The major immediate products of dioxane ring opening were shown to be $CH_2CHOCH_2CH_2OH$ and $CH_3CH_2OCH_2CHO$, which subsequently decompose at the central bond to radical and molecular products.

II.B. Non-Born–Oppenheimer Chemistry

We have carried out direct electronically nonadiabatic non-Born–Oppenheimer (NBO) trajectory simulations to predict product branching of activated H_2OO^* , where spin-allowed isomerization to $HOOH$ competes with spin-forbidden O–O bond scission to give $H_2O + {}^3O$. The contribution of the spin-forbidden processes was predicted to be only 2%, and this spin-forbidden channel is therefore not likely to significantly impact the quantitative modeling of combustion systems. The spin-forbidden NBO trajectories were analyzed in detail. These studies showed that the use of simple statistical models to calculate spin-forbidden kinetics may lead to significant errors due to the neglect of multidimensional dynamics and (de)coherence between successive NBO events.

With Truhlar, detailed descriptions of our most accurate and well-validated multistate NBO trajectory methods have been given in a recent book chapter. This chapter complements the release of our direct trajectory code DiNT (freely available at <http://www.sandia.gov/~ajasper/dint/>), which has been interfaced with the Gaussian and Molpro quantum chemistry packages.

The effect of spin-orbit splitting on barrierless association rate coefficients was quantified for six hydrocarbon radical–halogen atom reactions ($R + X$, with $R =$ methyl and allyl, $X = F, Cl, \text{ and } Br$). For five of the six reactions, spin-orbit splitting resulted in only a small (5–15%) perturbation to the nonrelativistic rate. For one reaction (allyl + Br), the effect was much larger, lowering the rate by a factor of 2. For this reaction, spin-orbit splitting had a nonperturbative effect on the barrierless kinetics, shifting the transition states to shorter fragment separations.

II.C. Quantum Chemistry

In collaboration with Richard Dawes (at Missouri University of Science and Technology and while he was at Sandia as a postdoctoral researcher), the interpolated moving least squares (IMLS) method for fitting analytic potential energy surfaces to automatically grown ab initio data was developed, and several applications were made. Vibrational states of the S_2 state of CDF were calculated on an IMLS surface generated from dynamically weighted state averaged MRCI+Q/CBS ab initio data. Good agreement with the experimental vibrational spectroscopy was obtained. Hyperthermal $O + HCl$ collisions were studied on global IMLS potential energy surfaces for the ground and first excited electronic states. The two states predict different branching ratios to the OCl and OH products, and this observation was rationalized in terms of differences in the attractive potential near the H atom of the reactant diatom. The first excited state of HO_2 was studied using high-level quantum chemistry and an IMLS fit. The van der Waals interaction of the N_2O dimer was

characterized using a series of high-level quantum chemistry calculations. Sensitivities of the quantum chemistry calculations to the choice of basis set, complete-basis-set extrapolation scheme, and treatment of electron correlation were studied in detail. The resulting fitted four-dimensional IMLS surface was used in rovibrational energy level and tunneling lifetime calculations; the results of these calculations are in good agreement with available experimental results for the N₂O dimer.

III. Future Work

III.A. Theoretical Kinetics

We will continue to make quantitative kinetics predictions for important elementary combustion reactions. Several applications are underway, including a collaboration with Tranter studying cyclopentane decomposition and its associated chemistry. In another collaboration with Osborn and Klippenstein, we are studying the phenyl + propargyl reaction.

More generally, we are developing new transition state theory strategies for systems that are currently not well described by statistical theories. For example, barrierless abstraction reactions pose challenges to current theories. For these reactions variable reaction coordinate TST is appropriate for characterizing the kinetics at low temperatures, but the assumptions involved in this approach are not suitable at higher temperatures where the reacting fragments are significantly distorted from their isolated geometries at the important dynamical bottlenecks. A two transition state approach will be applied to study these systems. As another example, we are developing practical schemes for sampling global dividing surfaces with multiple pathways connecting the same set of reactants and products.

Semiclassical Monte Carlo based approaches for predicting vibrational anharmonicities are being developed. The applicability and accuracy of these approaches is improved via direct coupling with quantum chemistry codes for the evaluation of the potential energy surface. Numerical evaluations of the kinetic energy operator allow for the use of arbitrary curvilinear coordinates, and these methods may therefore be applied to systems with nonlocal vibrations, such as torsions. Path integral and semiclassical zero point corrections are being pursued. The accuracy of separable-mode and reduced-dimensional models is being studied.

We will continue to develop our trajectory-based methods for studying energy transfer. In addition to providing improved theoretical kinetics for pressure dependent reactions involving these species, the proposed systematic studies of energy transfer will be used to guide the development of more complete models and predictive rules for parameterizing collisional energy transfer models in master equation calculations. Applications to radical decomposition kinetics and to H₂C₂ isomerization are underway.

III.B. Non-Born–Oppenheimer Chemistry

A major component of future work will involve the application of our NBO molecular dynamics (MD) methods to polyatomic systems. Furthermore, we will develop, validate, and quantify the accuracy of new and existing statistical theories for studying NBO processes. Existing statistical methods can be qualitatively useful but are not generally reliable for making quantitative predictions, as they make several simplifying assumptions of unknown accuracy, such as: treating the nonadiabatic event as occurring in only one nuclear dimension, assuming the nonadiabatic dynamics is localized to some predetermined crossing seam, and using perturbative methods for calculating electronic transition probabilities (e.g., the Landau-Zener approximation). Some physics is often neglected entirely, such as electronic (de)coherence between successive NBO events. We propose to test existing statistical models and to develop improved models using our NBO MD methods, which include explicit treatments of global multidimensional electronic coupling and (de)coherence. These simulations will be carried out using direct evaluations of the coupled potential energy surfaces. The results of the NBO trajectories will be analyzed to characterize the fundamental physics of nonadiabatic events, to test the assumptions used by existing statistical models, and to inform the

development of new models and codes. Initial targets of study include those from a variety of different kinds of NBO reactions: spin-forbidden intersystem crossing reactions ($O(^3P) + \text{alkene}$), spin-orbit-coupled internal conversion (halogen atom-radical molecule addition reactions), and ultrafast decay via conical intersections (the photodissociation of NH_3).

IV. Publications supported by this project since 2010

1. **Separability of tight and roaming pathways to molecular decomposition.** L. B. Harding, S. J. Klippenstein, and A. W. Jasper, *J. Phys. Chem. A*, submitted (2012).
2. **Hydrogen-assisted isomerizations of fulvene to benzene and of larger cyclic aromatic hydrocarbons.** A. W. Jasper and N. Hansen, *Proc. Combust. Inst.*, submitted (2012).
3. **Chemical structures of low-pressure premixed methylcyclohexane flames as benchmarks for the development of a predictive combustion chemistry model.** S. A. Skeen, B. Yang, A. W. Jasper, W. J. Pitz, and N. Hansen, *Energy & Fuels* 25, 5611 (2011).
4. **Identification of tetrahydrofuran reaction pathways in premixed flames.** T. Kasper, A. Lucassen, A. W. Jasper, W. Li, B. Yang, P. R. Westmoreland, K. Kohse-Höinghaus, B. Yang, J. Wang, T. A. Cool, and N. Hansen, *Z. Phys. Chem.* 225, 1237 (2011).
5. **Theoretical unimolecular kinetics for $CH_4 + M \rightarrow CH_3 + H + M$ in eight baths, $M = He, Ne, Ar, Kr, H_2, CO, N_2,$ and CH_4 .** A. W. Jasper and J. A. Miller, *J. Phys. Chem. A* 115, 6438 (2011).
6. **The vibration-rotation-tunneling spectrum of the polar and T-shaped-N-in isomers of $(NNO)_2$.** X.-G. Wang, T. Carrington, Jr., R. Dawes, A. W. Jasper, *J. Mol. Spectrosc.* 53, 6438 (2011).
7. **Non-Born-Oppenheimer molecular dynamics for conical intersections, avoided crossings, and weak interactions.** A. W. Jasper and D. G. Truhlar, in *Conical Intersections: Theory, Computation, and Experiment*, edited by W. Domcke, D. R. Yarkony, and H. Koppel (World Scientific, 2011).
8. **Roaming radicals in the thermal decomposition of dimethyl ether: Experiment and theory.** R. Sivaramakrishnan, J. V. Michael, A. F. Wagner, R. Dawes, A. W. Jasper, L. B. Harding, Y. Georgievskii, and S. J. Klippenstein, *Combust. Flame* 158, 618 (2011).
9. **A shock tube and theoretical study on the pyrolysis of 1,4-dioxane.** X. Yang, A. W. Jasper, B. R. Giri, J. H. Kiefer, and R. S. Tranter, *Phys. Chem. Chem. Phys.* 13, 3686 (2011).
10. **Global potential energy surface, vibrational spectrum, and reaction dynamics of the first excited (A^2A') state of HO_2 .** A. Li, D. Xie, R. Dawes, A. W. Jasper, J. Ma, and H. Guo, *J. Chem. Phys.* 133, 144306 (2010).
11. **Nitrous oxide dimer: A new potential energy surface and rovibrational spectrum of the nonpolar isomer.** R. Dawes, X.-G. Wang, A. W. Jasper, T. Carrington, Jr., *J. Chem. Phys.* 133, 134304 (2010).
12. **The role of excited electronic states in hypervelocity collisions: Enhancement of the $O(^3P) + HCl \rightarrow OCl + H$ reaction channel.** A. J. Binder, R. Dawes, A. W. Jasper, J. P. Camden, *J. Phys. Chem. Lett.* 1, 2940 (2010).
13. **The effect of spin-orbit splitting on the association kinetics of barrierless halogen atom-hydrocarbon radical reactions.** A. W. Jasper, S. J. Klippenstein, and L. B. Harding, *J. Phys. Chem. A* 114, 5759 (2010).
14. **Theoretical and experimental spectroscopy of the S_2 state of CHF and CDF: Dynamically weighted multireference configuration interaction calculations for high-lying electronic states.** R. Dawes, A. W. Jasper, C. Tao, C. Richmond, C. Mukarakate, S. H. Kable, and S. A. Reid, *J. Phys. Chem. Lett.* 1, 641 (2010).

Probing the Reaction Dynamics of Hydrogen-Deficient Hydrocarbon Molecules and Radical Intermediates via Crossed Molecular Beams

Ralf I. Kaiser

Department of Chemistry, University of Hawai'i at Manoa, Honolulu, HI 96822

ralfk@hawaii.edu

1. Program Scope

The major goals of this project are to explore experimentally in crossed molecular beams experiments the reaction dynamics and potential energy surfaces (PESs) of hydrocarbon molecules and their corresponding radical species which are relevant to combustion processes. The reactions are initiated under single collision conditions by crossing two supersonic reactant beams containing radicals and/or closed shell species under a well-defined collision energy and intersection angle. By recording angular-resolved time of flight (TOF) spectra, we obtain information on the reaction products, intermediates involved, on branching ratios for competing reaction channels, on the energetics of the reaction(s), and on the underlying reaction mechanisms. These data are of crucial importance to understand the formation of carbonaceous nanostructures as well as of polycyclic aromatic hydrocarbons and their hydrogen deficient precursors in combustion flames.

2. Recent Progress

2.1. Formation of Resonantly Stabilized Free Radicals (RSFRs)

The energetics and dynamics involved in the formation of resonantly stabilized free radicals (RSFRs) are of paramount importance in untangling the formation of soot particles, polycyclic aromatic hydrocarbons (PAHs), and their hydrogen deficient precursors from the 'bottom up' in combustion processes. Here, we conducted crossed molecular beam experiments of ground state carbon atoms and of ground and excited state dicarbon molecules, $C_2(X^1\Sigma_g^+/a^3\Pi_u)$, with vinylacetylene (C_2H_3CCH ; C_4H_4) and combined the scattering experiments with electronic structure calculations. These investigations suggest the formation of three key resonantly stabilized free radicals: *i*- C_3H_3 ($H_2CCCCCH$) and *n*- C_3H_3 ($HCCCCHCCH$) as well as *i*- C_6H_3 ($H_2CCCCCCH$) upon reaction of vinylacetylene with atomic carbon and dicarbon, respectively. Note that *i*- C_3H_3 and *i*- C_6H_3 are higher homologues of the well-known propargyl radical C_3H_3 (H_2CCCH).

2.2. Unimolecular Decomposition of Resonantly Stabilized Free Radicals (RSFRs)

Besides an investigation of the formation of RSFRs, it is also important to untangle the unimolecular decomposition of RSFRs and their isomers to gain information on the stability of RSFRs in combustion systems. We accessed distinct sections of the C_3H_3 potential energy surface (PES) in the crossed beam reactions of ground state methylidyne radicals, $CH(X^2\Pi)$, with acetylene, $C_2H_2(X^1\Sigma_g^+)$, and via the atom – radical reaction of ground state carbon atoms, $C(^3P_j)$, with the vinyl radical, $C_2H_3(X^2A')$. In case of the methylidyne – acetylene system, product isomers and intermediates were also identified by utilizing deuterated reactants. At a collision energy of 16.8 kJmol^{-1} , competing atomic and molecular hydrogen loss pathways leading to C_3H_2 and C_3H isomers were identified with fractions of $91\pm 5 \%$ and $9\pm 2 \%$, respectively. Studies of the methylidyne – D2-acetylene and D1-methylidyne – acetylene systems identified four competing channels following atomic 'hydrogen' (H/D) and molecular 'hydrogen' ($H_2/D_2/HD$) losses. Considering the atomic carbon – vinyl system, the reaction dynamics involved a complex forming reaction mechanism initiated by the barrier-less addition of the ground state carbon atom to the carbon-carbon-double bond of the vinyl radical forming a cyclic C_3H_3 radical intermediate. The latter decomposed to cyclopropenylidene ($c\text{-}C_3H_2$) plus atomic hydrogen.

2.3. Formation of Aromatic Radicals (ARs)

We investigated a route to potentially form the phenyl radical in combustion flames via the reaction of 1,3-butadiene ($C_2H_3C_2H_3$) with dicarbon molecules $C_2(X^1\Sigma_g^+/a^3\Pi_u)$. Crossed molecular beam experiments of dicarbon molecules in their $X^1\Sigma_g^+$ electronic ground state and in the first electronically excited $a^3\Pi_u$ state were conducted with 1,3-butadiene and two partially deuterated counterparts at collision energies up

to 33.7 kJmol⁻¹. Combining the scattering experiments with electronic structure and RRKM calculations, our investigation reveals that the phenyl radical is formed predominantly on the triplet surface via indirect scattering dynamics. Initiated by a barrier-less addition of triplet dicarbon to one of the terminal carbon atoms of 1,3-butadiene, the collision complex undergoes trans-cis isomerization followed by ring closure and hydrogen migration prior to hydrogen atom elimination ultimately forming the phenyl radical. On the singlet surface, smaller contributions of phenyl radical could not be excluded; experiments with partially deuterated 1,3-butadiene indicate the formation of the thermodynamically less stable H₂CCHCCCCH₂ isomer. This study presents the first experimental evidence – contemplated by theoretical studies – that under single collision conditions an aromatic hydrocarbon molecule can be formed in a bimolecular gas phase reaction via reaction of two acyclic molecules involving cyclization processes at collision energies relevant to combustion flames.

2.4. Reactions of the Aromatic Phenyl Radical: PAH Formation

Chemical reaction networks modeling the formation of PAHs in combustion flames imply that the phenyl radical (C₆H₅) presents one of the most important transient species involved in the formation and complexation of PAHs. However, despite impressive kinetic data, the reaction products formed in bimolecular collisions of phenyl radicals with unsaturated hydrocarbons have remained elusive. Therefore, we engaged a systematic research program to investigate the reaction dynamics of phenyl radicals with unsaturated hydrocarbons under single collision conditions as provided in crossed molecular beam experiments over a wide range of collision energies from about 40 to 200 kJmol⁻¹. Reactions at higher collision energies from 80 to 200 kJmol⁻¹ tied up some loose ends from the previous funding period. Crossed beam experiments at lower collision energies focused on the reaction dynamics of phenyl radicals with hydrocarbon molecules accessing the C₉H_x (x=8,10) and C₁₀H_x (x = 6, 8,10) PESs and, hence, investigating the formation of bicyclic aromatic species holding the *indene* and *naphthalene* carbon skeletons. This was achieved by crossing supersonic beams of phenyl radicals with allene (H₂CCCH₂), methylacetylene (CH₃CCH), and propylene (CH₃C₂H₃) (*indene core*) as well as diacetylene (HCCCCH), vinylacetylene (HCCC₂H₃), and 1,3-butadiene (C₂H₃C₂H₃) (*naphthalene core*). Most important, at lower collision energies of 40–50 kJmol⁻¹, the crossed beam experiments of phenyl with methylacetylene (CH₃CCH) and allene (H₂CCCH₂) as well as with vinylacetylene (C₂H₃CCH) depicted for the very first time that ***polycyclic aromatic hydrocarbons indene (C₉H₈) and naphthalene (C₁₀H₈) are formed as a result of a single collision event between the aromatic phenyl radical and a hydrogen-deficient hydrocarbon molecule*** (Fig. 1). These lower collision energies lead to an enhanced life time of the initial collision complex allowing the latter to isomerize via hydrogen migration(s) and/or cyclization ultimately leading to PAH formation such as indene and naphthalene through hydrogen loss.

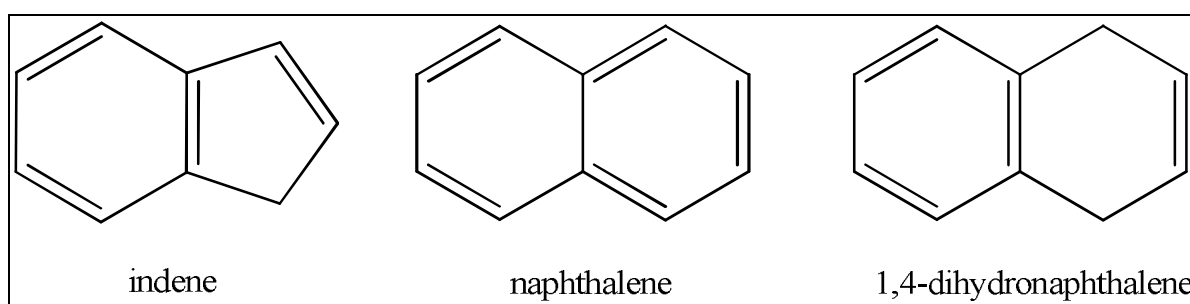


Fig. 1: Structures of the indene (C₉H₈) and the naphthalene (C₁₀H₈) molecules formed under single collision conditions via reactions of the phenyl radical (C₆H₅) with methylacetylene/allene (CH₃CCH/H₂CCCH₂) and with vinylacetylene (C₂H₃CCH). The recent data analysis of the crossed beam reaction of phenyl radicals with 1,3-butadiene suggests the formation of 1,4-dihydronaphthalene (C₁₀H₁₀).

2.5. PAH Species – A Photoionization Study at the ALS

To yield further insights on the formation of PAHs under combustion relevant conditions (pressure, temperature, reactant molecules), we commissioned in collaboration with Musa Ahmed (LBNL) at the Chemical Dynamics Beamline a high temperature ‘chemical reactor’. A ‘directed synthesis’ of the PAHs is performed *in situ* in a supersonic molecular beam through reaction of pyrolytically generated phenyl radicals (C_6H_5) with hydrocarbons inside a heated silicon carbide tube (‘chemical reactor’). The PAHs together with their acyclic isomers formed are then photoionized by vacuum ultraviolet (VUV) light from the Advanced Light Source at various photon energies from 7.5 to 12 eV to record photoionization efficiency (PIE) curves. Based on known PIE curves of the individual PAHs and their acyclic isomers, the recorded PIE curves are then simulated theoretically to extract the nature of the products formed and their branching ratios over a range of combustion-relevant reaction vessel temperatures (1,000-2,000 K) and pressures (few 100 Torr to a few 1,000 Torr). By selecting the reactants, allene (H_2CCCH_2), methylacetylene (CH_3CCH), propylene ($CH_3C_2H_3$), and 1,3-butadiene ($C_2H_3C_2H_3$), these studies access the important C_9H_x ($x=8,10$) and $C_{10}H_x$ ($x=6,8,10$) potential energy surfaces (PESs), among them are the crucial combustion intermediates with indene and naphthalene cores. To date, no experiment has been conducted in which an individual PAH (like) species is formed via a gas phase reaction under well-defined conditions in a high temperature chemical reactor. These studies suggest the formation of indene (methylacetylene/allene) and 1,4-dihydronaphthalene (1,3-butadiene) molecules together with their acyclic isomers.

3. Future Plans

Further experiments are aimed to understand the formation mechanisms of prototype bicyclic polycyclic aromatic hydrocarbons (PAHs) and their successive growth to tricyclic PAHs in combustion processes of hydrocarbon-based fuel, i.e. the formation of complex PAHs such as anthracene/phenanthrene ($C_{14}H_{10}$), i.e. prototype PAHs with three six-membered rings, and fluorene/1H-benz[f]indene/1H-benz[e]indene, i.e. prototype PAHs with two six- and one five-membered ring, as well as of 1H-phenalene ($C_{13}H_{10}$).

4. Acknowledgements

This work was supported by US Department of Energy (Basic Energy Sciences; DE-FG02-03-ER15411).

5. Publications Acknowledging DE-FG02-03ER15411 (7/2009 – 7/2012)

- P1. X. Gu, F. Zhang, R.I. Kaiser, *A Crossed Molecular Beam Study of the Phenyl Radical Reaction with 1,3-Butadiene and its Deuterated Isotopomers*. The Journal of Physical Chemistry A 113, 998-1006 (2009).
- P2. X. Gu, R.I. Kaiser, *Reaction Dynamics of Phenyl Radicals in Extreme Environments - A Crossed Molecular Beam Study*. Acc. Chem. Res. 42, 290-302 (2009).
- P3. X. Gu, F. Zhang, R.I. Kaiser, V.V. Kislov, A.M. Mebel, *Reaction Dynamics of the Phenyl Radical with 1,2-Butadiene*. Chemical Physics Letters 474, 51-56 (2009).
- P4. R.I. Kaiser, F. Zhang, X. Gu, V.V. Kislov, A.M. Mebel, *Reaction Dynamics of the Phenyl Radical (C_6H_5) with 1-Butyne ($HCCC_2H_5$) and 2-Butyne (CH_3CCCH_3)*. Chemical Physics Letters 481, 46-53 (2009).
- P5. R.I. Kaiser, A.M. Mebel, O. Kostko, M. Ahmed. *On the Ionization Potentials of C_4H_3 Isomers*. Chemical Physics Letters 485, 281-285 (2010).
- P6. R.I. Kaiser, *Reaction Dynamics of Carbon-Centered Radicals in Extreme Environments Studied by the Crossed Molecular Beams Technique*. in: Carbon-Centered Radicals: Structure, Dynamics and Reactivity. Malcolm D. E. Forbes, Editor, Wiley, p. 221-248 (2010).

- P7. F. Zhang, B. Jones, P. Maksyutenko, R. I. Kaiser, C. Chin, V.V. Kislov A.M. Mebel, *Formation of the Phenyl Radical [$C_6H_5(X^2A_1)$] under Single Collision Conditions – A Crossed Molecular Beam and Ab Initio Study*. JACS 132, 2672-2683 (2010).
- P8. O. Kostko, J. Zhou, B.J. Sun, J.S. Lie, A.H.H. Chang, R.I. Kaiser, M. Ahmed, *Determination of ionization energies of C_nN ($n=3-14$) clusters: Vacuum-ultraviolet (VUV) photoionization experiments and theoretical calculations*, ApJ 717, 674-682 (2010).
- P9. P. Maksyutenko, F. Zhang, X. Gu, R.I. Kaiser, *A Crossed Molecular Beam Study on the Reaction of Methylidyne Radicals [$CH(X^2\Pi)$] with Acetylene [$C_2H_2(X^1\Sigma_g^+)$] – Competing $C_3H_2 + H$ and $C_3H + H_2$ Channels*. Physical Chemistry Chemical Physics 13, 240-252 (2011).
- P10. D.S.N. Parker, F. Zhang, Y. Seol Kim, R. I. Kaiser, A.M. Mebel. *On the Formation of the Resonantly Stabilized C_3H_3 Radicals - A Crossed Beam and Ab Initio Study of the Reaction of Ground State Carbon Atoms with Vinylacetylene*. The Journal of Physical Chemistry A 115, 593-601 (2011).
- P11. F. Zhang, R.I. Kaiser, V. Kislov, A.M. Mebel, A. Golan, M. Ahmed, *A VUV Photoionization Study of the Formation of the Indene Molecule and its Isomers*. The Journal of Physical Chemistry Letters 2, 1731-1735 (2011).
- P12. R.I. Kaiser, M. Goswami, P. Maksyutenko, F. Zhang, Y.S. Kim, A.M. Mebel, *A Crossed Molecular Beams and Ab Initio Study on the Formation of C_6H_3 Radicals - An Interface between Resonantly Stabilized (RSFRs) and Aromatic Radicals (ARs)*. The Journal of Physical Chemistry A 115, 10251-10258 (2011).
- P13. D.S.N. Parker, F. Zhang, R.I. Kaiser, *Phenoxy Radical (C_6H_5O) Formation under Single Collision Conditions from Reaction of the Phenyl Radical (C_6H_5 , X^2A_1) with Molecular Oxygen (O_2 , $X^3\Sigma_g^-$) – The Final Chapter?* The Journal of Physical Chemistry A 115, 11515-11518 (2011).
- P14. D.S.N. Parker, F. Zhang, R. I. Kaiser, V. Kislov, A.M. Mebel, *Indene Formation under Single Collision Conditions from Reaction of Phenyl Radicals with Allene and Methylacetylene – A Crossed Molecular Beam and Ab Initio Study*. Chemistry – An Asian Journal [Y.T. Lee Special Issue] 6, 3035-3042 (2011).
- P15. A.V. Wilson, D. S. N. Parker, F. Zhang, R.I. Kaiser, *Crossed Beam Study of the Atom-Radical Reaction of Ground State Carbon ($C(^3P_j)$) with the Vinyl Radical (C_2H_3 , X^2A')*. Physical Chemistry Chemical Physics 14, 477-481 (2012).
- P16. R.I. Kaiser, X. Gu, F. Zhang, P. Maksyutenko, *Crossed Beams Reactions of Methylidyne [$CH(X^2\Pi)$] with D2-Acetylene [$C_2D_2(X^1\Sigma_g^+)$] and of D1-Methylidyne [$CD(X^2\Pi)$] with Acetylene [$C_2H_2(X^1\Sigma_g^+)$]*. Physical Chemistry Chemical Physics 14, 575-588 (2012).
- P17. D. Parker, F. Zhang, R.I. Kaiser, V. Kislov, A.M. Mebel, A.G.G.M. Tielens, *Low Temperature Formation of Naphthalene and Its Role in the Synthesis of PAHs in the Interstellar Medium*. Proceedings National Academy of Sciences USA (PNAS) 109, 53-58 (2012).
- P18. R.I. Kaiser, D. Parker, M. Goswami, F. Zhang, V. Kislov, A.M. Mebel, *Crossed Beam Reaction of Phenyl and D5-Phenyl Radicals with Propene and Deuterated Counterparts – Competing Atomic Hydrogen and Methyl Loss Pathways*. Physical Chemistry Chemical Physics 14, 720-729 (2012).
- P19. D.S.N. Parker, F. Zhang, Y. S. Kim, R. I. Kaiser, A. Landera, A. M. Mebel, *On the Formation of Phenyl diacetylene (C_6H_5CCCCH) and D5-Phenyl diacetylene (C_6D_5CCCCH) Studied under Single Collision Conditions*. Physical Chemistry Chemical Physics 14, 2997-3003 (2012).
- P20. Kaiser, D.S.N. Parker, F. Zhang, A. Landera, V. V. Kislov, A.M. Mebel, *Formation of PAHs and their Derivatives under Single Collision Conditions - The 1,4-Dihydronaphthalene Molecule as a Case Study*. The Journal of Physical Chemistry A (in press 2012).
- P21. R.I. Kaiser, F. Zhang, A. M. Mebel, A. Golan, M. Ahmed, *A VUV Photoionization Study on the Formation of Primary and Secondary Products in the Reaction of the Phenyl Radical with 1,3-Butadiene under Combustion Relevant Conditions*. Physical Chemistry Chemical Physics (submitted 2012).

DYNAMICAL ANALYSIS OF HIGHLY EXCITED MOLECULAR SPECTRA

Michael E. Kellman

Department of Chemistry, University of Oregon, Eugene, OR 97403

kellman@uoregon.edu

PROGRAM SCOPE:

The highly excited vibration-rotation dynamics of small molecular species, including those approaching the threshold of reaction, are crucial to understanding fundamental processes important for combustion. The goal of our program is to develop theoretical tools to analyze spectra and dynamics of these highly excited systems. A constant theme is the use of effective spectroscopic fitting Hamiltonians to make the link between experimental data and theoretical dynamical analysis. We emphasize particularly the role of bifurcations and the “birth of new modes in bifurcations from the low energy normal modes.” A new focus has been systems approaching and undergoing intramolecular isomerization reactions. We have been developing new generalizations of the effective Hamiltonian, called “polyad-breaking Hamiltonians,” to deal with spectra of isomerizing systems. In our most recent work we have extended these investigations to consider time-dependent dynamics, including the isomerization process.

RECENT PROGRESS AND FUTURE PLANS: The progress described below is in collaboration with postdoctoral associates George Barnes and Vivian Tyng. Our current research is pursuing two main directions.

POLYAD BREAKING GENERALIZED EFFECTIVE HAMILTONIANS.

Generalized spectroscopic Hamiltonian with polyad breaking. This work has been primarily in collaboration with Dr. George Barnes. A recent focus of our work is systems in which the standard spectroscopic polyad approximation breaks down. This involves a major extension of the standard effective spectroscopic fitting Hamiltonian. The Hamiltonian used in virtually all existing spectral fits invokes an approximate conserved quantity known as the polyad or total quantum number. In a recent step, initiated with two papers [3,4], we have been concerned with a new and difficult question of principle: whether it is possible to construct an effective Hamiltonian to encompass multiple potential energy minima, especially in a system that does not have two simple uncoupled modes as a zero-order limit. An example is a molecule that shifts between two isomeric forms, each possessing its own potential minimum. This almost surely requires a polyad-breaking Hamiltonian, and even so it has been very much open to question whether it can be done at all. We have been investigating this problem using an example from combustion reaction systems. One of the most important elementary combustion species is the hydroperoxyl radical HO₂. In its equilibrium configuration it has a bent H—O—O structure. At very high energies the system can make transitions over a saddle in which the H atom is situated symmetrically above the O—O in an isosceles triangle. In our current work we are concerned with this isomerization pathway. At still higher energies, the molecule can assume a linear form, and at even higher energies, it can dissociate into either HO + O or O₂ + H.

We have devised a simplified model for HO₂ based on a high level ab initio potential energy surface of Guo and coworkers. Our model includes two vibrational coordinates, which may be designated as bend and O—H stretch modes. That is, we remove the

O—O coordinate, taking a slice of the full-dimensional potential surface. The resulting potential encompasses both the lowest isomerization pathway and the lowest dissociation channel of the system. The resulting model potential, has similar features to the full three dimensional PES. In order to test the generalized spectroscopic fitting Hamiltonian, we obtain a set of essentially exact vibrational levels from the model potential and use these as "data". These levels result from a discrete variable representation (DVR) calculation. In Refs. [3,4] we show that spectroscopic fitting Hamiltonians are capable of reproducing large scale vibrational structure above the isomerization barrier. Good fits for below barrier states are obtained from just a diagonal Hamiltonian, but there is a severe breakdown above the barrier. Two resonances, the 2:1 and 3:1, are necessary to describe the pertinent physical features of the system and hence a polyad-breaking Hamiltonian is required. We further illustrate, through the use of approximate wave functions, that inclusion of additional coupling terms yield physically unrealistic results despite an improved agreement with the exact energy levels. Insight into the dynamical nature of isomerization is also gained through classical trajectories. Contrary to physical intuition the bend mode is not the initial "reaction mode," but rather isomerization requires excitation in both the stretch and bend modes. The success of our new Hamiltonian is exemplified in Fig.1 which

shows a comparison of the exact wave function for an isomerizing state with the wave functions obtained with various refinements of the effective Hamiltonian, demonstrating that only our "best" effective Hamiltonian gives good results.

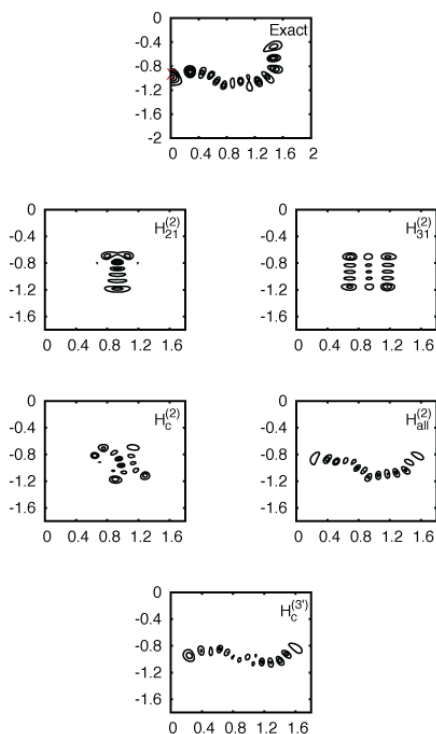


Fig. 1. A comparison of squared wave functions from various Hamiltonians for an isomerizing state. The best comparison is between the Exact state from the PES, top; and our best polyad-breaking effective Hamiltonian, bottom. In contrast, polyad Hamiltonians and some polyad-breaking Hamiltonians (middle panels) can give poor results.

Time dependent dynamics of the generalized effective Hamiltonian. In the latest phase of our work on generalized effective Hamiltonians, we are investigating the physical nature of the quantum mechanical states [5,6]. The problem is that the effective Hamiltonian uses an abstract zero-order basis – by itself, it gives no way of describing the states in the physical coordinate space of the system. In recent work [6] we present a method of obtaining the coordinate space representation of the abstract zero order basis (ZOB) of a spectroscopic effective Hamiltonian. The ZOB is an abstract basis which is the "ideal" basis for a given form and parameterization of the spectroscopic Hamiltonian. Without a physical model there is no way to transform this abstract basis into a coordinate representation. In Ref. [6] we present a method that relies on a set

of converged eigenfunctions obtained from a variational calculation on a potential surface. We make a one-to-one correspondence between the energy eigenfunctions of the effective Hamiltonian and those of a model potential surface. Through this correspondence we construct a physical representation of the abstract ZOB. The ZOB basis is a *time-dependent* basis – a point which is obvious from the fact that the ZOB states are superpositions of the energy eigenfunctions – but also something that is not widely thought about. We find that the time dependent ZOB basis shows states with both conventional low-energy characteristics, with little time-dependence, in terms of wavefunctions assignable with zero-order quantum numbers; and unconventional wildly time-varying “gnarly” ZOB states at higher energies – see Fig. 2 bottom left – that reflect the highly chaotic, multiple-well nature of the potential in regions of the isomerization process. It is this automatic built-in flexibility that allows extension of the effective Hamiltonian to polyad-breaking and highly chaotic multiple well behavior. The “gnarly” state at bottom left in Fig. 2 actually shows regular, “understandably conventional” behavior at certain later times – see Fig. 2 right.

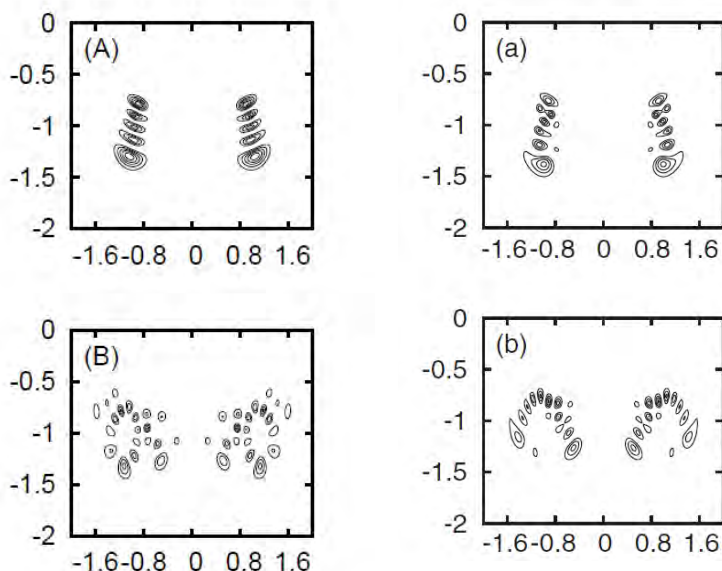


Fig. 2. Left: The squared amplitude of the $|4 0\rangle$ and $|5 0\rangle$ spectroscopic Hamiltonian ZOB functions in panels A and B, respectively. $|4 0\rangle$ illustrates a “conventional” basis function, while $|5 0\rangle$ illustrates an “unconventional” basis function.

Right: Two snapshots of the time evolution of the squared amplitude of the $|5 0\rangle$ spectroscopic ZOB function as propagated on the potential surface. The $t = 0$ snapshot of this state is shown in Left (B). The snapshots on right are at $t = 0.765$ ps and $t = 0.830$ ps for panels (a) and (b), respectively. These plots show that although the ZOB at $t = 0$ appears unconventional, in truth it contains a linear combination of a conventional form and a form understandable in terms of a “horseshoe” shape periodic orbit.

CRITICAL POINTS BIFURCATION ANALYSIS OF EFFECTIVE SPECTROSCOPIC HAMILTONIANS.

In recent years we have successfully completed several investigations using our method of critical points bifurcation analysis of effective spectroscopic Hamiltonians [1,2,7]. In our latest work, we

are performing a critical points bifurcation analysis for the first time for a rotation-vibration effective Hamiltonian, using a recent spectroscopic Hamiltonian for CO₂ fit to experimental data.

We are now successfully completing the critical points analysis of rotation-vibration dynamics of CO₂ on the effective Hamiltonian fit to experimental data. The analysis gives relatively simple, intelligible dynamics, comparable to but significantly extending what has been obtained with pure vibrational dynamics. At $J = 0$ there is only the bifurcation tree of normal modes and Fermi resonance modes. Then, as J increases, we find a principal "Coriolis mode" that bifurcates out of one of the Fermi resonance modes at very low J , with further finer branching of the tree into Coriolis modes with increasing J .

In this study, work remains to be done in the physical interpretation of the results of the critical points analysis. What is the physical nature of the rotation-vibration motion in the new bifurcation rotation-vibration "modes" of the molecule? A good starting point is the standard picture of the rotation-vibration motion of a symmetric top. In the new Coriolis modes of CO₂ determined in the bifurcation analysis, things will be somewhat but not altogether different from the symmetric top; and also with some similarities to the asymmetric top. In the critical points Coriolis modes, the molecule "locks" into certain configurations that involve combinations of the zero-order vibrational angle variables. The full motion of the molecule separates into a resonant periodic vibration (due to the combined effects of Fermi and Coriolis couplings); and a periodic precession-like rotational motion. In the body-fixed frame, the resonant periodic vibration involves the four vibrational modes including vibrational angular momentum and, unlike the pure Fermi resonance problem, the antisymmetric stretch. We hope that animations will dramatically simplify the visualization, following the example of our animations of the new bending modes born in bifurcations of acetylene.

Recent publications related to DOE supported research:

1. S. Yang and M.E. Kellman, "Resonance induced spectral tuning", *Phys. Rev. A.* 81, 062512 (2010).
2. V. Tyng and M.E. Kellman, "The Bifurcation Phase Diagram For C₂H₂ Bending Dynamics Has A Tetracritical Point With Spectral Patterns", *J. Phys. Chem. A.* 114, 9825–9831 (2010).
3. G. L. Barnes and M.E. Kellman, "Effective Spectroscopic Hamiltonian for Multiple Minima with Above Barrier Motion: Isomerization in HO₂", *J. Chem. Phys.* 133, 101105 (2010).
4. G.L. Barnes and M.E. Kellman, "Detailed Analysis of Polyad-Breaking Spectroscopic Hamiltonians for Multiple Minima with Above Barrier Motion: Isomerization in HO₂", *J. Chem. Phys.* 134, 074108 (2011).
5. G.L. Barnes and M.E. Kellman, "Effective Hamiltonian for femtosecond vibrational dynamics" *J. Chem. Phys.* 135, 144113 (2011).
6. G.L. Barnes and M.E. Kellman, "Visualizing the Zero Order Basis of the Spectroscopic Hamiltonian," *J. Chem. Phys.* 136, 024114 (2012).
7. J. Ma, D. Xu, H. Guo, V. Tyng, and M.E. Kellman, "Isotope effect in normal-to-local transition of acetylene bending modes" *J. Chem. Phys.* 136, 014304 (2012).

Time-Resolved Optical Diagnostics

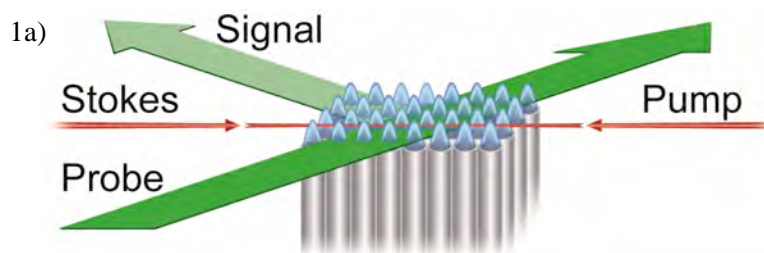
Christopher J. Kliewer (PI)
Combustion Research Facility, Sandia National Laboratories
P.O. Box 969, MS 9055
Livermore, CA 94551-0969
cjkliew@sandia.gov

Program Scope

This program focuses on the development of innovative laser-based techniques for measuring temperature and concentrations of important combustion species as well as the investigation of fundamental physical and chemical processes that directly affect quantitative application of these techniques. Our development efforts focus on crossed-beam approaches such as time-resolved nonlinear wave-mixing. A critical aspect of our research includes the study of fundamental spectroscopy, energy transfer, and photochemical processes. This aspect of the research is essential to the development of accurate models and quantitative application of techniques to the complex environments encountered in combustion systems. These investigations use custom-built tunable picosecond (ps) and commercial femtosecond lasers, which enable efficient nonlinear excitation, provide high temporal resolution for pump/probe studies of collisional processes, and are amenable to detailed physical models of laser-molecule interactions.

Recent Progress

High-spatial-resolution 1D RCARS imaging in flames: A disadvantage of the standard BOXCARS phase-matching scheme employed in CARS experiments is the lack of spatial resolution in the probe volume along the beam-propagation dimension. The length of the probed volume in this dimension is termed the “interaction length”. Most of our CARS measurements have resulted in interaction lengths of 2-3 mm, and this is common within the CARS community. In many situations higher resolution is required to avoid spatially averaging over important combustion features. The interaction length can be reduced by using a large-angle phase matching configuration. However, CARS signal intensity decreases quadratically as the interaction length is reduced. Thus, a reduction in interaction length from 2 mm to 200 μm would correspond to a 100-fold decrease in CARS signal intensity. I have demonstrated a novel 1D imaging phase-matching configuration to address these shortcomings, depicted in Figure 1a. The pump and Stokes pulses are not stretched into sheets, but instead are counter-propagated and focused to $\sim 150 \mu\text{m}$ symmetrically. The phase-matching condition for the wavelengths used then requires the narrowband probe to intersect this excited coherence at 33° to the Stokes beam. This configuration has two major advantages. First, the probe crosses the pump and Stokes pulses at such a steep angle the interaction length is reduced to $< 200 \mu\text{m}$, corresponding to an order of magnitude increase in spatial resolution. Second, the corresponding loss in CARS signal is mitigated by the fact that both the pump and Stokes beams are tightly focused in this geometry ($150 \mu\text{m}$) as opposed to being expanded to form sheets ($\sim 20000 \mu\text{m}$) thereby increasing the irradiance of the coherence preparation pulses each by a factor of 130. Figure 1 displays the results of using this experimental scheme to investigate a methane/air flame at the lean flammability limit over a custom burner. The small features of the flame structures in this burner would be highly spatially averaged if probed with a standard CARS phase-matching geometry. However, as shown in Figure 1b-c the structures are well-resolved using this new technique.



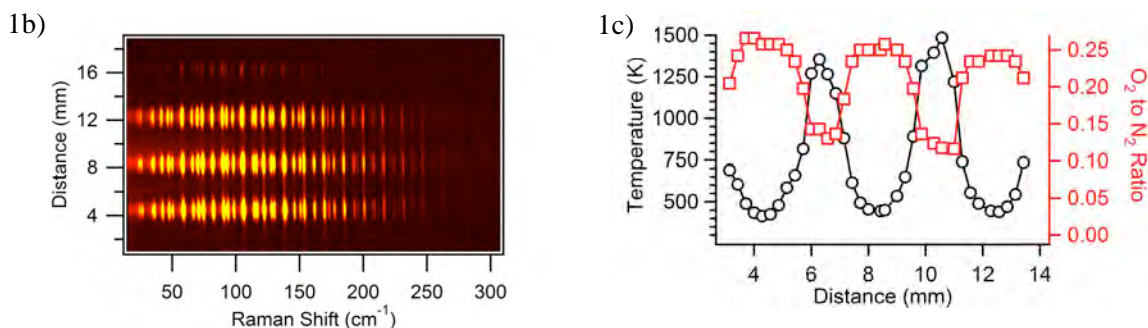


Figure 1. Panel (a) displays the high-spatial-resolution phase matching scheme employed in the 1D RCARS measurements over a methane/air burner. Panel (b) displays the RCARS CCD image obtained during the experiment. By analyzing spectra from single pixel rows in the CCD image, profiles for temperature and $[\text{O}_2]/[\text{N}_2]$ ratio are obtained and depicted in panel (c).

Development of $\text{N}_2\text{-H}_2$ collisional broadening model for RCARS measurements: One of the difficulties in the quantitative interpretation of CARS signal is its sensitivity to the J -dependent Raman linewidths. In frequency-domain CARS the signal intensity for a specific Raman transition scales as $1/\gamma^2$ where γ is the Raman linewidth. The Raman linewidth for a given molecular transition is sensitive to the temperature, pressure, and the molecule's collision partner(s). Both experimental and theoretical work over the past decades therefore has been dedicated to the measurement and modeling of rotational and rovibrational Raman linewidths for combustion-relevant species such as N_2 , O_2 , CO , CO_2 , H_2O and small fuel molecules. N_2 is the most commonly probed molecule in CARS measurements, as it is present in high concentration in all air-breathing combustion processes. High-resolution data have been used to construct phenomenological linewidth models, such as the modified exponential gap (MEG) model^A or Energy Corrected Sudden (ECS)^B model, to extrapolate the high-resolution data set to arbitrary temperature.

We previously demonstrated in our laboratory a technique for measuring coherence decays directly in the time-domain^{C,6}. This measurement is accomplished by preparing pure-rotational coherences in the probed molecules and then delaying the probe pulse in time. By tracking the signal decay as a function of probe delay, the coherence dephasing rate is measured directly in the time domain. This technique is made possible by the use of a picosecond probe laser pulse, which provides sufficient spectral resolution to isolate individual S-branch rotational transitions and simultaneously provide enough time-resolution to resolve the coherence decays that are on the order of 60 ps (N_2 at 1 bar and 295K). The frequency-domain Raman linewidth can thus be calculated from the time-domain dephasing data. We demonstrated that our time-domain measurements agreed well with reported high-resolution inverse Raman spectroscopy (IRS) data on the Raman linewidth for N_2 self-broadening.⁴ In collaboration with both Per-Erik Bengtsson from Lund University and Pierre Joubert of the Universite Franche we have analyzed a substantial coherence decay data set for various mixtures of N_2 and H_2 from 295K – 1500K. It has previously been shown that taking account of the $\text{N}_2 - \text{H}_2$ line-broadening coefficient is important for accurate thermometry in rich flames.^D We have used these data to develop a Raman linewidth model for use with pure-rotational CARS in flames with significant H_2 concentrations, such as diffusion flames.¹

Figure 2 displays the measured $\text{N}_2\text{-H}_2$ broadening coefficients from our laboratory, as compared with semi-classical line-broadening calculations performed in the group of Pierre Joubert and the linewidths for pure $\text{N}_2\text{-N}_2$ collisions as calculated by the ECS phenomenological linewidth model^B. These measured $\text{N}_2\text{-H}_2$ broadening coefficients were included in the CARS fitting code by modifying the linewidth calculation according to a model linearly weighted in $[\text{H}_2]$ concentration:

$$\Gamma_{J,J+2}^{\text{N}_2} = [\text{N}_2] \cdot \Gamma_{J,J+2}(\text{N}_2 - \text{N}_2) + [\text{H}_2] \cdot \Gamma_{J,J+2}(\text{N}_2 - \text{H}_2) \quad \text{Eq. 1}$$

This model resulted in improved thermometry in H_2 -rich environments, demonstrated in Figure 2b.

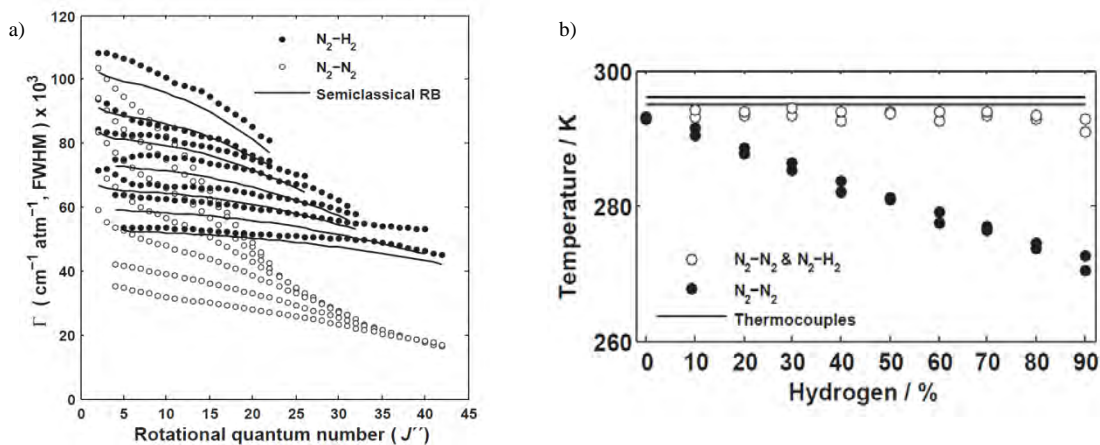


Figure 2. (a) $\text{N}_2\text{-H}_2$ broadening coefficients at temperatures of 294 K, 395 K, 495 K, 661 K, 868 K, and 1116 K (top to bottom) determined from time-domain coherence decay measurements. The open circles are the linewidths for pure $\text{N}_2\text{-N}_2$ collisional dephasing, and the closed black circles are the $\text{N}_2\text{-H}_2$ linewidths. The black lines represent the $\text{N}_2\text{-H}_2$ linewidths calculated from the semiclassical RB calculations of the system at the same temperatures. (b) The evaluated temperature for RCMRS measurements in a vessel containing differing concentrations of H_2 where the open-circle data were evaluated using the measured $\text{N}_2\text{-H}_2$ broadening coefficients, and the closed-circle data resulted from evaluation with the pure $\text{N}_2\text{-N}_2$ calculated linewidths from the ECS scaling law.

In-situ measurement of total collisional dephasing in flames: We have demonstrated that it is possible to obtain highly accurate measurements of broadening coefficients using the time-resolved CARS method, and this information resulted in improved CARS analysis for the diagnostics community. However, a unique ability of this measurement technique is the capability to measure the total collisional dephasing rate *in-situ* in an applied flame measurement. This approach requires the use of ps or fs lasers, but allows for accurate thermometry in flame environments, where very little is known about the collisional dephasing of the N_2 coherences because of the presence of colliders such as fuel molecules and H_2 , which can greatly perturb the J -dependence of the N_2 Raman linewidths. We have demonstrated *in-situ* measurement of Raman linewidth during CARS analysis of a highly sooting ethylene diffusion flame.² A systematic temperature correction of as much as 125K in evaluated temperatures was found on the fuel-side of the flame front, demonstrating both the importance and capability of measuring broadening coefficients, especially when there is no *a priori* knowledge regarding flame composition or pressure.

Future Work

In-situ single-shot CARS measurement of local collisional dephasing rates: We have demonstrated the significance of employing a linewidth model which correctly account for all of the collision partners of the probed molecule. Further, we have demonstrated the ability to collect this data *in-situ* while probing combustion. However, the technique used requires a probe-delay scan in order to collect this data. A delay scan is not suitable for probing turbulent combustion flow fields where the local mixture fraction can vary dramatically from laser shot to laser shot. We are currently implementing a scheme whereby the local broadening coefficients can be extracted from data obtained during a single laser shot. We achieve this by splitting the CARS probe beam into four separate beams, separated in time by an appropriate time delay for monitoring the coherence decay. These probe beams are then sent to the CARS probe volume at different folded BOXCARS angles, separating the signal generated from each of the four probes on the CCD detector. This technique allows for single-shot *in-situ* measurement of coherence decays, therefore leaving only molecular parameters and the Boltzmann distribution to the fitting routine. Further, because all of the probe delay measurements are generated from the same laser pulse, the measurement is intrinsically corrected for fluctuations in laser pulse energy. This capability will greatly enhance our ability to

accurately characterize the evolution of temperature and major species concentration in turbulent flame environments.

Validation of the time-domain CARS model at high pressures: We will continue to develop the time-domain CARS code for use in the general CARS community. This will require further model-validation experiments. We plan to explore how the CARS signal intensity depends on Raman linewidth for ultrafast pulses (ps and fs pulses) at pressures up to 50 atm at 1000K utilizing a recently constructed high pressure / high temperature cell. At atmospheric pressure, ns CARS signal intensity depends on the Raman linewidth as $1/\gamma^2$ where γ is the linewidth. However, the average time between molecular collisions at room temperature and atmospheric pressure is on the order of picoseconds. As the probe pulse gets shorter in time, the CARS signal intensity will become less linewidth dependent, eventually approaching a linewidth-independent signal intensity if the probe pulse is shorter than collision times. Chirped-probe pulse fs-CARS has been demonstrated by Professor Robert Lucht at Purdue, in collaboration with colleagues at WPAFB, to be a collision-free measurement for probing N₂ thermometry.^E In this manner, it has also been shown that collision-free measurements can be made with hybrid fs pump / ps probe rotational CARS at relatively low pressure.^F However, as the pressure increases, the collisional dephasing becomes fast enough to affect signal generation even with probe pulses which are just a few ps in duration, the minimum pulse-length for spectrally resolved CARS. The time-dependent collisional dynamics involved here must be more fully understood, especially as ps-CARS and fs-CARS are to be applied at elevated pressures.

Hybrid fs/ps RCARS using independent phase-locked lasers: We will perform hybrid fs/ps rotational CARS measurements using our new 10 kHz fs laser to excite rotational coherences and our custom-built ps laser to probe the excited coherences with high spectral resolution, sufficient to resolve individual rotational transitions in the frequency domain. The fs and ps lasers are both phase-locked to an RF source allowing for time synchronization of the pulses. These proof-of-principle experiments pave the way for high-repetition rate (1-10 kHz) rotational CARS thermometry and species concentration experiments in flames with signal levels sufficient for the simultaneous *in-situ* single-shot determination of broadening coefficients as described above. High repetition rate 1D rotational CARS imaging of a large field (2 cm) should also be made possible with this technique.

References

- A. M. L. Koszykowski, L. A. Rahn, R. E. Palmer, M. E. Coltrin, *J. Chem. Phys.* **91**, 41–46 (1987).
- B. P. Joubert, J. Bonamy, L. Gomez, D. Bermejo, *J. Raman Spectrosc.* **39**, 707 (2008).
- C. T. Seeger, J. Kiefer, A. Leipertz, B.D. Patterson, C.J. Kliewer, T.B. Settersten, *Opt. Lett.* **34**, 3755 (2009)
- D. A. Bohlin, F. Vestin, P. Joubert, J. Bonamy, P.E. Bengtsson, *J. Raman Spec.* **40**, 788 (2009)
- E. S. Roy, D.R. Richardson, W.D. Kulatilaka, R.P. Lucht, J.R. Gord, *Opt. Lett.* **34**, 3857-3859 (2009)
- F. J. Miller, C. Dedic, S. Roy, J. Gord, T. Meyer, *Opt. Exp.* **20**, 5003 (2012)

Publications and submitted journal articles supported by this BES project (2010-present)

1. A. Bohlin, E. Nordstrom, M. Dhyne, B. D. Patterson, P. Joubert, P.-E. Bengtsson, and C. J. Kliewer, "Direct measurement of S-branch N₂-H₂ Raman linewidths using time-resolved pure rotational coherent anti-Stokes spectroscopy," *J. Chem. Phys.* submitted (2012)
2. Y. Gao, A. Bohlin, T. Seeger, P.-E. Bengtsson, and C. J. Kliewer, "In-situ determination of N₂ broadening coefficients in flames for rotational CARS thermometry," *Proc. Comb. Instit.* accepted (2012)
3. C. J. Kliewer, "High-spatial-resolution one-dimensional rotational coherent anti-Stokes Raman spectroscopy imaging using counterpropagating beams" *Opt. Lett.* **37**, 229 (2012)
4. C. J. Kliewer, A. Bohlin, E. Nordstrom, B. D. Patterson, P.-E. Bengtsson, and T. B. Settersten, "Time-domain measurements of S-branch N₂-N₂ Raman linewidths using picosecond pure rotational coherent anti-Stokes Raman spectroscopy," *Appl. Phys. B*, accepted (2012)
5. C. J. Kliewer, Y. Gao, T. Seeger, B. D. Patterson, R. L. Farrow, and T. B. Settersten, "Quantitative one-dimensional imaging using picosecond dual-broadband pure-rotational CARS" *Appl. Opt.* **50**, 1770 (2011).
6. C. J. Kliewer, T. Seeger, Y. Gao, J. Kiefer, B. D. Patterson, and T. B. Settersten, "Picosecond time-resolved pure-rotational CARS in sooting flames," *Proc. Comb. Instit.* **33**, 831 (2011).
7. T. Seeger, J. Kiefer, Y. Gao, B. D. Patterson, C. J. Kliewer, and T. B. Settersten, "Suppression of Raman-resonant interferences in rotational CARS using time-delayed picosecond probe pulses," *Opt. Lett.* **35**, 2040 (2010).

ARGONNE-SANDIA CONSORTIUM ON HIGH-PRESSURE COMBUSTION CHEMISTRY

Stephen J. Klippenstein (PI), Michael J. Davis, Lawrence B. Harding, Joe V. Michael,
James A. Miller, Branko Ruscic, Raghu Sivaramakrishnan, Robert S. Tranter
Chemical Sciences and Engineering Division, Argonne National Laboratory, Argonne, IL, 60439
sjk@anl.gov

Craig A. Taatjes (PI), Ahren W. Jasper, David L. Osborn, Leonid Sheps, Judit Zádor
Combustion Research Facility, Mail Stop 9055, Sandia National Laboratories
Livermore, CA 94551-0969
cataatj@sandia.gov

Program Scope

The goal of this project is to explore the fundamental effects of high pressure on the chemical kinetics of combustion and to use that knowledge in the development of accurate models for combustion chemistry at the high pressures of current and future engines. Such accurate chemical models will aid in the effective use of novel alternative fuels, in the development of advanced engine designs, and in the reduction of pollutants. We design and implement novel experiments, theory, and modeling to probe high-pressure combustion kinetics from elementary reactions, to submechanisms, to flames. The work focuses on integrating modeling, experiment, and theory (MET) through feedback loops at all levels of chemical complexity. We are currently developing and testing the methodology for propane and 1-butanol as key prototype fuels, and will extend this approach to a general fundamental theory of pressure effects. The consortium expands and enhances collaborations between Argonne's Dynamics in the Gas Phase Group and the Combustion Chemistry Group in Sandia's Combustion Research Facility and also interacts closely with the Princeton-led Combustion Energy Frontier Research Center (CEFRC).

Recent Progress

Experimental Developments

High pressure, miniature high repetition rate shock tube: A novel miniature high repetition rate shock tube, HRRST, for high pressure, high temperature chemical kinetic studies has been developed to take advantage of advanced diagnostic techniques that are available at DOE user facilities, including the Advanced Photon Source (APS) and Advanced Light Source (ALS). Lab tests confirmed that well-formed incident shock waves are produced and that the reaction zone behind the reflected shock wave persists for $\sim 130 \mu\text{s}$; sufficient for kinetic and mechanistic studies at practical combustion conditions.

Recently, the first ever experiments with a chemical kinetics shock tube at a synchrotron were performed at beamline 7-BM at the APS with the HRRST. These experiments examined the formation of boundary layers, which are significant in a small bore shock tube, with X-ray absorption spectroscopy. To maximize observation of the boundary layers, a shaped plug was installed that filled half the bore of the tube. Additional experiments performed without the plug demonstrated that the density changes across the incident and reflected shock waves are in very good agreement with predictions from normal shock wave theory again confirming that well-formed shocks with predictable characteristics are being formed. The experiments probing boundary layer formation are currently being interpreted.

Absolute OH concentrations from high-pressure Laser-Induced Fluorescence: Laser-Induced Fluorescence (LIF) detection offers exceptional sensitivity and high time resolution, making it a natural choice for probing many important combustion species. Quantification of the observed LIF signal to obtain absolute concentrations, however, is not trivial. We recently developed and optimized a calibration scheme for LIF detection of the OH radical at high pressures, enabling determination of their absolute concentration. Our method relies on known standards of OH radical concentrations, produced with unit yield by the well-known reaction $\text{O}(^1\text{D}) + \text{H}_2\text{O} \rightarrow 2 \text{OH}$. Experimental LIF signals are corrected for

fluorescence quenching by measuring the quenching rates separately. With this scheme in hand, we obtained the OH radical yield in propane oxidation reactions (see below).

Propane Oxidation and Combustion

Our efforts to develop a comprehensive first principles model for propane oxidation are proceeding along many fronts. We have performed high level theoretical analyses for a number of the key elementary reactions. We have made measurements of OH radical concentrations arising from propyl radical oxidation at high pressures. We are developing submodels to explain these experimental observations as well as a global model to predict propane combustion properties. Sensitivity analyses are being applied to these models as well as to the theoretical estimates.

H + propane and ethane: The reactions of H/D with C₂H₆ and C₃H₈ have been studied with both shock tube experiments and ab-initio transition state theory calculations. The reflected shock wave measurements at pressures of 0.3-1 atm over the 1128–1299 K temperature range represent the first direct measurements at combustion relevant temperatures (>1000 K). Ab initio TST predictions obtained at the CCSD(T)/aug-cc-pv ∞ z//MP2/6-311++G(d,p) level are in good agreement with the present experiments, with lower temperature literature data, and with ATcT values for the reaction enthalpies.

Chemistry of HO₂ + alkene reactions: At high pressures, HO₂ becomes the most important radical carrier in combustion. The major bimolecular channel of alkyl + O₂ reactions is alkene + HO₂, but in the reverse direction, the most important products of the alkene + HO₂ reactions are alkylperoxy radical, OH radical + cyclic ether, and the corresponding hydroperoxyalkyl (QOOH) species. Moreover, abstraction of allylic hydrogens can compete with addition. We studied seven unsaturated compounds (ethene, propene, 1-butene, trans-2-butene, isobutene, cyclohexene and ethenol) + HO₂ reactions using *ab initio* transition state theory. Using multiple-well master equations, pressure-dependent branching fractions and rate coefficients were calculated between 300 and 1200 K. We also showed that the pressure dependence of these rate coefficients is large enough to have an impact on ignition delay times in realistic systems.

OH + propene chemistry at high pressures: Addition of OH to the double bond is dominant at low temperatures in this prototypical reaction; at higher temperatures it diminishes in importance due to back dissociation of the C₃H₇O adducts, while H abstraction becomes increasingly important. Despite many previous studies, this reaction has not been characterized at intermediate temperatures, where the interaction of the competing pathways is especially pronounced and back dissociation of the adduct is most evident. In collaboration with researchers at Karlsruhe in Germany, we investigated the OH + propene reaction at pressures from 2.8 to 95 bar, focusing on the intermediate ~ 600-750 K temperature range. We analyzed the measured OH time profiles using recent theoretical results, and presented a simplified set of reactions, validated over a broad set of temperatures and pressures, that can be used in smaller combustion models for propene + OH.

Roaming radicals in isobutane and neopentane: Statistical theory predicts that, due to stronger long-range attractions, the roaming mechanism will be of increased importance in larger molecules. We have explored this prediction with experimental measurements of the H-atom branching fractions for shock tube based studies of the decomposition of iso-butane and neo-pentane. Theoretical work was used to delineate the possible contribution from other decomposition channels. For iso-butane the roaming branching was estimated to be ~ 0.16 ± 0.05, while for neo-pentane it was 0.21 ± 0.05; verifying the prediction of increased roaming fraction for these larger alkanes.

C₃H₆OOH + O₂: The reaction of C₃H₆OOH with O₂ provides a prototypical example of the second O₂ addition, which has been postulated to be responsible for low-temperature chain branching in hydrocarbon oxidation. High-level *ab initio* calculations of the C₃H₇O₂ and C₃H₇O₄ potential energy surfaces were coupled with RRKM master equation methods to compute the temperature- and pressure-dependence of the rate coefficients. Variable reaction coordinate transition-state theory was used to characterize the barrierless transition states. A simple kinetic mechanism indicates that chain branching through this reaction is maximized for temperatures of 600-900 K and pressures of 0.1-10 atm. These thermal rate predictions are central to our development of a submodel for propyl radical oxidation.

Uncertainty in propyl radical + O₂ theoretical kinetics: We have used global uncertainty analysis to study the propagation of uncertainties in fundamental theoretical parameters through to uncertainties in

the predicted temperature and pressure dependent phenomenological rate coefficients for the n-propyl + O₂ reaction. The number of sensitive parameters and the output variance increase with the number of transition states that are crossed. We find rates at 3 σ variances that typically differ from the most frequent values by factors of 4-6, with the uncertainties decreasing with increasing temperature. For well skipping reactions, there are more parameters that contribute significantly to the variance, the second-order sensitivities are greater, and the global uncertainties increased with increasing pressure. For other reactions, the uncertainties decrease with increasing pressure.

Experimental and computational studies of propane oxidation: Propane oxidation is an important benchmark reaction for understanding low-temperature autoignition of alkanes, because 1-propyl radicals are the smallest radicals that react in significant proportion by pathways that involve QOOH radicals. The subsequent fate of QOOH is governed by the pressure-dependent competition between unimolecular decomposition and second O₂ addition to form OOQOOH. We recently measured the OH radical yield in chlorine-initiated propane oxidation at 2 and 8 bar. Although the total OH yield is small, it shows a significant increase (by a factor of ~20) in the temperature range 600-670 K. Preliminary modeling results, based on an updated chemical mechanism that includes OOQOOH formation and decomposition, qualitatively confirm this trend, although the modeled OH radical yield is substantially smaller than in the experiment. This modeling effort incorporates our theoretical predictions for various reactions of both primary and secondary importance.

Energy Transfer

Pressure-dependent unimolecular rate coefficients were obtained via master equation calculations, with nonempirical energy transfer parameters predicted using trajectories. For CH₄ decomposition in the baths He, Ne, Ar, Kr, H₂, N₂, CO, and CH₄, the predicted rate coefficients were shown to agree with available experiments within a factor of two. The neglect of vibrational anharmonicity and approximations in the energy transfer model were identified as the dominant sources of uncertainty. Trends in the energy transfer efficiencies were studied for hydrocarbon targets as large as C₆H₁₂, where the relative bath gas efficiencies were shown to be a function of temperature and to increase systematically with respect to the number of carbon atoms.

Butanol Combustion

1-hydroxybutyl + O₂: We performed quantum chemical and time-dependent multiple-well master-equation calculations on the reactions of O₂ with 1-hydroxy-(1/2/3/4)-butyl radicals derived from 1-butanol, a promising next-generation biofuel. Our goal is to develop a rigorous model of the pressure-dependence of the initial reactions in low-temperature 1-butanol oxidation, capable of predicting the chemistry under relevant in-cylinder conditions. To validate the model, we will compare our predicted rate coefficients and product branching ratios with experimental results over a broad pressure range, including planned high-pressure Multiplexed Photoionization Mass Spectrometry (HP-MPIMS) and OH LIF studies at high pressures.

Future Directions

HRRST Developments: Following the success of the XAS experiments, the HRRST is being coupled to an electron impact ionization time-of-flight mass spectrometer in the lab. Initial experiments will be performed on the dissociation of 1,1,1-trifluoroethane and cyclohexene, which provide well-validated tests for our apparatus. We will also conduct experiments at the ALS, in December of this year. In these experiments PIMS will be used to obtain time and species dependent data. By operating the shock tube at high pressures and with dilute reagent mixtures it should be possible to study oxidation reactions relevant to ignition and development of the initial radical pool, as well as pyrolytic chemistry. The resolution of the molecular and radical products in PIMS/HRRST studies of the high temperature pyrolysis of acetaldehyde and dimethyl ether will be performed over a broad pressure range in order to further delineate the role of the roaming radical mechanism in these reactions.

HP-MPIMS Developments: We continue our efforts at optimizing the HP-MPIMS reactor, designed to investigate photolytically initiated chemical reactions up to 100 bar and up to 1000 K. The reactor couples molecular beam sampling to a mass spectrometer with a tunable synchrotron ionization source

and enables isomer-specific detection of reaction intermediates and products. Initial tests of this reactor highlighted important challenges, the main one being heterogeneous surface chemistry at elevated temperatures, leading to sample decomposition and unwanted wall reactions. This problem, which limits the experimental ranges of both the HP-MPIMS reactor and the LIF detection apparatus, is particularly severe for studies that use halogen-containing radical precursors for photolytic initiation of reactions. Tests are currently underway to replace the first-generation HP-MPIMS reactor with a new design whose wetted parts are more chemically inert, employing glass or fused silica inserts and shaped fused silica sampling nozzles. Such improvements will also be employed in modifications of the high-pressure LIF cell that incorporate chemically inert inserts to reduce wall reactions.

Low-Temperature Autoignition Chemistry: Improvements in instrumentation will extend the range of possible experimental conditions to higher temperatures and pressures, enable broader comparisons with theory for propane oxidation studies, and open the door for experiments on larger alkanes. We will investigate the high-pressure autoignition chemistry of butanol by HP-MPIMS and by OH radical yield measurements. In addition, we plan studies of the pressure and temperature dependence of the reaction of OH with butene. In analogy to the OH + propene work (see above), we will measure rate coefficients for the unimolecular dissociation of β -hydroxybutyl radicals for comparison with theoretical predictions and for validation of butanol combustion models.

We are continuing to work on the development of an accurate mechanism for the combustion and oxidation of propane at high-pressures over a range of temperatures. Theoretical kinetics predictions will be obtained for the following reactions: C_3H_7 decomposition, $C_3H_8 + O_2$, $C_3H_8 + HO_2$, and $C_3H_7O_2 + HO_2$.

Theory Developments: We are working at coupling 2-dimensional master equation solutions with direct trajectory simulations of collision-induced energy and angular momentum transition probabilities in order to obtain fully ab initio pressure dependent rate estimates. We also continue our work on understanding the radical-complex mechanism, focusing initially on the $CH_3 + O_2$ reaction.

DOE Supported Publications, 2010-Present

1. **Theoretical Rate Coefficients for Allyl + HO₂ and Allyloxy Decomposition**, C. F. Goldsmith, S. J. Klippenstein, and W. H. Green, *Proc. Comb. Inst.*, **33**, 273-282 (2011).
2. **Role of Peroxy Chemistry in the High Pressure Ignition of n-Butanol - Experiments and Detailed Kinetic Modelling** S. Vranckx, K. A. Heufer, C. Lee, H. Olivier, L. Schill, W. A. Kopp, K. Leonhard, C. A. Taatjes, R. X. Fernandes, *Combust. Flame* **158**, 1444-1455 (2011).
3. **Shock Tube and Theoretical Studies on the Thermal Decomposition of Propane: Evidence for a Roaming Radical Channel**, R. Sivaramakrishnan, M.-C. Su, J. V. Michael, S. J. Klippenstein, L. B. Harding, and B. Ruscic, *J. Phys. Chem. A*, **115**, 3366-3379 (2011).
4. **Theoretical Unimolecular Kinetics for CH₄ + M → CH₃ + H + M in Eight Baths, M = He, Ne, Ar, Kr, H₂, N₂, CO, and CH₄** A. W. Jasper and J. A. Miller, *J. Phys. Chem. A*, **115**, 6438-6455 (2011).
5. **Competing channels in the propene + OH reaction: Experiment and validated modeling over a broad temperature and pressure range**. C. Kappler, J. Zádor, O. Welz, R. X. Fernandes, M. Olzmann, C. A. Taatjes, *Z. Phys. Chem.* **225**, 1271-1293 (2011).
6. **Pressure Dependent OH Yields in Alkene + HO₂ Reactions: A Theoretical Study** J. Zador, S. J. Klippenstein, and J. A. Miller, *J. Phys. Chem. A*, **115**, 10218-10225 (2011).
7. **High-Temperature Rate Constants for H/D + C₂H₆ and C₃H₈**, R. Sivaramakrishnan, J. V. Michael, and B. Ruscic, *Int. J. Chem. Kinet.* **44**, 194-205 (2012).
8. **On the Role of O₂ + QOOH in Low-Temperature Ignition of Alkanes I: Temperature and Pressure Dependent Rate Coefficients**, C. F. Goldsmith, W. H. Green, and S. J. Klippenstein, *J. Phys. Chem. A*, **116**, 3325-3346 (2012).
9. **Uncertainty Propagation in the Derivation of Phenomenological Rate Coefficients from Theory: A Case Study of Propyl Radical Oxidation**, C. F. Goldsmith, A. S. Tomlin, and S. J. Klippenstein, *Proc. Comb. Inst.*, *in press* (2012).
10. **Shock Tube Explorations of Roaming Radical Mechanisms: The Decompositions of Iso-Butane and Neo-Pentane**, R. Sivaramakrishnan, J. V. Michael, L. B. Harding, and S. J. Klippenstein, *J. Phys. Chem. A*, *in press* DOI: 10.1021/jp210959j (2012).

THEORETICAL CHEMICAL KINETICS

Stephen J. Klippenstein
Chemical Sciences and Engineering Division
Argonne National Laboratory
Argonne, IL, 60439
sjk@anl.gov

Program Scope

The focus of this program is the theoretical estimation of the kinetics of elementary reactions of importance in combustion chemistry. The research involves a combination of *ab initio* quantum chemistry, variational transition state theory (TST), classical trajectory simulations, and master equation calculations. We apply these methods to reactions of importance in various aspects of combustion chemistry including (i) polycyclic aromatic hydrocarbon (PAH) formation, (ii) hydrocarbon oxidation, and (iii) NO_x chemistry. We are also interested in a detailed understanding of the limits of validity of and, where feasible, improvements in the accuracy of specific implementations of transition state theory. Detailed comparisons with experiment and with other theoretical methods are used to explore and improve the predictive properties of the transition state theory models. Dynamics simulations are performed as a means for testing the statistical assumptions, for exploring reaction mechanisms, and for generating theoretical estimates where statistical predictions are clearly inadequate. Master equation simulations are used to study the pressure dependence of the kinetics and to obtain phenomenological rate coefficients for use in kinetic modeling.

Recent Progress

Roaming Radical Kinetics

In collaboration with Harding and Georgievskii we presented a statistical theory for the effect of roaming pathways on product branching fractions in both unimolecular and bimolecular reactions [21]. The analysis employs a separation into three distinct steps: (i) the formation of weakly interacting fragments in the long-range/van der Waals region of the potential via either partial decomposition (for unimolecular reactants) or partial association (for bimolecular reactants), (ii) the roaming step, which involves the reorientation of the fragments from one region of the long-range potential to another, and (iii) the abstraction, addition, and/or decomposition from the long-range region to yield final products. The branching between the roaming induced channel(s) and other channels is obtained from a steady state kinetic analysis for the two (or more) intermediates in the long-range region of the potential. This statistical theory for the roaming induced product branching is illustrated through explicit comparisons with reduced dimension trajectory simulations for the decompositions of H₂CO, CH₃CHO, CH₃OOH, and CH₃CCH. In each instance, at low energy the statistical analysis accurately reproduces the branching obtained from the trajectory simulations. At higher energies, e.g., above 1 kcal/mol, increasingly large discrepancies arise, apparently due to a dynamical biasing towards continued decomposition of the incipient molecular fragments (for unimolecular reactions). Overall, the statistical theory based kinetic analysis is found to provide a useful framework for interpreting the factors that determine the significance of roaming pathways in varying chemical environments.

Recent studies have questioned the separability of the tight and roaming mechanisms to molecular decomposition. In collaboration with Harding and Jasper [26] we have explored this issue for a variety of reactions including $\text{MgH}_2 \rightarrow \text{Mg} + \text{H}_2$, $\text{NCN} \rightarrow \text{CNN}$, $\text{H}_2\text{CO} \rightarrow \text{H}_2 + \text{CO}$, $\text{CH}_3\text{CHO} \rightarrow \text{CH}_4 + \text{CO}$, and $\text{HNNOH} \rightarrow \text{N}_2 + \text{H}_2\text{O}$. Our analysis focuses on the role of the second order saddle point in defining global dividing surfaces that encompass both tight and roaming saddle points. The second order saddle points define an energetic criterion for separability of the two mechanisms. Furthermore, plots of the differential contribution to the reactive flux along approximate minimum energy ridge paths (MERP) provide a dynamic criterion for separability. The minimum in the differential reactive flux in the neighborhood of the second order saddle point plays the role of a mechanism divider, with the presence of a strong minimum indicating that the roaming and tight mechanisms are dynamically distinct. Overall, our calculations suggest that the two mechanisms are generally distinct over broad ranges of energy covering most kinetically relevant regimes.

H₂/O₂ Mechanism

A wide variety of sources provide information on elementary rate constants including rate constant measurements, global combustion experiments, and theoretical kinetics calculations. In collaboration with Burke and Harding [24] we have developed a framework for integrating the information from distinct data types in a self-consistent manner; encapsulating behavior across a wide range of chemically relevant scales from fundamental molecular interactions to global combustion phenomena. The resulting kinetic model consists of a set of theoretical kinetics parameters (with constrained uncertainties), which in turn can be related through kinetics calculations to *T/P/M*-dependent rate constants (with propagated uncertainties), and then through physical models to combustion behavior (with propagated uncertainties). This direct incorporation of theory in combustion model development is expected to yield more reliable extrapolation of limited data to conditions outside the validation set, which is particularly useful for extrapolating to engine-relevant conditions where relatively limited data are available. We have demonstrated several key features of the approach for the H_2O_2 decomposition mechanism. The analysis yields a quantitative explanation for the apparent anomalous temperature dependence of $\text{OH} + \text{HO}_2 \rightarrow \text{H}_2\text{O} + \text{O}_2$ – in a manner consistent with experimental data covering the entire temperature range and *ab initio* transition-state theory within their associated uncertainties. Interestingly, we do find a rate minimum near 1200 K, although the temperature dependence is substantially less pronounced than previously suggested. A related study of the $\text{OH} + \text{OH} \rightarrow \text{O} + \text{H}_2\text{O}$ reaction suggested a modification to the CCSD(T)/CBS barrier height that turned out to be in good agreement with subsequent high level calculations.

Hydrocarbon Oxidation

In collaboration with Glowacki (Bristol) and the Pilling/Seakins (Leeds) group we have studied the effect of reaction occurring during vibrational relaxation for the acetylene + OH + O₂ reaction. Acetylene (R) oxidation begins with OH addition to make $\cdot\text{ROH}$, which subsequently undergoes association with O₂ to form an RO₂ peroxy radical with prompt product channels leading to either (i) formic acid + HCO or (ii) glyoxal + OH depending on the isomeric state of the $\cdot\text{ROH}$ complex. Using a detailed theoretical model, we show that the product ratio is determined by the excited vibrational quantum state distribution of $\cdot\text{ROH}$ at the moment it reacts with O₂. Experimentally, we are able to “tune” the degree of vibrational excitation within the

nascent $\cdot\text{ROH}$, and show that under atmospheric conditions, O_2 “intercepts” $\sim 25\%$ of the excited $\cdot\text{ROH}$ before its vibrational quantum states have fully relaxed. The interception of excited-state radicals by O_2 is likely common to a range of peroxy radical formation reactions in Earth’s atmosphere at ambient temperatures and pressures. More importantly for combustion purposes, a similar interception of excited state radicals may play an important role in the second O_2 addition to QOOH radicals. In particular, the initial population of QOOH radicals formed from $\text{R} + \text{O}_2$ reactions is much greater than the equilibrium population that evolves over many collisions. Correspondingly, the net reactive flux through $\text{QOOH} + \text{O}_2$ may be much greater than predicted by traditional master equation simulations if the hot RO_2/QOOH radicals react with O_2 prior to equilibration.

Future Directions

We are working at improving the accuracy of our TST predictions via (i) higher level treatments of the energies using Heat and W4 like methods (in collaboration with Ruscic), (ii) direct Monte Carlo integration of the torsional mode contributions, (iii) improved tunneling treatments based on higher order local expansions of the potential energy surface. We are also collaborating with Allen (Georgia) on a high level study of the $\text{H} + \text{H}_2\text{O}_2$ reaction and on multi-reference CCSD(T) calculations of the reaction path potential for radical-radical abstractions. A collaboration with Cavallotti (Milan) is exploring the kinetics of $^1\text{CH}_2$ addition to various unsaturated hydrocarbons using our variable reaction coordinate transition state theory methods.

DOE Supported Publications, 2010-Present

1. **On the Temperature Dependence of Two Key Interstellar Reactions of H_3^+ : $\text{O}(^3\text{P}) + \text{H}_3^+$ and $\text{CO} + \text{H}_3^+$** , S. J. Klippenstein, Y. Georgievskii, and B. J. McCall, *J. Phys. Chem. A*, **114**, 278-290 (2010).
2. **Direct Observation of Roaming Radicals in the Thermal Decomposition of Acetaldehyde**, R. Sivaramakrishnan, J. V. Michael, and S. J. Klippenstein, *J. Phys. Chem. A*, **114**, 755-764 (2010).
3. **Roaming Radical Kinetics in the Decomposition of Acetaldehyde**, L. B. Harding, Y. Georgievskii, and S. J. Klippenstein, *J. Phys. Chem. A*, **114**, 765-777 (2010).
4. **Reactions between Resonance Stabilized Radicals: Propargyl + Allyl**, J. A. Miller, S. J. Klippenstein, Y. Georgievskii, L. B. Harding, W. D. Allen, and A. C. Simmonett, *J. Phys. Chem. A*, **114**, 4881-4890 (2010).
5. **D-Atom Products in Predissociation of $\text{CD}_2\text{CD}_2\text{OH}$ from the 202-215 nm Photodissociation of 2-bromoethanol**, L. W. Edwards, M. Ryazanov, H. Reisler, and S. J. Klippenstein, *J. Phys. Chem. A*, **114**, 5453-5461 (2010).
6. **The Effect of Spin-Orbit Splitting on the Association Kinetics of Barrierless Halogen-Atom-Hydrocarbon Radical Reactions**, A. W. Jasper, S. J. Klippenstein, and L. B. Harding, *J. Phys. Chem. A*, **114**, 5759-5768 (2010).
7. **Formation of CH_2NH and NH_3 in Titan’s Upper Atmosphere**, R. V. Yelle, V. Vuitton, P. Lavvas, S. J. Klippenstein, M. Smith, S. Horst, and J. Cui, *Faraday Discussions*, **147**, 31-49 (2010).
8. **An Experimental and Theoretical Investigation of the Self-Reaction of Phenyl Radicals**, R. S. Tranter, S. J. Klippenstein, L. B. Harding, B. R. Giri, X. Yang, and J. H. Kiefer, *J. Phys. Chem. A*, **114**, 8240-8261 (2010).
9. **Theoretical Validation of Chemical Kinetic Mechanisms: Combustion of Methanol**, R. T. Skodje, A. S. Tomlin, S. J. Klippenstein, L. B. Harding, and M. J. Davis, *J. Phys. Chem. A*, **114** 8286-8301 (2010).

10. **Exploring the Role of PAHs in the Formation of Soot: Pyrene Dimerization**, H. Sabbah, L. Biennier, S. J. Klippenstein, I. R. Sims, and B. R. Rowe, *J. Phys. Chem. Lett.*, **1**, 2962-2967 (2010).
11. **Rate Constants for The Thermal Decomposition of Ethanol and its Bimolecular Reactions with OH and D: Reflected Shock Tube and Theoretical Studies**, R. Sivaramakrishnan, M.-C. Su, J. V. Michael, S. J. Klippenstein, L. B. Harding, and B. Ruscic, *J. Phys. Chem. A*, **114**, 9425-9439 (2010).
12. **Roaming Radical Pathways for the Decomposition of Alkanes**, L. B. Harding and S. J. Klippenstein, *J. Phys. Chem. Lett.*, **1**, 3016-3020 (2010).
13. **Uncertainty Driven Theoretical Kinetics Studies for CH₃OH Ignition: HO₂ + CH₃OH and O₂ + CH₃OH**, S. J. Klippenstein, L. B. Harding, M. J. Davis, A. S. Tomlin, and R. T. Skodje, *Proc. Comb. Inst.*, **33**, 351-357 (2011).
14. **Ab Initio Kinetics for the Decomposition of Monomethylhydrazine (CH₃NHNH₂)**, P. Zhang, S. J. Klippenstein, H. Sun, and C. K. Law, *Proc. Comb. Inst.*, **33**, 425-432 (2011).
15. **Roaming Radicals in the Thermal Decomposition of Dimethyl Ether: Experiment and Theory**, R. Sivaramakrishnan, J. V. Michael, A. F. Wagner, R. Dawes, A. W. Jasper, L. B. Harding, Y. Georgievskii, and S. J. Klippenstein, *Comb. Flame*, **158**, 618-632 (2011).
16. **The Role of NNH in NO Formation and Control**, S. J. Klippenstein, L. B. Harding, P. Glarborg, and J. A. Miller, *Comb. Flame*, **158**, 774-789 (2011).
17. **Near-Threshold H/D Exchange in CD₃CHO Photodissociation** B. R. Heazlewood, A. T. Maccarone, D. U. Andrews, D. L. Osborn, L. B. Harding, S. J. Klippenstein, M. J. T. Jordan, and S. H. Kable, *Nature Chem.*, accepted (2011).
18. **Insights into the Role of PAH Condensation in Haze Formation in Jupiter's Atmosphere**, L. Biennier, H. Sabbah, V. Chandrasekaran, S. J. Klippenstein, I. R. Sims, and B. R. Rowe, *Astronomy and Astrophysics*, **532**, A40, 10.1051, (2011).
19. **Long-Range Interaction Potential of Open Shell Atoms with Neutral Molecules: Application to the Calculation of the Rate Constant for the C₂H + O(³P) Reaction** Y. Georgievskii and S. J. Klippenstein *IAU Symp. 280 (The Molecular Universe), Proceedings*, Eds. J. Cernicharo and R. Bachiller, doi:10.1017/S1743921311025129 (2011).
20. **Combustion Chemistry: Important Features of the C₃H₅ Potential Energy Surface, Including Allyl Radical, Propargyl + H₂, Allene + H, and Eight Transition States** B. S. Narendrapurapu, A. C. Simmonett, H. F. Schaefer III, J. A. Miller, and S. J. Klippenstein, *J. Phys. Chem. A*, **115**, 14209-14214 (2011).
21. **Statistical Theory for the Kinetics and Dynamics of Roaming Reactions** S. J. Klippenstein, Y. Georgievskii, and L. B. Harding, *J. Phys. Chem. A*, **115**, 14370-14381 (2011).
22. **Rapid Association Reactions at Low Pressure: Impact on the Formation of Hydrocarbons on Titan**, V. Vuitton, R. V. Yelle, P. Lavvas, and S. J. Klippenstein, *Astrophys. J.*, **744**, 11:1-7 (2012).
23. **Exploring Formation Pathways of Aromatic Compounds in Laboratory-Based Model Flames of Aliphatic Fuels**, N. Hansen, J. A. Miller, S. J. Klippenstein, P. R. Westmoreland, and K. Kohse-Hoinghaus, *Combust. Expl. and Shockwaves*, in press (2012).
24. **A Quantitative Explanation for the Apparent Anomalous Temperature Dependence of OH + HO₂ = H₂O + O₂ through Multi-Scale Modeling** M. P. Burke, S. J. Klippenstein, L. B. Harding, *Proc. Comb. Inst.*, in press (2012).
25. **Comment on "Automatic Estimation of Pressure-Dependent Rate Coefficients"**, J. A. Miller, S. J. Klippenstein, *Phys. Chem. Chem. Phys.*, submitted (2012).
26. **Separability of Tight and Roaming Pathways to Molecular Decomposition**, L. B. Harding, S. J. Klippenstein, and A. W. Jasper, *J. Phys. Chem. A*, submitted (2012).

Theoretical modeling of spin-forbidden channels in combustion reactions

Anna I. Krylov

Department of Chemistry, University of Southern California,
Los Angeles, CA 90089-0482

krylov@usc.edu

1 Scope of the project

The goal of our research is to develop predictive theoretical methods, which can provide crucial quantitative data (e.g., rate constants, branching ratios, heats of formation), identify new channels and refine reaction mechanisms. Specifically, we are developing tools for computational studies of spin-forbidden and non-adiabatic pathways of reactions relevant to combustion, and applying these tools to study electronic structure and reactions of open-shell and electronically excited species involved in these processes.

2 Summary of recent major accomplishments

During the past year, we conducted several computational studies of open-shell and electronically excited species. The common theme in these studies is interactions between states of different character and intersections between the corresponding potential energy surfaces (PESs). We also continued to develop computational methods for modeling electronic structure and spectroscopy of open-shell species. In 2011-2012, the DOE support has been acknowledged in four publications¹⁻⁴ and two more papers are under review.^{5,6}

Some of the recent results are highlighted below.

2.1 Spectroscopy and dynamics of hydroxy-methyl radical

In collaboration with Prof. Hanna Reisler's and Joel Bowman's group, we investigated dynamics of energetic CH_2OH radicals.¹ We developed a global PES fitted to *ab initio* calculations. The PES includes CH_2OH and CH_3O minima, dissociation products, and all relevant barriers. Using this PES, we applied quasi-classical molecular dynamics calculations to study the dissociation of the hydroxymethyl radical and its isotopolog, CD_2OH , following the excitation of high OH stretch overtones. The PES analysis shows that the transition states for OH bond fission and isomerization are both very close in energy to the excited vibrational levels reached in recent experiments and involve significant geometry changes relative to the CH_2OH equilibrium structure. In particular, the OH stretch is strongly

structure methods, we computed adiabatic and vertical IEs of the ground and first four excited states of α -pyranose (Fig. 2), the structure that dominates in the gas phase. A clear picture of the dissociative photoionization dynamics of deoxyribose emerges from the fragmentation pattern recorded using mass spectrometry and from ab initio molecular dynamics calculations. The experimental threshold $9.4 (\pm 0.05)$ eV for neutral water elimination upon ionization is captured well in the calculations, and qualitative insights are provided by molecular orbital analysis and molecular dynamics snapshots along the reaction coordinate.

2.3. Implementation and benchmarking of non-collinear SF-TDDFT

Many of the so-called “multi-reference” situations, which are common in molecules with stretched bonds and unpaired electrons, can be efficiently described by robust and efficient single-reference approaches based on equation-of-motion (EOM) or linear response formalisms. In particular, electronic states of polyradicals can be described as spin-flipping excitation from well-behaved high-spin reference states, which is exploited in the spin-flip (SF) approach.

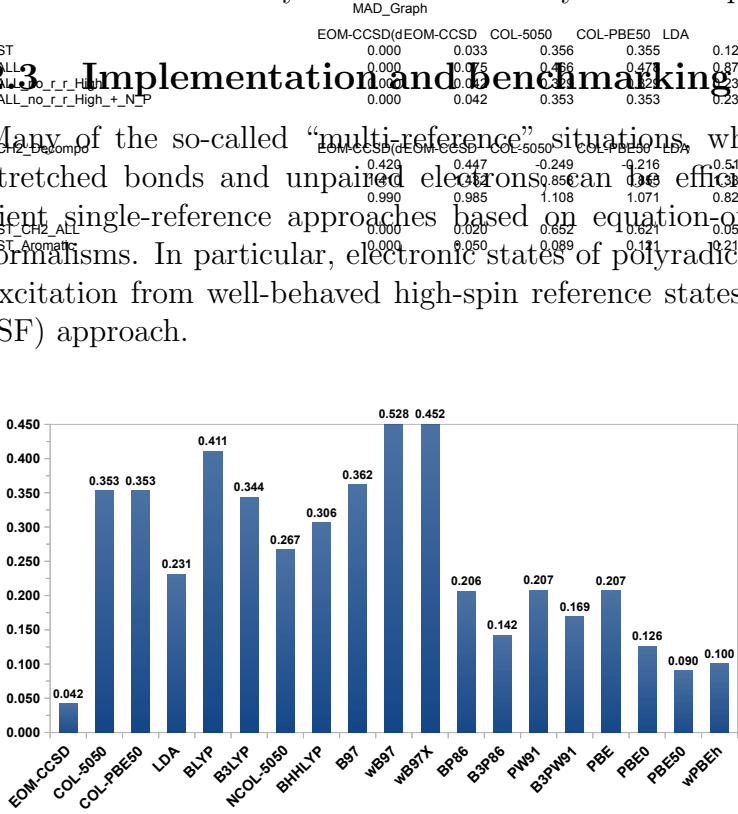


Figure 3: MAD (eV) for 41 gaps between low-lying electronic states in various atomic and molecular systems. The best performance is observed for PBE50 (MAD=0.09 eV). Larger errors for 5050 and BHHLYP are due to the same-center diradicals; for all other cases these functionals exhibit much smaller errors (~ 0.1 eV).

When implemented within DFT, the SF method extends DFT to systems with extensive electronic degeneracies, such as diradicals, triradicals, and even transition metals. We implemented⁵ a general non-collinear variant of SF-TDDFT, which improved the accuracy of original (collinear) SF-TDDFT. We also performed extensive benchmark calculations focusing on energy gaps in a variety of diradicals and open-shell atoms (41 energy gaps). The performance of local, generalized gradient approximation, hybrid, and range-separated functionals for these energy gaps has been carefully evaluated. A consistently good performance is observed for the PBE family, in particular PBE0 and PBE50, which yield mean average deviations (MAD) of 0.126 and 0.090 eV, respectively. In most cases, the performance of original (collinear) SF-TDDFT with 5050 functional is also satisfactory (as compared to non-collinear variants), except for the same-center diradicals where both collinear and non-collinear SF variants that use LYP or B97 exhibit large errors.

2.4 Using charge stabilization method in EOM-DIP calculations

Charge stabilization improves the numeric performance of double ionization potential equation-of-motion (EOM-DIP) method when using unstable (autoionizing) dianion references.³ However, the stabilization potential introduces an undesirable perturbation to the target states' energies. We introduced and benchmarked two approaches for removing the perturbation caused by the stabilization.⁶ The benchmark calculations of excitation energies in selected diradicals illustrated that the so-called core correction based on evaluating the perturbation in a small basis set is robust and yields reliable EOM-DIP values, i.e., the errors of 0.0 - 0.3 eV against a similar-level coupled-cluster approach.

3 Current developments and future plans

Currently, we are pursuing modeling of electronic structure and dynamics of several radicals relevant to combustion. In collaboration with Prof. Hai Wang, we are applying SF-DFT to characterize different pathways in combustion of aromatic hydrocarbons. We are working on improving numeric stability of analytic gradients for non-collinear SF-TDDFT. We are also developing complex-scaled EOM-CC for treating resonance states and photoionization cross sections.

References

- [1] E. Kamarchik, C.P. Rodrigo, J.M. Bowman, H. Reisler, and A.I. Krylov, Overtone-induced dissociation and isomerization dynamics of the hydroxymethyl radical (CH_2OH and CD_2OH). Part I: A theoretical study, *J. Chem. Phys.* **136**, 084304 (2012).
- [2] D. Ghosh, A. Golan, L.K. Takahashi, A.I. Krylov, and M. Ahmed, A VUV photoionization and ab initio determination of the ionization energy of a gas phase sugar (deoxyribose), *J. Phys. Chem. Lett.* **3**, 97 (2012).
- [3] T. Kuś and A.I. Krylov, Using the charge stabilization technique in the double ionization potential equation-of-motion calculations with dianion references, *J. Chem. Phys.* **135**, 084109 (2011).
- [4] K. Khistyayev, K.B. Bravaya, E. Kamarchik, O. Kostko M. Ahmed, and A.I. Krylov, The effect of microhydration on ionization energies of thymine, *Faraday Discuss.* **150**, 313 (2011).
- [5] Y.A. Benrnard, Y. Shao, and A.I. Krylov, General formulation of spin-flip time-dependent density functional theory using non-collinear kernels: Theory, implementation, and benchmarks, *J. Chem. Phys.* (2012), submitted.
- [6] T. Kuś and A.I. Krylov, De-perturbative corrections for charge-stabilized double ionization potential equation-of-motion coupled-cluster method, *J. Chem. Phys.* (2012), submitted.

SYNCHROTRON STUDIES OF COMBUSTION RADICAL REACTIONS AND AEROSOL CHEMISTRY

Stephen R. Leone, Musahid Ahmed, Kevin Wilson, Fabien Goulay, Theodora Nah,
Jessica Lockyear, Denisia Popolan, Amir Golan, and Jordy Bouwman
Lawrence Berkeley National Laboratory and Departments of Chemistry and Physics
University of California, Berkeley, California 94720
(510) 643-5467 srl@berkeley.edu

I. Scope of the Project

Combustion is a complex process involving short-lived radicals, highly excited states, transport processes, heterogeneous chemistry, fluid dynamics, and energy transfer. Vacuum ultraviolet (VUV) light from the Chemical Dynamics Beamline of the Advanced Light Source (ALS) provides a powerful tool to selectively investigate the individual component processes involved in combustion with the aim to better understand the process as a whole. One apparatus for gas phase reactions is the multiplexed photoionization mass spectrometer, which was co-constructed with David Osborn and Craig Taatjes of the Sandia Combustion Research Facility. Employing this technique it is possible to detect the products formed when radical species (for example C_2H , CH , C_3H_3 and C_5H_5) react with molecules. Isomerically defined products from combustion reactions are detected and branching ratios estimated.

The role of heterogeneous chemistry in the combustion process becomes important since fuels are injected directly into combustion chambers and can coat cylinder walls, valves, and injectors with a liquid film, leading to stochastic variations in engine ignition. An aerosol mass spectrometer that employs flash vaporization together with photoionization time-of-flight mass spectrometry is used to study aerosol heterogeneous chemistry. The chemistry of organic particulate species with reactive radicals involved in combustion are explored. Moreover, these data can provide information on the environmental impact of aerosol reactions and oxidation.

II. Recent Progress

A. Gas-Phase Chemistry – C_2H + Allene

The C_2H + allene reaction was investigated at room temperature to obtain isomer branching ratios. The major channel is found to be addition followed by H-elimination, similar to the conclusion in prior studies of this system. In contrast to previous work, four isomers contribute to this channel rather than three. Specifically, the major product isomers are 1,4-pentadiyne (30-45%), ethynylallene (35-45%) and methyldiacetylene (20-25%). An additional isomer, pentatetraene, accounts for 10 % of the signal. It has been theoretically predicted that formation of pentatetraene should be five times more likely than that of methyldiacetylene, different from the branching ratios determined here.

B. CH + Acetaldehyde

Aldehydes are very important intermediates in the combustion of hydrocarbons and are recognized to promote combustion processes. In homogeneous charge compression ignition (HCCI) engines the addition of aldehyde enhances the ignition process by promoting the preflame reaction of the main fuel region. The products of the reaction of the CH radical with acetaldehyde are studied at room temperature. Several reaction channels are observed in these experiments, resulting from direct hydrogen abstraction, CH insertion and CH addition. Direct abstraction of the hydrogen atom on the carbonyl group produces the acetyl radical. Insertion of the CH radical to the C-H bond of the methyl group of the acetaldehyde followed by CH_3 -elimination leads to the formation of ketene. Addition of the CH radical onto the π -electron system of the carbonyl forms a cyclic adduct that dissociates to form C_3H_4O isomers and an H

atom. Photoionization efficiency curves show that methylketene, acrolein and cyclopropanone are the main C_3H_4O reaction products. By selective deuteration of the CH radicals and acetaldehyde molecules it is possible to gain very detailed information about the reaction mechanism. Following CH addition to acetaldehyde, acrolein is formed by loss of a hydrogen atom from the methyl group while all the other C_3H_4O isomers are formed by loss of the H atom from the CH radical. Such a level of detail allows the prediction of the reaction products of CH reactions with larger molecules containing a carbonyl group.

C. CH + acrolein

One of the principle products of the reaction between CH and acetaldehyde is acrolein. Acrolein presents an interesting case study since it contains both C=C and C=O bonds, thus we can probe the competition of insertion or cycloaddition to these unsaturated sites. Investigations of the reactivity of CH with acrolein show a number of channels, some analogous to those observed with acetaldehyde and some differing. Current analysis suggests that H-, CH_3 -, HCO-, C_2H_4 - and CH_2O -elimination channels take place, following addition of the reactants, yielding C_4H_4O , C_3H_2O , C_3H_4 , C_2HO and C_3H_3 , respectively, as partner products. By analysis of the photoionization efficiency curve, the signal corresponding to C_3H_4 is attributed to allene, propyne and cyclopropene. Moreover, C_3H_3 is unequivocally determined to be the propargyl radical, a precursor to benzene formation in combustion. Interestingly, these two channels exhibit conversion of a double bond on the reactant to a product containing a triple bond, a result with potential implications for further molecular-growth reactions.

D. Heterogeneous Chemistry - OH + Unsaturated Fatty Acid Particles

The heterogeneous reaction of OH radicals, in the presence of O_2 , with sub-micron oleic acid, linoleic acid and linolenic acid particles is measured in a photochemical flow reactor using H_2O_2 as a photolytic precursor of OH. These experiments explore how surface OH addition reactions initiate chain reactions that rapidly transform the chemical composition of the particle. Oleic acid, linoleic acid and linolenic acid, which have one, two and three double bonds respectively, are long chain unsaturated fatty acids. These unsaturated fatty acid molecules are similar in structure to the long chain alkyl (methyl, ethyl, or propyl) esters typically found in biodiesel, thus making them reasonable model systems to explore the fundamental heterogeneous reactions between hydrocarbon droplets and gas phase radicals and molecules. Kinetic measurements find that the uptake coefficient for OH on these unsaturated fatty acid particles in the absence and presence of O_2 is larger than unity, providing evidence for particle phase secondary radical chain chemistry, which may accelerate the rate of particle oxidation. The extent of secondary chemistry can be controlled by the concentrations of oxygen and hydrogen peroxide in the system. In addition, the reactive uptake coefficient is inversely proportional to the concentration of OH, signaling a chain termination step that competes with the chain propagation steps. Elemental mass spectrometric analysis reveals that on average only 0.4, 0.46 and 0.59 O atoms is added per reactive loss of oleic acid, linoleic acid and linolenic acid, respectively, thereby indicating that OH addition to the double bond is not be the main reaction pathway that consumes the molecular species. Using a sequential oxidation model, the non-oxidative secondary chain reactions accelerate the reactive depletion rate of the molecular species.

E. Gas-Phase Radicals with Saturated and Unsaturated Hydrocarbon Particles

Reactions are investigated to explore direct H-atom abstraction versus competing addition-elimination reaction mechanisms. Squalane molecules (no double bonds) and squalene (six C=C double bonds) are similar in structure to the long chain alkyl esters found in biodiesel fuel. Gas

phase radicals (CH_3 and I) are generated along the length of a flow tube reactor by photolysis of CH_3I . Although the CH_3 radical is an important intermediate in combustion, subsequent gas phase reactions of methyl with residual O_2 rapidly remove CH_3 from the flow tube, making it difficult to study without further improvements to the apparatus. Therefore the simple atomic radical, I , is used to understand the reaction mechanism that is initiated via a gas phase I atom regarding heterogeneous H abstraction reaction versus radical addition to $\text{C}=\text{C}$ double bonds at the surface of the sub-micron droplets. Preliminary results show no evidence for product formation after the reaction of I radicals with saturated hydrocarbon squalane droplets. In contrast, unsaturated squalene droplets react with I radicals revealing evidence of squalene H atom loss. Products corresponding to $\text{Sq}(\text{CH}_3)_n$ and $\text{SqI}(\text{CH}_3)_n$ ($n=0-3$) are identified, following reaction of the squalene radical species with the residual methyl iodide. The observed reactions are primarily attributed to I atom initiation and the reaction products such as $\text{Sq}(\text{CH}_3)_n$ and $\text{SqI}(\text{CH}_3)_n$ are secondary chemistry reaction products. Experiments using $(\text{CH}_3)_2\text{CO}$ as precursor for the CH_3 and CH_3CO radicals are also performed and reveal significant differences with respect to the experiments in which CH_3I is used as radical precursor. Experiments are underway to understand the mechanisms occurring using different radical precursors. The goal is to construct a detailed heterogeneous reaction dataset and to examine how the heterogeneous reaction rate of I atoms compares with previous measurements of Cl atom initiation.

III. Future Plans

Proposed gas-phase studies will extend the existing work by focusing on understanding reactions of the CH radical, with a view to predicting outcomes of interactions in real combustion environments. In particular, we are examining the trends of insertion and cycloaddition reactions of the CH radical with oxygenated hydrocarbons, which are involved in the processes of biofuel combustion. Products of the reaction of CH with oxirane ($\text{c-C}_2\text{H}_4\text{O}$) and dimethyl ether (CH_3OCH_3) will be investigated since the former class of species has been shown to be an important intermediate in combustion and the latter has recently received interest as an alternative biofuel. Biodiesel comprises long chain fatty acid methyl esters and it is for this reason that reactions of CH with methyl propionate, methyl acrylate and methyl propiolate will also be studied. These three esters represent tenable analogues of biodiesel molecules and also allow us to probe the effect of bond saturation on products formed. Several aspects of the combustion reaction of methyl esters are very similar to those of large alkanes or alkenes due to the common alkyl chains, but the mechanisms of methyl ester reactions tend to be more complex due to the size of these fuel molecules as well as the availability of oxygen-containing functional groups. In this context, the construction of a jet stirred reactor (JSR) for future gas phase and heterogeneous chemistry is planned. The JSR currently represents the best way to realistically simulate the chemical transformations in combustion engines under well-defined conditions of temperature and pressure. The jet-stirred reactor will be utilized for the goal of studying heterogeneous chemistry of methyl esters. In particular, high temperature (500-1100 K) and high pressure (1-10 atm) oxidation reactions of methyl stearate, methyl oleate, and methyl linoleate will be investigated. This series of molecules, differing by the number of unsaturated bonds, will be used to investigate the dependence of aerosol volatilization on molecular structure. This will be investigated for a range of droplet-oxidizer concentrations.

IV. Recent Publications Citing DOE Support (2010-2012)

S. H. Kessler, T. Nah, K. E. Daumit, J. D. Smith, S. R. Leone, C. E. Kolb, D. R. Worsnop, K. R. Wilson and J. H. Kroll, "OH-Initiated Heterogeneous Aging of Highly Oxidized Organic Aerosol", *J. Phys. Chem. A* (in press).

- J. Bouwman, F. Goulay, S. R. Leone and K. R. Wilson, "Bimolecular Rate Constant and Product Branching Ratio Measurements for the Reaction of C_2H with Ethene and Propene at 79 K", *J. Phys. Chem. A*, DOI: 10.1021/jp301015b
- F. Goulay, A. J. Trevitt, J. D. Savee, J. Bouwman, D. L. Osborn, C. A. Taatjes, K. R. Wilson and S. R. Leone, "Product Detection of the CH Radical Reaction with Acetaldehyde", *J. Phys. Chem. A*, DOI: 10.1021/jp2113126
- F. Zhang, R. I. Kaiser, A. Golan, M. Ahmed and N. Hansen, "A VUV Photoionization Study of the Combustion-Relevant Reaction of the Phenyl Radical (C_6H_5) with Propylene (C_3H_6) in a High Temperature Chemical Reactor," *J. Phys. Chem. A* (in press).
- F. Zhang, R. I. Kaiser, V. V. Kislov, A. M. Mebel, A. Golan and M. Ahmed, "A VUV Photoionization Study of the Formation of the Indene Molecule and Its Isomers," *J. Phys. Chem. Lett.* **2**, 1031 (2011).
- A. G. Vasiliou, K. M. Piech, X. Zhang, M. R. Nimlos, M. Ahmed, A. Golan, O. Kostko, D. L. Osborn, J. W. Daily, J. F. Stanton, and G. B. Ellison, "The Products of the Thermal Decomposition of CH_3CHO " *J. Chem. Phys.* **135**, 014306 (2011).
- F. Goulay, S. Soorkia, G. Meloni, D. L. Osborn, C. A. Taatjes and S. R. Leone, "Detection of Pentatetraene by Reaction of the Ethynyl Radical (C_2H) with Allene ($CH_2=C=CH_2$) at Room Temperature", *Phys. Chem. Chem. Phys.* **13**, 20820 (2011).
- A. J. Trevitt, S. Soorkia, J. D. Savee, T. S. Selby, D. L. Osborn, C. A. Taatjes, and S. R. Leone, "Branching Fractions of the $CN + C_3H_6$ Reaction Using Synchrotron Photoionization Mass Spectrometry: Evidence for the 3-Cyanopropene Product," *J. Phys. Chem. A* **115**, 13467 (2011).
- S. Soorkia, C.-L. Liu, J. D. Savee, S. J. Ferrell, S. R. Leone, and K. R. Wilson, "Airfoil Sampling of a Pulsed Laval Beam with Tunable Vacuum Ultraviolet Synchrotron Ionization Quadrupole Mass Spectrometry: Application to Low Temperature Kinetics and Product Detection," *Rev. Sci. Instrum.* **82**, 124102 (2011).
- S. H. Kessler, T. Nah, A. J. Carrasquillo, J. T. Jayne, D. R. Worsnop, K. R. Wilson and J. H. Kroll, "Formation of Secondary Organic Aerosol from the Direct Photolytic Generation of Organic Radicals", *J. Phys. Chem. Lett.* **2**, 1295 (2011).
- C.-L. Liu, J. D. Smith, D. L. Che, M. Ahmed, S. R. Leone, and K. R. Wilson, "The Direct Observation of Secondary Radical Chain Chemistry in the Heterogeneous Reaction of Chlorine Atoms with Submicron Squalane Droplets", *Phys. Chem. Chem. Phys.* **13**, 8993 (2011).
- S. R. Leone, M. Ahmed, and K. R. Wilson, "Chemical Dynamics, Molecular Energetics, and Kinetics at the Synchrotron," *Phys. Chem. Chem. Phys.* **12**, 6564 (2010).
- S. Soorkia, A. J. Trevitt, T. M. Selby, D. L. Osborn, C. A. Taatjes, K. R. Wilson and S. R. Leone, "Reaction of the C_2H Radical with 1-Butyne (C_4H_6): Low-Temperature Kinetics and Isomer-Specific Product Detection," *J. Phys. Chem. A* **114**, 3340 (2010).
- S. Soorkia, C. A. Taatjes, D. L. Osborn, T. M. Selby, A. J. Trevitt, K. R. Wilson and S. R. Leone, "Direct Detection of Pyridine Formation by the Reaction of CH (CD) with Pyrrole: a Ring Expansion Reaction," *Phys. Chem. Chem. Phys.* **12**, 8750 (2010).
- A. J. Trevitt, F. Goulay, C. A. Taatjes, D. L. Osborn, and S. R. Leone, "Reactions of the CN Radical with Benzene and Toluene: Product Detection and Low Temperature Kinetics," *J. Phys. Chem. A* **114**, 1749 (2010).
- R. I. Kaiser, A. Mebel, O. Kostko and M. Ahmed, "On the Ionization Energies of C_4H_3 Isomers," *Chem. Phys. Lett.* **485**, 281 (2010)
- R. I. Kaiser, B. J. Sun, H. M. Lin, A. H. H. Chang, A. Mebel, O. Kostko and M. Ahmed "An Experimental and Theoretical Study on the Ionization Energies of Polyynes ($H-(CC)_n-H$; $n = 1 - 9$)," *Astrophys. J.* **719**, 1884 (2010).
- O. Kostko, J. Zhou, A. Chang, B. J. Sun, J. S. Lie, A. H. H. Chang, R. I. Kaiser and M. Ahmed "Determination of Ionization Energies of C_nN ($n=3-12$) Clusters: Vacuum-Ultraviolet (VUV) Photoionization Experiments and Theoretical Calculations," *Astrophys. J.* **717**, 674 (2010)

INTERMOLECULAR INTERACTIONS OF HYDROXYL RADICALS ON REACTIVE POTENTIAL ENERGY SURFACES

Marsha I. Lester
Department of Chemistry
University of Pennsylvania
Philadelphia, PA 19104-6323
milester@sas.upenn.edu

I. Program Scope

Hydroxyl radicals are important in combustion and atmospheric environments, where they are often detected by laser-induced fluorescence (LIF) on the $A^2\Sigma^+ - X^2\Pi$ band system. However, collision partners known to quench electronically excited OH $A^2\Sigma^+$ radicals are ubiquitous in these environments. Thus, great effort has been made to quantify the rates and/or cross sections for collisional quenching, so that its effects on LIF signals may be taken into account to allow an accurate determination of OH concentrations. Despite extensive kinetic measurements, fundamental questions remain regarding the fate of the collisionally quenched molecules and the *mechanism* by which these nonadiabatic processes occur. The experimental work carried out under DOE-BES funding in the Lester laboratory is aimed at understanding the fundamental chemical dynamics governing quenching of OH $A^2\Sigma^+$ by molecular partners ($M = H_2, O_2, N_2, CO, CO_2, H_2O$) of significance in combustion environments.

II. Recent Progress

A. A new spectroscopic window on hydroxyl radicals using UV+VUV resonant ionization

Although OH is readily detected using LIF on the $A^2\Sigma^+ - X^2\Pi$ transition, a quantum state-selective ionization scheme has been a long-standing goal. The development of a sensitive ionization scheme for OH is essential for the application of techniques such as velocity-map ion imaging to the study of fundamental reaction, photodissociation and inelastic collision dynamics. OH has an adiabatic ionization potential (IP) of 13.017 eV. 2+1 REMPI detection of OH radicals via the $D^2\Sigma^-$ and $3^2\Sigma^-$ states has been demonstrated, but has seen only limited applications, because the ion signals are relatively weak due to fast predissociation ($\tau = 40 - 400$ ps) of the intermediate Rydberg states.¹ We have recently developed an alternative 1+1' MPI detection scheme: a first UV photon prepares the relatively long-lived ($\tau_{\text{rad}} \sim 700$ ns) and spectroscopically well-characterized $A^2\Sigma^+$ valence state as the resonant intermediate state and a subsequent VUV photon provides sufficient energy to ionize.² The fixed frequency VUV at 118.2 nm (10.490 eV) is obtained by frequency tripling the 3rd harmonic output of a Nd:YAG laser in rare gas mixtures.

The 1+1' MPI scheme accesses autoionizing Rydberg states that converge on the $OH^+ A^3\Pi$ ion state. Jet-cooled MPI spectra on the A-X (1,0) and (2,0) bands show anomalous rotational line intensities, while initial excitation on the (0,0) band does not lead to detectable OH^+ ions. The onset of ionization with the (1,0) band is attributed to an energetic threshold; the combined UV+VUV photon energies are above the first member of the autoionizing ($A^3\Pi$) *nd* Rydberg series.³ Comparison of the OH 1+1' MPI signal with that from single photon VUV ionization of NO, indicates that the cross section for photoionization from OH $A^2\Sigma^+$, $v' = 1$ is on the order of 10^{-17} cm². Recent studies are focused on a detailed comparison of REMPI vs. LIF intensities for various OH A-X lines, which avoids complications due to temperatures (population) or line strengths (saturation). The ratio of REMPI to LIF yields an enhancement profile for A-X (1,0) excitation that coincides with the OH [$A^3\Pi$, 3d], $v = 0$ Rydberg feature. Future studies will replace the fixed frequency VUV excitation with tunable light and, in collaboration with Steve Pratt, we plan to examine at the e^- kinetic energy distribution.

B. Outcomes of collisional quenching of electronically excited OH $A^2\Sigma^+$ radicals

1. Reactive quenching of OD $A^2\Sigma^+$ by H₂

The H- and D-atom products from collisional quenching of OD $A^2\Sigma^+$ by H₂ have been characterized through Doppler spectroscopy using two-photon ($2^2S \leftarrow\leftarrow 1^2S$) laser-induced fluorescence.⁴ Partial deuteration enables separation of the channel forming H + HOD products, which accounts for 75% of reactive quenching events, from the D + H₂O product channel. The Doppler profiles, along with those reported previously for other isotopic variants,⁵ are transformed into product translational energy distributions using a robust fitting procedure based on discrete velocity basis functions. The product translational energy distribution for the H-atom channel is strongly peaked at low energy (below 0.5 eV) with a long tail extending to the energetic limit. By contrast, the D-atom channel exhibits a small peak at low translational energy with a distinctive secondary peak at higher translational energy (approximately 1.8 eV) before falling off to higher energy. In both cases, most of the available energy flows into internal excitation of the water products. Similar distributions are obtained upon reanalysis of D- and H-atom Doppler profiles, respectively, from reactive quenching of OH $A^2\Sigma^+$ by D₂. The sum of the translational energy distributions for H- and D-atom channels is remarkably similar to that obtained for OH $A^2\Sigma^+$ + H₂, where the two channels cannot be distinguished from one another. The product translational energy distributions from reactive quenching are compared with those obtained from a previous experiment performed at higher collision energy,⁶ quasiclassical trajectory calculations of the post-quenching dynamics,^{7,8} and a statistical model. There is now an extensive experimental data set on the reactive and nonreactive outcomes of collisional quenching for OH $A^2\Sigma^+$ + H₂ and two of its isotopic variants. Full dimensional coupled dynamics on the relevant potential energy surfaces are in progress (Joel Bowman, Don Truhlar, and coworkers) to more fully understand the nonadiabatic dynamics.

2. Reactive quenching of OH $A^2\Sigma^+$ by O₂ and CO

Recently, we examined the reactive quenching channels for OH $A^2\Sigma^+$ + O₂ and CO producing H- and O-atom products. Previously, we investigated the OH $X^2\Pi$ product state distribution from nonreactive quenching of OH $A^2\Sigma^+$ by O₂, which showed a significant degree of rotational excitation but minimal vibrational excitation.⁹ Branching fraction measurements revealed that 40% of the products are OH $X^2\Pi$ ($v''=0, 1$) and indicated that reactive quenching is significant. In our latest work, we observe both of the energetically accessible reactive channels: O (3P_1) + HO₂ (X^2A'' , A^2A') and H (2S) + O₃ (X^1A_1). Similarly, for quenching of OH $A^2\Sigma^+$ by CO, we observe both of the energetically accessible reactive channels: H (2S) + CO₂ ($X^1\Sigma_g^+$) and O (3P_1) + HCO (X^2A'). In addition, we have searched, but have been unable to detect, OH $X^2\Pi$ ($v''=0, 1$) products from nonreactive quenching.

Doppler profiles of the H-atom fragments are analyzed to obtain the average kinetic energy and, as indicated, the percentage of available energy released as translation to H + O₃ (35%) or H + CO₂ (6%) products. For O-atom products, we lack the laser resolution required for Doppler measurements, but we are able to show a nearly statistical fine structure distribution. Most interesting is the branching fraction to the reactive channels: For OH $A^2\Sigma^+$ + O₂, we demonstrate that O + HO₂ is the dominant channel (48%) and H + O₃ is a minor channel (12%). For OH $A^2\Sigma^+$ + CO, we show that the O + HCO channel (75%) is most significant with the balance resulting in H + CO₂ products (25%). To understand the mechanism for reactive quenching in the OH $A^2\Sigma^+$ + CO system, we are collaborating with David Yarkony to elucidate the nature of the conical intersection region that leads to O + HCO products. Our theoretical work builds on electronic structure and classical trajectory calculations carried out 20 years ago by Vegiri and Farantos,¹⁰ who suggested that the most important pathway involved a C_{2v} configuration leading to the formyloxyl radical (HCO₂).

3. Nonreactive quenching of OH A²Σ⁺ by Kr

Finally, we are taking a brief look at the OH X²Π (v''=0-2) products, again finding highly rotationally excited OH X²Π (v''=0), resulting from quenching of OH A²Σ⁺ by Kr. Ongoing theoretical work by Millard Alexander and coworkers has shown strong nonadiabatic coupling between the OH (A²Σ⁺, X²Π) + Kr potentials of A' symmetry for a crossing (linear) or avoided crossing (non-linear) in Kr-O-H orientations, but not in Kr-H-O configurations where the crossing lies at very high energy. This 3D system seems to mirror many of the nonadiabatic effects we have unraveled in HO-H₂ (6D), making it more tractable for dynamical calculations.

III. Future Plans

Our ongoing research is focused on the *outcomes* of collisional quenching of electronically excited OH A²Σ⁺ radicals. Specifically, the experimental studies are examining reactive quenching processes that generate chemically distinct products as well as nonreactive quenching processes that return OH A²Σ⁺ radicals to their ground X²Π electronic state, the latter with an emphasis on the energy transferred to the collision partner. The observed product state distributions from reactive and nonreactive quenching processes are used to identify the forces acting on the nuclei as the system switches from the electronically excited to ground state potential energy surface. The systems investigated and experimental methods utilized are being expanded to probe previously unobserved outcomes of collisional quenching. Finally, collaborations are being developed with theoretical groups to obtain a comprehensive model for quenching consistent with kinetic rate measurements, product branching ratios, quantum state distributions, and kinetic energy release.

IV. References

1. M. E. Greenslade, M. I. Lester, D. C. Radenovic, A. J. A. van Roij and D. H. Parker, *J. Chem. Phys.* **123**, 074309 (2005); M. P. J. van der Loo and G. C. Groenenboom, *J. Chem. Phys.* **123**, 074310 (2005).
2. J. M. Beames, F. Liu, M. I. Lester, and C. Murray, *J. Chem. Phys.* **134**, 241102 (2011).
3. J. D. Barr, A. De Fanis, J. M. Dyke, S. D. Gamblin, N. Hooper, A. Morris, S. Stranges, J. B. West and T. G. Wright, *J. Chem. Phys.* **110**, 345 (1999).
4. J. H. Lehman, J. Bertrand, T. A. Stephenson, and M. I. Lester, *J. Chem. Phys.* **135**, 144303 (2011).
5. D. T. Anderson, M. W. Todd, and M. I. Lester, *J. Chem. Phys.* **110**, 11117 (1999); M. W. Todd, D. T. Anderson, and M. I. Lester, *J. Phys. Chem. A* **105**, 10031 (2001).
6. M. Ortiz-Suárez, M. F. Witinski, and H. F. Davis, *J. Chem. Phys.* **124**, 201106 (2006).
7. B. Fu, E. Kamarchik, and J. M. Bowman, *J. Chem. Phys.* **133**, 164306 (2010); E. Kamarchik, B. N. Fu, and J. M. Bowman, *J. Chem. Phys.* **132**, 091102 (2010).
8. J. H. Lehman, L. P. Dempsey, M. I. Lester, B. Fu, E. Kamarchik, and J. M. Bowman, *J. Chem. Phys.* **133**, 164307 (2010).
9. L. P. Dempsey, T. D. Sechler, C. Murray and M. I. Lester, *J. Phys. Chem. A* **113**, 6851-6858 (2009).
10. A. Vegiri and S. C. Farantos, in *Selectivity in Chemical Reactions*, edited by J. C. Whitehead (Kluwer Academic Publishers, 1988), pp. 393; *ibid.*, *Mol. Phys.* **69**, 129 (1990).

V. Publications supported by this project 2010-2012

1. J. M. Beames, F. Liu, M. I. Lester, and C. Murray, "Communication: A new spectroscopic window on hydroxyl radicals using UV+VUV resonant ionization", [*J. Chem. Phys.* **134**, 241102 \(2011\)](#).
2. J. H. Lehman, J. Bertrand, T. A. Stephenson, and M. I. Lester, "Reactive quenching of OD A²Σ⁺ by H₂: Translational energy distributions for H- and D-atom product channels", [*J. Chem. Phys.* **135**, 144303 \(2011\)](#).

3. J. H. Lehman, L. P. Dempsey, M. I. Lester, B. Fu, E. Kamarchik, and J. M. Bowman, "Collisional quenching of OD $A^2\Sigma^+$ by H_2 : Experimental and theoretical studies of the state-resolved OD $X^2\Pi$ product distribution and branching fraction", *J. Chem. Phys.* **133**, 164307 (2010).
4. P. Soloveichik, B. A. O'Donnell, M. I. Lester, A. B. McCoy, and J. S. Francisco, "Infrared spectrum and stability of the H_2O -HO complex: Experiment and theory", *J. Phys. Chem. A* **114**, 1529-1538 (2010).

Theoretical Studies of Molecular Systems

William A. Lester, Jr.
Chemical Sciences Division,
Ernest Orlando Lawrence Berkeley National Laboratory and
Kenneth S. Pitzer Center for Theoretical Chemistry
Department of Chemistry, University of California, Berkeley
Berkeley, California 94720-1460
walester@lbl.gov

Program Scope

This research program is directed at extending fundamental knowledge of atoms and molecules. The approach combines the use of ab initio basis set methods and the quantum Monte Carlo (QMC) method to describe the electronic structure and energetics of systems of primarily combustion interest.

Recent Progress

a) Nature of diradical states of graphene at correlated levels of theory (joint with the Frenklach group)

For larger polyaromatic hydrocarbons (PAHs), it is important to correctly identify the nature of the ground state in view of the possibility of there being multi-configurational open-shell states with energy close to that of the ground state. The implications of spin-polarization for the model systems also need to be investigated. It is important here to clarify how interior and exterior (edge) regions, and exterior regions of different types (zigzag/armchair) of a finite-size graphene patch contribute to spin-polarization so that it is clear what kinds of effects must be considered in model studies.

A family of small graphene patches, i.e., rectangular PAHs, that display both zigzag and armchair edges, was investigated to establish their ground state electronic structure. Both broken symmetry DFT and plane wave DFT were used to characterize the onset of diradical character via relative energies of open-shell and closed-shell singlet states. The perfect pairing (PP) active space approximation of

coupled cluster theory was used to characterize diradical character on the basis of promotion of electrons from occupied to unoccupied molecular orbitals. The role of zigzag and armchair edges in the formation of open-shell singlet states was elucidated. In particular, it is found that elongation of the former results in increase of diradical character whereas elongation of the latter leads to decrease of diradical character. Analysis of orbitals from PP calculations suggests that diradical states are formally Mobius aromatic multiconfigurational systems.

b) *Thermal Decomposition of Pentacene Oxyradicals* (joint with the Frenklach group)

The energetics and kinetics of the thermal decomposition of pentacene oxyradicals were studied using a combination of ab initio electronic structure theory and energy-transfer master equation modeling. The rate coefficients of pentacene oxyradical decomposition were computed for the range of 1500 to 2500 K and 0.01 to 10 atm and found to be both temperature and pressure dependent. The computational results reveal that oxyradicals with oxygen attached to the inner rings are kinetically more stable than those with oxygen attached to the outer rings. The latter decompose to produce CO at rates comparable to those of phenoxy radical, while CO is unlikely to be produced from oxyradicals with oxygen bonded to the inner rings.

c) *Quantum Monte Carlo Simulation of X-ray Absorption Spectrum of Pyrrole at the Nitrogen K-edge*

In this study the fixed-node diffusion Monte Carlo (FNDMC) was used to simulate the x-ray absorption spectrum of a gas-phase pyrrole molecule at the nitrogen K-edge. Ground state Kohn-Sham determinant and singly occupied natural orbitals (SONO) from configuration interaction with single excitations (CIS) calculations of the five lowest valence-excited triplet states were used to construct the independent-particle part of trial wave functions of the core-excited states. Assessment of the performance of alternative sources of independent-particle components in the FNDMC treatment of core-excited states is perceived as a natural extension of the present study. It was demonstrated that the FNDMC can yield the

ionization potential (IP) within 0.3 eV from the experimental value of 406.1 ± 0.1 eV. The energies of transitions to anti-bonding virtual orbitals match experimental spectrum after alignment of IP values and agree with the existing assignments. Overall, the reported results are encouraging enough to consider systematic application of FNDMC to simulations of x-ray absorption spectra of molecular systems.

Future Plans

The present level of development of the two central QMC approaches, variational Monte Carlo (VMC) and FNDMC, is sufficiently high that they can be used routinely to compute ground state energies of molecular systems. Certain basic and methodological aspects of QMC still need refinement and development, especially for electronically excited states and open-shell systems. Future research incorporates these aspects. The first direction is system-specific research that aims to address issues relevant to experimental investigations carried out by CSD PIs. This direction is primarily dedicated to utilization of existing QMC methodology for computations of various energetic characteristics of molecules, such as reaction energies, reaction barriers, electron affinities and detachment energies. FNDMC is a reliable source of these values even with the simplest available trial wave functions of Hartree-Fock (HF) or Kohn-Sham (KS-DFT) quality. The second direction is directed at the extension of the FNDMC method to the domain of problems that previously have not been addressed by the approach.

Exploration of reactions on graphene edges will continue in collaboration with Michael Frenklach's group. One of the immediate goals is to investigate reaction of PAH arm-chair sites.

DoE Supported Publications (2010-2012)

1. D. Y. Zubarev, D. Domin, and W. A. Lester, Jr., "Quantitative Characteristics of Qualitative Localized Bonding Patterns," *J. Phys. Chem. A* **114**, 3074 (2010).

2. D. Y. Zubarev, N. Robertson, D. Domin, J. McClean, J. Wang, W.A. Lester, Jr., R. Whitesides, X. You, and M. Frenklach, "Local Electronic Structure and Stability of Pentacene Oxyradicals," *J. Phys. Chem. C* **114**, 5429 (2010).
3. W. A. Lester, Jr., "Quantum Monte Carlo for Electronic Structure," in *Practical Aspects of Computational Chemistry*, J. Leszczynski and M. K. Shukla, Eds., Springer 315 (2010).
4. D. Yu. Zubarev, N. Robertson, D. Domin, J. McClean, J. H. Wang, W. A. Lester, Jr., R. Whitesides, X. You, M. Frenklach, "Polyaromatic Hydrocarbon Oxyradical Stability," *J. At. Mol. Sci.* **1**, 48 (2010).
5. J. Wang, D. Domin, B. Austin, D. Zubarev, J. McClean, M. Frenklach, T. Cui, and W. A. Lester, Jr., "A Diffusion Monte Carlo Study of the O-H Bond Dissociation of Phenol," *J. Phys. Chem. A* **114**, 9832 (2010).
6. M. R. Philpott, S. Vukovic, Y. Kawazoe, and W. A. Lester, Jr., "Edge Versus Interior in the Chemical Bonding and Magnetism of Zigzag Edged Triangular Graphene Molecules," *J. Chem. Phys.* **133**, 044708 (2010).
7. J. Wang, D. Yu. Zubarev, M. R. Philpott, S. Vukovic, W. A. Lester, Jr., T. Cui, Y. Kawazoe, "Onset of Diradical Character in Small Nanosized Graphene Patches," *Phys. Chem. Chem. Phys.* **12**, 9839 (2010).
8. L. Castiglioni, S. Vukovic, P. E. Crider, W. A. Lester, Jr., and D. M. Neumark, "Intramolecular Competition in the Photodissociation of C₃D₃ Radicals at 248 and 193 nm," *Phys. Chem. Chem. Phys.* **12**, 10714 (2010).
9. X. You, R. Whitesides, D. Zubarev, W. A. Lester, Jr., and M. Frenklach, "Bay-capping Reactions: Kinetics and Influence on Graphene-Edge Growth," *Proc. Combust. Inst.* **33**, 685 (2011).
10. D. Yu. Zubarev, X. You, J. McClean, W. A. Lester, Jr., and M. Frenklach, "Patterns of local aromaticity in graphene oxyradicals," *J. Mater. Chem.* **21**, 3404 (2011).
11. X. You, D. Yu. Zubarev, W. A. Lester, Jr., and M. Frenklach, "Thermal decomposition of pentacene oxyradicals," *J. Phys. Chem. A* **115**, 14184 (2011).
12. D. Yu. Zubarev, X. You, M. Frenklach, and W. A. Lester, Jr., "Delocalization effects in pristine and oxidized graphene substrates," in *Advances in the Theory of Quantum Systems in Chemistry and Physics* (P. E. Hoggan, E. J. Brändas, J. Maruani, P. Piecuch, and G. Delgado-Barrio, Eds.), *Progress in Theoretical Chemistry and Physics*, Vol. 22, Springer, Dordrecht, 2012, Chapter 29, p. 553.
13. D. Yu. Zubarev, B. M. Austin, and W. A. Lester, Jr., "Practical Aspects of Quantum Monte Carlo for the Electronic Structure of Molecules," in *Practical Aspects of Computational Chemistry: Methods, Concepts and Applications*, J. Leszczynski and M. K. Shukla, Eds., Springer, 2012.
14. B. M. Austin, D. Yu. Zubarev, and W. A. Lester, Jr., "Quantum Monte Carlo and Related Approaches," *Chem. Rev.* **112**, 263 (2012).
15. D. E. Edwards, X. You, D. Yu. Zubarev, W. A. Lester, Jr., and M. Frenklach, "Thermal decomposition of graphene armchair oxyradical," accepted to the 34th Symp. (Int.) Combust., 2012.

Development of Kinetics for Soot Oxidation at High Pressures Under Fuel-Lean Conditions

JoAnn S. Lighty

Department of Chemical Engineering, University of Utah, jlighty@utah.edu

Randall Vander Wal

Dept. of Energy and Mineral Engineering, Pennsylvania State University, ruv12@psu.edu

Project Scope

The focus of the proposed research is to develop kinetic models for soot oxidation with the hope of developing a validated, predictive, multi-scale, combustion model to optimize the design and operation of evolving fuels in advanced engines for transportation applications. The work focuses on the relatively unstudied area of the fundamental mechanism for soot oxidation. The objectives include understanding of the kinetics of soot oxidation by O₂ under high pressure which require: 1) development of intrinsic kinetics for the surface oxidation, which takes into account the dependence of reactivity upon nanostructure and 2) evolution of nanostructure and its impact upon oxidation rate and 3) inclusion of internal surface area development and possible fragmentation resulting from pore development and /or surface oxidation. These objectives will be explored for a variety of pure fuel components and surrogate fuels.

This project is a joint effort between the University of Utah (UU) and Pennsylvania State University (Penn State). The work at the UU focuses on experimental studies using a Two-Stage burner and high- pressure TGA. Penn State will provide HRTEM images and guidance in the fringe analysis algorithms and parameter quantification for the images.

Recent Progress

Fuel components

At this time, experiments are being conducted using pure n-dodecane and m-xylene, a simple jet fuel surrogate, as well as a mixture of them to study synergies between components. In the future, n-dodecane with the addition of butanol will be used for an oxygenated diesel.

Oxidation Studies

TGA studies were performed with soot samples. Soot was generated in a flat-flame, premixed burner under heavily-sooting conditions and captured on a water-cooled stabilization plate which was located 5 cm above the burner surface. The collected soot was crushed into a powder and oxidized using a Cahn TherMax 500 high pressure TGA. An inert material was used in all the tests to minimize thermal and mass transfer effects by decreasing the stagnant region between the top surface of the soot and the entrance of the crucible. Experiments were performed with 10 mg of sample and a volumetric flow rate of 1 L/min. Two total pressures of the system were evaluated (1 and 10 atm) and the O₂ concentrations varied between 10 and 21%.

Figure 1 shows a typical thermogram obtained from the TGA for 1 and 10 atm. An initial weight loss of roughly 1 mg was recorded during the temperature ramp before introduction of the oxidizing gas, followed by a quasi-linear weight loss until the end of combustion. The high-pressure test showed an increased in weight due to the pressurization of the system; however, weight stabilization was achieved as soon as the system reached the desired pressure.

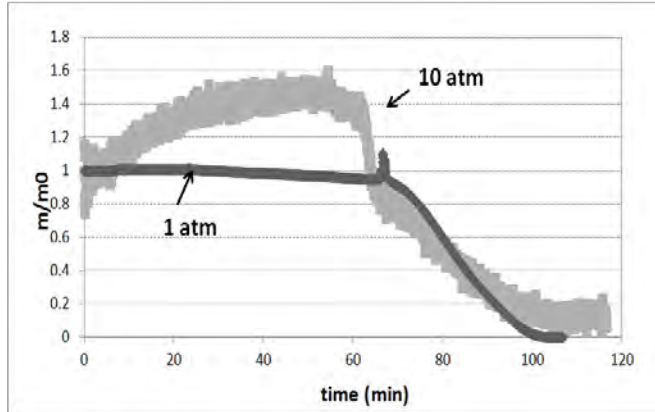


Figure 1. Weight loss versus time, for soot sample at 600 °C, 10% O₂, 1 and 10 atm.

From TGA mass loss data, the activation energy (E_a) and frequency factor (A) were obtained by using the following equations:

$$\frac{dmc}{mc} = -k_c P_{O_2}^n dt \quad k_c = A \cdot \exp\left(\frac{-E_a}{R \cdot T}\right)$$

where mc is the actual soot mass, t is the time, k_c is the reaction rate constant, P_{O_2} is the partial pressure of oxygen, and n is the reaction order of oxygen. After extracting each rate constant at four different temperatures and plotting them against inverse temperature, the activation energy (E_a) and frequency factor (A) were obtained by linear regression.

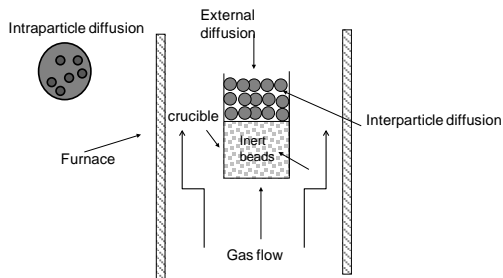


Figure 2. Schematic representation of the oxygen diffusion limitation inside the crucible in the TGA soot oxidation experiment.

A schematic representation of the oxygen diffusion limitation inside the crucible is shown on Figure 2. Mass transfer corrections were required for experiments evaluated at 10 atm. A simplified model based on effectiveness factors accounting for internal and external diffusion limitations was applied in order to account for limitation of oxygen transfer [1, 2].

Table 2 presents the kinetic parameters obtained in this study. The comparison of the activation energy before corrections shows no significant differences for different soot samples under atmospheric conditions, and the values were found to be in the range reported by Ciambelli et al. [3], Otto et al. [4] and Neeft et al. [5] for experiments where kinetics control. The activation energy for the standard Carboxen was also found to be in the range previously reported [6]. As seen in the table, the effects of mass transfer were more profound for the experiments performed under pressure, as evidenced by the differences between the before and after corrections activation energy.

Table 2. kinetic parameters obtained from TGA experiments.

Soot sample	% O ₂	total pressure (atm)	Ea(KJ/mol)		A(1/s)
			before corrections	after corrections	
Carboxen	10	1	140.61	141.75	2.06E+08
Carboxen	10	10	93.79	142.09	1.28E+09
m-xylene/n_dodecane	10	1	148.75	147.69	4.19E+08
m-xylene/n_dodecane	10	10	59.67	162.26	8.72E+07
m-xylene	10	1	154.73	160.33	3.77E+08
m-xylene	21	10	129.04	163.76	2.43E+08
n-dodecane	10	1	161.34	162.45	6.08E+07
n-dodecane	10	10	102.79	164.61	2.24E+08

A challenge is to determine a methodology to investigate nanostructure in the TGA experiments. This requires that the soot be deposited on grids and placed in the TGA or soot is somehow redeposited on the grid after oxidation for a certain period of time. Both of these methods are currently under development. The later has not been totally successful. The former method has been tested with E85 fuel-blend soot from an engine. The soot was deposited on a gold grid versus the standard lacey carbon. Figure 3 illustrates the HR-TEM images from this soot from the engine. As seen in this figure, the images have a disorganized nanostructure organization among lamella and look fairly amorphous.

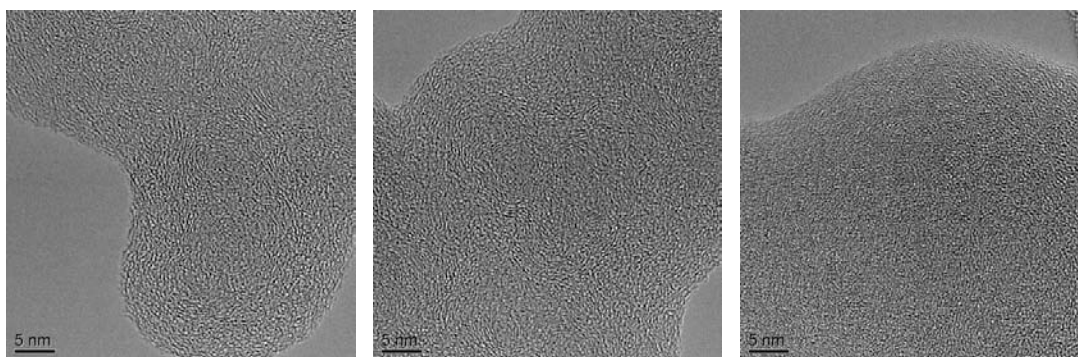


Figure 3. Representative HR-TEM Images of soot for the E85 fuel blend.

The grids were then exposed to air under a temperature ramp of 10°C per min up to 550°C. The resulting structure showed a more graphitic organization after this oxidation (Figure 4).

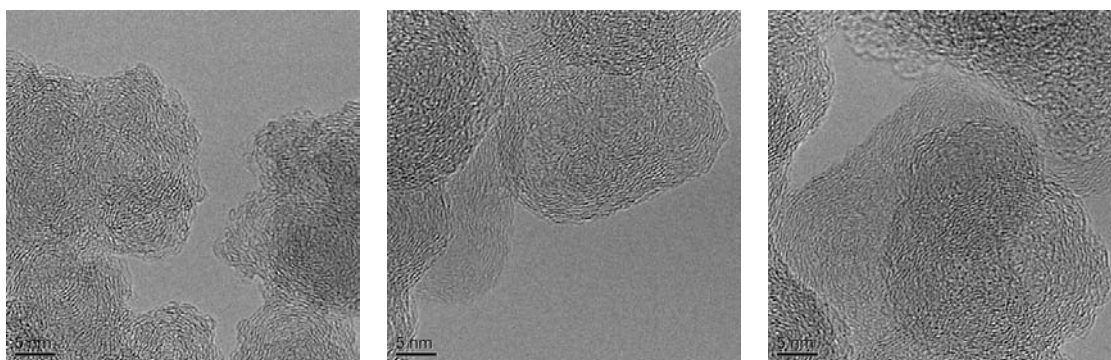


Figure 4. Representative HR-TEM Images of soot after TGA oxidation for the E85 fuel blend.

As demonstrated below (Figure 5), based on image analysis, the fringe length increased for the TGA-oxidized soot. This is seen in the third panel where the length for the engine soot is subtracted from the more oxidized soot. The number is positive for the longer fringe lengths.

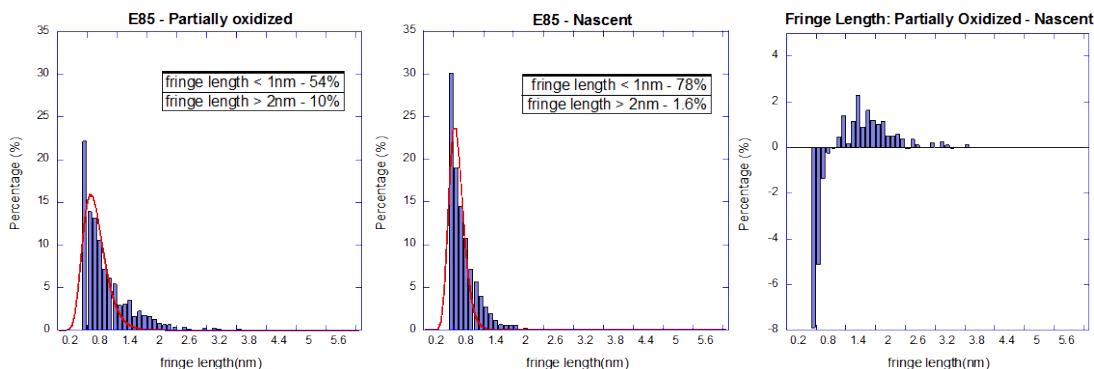


Figure 5. Fringe lengths and difference histogram for the nascent and TGA-oxidized samples.

There was also a decrease in fringe tortuosity for the TGA-oxidized soot suggesting a “flattening” of the structure. These results illustrated that the methodology can capture changes in the structure of the soot with oxidation.

Future Plans

Future work will continue with the development of a methodology to investigate the nanostructure from TGA runs. In addition, the oxygenated fuels will be evaluated in the TGA system under different pressures. At this point, based on nanostructure and obtained activation energies, we will either continue testing in the high-pressure TGA or the two-state burner. If pressure effects remain to be minimal, the two-stage burner offers a higher temperature and larger temperature range of study.

References

- [1] J. Song, J. Chung-Hwan, and A. Boehman. Impacts of Oxygen Diffusion on the Combustion Rate of In-Bed Soot Particles. *Energy & Fuels*, 24:2418-2428, 2010.
- [2] Q. Song, B. He, Q. Yao, Z. Meng, and C. Che. Influence of Diffusion on Thermogravimetric Analysis of Carbon Black Oxidation. *Energy & Fuels*, 20: 1895-1900, 2006.
- [3] P. Ciambelli, P. Corbo, M. Gambino, V. Palma, and S. Vaccaro. Catalytic combustion of carbon particulate. *Catalysis Today*, 53:99, 1996.
- [4] K.Otto, M.H. Sieg, M. Zinbo, and L. Baartosiewicz. The oxidation of soot deposits from Diesel engines, SAE paper 1981.
- [5] J.P. A. Neeft, T.X. Nijhuis, M. Makkee, and J.A. Moulijn. Kinetics of the oxidation of diesel soot. *Fuel*, 76:1129-36, 1997.
- [6] L.H. Sorensen, E. Gjernes, T. Jessen, and J. Fjellerup. Determination of reactivity parameters of model carbons, cokes and flame-chars. *Fuel*, 75: 31-38, 1996.

Advanced Nonlinear Optical Methods for Quantitative Measurements in Flames

Robert P. Lucht

School of Mechanical Engineering, Purdue University

West Lafayette, IN 47907-2088

Lucht@purdue.edu

I. Program Scope

Nonlinear optical techniques such as laser-induced polarization spectroscopy (PS), resonant wave mixing (RWM), and coherent anti-Stokes Raman scattering (CARS) are techniques that show great promise for sensitive measurements of transient gas-phase species, and diagnostic applications of these techniques are being pursued actively at laboratories throughout the world. The objective of this research program is to develop and test strategies for quantitative concentration and temperature measurements using nonlinear optical techniques in flames and plasmas. We have continued our fundamental theoretical and experimental investigations of these nonlinear optical techniques.

We have also continued our theoretical and experimental efforts to investigate the potential of femtosecond (fs) laser systems for sensitive and accurate measurements in gas-phase media. The main advantage of using ultrafast laser systems is the data rate of the measurements is orders of magnitude higher than with nanosecond Q-switched Nd:YAG laser systems. However, this enhanced data rate is useful only if sufficient signal can be obtained on a single laser shot and if the signal can be analyzed to determine parameters of interest. Our initial efforts have been focused on fs CARS, although the systems will be useful for a wide range of future diagnostic techniques involving two-photon transitions. During 2010 we purchased a Coherent ultrafast laser system for nonlinear optical experiments. The new laser system is currently installed in the Applied Laser Spectroscopy Laboratory at Purdue University.

Over the past year we have concentrated on polarization spectroscopy measurements of atomic hydrogen in flames and on fs CARS temperature and concentration measurements at data rates of 5 kHz. We developed and optimized a new laser system for the PS measurements of atomic hydrogen featuring two injection-seeded optical parametric generator/pulsed dye amplifier (OPG/PDA) systems at 656 nm and 486 nm. This new system allows us to correct for the effect of intensity fluctuations on the generation of nonlinear optical signals.

We are investigating the physics of these processes by direct numerical integration (DNI) of the time-dependent density matrix equations for the resonant interaction. Significantly fewer restrictive assumptions are required using this DNI approach compared with the assumptions required to obtain analytical solutions. Inclusion of the Zeeman state structure of degenerate levels has enabled us to investigate the physics of PS and of polarization effects in DFWM and ERE CARS. We are concentrating on the accurate simulation of two-photon processes, including Raman transitions, where numerous intermediate electronic levels contribute to the two-photon transition strength. The DNI numerical methods can be extended to the calculation of the interaction of laser pulses as short as 50 fs simply by decreasing the integration time step (for pulses shorter than this the rotating wave approximation will no longer be valid and the density matrix equations will need to include terms that are negligible for longer pulses).

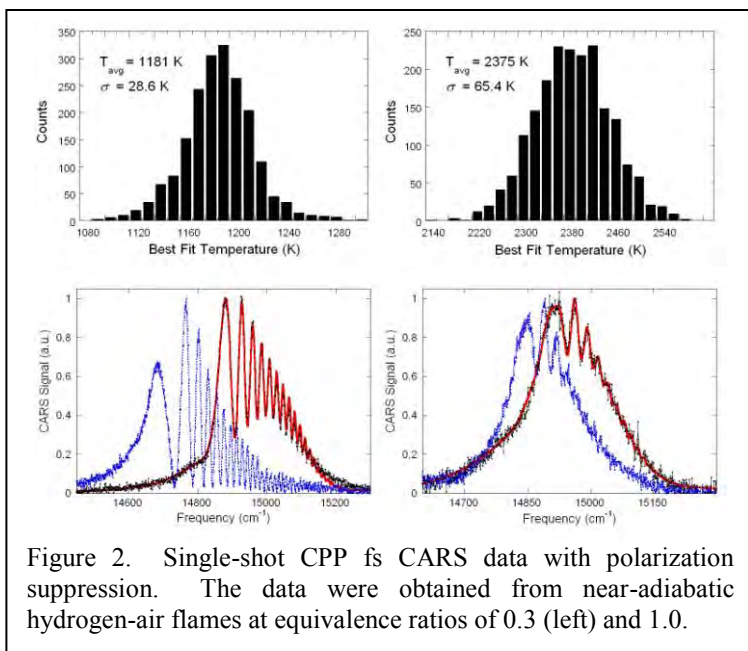
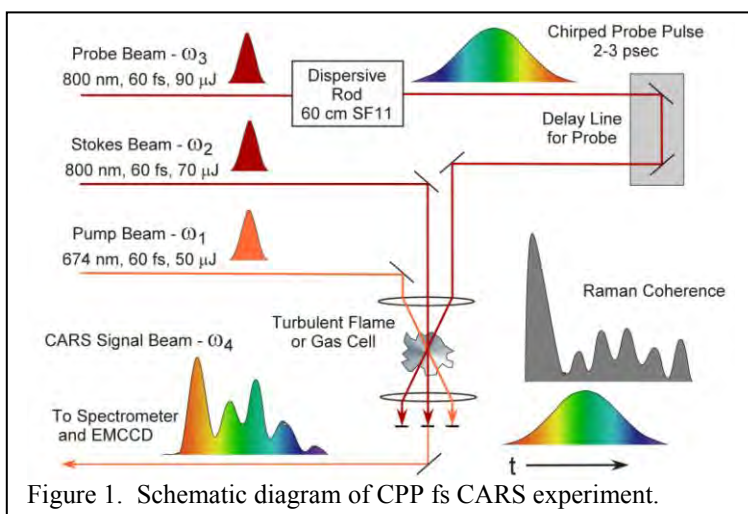
In November of 2011 we moved into the new 2800-square-foot Applied Spectroscopy Laboratory in the new Gatewood Wing of the Mechanical Engineering Building. The new lab is in the basement and features excellent temperature and relative humidity control and exhaust facilities for running flames up to a heat output of 150 kW. The stability of the lab temperature and relative humidity is crucial for stable operation of our Coherent ultrafast laser system.

II. Recent Progress

A. Femtosecond CARS Calculations and Experiments

Fs CARS offers several major potential advantages compared with nanosecond (ns) CARS; i.e., CARS as usually performed with nanosecond pump and Stokes lasers. These potential advantages include an elimination of collisional effects in the signal generation and the capability of performing real-time temperature and species measurements at data rates of 1 kHz or greater as compared to 10-50 Hz for ns CARS. During the past year single-laser-shot temperature measurements at a data rate of 5 kHz were performed in near-adiabatic laminar flames and in a turbulent jet diffusion flame.

Our new ultrafast laser system operates at 5 kHz with a fundamental pulse width of 60 fs and energy of over 2 mJ. The fundamental 800-nm pulse is Fourier-transform-limited to within a few percent. The fundamental 800-nm beam is used as the probe beam for our chirped-pulse-probe (CPP) fs CARS experiments as shown in Fig. 1. The greatly increased pulse energy of the chirped-pulse-probe beam results in a significant increase in the signal-to-noise ratio of the single-pulse measurements. This has enabled us to obtain single-shot spectra with high signal-to noise ratios using



polarization suppression of the nonresonant background in flames, even at stoichiometric conditions [P6]. Temperature histograms and typical single-shot spectra obtained from hydrogen-air flames with equivalence ratio of 0.3 and 1.0 and calculated adiabatic flame temperatures of 1189 K and 2382 K, respectively, are shown in Fig. 2. Single-shot spectra with (red) and without (blue) nonresonant background suppression are also shown in Fig. 2.

The physics of the CPP fs CARS process was previously analyzed using a time-dependent density matrix analysis. The time-dependent density matrix equations for the fs CARS process were formulated and manipulated into a form suitable for solution by direct numerical integration (DNI). The temporal shapes of the pump, Stokes, and probe laser pulses are specified as an input to the DNI calculations. Based on these numerical results, a much faster fitting code was developed to generate synthetic CPP fs CARS spectra. The parameters in the fitting code were varied to obtain the best fit theoretical spectrum for a given experimental spectrum, and temperature was determined as one of the best-fit parameters. This code

is described in detail in publication P4.

B. Polarization Spectroscopy and Six-Wave Mixing: Experiments and Modeling Efforts

We are continuing our collaborative efforts with Dr. Thomas B. Settersten at Sandia's Combustion Research facility on six-wave mixing (6WM) spectroscopy and polarization spectroscopy of atomic hydrogen. The DNI computer code for the calculation of 6WM and PS signals from atomic hydrogen was significantly modified to incorporate all of the different possible photon mixing processes that can potentially contribute to both the 6WM and PS signals. The modeling of collisional processes in atomic hydrogen has also been modified to account for coherence transfer as well as population transfer.

We have developed a new experimental apparatus for the atomic hydrogen experiments featuring OPGs seeded at 1313 nm and 772 nm with signal outputs at 486 nm and 656 nm, respectively. This system is shown in Fig. 3 and described in detail in P5. The signals beams from the OPGs are amplified using PDAs, and the 486-nm beam is then frequency-doubled to 243 nm for two-photon excitation of the 1S-2S resonance. The 656-nm beam is used to probe the 2S-3P transition using polarization spectroscopy. The 656-nm beam is split into a relatively strong circularly polarized pump beam and a linearly polarized probe beam. For each laser pulse, the waveforms for the signal photomultiplier and photodiodes to monitor the 243-nm pump beam energy, the 656-nm pump beam energy, and the 656-nm probe beam energy are captured a fast digital oscilloscope. The data are post-processed to remove data where the laser energies differ from the average energies by more than a certain set threshold amount. This is effective because all the pulses are single-frequency-mode with frequency bandwidths of approximately 200 MHz. We have used this system in the past year for an extensive investigation of atomic hydrogen PS line shapes in near-adiabatic hydrogen-air flames.

III. Future Work

We will continue to perform fs CARS experiments in our laboratory using the new Coherent ultrafast laser system. This system is significantly more powerful and capable than the system at WPAFB that has been used for CPP fs CARS measurements to date. Our studies of polarization suppression and concentration measurements using CPP fs CARS will continue. We have begun to explore the potential of using CPP fs CARS for accurate concentration measurements for water vapor, a very hard species to measure using ns CARS. We will also investigate the potential for measuring mixtures of hydrocarbon species.

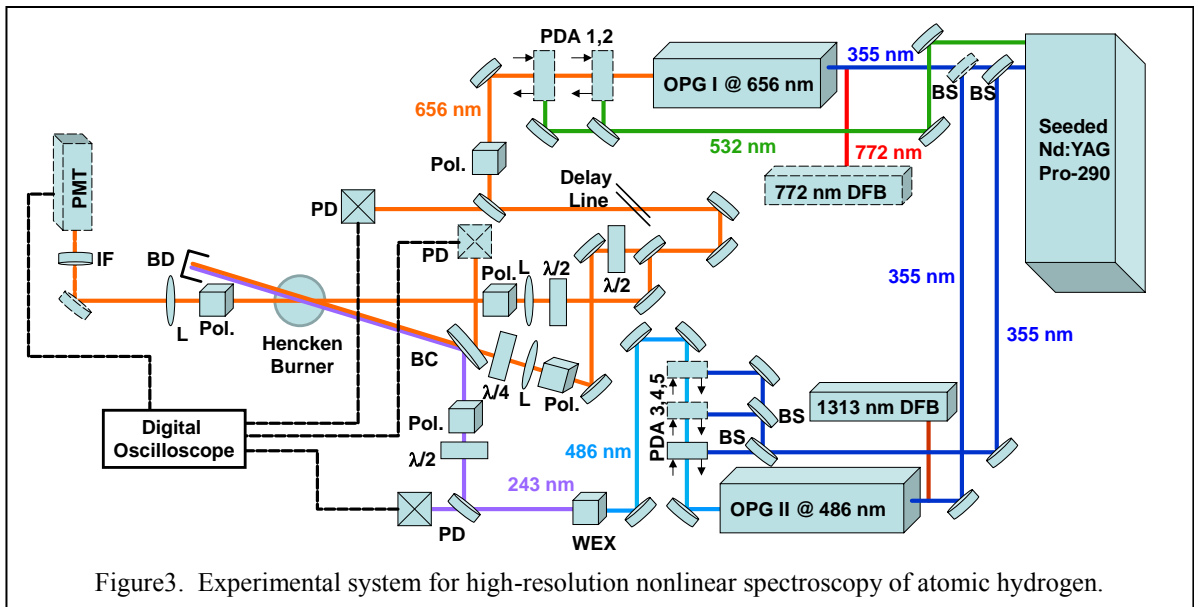


Figure3. Experimental system for high-resolution nonlinear spectroscopy of atomic hydrogen.

Our investigation of the physics of two-photon, two-color PS and 6WM measurements of atomic hydrogen will continue in collaboration with Tom Settersten at Sandia. We have developed a new experimental apparatus for these measurements and collected extensive line shape and concentration data for atomic hydrogen. We will use the density matrix code for two-color PS for comparison and interpretation of the data. We have also purchased the optics and injection-seed lasers needed of two-color PS or 6WM of carbon monoxide, and will begin these experiments soon.

We plan to pursue further theoretical and experimental investigations of the ERE CARS process for species such as NO, OH, and CH, especially at higher pressures where collisional narrowing may result in significant improvement in the detection limits. The DNI code for single-pulse, broadband Stokes ERE CARS will be used to further explore the physics of the single-pulse ERE CARS process. The EIT-like behavior of the ERE CARS saturation process is of significant interest.

IV. Refereed publications and submitted journal articles supported by this project 2010-2012

1. N. Chai, R. P. Lucht, W. D. Kulatilaka, S. Roy, and J. R. Gord, "Electronic-Resonance-Enhanced Coherent Anti-Stokes Raman Scattering Spectroscopy of Nitric Oxide: Nonperturbative Time-Dependent Modeling and Saturation Effect," *Journal of Chemical Physics* **133**, Article Number 084310 (2010).
2. D. R. Richardson, R. P. Lucht, S. Roy, W. D. Kulatilaka, and J. R. Gord, "Single-Laser-Shot Femtosecond Coherent Anti-Stokes Raman Scattering Thermometry at 1000 Hz in a Driven H₂-Air Flame," *Proceedings of the Combustion Institute* **33**, 839-845 (2011).
3. S. Roy, R. P. Lucht, and J. R. Gord, "Orientation and Alignment Dynamics During Generation of Laser-Induced Polarization Spectroscopy (LIPS) Signal," *JOSA B* **28**, 208-219 (2011).
4. D. R. Richardson, R. P. Lucht, S. Roy, W. D. Kulatilaka, and J. R. Gord, "Theoretical Modeling of Single-Laser-Shot, Chirped-Probe Pulse Femtosecond Coherent Anti-Stokes Raman Scattering Thermometry," *Applied Physics B* **104**, 699-714(2011).
5. A. H. Bhuiyan, A. Satija, S. V. Naik, and R. P. Lucht, "High-Resolution Polarization Spectroscopy Based System for H-atom Detection," *Optics Letters*, submitted for publication (2012).
6. D. R. Richardson, D. Bangar, and R. P. Lucht, "Femtosecond Coherent Anti-Stokes Raman Scattering Temperature Measurements at 5kHz with Polarization Suppression of the Nonresonant Background," *Optics Express*, submitted for publication (2012).

Time-Resolved Infrared Absorption Studies of Radical Reactions

R. G. Macdonald
Chemistry Division
Argonne National Laboratory
Argonne, IL 60439
Email: rgmacdonald@anl.gov

Background

Information about the dynamics of radical-radical reactions is sparse. However, these processes are important in combustion being either chain propagating or terminating steps as well as potentially producing new molecular species. For almost all radical-radical reactions, multiple product channels are possible, and the determination of product channels will be a central focus of this experimental effort. In the current experiments, both transient species are produced by excimer laser photolysis of suitable photolytes, and if possible, two species are detected simultaneously using different continuous-wave laser sources operating in the red, near infrared and infrared spectral regions. This approach allows for the direct determination of the second-order rate constant under any concentration conditions if the appropriate absorption cross sections have been measured. The time dependence of individual ro-vibrational states of the reactants and/or products is followed by frequency- and time-resolved absorption spectroscopy. The simultaneous detection of multiple species ensures that species concentration profiles can be normalized to a common set of reaction conditions. In order to determine branching ratios and second-order rate constants, it is necessary to measure state-specific absorption coefficients and transition moments of radicals. These measurements play an important role in this experimental study.

Recent Results

The old rectangular reaction chamber has been replaced by a new stainless steel cylindrical chamber, approximately 120 x 15 cm. The new chamber is heated by 6 barrel heaters divided into 3 zones. Three PID controllers provide uniform heating along the length of cylinder. Brewster-angle CaF₂ windows admit the UV laser photolysis and probe laser radiation. The window holders are heated by separate heating elements. The gases are mixed before entering the reaction chamber, and admitted through narrow stainless steel tubing along the axis of the chamber. This arrangement provides mixing and preheating of the flowing gases. The laser radiation passes through the center of the chamber remote from the walls. Temperatures over 300 C can be reached. Preliminary work has been initiated to measure the temperature dependence of the NH₂ + NH₂ and NH₂ + H recombination reactions with several third bodies.

NH₂(X²B₁) + NH₂(X²B₁) Recombination

The NH₂ + NH₂ reaction is an ideal system to study the influence of different third bodies on a simple radical-radical recombination reaction. The theoretical calculations of Klippenstein *et al* (*J. Phys. Chem. A* **2009**, *113*, 10241) show that near 300 K bimolecular rate processes make little contribution to the removal process of NH₂;

furthermore, these workers have calculated the low and high pressure limits for this system. The reaction system is quite straightforward:



Both NH_2 and NH_3 are monitored simultaneously following the photolysis laser pulse. At pressures < 5 Torr, the loss of NH_3 provides a direct measure of the NH_2 radical concentration. Because the Doppler width of the NH_2 transition is over a factor of four times larger than the infrared NH_3 transition, it is possible to extend these measurements to over 20 Torr, and use the initial NH_2 concentration to calibrate the NH_3 concentration. With the extended mode hop free tuning range of the new dual cavity OPO laser, it is straightforward to determine the NH_3 concentration by recording on and off line laser intensity.

Depending on the third body, at pressures greater than 5 Torr, the NH_3 temporal profiles were sensitive to the recombination rate reaction:



Figure 1 shows the simultaneous determination of the removal of NH_2 by both reactions 2 and 3 at total pressures of 7.02 and 20.82 Torr of CF_4 . The solid line provides the best fit to the data set after several iterations to determine the bimolecular rate constants for reactions 1 and 2. The dotted green line is the calculated model profile for the H atom temporal concentration profile. Diffusion is the major loss process for H atoms. The blue dotted line and black dash-dot line shows the variation in the H atom concentration by $\pm 50\%$ in the first-order diffusion rate constant. However, the NH_2 concentration is rate limiting and the value of k_3 is only changed by $\mp 10\%$.

Fall-off behavior was observed for the pressure dependence of k_1 , and the data was fit to obtain the optimum Troe parameters, k_{inf} , k_0 and F_{cent} . The data was not sensitive to k_{inf} and it was fixed at the theoretical value predicted by Klippenstein et al ($k_{\text{inf}}^1 = 7.9 \times 10^{-11} \text{ cm}^3 \text{ molecule}^{-1} \text{ s}^{-1}$). The results are summarized in Table 1. Also included in Table 1 is the relative efficiency for each third body relative to He.

Table 1. Summary of the Troe fits for k_1 with $k_{\text{inf}}^1 = 7.9 \times 10^{-11} \text{ cm}^3 \text{ molecule}^{-1} \text{ s}^{-1}$.

third body (M)	$k_0^1(\text{M}) (\times 10^{-29})^a$	$F_{\text{cent}}(\text{M})$	$k_0^1(\text{M})/k_0^1(\text{He})$
He	2.8	0.47	1.0
Ne	2.7	0.34	0.96
Ar	4.4	0.41	1.6
N_2	5.7	0.61	2.0
CH_4	9.4	0.61	3.4
C_2H_6	15	0.80	5.4
CO_2	8.6	0.66	3.1
CF_4	11	0.55	3.9
SF_6	19	0.52	6.8

^aunits $\text{cm}^6 \text{ molecule}^{-2} \text{ s}^{-1}$.

The data was not reliable enough to determine the pressure dependence of k_2 . It was assumed that k_2 was in the pure three-body pressure regime, and was linearly dependent on pressure. The results are summarized in Table 2. Also included in Table 2 is the relative recombination efficiency for each third body compared to N_2 and the last column compares the relative rate constants for reaction 1 and 2 in the low-pressure limit for each collision partner.

Table 2. Summary of the low-pressure recombination rate constant for k_2 .

third body	$k_0^2(\text{M}) (\times 10^{30})^a$	$k_0^2(\text{M})/k_0^2(\text{N}_2)$	$k_0^1(\text{M})/k_0^2(\text{M})$
N_2	2.3	1.0	25
CH_4	6.0	2.6	16
C_2H_6	11.	4.8	13
CO_2	6.5	2.8	13
CF_4	8.3	3.6	13
SF_6	14.	6.2	13

^a Units $\text{cm}^6 \text{molecules}^{-2} \text{s}^{-1}$

Publications 2009-present.

Determination of the rate constants for the radical-radical reactions $NH_2(X^2B_1) + NH(X^3\Sigma^-)$ and $NH_2(X^2B_1) + H(^2S)$ at 293 K, Mi-Kyung Bahng and R. G. Macdonald, J. Phys. Chem. A **113**, 2415-2423 (2009).

Determination of the rate constants for the radical-radical reactions $NH_2(X^2B_1) + NH_2(X^2B_1)$ Recombination Reaction with Collision Partners He, Ne, Ar, and N_2 at Low Pressures and 296 K. Part 1, G. Altinay and R. G. Macdonald, J. Phys. Chem. **2012**, 116, 1353-1367.

Determination of the rate constants for the radical-radical reactions $NH_2(X^2B_1) + NH_2(X^2B_1)$ and $NH_2(X^2B_1) + H$ Recombination Reactions with Collision Partners CH_4 , C_2H_6 , CO_2 , CF_4 , and SF_6 at Low Pressures and 296 K. Part 2, G. Altinay and R. G. Macdonald, J. Phys. Chem. A, **2012**, 116, 2161-2176.

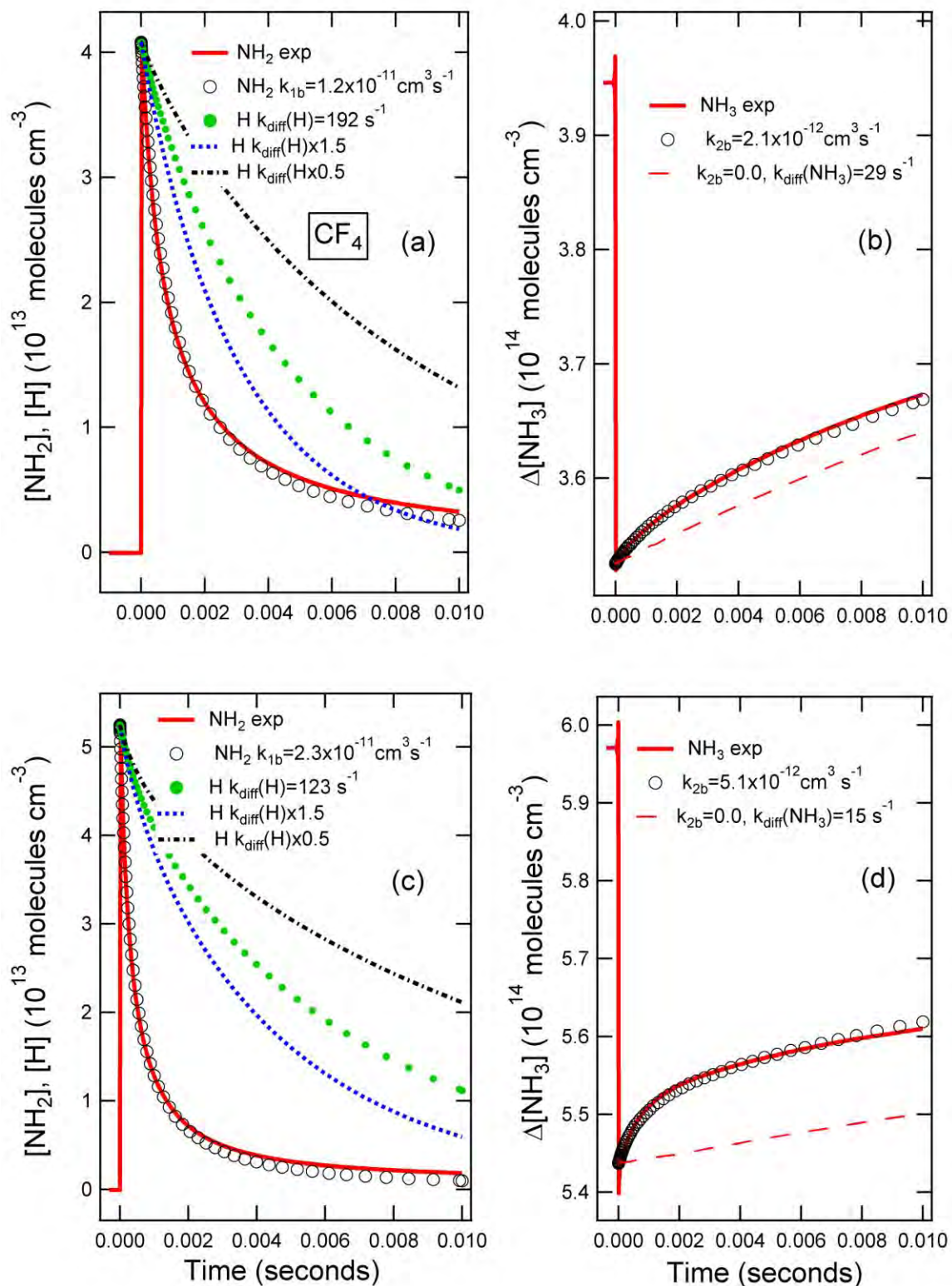


Figure 1. The simultaneous measurement of reactions 1 and 2 is shown for CF_4 as a third body. Panels (a) and (c) were for $P_{\text{CF}_4} = 7.02$ and $P_{\text{NH}_3} = 0.012$ Torr. Panels (c) and (d) for $P_{\text{CF}_4} = 20.82$ and $P_{\text{NH}_3} = 0.018$ Torr. In each panel the experimental profile is shown by the open circles every 10^{th} point and the solid red curve the optimum fit to the data.

Theoretical studies of chemical reactions related to the formation and growth of polycyclic aromatic hydrocarbons and molecular properties of their key intermediates

Alexander M. Mebel

Department of Chemistry and Biochemistry, Florida International University
Miami, Florida 33199. E-mail: mebela@fiu.edu

Program Scope

In this project, we investigate complex chemical mechanisms of PAH formation and growth via theoretical studies of their critical elementary reactions. Our primary objectives include (i) to unravel reaction mechanisms through detailed, accurate, and reliable calculations of pertinent potential energy surfaces (PESs); (ii) to compute rate constants for individual reaction steps and total absolute reaction rate constants and product branching ratios depending on reaction conditions, such as collision energy or temperature and pressure; (iii) to characterize molecular, energetic, and spectroscopic parameters of various possible reaction intermediates and products including their enthalpies of formation, geometric structure, vibrational frequencies and rotational constants, as well as photoionization and photoexcitation spectra. To achieve these goals, we employ chemically accurate ab initio and density functional calculations (using CCSD(T)/CBS, G3, G4, and explicitly correlated methods) of the PESs of these reactions which are then utilized for statistical (TST and RRKM/Master Equation) computations of absolute reaction rate constants and product branching ratios. The underlying theme of the current project period concerns the reactions of phenyl and cyclopentadienyl radical, which are able to produce the smallest PAH and CP-PAH molecules, naphthalene and indene, respectively. In addition, we investigate a variety of oxidation reactions competing with the PAH growth.

Recent Progress

Reactions of phenyl radical with unsaturated hydrocarbons, C₃H₄, C₃H₆, C₄H₂, C₄H₄ (vinylacetylene), and C₄H₆ (1,3-butadiene) – potential pathways to the formation of the simplest PAH molecules. We have employed chemically accurate ab initio calculations to investigate PESs for the reactions of phenyl radical with C₃ and C₄ unsaturated hydrocarbons and utilized the computed surfaces for kinetics calculations (RRKM and RRKM/ME) to predict reaction rate constants and product branching ratios under various conditions, including single-collision conditions (at the zero-pressure limit) and thermal conditions (at finite pressures and temperatures relevant to combustion flames). These theoretical studies were carried out in collaboration with Ralf Kaiser's group at the University of Hawaii and Musa Ahmed's group at LBL who studied these reactions in crossed molecular beams experiments and using high-temperature chemical reactor measurements under combustion-like conditions with product distributions probed utilizing tunable VUV radiation from the Advanced Light Source. In theoretical studies of C₆H₅ + C₃H₆, we also collaborated with William Green's group at MIT.

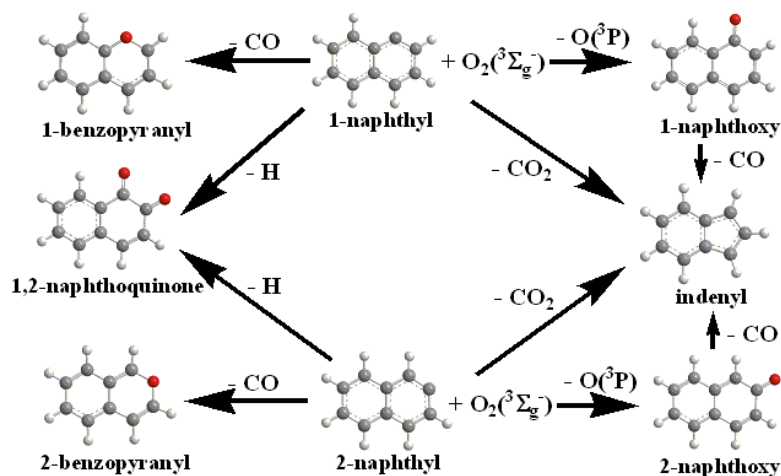
For C₆H₅ + C₃H₄, we refined the B3LYP PES available in the literature using higher level G3(MP2,CC) calculations in order to evaluate relative energies of the reaction intermediates, transition states, and products with chemical accuracy and then computed product branching ratios under single-collision conditions at collision energies of 0-14 kcal/mol. The results indicated that the reaction of C₆H₅ with allene almost exclusively produces indene + H. The reaction of phenyl with methylacetylene also gives indene as the dominant product, but it can

additionally form 1-phenyl-1-propyne as a minor but significant product, especially at high collision energies where its yield reaches 10-15%. The theoretical calculations corroborated the experimentally observed reaction dynamics showing that both reactions are indirect, proceed via the same collision complex, which has a long lifetime, and form indene in high yields. The theoretical study, together with the use of deuterium-substituted reactants in experiment, helped to identify the reaction pathway to indene. The calculations also assisted in the interpretation of the reaction mechanisms and branching ratios observed in a high-temperature chemical reactor under combustion-like conditions (300 Torr, 1200–1500 K). We concluded that the indene molecule can be easily formed in combustion flames as a result of a single collision event between C_6H_5 and C_3H_4 .

We have described the PES for the $C_6H_5 + C_3H_6$ reaction and RRKM calculations of products branching ratios under single-collision conditions in the last year abstract (for the 32nd Annual Combustion Research Meeting). According to our recent RRKM-ME calculations, the H abstraction channels are found to be kinetically preferable at temperatures relevant to combustion and to contribute 55-75% to the total product yield in the 1000-2000 K temperature range, with allyl radical + benzene being the major product (~45%). The relative contributions of phenyl addition channels are calculated to be ~35% at 1000 K, decreasing to ~15% at 2000 K, with styrene + CH_3 and 3-phenylpropene + H being the major products. Collisional stabilization of $C_6H_5 + C_3H_6$ addition complexes is computed to be significant only at temperatures up to 1000-1200 K, depending on the pressure, and maximizes at low temperatures of 300-700 K reaching up to 90% of the total product yield. At $T > 1200$ K collisional stabilization becomes negligible, whereas the dissociation products, styrene plus methyl and 3-phenylpropene + H, account for up to 45% of the total product yield. The production of bicyclic aromatic species including indane C_9H_{10} is found to be negligible. Alternatively, the formation of a PAH molecule, indene C_9H_8 , can be accomplished through secondary reactions after activation of a major product of the $C_6H_5 + C_3H_6$ addition reaction – 3-phenylpropene by direct hydrogen abstraction by small radicals, such as H, OH, CH_3 , etc. It is shown that at typical combustion temperatures 77-90% of C_9H_9 radicals formed by H-abstraction from 3-phenylpropene undergo a closure of a cyclopenta ring via low barriers and then lose a hydrogen atom producing indene. This results in an upper estimate of 7.0-14.5% for the indene yield relative to the initial $C_6H_5 + C_3H_6$ reactants within the 1000-2000 K temperature range.

Our theoretical ab initio/RRKM calculations of PESs and product branching ratios under single-collision conditions for the reactions of C_6H_5 with diacetylene, vinylacetylene, and 1,3-butadiene combined with crossed molecular beams experiments showed that these reactions produce phenyldiacetylene, naphthalene and phenylvinylacetylenes, and 1,4-dihydronaphthalene and 1-phenyl-1,3-butadiene, respectively. While the $C_6H_5 + C_4H_2$ reaction is hindered by a ~1 kcal/mol barrier, the additions of phenyl radical to the terminal CH_2 groups in C_4H_4 and C_4H_6 appear to be barrierless according to our calculations. Thus, the $C_6H_5 +$ vinylacetylene/1,3-butadiene reactions may form the PAH molecules naphthalene and 1,4-dihydronaphthalene even under low-temperature conditions.

Oxidation of naphthyl radicals. PESs of the reactions of 1- and 2-naphthyl radicals with molecular oxygen have been investigated at the G3(MP2,CC)//B3LYP/6-311G** level of theory. Both reactions are shown to be initiated by barrierless addition of O_2 to the respective radical sites of $C_{10}H_7$. The end-on O_2 addition leading to 1- and 2-naphthylperoxy radicals exothermic by 45–46 kcal/mol is found to be more preferable thermodynamically than the side-on addition. At the



subsequent reaction step, the chemically activated 1- and 2- $C_{10}H_7OO$ adducts can eliminate an oxygen atom leading to the formation of 1- and 2-naphthoxy radical products, respectively, which in turn can undergo unimolecular decomposition producing indenyl radical + CO via the barriers of 57.8 and 48.3 kcal/mol and with total reaction endothermicities of 14.5 and 10.2 kcal/mol, respectively.

Alternatively, the initial reaction adducts can feature an oxygen atom insertion into the attacked C_6 ring leading to bicyclic intermediates **a10** and **a10'** (from 1-naphthyl + O_2) or **b10** and **b10'** (from 2-naphthyl + O_2) composed from two fused six-member C_6 and seven-member C_6O rings. Next, **a10** and **a10'** are predicted to decompose to C_9H_7 (indenyl) + CO_2 , 1,2- $C_{10}H_6O_2$ (1,2-naphthoquinone) + H, and 1- C_9H_7O (1-benzopyranyl) + CO, whereas **b10** and **b10'** would dissociate to C_9H_7 (indenyl) + CO_2 , 2- C_9H_7O (2-benzopyranyl) + CO, and 1,2- $C_{10}H_6O_2$ (1,2-naphthoquinone) + H. Based on this, the 1-naphthyl + O_2 reaction is concluded to form the following products (with the overall reaction energies given in parentheses): 1-naphthoxy + O (-15.5 kcal/mol), indenyl + CO_2 (-123.9 kcal/mol), 1-benzopyranyl + CO (-97.2 kcal/mol), and 1,2-naphthoquinone + H (-63.5 kcal/mol). The 2-naphthyl + O_2 reaction is predicted to produce 2-naphthoxy + O (-10.9 kcal/mol), indenyl + CO_2 (-123.7 kcal/mol), 2-benzopyranyl + CO (-90.7 kcal/mol), and 1,2-naphthoquinone + H (-63.2 kcal/mol). Simplified kinetic calculations using transition state theory computed rate constants at the high pressure limit indicate that the $C_{10}H_7O + O$ product channels are favored at high temperatures, while the irreversible oxygen atom insertion first leading to the **a10** and **a10'** or **b10** and **b10'** intermediates and then to their various decomposition products is preferable at lower temperatures. Among the decomposition products, indenyl + CO_2 are always most favorable at lower temperatures, but the others, 1,2- $C_{10}H_6O_2$ (1,2-naphthoquinone) + H (from **a10** and **b10'**), 1- C_9H_7O (1-benzopyranyl) + CO (from **a10'**), and 2- $C_{10}H_7O$ (2-benzopyranyl) + O (from **b10** and minor from **b10'**), may notably contribute or even become major products at higher temperatures.

Future Plans

We plan to complete theoretical kinetics studies of the $C_6H_5 + C_4H_4/C_4H_6$ reactions for combustion applications, via multichannel-multiwell RRKM-ME calculations of the absolute reaction rate constants and relative product yields (including all possible phenyl addition and H abstraction channels) at different temperatures and pressures relevant to combustion. We are also now in position to carry out RRKM-ME calculations for the reaction of oxidation of naphthyl radical, $C_{10}H_7 + O_2$. We will continue to investigate PESs relevant to the formation of larger PAH molecules (anthracene, phenanthrene, chrysene, pyrene, benzopyrene, etc.) via the HACA mechanism with the goal to understand a relatively high abundance of the most carcinogenic PAH isomers. Finally, calculations are underway to evaluate product branching ratios in photodissociation and unimolecular thermal decomposition of benzyne and phenyl radical.

DOE/BES sponsored publications (2010-2012)

1. Kaiser R.I., Mebel A.M., Kostko O., Ahmed M., “On the Ionization Energies of C₄H₃ Isomers”, *Chem. Phys. Lett.*, 2010, 485, 281-285.
2. Zhang F., Jones B., Maksyutenko P., Kaiser R.I., Chin C., Kislov V.V., Mebel A.M., “Formation of the Phenyl Radical [C₆H₅(X²A₁)] under Single Collision Conditions – A Crossed Molecular Beam and Ab Initio Study”, *J. Am. Chem. Soc.*, 2010, 132, 2672-2683.
3. Sebree J.A., Kislov V.V., Mebel A.M., Zwier T.S., “Spectroscopic and Thermochemical Consequences of site-specific H-atom addition to Naphthalene”, *J. Phys. Chem. A*, 2010, 114, 6255–6262.
4. Kislov V.V., Mebel A.M., “Ab Initio/RRKM-ME Study on the Mechanism and Kinetics of the Reaction of Phenyl Radical with 1,2-Butadiene”, *J. Phys. Chem. A*, 2010, 114, 7682-7692.
5. Sebree J.A., Kislov V.V., Mebel A.M., Zwier T.S., “Isomer Specific Spectroscopy of C₁₀H_n, n = 8-12: Exploring Pathways to Naphthalene in Titan’s Atmosphere”, *Faraday Disc.*, 2010, 147, 231-249.
6. Parker D.S.N., Zhang F., Kim, Y.S. Kaiser R.I., Mebel A.M., “On the Formation of Resonantly Stabilized C₅H₃ Radicals -A Crossed Beam and Ab Initio Study of the Reaction of Ground State Carbon Atoms with Vinylacetylene”, *J. Phys. Chem. A*, 2011, 115, 593-601.
7. Zhang F., Kaiser R.I., Kislov V.V., Mebel A.M., Golan A., Ahmed M., “A VUV Photoionization Study of the Formation of the Indene Molecule and Its Isomers”, *J. Phys. Chem. Lett.*, 2011, 2, 1731-1735.
8. Kaiser R.I., Goswami M., Maksyutenko P., Zhang F., Kim Y.S., Landera A., Mebel A.M., “A Crossed Molecular Beams and Ab Initio Study on the Formation of C₆H₃ Radicals - An Interface between Resonantly Stabilized (RSFRs) and Aromatic Radicals (ARs)”, *J. Phys. Chem. A.*, 2011, 115, 10251-10258.
9. Parker D.S.N., Zhang F., Kaiser R.I., Kislov V.V., Mebel A.M., “Indene Formation under Single Collision Conditions from Reaction of Phenyl Radicals with Allene and Phenylacetylene – A Crossed Molecular Beam and Ab Initio Study”, *Chem. Asian J.*, 2011, 6, 3035-3042.
10. Kaiser R.I., Goswami M., Zhang F., Parker D., Kislov V.V., Mebel A.M., Aguilera-Iparraguirre J., Green W.H., “Crossed Beam Reaction of Phenyl and D₅-Phenyl Radicals with Propene and Deuterated Counterparts – Competing Atomic Hydrogen and Methyl Loss Pathways”, *Phys. Chem. Chem. Phys.*, 2012, 14, 720-729.
11. Parker D.S.N., Zhang F., Kaiser R.I., Landera A., Kislov V.V., Mebel A.M., Tielens A.G.G.M., “Low Temperature Formation of Naphthalene and its Role in the Synthesis of PAH in the Interstellar Medium”, *Proc. Nat. Acad. Sci.*, 2012, 109, 53-58.
12. Parker D.S.N., Zhang F., Kim Y.S., Kaiser R.I., Landera A., Mebel A.M., “On the Formation of Phenyl diacetylene (C₆H₅CCCCH) and D₅-Phenyl diacetylene (C₆D₅CCCCH) Studied under Single Collision Conditions”, *Phys. Chem. Chem. Phys.*, 2012, 14, 2997-3003.
13. Zhou C.-W., Kislov V.V., Mebel A.M., “The Reaction Mechanism of Naphthyl Radicals with Molecular Oxygen. I. A Theoretical Study of the Potential Energy Surface”, *J. Phys. Chem. A*, 2012, 116, 1571–1585.
14. Kislov V.V., Mebel A.M., Aguilera-Iparraguirre J., Green W.H., “The Reaction of Phenyl Radical with Propylene as a Possible Source of Indene and Other Polycyclic Aromatic Hydrocarbons: An Ab Initio/RRKM-ME Study”, *J. Phys. Chem. A*, 2012, 116, in press, DOI: 10.1021/jp212338g.
15. Kaiser R.I., Parker D.S.N., Zhang F., Landera A., Kislov V.V., Mebel A.M., “PAH Formation under Single Collision Conditions - Reaction of Phenyl Radical and 1,3-Butadiene to Form 1,4-Dihydronaphthalene”, *J. Phys. Chem. A*, 2012, 116, in press, DOI: 10.1021/jp301775z.

FLASH PHOTOLYSIS-SHOCK TUBE STUDIES

Joe V. Michael

Chemical Sciences and Engineering Division
Argonne National Laboratory, Argonne, IL 60439
E-mail: jmichael@anl.gov

The scope of the program is to measure, with the ANL flash photolysis reflected shock tube technique, high-temperature thermal rate constants for use in high-temperature combustion. This year we have concentrated on reactions where H(or D) is either a reactant or product using H/D-atom atomic resonance absorption spectrometry (ARAS) as the detection technique.^{1,2}

The thermal dissociation of dimethyl ether has been studied with a combination of reflected shock tube experiments and ab initio dynamics simulations coupled with transition state theory based master equation calculations.³ The experiments use H-atom ARAS detection to measure both the total decomposition rate and the branching ratio of radical products to molecular products. The molecular products arise mostly from roaming as suggested by theory. The experiments also give rate constants for H + CH₃OCH₃. An evaluation of the available experimental results for this abstraction can be expressed by a three parameter Arrhenius expression as,

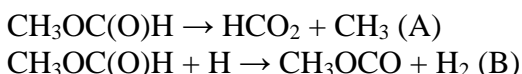
$$k = 6.54 \times 10^{-24} T^{4.13} \exp(-46953/T) \text{ cm}^3 \text{ molecule}^{-1} \text{ s}^{-1}$$

The CH₃OCH₃ potential energy surface was explored with high-level ab initio electronic structure theory. The dynamics of roaming versus radical formation was studied with a reduced dimensional trajectory approach. The requisite potential energy surface was obtained from an interpolative moving least squares fit to wide-ranging ab initio data for the long-range interactions between methyl and methoxy. The predicted roaming and radical micro-canonical fluxes are incorporated in a master equation treatment of the temperature and pressure dependence of the dissociation process. The tight (i.e., non-roaming) transition states leading to a variety of additional molecular fragments were also included in the master equation analysis but predict a negligible contribution to product formation. The final theoretical results reliably reproduce the measured dissociation rate to radical products reported here and are well reproduced over the 500–2000 K temperature range and the 0.01–300 bar pressure range by the following modified Arrhenius parameters in the Troe falloff format:

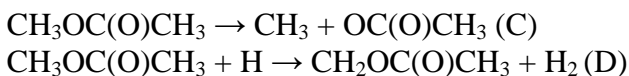
$$\begin{aligned} k_1^\infty &= 2.33 \times 10^{19} T^{-0.661} \exp(-42345/T) \text{ s}^{-1} \\ k_1 &= 2.86 \times 10^{35} T^{-11.4} \exp(-46953/T) \text{ cm}^3 \text{ molecule}^{-1} \text{ s}^{-1} \\ F_{\text{cent}} &= \exp(-T/880) \end{aligned}$$

The experimentally observed branching ratio of 0.19 ± 0.07 provides a direct measure of the contribution from the roaming radical mechanism. The theoretical analysis predicts a much smaller roaming contribution of 0.02.

Responding to the need for absolute rate data for biofuels, we studied the high temperature thermal decompositions of methylformate (MF) and methylacetate (MA).⁴ The formation of H-atoms was measured behind reflected shock waves again using the ARAS method. The experiments span a T-range of 1194 - 1371 K at pressures ~ 0.5 atm. H-atom profiles were simulated using a detailed chemical kinetics mechanism for MF and MA thermal decompositions. The simulations were used to derive rate constants for sensitive decomposition and H-abstraction reactions in both molecules. Figure 1 shows representative H-atom profiles and model simulations from methyl formate decomposition experiments. In methylformate, the most sensitive reactions that determine H-atom profiles are:



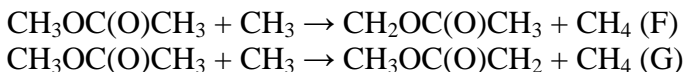
where H is formed from $\text{HCO}_2 \rightarrow \text{H} + \text{CO}_2$. In methylacetate the most sensitive reactions affecting H-atom formation are:



Minor sensitivity was observed for the energetically higher lying bond fission,



and H-atom abstractions from MA by CH_3 ,



Unlike MF (where H-atoms are formed instantaneously at high-temperatures from (A)), in MA, H-atoms form from CH_3 radicals (through $\text{CH}_3 + \text{CH}_3 \rightarrow \text{C}_2\text{H}_4 + 2\text{H}$) generated primarily through the C-O bond fission channel (C) with minor contributions from (E). A master equation analysis was performed using CCSD(T)/cc-pv ∞ z//B3LYP/6-311++G(d,p) energetics and molecular properties for all thermal decomposition processes in both MF and MA. Figure 2 depicts the experimentally measured rate constants from the present experiments for channel (C). The theoretical predictions shown here are in good agreement with the present⁴ and prior⁵ experimentally derived rate constants for the major bond fission, channel (C). TST calculations using CCSD(T)/cc-pv ∞ z//MP2/aug-cc-pvtz energies and molecular properties for reactions (B) and (D) (the only sensitive abstraction processes in MF and MA) are in good agreement with the experimental rate constants. The theoretically derived rate constants for these processes can be represented by modified Arrhenius expressions for the bond fissions at 0.5 atm over the T-range 1000-2000 K and for the bimolecular abstractions over the 500 - 2000 K regime.

$$\begin{aligned} k_A(T) &= 9.79 \times 10^{68} T^{15.95} \exp(-57434 \text{ K}/T) \text{ s}^{-1} \\ k_B(T) &= 5.67 \times 10^{-19} T^{2.50} \exp(-3188 \text{ K}/T) \text{ cm}^3 \text{ molecule}^{-1} \text{ s}^{-1} \end{aligned}$$

$$k_C(T) = 1.42 \times 10^{84} T^{19.60} \exp(-63608 \text{ K}/T) \text{ s}^{-1}$$

$$k_D(T) = 1.18 \times 10^{18} T^{2.58} \exp(-3714 \text{ K}/T) \text{ cm}^3 \text{ molecule}^{-1} \text{ s}^{-1}$$

$$k_E(T) = 1.90 \times 10^{82} T^{19.30} \exp(-64724 \text{ K}/T) \text{ s}^{-1}$$

Our theoretical predictions for MA + CH₃ give over the *T*-range 500-2000 K,

$$k_F(T) = 2.117 \times 10^{-25} T^{3.93} \exp(-4440 \text{ K}/T) \text{ cm}^3 \text{ molecule}^{-1} \text{ s}^{-1}$$

$$k_G(T) = 3.403 \times 10^{-25} T^{3.88} \exp(-4149 \text{ K}/T) \text{ cm}^3 \text{ molecule}^{-1} \text{ s}^{-1}$$

To our knowledge this is the first study providing experimentally derived rate constant values for the primary bond fission and abstraction reactions in MF and MA.

This work was supported by the U. S. Department of Energy, Office of Basic Energy Sciences, Division of Chemical Sciences, Geosciences, and Biosciences, under Contract No. DE-AC02-06CH11357.

References

- ¹ S.S. Kumaran, J.J. Carroll, and J.V. Michael, Proc. Combust. Inst. **27**, 125 (1998).
- ² S.L. Mielke, K.A. Peterson, D.W. Schwenke, B.C. Garrett, D.G. Truhlar, J.V. Michael, M.-C. Su, J.W. Sutherland, Phys. Rev. Lett. **91**, 063201 (2003).
- ³ R. Sivaramakrishnan, J.V. Michael, A.F. Wagner, R. Dawes, A.W. Jasper, L.B. Harding, Y. Georgievskii, and S.J. Klippenstein, Combust. and Flame **158**, 618-632 (2011).
- ⁴ S. Peukert, R. Sivaramakrishnan, M.-C. Su, and J.V. Michael, Combust. and Flame, dx.doi.org/10.1016/j.combustflame.2012.03.007.
- ⁵ A. Farooq, D. F. Davidson, R. K. Hanson, L. K. Huynh, A. Violi, Proc. Combust. Inst. **32**, 247-253 (2009).

PUBLICATIONS FROM DOE SPONSORED WORK FROM 2010-2012

- *The Direct Observation of Roaming Radicals in the Thermal Decomposition of Acetaldehyde*, R. Sivaramakrishnan, J.V. Michael, and S.J. Klippenstein, J. Phys. Chem. A **114**, 755-764 (2010).
- *The Thermal Decomposition of Ethanol and its Bimolecular Reactions with OH and D: Reflected Shock Tube and Theoretical Studies*, R. Sivaramakrishnan, M.-C. Su, J.V. Michael, S.J. Klippenstein, L.B. Harding, and B. Ruscic, J. Phys. Chem. A **114**, 9425-9439 (2010).
- *H- and D-atom Formation from the Pyrolysis of C₆H₅CH₂Br and C₆H₅CD₂Br: Implications for High-Temperature Benzyl Decomposition*, R. Sivaramakrishnan, M.-C. Su, and J.V. Michael, Proc. Combust. Inst. **33**, 243-250 (2011).
- *Pyrolysis of C₆D₅CH₃: Rate Constants and Branching Ratios in the High Temperature Thermal Decomposition of Toluene*, R. Sivaramakrishnan and J.V. Michael, Proc. Combust. Inst. **33**, 225-232 (2011).

- *Roaming Radicals in the Thermal Decomposition of Dimethyl Ether: Experiment and Theory*, R. Sivaramakrishnan, J.V. Michael, A.F. Wagner, R. Dawes, A.W. Jasper, L.B. Harding, Y. Georgievskii, and S.J. Klippenstein, *Combust. and Flame* **158**, 618-632 (2011).
- *Experiment and Theory on Methyl Formate and Methyl Acetate Kinetics at High Temperatures: Rate Constants for H-atom Abstraction and Thermal Decomposition*, S.L. Peukert, R. Sivaramakrishnan, M.-C. Su, and J. V. Michael, *Combust. and Flame*, dx.doi.org/10.1016/j.combustflame.2012.03.007.
- *The Thermal Decomposition of o-Xylyl Radicals using H-ARAS*, R. Sivaramakrishnan and J.V. Michael, in preparation.
- *High Temperature Rate Constants for H/D + Methylformate and Methylacetate*, S. Peukert, R. Sivaramakrishnan, M.-C. Su, and J.V. Michael, *Proc. Combust. Inst.* **34**, accepted.

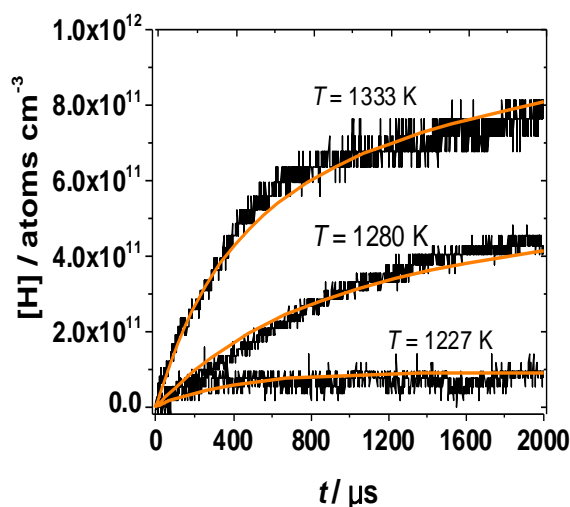


Figure 1: H-atom profiles produced from the pyrolysis of $\text{CH}_3\text{OC}(\text{O})\text{H}$. [—]: H-atom profiles simulated with the reaction model to obtain k_A .

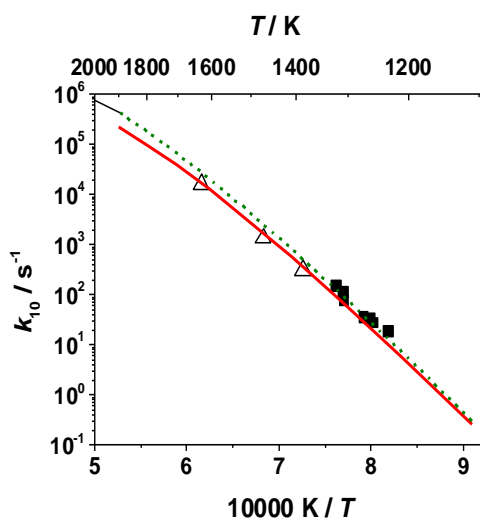


Figure 2: Rate constants for the reaction $\text{CH}_3\text{OC}(\text{O})\text{CH}_3 \rightarrow \text{CH}_3 + \text{OC}(\text{O})\text{CH}_3$. [■] – k_C from modeling the present H ARAS experiments, ($P_5 \sim 0.5$ atm); [Δ] – k_C values derived from modeling the measured CO_2 profiles from Farooq et al.⁵ ($P_5 \sim 1.5$ atm). [—] – Theory (present work), 0.5 atm; [---] – Theory (present work), 1.5 atm.

Particle Diagnostics Development

H. A. Michelsen

Sandia National Labs, MS 9055, P. O. Box 969, Livermore, CA 94551

hamiche@sandia.gov

I. Program Scope

Combustion processes often produce solid carbon particles, i.e., soot. These particles may be oxidized to form gas-phase species or released into the exhaust stream, where they can be coated with liquid coatings. These coatings can be comprised of any of a number of components, including unburned fuel, lube oil, sulfuric acid, water, and other combustion by-products.^{1,2} The research program described here focuses on the development of optical diagnostics for soot particles in combustion environments and combustion exhaust plumes. The goal of this work is *in situ* measurements of volume fraction, size, composition, and morphology of combustion-generated particles with fast time response and high sensitivity. Measurement techniques are targeted for studies of soot formation and evolution and must be versatile enough to probe particles throughout their entire life cycle. Techniques are being developed for detection and characterization of particles in combustion environments from incipient particles that are 2-20 nm in diameter and composed of condensed large organic species to mature soot particles composed of aggregates of carbonaceous primary particles resembling polycrystalline graphite. Diagnostics are also being developed for characterization of inhomogeneous exhaust particles.

II. Recent Progress

Our work has focused on developing a detailed understanding of the chemical and physical mechanisms that influence the applicability of laser-based techniques for soot detection under a wide range of conditions. In recent work, for instance, we have investigated the optical properties of soot in a flame. Using a combination of laser-induced incandescence (LII), extinction, and particle temperature measurements from spectrally and temporally resolved radiative emission, we have studied the wavelength and temperature dependence of the scattering and absorption cross-sections of soot. We have used these results in a model that describes the energy- and mass-balance equations for laser-heated soot and compared the model predictions of time-resolved incandescence signals and particle temperatures to observed LII and temperature temporal profiles. We have also built a particle-beam chamber for focusing and coating soot particles and measuring their optical properties under controlled conditions. We have used this chamber to measure LII of flame-generated soot under low-pressure conditions.

A. Aerodynamic Focusing of Soot in a Particle Beam

LII is used extensively to characterize soot in various combustion environments. This technique generally involves heating soot with a pulsed laser and recording the resulting blackbody emission. The intensity of the incandescence is used to measure the soot volume fraction, and the decay rate of the LII signal after the laser pulse provides information about the primary-particle size of the soot aggregate. The temporal evolution of the LII signal depends strongly on the laser spatial and temporal profiles, temporal and spectral response of the detection system, and surrounding gas-phase environment. Although LII is a promising technique for characterizing and quantifying soot, reliable application under a wide range of combustion environments requires a better understanding of experimental factors that influence the signal and the underlying physical mechanisms involved in signal generation.

Models have been developed to reproduce and predict the temporal profile of soot emission over a wide range of laser fluences. These models solve the mass- and energy-balance equations during and after the laser pulse by considering the most important physical and chemical processes expected to occur during LII, including laser absorption, radiative and conductive cooling, sublimation, non-thermal ablation, phase-changes, and surface chemistry. Predictions from these models have been compared with experimental LII profiles from soot generated in diffusion and premixed flames. Models have also been developed to predict the LII signal evolution under more extreme environments, such as very dense media, high-pressure environments, and high-vacuum conditions. Nevertheless, large uncertainties in predicting LII signals still remain. The most significant of these uncertainties stem from an incomplete understanding of mass-loss processes, conductive cooling, and temperature and wavelength dependencies of the soot optical properties. The development of LII as a quantitative tool for soot characterization

requires a better understanding of these phenomena. Narrowing these uncertainties will require careful studies of LII data obtained under broad and very well controlled experimental conditions.

Our studies of LII of flame-generated soot under low-pressure conditions and with coatings require the generation of a stable soot-particle beam. We generate such a beam using an ethylene co-flow diffusion flame combined with an aerodynamic-lens system. A schematic diagram of the experimental setup is shown in Fig. 1. Particle beams generated by aerodynamic-lens systems (1) are collimated, allowing for directional control of sampled particles, (2) are concentrated, thereby improving detection sensitivity for low-density samples, and (3) have high-flow rates, enabling rapid-sampling rates for better particle statistics over short timescales. These systems are characterized by a series of orifices (known as aerodynamic lenses), with sequentially smaller diameters, upstream of a differentially pumped nozzle. There is no differential pumping between these aerodynamic lenses, except for pressure drops across the first and final orifices. Particles of decreasing aerodynamic size are focused along the axis with each lens of decreasing diameter³⁻⁶ and remain focused and collimated when introduced into the final vacuum chamber.

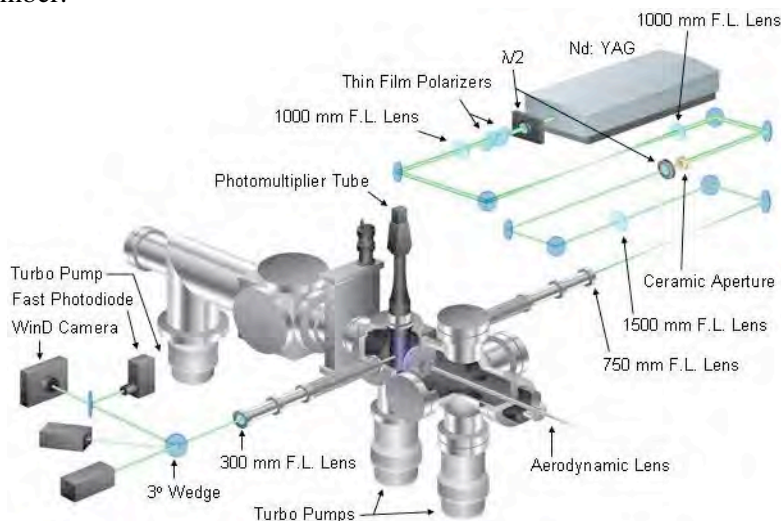


Figure 1. Schematic diagram of the experimental setup.

Detailed characterization of aerodynamic-lens-system design has generally been limited to studies of spherical particles. Soot particles have a non-spherical branched-chain morphology, which may be significantly more susceptible than spherical particles to perturbations from Brownian motion and aerodynamic-lift forces during expansion, and thus may not focus as well as spherical particles^{3,4,7-12}. Such effects have been demonstrated experimentally for non-spherical salt particles^{4,8,9,11,12}, but studies on soot particles are limited^{12,13}.

We have compared soot-focusing characteristics of three similar aerodynamic-lens systems in common use³⁻⁵. We compared a three-element system (McMurry D configuration⁴) with two five-element systems (McMurry E configuration⁴ and Aerodyne configuration⁵). We extracted soot from a co-flow ethylene diffusion flame, focused it using these aerodynamic-lens systems, and measured the associated divergence angles. We used light-scattering techniques to image the particle beams onto a CCD camera in order to infer divergence angles and transmission electron microscopy (TEM) images to characterize the particles focused in the beams.

Figure 2 shows a TEM image of a typical particle sampled in the particle beam down stream of the exit nozzle. Dimensions are shown on the left and top axes. The particle demonstrates morphology characteristic of mature soot particles generated in a flame. Primary particles in the size range of 20-40 nm are covalently bound to form an aggregate with a geometric mean diameter of ~180 nm. A large number of these particles have been collected and individually analyzed to produce a statistical sample of the particles that form the particle beam. An example of the size distribution derived from this analysis is shown in Fig. 3. A lognormal fit to this distribution (also shown in this figure) yields a mean diameter of 66.27 ± 1.73 nm. This sample was collected on the outer edges of the particle beam where the particles tend to be smaller and less well focused. Particles collected near the center of the beam tend to be more similar in size to the particle shown in Fig. 2.

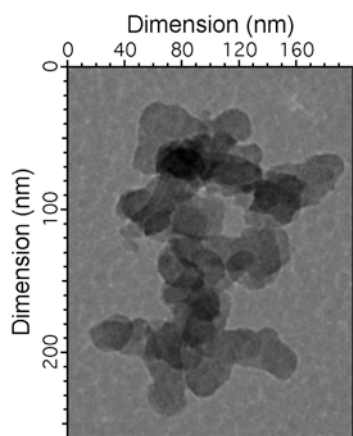


Figure 2. Transmission electron microscopy (TEM) image of a soot particle at the detection region following the aerodynamic-lens system.

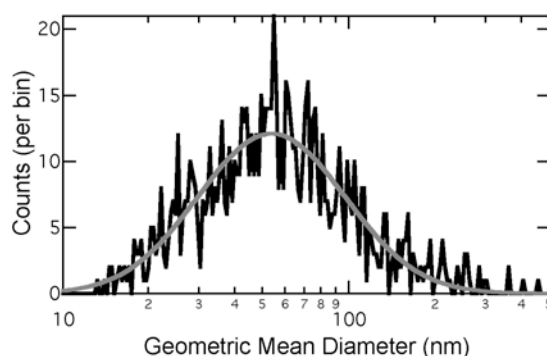


Figure 3. Particle size distribution of the particle beam after exiting the aerodynamic-lens system. The size distribution was derived from TEM images (black line). The distribution is well fit by a lognormal function (gray line), which yields a mean diameter of 66.27 ± 1.73 nm and a full width at half max of 80 nm.

Figure 4 shows a compilation of the scattering images for the particle beam produced by the Aerodyne configuration⁵ in the lower panel and an analysis of the beam radius as a function of distance from the exit nozzle in the upper panel. For the Aerodyne configuration⁵ these results yield a divergence angle of 3.25 mrad, solid angle of 3.31×10^{-5} sr, and an inferred radius at the exit nozzle of 0.256 mm. These results are similar to those of the McMurry D configuration⁴ (3.12 mrad, 3.07×10^{-5} sr, 0.230 mm) and E configuration⁴ (3.37 mrad, 3.58×10^{-5} sr, 0.196 mm). Our beam divergences are larger than those of Slowik et al.¹³ who measured a solid angle of 9.2×10^{-6} sr for flame generated soot using the Aerodyne configuration. The differences between their results and ours may be explained by the differences in size distributions. Slowik et al.¹³ size selected their particles to have a mean mobility diameter of 350 nm. Because their particle distribution was narrower and larger on average, the expected solid angle of the focused beam is smaller.

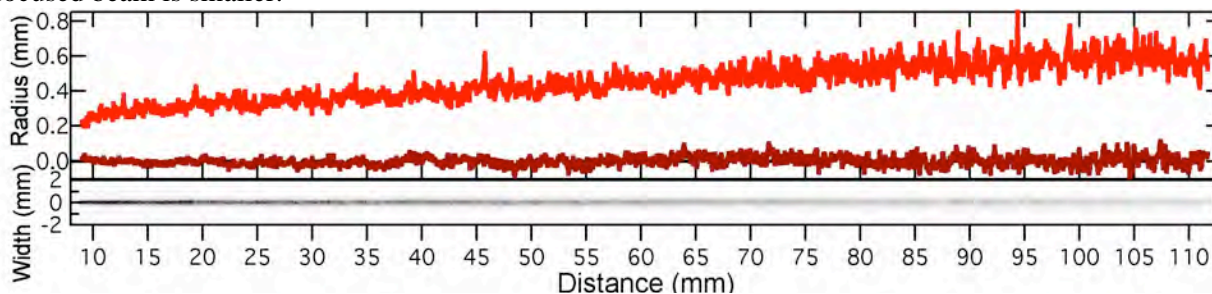


Figure 4. Particle beam (top) radius and (bottom) image as a function of distance from the exit nozzle for the Aerodyne configuration

III. Future Work

Current work builds on these results and extends them to combustion-generated particles with inorganic and organic coatings representative of particles found in exhaust plumes. In order to simulate exhaust-plume particulates, we have modified our flow-tube system to allow controlled deposition of a coating with low volatility on flame-generated soot. The thickness of the coating can be varied, and the particles collected for analysis by TEM or analyzed in situ with an aerosol mass spectrometer that is under construction. Coatings investigated to date have been selected for diagnostic development for diesel exhaust and include sulfuric acid, heptamethylnonane, and oleic acid. These experiments are currently limited by our inability to determine the mass loading of particle coatings. Developing an understanding of the cause and magnitude of the effects of coatings will require characterization of the particle coatings. Coating the particles increases the mean aggregate size as measured by a scanning mobility particle sizer (SMPS), but measurements of mobility diameter provided by the SMPS do not provide a quantitative measure of the volatile coating fraction either by volume or by mass. In order to measure the volatile fraction, we will build a chamber that includes a temperature-controlled oscillating crystal microbalance for differential mass measurements on coated and evaporatively dried particles.

We are also working on a SISGR project led by Prof. Angela Viola to develop a validated predictive multiscale model to describe the chemical composition of soot nanoparticles in premixed and diffusion flames. This project closely couples experimental investigations of soot precursors and incipient particle characteristics with the development of a predictive model for the chemical composition of soot nanoparticles. The co-investigators on the project are Profs. Angela Violi (University of Michigan) and Bernhard Schlegel (Wayne State University) for model development and Drs. Hope Michelsen (Sandia), Nils Hansen (Sandia), and Kevin Wilson (LBNL ALS) for experimental investigations.

Experimental and modeling studies are being carried out for several low- and atmospheric pressure flames fueled by acetylene, ethylene, and propane. A new counter-flow burner and sampling probe has been designed and built for this project. Polycyclic aromatic hydrocarbons (PAHs) and small soot particles are extracted from the counter-flow flames via a microprobe. The flames vary from lean to rich conditions in order to cover a wide range of practical conditions. The composition of incipient particles is measured using the aerosol mass spectrometer developed by Kevin Wilson and coworkers at the ALS. The corresponding particle size distributions are measured using an SMPS. Angela Violi and coworkers use the experimental results in the development and validation of a predictive multiscale soot model.

IV. References

1. Kittelson, D. B. *J. Aerosol Sci.* **1998**, *29*, 575.
2. Lighty, J. S.; Veranth, J. M.; Sarofim, A. F. *J. Air Waste Management Assoc.* **2000**, *50*, 1565.
3. Liu, P.; Ziemann, P. J.; Kittelson, D. B.; McMurry, P. H. *Aerosol Sci. Technol.* **1995**, *22*, 293.
4. Liu, P.; Ziemann, P. J.; Kittelson, D. B.; McMurry, P. H. *Aerosol Sci. Technol.* **1995**, *22*, 314.
5. Zhang, X.; Smith, K. A.; Worsnop, D. R.; Jimenez, J.-L.; Jayne, J. T.; Kolb, C. E.; Morris, J.; Davidovits, P. *Aerosol Sci. Technol.* **2004**, *38*, 619.
6. Vidal-de-Miguel, G.; Fernandez de la Mora, J. *Aerosol Sci. Technol.* **2012**, *46*, 287.
7. Dahneke, B. E.; Cheng, Y. S. *J. Aerosol Sci.* **1979**, *10*, 257.
8. Schreiner, J.; Voigt, C.; Mauersberger, K.; McMurry, P. H.; Ziemann, P. *J. Aerosol Sci. Technol.* **1998**, *29*.
9. Jayne, J. T.; Leard, D. C.; Zhang, X.; Davidovits, P.; Smith, K. A.; Kolb, C. E.; Worsnop, D. R. *Aerosol Sci. Technol.* **2000**, *33*, 49.
10. Kane, D. B.; Johnston, M. V. *Environ. Sci. Technol.* **2000**, *34*, 4887.
11. Kane, D. B.; Oktem, B.; Johnston, M. V. *Aerosol Sci. Technol.* **2001**, *34*, 520.
12. Huffman, J. A.; Jayne, J. T.; Drewnick, F.; Aiken, A. C.; Onasch, T. B.; Worsnop, D. R.; Jimenez, J. L. *Aerosol Sci. Technol.* **2005**, *39*, 1143.
13. Slowik, J. G.; Stainken, K.; Davidovits, P.; Williams, L. R.; Jayne, J. T.; Kolb, C. E.; Worsnop, D. R.; Rudich, Y.; DeCarlo, P. F.; Jimenez, J.-L. *Aerosol Sci. Technol.* **2004**, *38*, 1206.

V. Publications and submitted journal articles supported by this project 2010-2012

1. S. A. Skeen, B. Yang, H. A. Michelsen, J. A. Miller, A. Violi, and N. Hansen, "Studies of laminar opposed-flow diffusion flames of acetylene at low pressures with photoionization mass spectrometry", *Thirty fourth International Symposium on Combustion*, (Warsaw, Poland, July 29-August 3, 2012) in press.
2. H. A. Michelsen, P. E. Schrader, and F. Goulay, Erratum to "Wavelength and temperature dependences of the absorption and scattering cross sections of soot" [*Carbon* 48 (2010) 2175-2191], *Carbon* **50**, 740 (2011).
3. J. M. Headrick, F. Goulay, P. E. Schrader, and H. A. Michelsen, "High-vacuum time-resolved laser-induced incandescence of flame-generated soot", *Appl. Phys. B* **104**, 439-450 (2011).
4. H. A. Michelsen, P. E. Schrader, and F. Goulay, "Wavelength and temperature dependences of the absorption and scattering cross sections of soot", *Carbon* **48**, 2175-2191 (2010).
5. F. Goulay, P. E. Schrader, and H. A. Michelsen, "Effect of the wavelength dependence of the emissivity on inferred soot temperatures measured by spectrally resolved laser-induced incandescence", *Appl. Phys. B* **100**, 655-663 (2010).
6. F. Goulay, L. Nemes, P. E. Schrader, and H. A. Michelsen, "Spontaneous emission from $C_2(d^3\Pi_g)$ and $C_3(A^1\Pi_u)$ during laser irradiation of soot particles", *Mol. Phys.* **108**, 1013-1025 (2010).

Detection and Characterization of Free Radicals Relevant to Combustion Processes

Terry A. Miller

Laser Spectroscopy Facility, Department of Chemistry

The Ohio State University, Columbus OH 43210, email: tamiller@chemistry.ohio-state.edu

1 Program Scope

Combustion processes have been studied for many years, but the chemistry is very complex and yet to be fully understood. Moreover new fuels have introduced modifications to traditional mechanisms. Modern computer codes for modeling typically employ hundreds of reaction steps with a comparable number of chemical intermediates. The predictions of such models are obviously limited by the dynamical and mechanistic data that are input. Spectroscopic identifications and diagnostics for the chemical intermediates in the reaction mechanisms constitute an important experimental benchmark for the models, as well as providing molecular parameters that are “gold standards” against which quantum chemistry computations of molecular properties may be judged. Our recent work has emphasized the spectroscopy of reactive organic peroxy radicals which are known to be key intermediates in combustion reactions.

2 Recent Progress

Our earlier cavity ringdown spectroscopic (CRDS) studies mainly involved the $\tilde{A} - \tilde{X}$ absorptions of simple alkyl peroxy radicals. Recent studies have included unsaturated and hydroxy-substituted peroxies and reactive intermediates produced from the peroxies in subsequent steps of combustion mechanisms. We have reported the $\tilde{A} - \tilde{X}$ absorption spectra of the β -hydroxy ethyl peroxy (β -HEP) radical and most recently we have observed the corresponding spectrum of β -hydroxy propyl peroxy (β -HPP) radical. These species are important intermediates in the oxidation of biofuels like ethanol and propanol. They also represent model systems for the OH-initiated oxidation of atmospherically important olefins, such as ethylene, isoprene, and terpenes.

In combustion mechanisms, not only are alkyl peroxy radicals, ROO \cdot , important, but also their peroxide isomers, \cdot QOOH (Q=R less one H), in which a H atom bonded to carbon has transferred to the OO moiety. An analogous reaction is possible with the hydroxy substituted alkyl peroxy radicals, HOR'OO \cdot , isomerizing to the alkoxy peroxides, \cdot Q'OOH (Q'=OR'), by H-atom transfer from OH to OO.

Below we describe our recently completed analysis of the CRDS spectrum of β -HPP. We then discuss spectral observations closely connected to the photo-activation of the HOR'OO $\cdot \rightarrow \cdot$ Q'OOH isomerization process. Finally we discuss recent results from our dual wavelength (2 λ -CRDS) spectrometer that suggest it could be used to measure radical-radical reaction kinetics.

2.1 The $\tilde{A} - \tilde{X}$ Electronic Spectroscopy of β -HPP

The HPP radical can exist in several isomeric forms, α (1,1- or 2,2-HPP) or β (2,1- or 1,2- HPP). These forms and the reactions leading to them are shown in Fig. 1. Two separate routes are indicated: Cl atom attack on 2-propanol and photolysis of iodohydrin. The α -HPP isomers generally decompose under our ambient conditions to form HO $_2$. Its well-known $\tilde{A} - \tilde{X}$ spectrum is readily detected by our CRDS apparatus creating an interference to the spectrum of β -HPP, which is also produced by Cl atom attack. Therefore photolysis of iodohydrin is the preferred method for producing the radical, with Cl atom attack providing an independent way to produce β -HPP and verify the carrier of the observed spectrum. While photolysis is the cleaner production method, it requires the

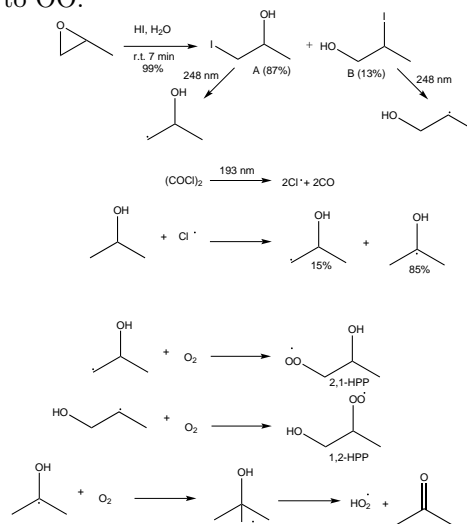


Figure 1: Reaction scheme for producing β -HPP radicals including synthesis of two isomers (A, B) of iodohydrin. The last reaction shows production and destruction of 2,2-HPP; the reaction for 1,1-HPP is equivalent.

are present. There may also be a shift in the OH overtone line which could be attributable to the absorption of the $\cdot\text{QOOH}$ species. However at present the shift is comparable to experimental error and further work is necessary to establish a spectral observation of $\cdot\text{QOOH}$.

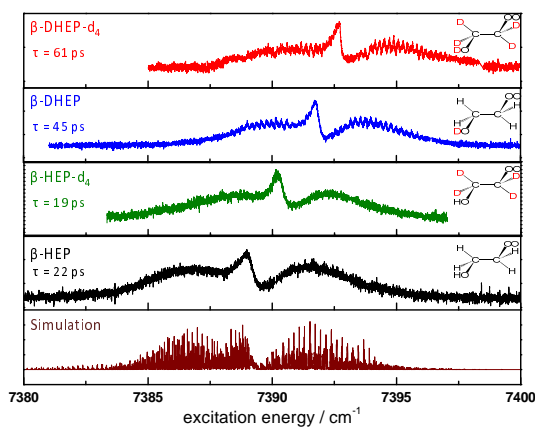


Figure 4: Experimental $\tilde{A} - \tilde{X}$ spectra of β -HEP isotopologues, demonstrating the differently resolved rotational contours. The β -HEP simulation assumes instrumental resolution of 200 MHz.

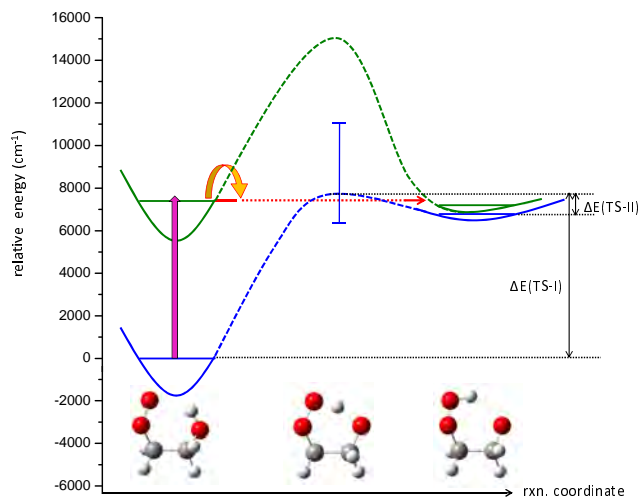


Figure 5: A qualitative diagram describing the isomerization of β -HEP on the \tilde{X} state PES, the $\Delta E(\text{TS-I})$ and $\Delta E(\text{TS-II})$ denote the energy differences between the transition state and reactant and product respectively.

2.2 Absolute Concentrations and Reaction Kinetics via CRDS Spectroscopy

Last year we reported experiments on ethyl peroxy using our dual wavelength (2λ -CRDS) spectrometer which obtained the peak absorption cross-section, σ_p , for its G conformer and from that the magnitude of the transition dipole moment, $|\mu^G|$. Using this information, we have performed initial experiments designed to enable the measurement of peroxy radical-radical reaction kinetics with a modification of our 2λ -CRDS spectrometer.

The $\tilde{A} \leftarrow \tilde{X}$ absorption spectra of peroxy radicals offers two significant advantages for following their chemistry compared to the traditionally used $\tilde{B} \leftarrow \tilde{X}$ transition. First, despite its weakness, the $\tilde{A} - \tilde{X}$ transition can be successfully observed and quantified by means of CRDS spectroscopy which allows for accurate measurement of species concentrations, given a known absorption cross-section, σ_p . Second, due to the relatively sharp structure of the transition, one can measure uniquely concentrations of different chemical species and their isomers and conformers, even when several members of the same chemical family are present.

To monitor concentrations as a function of time and hence the kinetic decay of the reactive species we have modified our 2λ -CRDS apparatus to perform time-resolved spectroscopy using a CW laser. A schematic diagram of the apparatus is shown in Fig. 6. The radiation of a CW external cavity diode laser (ECDL) passes through an optical isolator (OI), acousto-optical modulator (AOM) operating as a switch, and is mode-matched to the CRDS cavity. The frequency of the ECDL is periodically scanned over a single cavity resonance coinciding with an absorption peak of the radical of interest at a repetition rate of ≈ 2 kHz (limited by mechanical properties of the laser). The laser frequency matches the resonance of the cavity twice a period, resulting in observation of a ring-down curve every $\approx 250 \mu\text{s}$. The feedback circuit dynamically “locks” the laser frequency to the cavity mode by compensating for the effects of slow drift of the cavity length or laser frequency. The use of a high repetition rate sweep of the CW laser has two major advantages. It allows the monitoring of the complete time evolution of a given set of radicals following production. It also has a duty factor of the order of unity, allowing fast data acquisition.

The reaction of interest is initiated with the production of a reactive species by an excimer laser photolysis pulse. A sequence of ring-down curves of duration $\approx 200 \mu\text{sec}$ are recorded over a time period of 40-70 msec, from prior to the excimer firing to a time when the reaction has effectively gone to completion. An example of such data is given in Fig. 7. Panel (a) shows the photodetector output for 40 ms, which contains about 140 individual ring-down curves. The vertical red arrow indicates the time of the photolysis laser pulse. The absorption $A(t)$ is

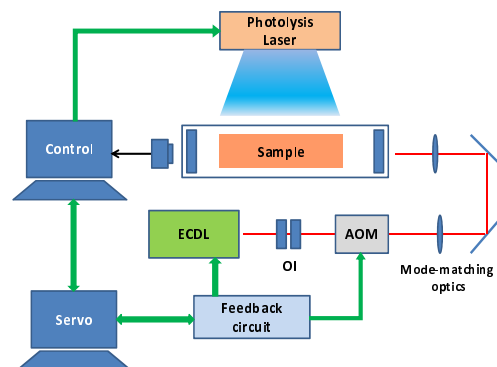


Figure 6: Schematic design of the CW arm of the 2λ -CRDS spectrometer. See text for details.

calculated from the fit time constants of each ringdown curve (see panel (b)) and converted with the known σ_p to a concentration which is plotted vs time in panel (c). Preliminary values for the rate constant for the ethoxy peroxy self-reaction are consistent with previous results but hold the promise of being considerably more precise.

3 Future Directions

Efforts will continue to obtain the spectra of, and thereby provide diagnostics for, other important reactive intermediates in combustion chemistry. One of our first targets will be the 1,2 β -HPP as this isomer is preferentially produced by OH attack on propene. We plan to investigate the hydroxy peroxy derivatives of other key dienes, e.g. butadiene and isoprene, as all these species are particularly important in tropospheric chemistry.

An area of interest closely related to the peroxy radicals is their peroxide isomers, $\cdot\text{QOOH}$ or $\cdot\text{Q}'\text{OOH}$. These radicals play critically important roles for chain branching in low temperature combustion. In terms of detection the alkoxy functionality, $\text{RO}\cdot$, provides a much more favorable spectroscopic chromophore than does $\text{Q}\cdot$. Efforts to observe directly either or both species are on-going.

The initial radical-radical kinetic measurements with our 2 λ -CRDS apparatus modified with a CW laser on one arm are quite encouraging. Since the ethoxy self-reaction was chosen for initial experiments, there was no need for any measurement with the second arm. For reactions between two different peroxy radicals, the concentrations of both species need to be determined simultaneously. This requirement can easily be met with a laser in the second arm tuned to the separate resonance frequency of the second radical. A pulsed laser suffices for the required initial concentration measurement, but if the entire time-dependent decay curve of the second radical is needed, it can be acquired by using another CW laser in the second arm. Work will continue to improve the apparatus and commence kinetic measurements of reactions between disparate radicals.

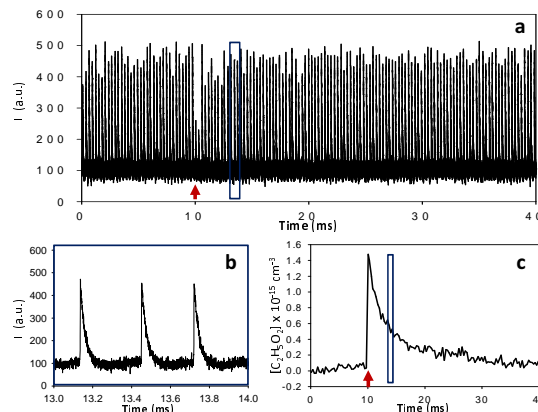


Figure 7: An example of the experimental data for kinetic measurements obtained with the CW-2 λ -CRDS spectrometer. Panel (a) shows the light intensity, $I(t)$, measured by the photodiode in Fig. 6. Panel (b) show an expanded view of the portion of panel (a) outlined with a blue rectangle, containing three individual ring-down curves. The decay time of each ring-down is used to calculate the absorption $A(t)$ and corresponding concentration, which is shown in panel (c). The vertical red arrow indicates the firing of the photolysis laser.

Publications Supported by DOE (2010-2012)

- [1] "The $\tilde{A} - \tilde{X}$ Absorption of Vinyloxy Radical Revisited: Normal and Herzberg-Teller Bands Observed Via Cavity Ringdown Spectroscopy," P. S. Thomas, R. Chhantyal-Pun, N. D. Kline, and T. A. Miller, *J. Chem. Phys.* **132**, 114302 (2010).
- [2] "Cavity Ringdown Spectroscopy of the NIR $\tilde{A} - \tilde{X}$ Electronic Transition of Allyl Peroxy Radical ($\text{H}_2\text{C}=\text{CH}-\text{CH}_2\text{OO}\cdot$)," P. S. Thomas and T. A. Miller, *Chem. Phys. Lett.* **491**, 123 (2010).
- [3] "Observation of the $\tilde{A} - \tilde{X}$ Electronic Transition of the β -Hydroxyethylperoxy Radical," R. Chhantyal-Pun, N. D. Kline, P. S. Thomas, and T. A. Miller, *J. Phys. Chem. Lett.* **1**, 1846 (2010).
- [4] "Measurement of the Absolute Absorption Cross Sections of the $\tilde{A} \leftarrow \tilde{X}$ Transition in Organic Peroxy Radicals by Dual Wavelength Cavity-Ringdown Spectroscopy," D. Melnik, R. Chhantyal-Pun, and T. A. Miller, *J. Phys. Chem. A* **114**, 11583 (2010).
- [5] "Cavity Ringdown Spectroscopy of Peroxy Radicals: The $\tilde{A} - \tilde{X}$ Absorption of Propargyl Peroxy ($\text{H}-\text{C}=\text{C}-\text{CH}_2\text{OO}\cdot$)," P. S. Thomas, N. D. Kline, and T. A. Miller, *J. Phys. Chem. A* **114**, 12437 (2010).
- [6] "The $\tilde{A} - \tilde{X}$ Absorption of Cyclopentadienyl Peroxy Radical ($c\text{-C}_5\text{H}_5\text{OO}\cdot$): A Cavity Ringdown Spectroscopic and Computational Study," P. S. Thomas and T. A. Miller, *Chem. Phys. Letts.* **514**, 196 (2011).
- [7] "The Electronic Transition Moment for the 0_0^0 Band of the $\tilde{A} - \tilde{X}$ Transition in the Ethyl Peroxy Radical," D. Melnik, P. S. Thomas, and T. A. Miller, *J. Phys. Chem. A* **115**, 13931 (2011).
- [8] "Spectroscopic Studies of the $\tilde{A} - \tilde{X}$ Electronic Spectrum of the β -Hydroxyethylperoxy Radical: Structure and Dynamics," M.-W. Chen, G. M. P. Just, T. Codd, and T. A. Miller, *J. Chem. Phys.* **135**, 184304 (2011).
- [9] "Analysis of the $\tilde{A} - \tilde{X}$ Electronic Transition of the 2,1-Hydroxypropylperoxy Radical Using Cavity Ringdown Spectroscopy," N. D. Kline and T. A. Miller, *Chem. Phys. Letts.* **530**, 16 (2012).

Reaction Dynamics in Polyatomic Molecular Systems

William H. Miller

Department of Chemistry, University of California, and
Chemical Sciences Division, Lawrence Berkeley National Laboratory
Berkeley, California 94720-1460
millerwh@berkeley.edu

I. Program Scope or Definition

The goal of this program is the development of theoretical methods and models for describing the dynamics of chemical reactions, with specific interest for application to polyatomic molecular systems of special interest and relevance. There is interest in developing the most rigorous possible theoretical approaches and also in more approximate treatments that are more readily applicable to complex systems.

II. Recent Progress

Research efforts are being focused on the problem of how to add quantum mechanical effects to the classical molecular dynamics (MD) simulations that are now so ubiquitously applied to all types of dynamical processes in complex molecular systems, e.g., chemical reactions in clusters, nano-structures, molecules on or in solids, bio-molecular systems, etc. Semiclassical (SC) theory — since it is based on the classical trajectories of the molecular system — is a natural way to approach the problem, and one knows from much work¹ in the early 1970's that SC theory describes *all* quantum effects in molecular dynamics at least qualitatively, and typically quite quantitatively; the primary challenge is thus to develop methods for implementing it for large molecular systems. In this regard, the 'initial value representation'² (IVR) of SC theory has emerged as the most useful starting point since it replaces the non-linear boundary value problem of earlier SC approaches by a Monte Carlo average over the initial conditions of classical trajectories, a procedure more amenable to systems with many degrees of freedom.³

Since quantum effects in transitions between different electronic states can obviously be very significant, one of the most important applications of the SC-IVR approach is to such non-adiabatic processes. This is made possible by the model of electronic states introduced by Meyer and Miller⁴ (MM) [which Stock and Thoss⁵ (ST) later showed to be an *exact representation*] whereby each electronic state becomes a classical degree of freedom (a harmonic oscillator). This allows both nuclear and electronic degrees of freedom to be treated by SC-IVR methods in a unified and completely consistent fashion. A variety of applications of this approach have demonstrated its usefulness.⁶⁻⁸ One particularly interesting aspect is that even though the classical trajectories that are determined by the MMST vibronic Hamiltonian are 'Ehrenfest trajectories', they emerge (correctly) on one potential energy surface (PES) or another, unlike the traditional Ehrenfest model itself which has them emerging on an average PES. This comes about because of coherence effects that are contained in the SC description.⁷

An even more ambitious classical model for electronic degrees of freedom was introduced later by Miller and White⁹ (MW): here the creation/annihilation operators for each single-particle state in the second-quantized many-electron Hamiltonian operator,

$$\hat{H}_{el} = \sum_{ij} \langle i | j \rangle a_i^\dagger a_j + \frac{1}{2} \sum_{ijkl} \langle ij | kl \rangle a_i^\dagger a_j^\dagger a_l a_k , \quad (1)$$

are replaced by functions of classical action-angle variables (n_i, q_i). Since the 1- and 2-electron matrix elements are functions of the nuclear coordinates \mathbf{R} of the molecular system, the resulting classical electronic Hamiltonian is also a function of nuclear coordinates, and the complete classical vibronic Hamiltonian is obtained by adding the nuclear kinetic energy to it,

$$H(\mathbf{P}, \mathbf{R}, \mathbf{n}, \mathbf{q}) = \sum_k \frac{\mathbf{P}_k^2}{2m_k} H_{el}(\mathbf{n}, \mathbf{q}; \mathbf{R}) , \quad (2)$$

where \mathbf{P}_k are the nuclear momenta and $\{m_k\}$ their corresponding masses.

This ‘classical second-quantized’ electronic Hamiltonian (with no nuclear degrees of freedom) has recently been applied the resonant level (Landauer) model as a simple example of quantum transport.¹⁰ It consists of a single quantum dot state coupled to two electrodes (left and right) according to the electronic Hamiltonian

$$\hat{H} = \varepsilon_0 \hat{a}_0^\dagger \hat{a}_0 + \sum_{k=1}^N \varepsilon_k \hat{a}_k^\dagger \hat{a}_k + \sum_{k=1}^N t_k (\hat{a}_0^\dagger \hat{a}_k + \hat{a}_k^\dagger \hat{a}_0) , \quad (3)$$

where ε_0 is the energy of the isolated quantum dot (which is used to model a gate voltage), ε_k is the energy of level k of the electrode, and t_k the coupling between the dot and electrode mode k ; the classical electronic Hamiltonian corresponding to this is

$$H(n, q) = \varepsilon_0 n_0 + \sum_{k=1}^N \varepsilon_k n_k + \sum_{k=1}^N t_k \sqrt{n_0 - n_0^2 + \frac{1}{2}} \\ \times \sqrt{n_k - n_k^2 + \frac{1}{2}} \cos(q_0 - q_k) . \quad (4)$$

In this initial application the calculations were carried out at the primitive ‘quasi-classical’ level, i.e., purely classically. The correct quantum initial conditions are thus imposed by setting the initial action variable n_i to be 0 or 1 such that its expectation value, $\langle n_i \rangle$, averaged over the set of initial conditions, satisfies the Fermi distribution

$$f(\varepsilon_i - \mu_i) = (1 + e^{\beta(\varepsilon_i - \mu_i)})^{-1} , \quad (5)$$

where μ_i is the chemical potential of the lead in which mode i is located and $\beta = 1/T$ is the inverse temperature. (The angle variable q_i is selected at random between 0 and 2π .)

Figure 1 shows some sample results, displaying extremely close agreement with the correct quantum results. Similarly good agreement has been found for various values of the other parameters (different values of the gate voltage, the chemical potentials of the leads, and the different temperatures).

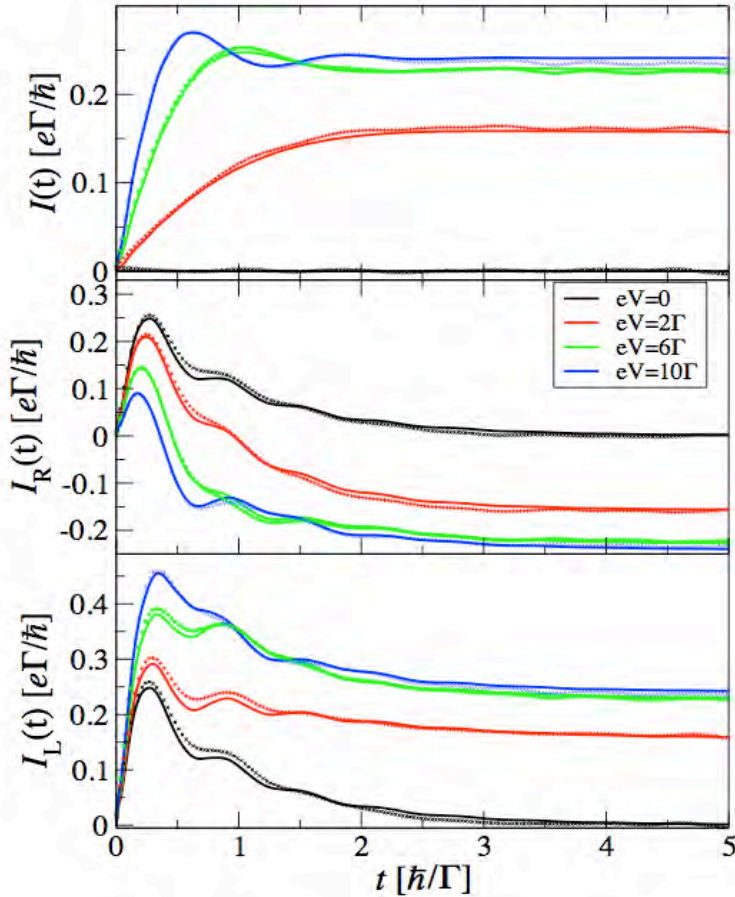


Figure 1. Plots of the left (lower panel), right (middle panel), and total (upper panel) transient current for different values of the source-drain voltage $eV = \mu_L - \mu_R$. Other model parameters are: $T = \Gamma/3$, $\epsilon_0 = 0$, and $N_L = N_R = 400$. Solid line and symbols correspond to exact quantum mechanical and semiclassical results, respectively.

III. Future Plans

Though the initial application of this ‘classical second-quantized’ electronic Hamiltonian are very encouraging, it is important to apply it to more general electronic models to see how well it can describe the effects of electron correlation. One such effect is ‘coulomb blockade’, and it will be interesting to see if this classical model can describe it well.

There are also various ways of building in the proper antisymmetry structure of the fermionic operators. MW gave one way to do this, but there are others that are being considered. It will be interesting to see if one particular approach emerges as the most useful.

References

1. For reviews, see W. H. Miller, *Adv. Chem. Phys.* **25**, 69-177 (1974); **30**, 77-136 (1975).
2. W. H. Miller, *J. Chem. Phys.* **53**, 1949-1959 (1970).
3. For reviews, see (a) W. H. Miller, *J. Phys. Chem. A* **105**, 2942-2955 (2001); (b) W. H. Miller, *Proceedings of the National Academy of Sciences*, **102**, 6660-6664 (2005); (c) W. H. Miller, *J. Chem. Phys.* **125**, 132305.1-8 (2006).
4. H. D. Meyer and W. H. Miller, *J. Chem. Phys.* **71**, 2156-2169 (1979).
5. G. Stock and M. Thoss, *Phys. Rev. Lett.* **78**, 578-581 (1997).
6. G. Stock and M. Thoss, *Adv. Chem. Phys.* **134**, 243 (2005).
7. W. H. Miller, *J. Phys. Chem.* **113**, 1405-1415 (2009).
8. D. F. Coker and L. Xiao, *J. Chem. Phys.* **102**, 496-510 (1995).
9. W. H. Miller and K. A. White, *J. Chem. Phys.* **84**, 5059-5066 (1986).
10. See DOE Publication 7 below.

IV. 2010 - 2012 (to date) DOE Publications

1. G. Tao and W. H. Miller, Semiclassical description of electronic excitation population transfer in a model photosynthetic system, *J. Phys. Chem. Lett.* **1**, 891-894 (2010).
2. A. L. Kaledin, C. W. McCurdy, W. H. Miller, A semiclassical correction for quantum mechanical energy levels, *J. Chem. Phys.* **133**, 054101.1-6 (2010).
3. D. Lambrecht, K. Brandhorst, W. H. Miller, C. W. McCurdy, and M. Head-Gordon, A kinetic energy fitting metric for resolution of the identity second-order Möller-Plesset perturbation theory, *J. Phys. Chem. A* **115**, 2794-2801 (2011).
4. J. Liu and W. H. Miller, An approach for generating trajectory-based dynamics which conserves the canonical distribution in the phase space formulation of quantum mechanics. I. Theories, *J. Chem. Phys.* **134**, 104101.1-14 (2011).
5. J. Liu and W. H. Miller, An approach for generating trajectory-based dynamics which conserves the canonical distribution in the phase space formulation of quantum mechanics. II. Thermal Correlation Functions, *J. Chem. Phys.* **134**, 104102.1-19 (2011).
6. J. Liu, Two more approaches for generating trajectory-based dynamics which conserves the canonical distribution in the phase space formulation of quantum mechanics, *J. Chem. Phys.* **134**, 194110.1-9 (2011).
7. D. W. H. Swenson, T. Levy, G. Cohen, E. Rabani and W. H. Miller, Application of a semiclassical model for the second-quantized many-electron Hamiltonian to nonequilibrium quantum transport: The resonant level model, *J. Chem. Phys.* **134**, 164103.1-8 (2011).
8. G. Tao and W. H. Miller, Time-dependent importance sampling in semiclassical initial value representation calculations for time correlation functions, *J. Chem. Phys.* **135**, 024104.1-9 (2011).
9. J. Liu, B. J. Alder and W. H. Miller, A semiclassical study of the thermal conductivity of low temperature liquids, *J. Chem. Phys.* **135**, 114105.1-10 (2011).
10. J. Liu, W. H. Miller, G. S. Fanourgakia, S. S. Xanthas, I. Sho, and S. Saito, Insights in quantum dynamical effects in the infrared spectroscopy of liquid water from a semiclassical study with an ab initio-based force field, *J. Chem. Phys.* **135**, 244503.1-14 (2011).

Dynamics of Activated Molecules

Amy S. Mullin

Department of Chemistry and Biochemistry, University of Maryland

College Park, MD 20742

mullin@umd.edu

I. Program Scope

The focus of my research program is to investigate collisional energy transfer of molecules with large amounts of internal energy. Collisional energy transfer is ubiquitous in gas-phase chemistry and can have important effects on overall reaction rates and branching ratios. However there are substantial challenges to making detailed experimental measurements of molecular energy transfer at energies that are relevant to chemistry under combustion conditions. High energy molecules contain extremely large densities of states, are of transient nature and have poorly understood interactions with other molecules. Currently, there are no first-principle theories of collisional energy transfer and the lack of fundamental knowledge often results in cursory and insufficient treatments in reactive models. A goal of my research is to gain new insights into the microscopic details of relatively large complex molecules at high energy as they undergo quenching collisions and redistribute their energy.

We use state-resolved transient IR absorption to characterize the energy transfer pathways that are responsible for the collisional cooling of high energy molecules. To overcome the inherent difficulties in developing a molecular level understanding of collisions involving high energy molecules, we use high-resolution IR probing to measure population changes in small collision partners that undergo collisions with the high energy molecules. Using this technique, we have performed in-depth spectroscopic studies that provide a greater understanding of high energy molecules and their collisional energy transfer. In the past five years we have developed the means to measure the full range of rotational states of the scattered molecules and their velocity distributions. This type of data is combined with rate constant measurements to reveal the mechanisms of the important energy flow pathways.

A number of our studies have identified the dynamics associated with “weak” and “strong” collisions that relax high energy molecules. The terms “weak” and “strong” are qualitative descriptors that refer to collisions leading to small- ΔE and large- ΔE energy transfer, based historically on Hirschelwood’s strong collision assumption. Strong collisions account for approximately 10% of all collisions and have been studied using transient IR probing for a number of years. The dynamics associated with “strong” collisions of high energy molecules with small bath molecules such as DCl and CO₂ involve scattered molecules with large energy gains in both rotation and translation. We understand these results in terms of impulsive collisions that may or may not involve chattering multi-encounter collisions. The other 90% of collisions are “weak” collisions that impart little or no rotational energy to the energy-accepting molecule and include elastic collisions. The “weak” collisions result in only modest translational energy in the scattered molecules.

The ability to measure the full distribution of scattered molecules allows us to ask even more fundamental questions about the underlying molecular features that are responsible for the observed energy transfer behavior. One such question is how the rotational energy structure of the energy-accepting bath molecule affects the energy exchange dynamics in collisions of highly excited molecules. To answer this question, we have measured energy gain profiles for HCl following collisions of pyrazine (C₄H₄N₂, $E_{\text{vib}}=38000 \text{ cm}^{-1}$). We compare our results to previously reported studies on the dynamics of DCl collisions with pyrazine. These experiments are expected to provide information about the importance of energy gaps and angular momentum gaps in collisional energy transfer, as well as establishing important benchmarks for the development of new models that account for energy partitioning in molecular collisions.

II. Recent Progress

A. Construction of a mid-IR OPO based transient absorption spectrometer

Initially we used a mid-IR diode laser based transient absorption spectrometer to measure the energy gain profiles for HCl from collisions with pyrazine (E_{vib}). The fundamental vibrational transition of HCl is at $\lambda=3.4 \mu\text{m}$, which lies at the blue edge of the output range for lead-salt diode lasers. In this wavelength region, the diode laser output is quite unstable, both in terms of intensity and optical frequency. While we were able to measure transient absorption features (including Doppler-broadened line profiles) using the diode laser, the low signal to noise levels severely limited our ability to quantify the dynamics. To overcome this problem, we built a new transient absorption spectrometer based on a mid-IR optical parametric oscillator (OPO) that provides high resolution (0.0001 cm^{-1}) and intense (up to 1W) tunable IR light with $\lambda=2.5\text{-}3.9 \mu\text{m}$.

A comparison of results for HCl-pyrazine(E_{vib}) collisions collected with the OPO and with the diode laser is presented here. Fig.1 shows transient absorption for HCl($v=0, J=7$) collected at a total pressure of 10 mTorr (the time between collisions is $\sim 6 \mu\text{s}$), with a S/N improvement close to 250 for the OPO-based instrument. Transient Doppler-broadened line profiles for pure appearance of high- J rotational states (as for $J=7$ of HCl in Fig. 2) also have improved S/N.

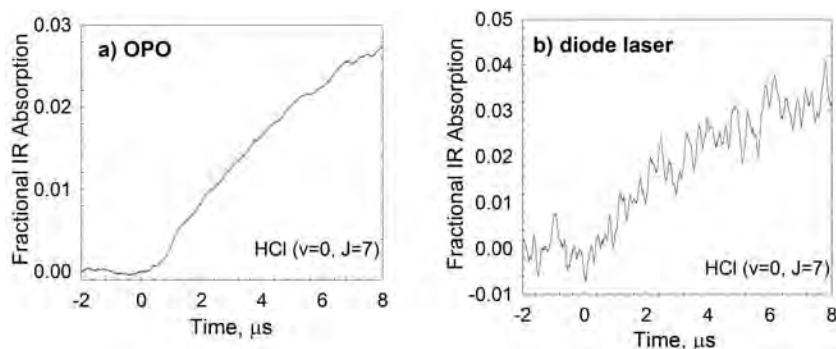


Fig. 1. Transient IR absorption signals for HCl ($v=0, J=7$) following collisions with pyrazine (E_{vib}) collected with a) the new OPO-based spectrometer and b) our previous diode laser-based instrument.

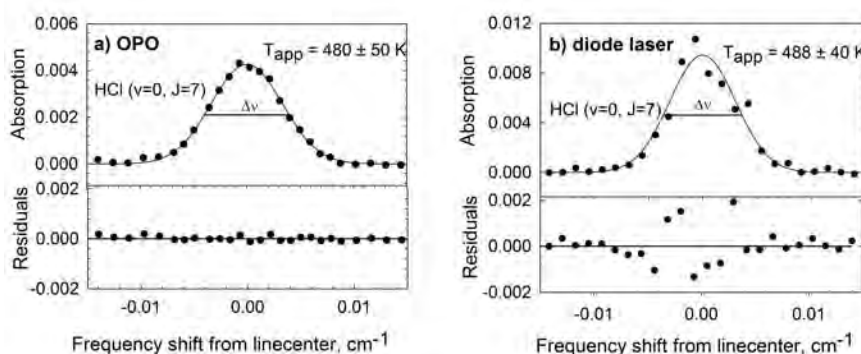


Fig. 2. Doppler-broadened transient line profiles for HCl ($v=0, J=7$) collected $1 \mu\text{s}$ following collisions with pyrazine (E_{vib}) collected with a) the new OPO-based spectrometer and b) our previous diode laser-based instrument.

The improved signal levels with the OPO system make it possible to discern concurrent depletion of initial thermal population (at line center) from the appearance of scattered molecules (in the wings of the Doppler- profile). This level of instrumental sensitivity is required to measure the outcome of small ΔE_{rot}

collisions. Fig. 3 shows the transient Doppler-broadened line profile for HCl $J=4$. No clear appearance signals could be seen previously with the diode laser spectrometer.

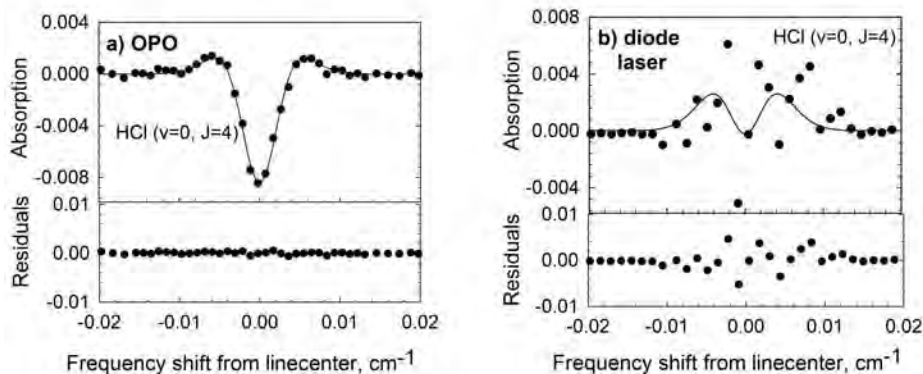


Fig. 3. Doppler-broadened transient line profiles for HCl ($v=0$, $J=4$) collected $1 \mu\text{s}$ following collisions with pyrazine (E_{vib}) collected with a) the new OPO-based spectrometer and b) our previous diode laser-based instrument. A double Gaussian fit to the OPO data characterizes scattering into the $J=4$ state due to collisions, while the diode laser data has large scatter.

B. Energy gain profiles of scattered HCl ($v=0$, J)

We have made substantial progress in characterizing the nascent rotational and translational energy profiles for the $J=2$ -13 states of HCl following collisions with pyrazine (E_{vib}). Fig. 4 shows the scattered HCl molecules are rotationally hot (with $T_{\text{rot}} = 937 \pm 95 \text{ K}$). This result is very similar to results for DCI collisions (where we found that $T_{\text{rot}} = 880 \pm 90 \text{ K}$). In collisions of both HCl and DCI with pyrazine (E_{vib}), a similar amount of rotational energy is gained by the energy-acceptor. This result indicates that the difference in the rotational state density of the HCl and DCI does not impact the rotational energy gain. This is likely due to the large available energy in pyrazine (E_{vib}). It may be that energy gain differences are observed at lower internal energies of pyrazine.

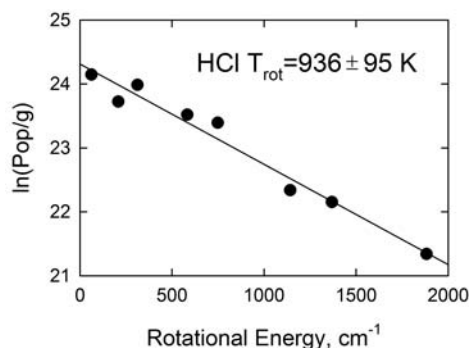


Fig. 4. Nascent rotational distribution of HCl at $1 \mu\text{s}$ following collisions with pyrazine (E_{vib}).

We have also measured the J -dependent translational energy distributions for HCl/pyrazine(E_{vib}) collisions. The results are shown in Fig. 5 for appearance of scattered molecules and depletion of the initial HCl states that are thermally populated at 300 K. The depletion measurements show initial temperatures of 230-250 K, indicating that slightly cooler than ambient molecules are favored in the energy transfer. Similar behavior was seen previously for DCI/pyrazine collisions. Appearance line widths show that the scattered molecules have translational energy that is greater than the pre-collision value for all HCl J -states observed, indicating that rotational and translational energy are coupled in the relaxation mechanism for pyrazine (E_{vib}) and HCl. However, for HCl collisions, the translational energy

of the scattered molecules is *inversely* related to the final HCl rotational state. The opposite behavior was observed for DCI collisions. The HCl and DCI results are compared in Fig. 5. The DCI behavior was understood in terms of strong impulsive collisions that imparted both rotation and translational energy. The HCl results indicate a different mechanism wherein the HCl energy gain is primarily either rotational or translational, not both concurrently. This result is highly unusual given that every other collision system of this type studied to date shows either J-independent recoil velocities (H₂O and HOD) or recoil velocities that increase with increasing rotation (DCI and CO₂). The previous observations are consistent with an impulsive collision mechanism involving either very light molecules (H₂O and HOD with small moments of inertia) or heavier molecules (DCI and CO₂). We are currently developing a microscopic picture to explain the HCl results.

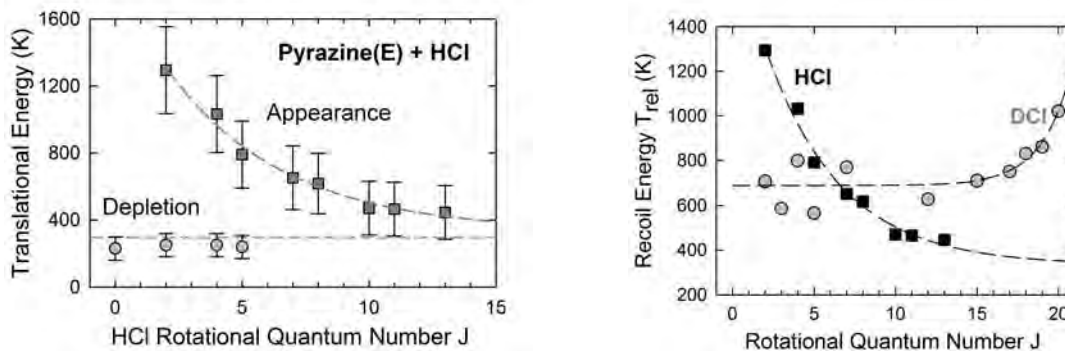


Fig. 5. Nascent translational energies for collisions of pyrazine (E_{vib}) with HCl (left) and compared to DCI (right).

III. Future Work

We will continue our studies on the energy transfer dynamics of highly excited molecules in collisions with HCl. We also plan new studies that will address how internal energy content in high energy molecules affects their collision rates. We have seen that collision rates of water and HOD with high energy molecules are as large as 3 times larger than Lennard-Jones collision rates. In the case of water collisions, it is likely that strong hydrogen bonding is a major factor for the enhanced collision rates. For CO₂ collisions, it is not clear whether the donor energy content enhances the collision rate or whether the Lennard-Jones model is in error by a factor of two. We plan to investigate this issue by measuring full energy transfer distributions for additional donor molecules with a wide range of internal energies.

IV. Publications supported by this project 2010-2012

1. D. K. Havey, J. Du and A. S. Mullin, Full state-resolved energy gain profiles of CO₂ (J=2-80) from collisions with highly vibrationally excited molecules. I. Relaxation of pyrazine ($E=37900\text{ cm}^{-1}$)” J. Phys. Chem. A **114**, 1569-80 (2010)
2. J. Du, N. A. Sassin, D. K. Havey, K. Hsu and A. S. Mullin, “Full energy gain profiles of CO₂ from collisions with highly vibrationally excited molecules. II. Energy dependent pyrazine ($E=32700$ and 37900 cm^{-1}) relaxation” in preparation.
3. J. Du, D. K. Havey, S. W. Teitelbaum and A. S. Mullin, “Full energy gain profiles of CO₂ from collisions with highly vibrationally excited molecules. III. 2-Methylpyridine, 2,6-dimethylpyridine and 3,5-dimethylpyridine ($E\sim 38500\text{ cm}^{-1}$) relaxation” in preparation.
4. G. Echibiri, M. Smarte, W. Walters and A. S. Mullin, “Using a frequency stabilized CW mid-IR OPO for high resolution transient IR absorption spectroscopy” submission in May 2012 for Optics Express.
5. G. Echibiri, M. Smarte, W. Walters, J. Cleveland and A. S. Mullin, “Unusual isotope effects in collisions of pyrazine(E_{vib}) + HCl and DCI: Evidence of strong interactions”, in preparation for a Letter in the Journal of Physical Chemistry.

Reacting Flow Modeling with Detailed Chemical Kinetics

Habib N. Najm

Sandia National Laboratories
P.O. Box 969, MS 9051, Livermore, CA 94551
hnnajm@sandia.gov

I. Program Scope

The goal of this research program is to improve our fundamental understanding of reacting flow, thereby advancing the state of the art in predictive modeling of combustion. The work involves: (1) Using computations to investigate the structure and dynamics of flames using detailed chemical kinetics; (2) Developing techniques for analysis of multidimensional reacting flow; (3) Developing numerical methods for the efficient solution of reacting flow systems of equations with detailed kinetics and transport; (4) Developing massively parallel codes for computing large scale reacting flow with detailed kinetics; and (5) Developing numerical methods for uncertainty quantification in reacting flow computations, including methods for the construction of uncertain chemical models from experimental data.

II. Recent Progress

A. Reacting Flow Computations, Analysis, and Model Reduction

We continued our work on studying the detailed structure of n-heptane/air edge flames in 2D rectangular geometry. Additional computations were carried out exploring the effect of increasing the equivalence ratio in the fuel stream. With highly rich fuel-stream, we observed the transition to a flame structure more closely resembling a pure diffusion flame in terms of heat-release rate structure and species profiles. A change in propagation speed of the edge flame was observed consistent with theoretical predictions in the literature. Moreover, employing Computational Singular Perturbation (CSP) analysis, important reaction pathways were studied over a range of equivalence ratio variation.

We also continued working on validating our axisymmetric low-Mach number reacting flow solver. The method of manufactured solutions was employed, allowing the comparison of the output of the flow solver with analytic (manufactured) solutions to verify the solver and establish its convergence rate. Expected second order convergence rate with respect to the analytical solution was demonstrated. We used the axisymmetric solver to compute a lifted methane/air jet flame. The jet configuration was chosen according to prior work in the literature for which results of computations and experimental data are available. After further validating our results, this configuration will be used for time-dependent forced flame studies. Our computation was performed on a 3.2 cm by 6.4 cm domain using the detailed gri3.0 reaction mechanism.

We also used the axisymmetric code to compute a low-pressure nonpremixed methane/oxygen jet flame with helium dilution. This computation is a collaboration with J. Frank to assist in the analysis of experimental X-ray spectra of such a flame obtained at the Advanced Light Source of Lawrence Berkeley National Laboratory. Despite the large thickness of this low pressure flame, its particular composition with helium dilution is, in fact, numerically challenging in the context of low Mach number reacting flow (ρu)-projection algorithms. This is primarily because of the large density ratio across the flame. Stable computations were feasible, albeit only with very small time-steps, $\mathcal{O}(10)$ ns. We plan to explore this issue in the context of u -projection schemes in future work. (with J. Frank)

We continued our work on the CSP analysis of explosive modes for the ignition of n-heptane, iso-octane, and toluene air mixtures. Explosive modes are found in chemical systems undergoing ignition processes and can be analyzed with respect to time scales and contributing chemical reactions. We studied pure n-heptane, iso-octane, and toluene ignition at elevated pressures as well as a mixture of n-heptane and iso-octane. In all cases, explosive modes during the individual ignition stages could be identified and specific reactions participating in the explosive behavior were found. A distinct difference in the mechanism leading to the first and second ignition stages can be seen. The explosive mode structure was similar for the pure fuels as for the fuel mixtures. (with W. Pitz)

B. Uncertainty Quantification in Reacting Flow

We had previously developed a “Data Free Inference” (DFI) approach for reconstructing the joint PDF on model parameters given partial information on these parameters, in the absence of the raw data from which this summary information was derived. We had also begun to apply this method in the context of a simple chemical system with a single irreversible global reaction step. The algorithm employs a nested pair of Markov Chain Monte Carlo (MCMC) chains with the objective of exploring a large number of hypothetical data sets that are *consistent* with the given information. The outer chain provides a random walk on the data space, where every step is a proposed data set. The inner chain employs MCMC to discover the posterior density on the model parameters given each proposed data set, to be used in the consistency check in the outer chain. The posteriors from all explored consistent data sets are subsequently averaged/pooled to provide a consensus posterior. The geometry of the problem in the data space allows for the utilization of independently parallel outer chains, greatly reducing computational wall clock time. We recently explored the convergence of the algorithm as a function of the number of data sets, more specifically the number of outer chains. We find statistical convergence in the Kullbeck-Leibler divergence between pooled posteriors, as the number of data sets is increased. This is important, as there is no expectation of good mixing in the outer MCMC, but rather the goal is to provide sufficient coverage of the data space. Further, it is curious that, while the nominal and quantile parameter statistics exhibit observable variability among data sets, as per the chosen acceptance criteria, the correlation structure is quite stable, exhibiting very small variability. This suggests that this structure is inherently constrained by the fit and/or noise model structure.

Quantum mechanical methods are an important tool for obtaining kinetic information of elementary chemical reactions. So far, validation of these methods has always involved the comparison of obtained rate coefficients with experimental data. To be predictive, the uncertainty in the results of these methods has to be examined. We started a collaboration with J. Zádor using Bayesian methods to study the uncertainties involved in rate coefficients obtained from transition-state theory. We studied the hydrogen abstraction from iso-propanol by OH, an important reaction of the ignition chemistry of this alcohol. We found the main parameters causing the uncertainty of rate coefficients in this case, studied the variance of these parameters resulting from different methods of quantum-chemical calculations, and obtained an estimate of overall uncertainty of the resulting rate coefficients. (with J. Zádor)

With the current trend toward developing increasingly large reaction mechanisms for modeling the combustion of application-relevant fuels, the need for *efficient* uncertainty quantification (UQ) methods becomes significant. These chemical models include hundreds of species and thousands of reactions. Most of the reaction rates were not measured and modelers have to rely on rate rules to build their reaction mechanisms. By using rate rules, the kinetic parameters of a certain reaction are derived from those of a similar but previously measured reaction. This procedure introduces correlations between the kinetic parameters in a model which should be considered in UQ analysis. These correlations are generally important to account for from an accuracy perspective, given the rate-rules defining interdependence of rate constants. They also are of key importance in decreasing the number of degrees of freedom in the uncertain input space, particularly in the limit of large mechanisms where the curse of dimensionality is in full force. We started studying the effect of these correlations in the case of the ignition of a propane/ethane air mixture using only one rate rule for the hydrogen abstraction from propane and ethane by OH. Consistent with our previous experience with simpler chemical models, we observed bimodal probability density function (PDF) structures for state variables such as temperature or species concentration, during the fast ignition transient. We found an effect of the correlation on the PDF of ignition delay time, whose amplitude depends on the degree of uncertainty in the rate parameters. (with W. Pitz)

We also worked on CSP analysis of uncertain ODE systems, with an eye towards the use of such dynamical analysis for chemical model reduction under uncertainty. In a context with relatively small uncertainty, we found that the underlying nominal slow manifold formed a good approximation of the stochastic eigenvectors. In this context, the slow/fast subspaces corresponding to this manifold provided a useful eigenbasis for CSP-based model reduction. We are exploring the large-uncertainty limit in other work, and expect to apply it in the context of CSP-based chemical model reduction in future work.

One of the challenges with UQ in reacting flow is related to the transient time dynamics of both flow and chemical features. For example, in ignition, the uncertainty in ignition time leads to a range of state-variable time-profiles whose representation using polynomial chaos (PC), or any other functional, expansions can be quite challenging, requiring high order. We have explored the utility of preconditioning in this context, employing random time shifts that are adapted to the uncertain solution structure. We have shown that this preconditioning can have a significant effect in reducing the challenges with representation of the uncertain solution, allowing the

use of low-order expansions. This finding, in a zero-dimensional spatial context, will need to be appropriately extended to the partial differential equation context, allowing appropriate preconditioning of multidimensional flame solutions, to be of more general benefit in reacting flow computations under uncertainty.

III. Future Plans

A. Reacting Flow Computations, Analysis, and Model Reduction

We now have two mature reacting flow codes for low Mach number reacting flow in 2D, an axisymmetric fixed uniform-mesh second-order code, and a rectangular-geometry high-order adaptive mesh refinement (AMR) code. Both approaches will be further honed going forward in time. We are interested in moving towards 4th order spatial order for the axisymmetric formulation. Further, the AMR code is being used, in the context of an ongoing collaboration, by a PhD student at MIT for his thesis research on reacting flow. This application in a new setting is driving us towards yet more flexibility in code structure and use.

We have started computations of an axisymmetric n-heptane jet flame, using a simplified 66-species n-heptane model developed using CSP analysis. The degree of stiffness, and associated computational challenges, with the detailed n-heptane model leads to significant time-step limitations, even with optimized operator-split explicit-implicit time integration strategies. The present simplified mechanism computations will form the starting point for subsequent use of the more detailed n-heptane models in this flame.

We will continue to work on the general area of chemical model reduction. Our hitherto model reduction relying on CSP/dynamical-analysis pursues a simplified mechanism that inherently captures the correct dynamical structure of the detailed starting mechanism. It does this using a database of flame or ignition solutions, and ensures that species/reactions that have dominant importance in decoupled fast/slow subspaces, over the union of states in the database, are retained in the simplified mechanism. This strategy works well, delivering a spectrum of simplified mechanisms depending on specified importance index thresholds. However, recent preliminary studies indicate that, at least from an error-analysis perspective relative to the detailed mechanism, the CSP-simplified mechanism is not *optimal*. In other words, for a specification of a requisite simplified mechanism with N -species, one can find an alternate N -species-mechanism with error lower than that corresponding to the N -species-mechanism discovered with our present analysis. The question then, is whether the present strategy can be altered towards more optimal performance. Specifically, it is of interest to explore L1-constrained optimization strategies in the present context, with application to a dynamical-analysis context for model reduction. The application of L1-constraints in optimization is effectively done using compressive sensing (CS) methods. CS methods have been used in L2-error minimization with L1-constraints, arriving at optimal models of a given requisite sparsity (*i.e.* chosen N -value in the present context). The question of interest is whether this formalism can be extended to a CSP/dynamical-analysis context for chemical model reduction.

B. Uncertainty Quantification in Reacting Flow

We will continue to explore the utility of DFI in chemical kinetic models for flames. We plan to move beyond the present demonstration in a single-step global mechanism towards a detailed chemical kinetic model with reversible elementary step reactions. Our first foray in this direction will be in the context of a hydrogen mechanism. We will apply DFI to each reaction, discovering inherent correlations in its parameters. We will also apply it towards discovery of correlations among parameters of different reactions where associated experiments dictate such dependences. Further, it is of interest to demonstrate DFI in other contexts, e.g. where different types of information, beside nominals/marginal-bounds is known from published literature. This includes, the handling of conditional bounds, as well as dealing with general error-bar specifications in processed data products.

From another perspective, the forward propagation of uncertainty in chemical models is strongly challenged by the curse of dimensionality. The forward UQ problem, relying on practical non-intrusive Galerkin PC methods, is essentially an integration problem. Thus, with N -uncertain parameters, and $N \gg 1$, the forward UQ challenge is one of evaluating high-dimensional integrals. Despite the availability of generalized sparse quadrature methods, it is imperative that dimensionality is reduced for practical UQ in chemical/reacting-flow models. Sensitivity analysis (SA) can be used to eliminate reactions/parameters that have little impact on a given quantity of interest. However, allowing for large uncertainty means that *global* SA methods are needed, and these offer the same degree of difficulty as forward UQ methods. In other words, to properly estimate global sensitivities over the

range of variation of each parameter, full coverage of the N -dimensional space is needed. In this context, we will explore the utility of Bayesian compressive sensing (BCS) methods for discovering a sparse surrogate for a chemical model observable over the range of uncertain parameters. This approach proposes a PC-surrogate over the space of interest, and then, using a set of incoherent samples of the detailed model response, discovers a sparse PC-surrogate employing L1-constrained optimization via the use of Laplace priors and an iterative algorithm that pursues evidence maximization. We have explored the use of these methods in other contexts for discovering accurate sparse PC surrogates, and plan to extend them to chemical models.

Finally, model reduction under uncertainty remains a matter of significant interest. We have several of the necessary pieces in hand at this time. We have reduction strategies for deterministic models that rely on eigen-analysis of the system Jacobian. We have demonstrated eigen-analysis of uncertain/stochastic Jacobians using Galerkin PC methods. We have also explored the use of CSP in uncertain ODE systems, and the evaluation of stochastic importance indices. Accordingly, we are ready to apply CSP methods for model reduction under large uncertainty. We plan to work towards this goal. It is particularly of interest to evaluate the quality of different reduced models in a Bayesian/information-theoretic context given the underlying uncertainties in the detailed model. Further, it should be clear that uncertainty in the detailed model should inform the choice of meaningful error thresholds to be imposed on the simplified models. These and other trade-offs/considerations, will be of interest going forward in this context.

IV. BES-Supported Published/In-Press Publications [2010-2012]

- [1] Prager, J., Najm, H.N., and Zádor, J., Uncertainty Quantification in the *ab initio* Rate-Coefficient Calculation for the $\text{CH}_3\text{CH}(\text{OH})\text{CH}_3 + \text{OH} \rightarrow \text{CH}_3\text{C}^*(\text{OH})\text{CH}_3 + \text{H}_2\text{O}$ Reaction, *Proc. Comb. Inst.* (2012) in press.
- [2] Prager, J., Najm, H.N., Valorani, M., and Goussis, D., Structure of n-Heptane/Air Triple Flames in Partially-Premixed Mixing Layers, *Combustion and Flame*, 158:2128–2144 (2012).
- [3] Debusschere, B.J., Marzouk, Y.M., Najm, H.N., Rhoads, B., Goussis, D.A., and Valorani, M., Computational Singular Perturbation with Non-Parametric Tabulation of Slow Manifolds for Time Integration of Stiff Chemical Kinetics, *Combustion Theory and Modelling*, 16(1):173–198 (2012).
- [4] Berry, R.D., Najm, H.N., Debusschere, B.J., Adalsteinsson, H., and Marzouk, Y.M., Data-free inference of the joint distribution of uncertain model parameters, *Journal of Computational Physics*, 231:2180–2198 (2012).
- [5] Alexanderian, A., Maître, O.P. Le, Najm, H.N., Iskandarani, M., and Knio, O.M., Multiscale stochastic preconditioners in non-intrusive spectral projection, *J. Sci. Comp.*, 50:306–340 (2012).
- [6] Salloum, M., Alexanderian, A., Maître, O.P. Le, Najm, H.N., and Knio, O.M., Simplified CSP Analysis of a Stiff Stochastic ODE System, *Computer Methods in Applied Mechanics and Engineering*, 217-220:121–138 (2012).
- [7] Sunday, B.E., Berry, R.D., Najm, H.N., and Debusschere, B.J., Eigenvalues of the Jacobian of a Galerkin-Projected Uncertain ODE System, *SIAM J. Sci. Comp.*, 33:1212–1233 (2011).
- [8] Najm, H.N., Uncertainty Quantification in Fluid Flow, in *Turbulent Combustion Modeling: Advances, New Trends and Perspectives* (T. Echehki and N. Mastorakos, Eds.), Springer-Verlag, Berlin, 2011, , pp. 381–407.
- [9] Ray, J., Armstrong, R., Safta, C., Debusschere, B.J., Allan, B.A., and Najm, H.N., Computational frameworks for advanced combustion simulations, in *Turbulent Combustion Modeling: Advances, New Trends and Perspectives* (T. Echehki and N. Mastorakos, Eds.), Springer-Verlag, Berlin, 2011, , pp. 409–437.
- [10] Najm, H.N., Valorani, M., Goussis, D.A., and Prager, J., Analysis of Methane-Air Edge Flame Structure, *Combustion Theory and Modelling*, 14(2):257–294 (2010).
- [11] Safta, C., Ray, J., and Najm, H.N., A High-Order Low-Mach Number AMR Construction for Chemically Reacting Flows, *J. Comput. Phys.*, 229(24):9299–9322 (2010).

Spectroscopy, Kinetics and Dynamics of Combustion Radicals

David J. Nesbitt

*JILA, University of Colorado and National Institute of Standards and Technology, and
Department of Chemistry and Biochemistry, University of Colorado, Boulder, Colorado*

Spectroscopy, kinetics and dynamics of jet cooled hydrocarbon transients relevant to the DOE combustion mission have been explored, exploiting i) high resolution IR lasers, ii) slit discharge sources for formation of jet cooled radicals, and iii) high sensitivity detection with direct laser absorption methods and near the quantum shot noise limit. What makes this combination powerful is that such transients can be made under high concentrations and pressures characteristic of actual combustion conditions, and yet with the resulting species rapidly cooled ($T \approx 10\text{-}15\text{K}$) in the slit supersonic expansion. Combined with the power of IR laser absorption methods, this provides novel access to spectral detection and study of many critical combustion species. Highlights from work over the last year are summarized below.

1. High Resolution IR Spectroscopy of Open Shell Aromatics: Phenyl Radical

We have quite recently redoubled our efforts in exploring IR spectroscopy of jet cooled phenyl radical (C_6H_5) in the CH stretching region, building on and extending our earlier efforts¹ with considerably improved S/N. Phenyl is a highly reactive 6-membered organic hydrocarbon ring intermediate formed from homolytic cleavage of a CH bond in benzene. By virtue of its overall reactivity, this radical plays a central role in combustion, especially for fossil fuels typically rich in aromatics. It is the classic prototype of an open shell aromatic species, achieving partial stabilization of the radical due to resonance structures arising from electron delocalization around the ring. This radical stabilization

also makes it a prime target intermediate for ring formation in complex combustion processes, which identifies phenyl as a crucial species in mediating the early stages of soot formation. Fig. 1 shows a rotationally resolved spectrum of the in-phase asymmetric CH stretch band in phenyl radical obtained with significantly improved S/N, one of 3 bands currently being explored with sufficient IR intensity to observe and analyze. Rigorous assignment of these spectra has been confirmed via precision 2-line ground state combination differences from radio frequency spectroscopy of Thaddeus and coworkers.² It is worth stressing that the ability to obtain rovibrationally resolved spectra for such a large but fundamental aromatic species represents a critical milestone for spectroscopic study, detection and analysis of even more complex aromatic combustion radical intermediates implicated in the soot formation process.

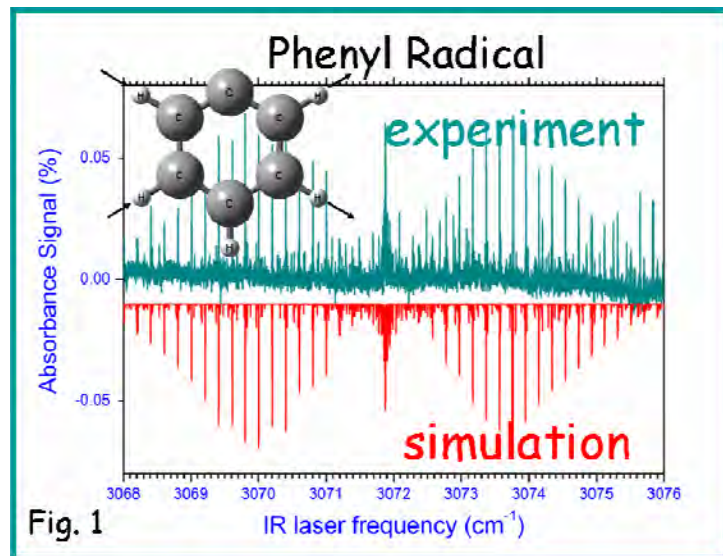


Fig. 1

2. Non-Born Oppenheimer Rovibronic Dynamics in Ethynyl (C_2H) Radical

Ethynyl radical (C_2H) is a particularly important reactive intermediate in combustion as well as interstellar chemistry, specifically postulated to play a role in polycyclic aromatic hydrocarbons (PAHs) and the path toward soot formation. What makes C_2H particularly interesting is the presence of low lying electronically excited states, in which the quantum states due to vibrations of the C_2H framework are imbedded and can lead to anomalously strong vibronic mixing dynamics. In order to explore these non-adiabatic effects, we have undertaken a spectroscopic reinvestigation of C_2H under sub-Doppler conditions of the slit jet apparatus.^{3,4} Of particular dynamical interest is vibronic coupling between the electronically excited $\tilde{A}^2\Pi$ state and highly excited vibrational states in the ground state of this radical, which is responsible for the rich complexity observed in the near IR spectrum. To

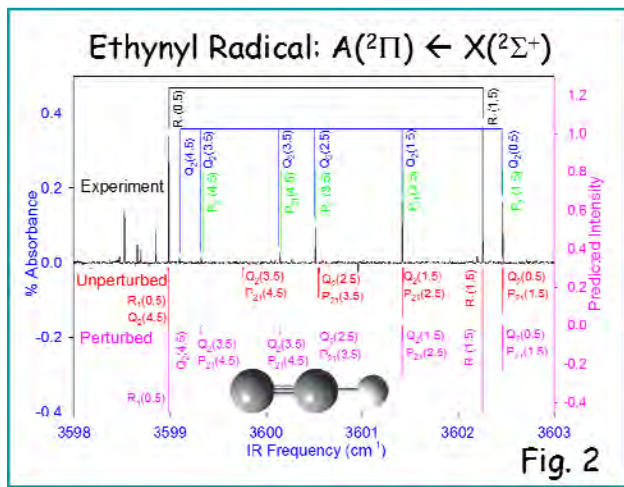


Fig. 2

explore this further, a high resolution infrared spectrum of the origin band region near 3600 cm^{-1} of jet-cooled ethynyl radical (C_2H) has been obtained and analyzed in detail (Fig. 2), which exhibits a strong, parity specific rotational crossing in the excited spin orbit $F_2^2\Pi_{1/2}$ state. By incorporating this Σ - Π Coriolis coupling into the unperturbed Hamiltonian model (containing only rotational, spin-rotational, spin-orbit, and lambda-doubling contributions), we are able to fit the observed $^2\Pi$ - $^2\Sigma^+$ origin band to a standard deviation of 15 MHz, i.e., essentially the experimental limit. By virtue of the high frequency precision, these data permitted a direct determination of the band origin (ν_{pert}) and rotational constant (B_{pert}) for the perturbing “dark” $^2\Sigma^+$ state. Furthermore, since the vibrational density of states is still relatively modest in C_2H at 3600 cm^{-1} , we have successfully identified the dark state by comparison with high quality predictions of Tarroni and Carter. Indeed, the results unambiguously indicate the source of strong vibronic coupling arising from a fortuitous near resonant “avoided crossing” between the $F_2^2\Pi_{1/2}$ state and the high overtone $^2\Sigma^+$ ($0,8^0,0$) state with 8 quanta of CH bending excitation. By way of further confirmation, the rotational constants observed from this high resolution analysis are in excellent agreement with the UV dispersed fluorescence studies of Hsu *et al.*⁵

3. Ab Initio Rovibrational Dynamics of $H_2 + H_2O$

A first principles description of combustion processes requires a detailed understanding of state-to-state collisional energy transfer dynamics, which in turn requires high quality multidimensional intra/intermolecular potential energy surfaces for reactants and products, benchmarked against high quality experimental data. Toward this end, we have explored $H_2 + H_2O$ interactions by a synergistic combination of i) *ab initio* calculations, ii) exact multidimensional quantum dynamics and iii) high

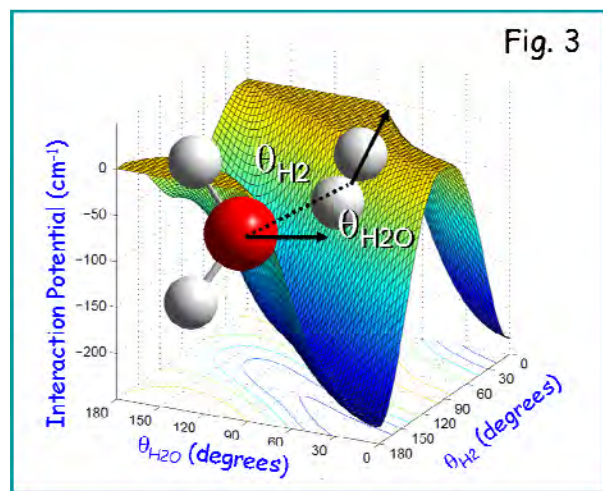


Fig. 3

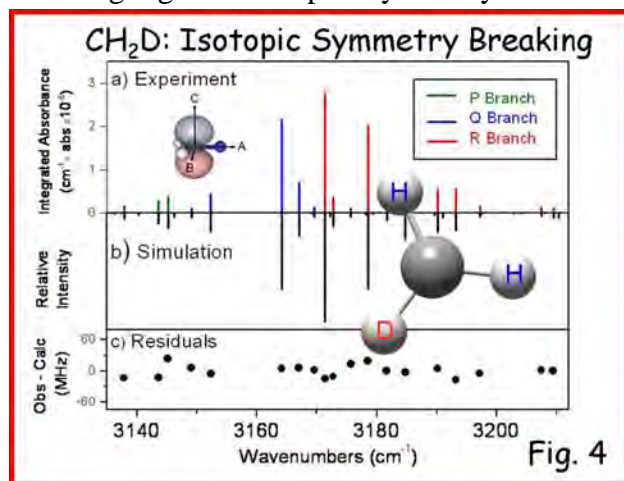
resolution spectroscopy of the corresponding $\text{H}_2\text{-H}_2\text{O}$ and $\text{D}_2\text{-H}_2\text{O}$ complexes.^{6,7} Specifically, jet cooled $\text{H}_2\text{O-H}_2$ and $\text{H}_2\text{O-D}_2$ complexes are formed by pulsed supersonic expansion through a slit valve and detected via direct absorption of high resolution IR light in the 6.2 μm region corresponding to ν_2 bending of the H_2O chromophore. High resolution rotational structure for each of the $\text{H}_2\text{O-H}_2$ and $\text{H}_2\text{O-D}_2$ complexes is observed, which can be unambiguously assigned to progressions in the $K_a = 0 \leftarrow 0$ and $1 \leftarrow 1$ manifolds arising from i) overall rotation and ii) large amplitude internal rotor motion in the complex. From a theoretical perspective, a 5D intermolecular potential is obtained (a 2D slice of which is shown in Fig. 3) from a state-of-the-art 9 D *ab initio* potential energy surface (PES) by averaging over the ground state vibrational wave functions of H_2O and H_2/D_2 . On this PES, we calculate the bound rovibrational levels for total angular momentum $J = 0\text{-}3$, based on a coupled free rotor basis for the hindered internal rotations (with permutation/inversion symmetry associated with the para/ortho (p/o) nature of both H_2O and H_2/D_2), and a discrete variable representation (DVR) in the intermolecular distance R . Agreement between experiment and theory is quantitative ($< 0.1\%$ in B_{rot}), providing an extremely successful test of the $\text{H}_2 + \text{H}_2\text{O}$ potential energy surface from a rigorous, first principles perspective.

4. Isotopic Symmetry Breaking in the C-H Stretching Manifold of Methyl Radical

Methyl (CH_3) represents a critical radical species in the combustion of hydrocarbon fuels, which provides motivation for a detailed understanding of its molecular properties. To address these issues, we have obtained⁸ first high resolution sub-Doppler IR spectra of CH_2D radical in both the symmetric/antisymmetric C-H stretching regions. Isotopic “symmetry

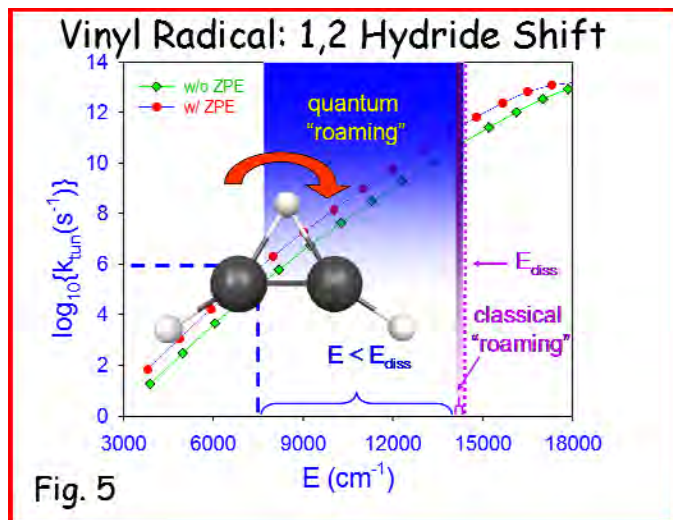
breaking” in the CH_2D radical by partial H/D substitution has been exploited to localize CD vs. CH vibrational motion, lower the point group symmetry from D_{3h} to C_{2v} , and thereby permit investigation of unimolecular vibrational coupling dynamics in unprecedented detail. At our resolution, the spectral structure is rovibrationally fully resolved and can be fit to a Watson asymmetric top Hamiltonian to yield rotational/centrifugal constants and vibrational band origins. An asymmetric top stick spectrum for the observed rotational lines of CH_2D is shown in Fig. 4 along with residuals from a least squares fit simulation. However, in

addition, the transverse velocity distribution along the laser probe direction is collisionally quenched in the slit jet expansion, thus yielding complete sub-Doppler resolution of spin-rotation structure and even partial resolution of nuclear hyperfine structure for each rovibrational line. Global least-squares fits to the line shapes provide additional information on spin-rotation and nuclear hyperfine constants, which both complement and clarify previous FTIR studies of CH_2D in the out of plane bending region. We have successfully exploited a harmonically coupled Morse oscillator model Hamiltonian for systematic analysis over the entire isotopomeric $\text{CH}_m\text{D}_{3-m}$ series, which now provides a remarkably quantitative framework for predicting in-plane stretching dynamics in this fundamental combustion radical.



5. Quantum “Roaming” and 1,2 H atom Shift Dynamics in Vinyl Radical

The vinyl radical C_2H_3 is a critically important species in combustion and hydrocarbon plasma chemistry. A particularly interesting dynamical is the presence of multiple first order saddle points, the lowest of which is a planar Y-shaped structure of C_{2v} symmetry, however, there is also a 1,2 hydride shift pathway at much higher energies (i.e., $18,000\text{ cm}^{-1}$). What makes these higher isomerization barriers particularly intriguing is that quantum tunneling can occur despite the fact that the classical 1,2, shift barrier is above the homolytic limit for CH bond cleavage. To address this issue, we have calculated splittings associated with large amplitude 1,2 H-atom migration for vinyl radical via two completely independent approaches, i) full-D *ab initio* potential energy surface (CCSD(T)/aug-cc-pVTZ) and ii) “intrinsic reaction paths” (CCSD(T)/aug-cc-pVnZ/CBS), yielding results in remarkable quantitative agreement over a 10-order dynamic range of tunneling lifetimes.⁹ Most importantly, this work predicts 1,2 hydride shift dynamics in vinyl radical to exhibit



exponential growth with internal vibrational excitation, specifically achieving $> 1\text{ MHz}$ rates relevant to low pressure combustion at energies above $E \approx 7500\text{ cm}^{-1}$, i.e., far below the CH bond dissociation limit (see Fig. 5). These results suggest such “quantum isomerization” dynamics to be in competition with “roaming,” which is classically restricted to a narrow window of energies at the dissociation limit. Furthermore, integrated over a Boltzmann distribution of thermal energies, these microcanonical tunneling rates are consistent with sub μsec time scales for 1,2 hydride shift dynamics at $T > 1400\text{ K}$, with particular relevance for combustion modeling of low pressure flames.

- ¹ E. N. Sharp, M. A. Roberts, and D. J. Nesbitt, *Phys. Chem. Chem. Phys.* **10**, 6592 (2008).
- ² R. J. McMahon, M. C. McCarthy, C. A. Gottlieb, J. B. Dudek, J. F. Stanton, and P. Thaddeus, *Astrophys. J.* **590**, L61 (2003).
- ³ E. N. Sharp-Williams, M. A. Roberts, and D. J. Nesbitt, *J. Chem. Phys.* **134** (2011).
- ⁴ E. N. Sharp-Williams, M. A. Roberts, and D. J. Nesbitt, *Phys. Chem. Chem. Phys.* **13**, 17474 (2011).
- ⁵ Y.-C. Hsu, Y.-J. Shiu, and C.-M. Lin, *J. Chem. Phys.* **103**, 5919 (1995).
- ⁶ A. van der Avoird, Y. Scribano, A. Faure, M. J. Weida, J. R. Fair, and D. J. Nesbitt, *Chem. Phys.* (in press).
- ⁷ A. van der Avoird and D. J. Nesbitt, *J. Chem. Phys.* **134**, 044314 (2011).
- ⁸ M. A. Roberts, C. Savage, F. Dong, E. N. Sharp-Williams, A. B. McCoy, and D. J. Nesbitt, *J. Chem. Phys.* (submitted).
- ⁹ A. R. Sharma, J. M. Bowman, and D. J. Nesbitt, *J. Chem. Phys.* **136**, 034305 (2011).

Radical Photophysics and Photochemistry

Daniel Neumark
Chemical Sciences Division
Lawrence Berkeley National Laboratory
Berkeley, CA 94720

This project applies complementary experimental techniques to study the spectroscopy and photodissociation of free radicals, with a particular focus on species that play a key role in combustion chemistry. These experiments also provide fundamental new insights into the chemical dynamics of free radicals. These species, owing to their high reactivity, present unique experimental challenges that are absent for closed shell molecules. The experiments are carried out on two instruments: a fast radical beam instrument (FRBM) and a molecular beam apparatus.

Recent experiments have focused on photodissociation of free radicals, hydrocarbons, and negative ions. Molecular beam photodissociation experiments were carried out on the phenyl and *t*-butyl radicals, both of which were generated by flash pyrolysis. The ultraviolet photodissociation of isobutene was also investigated. Our fast radical beam instrument was used to investigate the dynamics of the photoexcited propargyl and propynyl radicals, both of which are C₃H₃ isotopomers. The competition between dissociation and isomerization of these species was the focus of a collaborative experimental and theoretical effort with Bill Lester. Finally, the two- and three-body dissociation dynamics of the I₂Br⁻ and I₂⁻(CO₂) anions were investigated.

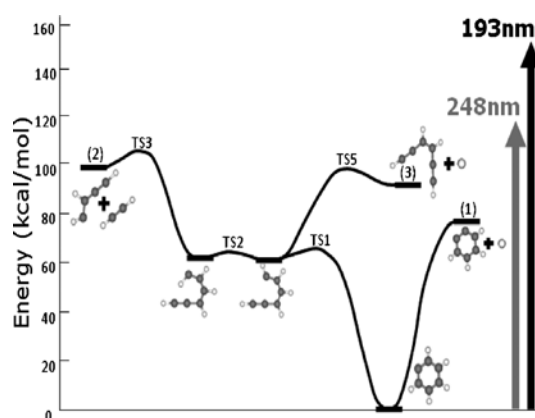


Fig. 1. Ground state potential energy surface for phenyl dissociation.

The phenyl radical, *c*-C₆H₅, plays a central part in the combustion chemistry of aromatic hydrocarbons. Its formation from the bimolecular reaction of smaller aliphatic species has been proposed to be the rate-limiting step in the production of larger aromatic molecules. The phenyl radical is an intermediate in the thermal decomposition of benzene, so its bimolecular reactivity and unimolecular decay kinetics are of considerable interest in formulating a complete mechanism for this process. These considerations motivated our experiments, in which the photodissociation of phenyl radical excited at 248 and 193 nm was investigated using photofragment translational spectroscopy. Fig. 1 shows relevant energetics for phenyl dissociation. At 248 nm, the only dissociation products observed were from H atom loss, attributed primarily to H + *o*-C₆H₄ (*ortho*-benzyne). The observed translational energy distribution was consistent with statistical decay on the ground state surface. At 193 nm, dissociation to H + C₆H₄ and C₄H₃ + C₂H₂ was observed. The C₆H₄ fragment can be either *o*-C₆H₄ or *i*-C₆H₄ resulting from decyclization of the phenyl ring. The C₄H₃ + C₂H₂ products dominate over the two H loss channels. Attempts to reproduce the observed branching ratio by calculations assuming ground state dynamics were unsuccessful. However, these calculations assumed that the C₄H₃ fragment was *n*-C₄H₃, and better agreement would be expected if the lower energy *i*-C₄H₃ + C₂H₂ channel were included.

Alkyl radicals are prototypical open-shell species that play a central role in combustion

chemistry. While the energetics, kinetics, and ground state spectroscopy of numerous smaller alkyl radicals are reasonably well understood, characterization of their electronic spectroscopy and photochemistry is complicated by their high reactivity and, in contrast to many other radicals, the general absence of low-lying, long-lived electronic states. We used photofragment translational spectroscopy to investigate the photochemistry of the simplest tertiary alkyl radical, the *t*-butyl radical ($t\text{-C}_4\text{H}_9$) in order to unravel its primary photochemistry and its dissociation dynamics subsequent to electronic excitation at 248 nm. The *t*-butyl radical was produced from flash pyrolysis of azo-*tert*-butane and dissociated at 248 nm. Two distinct channels of approximately equal importance were identified: dissociation to H + 2-methylpropene, and CH_3 + dimethylcarbene. Neither the translational energy distributions that describe these two channels nor the product branching ratio are consistent with statistical dissociation on the ground state, and instead favor a mechanism taking place on excited state surfaces.

Isobutene, $i\text{-C}_4\text{H}_8$, (2-methylpropene) is the smallest branched alkene. It plays a key role in combustion chemistry as an intermediate in the pyrolysis of iso-octane and in the oxidation of fuel additives such as MTBE and ETBE (methyl and ethyl *t*-butyl ether). The photodissociation of isobutene at 193 nm was investigated in order to gain new insights into its unimolecular photochemistry and dissociation dynamics. The results show that excitation at 193 nm results in two major photodissociation channels: H + C_4H_7 and CH_3 + CH_3CCH_2 . Translational energy distributions indicate that both channels result from statistical decay on the ground state surface. Although the CH_3 loss channel is 13 kcal/mol higher in energy, the CH_3 :H branching ratio was found to be 1.7 ± 0.5 , in reasonable agreement with RRKM calculations.

C_3H_3 radicals have been of interest for many years owing to their importance in combustion and interstellar chemistry. Of the various stable C_3H_3 isomers, propargyl (2-propynyl, H_2CCCH) has received the most attention. The photodissociation dynamics of both the propargyl radical and the higher-lying 1-propynyl isomer, H_3CCC , have been investigated at 248 nm and 193 nm using fast beam photofragment translational spectroscopy. In these experiments, radicals were produced from their respective anions by photodetachment at 540 nm and 450 nm (below and above the electron affinity of propynyl). The radicals were then photodissociated by 248 nm or 193 nm light. The recoiling photofragments were detected in coincidence with a time- and position-sensitive detector. Three channels were observed: D_2 loss, $\text{CD} + \text{C}_2\text{D}_2$, and $\text{CD}_3 + \text{C}_2$. The translational energy distributions for D_2 loss peaked at nonzero translational energy, consistent with ground state dissociation over small (<1 eV) exit barriers with respect to separated products. Translational energy distributions for the two heavy channels peaked near zero kinetic energy, indicating dissociation on the ground state in the absence of exit barriers.

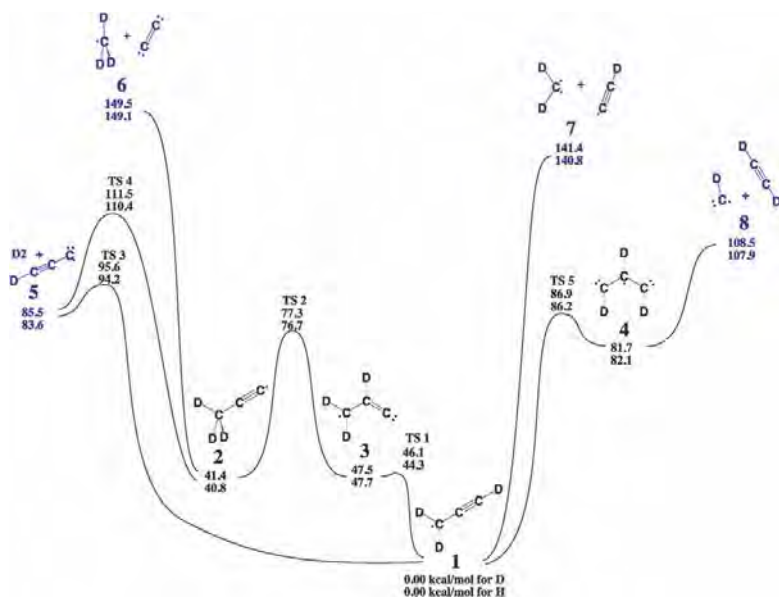


Fig. 2. Calculated isomerization and dissociation barriers for propargyl and propynyl radicals.

Motivated by this work, a theoretical study of the photodissociation of perdeuterated propargyl (D_2CCD) and propynyl (D_3CCC) radicals was carried out in collaboration with Bill Lester, focusing on the C-C bond cleavage and D_2 loss channels. High-level *ab initio* calculations were carried out, and RRKM rate constants were calculated for isomerization and dissociation pathways. The calculated energetics for this system are shown in Fig. 2. The reaction barriers, microcanonical rate constants and product branching ratios are consistent with the experimental findings, supporting the overall mechanism of internal conversion followed by statistical dissociation on the ground state surface. Loose transition states and very low exit barriers were found for two of the C-C bond cleavage channels and an additional $CD_2 + CCD$ channel, which had not been reported previously. The results probe the extent of propargyl and propynyl isomerization prior to dissociation at 248 and 193 nm and deliver a comprehensive picture of all ongoing molecular dynamics.

The vast majority of photodissociation experiments have focused on two-body dissociation; photodissociation into three fragments remains less explored largely owing to the difficulty of obtaining a complete picture of these complex decay pathways. However, photofragmentation into three (or more) fragments has been inferred in species such as H_3 , $COCl_2$, and glyoxal; three-body dissociation is also observed in collision-induced dissociation, dissociative photodetachment, and dissociative charge exchange. The mechanism by which these three-body dissociation reactions occur (concerted vs. sequential) is a topic of much interest in reaction dynamics. It is particularly fruitful to study these dynamics using fast beam dissociation experiments that are capable of making time- and position sensitive measurement of all coincident photofragments. This methodology offers a complete picture of the fragmentation and allows elucidation of both energetic and mechanistic information. Coincidence imaging has been used in this subtask to investigate the two- and three-body dissociation dynamics of prototypes I_2Br^- and $I_2^-(CO_2)$.

The photodissociation of gas-phase I_2Br^- was investigated using fast beam photofragment translational spectroscopy. Anions were photodissociated from 300 to 270 nm (4.13 - 4.59 eV) and the recoiling photofragments were detected in coincidence by a time- and position-sensitive detector. Both two- and three-body channels were observed throughout the energy range probed. Analysis of the two-body dissociation showed evidence for four distinct channels: $Br^- + I_2, I^- + IBr, Br + I_2^-$, and $I + IBr^-$. In three-body dissociation, $Br(^2P_{3/2}) + I(^2P_{3/2}) + I^-$ and $Br^- + 2I(^2P_{3/2})$ are produced primarily from a concerted decay mechanism. A sequential decay mechanism was also observed and attributed to formation of $Br^- + I_2(B^3\Pi_{0u}^+)$ followed by predissociation of the I_2 .

The three-body dissociation of $I_2^-(CO_2)$ following excitation of the I_2^- chromophore to the repulsive $A' ^2\Pi_{g,1/2}$ and $B^2\Sigma_{g,1/2}^+$ electronic states at 1.72 and 3.21 eV was also investigated with fast beam photofragment translational spectroscopy. The translational energy distributions for three-body dissociation provide a direct measurement of the CO_2 binding energy, yielding a value of 218 ± 10 meV. These distributions are vibrationally resolved and show that some CO_2 is produced with bend excitation. Dalitz plots show that the dominant three-body decay mechanism is asynchronous-concerted decay, in which the two bond cleavages are distinct but nearly simultaneous events.

In the future, the two radical photodissociation experiments along with anion slow electron velocity map imaging will be used to study the spectroscopy and photodissociation of free radicals, with a particular focus on species that play a key role in combustion chemistry. Specific target systems include radicals with relative low bond dissociation energies that take part in low-temperature (<1000 K) autoignition chemistry, particularly peroxy (RO_2) radicals, their as-yet unobserved QOOH isomers, and the radicals resulting from the subsequent

reactions of these species. Radicals such as benzyl and benzoyl are of interest as intermediates in the oxidation of aromatic hydrocarbons. Finally, resonance-stabilized radicals, including open chains (pentadienyl, heptadienyl, C_4H_3 , C_5H_3) and radicals comprising an intact aromatic ring (phenoxy, indenyl, phenalenyl), are of interest owing to their role in the growth of complex hydrocarbons such as PAH's in combustion.

Recent Publications:

P. E. Crider, L. Castiglioni, K. K. Kautzman, and D. M. Neumark, "Photodissociation of the Propargyl and Propynyl (C_3D_3) Radicals at 248 nm and 193 nm," *J. Chem Phys.* **130**, 044310, (2009).

W. A. Donald, R. D. Leib, M. Demireva, B. Negru, D. M. Neumark, and E. R. Williams, "Weighing' Photons with Mass Spectrometry: Effects of Water on Ion Fluorescence," *J. Am. Chem. Soc.* **132**, 6904, (2010).

B. Negru, S. J. Goncher, A. L. Brunsvold, G. M. P. Just, D. Park, and D. M. Neumark, "Photodissociation Dynamics of the Phenyl Radical via Photofragment Translational Spectroscopy," *J. Chem. Phys.* **133**, 074302, (2010).

L. Castiglioni, S. Vukovic, P. E. Crider, W. A. Lester, and D. M. Neumark, "Intramolecular Competition in the Photodissociation of C_3D_3 Radicals at 248 and 193 nm," *Phys. Chem. Chem. Phys.* **12**, 10714, (2010).

W. A. Donald, R. D. Leib, M. Demireva, B. Negru, D. M. Neumark, and E. R. Williams, "Average Sequential Water Molecule Binding Enthalpies of $M(H_2O)_{19-24}^{2+}$ ($M=Co, Fe, Mn, \text{ and } Cu$) Measured with Ultraviolet Photodissociation at 193 and 248nm," *J. Phys. Chem. A.* **115**, 2, (2011).

P. E. Crider, A. W. Harrison, D. M. Neumark, "Two-and Three-body Photodissociation Dynamics of the Diiodobromide (I_2Br^-) Anion," *J. Chem. Phys.* **134**, 134306, (2011).

B. Negru, G. M. P. Just, D. Park, and D. M. Neumark, "Photodissociation Dynamics of the t-butyl Radical via Photofragment Translational Spectroscopy at 248 nm," *Phys. Chem. Chem. Phys.* **13**, 8180, (2011).

A. W. Harrison, J. S. Lim, P. E. Crider, D. M. Neumark, "Three-body Photodissociation Dynamics of $I_2^-(CO_2)$," *Chem. Phys. Lett.* **512**, 30, (2011).

G. M. P. Just, B. Negru, D. Park, and D. M. Neumark, "Photodissociation of Isobutene at 193 nm," *Phys. Chem. Chem. Phys.* **14**, 675 (2012).

Determination of Accurate Energetic Database for Combustion Chemistry by High-Resolution Photoionization and Photoelectron Methods

C. Y. Ng

Department of Chemistry, University of California, Davis, California 95616

E-mail Address: cyng@chem.ucdavis.edu

I. Program Scope:

The main goal of this research program is to obtain accurate thermochemical data, such as ionization energies (IEs), 0 K dissociative photoionization thresholds or appearance energies (AEs), 0 K bond dissociation energies (D_0 's), and 0 K heats of formation (ΔH_{f0}° 's) for small and medium sizes molecular species and their ions of relevance to combustion chemistry. Accurate thermochemical data determined by high-resolution photoionization and photoelectron studies for selected polyatomic neutrals and their ions are also useful for benchmarking the next generation of *ab initio* quantum computational procedures.

II. Recent Progress:

The propargyl radical $\text{HC}\equiv\text{C}-\dot{\text{C}}\text{H}_2$ (C_3H_3), the smallest π -conjugated hydrocarbon radical, and its cation (C_3H_3^+) have been the subjects of numerous state-of-the-art experimental and theoretical investigations. Despite of the many previous studies, the agreement between the experimental determinations and theoretical predictions for the ionization energy for C_3H_3 [$\text{IE}(\text{C}_3\text{H}_3)$] was lacking. We have re-examined the $\text{IE}(\text{C}_3\text{H}_3)$ value by high-resolution vacuum ultraviolet (VUV) laser photoionization efficiency (PIE) and velocity-map-imaging-photoelectron (VMI-PE) measurements¹ of supersonically cooled C_3H_3 radicals for comparison with the $\text{IE}(\text{C}_3\text{H}_3)$ prediction² calculated by state-of-the-art CCSDTQ/CBS procedures.

The PFI-PE technique,³ which is based on the detection of near zero kinetic energy photoelectrons produced by delayed PFI of high- n ($n > 100$) Rydberg states populated by laser excitation, is a relatively low sensitivity method because high- n Rydberg states can be destroyed by stray electric field existing in the photoionization region. Recently, we have succeeded in performing high-resolution photoelectron measurements based on the VUV laser velocity-map-imaging-photoelectron (VMI-PE) method. This VMI-PE technique is highly sensitive because it is capable of measuring all photoelectrons with different velocities simultaneously. The nature of VMI measurements is that the velocity resolution (Δv) depends only on Δr , and is essentially constant across the image (i.e., for all the velocities), where r is the radial distance measured with respect to the center of the VMI-PE image on the imaging detector. Thus, the achievable bandwidth (ΔE) in terms of photoelectron kinetic energies is scaled as \sqrt{E} and can be significantly narrowed by lowering E . The VMI-threshold photoelectron

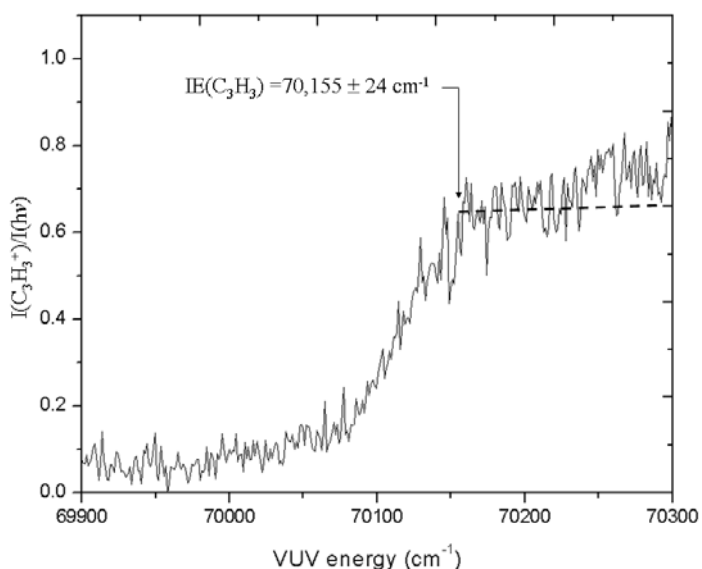


Fig. 1. The VUV PIE spectrum of $\text{C}_3\text{H}_3(\text{X}^2\text{B}_1)$ in the region of 69900-70300 cm^{-1} . The $\text{C}_3\text{H}_3(\text{X}^2\text{B}_1)$ sample was prepared by a pulsed supersonically cooled radical nozzle based on 193 nm photodissociation. The dashed horizontal line shows the estimated position the PIE plateau. Based on the conclusion obtained in the previous experiments, we have assigned the lowest VUV energy at 70155 cm^{-1} , where the PIE reaches the plateau value of the PIE step, as the $\text{IE}(\text{C}_3\text{H}_3)$.

(VMI-TPE) measurement, which employs the VMI arrangement to disperse the energetic or hot photoelectron background from the TPE detection by scanning the VUV laser energy across the photoelectron band of interest, is expected to yield the optimal energy resolution. This method of using tunable VUV laser for high-resolution VMI-TPE measurements has not been reported previously.

The ground electronic configuration for C_3H_3 is $\dots 7a_1^2 1b_2^2 1b_1^2 2b_2^2 2b_1^1$, giving rise to the $C_3H_3(X^2B_1)$ neutral ground state in the C_{2v} point group.⁵ The highest occupied $2b_1$ orbital is a π -type orbital covering the linear CCC structure of C_3H_3 ; and the ejection of the unpaired electron in the $2b_1$ orbital produces the $C_3H_3^+(X^+A_1)$ cation ground state. Based on the recent comparison of corresponding VUV-PIE and VUV-PFI-PE spectra near the first ionization thresholds of a series of diatomic and polyatomic molecules, we found that the IE value determined by the VUV-PFI-PE origin band is always in excellent agreement with the VUV energy of a sharp break along the rising PIE step. For many molecular systems, this PIE break position was found to coincide with the lowest VUV energy at which the PIE reaches the plateau of the PIE step. The identification of the sharp break allows the determination of the IE value with an error limit of 1-2 meV. The VUV laser PIE spectrum for $C_3H_3^+$ obtained in the present study is shown in Fig. 1. As observed in previous experiments, the VUV-PIE spectrum of C_3H_3 exhibits a sharp break at about $70,155\text{ cm}^{-1}$. At energies above this break, a PIE plateau is evident as estimated by the dashed horizontal line. After taking into account the experimental uncertainty due to a possible minor Stark shift correction, we have assigned the $IE(C_3H_3)$ as $70,155 \pm 24\text{ cm}^{-1}$ ($8.698 \pm 0.003\text{ eV}$) based on the VUV-PIE measurement.

The VUV-VMI-TPE spectrum was obtained by gating the TPE signal at the central image (or

detector) area as a function of VUV laser photoionization energy. For the purpose of energy calibration and the determination the dc Stark shift correction for VMI-TPE measurements, we have compared in Fig. 2 the VUV laser PFI-PE (blue curve) and VMI-TPE (red curve) spectra for the origin band of $C_6H_5Cl^+$. As shown in Fig. 2, the FWHMs for the VUV-VMI-spectrum obtained at the TPE energy resolution of 3 cm^{-1} and the VUV-PFI-PE spectrum measured using a PFI-PE energy resolution of $1.5\text{-}2.0\text{ cm}^{-1}$ are found to be similar and have the value of $\approx 26\text{ cm}^{-1}$. This observation confirms that the energy resolution achieved in the present VUV-VMI-TPE measurement is close to the instrumental resolution of 3 cm^{-1} . The spectral simulation of the VUV-PFI-PE band yields $IE(C_6H_5Cl) = 73172.1 \pm 1.6\text{ cm}^{-1}$, the value of which is marked by the peak position of the VUV-PFI-PE band. Discounting the contribution of hot photoelectrons, we estimate that the origin VUV-VMI-TPE band on the high energy side should have a profile as estimated by the dashed line of Fig. 2. For $F = 33.5\text{ V/cm}$ used in the present experiment, the Stark shift is expected to be -35 cm^{-1} . As shown in Fig. 2, the VUV-VMI-TPE intensity was found to drop sharply to the background level at the VUV energy of 73140 cm^{-1} . Since the latter value is 32 cm^{-1} lower than the $IE(C_6H_5Cl)$, we conclude that this observation is consistent with the classical Stark shift prediction. However, the peak position of the origin VUV-VMI-TPE band of $C_6H_5Cl^+$ is observed at 73155 cm^{-1} , indicating that the experimental Stark shift correction for the present VUV-VMI-TPE measurement of C_6H_5Cl is 17 cm^{-1} . Assuming that the Stark shift corrections are the

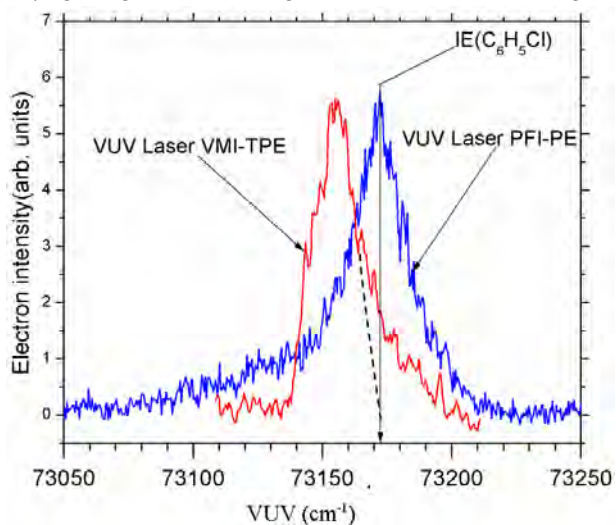


Fig. 2. Comparison of the VUV-VMI-TPE spectrum (red curve) and VUV-PFI-PE spectrum (blue curve) in the range of $73050\text{-}73250\text{ cm}^{-1}$ for the origin band of $C_6H_5Cl^+$. The peak energy of the VUV-PFI-PE band marks the $IE(C_6H_5Cl)$, which has been corrected for the Stark shift induced by the PFI field used for PFI-PE measurement. The difference of 17 cm^{-1} observed between the $IE(C_6H_5Cl)$ (or the peak position of the VUV-PFI-PE band) and the peak position of the VUV-VMI-TPE band at 73155 cm^{-1} is taken as the Stark shift correction for the present VUV-VMI-TPE measurements. The dashed curve is the estimated profile of the VUV-VMI-TPE band after discounting the contribution due to hot band photoelectron background.

same for the VUV-VMI-TPE measurements of C_6H_5Cl and C_3H_3 , the latter value is taken as the Stark shift correction for the $IE(C_3H_3)$ determination in the present VUV laser VMI-TPE measurement of C_3H_3 .

The top black spectra of Figs. 3(a) and 3(b) are the VUV-VMI-TPE spectra for the origin band of $C_3H_3^+$ measured at the respective TPE resolution of 3 and 8 cm^{-1} (FWHM). We have obtained the best simulated spectra [shown as the red spectra of Figs. 3(a) and 3(b)] for the VMI-TPE spectra by invoking the contributions of the N, O, P, Q, R, S, and T-branches, which correspond to the respective $\Delta J = J^+ - J'' = -3, -2, -1, 0, +1, +2,$ and $+3$ rotational branches. Individual contributions by these rotational branches are also shown in Figs. 3(a) and 3(b). The simulation yields a rotational temperature $T_{rot} = 75$ K for C_3H_3 . A Gaussian instrumental energy function with the FWHM of 3 cm^{-1} (7 cm^{-1}) was used in the simulation of the VMI-TPE spectrum of Fig. 3(a) [Fig. 3(b)].

This simulation also confirms the predicted photoelectron energy resolutions achieved in the present VMI-TPE measurements. The observed structure of the VMI-TPE spectra are mostly determined by the Q and P and R branches. The inclusion of higher rotational branches has the minor effect of broadening the origin band. The $IE(C_3H_3)$ defined by the energy for the $0_{00} \rightarrow 0_{0^+0^+}$ transition is determined to be 70139 cm^{-1} without the Stark shift correction. According to the simulation, the main peak for the VMI-TPE bands observed in Figs. 3(a) and 3(b) corresponds to the photoionization transition $K_a = 1 \rightarrow K_a^+ = 2$, which lies 27 cm^{-1} higher than the $IE(C_3H_3)$ value; and the shoulder of the VMI-TPE band corresponds to the $K_a = 1 \rightarrow K_a^+ = 0$ photoionization transition. Assuming that the Stark shift determined for the $C_6H_5Cl/C_6H_5Cl^+$ system is valid for the VUV-VMI-TPE measurement of the $C_3H_3/C_3H_3^+$ system, we arrive at the $IE(C_3H_3) = 70,156 \pm 4$ cm^{-1} (8.6982 ± 0.0005 eV). This value is in excellent agreement with the IE value obtained based on the VUV laser PIE measurement.

We have also reexamined the IE prediction of propargyl (C_3H_3) and allyl (CH_2CHCH_2) radicals using the CCSDTQ(full)/CBS method.² Both IE predictions, $IE(CH_2CCH) = 8.706$ eV and $IE(CH_2CHCH_2) = 8.144$ eV are found to compare favorably with the most recent experimental IE values of 8.6982 ± 0.0005 eV for propargyl radical¹ and 8.1314 ± 0.0003 (Ref. 1) and 8.1309 ± 0.0003 (Ref 4) eV for allyl radical determined by rotationally resolved photoelectron measurements.

III. Ongoing Studies

We are making progress in PIE, PFI-PE, and VUV-TPE-EI measurements on other radicals, such as phenyl (C_6H_5) and phenoxy (C_6H_5O) radicals. These experiments represent collaborative projects between

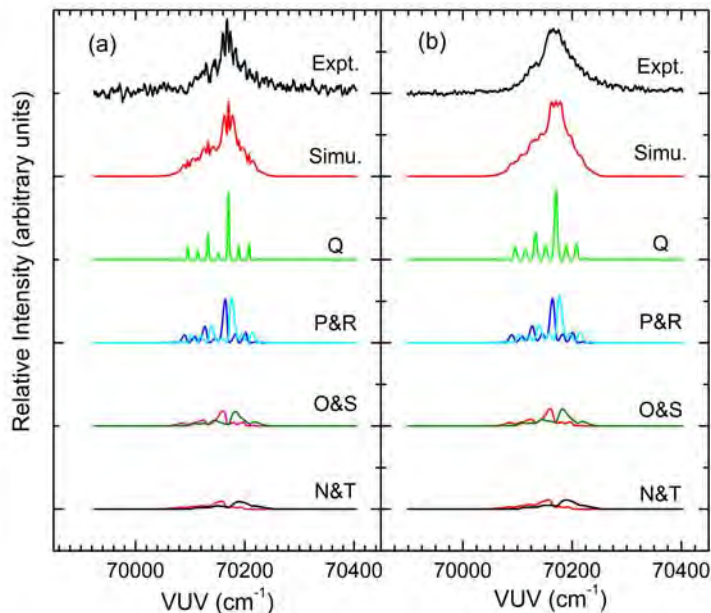


Fig. 3. Comparison of the VMI-TPE spectra (top spectra shown in black) for the origin band of $C_3H_3^+(X^1A_1)$ in the region of 69900-70400 cm^{-1} with the simulated spectra (second spectra from the top shown in red). The simulation is based on the selection rules $\Delta K_a = \text{odd}$ and $\Delta K_c = \text{even}$ and odd . Experimental and simulated spectra in (a) and (b) are obtained by using a Gaussian instrumental line-width of 3 and 7 cm^{-1} (FWHM), respectively. The simulated spectra are also calculated assuming a rotational temperature of 75 K and the branching ratios for the N : O : P : Q : R : S : T = 2 : 3 : 4 : 6 : 5 : 3 : 2. See also the text for detailed simulation procedures. Contributions by the Q, P&R, O&S, and N&T, branches are also shown in (a) and (b). The simulated spectra represent the sum of the corresponding contributions by the rotational branches.

our group and the groups of Dr. Xu Zhang (Jet propulsion Laboratory, NASA), and Prof. Barney Eillison (University of Colorado, Boulder). Using the IR-VUV-photoion and the VUV-VMI-PE techniques developed in our laboratory, we also plan to examine the vibrational bands for neutral C_3H_3 and C_3H_5 and their cations.

References:

1. Hong Gao, Yuntao Xu, Lei Yang, Chow-Sing Lam, Hailing Wang, Jingang Zhou, and C. Y. Ng, *J. Chem. Phys.* **135**, 224304 (2011).
2. K.-C. Lau and C. Y. Ng, *J. Chem. Phys.* **135**, 246101 (2011).
3. C. Y. Ng, *Ann. Rev. Phys. Chem.* **53**, 101 (2002).
4. M. Gasser, A. Bach, P. Chen, A. M. Schulenburg, P. Dietiker, and F. Merkt, *J. Chem. Phys.* **131**, 014304 (2009).

IV. Publications of DOE sponsored research (2010-present)

1. Y.-C. Chang, X. Shi, K.-C. Lau, Q. Yin, and C. Y. Ng, "Rovibronically selected and resolved two-color laser photoionization and photoelectron study of the nickel carbide cation", *J. Chem. Phys.* **133**, 054310 (2010).
2. Kai-Chung Lau, Yih-Chung Chang, Xiaoyu Shi, and C. Y. Ng, "High-level *ab initio* predictions of the ionization energy, bond dissociation energies and heats of formations for nickel carbide (NiC) and its cation (NiC⁺)", *J. Chem. Phys.* **133**, 114304 (2010).
3. Chow-Shing Lam, H. Wang, Yuntao Xu, Kai-Chung Lau, and C. Y. Ng, "A Vacuum-Ultraviolet Laser Pulsed Field Ionization-Photoelectron Study of Sulfur Monoxide (SO) and its Cation (SO⁺)", *J. Chem. Phys.* **134**, 144304 (2011).
4. Yih-Chung Chang, Hong Xu, Yuntao Xu, Zhou Lu, Yu-Hui Chiu, Dale J. Levandier, and C. Y. Ng, "Communication: Rovibrationally selected study of the $N_2^+(X; v^+ = 1, N^+ = 0-8) + Ar$ charge transfer reaction using the vacuum ultraviolet laser pulsed field ionization-photoion method", *J. Chem. Phys.* **134**, 201105 (2011).
5. Yang Pan, Hong Gao, Lei Yang, Jingang Zhou, C. Y. Ng, and W. M. Jackson, "Communication: Vacuum ultraviolet laser photodissociation studies of small molecules by the VUV laser photoionization time-sliced velocity-mapped ion imaging method", *J. Chem. Phys.*, **135**, 071101 (2011).
6. Hong Gao, Lei Yang, Yang Pan, Jingang Zhou, C. Y. Ng, and W. M. Jackson, "Time-sliced velocity-mapped imaging studies of the predissociation of single ro-vibronic energy levels of N_2 in the extreme ultraviolet region using vacuum ultraviolet photoionization", *J. Chem. Phys.* **135**, 134319 (2011).
7. Hong Gao, Yuntao Xu, Lei Yang, Chow-Sing Lam, Hailing Wang, Jingang Zhou, and C. Y. Ng, "High-resolution threshold photoelectron study of the propargyl radical by the vacuum ultraviolet laser velocity-map imaging method", *J. Chem. Phys.* **135**, 224304 (2011).
8. Hong Gao, Yu Song, Lei Yang, Xiaoyu Shi, Qingzhu Yin, C. Y. Ng, and W. M. Jackson, "Communication: Branching ratio measurement in the predissociation of $^{12}C^{16}O$ by time-slice velocity-map ion imaging in the vacuum ultraviolet region", *J. Chem. Phys.* **135**, 221101 (2011).
9. K.-C. Lau and C. Y. Ng, "Accurate *ab initio* predictions of ionization energies of propargyl radical: revisited", *J. Chem. Phys.* **135**, 246101 (2011).
10. Xiaoyu Shi, Huang Huang, Brian Jacobson, Yih-Chung Chang, Qing-Zhu Yin, and C. Y. Ng, "A high-resolution photoionization and photoelectron study of ^{58}Ni using a vacuum ultraviolet laser", *Astrophys. J.* **747**, 20 (2012).
11. Hong Gao, Yang Pan, Lei Yang, Jingang Zhou, C. Y. Ng, and W. M. Jackson, "Time-sliced velocity-map ion imaging studies of the photodissociation of NO in the extreme vacuum ultraviolet (EUV) region", *J. Chem. Phys.*, accepted.

LES of Turbulence-Chemistry Interactions in Reacting Multiphase Flows

Joseph C. Oefelein

Combustion Research Facility, Sandia National Laboratories

Livermore, CA 94551-0969

oefelei@sandia.gov

I. Program Scope

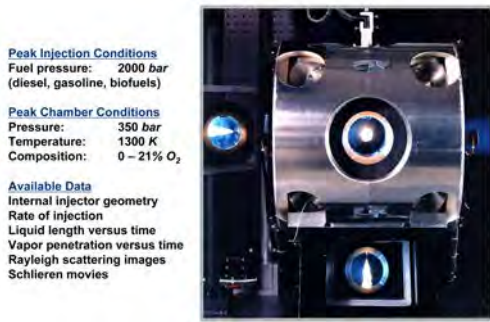
Application of the Large Eddy Simulation (LES) technique within the Diagnostics and Reacting Flows program at the CRF was initiated with two primary objectives. The first is to establish a set of high-fidelity computational benchmarks that identically match the geometry (i.e., experimental test section and burner) and operating conditions of selected experimental target flames. The second is to establish a scientific foundation for advanced model development. The goal is to provide a direct one-to-one correspondence between measured and modeled results at conditions unattainable using the Direct Numerical Simulation (DNS) technique by performing a series of detailed simulations that progressively incorporate the fully coupled dynamic behavior of reacting flows with detailed chemistry and realistic levels of turbulence. Our recent focal point has been aimed the fundamental issues related to high-pressure multiphase phenomena, with emphasis placed on the priority research directions identified in two recent DOE workshop reports: the Office of Science (SC) report of the Basic Energy Sciences (BES) *Workshop on Clean and Efficient Combustion of 21st Century Transportation Fuels*, and most recently the jointly sponsored SC-BES and Office of Energy Efficiency and Renewable Energy (EERE) Vehicle Technologies Program (VTP) *Workshop to Identify Research Needs and Impacts in Predictive Simulations for Internal Combustion Engines* (PreSICE).

II. Recent Progress

Our primary goals are to: 1) continue to develop our theoretical-numerical capabilities in LES through application of advanced subgrid-scale (SGS) models, 2) maximize the benefits of high performance computing through close collaboration with key DOE Office of Science computational facilities, and 3) continue to establish key links between DOE basic and applied research programs. All of the cases considered involve direct coupling with key target experiments and the common objective of establishing a one-to-one correspondence with these experiments while adhering to the strictest accuracy requirements for LES. These requirements include treatment of complex geometries, use of clean numerics with non-dissipative discretely-conservative differencing stencils and no artificial dissipation terms, high-quality grids, and science-based SGS models that are designed specifically for high-resolution applications.

One recent area of interest has been in the area of direct injection processes for high-pressure, low-temperature engine applications with emphasis on hydrocarbon fuels. As part of our BES effort, we are developing the fundamental science tools required for highly accurate treatment of the detailed real-fluid thermodynamics and transport processes associated with these flows. Injection of liquid fuel in systems where the working fluid exceeds the thermodynamic critical pressure of the liquid phase is not well understood. Depending on pressure, injected jets can exhibit two distinctly different sets of evolutionary processes. At low subcritical pressures, the classical situation exists where a well-defined molecular interface separates the injected liquid from ambient gases due to the presence of surface tension. Interactions between dynamic shear forces and surface tension promote primary atomization and secondary breakup processes that evolve from a dense state, where the liquid exists as sheets filaments or lattices intermixed with sparse pockets of gas; to a dilute state, where drop-drop interactions are negligible and dilute spray theory can be used. As ambient pressures approach or exceed the critical pressure of the liquid, however, the situation becomes quite different. Under these conditions, interfacial diffusion layers develop as a consequence of both vanishing surface tension forces and broadening gas-liquid interfaces. These interfaces eventually enter the continuum length scale regime and disappear as interfacial fluid temperatures rise above the critical temperature of the local mixture. Lack of inter-molecular forces, coupled with broadening interfaces, promotes diffusion dominated mixing processes prior to atomization. As a consequence, injected jets evolve in the presence of exceedingly large but continuous thermo-physical gradients in a manner that is markedly different from the classical modeling assumptions.

High-Pressure Combustion Vessel



LES Grid and Computational Domain

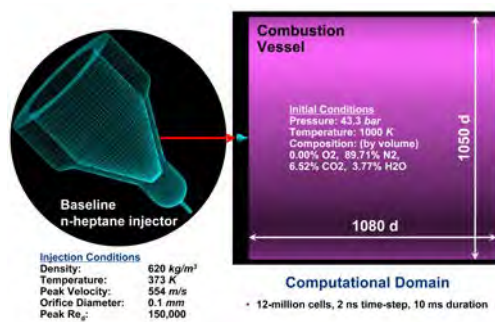


Figure 1: Photograph of the Sandia high-pressure combustion vessel (left) and computational domain used for LES (right). The injector is mounted at the head-end of the vessel, as indicated by the red arrow. The grid and operating conditions identically match the experiment. Conditions listed correspond to the Baseline n-Heptane experiment.

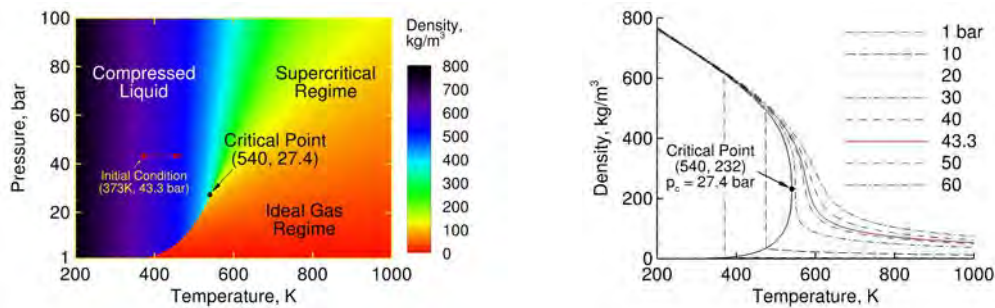


Figure 2: Thermodynamic characteristics of n-heptane showing key regimes and its initial state when injected into the combustion vessel. The jet enters as a compressed liquid and is heated at supercritical pressure.

Modeling either of the two extremes described above poses a variety of challenges. To enhance our understanding of these processes, we have performed a series of calculations using LES with a real-fluid model for detailed treatment of thermodynamics and transport. We have combined this with key experimental observations and the development of a detailed theoretical framework to explain the observed trends. We use the experimental data provided by Pickett *et al.* as part of the Engine Combustion Network (see www.ca.sandia.gov/ECN) using the “Baseline n-heptane” and “Spray-A (n-dodecane)” cases as key targets. Significant attention is focused on corroborating measured and modeled results as a function of distinctly different phenomenological processes that occur as a function of pressure. This is accomplished by rigorously treating the experimental geometry (injector and vessel) and operating conditions.

The experimental apparatus, corresponding computational domain, and key operating conditions for the Baseline n-Heptane case are shown in Fig. 1. The experiment involves a liquid n-heptane jet injected into a hot quiescent mixture of gaseous products. For the case considered here, all the oxygen has been consumed to prevent the onset of combustion so we can focus on thermo-physical processes associated with injection. Fuel is injected with an electronically controlled common rail injector at a pressure of 1540 bar and 373 K. The ambient gas composition in the vessel was conditioned to provide an inert composition of N₂, CO₂, and H₂O. The actual mole fractions of these components are summarized in Fig. 1. The thermodynamic characteristics of n-heptane are shown in Fig. 2. Its critical point is 540 K, 27.4 bar. Thus, n-heptane is injected into the chamber as a compressed liquid (i.e., supercritical with respect to pressure, subcritical with respect to temperature). LES calculations were performed using a grid with approximately 12-million cells. The transient jet was injected using boundary conditions that closely approximate the actual experimental conditions. The peak jet velocity is 554 m/s and corresponding jet Reynolds number is 150,000. The quasi-steady portion of the pulse lasts for 6.66 ms. At 6.69 ms the jet ramps down to zero velocity, with the end of injection occurring at 6.93 ms. The total integration time for the LES was 10 ms using a time-step of 2 ns.

Figure 3 provides a representative comparison of the mixture fraction distribution predicted using LES with the corresponding experimentally measured Rayleigh images. Note that the color maps and contour spacing used is identical for both the LES and measured data. In general, predictions agree well with the available experimental data. To perform a comprehensive analysis of the fuel mixing states, we used the time evolving fields given by the LES to map the relationship between mixture fraction (denoted here as ξ) and temperature. Here, $\xi = 1$ represents the fuel stream

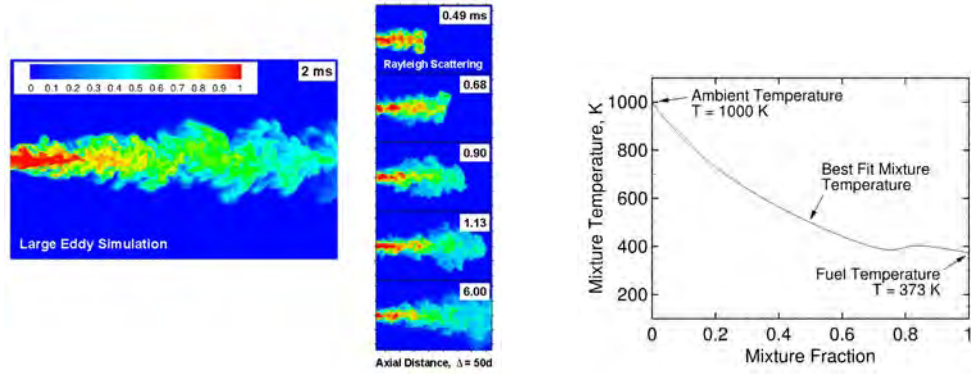


Figure 3: Comparison of mixture fraction predictions from LES (left) with measured Rayleigh images (center). Corresponding best fit mapping of temperature as a function of mixture fraction for the time evolving field (right).

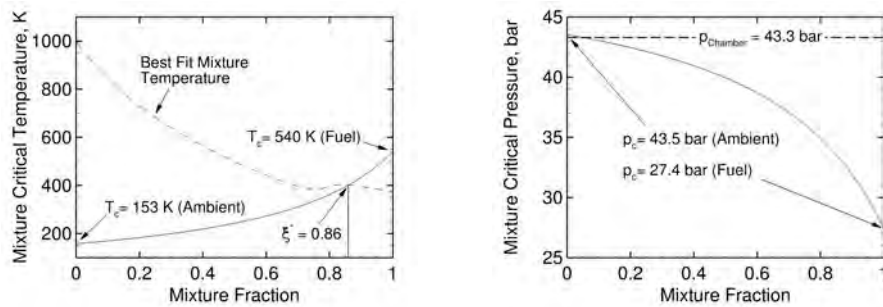


Figure 4: Mixture critical temperature and pressure of the time evolving field as a function of mixture fraction.

(C₇H₁₆) and $\xi = 0$ represents the “oxidizer” stream (N₂-CO₂-H₂O). A scatter plot of mixture temperature conditioned on mixture fraction was produced, which revealed that there was only slight variations in mixture temperature as a function of mixture fraction. Figure 3 also shows the resultant best fit relationship.

Having established the mapping between temperature and mixture fraction, we can now analyze how the state of the local mixture varies across key thermodynamic regimes. To accomplish this, we use the fundamental assumptions built into the real fluid model to calculate the mixture critical temperature and pressure as a function of mixture fraction. We then superimpose the best fit mixture temperature shown in Fig. 3 and the nominal ambient pressure chamber condition of 43.3 bar to identify key points of intersection. Figure 4 shows the results. Analysis of these data reveals two important features. First, the local mixture temperature is greater than the critical mixture temperature for all values of mixture fraction less than 0.86. Second, the nominal ambient chamber pressure is greater than the critical mixture pressure for all values of mixture fraction greater than 0.05.

Using the information given in Figs 3 and 4, we have plotted the entire envelope of mixture states on a thermodynamic regime diagram. Results are shown in Fig 5. Trends demonstrate that the mixing path associated with all states throughout the duration of injection never crosses the liquid/vapor regime (i.e., the mixture is never saturated). Instead, n-heptane is injected as a compressed liquid and the resultant local interfacial mixing layer dynamics occur at conditions that are locally supercritical. Surface tension effects are typically assumed to be negligible under such conditions, which implies that classical first order vapor-liquid phase transitions (as are typically assumed) do not occur. Instead, processes dominated by surface tension such as primary atomization, secondary breakup and the presence of distinct drops can become negligible.

We can now perform further analysis to understand details related to the actual time evolving mixture. Figure 5 shows a typical instantaneous LES field with iso-lines that mark the thermodynamic transition of the mixture from a compressed liquid to a supercritical state (black) and the separation between nonideal and ideal fluid behavior (white). Results demonstrate for the first time that the injected n-heptane enters the combustion chamber as a compressed liquid (not a spray) and is heated at supercritical pressure. This implies 1) that applying the ideal gas assumption just prior to autoignition in these types of flows is not valid, and 2) the classical view of spray atomization and secondary

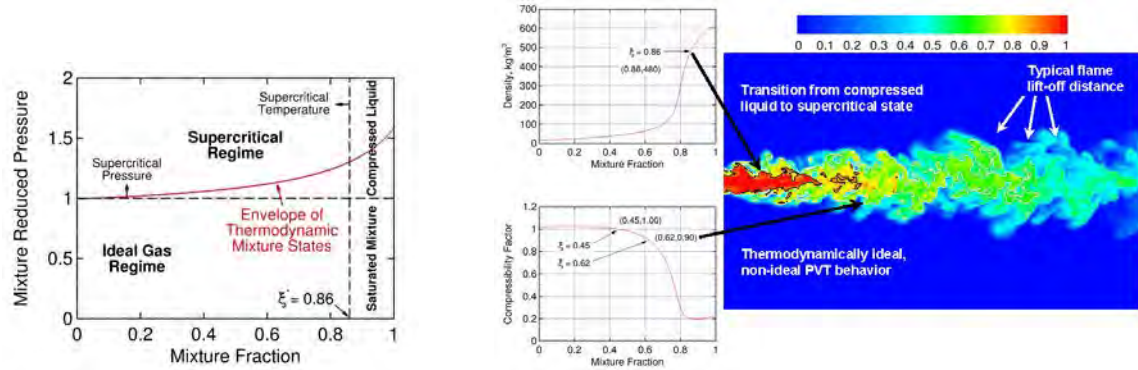


Figure 5: Envelope of mixture states predicted as a function of mixture fraction on right. LES field with iso-lines that mark the transition of the mixture from a compressed liquid to supercritical state (black) and separation between regions of nonideal and ideal fluid behavior (white) on left.

breakup processes as an appropriate model (as is widely assumed currently) is questionable. Instead, nonideal real-fluid behavior associated with the dense liquid jet must be taken into account.

III. Future Work

In addition to continuing to provide fundamental support for the work described above, we are planning a detailed series of studies on turbulent jet flames with varying amounts of localized extinction and different fuel mixtures. The first phase of this effort will focus on a series of partially premixed dimethyl ether/air jet flames that we have identified as target flames for the TNF Workshop. Our LES efforts will be closely coupled with Jonathan Frank's (Sandia) efforts. The goal is to expand our ongoing collaboration in coupling imaging measurements with LES to advance numerical simulation capabilities and to develop new methods for comparing simulations and experiments.

IV. BES Sponsored Publications (2010–2012)

1. G. Lacaze and J. C. Oefelein. A tabulated chemistry model for non-premixed combustion at high-pressure supercritical conditions. *Flow, Turbulence and Combustion*, 2012. In Press.
2. G. Lacaze and J. C. Oefelein. A non-premixed combustion model based on flame structure analysis at supercritical pressures. *Combustion and Flame*, 2012. In Press.
3. J. C. Oefelein, R. N. Dahms, G. Lacaze, J. L. Manin, and L. M. Pickett. Effects of pressure on the fundamental physics of fuel injection in diesel engines. *Proceedings of the 12th International Conference on Liquid Atomization and Spray Systems*, September 2-6 2012. Heidelberg, Germany.
4. B. Hu, M. P. Musculus, and J. C. Oefelein. The influence of large-scale structures on entrainment in a decelerating transient turbulent jet revealed by large eddy simulation. *Physics of Fluids*, 2012. In Press.
5. J. C. Oefelein, R. N. Dahms, and G. Lacaze. Detailed modeling and simulation of high-pressure fuel injection processes in diesel engines. *SAE International Journal of Engines*, 5(3):1–10, 2012. doi: 10.4271/2012-10-1258.
6. A. M. Kempf, B. J. Geurts, and J. C. Oefelein. Error analysis of large eddy simulation of the turbulent non-premixed Sydney bluff-body flame. *Combustion and Flame*, 158:2408–2419, 2011. doi: 10.1016/j.combustflame.2011.04.012.
7. J. C. Oefelein and G. Lacaze. Low-temperature injection dynamics and turbulent flame structure in high-pressure supercritical flows. *Proceedings of the 23rd International Colloquium on the Dynamics of Explosions and Reactive Systems*, July 24–29 2011. Irvine, California.
8. J. C. Oefelein and R. Sankaran. High-fidelity large eddy simulation of combustion for propulsion and power. *Proceedings of the SciDAC 2011 Meeting*, July 10-14 2011. Denver, Colorado. <http://press.mcs.anl.gov/scidac2011/>.
9. R. N. Dahms, L. M. Pickett, and J. C. Oefelein. A dense fluid approximation for the simulation of Diesel engine fuel injection processes. *Proceedings of the 23rd Annual Conference on Liquid Atomization and Spray Systems*, May 15-18 2011. Ventura, California.
10. J. H. Frank, S. A. Kaiser, and J. C. Oefelein. Analysis of scalar mixing dynamics in LES using high-resolution imaging of laser Rayleigh scattering in turbulent non-reacting jets and non-premixed jet flames. *Proceedings of the Combustion Institute*, 33:1373–1381, 2011.
11. J. C. Oefelein. A staggered dual-time all-Mach-number algorithm for LES of reacting flows. *CERFACS Colloquium on Multiphysics and Unsteady Simulations for Aeronautical Flows*, September 27-29 2010. Toulouse, France.
12. B. Hu, M. P. Musculus, and J. C. Oefelein. Large eddy simulation of a transient gas jet with emphasis on entrainment during deceleration. *SAE World Congress, Paper 2010-01-1133*, April 13-15 2010. Detroit, Michigan.

KINETICS AND DYNAMICS OF COMBUSTION CHEMISTRY

David L. Osborn

Combustion Research Facility, Mail Stop 9055

Sandia National Laboratories

Livermore, CA 94551-0969

Telephone: (925) 294-4622

Email: dlosbor@sandia.gov

PROGRAM SCOPE

The goal of this program is to elucidate mechanisms of elementary combustion reactions through the use of multiplexed optical spectroscopy and mass spectrometry. We developed a technique known as time-resolved multiplexed photoionization mass spectrometry (MPIMS), which is used to sensitively and selectively probe unimolecular and bimolecular reactions. This work is in collaboration with Craig Taatjes and many scientists from other institutions in the US and abroad. The Sandia-designed MPIMS instrument utilizes tunable vacuum ultraviolet light from the Advanced Light Source synchrotron at Lawrence Berkeley National Laboratory for sensitive, isomer-specific ionization of reactant and product molecules in chemical reactions.

As a complementary approach, we utilize time-resolved Fourier transform spectroscopy (TR-FTS) to probe multiple reactants and products with broad spectral coverage ($> 1000 \text{ cm}^{-1}$), moderate spectral resolution (0.1 cm^{-1}), and a wide range of temporal resolution (ns – ms). The inherently multiplexed nature of TR-FTS makes it possible to simultaneously measure product branching ratios, internal energy distributions, energy transfer, and spectroscopy of radical intermediates. Together with total rate coefficients, this additional information provides further constraints upon and insights into the potential energy surfaces that control chemical reactivity. Because of its broadband nature, the TR-FTS technique provides a global view of chemical reactions and energy transfer processes that would be difficult to achieve with narrow-band, laser-based detection techniques.

RECENT PROGRESS

Isomer-resolved mass spectrometry

The multiplexed chemical kinetics photoionization mass spectrometer operates both at Sandia National Laboratories (using a discharge lamp to create VUV radiation), and at the Chemical Dynamics Beamline of the Advanced Light Source (ALS) synchrotron of LBNL. The chemical reactor is based on the Gutman design,¹ which allows the study of photodissociation and bimolecular reactions at pressures of 1 – 10 Torr and temperatures of 300 – 1000 K.

While the study of chemical kinetics using PIMS is well-established, this apparatus has two unique features that make it especially powerful for chemical kinetics. First, the widely tunable, intense VUV radiation from the ALS enables isomer-specific ionization of product species. Second, the high repetition rate of the mass spectrometer allows us to take snapshots of the complete chemical composition in our reactor as a function of time at a repetition rate of 50 kHz. Mass resolution of $m/\Delta m \sim 1600$ has been achieved using a simple linear (i.e., not

reflectron) approach. This mass resolution has already been used to separate HCCO^+ from C_3H_5^+ (both nominally mass 41), CH_2OO vs. CH_2S , and will be increasingly valuable in separating other $\text{O} \leftrightarrow \text{CH}_4$ substitutions in larger hydrocarbons (e.g., acetone vs. butane, ketene vs. propene) in the chemistry of hydrocarbon oxidation.

The absolute photoionization cross Section of the propargyl (H_2CCCH) radical

The propargyl radical (H_2CCCH) is a key combustion intermediate in molecular weight growth chemistry. As more experiments attempt to measure concentrations of transient intermediates via photoionization, the need for accurate photoionization cross sections grows. However, the absolute number density of a free radical sample is time dependent due to loss via chemical reactions, making it challenging to obtain absolute photoionization cross sections. Our approach follows closely a method used by Neumark and co-workers,² in which a stable, closed-shell precursor molecule is photodissociated, yielding two free radical fragments in a 1:1 ratio, both of which are detected via photoionization. If the absolute photoionization cross section of one radical is known, the cross section of the partner radical may be determined from the ratio of signal strengths, properly corrected for instrumental factors.

For the propargyl radical, we chose two precursors: 1-butyne and 1,3-butadiene, both of which are known to produce $\text{H}_2\text{CCCH} : \text{CH}_3$ in a 1:1 ratio upon 193 nm photodissociation. We utilize the absolute photoionization cross section of the CH_3 radical, which has been measured with good agreement by three independent scientific teams.³ Using the MPIMS spectrometer for this measurement has two important advantages. First, the nascent radicals are thermalized rapidly to 300K via collisions with helium, ensuring that the thermal energy in each radical is small and well-determined. Second, the time-resolved signals of each radical can be used to extrapolate to signals that would be observed immediately following dissociation at $t \sim 0$. We obtain the values $\sigma(10.213 \text{ eV}) = 24.8 \pm 2.8 \text{ Mb}$ and $\sigma(10.413 \text{ eV}) = 24.2 \pm 2.4 \text{ Mb}$. These cross sections are approximately three times larger than the absolute cross section determined from photodissociation of propargyl chloride, in which the Cl atom was the reference radical. In our measurements, both the reference and the unknown radical can be measured at the same photoionization energy, eliminating the need to measure the VUV photon flux, thereby cancelling any systematic errors that may accompany such measurements.

The $\text{O}({}^3\text{P}) + \text{C}_3\text{H}_6$ reaction: Intersystem crossing plays a key role

Reactions of ground state oxygen atoms with unsaturated hydrocarbons are important reactions in some regions of flames. The primary loss channel for acetylene (HCCH) is reaction with $\text{O}({}^3\text{P})$, yielding the major product channel $\text{H} + \text{HCCO}$ and the minor channel ${}^3\text{CH}_2 + \text{CO}$. All evidence (experimental and theoretical) argues that this reaction takes place entirely on the triplet $\text{C}_2\text{H}_2\text{O}$ surface. By contrast, there is significant evidence that the reaction of $\text{O}({}^3\text{P})$ with ethene (C_2H_4) occurs on both the initial triplet and the singlet surface, despite the fact that all the atoms are light. The nonadiabatic interactions leading to the surprisingly facile intersystem crossing (ISC) are still not well understood.

Although the $O(^3P) + C_2H_4$ reaction is an important prototype reaction due to its small size and high degree of symmetry, we have chosen to study the $O(^3P) +$ propene (C_3H_6) reaction, which serves as a gateway to the richer chemical pathways available in larger alkenes. For example, in the propene reaction the oxygen atom may add to the central or the terminal carbon. These distinct entrance channels lead to different reaction pathways, and offer clues to the mechanism of ISC.

We have studied this reaction at a pressure of 4 torr and temperature of 300K, and with partially deuterated propenes for additional mechanistic insight. Under these low pressure conditions, stabilization of the C_3H_6O adduct is disfavored, and bimolecular reaction channels dominate. In addition to the expected $HCO + C_2H_5$ and $CH_3 +$ vinoxy (CH_2CHO) channels, we observe evidence for a new channel producing closed-shell singlet products $H_2 +$ methylketene (CH_3CHCO). This channel must be formed on the singlet potential energy surface and is a marker of intersystem crossing. We also have indirect evidence of the $H +$ methylvinoxy (CH_3CHCHO) channel. Using absolute photoionization cross sections, we determine branching ratios for these reaction channels and consider various pathways for their production in light of descriptions of the C_3H_6O potential energy surface in the literature. There is significant room for improvement in such calculations, and our experiments provide new observables with which new calculations could be compared.

A Direct Spectroscopic Investigation of the quasilinear propargylene diradical

In collaboration with W. C. Lineberger, R. J. McMahon, L. B. Harding, and J. F. Stanton, we have investigated the quasilinear diradical propargylene ($HCCCH$) by negative ion photoelectron spectroscopy and high level electronic structure calculations. Propargylene has been directly observed in low-pressure flames and is a fascinating species from a fundamental perspective. It can be considered as an ethynyl substituted methylene radical, i.e., $HC-CCH$. The richness of its electronic structure arises from the fact that the carbene center could be on either (or both) of the outer carbon atoms, leading to multiple valence bond structures of similar energy.

Previous investigations using cryogenic electron spin resonance and matrix isolation infrared spectroscopy have shown that the ground state of neutral $HCCCH$ is most appropriately described as a 1,3-diradical, yet its reactions resemble that of a carbene. The diradical structure is doubly-allylic, providing additional stabilization, but also leading to rather low frequency bending vibrations and a quasilinear structure. The technique of negative ion photoelectron spectroscopy complements these earlier investigations by allowing us to probe higher vibrational levels in each electronic state, revealing important clues about the shape of the neutral potential energy surfaces. We observe at least 4 electronic states of neutral $HCCCH$, including the $\tilde{X} (^3B)$, $\tilde{a} (^1A)$, and $\tilde{b} (^1B)$ states. This work is currently being prepared for publication.

Future Directions

Using TR-FTS, we will continue to investigate photodissociation reactions that show evidence for roaming dynamics. Following on the recent work of Suits and coworkers⁴ on acetone photodissociation, we plan to study production of C₂H₆ in this system.

A new modification of the MPIMS apparatus is the creation of a low temperature flow tube accessing the temperature range 230 – 300 K. This improvement will allow us to access a much broader range of reciprocal temperature space, providing more stringent tests of global mechanisms in combustion reactions. Our preliminary reactor design is promising, but will require modifications to achieve more uniform temperature profiles.

BES-sponsored publications, 2010 – present

- 1) “Direct kinetic measurements of the Criegee intermediate (CH₂OO) formed by reaction of CH₂I with O₂” O. Welz, J. D. Savee, D. L. Osborn, S. S. Vasu, C. J. Percival, D. E. Shallcross, and C. A. Taatjes, *Science* **335**, 204 (2012).
- 2) “Absolute photoionization cross-sections of some combustion intermediates” B. Yang, J. Wang, T. A. Cool, N. Hansen, S. Skeen, and D. L. Osborn, *International Journal of Mass Spectrometry* **309**, 118 (2012).
- 3) “Branching fractions of the CN + C₃H₆ reaction using synchrotron photoionization mass spectrometry: evidence for the 3-cyanopropene product” A. J. Trevitt, S. Soorkia, J. D. Savee, T. S. Selby, D. L. Osborn, C. A. Taatjes, S. R. Leone, *Journal of Physical Chemistry A* **115**, 13467 (2011).
- 4) “Detection of pentatetraene by reaction of the ethynyl radical (C₂H) with allene (CH₂=C=CH₂) at room temperature” F. Goulay, S. Soorkia, G. Meloni, D. L. Osborn, C. A. Taatjes, and S. R. Leone, *Physical Chemistry Chemical Physics* **13**, 20820 (2011).
- 5) “The products of the thermal decomposition of CH₃CHO” A. Vasilioiu, K. M. Piech, X. Zhang, M. R. Nimlos, M. Ahmed, A. Golan, O. Kostko, D. L. Osborn, J. W. Daily, J. F. Stanton, and G. B. Ellison, *Journal of Chemical Physics* **135**, 014306 (2011).
- 6) “Near-threshold H/D exchange in CD₃CHO photodissociation,” B. R. Heazlewood, A. T. Maccarone, D. U. Andrews, D. L. Osborn, L. B. Harding, S. J. Klippenstein, M. J. T. Jordan, and S. H. Kable, *Nature Chemistry* **3**, 443 (2011).
- 7) “Infrared emission following photolysis of methylisothiocyanate and methylthiocyanate,” E. A. Wade, J. L. Pore, and D. L. Osborn, *J. Phys. Chem. A* **115**, 014306 (2011).
- 8) “Reactions of the CN radical with benzene and toluene: product detection and low temperature kinetics,” A. J. Trevitt, F. Goulay, C. A. Taatjes, D. L. Osborn, and S. R. Leone, *J. Phys. Chem. A* **114**, 1749 (2010).
- 9) “Reaction of the C₂H radical with 1-butyne (C₄H₆): Low temperature kinetics and isomer-specific product detection,” S. Soorkia, A. J. Trevitt, T. M. Selby, D. L. Osborn, C. A. Taatjes, K. R. Wilson, and S. R. Leone, *J. Phys. Chem. A* **114**, 3340 (2010).
- 10) “Products of the benzene + O(³P) reaction,” C. A. Taatjes, D. L. Osborn, T. M. Selby, G. Meloni, A. J. Trevitt, E. Epifanovsky, A. Krylov, B. Sirjean, E. Dames, and H. Wang, *J. Phys. Chem. A* **114**, 3355 (2010).
- 11) “Direct detection of pyridine formation by the reaction of CH (CD) with pyrrole: a ring expansion reaction,” S. Soorkia, C. A. Taatjes, D. L. Osborn, T. M. Selby, A. J. Trevitt, K. R. Wilson, and S. R. Leone, *Phys. Chem. Chem. Phys.* **12**, 8750 (2010).
- 12) “Isomer-selective study of the OH initiated oxidation of isoprene in the presence of O₂ and NO. I. The minor inner OH-addition channel” E. E. Greenwald, B. Ghosh, K. C. Anderson, K. S. Dooley, P. Zou, T. Selby, D. L. Osborn, G. Meloni, C. A. Taatjes, F. Goulay, and S. W. North, *Journal of Physical Chemistry A* **114**, 3355 (2010).

References

- ¹ I. R. Slagle and D. Gutman, *J. Am. Chem. Soc.* **107**, 5342 (1985).
- ² J. C. Robinson, N. E. Sveum, and D. M. Neumark, *Chem. Phys. Lett.* **383**, 601 (2004).
- ³ C. A. Taatjes, D. L. Osborn, T. M. Selby, G. Meloni, H. Y. Fan, and S. T. Pratt, *J. Phys. Chem. A* **111**, 12417 (2008); B. Gans et al., *J. Phys. Chem. A* **114**, 3237 (2010); J. C. Loison, *J. Phys. Chem. A* **114**, 65151 (2010).
- ⁴ V. Goncharov, N. Herath, and A. G. Suits, *J. Phys. Chem. A* **112**, 9423 (2008).

Theoretical Studies of the Combustion Reactions of Asphaltene Model Compounds

Carol A. Parish

Department of Chemistry, University of Richmond

Richmond, VA 23173

cparish@richmond.edu

I. Program Scope

We seek to utilize theoretical methods to understand the gas phase structures and energies of the combustion and pyrolysis reactions of the molecular constituents of asphaltenes contained in oil sand and oil shale. Asphaltenes represent an untapped source of hydrocarbon fuels in North America; however, information about the molecular nature of these deposits has only recently become available.¹ Theoretical and experimental evidence suggests that asphaltenes are composed of molecules that contain 4-10 fused ring cores, with alkyl chain arms extending from the core. Sulfur and nitrogen may also be present.² Very little is known about the reaction pathways of these heteroaromatic species.

II. Summary of Recent Accomplishments Related to the Project

- **Mechanistic Study of the 2-Thienylmethyl + HO₂ Radical Recombination Reaction**

Radical recombination reactions are important in the combustion of fuel oils. Shale oil contains alkylated heteroaromatic species - the simplest example of which is the 2-thienylmethyl radical. The ab initio potential energy surface for the reaction of the 2-thienylmethyl radical with the HO₂ radical has been examined. Seventeen product channels corresponding to either addition/elimination or direct hydrogen abstraction have been characterized for the first time. Direct hydrogen abstract from HO₂ proceeds via a weakly bound van der Waals complex which leads to 2-methyl thiophene, 2-methylene-2,3-dihydrothiophene or 2-methylene-2,5-dihydrothiophene depending upon the 2-thienylmethyl radical reaction site. The addition pathway for the two radical reactants is barrierless with the formation of three adducts, as distinguished by HO₂ reaction at 3 different sites on the 2-thienylmethyl radical. The addition is exothermic by 37 ~ 55 kcal mol⁻¹ relative to the entrance channel and these excess energies are available to promote further decomposition or rearrangement of the adducts, leading to nascent products such as H, OH, H₂O and CH₂O. The reaction surfaces are characterized by relatively low barriers (most lower than 10 kcal mol⁻¹). Based upon a careful analysis of the overall barrier heights and reaction exothermicities, the formation of O₂, OH and H₂O are likely to be important pathways in the radical recombination reactions of 2-thienylmethyl + HO₂.

- **Mechanism for the Reaction of Thiophene and Methylthiophene with Singlet and Triplet Molecular Oxygen**

Mechanisms for the reaction of thiophene and 2-methylthiophene with molecular oxygen on both the triplet and singlet potential energy surfaces (PESs) have been investigated

using ab initio methods. Geometries of various stationary points involved in the complex reaction routes are optimized at the MP2/6-311++G(d, p) level. The barriers and energies of reaction for all product channels were refined using single-point calculations at the G4MP2 level of theory. For thiophene, CCSD(T) single point energies were also determined for comparison with the G4MP2 energies. Thiophene and 2-methylthiophene were shown to react with O₂ via two types of mechanisms, namely, direct hydrogen abstraction and addition/elimination. The barriers for reaction with triplet oxygen are all significantly large (i.e., > 30 kcal mol⁻¹), indicating that the direct oxidation of thiophene by ground state oxygen might be important only in high temperature processes. Reaction of thiophene with singlet oxygen via a 2+4-cycloaddition leading to endoperoxides is the most favorable channel. Moreover, it was found that alkylation of the thiophene ring (i.e., methyl-substituted thiophenes) is capable of lowering the barrier height for the addition pathway. The implication of the current theoretical results may shed new light on the initiation mechanisms for combustion of asphaltenes.

- **Singlet Oxygen (2+4) Cycloaddition to Heteroaromatic Compounds**

The 2+4 cycloaddition reactions of singlet molecular oxygen (¹Δ_g) with a series of aromatic heterocyclic compounds were investigated at both the MP2/6-311++G(d, p) and B3LYP/6-311++G(d, p) levels of theory. Several factors related to heteroaromatic ring structure were determined to affect the activation energy of the cycloaddition and the stability of the corresponding endoperoxide products. Such factors include: (1) the position of methyl substitution; (2) the number of methyl substituents; (3) the alkyl chain length of substituents; (4) the electronic structure of substituents and; (5) the type of heteroatom in the ring. In total, fourteen 2+4 cycloaddition routes were examined and in each case the mechanism is concerted. The order of reactivity toward O₂ (¹Δ_g) was determined to be: 2,3,4,5-tetramethylthiophene > 2,3,5-trimethylthiophene > 2,5-dimethylthiophene > 2-methylthiophene > 2-ethylthiophene > 2-propylthiophene > 3-methylthiophene > thiophene > benzothiophene > dibenzothiophene; and furan > pyrrole > thiophene > benzene. The stability of the endoperoxide products follows a similar trend. Each of the reaction pathways is initiated by the formation of a pre-reactive complex, formed by a van der Waals interaction between a C atom on the ring and an O atom on O₂. To the best of our knowledge, this type of VDW pre-reactive complex has not been identified in previous studies of cycloaddition reactions of singlet oxygen with arenes.

III. Future Work

Work is currently underway to characterize ground and excited states of heteroaromatic diradicals such as thiophene, fulvene and pyrrole. We are also pursuing a complete characterization of the singlet and triplet surfaces of the electrocyclization reaction

of (Z)-hexa-1,3,5-triene leading to *p*-benzyne as well as a characterization of the endo and exo-dig radical cyclization reactions.

IV. References

1. Mullins, O. C.; Sheu, E. Y.; Hammami, A.; Marshall, A. G. *Asphaltenes, Heavy Oils and Petroleomics*; Springer: New York, 2007.
2. Ruiz-Morales, Y.; Wu, X.; Mullins, O. C. *Energy and Fuels* **2007**, *21*, 944-952.

V. Recent publications and journal articles related to the project (undergraduate co-authors underlined).

1. "A Mechanistic Study of the 2-Thienylmethyl + HO₂ Radical Recombination Reaction," Xinli Song and Carol Parish,* *Journal of Physical Chemistry A*, **2011**, *115*, 14546-14557.

VI. Other recent publications and journal articles (undergraduate co-authors underlined).

1. "Halogen bonding in DNA base pairs," Anna J. Parker, John Stewart, Kelling Donald* and Carol Parish,* *Journal of the American Chemical Society*, **2012** *134*, 5165-5172.
2. "Evidence that the kinesin light chain contains tetratricopeptide repeat units." Sally Q. Fisher, Meredith Weck, Jenna E. Landers, Jeffrey Emrich, Shana A. Middleton, Jordan Cox, Lisa N. Gentile and Carol A. Parish,* *Journal of Structural Biology*, **2012**, *177*, 602-612.
3. "Challenging Disciplinary Boundaries in the First-Year: A New Introductory Integrated Science Course for STEM Majors", Gentile, L.*; Caudhill, L.; Fetea, M.; Hill, A.; Hoke, K.; Lawson, B.; Lipan, O.; Kerckhove, M.; Parish, C.; Stenger, K.; Szajda, D., "Challenging Disciplinary Boundaries in the First-Year: A New Introductory Integrated Science Course for STEM Majors," *Journal of College Science Teaching*, **2012**, *41*(5), 24-30.
4. "(rac)- 1,1'-Binaphthyl-based simple receptors designed for fluorometric discrimination of maleic and fumaric acids," Kumaresh Ghosh,* Tanushree Sen, Amarnedra Patra, John S. Mancini, Justin M. Cook and Carol A. Parish,* *Journal of Physical Chemistry B*, **2011**, *115*, 8597-8608.

The Dynamics of Large-Amplitude Motion in Energized Molecules

David S. Perry, Principal Investigator
Department of Chemistry, The University of Akron
Akron OH 44325-3601
DPerry@UAkron.edu

I. Program Scope

Chemical reactions, by definition, involve large-amplitude nuclear motion along the reaction coordinate that serves to distinguish reactants from products. Some reactions, such as roaming reactions and reactions proceeding through a loose transition state, involve more than one large amplitude degree of freedom. In principle, the exact quantum nuclear dynamics may be calculated, but such calculations are limited by practical considerations to a few degrees of freedom. Thus in systems larger than 3 or 4 atoms, one must define the active degrees of freedom and separate them in some way from the other degrees of freedom. In this project, we use large-amplitude motion in bound model systems to investigate the coupling of large-amplitude degrees of freedom to other nuclear degrees of freedom. This approach allows us to use the precision and power of high-resolution molecular spectroscopy to probe the specific coupling mechanisms involved, and to apply the associated theoretical tools. In addition to cavity ringdown experiments and calculations at the University of Akron, work on this project involves collaboration with Brooks Pate's group at the University of Virginia (CD-FTMW-IR spectroscopy of methanol and methylamine) and with Michel Herman of the Université Libre de Bruxelles (rotationally dependent vibrational dynamics of acetylene). The concepts developed in this project are finding application to the coupled torsional motions in poly(3-hexylthiophene) oligomers.

II. Recent Progress

A. Two-Dimensional Large-Amplitude Motion

The two-dimensional torsion-inversion potential energy surfaces of methylamine, protonated methanol, and ethyl radical have been investigated with partially optimized *ab initio* calculations [2]. All three molecules belong to the G_{12} molecular symmetry group and each has six equivalent minima. CH_3NH_2 has a high barrier to inversion ($\sim 1950 \text{ cm}^{-1}$), whereas in CH_3OH_2^+ the barrier is lower ($\sim 875 \text{ cm}^{-1}$). In $\text{CH}_3\text{CH}_2\cdot$, there is no barrier to inversion. The torsional barriers in these systems are about 704, 400, and 21 cm^{-1} respectively. The computed torsion-inversion surfaces were fit to a function of the form (Fig. 1),

$$V(\alpha, \tau) = \sum_{n=0}^4 \sum_{m=0}^{12} V_{m,3n} \tau^m \cos(3n\alpha), \quad (1)$$

where α , is the torsional angle, τ is the inversion angle, and $m+n = \text{even}$. Even though the three surfaces are quite different (Fig. 1(a)), we find that the torsion-inversion coupling is similar in strength (Fig. 1(b)). The dominant

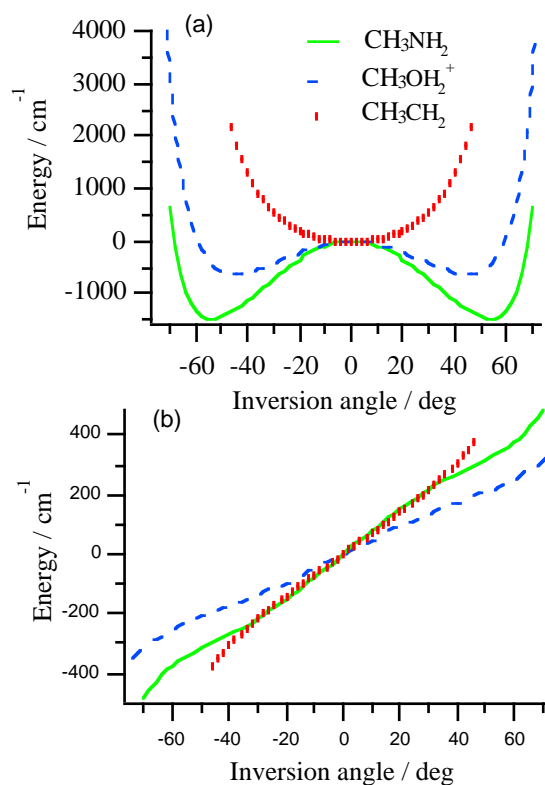


Fig. 1. *Ab initio* results at the CCSD(T)/6-311++G(3df,2p)//MP2/6-311++G(3df,2p) level on three CH_3XH_2 molecules. (a) The torsionally invariant part ($V_{m,0}$ terms) of the fitted potentials. (b) The $\cos 3\alpha$ part of the torsion-inversion coupling ($V_{m,3}$ terms).

torsion-inversion coupling term in all three cases has the form, $V_{1,3}\tau \cos 3\alpha$, with $V_{1,3}$ in the range 280 to 450 cm^{-1} .

The synthesis these results with those on methanol indicates that the coupling terms, whether torsion-vibration or torsion-inversion, have typical values that vary by less than a factor of two in a range of systems where the barriers to torsion or inversion vary by orders of magnitude.

Methylamine is our experimental prototype for these six-well G_{12} systems. Results to date include high-resolution slit-jet spectra of the ν_{11} asymmetric CH stretch (2965-3005 cm^{-1}) and the first FTMW-IR spectra in the ν_3 symmetric CH stretch region (Fig. 2). Whereas there is a single vibrational band in the ν_{11} region, Fig. 2 shows four distinct vibrational bands in the ν_3 region. The extra bands in the ν_3 region likely result, as in methanol [5,6], from interactions with bending combinations that serve as “doorway” states for intramolecular vibrational redistribution (IVR).

The torsion and inversion tunneling splittings in these bands contain information about the coupling the upper state vibrations to the large-amplitude degrees of freedom. The tunneling pattern involves four distinct species in the G_{12} group and the resultant splitting pattern is illustrated for the ground state on methylamine in Fig. 3. Our high resolution spectra for ν_{11} yield a pattern ($E_2 < A < B < E_1$) qualitatively different from the allowed range of patterns for the ground state. We have developed two different models of the torsion-inversion-vibration coupling, both of which also give patterns different from the ground state, but neither one agrees with the ν_{11} experiment. We are developing 5-dimensional quantum calculations of the nuclear motion on an ab initio potential energy surface to produce a first-principles result to compare with experiment.

B. Spectroscopy and Torsion-Vibration Coupling in the CH Stretch Region of Methanol

The three CH stretch fundamentals of methanol have been resolved at high resolution and assigned in detail, and those results have formed the foundation of our understanding of the torsion-vibration interactions in methanol. Nonetheless, there is a great deal of additional spectral complexity in

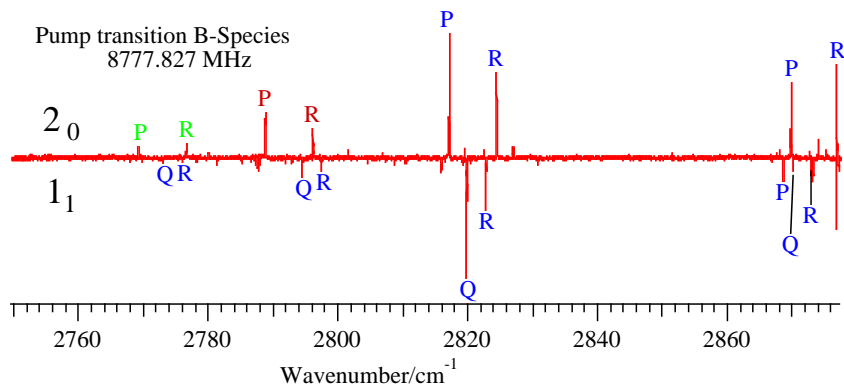


Fig. 2. Rotationally selected infrared spectrum of methylamine obtained at the University of Virginia with the coherence-converted population transfer Fourier transform microwave infrared technique (CCPT-FTMW-IR or FTMW-IR). The selected rotational states are $J_K = 2_0$ and 1_1 for the upward and downward pointing lines respectively.

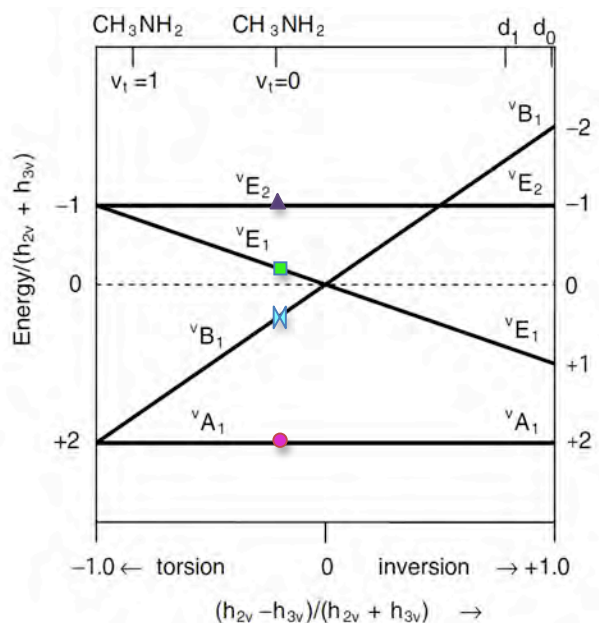
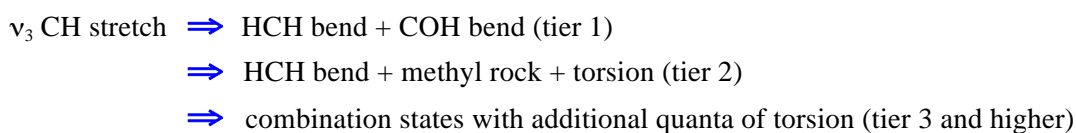


Fig. 3. The range of possible torsion-inversion tunneling patterns in G_{12} molecules according to Ilyushin, V. V., et al. [J. Mol. Spectrosc. 251(2008) 56]. The points indicate the observed ground state pattern for methylamine.

this region. To understand the responsible interactions, a new experimental technique for rotationally selected infrared spectra has been applied to obtain assignments for dozens of additional vibrational bands in the range 2700 – 3000 cm^{-1} for the E species of CH_3OH [5, 6] and CH_3OD [4].

The technique, developed at the University of Virginia, is coherence-detected Fourier transform microwave – infrared spectroscopy (CD-FTMW-IR). Population transfer induced by a pulsed IR laser is detected by FTMW spectroscopy using a sequence two microwave pulses. The first pulse converts the thermal population difference to a coherence using an approximate “ $\pi/2$ ” pulse. Then, an IR laser pulse interacts with the polarized sample. Finally, second microwave pulse with a 180° phase shift is applied to perform a “ $-\pi/2$ ” excitation. The sequence of two microwave pulses produces a null signal in the absence of the IR pulse and hence a flat baseline upon which the state-detected infrared transitions are observed.

In the ν_3 symmetric CH stretch region (2750 - 2890 cm^{-1}) of CH_3OH , a total of 12 interacting vibrations are observed [5]. By contrast, this region of CH_3OD is almost unperturbed. The pattern of the combined spectra can be explained by the following coupling pathway:



The higher frequency regions of both CH_3OH and CH_3OD (2890 - 3020 cm^{-1}) contain the asymmetric CH stretches (ν_2 and ν_9) plus 14 additional bands in each case that have been rotationally assigned [6]. The number of observed vibrational bands indicates that the CH stretch bright states couple first to the binary CH bend combinations, and then to higher order combinations of the normal modes, including torsional excitation.

The time-dependent interpretation of the frequency-resolved spectra shows three IVR time scales [6]. The fastest two time scales (~ 200 fs and 1-3 ps) are in qualitative agreement with the liquid phase time-resolved data, suggesting a common mechanism for the fastest relaxation processes in the liquid and gas phases. At longer times (>5 ps), the processes in the two phases necessarily differ because of energy transfer to solvent molecules in the liquid phase.

The OD stretch fundamental of CH_3OD (2710 - 2736 cm^{-1}) has resolved and assigned [4].

C. Rotational Dependence of the Intramolecular Dynamics in Acetylene

Acetylene high resolution infrared spectra (17,625 lines) have been analyzed and fit with precision up to 8900 cm^{-1} including high rotational levels [Amyay, B.; Herman, M.; Fayt, A.; Campargue, A.; Kassi, S. *J. Mol. Spectrosc.* 2011, 267, 80]. As part of this collaboration, the Herman group has extended the fit (882 additional lines) up to 13,000 cm^{-1} . The resulting spectroscopic Hamiltonian in the normal mode basis contains 155 off-diagonal terms representing four different coupling types: (i) anharmonic, (ii) vibrational l -resonance, (iii) rotational l -resonance, and (iv) Coriolis [3]. All of these couplings conserve the polyad quantum number, $N_r \equiv 5\nu_1 + 3\nu_2 + 5\nu_3 + \nu_4 + \nu_5$, and the ef and g/u symmetries. The rotational l -resonance couples states with differing values of the total vibrational angular momentum, $k = l_4 + l_5$. Only the Coriolis coupling mixes states with different numbers of stretching quanta, $N_s \equiv \nu_1 + \nu_2 + \nu_3$.

This detailed Hamiltonian provides an unprecedented opportunity to study the vibration-rotational dynamics up into the energy range above the onset of new kinds of vibrational motion, such as the local CH stretch, the local bender, and the counter rotator [work in this program by the Kellman and Field groups]. By computing time-dependent wavefunctions following different kinds of coherent excitations, we find hierarchies of sequentially coupled states that are populated on timescales ranging from 20 fs to 20 ps. The dynamics are mode-dependent with interior states relaxing faster than edge states, and the

local bender relaxing faster than the counter-rotator. The highest polyad investigated, $\{N_r = 18, e, g\}$ includes more than 1,400 coupled states. The time-dependent volume of phase space explored is measured both by the participation number and by the Shannon entropy. Since the Coriolis coupling is relatively weak, there are bottlenecks that result in slower and less complete exploration of parts of phase space that have different numbers of stretching quanta (Fig. 4).

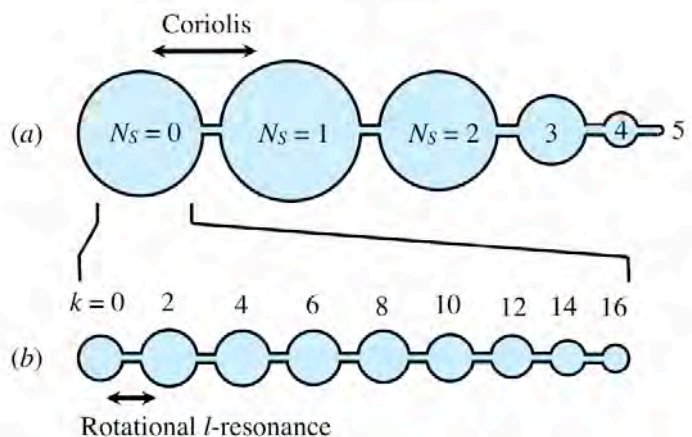


Fig. 4. Schematic of the acetylene phase space in the $N_r = 16$ polyad. Bottlenecks indicate weaker couplings. The areas of circles are proportional to the number of states in each region.

III. Future Work

The development of the continuous-wave cavity ringdown (CW-CRDS) and CD-FTMW-IR techniques will continue, targeting experiments on the CH manifolds in methylamine and methanol. The extension of the CD-FTMW-IR technique to the 48 GHz range has been tested and new capability for using high-frequency rotational transitions (~ 260 GHz) is being developed in the Pate group targeting applications to methanol and methylamine. The calculations on the CH_3XH_2 systems will be extended to include the coupling of the two large amplitude motions to CH stretch vibrations.

IV. Publications from this Project, 2009-2011

- [1] David S. Perry, The Adiabatic Approximation as a Diagnostic Tool for Torsion-Vibration Dynamics, *J. Mol. Spectrosc.* **257**(1), 1-10, 2009 (feature article), <http://dx.doi.org/10.1016/j.jms.2009.05.002>.
- [2] Ram S Bhatta, Amy Gao, David S Perry, A comparative ab initio study of torsion-inversion coupling in CH_3NH_2 , CH_3OH_2^+ and CH_3CH_2 , *J. Mol. Struct.: THEOCHEM* **941**, 22-29, 2009, <http://dx.doi.org/10.1016/j.theochem.2009.10.033>.
- [3] David Perry, Anthony Miller, B. Amyay, A. Fayt and M. Herman, Vibration-rotation alchemy in acetylene ($^{12}\text{C}_2\text{H}_2$), $X^1\Sigma_g^+$ at low vibrational excitation: From high resolution spectroscopy to fast intramolecular dynamics (invited article), *Mol. Phys.* **108**, 1115-1132, 2010, <http://dx.doi.org/10.1080/00268971003660874>.
- [4] Sylvestre Twagirayezu, David S. Perry, Justin L Neill and Matt T Muckle, Coherence-converted population transfer FTMW-IR double resonance spectroscopy of CH_3OD in the OD -stretch region, *J. Mol. Spectrosc.* **262**, 65-68 (2010), <http://dx.doi.org/10.1016/j.jms.2010.05.003>.
- [5] Sylvestre Twagirayezu, Trocia N. Clasp, David S. Perry, Justin L. Neill, Matt T. Muckle, Brooks H. Pate, Vibrational coupling pathways in methanol as revealed by coherence-converted population transfer FTMW-IR double resonance spectroscopy, *J. Phys. Chem. A* **114**, 6818-6828 (2010), <http://dx.doi.org/10.1021/jp1019735>.
- [6] Sylvestre Twagirayezu, Xiaoliang Wang, David S. Perry, Justin L. Neill, Matt T. Muckle, Brooks H. Pate, Li-Hong Xu, IR and FTMW-IR Spectroscopy and Vibrational Relaxation Pathways in the CH Stretch Region of CH_3OH and CH_3OD , *J. Phys. Chem. A* **115**, 9748-9763 (2011), <http://dx.doi.org/10.1021/jp202020u>.

New Single- and Multi-Reference Coupled-Cluster Methods for High Accuracy Calculations of Ground and Excited States

Piotr Piecuch

Department of Chemistry, Michigan State University
East Lansing, MI 48824
piecuch@chemistry.msu.edu

I. Program Scope

This research program focuses on the development and applications of new generations of *ab initio* electronic structure methods and computer codes, exploiting the exponential coupled-cluster (CC) wave function ansatz, which can provide an accurate description of chemical reaction pathways, radicals, biradicals, potential energy surfaces (PESs), properties other than energy, and electronic excitations in molecular species. The goal is to design and apply affordable computational methods that enable precise modeling of molecular processes and properties relevant to combustion, catalysis, light harvesting, photochemistry, and photobiology. Among the most promising methods developed in this program are (i) the renormalized CC and equation-of-motion CC (EOMCC) approaches, and the low-order scaling, local correlation extensions of the conventional and renormalized CC methods to larger molecular systems involving hundreds of correlated electrons, (ii) the active-space CC and EOMCC methods, and (iii) the genuine multi-reference CC (MRCC) theories. The main focus is on methods that can balance high accuracy with the relative ease of use and relatively low computer costs compared to other quantum-chemistry approaches that aim at similar accuracies, so that one can study chemical processes and phenomena involving complex molecular problems with dozens or hundreds of non-hydrogen atoms, in addition to the more traditional smaller systems. The renormalized CC methods and their open-shell, local correlation, and excited-state generalizations extend the standard single-reference theories to multi-reference situations created by radicals, biradicals, bond breaking, and two-electron excitations with an ease of a black-box calculation that can be performed by non-experts. The active-space CC and EOMCC approaches, and their open-shell generalizations via the electron attached (EA) and ionized (IP) theories as well as the genuine MRCC methods have the flexibility that enables accurate *ab initio* calculations for all kinds of closed- and open-shell electronic states, with manageable computer costs, including systems characterized by strong electronic near-degeneracies that cannot be handled by single-reference approaches. All methods pursued in this program can effectively utilize modern multi-node computer architectures and are well suited for pursuing novel coding strategies, such as the automated and parallel computer implementations. They address two main challenges of electronic structure theory, which are (i) the development of practical and systematically improvable computational schemes that can provide a balanced and accurate description of closed- and open-shell systems, and the rapidly changing electron correlation effects along reaction coordinates and in electronic excitations, and (ii) the development of algorithms that can reduce prohibitive costs of traditional high-accuracy *ab initio* calculations by orders of magnitude by directly attacking the scaling laws that define the dependence of computer costs on the system size. Methods developed in this program are shared with the community by incorporating them in the GAMESS package.

II. Recent Progress (2010-2012)

We introduced the generalization of the previously developed biorthogonal method of moments of coupled-cluster (MMCC) equations that resulted in the left-eigenstate completely renormalized (CR) CC or EOMCC approaches, such as CR-CC(2,3) or CR-EOMCC(2,3) [4,6,8,11,14], which enables one to correct the CC/EOMCC energies obtained with the arbitrary, conventional as well as unconventional, truncations in the cluster operator T and the EOM excitation operator R_μ for essentially any subset of the missing many-electron correlation effects of interest [11,12]. The resulting moment expansions, defining the Flex-MMCC and CC($P;Q$) formalisms [11,12], enable one to contemplate a variety of novel *ab initio* schemes for high accuracy calculations of ground- and excited-state molecular PESs. Among them is the CC($t;3$), CC($t,q;3$), CC($t,q;3,4$), etc. hierarchy, in which energies obtained in the active-space CC/EOMCC calculations (see [5] for a review), such as CCSDt/EOMCCSDt or CCSDtq/EOMCCSDtq,

which recover much of the non-dynamical and some dynamical electron correlation effects, are corrected for the higher-order, primarily dynamical, correlations, such as triples (3) or triples and quadruples (3,4) missing in the active-space CC/EOMCC considerations, using the non-iterative corrections which are operationally similar to those of CR-CC/CR-EOMCC [11,12]. The potential advantages of the Flex-MMCC and CC($P;Q$) formalisms were illustrated by the numerical tests of the new CC(t;3) scheme, in which one corrects the results of the CC calculations with singles, doubles, and active-space triples, termed CCSDt, for the remaining effects due to connected triple excitations missing in CCSDt [11,12]. By examining bond breaking in the HF, F₂, and F₂⁺ molecules, and challenging MR problems of the automerization of cyclobutadiene and isomerization of bicyclo[1.1.0]butane to trans-but-1,3-diene involving strongly biradical transition states, we showed that CC(t;3) greatly improves the CCSD(T), CCSD(2)_T, Λ -CCSD(T), CR-CC(2,3), CCSDt, and CCSD(T)-h results, providing PESs that agree with those obtained with full CCSDT to within ~ 0.1 millihartree for total energies and ~ 0.1 kcal/mol for relative energies at the small fraction of the computer costs of the CCSDT calculations, which are competitive with the sophisticated MRCC and Quantum Monte Carlo (QMC) calculations.

We implemented the rigorously size-intensive modification of the previously developed (see [11,14] for reviews) CR-EOMCC(2,3) approach, termed δ -CR-EOMCC(2,3) [6,8], which corrects the EOMCCSD energies for the effect of triple excitations using the non-iterative N^7 steps similar to those used in CCSD(T) and CR-CC(2,3), offering great improvements in the EOMCCSD results. The δ -CR-EOMCC(2,3) codes, along with the extension of the EOMCCSD routines to open shells, were incorporated in GAMESS as additions to a variety of the CC and EOMCC options that we developed for GAMESS in the past. In our continuing effort to examine the utility of the CR-EOMCC methodology, we showed that CR-EOMCC(2,3) provides excellent results for the low-lying singlet and triplet states of biradical species, such as methylene, where the CR-EOMCC(2,3) results for the adiabatic excitation and total energies extrapolated to the complete basis set limit, including states dominated by two-electron transitions, are in perfect agreement with the converged QMC and the available experimental data, eliminating, in particular, large errors in the EOMCCSD results [4]. We used the δ -CR-EOMCC(2,3) approach to examine shifts in the $\pi \rightarrow \pi^*$ excitation energy in cis-7-hydroxyquinoline (cis-7HQ) induced by hydrogen bonding, on the order of 500-2000 cm⁻¹, along with the corresponding excitation energies, on the order of 30,000 cm⁻¹, obtained in the frozen-density embedding theory (FDET) and supermolecular time-dependent density functional theory (TDDFT) calculations, and in experiment [6,8]. By considering eight complexes of cis-7HQ with up to three small hydrogen-bonded molecules, we demonstrated that the spectral shifts resulting from the FDET calculations employing non-relaxed environment densities and their δ -CR-EOMCC(2,3) counterparts are in excellent agreement with one another and experiment (to within 100 cm⁻¹ or 15 % on average), whereas the analogous shifts obtained in the supermolecular TDDFT calculations do not agree with the δ -CR-EOMCC(2,3) data, producing large errors (39% on average). The δ -CR-EOMCC(2,3) excitation energies match the experimental ones to within a few hundred cm⁻¹. We have continued applying the CR-CC/CR-EOMCC methods to important chemical and spectroscopic problems, including, for example, accurate modeling of JP-10 (*exo*-tetrahydrodicyclopentadiene) high temperature oxidation [10], and incorporated CR-CC(2,3), as a substitute for conventional CCSD(T), into a correlation consistent composite approach (ccCA) for thermodynamic properties and reaction paths [13]. We demonstrated that the new ccCA-CC(2,3) method, incorporated in GAMESS, produces a mean absolute deviation of 1.7 kcal/mol for predicted heats of formation at 298 K, based on calibration with the G2/97 set of 148 molecules, while significantly improving the performance of the CCSD(T)-based ccCA approaches in calculations involving more demanding radical and diradical species [13]. We also used the EOMCC methodology, along with a variety of MR and TD-DFT methods, to provide insights into the electronic structure of the low-lying excited states of methylcobalamin, showing that its S_1 state should be interpreted as the metal-to-ligand charge transfer transition, in agreement with transient absorption spectroscopy measurements [16].

We have continued our work on extending the active-space CC and EOMCC theories, reviewed in [5], to ground and excited states of radicals and other valence systems by combining them with the

EA/IP EOMCC methodology [5,7,9]. We demonstrated an excellent performance, in terms of accuracy and computational efficiency, of the active-space EA-EOMCCSD(3p2h) and IP-EOMCCSD(3h2p) approaches in calculations of the excitation energies in CNC, C₂N, N₃, and NCO, where some of the low-lying excited states have a significant MR character, particularly in the case of CNC and C₂N, causing major problems to EOMCCSD and EA-EOMCCSD(2p1h). We showed that the active-space EA/IP EOMCC schemes, which use small subsets of higher-than-2p1h and 2h1p excitations, reproduce the results of their parent methods, where all such excitations are included, while requiring a computational effort similar to CCSD. This applies to excitation energies and ground- and excited-state geometries [7]. We completed our work on incorporating the EA-EOMCCSD(2p1h), IP-EOMCCSD(2h1p), and full and active-space EA-EOMCCSD(3p2h) and IP-EOMCCSD(3h2p) codes in the official GAMESS distribution. This allowed us to perform the scalar relativistic IP- and EA-EOMCC calculations with up to 3h2p and 3p2h excitations, using the spin-free part of the second-order Douglas-Kroll-Hess (DKH2) Hamiltonian, along with the corresponding SAC-CI calculations, for the valence excitation spectra of the CuCl₄²⁻ and CuBr₄²⁻ complexes [9]. We demonstrated that the DKH2-based IP-EOMCC and SAC-CI methods reproduce the observed UV-vis photoabsorption spectra of CuCl₄²⁻ and CuBr₄²⁻ in both peak positions and intensities, allowing us to provide a rigorous assignment of the observed strong bands and weaker shoulder transitions, and showing that relativity affects excitation energies and geometries.

We have continued our work on the development of the local correlation CCSD, CCSD(T), and CR-CC(2,3) approaches, and their multi-level extensions, which exist under the common term of ‘cluster-in-molecule’ (CIM) methods [1-3,15]. The resulting CIM-CCSD, CIM-CCSD(T), and CIM-CR-CC(2,3) methods, and their CIM-MP_n analogs use orthonormal localized orbitals and enable high-accuracy calculations for systems with hundreds of correlated electrons. Our CIM-CC and CIM-MP2 codes, which we have incorporated in the GAMESS package (the official release planned in the future), are characterized by the linear scaling of the CPU time with the system size when a single-level CIM-CC or CIM-MP2 approach is used, memory requirements that do not grow with the size of the system, coarse-grain parallelism, which can be further enhanced by the fine-grain parallelism of each CIM subsystem calculation, and the purely non-iterative character of the local triples and other perturbative corrections to correlation energy. They enable one to combine affordable canonical *ab initio* calculations, such as MP2 or CCSD, with a local CIM approach to handle higher-order correlation effects, such as the triples corrections of CCSD(T) and CR-CC(2,3) [15]. Another possibility is represented by the intrinsically multi-level local correlation theories exploiting the CIM framework that combine high-level CC methods, such as CR-CC(2,3), to treat, for example, the reactive part of a large molecular system with the lower-order (e.g., MP2) scheme(s) to handle the chemically inactive regions without splitting it into *ad hoc* fragments and saturating dangling bonds [1]. We applied CIM-CR-CC(2,3), combined with the embedded cluster QM/MM method called SIMOMM, to the etching and diffusion of atomic oxygen on the Si(100) surface, obtaining accurate information about the activation barriers and energetics characterizing these processes [3]. Thanks to the use of CIM-CC, we could perform the CR-CC(2,3)-level calculations for clusters as large as Si₁₅H₁₆O [3]. The results of multi-level CIM-CC/MP2 calculations for bond breaking in large alkanes and the reactions between the bis(2,4,4-trimethylpentyl)dithiophosphinic acid and water or water dimer (important for nuclear waste management) are outstanding [1]. We also performed the unprecedented calculations for the Co-methyl bond dissociation in methylcobalamin [15]. Our local CIM-CR-CC(2,3) method combined with canonical CCSD allowed us to produce the entire Co-methyl bond breaking curve and the dissociation energy in the 37-38 kcal/mol range. Experiment gives 37±3 or 36±4 kcal/mol, and DFT approaches give all kinds of values between -2 and 41 kcal/mol. Thanks to the availability of the CR-CC(2,3)-level results, obtained with the help of CIM, we were able to provide recommendations regarding the proper way of performing DFT calculations for cobalamins and information about the suitable choices of active orbitals for MR calculations [15]. We improved the orbital subsystem design in the CIM-CC methodology, which is particularly relevant for large weakly bound molecular clusters, while helping the description of covalently bound systems [2].

III. Immediate Future Plans (2012/2013)

- Development of the active-space doubly electron attached (DEA) and ionized (DIP) EOMCC methods.

- Development of hybrid CC and EOMCC schemes based on the CC($P;Q$) formalism.
- Development of the PES extrapolation procedure based on the concept of correlation energy scaling that uses lower-order methods to calculate correlation energy scaling factors for high-level calculations.
- New studies of radical and biradical reactions, and molecular electronic spectra.

IV. Publications and submitted journal articles supported by this project (2010-2012)

1. W. Li and P. Piecuch, "Multi-level Extension of the Cluster-in-Molecule Local Correlation Methodology: Merging Coupled-Cluster and Møller-Plesset Perturbation Theories," *J. Phys. Chem. A* **114**, 6721-6727 (2010).
2. W. Li and P. Piecuch, "Improved Design of Orbital Domains within the Cluster-in-Molecule Local Correlation Framework: Single-Environment Cluster-in-Molecule Ansatz and its Application to Local Coupled-Cluster Approach with Singles and Doubles," *J. Phys. Chem. A* **114**, 8644-8657 (2010).
3. P. Arora, W. Li, P. Piecuch, J.W. Evans, M. Albao, and M.S. Gordon, "Diffusion of Atomic Oxygen on the Si(100) Surface," *J. Phys. Chem. C* **114**, 12649-12658 (2010).
4. J.R. Gour, P. Piecuch, and M. Włoch, "Comparison of the Completely Renormalized Equation-of-Motion Coupled-Cluster and Quantum Monte Carlo Results for the Low-Lying Electronic States of Methylene," *Mol. Phys.* **108**, 2633-2646 (2010).
5. P. Piecuch, "Active-space coupled-cluster methods," *Mol. Phys.* **108**, 2987-3015 (2010).
6. G. Fradelos, J.J. Lutz, T.A. Wesolowski, P. Piecuch, and M. Włoch, "Embedding vs Supermolecular Strategies in Evaluating the Hydrogen-Bonding-Induced Shifts of Excitation Energies," *J. Chem. Theory Comput.* **7**, 1647-1666 (2011).
7. J.A. Hansen, P. Piecuch, J.J. Lutz, and J.R. Gour, "Geometries and Adiabatic Excitation Energies of the Low-Lying Valence States of CNC, C₂N, N₃, and NCO Studied with the Electron-Attached and Ionized Equation-of-Motion Coupled-Cluster Methodologies," *Phys. Scr.* **84**, 028110 (2011) (17 pp).
8. G. Fradelos, J.J. Lutz, T.A. Wesolowski, P. Piecuch, and M. Włoch, "Shifts in Excitation Energies Induced by Hydrogen Bonding: A Comparison of the Embedding and Supermolecular Time-Dependent Density Functional Theory Calculations with the Equation-of-Motion Coupled-Cluster Results," in: *Progress in Theoretical Chemistry and Physics*, Vol. 22, edited by P.E. Hoggan, E. Brändas, J. Maruani, P. Piecuch, and G. Delgado-Barrio (Springer, Dordrecht, 2012), pp. 219-248.
9. M. Ehara, P. Piecuch, J.J. Lutz, and J.R. Gour, "Symmetry-Adapted-Cluster Configuration-Interaction and Equation-of-Motion Coupled-Cluster Studies of Electronically Excited States of Copper Tetrachloride and Copper Tetrabromide Dianions," *Chem. Phys.*, in press, corrected proof (2012); accepted manuscript available online 29 September 2011, doi:10.1016/j.chemphys.2011.09.022.
10. G.R. Magoon, J. Aguilera-Iparraguirre, W.H. Green, J.J. Lutz, P. Piecuch, O.O. Oluwole, and H.-W. Wong, "Detailed Chemical Modeling of JP-10 (*exo*-tetrahydrodicyclopentadiene) High Temperature Oxidation: Exploring the Role of Biradical Species in Initial Decomposition Steps," *Int. J. Chem. Kin.* **44**, 179-193 (2012).
11. J. Shen and P. Piecuch, "Biorthogonal Moment Expansions in Coupled-Cluster Theory: Review of Key Concepts and Merging the Renormalized and Active-Space Coupled-Cluster Methods," *Chem. Phys.*, in press (2012); accepted manuscript available online 3 December 2011, doi:10.1016/j.chemphys.2011.11.033.
12. J. Shen and P. Piecuch, "Combining Active-Space Coupled-Cluster Methods with Moment Energy Corrections via the CC($P;Q$) Methodology, with Benchmark Calculations for Biradical Transition States," *J. Chem. Phys.* **136**, 144104-1 - 144104-16 (2012).
13. S.A. Nedd, N.J. De Yonker, A.K. Wilson, P. Piecuch, and M.S. Gordon, "Incorporating a Completely Renormalized Coupled Cluster Approach into a Composite Method for Thermodynamic Properties and Reaction Paths," *J. Chem. Phys.* **136**, 144109-1 - 144109-13 (2012).
14. P. Piecuch, M. Włoch, J.R. Gour, W. Li, and J.J. Lutz, "Dealing with Chemical Reaction Pathways and Electronic Excitations in Molecular Systems via Renormalized and Active-Space Coupled-Cluster Methods," in: AIP Conference Proceedings, Vol. XXX, edited by T.E. Simos and G. Maroulis (American Institute of Physics, Melville, NY, 201X), pp. XX-XXX, in press.
15. P.M. Kozłowski, M. Kumar, P. Piecuch, W. Li, N.P. Bauman, J.A. Hansen, P. Lodowski, and M. Jaworska, "The Cobalt-Methyl Bond Dissociation in Methylcobalamin: New Benchmark Analysis Based on Density Functional Theory and Completely Renormalized Coupled-Cluster Calculations," *J. Chem. Theory Comput.*, Just Accepted Manuscript, doi: 10.1021/ct300170y, Publication Date (Web): 17 April 2012.
16. K. Kornobis, N. Kumar, P. Lodowski, M. Jaworska, P. Piecuch, J.J. Lutz, B.M. Wong, and P.M. Kozłowski, "Electronic Structure of the S₁ State in Methylcobalamin: Insight from CASSCF/MC-XQDPT2, EOM-CCSD, and TD-DFT Calculations," *J. Chem. Theory Comput.*, submitted, in revision (2012).

Kinetic Modeling of Combustion Chemistry

W.J. Pitz and C. K. Westbrook
Physical and Life Sciences Directorate
Lawrence Livermore National Laboratory
Livermore, CA 94550
pitz1@llnl.gov

I. Program Scope

We develop chemical kinetic reaction mechanisms to describe the combustion of hydrocarbon and biofuels. These mechanisms are validated through comparisons between computations and experiments in carefully controlled laboratory-scale facilities including laminar flames, shock tubes, stirred reactors and rapid compression machines, then used to understand more complex combustion phenomena in practical engines and other combustion systems. Chemical systems and fuels are chosen for analysis because they represent practical fuels used in transportation and other energy devices. We strive to identify key reactions that need further study by DOE BES researchers. We do attempt to anticipate kinetic modeling needs of the DOE combustion community, so other researchers can have useful reaction mechanisms to use in their programs. Our resulting kinetic mechanisms are routinely available on the LLNL web page at https://www-pls.llnl.gov/?url=science_and_technology-chemistry-combustion and provide a valuable service to the combustion community.

II. Recent Progress

A. Chemical kinetic modeling of biofuels

During the past several years, we have extended our kinetic modeling capabilities to model the reactions in large methyl ester fuels which are the primary components of biodiesel fuels [3,6,9]. Many biodiesel fuels consist almost entirely of the same five methyl esters: methyl palmitate, methyl stearate, methyl oleate, methyl linoleate and methyl linolenate. Last year we published the first chemical kinetic model for all these components. Subsequently, we have used this model to simulate many different types of biodiesel derived from vegetable oils and animal fat [9]. Using jet stirred reactor (JSR) simulations, we were able to correlate the fuel conversion of different types of biodiesel with cetane number, which is used to rate ignition properties of diesel fuels. Fuel conversion at low temperature is controlled by the relative amounts of the five methyl esters that comprise the biodiesel fuel. Three of the five methyl esters are unsaturated, containing double bonds on the long carbon chain of the methyl ester component. These double bonds inhibit low temperature chemistry because of the low R-O₂ bond strength at the allylic sites. Biodiesel fuels such as linseed oil with large amounts of unsaturated methyl esters (dotted line in Fig. 1), have low conversion rates with limited low temperature chemistry and relatively low cetane numbers. Biodiesel fuels like palm oil with large amounts of methyl esters with no double bonds on the carbon chain (like methyl palmitate and methyl stearate) have ample low temperature chemistry with high conversion rates in the JSR relevant to diesel engine ignition and high cetane numbers. This can be seen by the computed fuel conversion curve of palm oil methyl ester represented by the dashed line in Fig. 1.

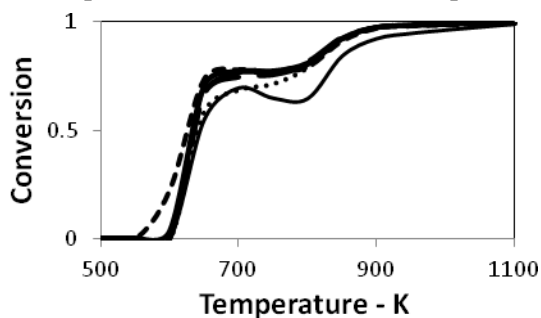


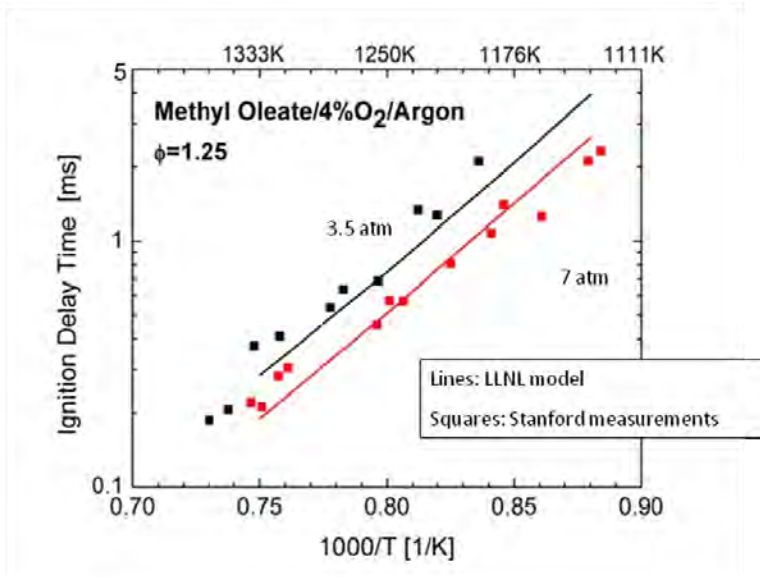
Figure 1: Computed conversion of selected biodiesel fuels, including palm, soy, rapeseed, peanut, olive, jatropha, sunflower and linseed methyl ester fuels. Fastest is palm oil methyl ester (dashed line), dotted line is linseed oil methyl ester, the lowest solid line is cetane no. 20 primary reference fuel. The remaining lines for soy, rapeseed, peanut, olive, jatropha, and sunflower methyl ester fuels cannot be distinguished from each other.

Real methyl ester components in biodiesel have high molecular weights and low vapor pressures which makes it experimentally challenging to provide

experimental data to validate their associated detailed chemical kinetic mechanisms. Recently, shock tube experimentalists have been able to overcome these challenges [19] and provide ignition times for these real biodiesel fuel components in a shock tube. This development has allowed validation of our high molecular weight methyl ester component models. Figure 2 shows a comparison of our chemical kinetic model for methyl oleate (which has one double bond) with ignition delay times measured at Stanford University [19]. With new improvements in the estimates of the methyl oleate decomposition rate constants, the model was able to reproduce experiments quite well.

Figure 2: The shock tube ignition delay times of methyl oleate, an unsaturated component contained in real diesel fuel [19]. Measurements made in the Stanford aerosol shock tube.

In addition, studies of small unsaturated methyl ester fuels have been carried out in collaboration with experimental projects elsewhere; and this work provides an independent opportunity to explore the kinetic features of the ester moiety and the effect of inclusion of double bonds on the carbon chain.



We are also developing chemical kinetic models for other biofuels

including butanols and pentanols. These fuels have advantages over the conventional biofuel ethanol for displacement of gasoline because of their higher energy densities. We have developed a detailed model for the four butanol isomers and validated it by comparison to experimental data from a low-pressure flame, a jet stirred reactor, a rapid compression machine, and shock tubes. Figure 3 shows a comparison of the ignition behavior of the four isomers of butanol compared to ignition times in a shock tube at pressures relevant to internal combustion engines [10]. This work shows that by collaborating with many different research groups, we are now able to simulate the ignition of these butanol isomers quite well.

We have been developing chemical models for the pentanol isomers. Based on our model development, the butanol and pentanol fuels exhibit some low temperature chemistry that reduces the ignition delay times at low temperature, but not enough to yield negative temperature coefficient behavior (Fig. 3). Low temperature reactions occur in spite of the pronounced influence of the alpha hydroxy alkyl radical formed by most of these alcohols. This radical reacts easily with molecular oxygen to form an aldehyde and an HO₂ radical, a path that inhibits conventional low temperature branching. The rate of this key reaction is only available for the case of alpha-hydroxyethyl + O₂ and is needed for other alpha hydroxy alkyl radicals produced by higher molecular weight alcohols that are the focus of future biofuels.

B. Chemical kinetic modeling of iso-alkanes in conventional and renewable fuels

Conventional fuels such as diesel and jet fuel, and bio-derived fuels such as hydrotreated renewable fuels contain large amounts of lightly branched iso-alkanes. Until recently, very few chemical kinetic models and experimental data have existed for these fuels and we have made considerable effort over the last two years to fill this gap. We have developed chemical kinetic models for singly methylated and di-methylated alkanes and compared the results of the models to experimental data taken by research collaborators in shock tubes, rapid compression machine, jet stirred reactor, flow reactor and flames [7,12,13-16]. We have compared our chemical kinetic models for four different C8 iso-alkanes with experimental data taken in a high-pressure shock tube at Rensselaer Polytechnic Institute (Fig. 4) [13].

The agreement between the model and experiment is reasonable although some improvements can be made. The largest discrepancy is around 900K where the ignition delay time is mainly controlled by the reaction rate of the fuel with HO₂ radicals. More accuracy for the associated rate constants is needed.

III. Future Work

We will continue to validate our methyl ester, alcohol, and iso-alkane models as new experimental data become available from research collaborators and from the literature. We will also explore the effect of the presence of double bonds in the carbon chain on the ignition of methyl esters. To isolate this effect, we will study the effect of the presence and position of double bonds in straight chain hydrocarbons which have no ester group.

We will continue to extend our detailed chemical kinetic models to components of higher molecular weight that are more representative of transportation fuels such as jet and diesel fuels. Models for higher molecular components are

especially needed for aromatics and cycloalkane chemical classes.

As more accurate rate constants as a function of pressure and temperature become available from computational and fundamental reaction rate studies, we will test and implement these new rate constants in our models. One particular focus will be the RO₂ and O₂QOOH isomerization reactions which are the keys to low temperature combustion rates and product distributions.

Acknowledgements: This work was performed under the auspices of the U.S. Department of Energy by Lawrence Livermore National Laboratory under

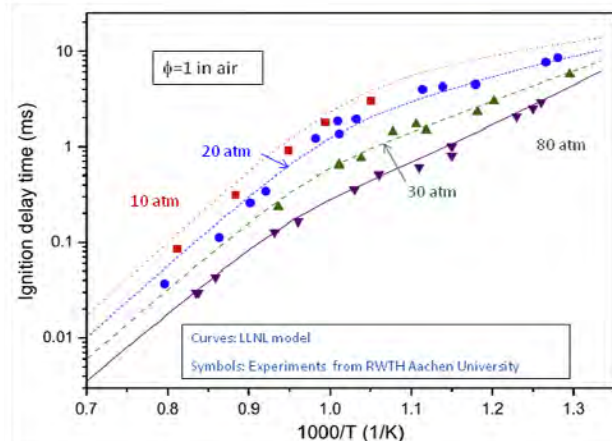


Figure 3: The shock tube ignition of 1-butanol over a range of temperatures at different elevated pressures [10].

Contract DE-AC52-07NA27344.

IV. References and Journal articles supported by this project 2010-2012

1. P.S. Veloo, Y.L. Wang, F.N. Egolfopoulos and C.K. Westbrook, "A comparative experimental and computational study of methanol, ethanol, and *n*-butanol flames", *Combust. Flame* 157, 1989-2004 (2010).
2. K. Kohse-Hoinghaus, P. Oswald, T.A. Cool, T. Kasper, N. Hansen, F. Qi, C.K. Westbrook and P.R. Westmoreland, "Biofuel Combustion Chemistry: From Ethanol to Biodiesel", *Angew. Chem. Int. Ed.* 49, 3572-3597 (2010).
3. C.V. Naik, C.K. Westbrook, O. Herbinet, W.J. Pitz, and M. Mehl, "Detailed chemical kinetic reaction mechanism for biodiesel components methyl stearate and methyl oleate", *Proc. Combust. Inst.* 33, 383-389 (2011).
4. M. Mehl, W.J. Pitz, C.K. Westbrook, and H.J. Curran, "Kinetic modeling of gasoline surrogate components and mixtures under engine conditions", *Proc. Combust. Inst.* 33, 193-200 (2011).
5. M. Mehl, W.J. Pitz, C.K. Westbrook, K. Yasunaga, C. Conroy, and H.J. Curran, "Autoignition behavior of unsaturated hydrocarbons in the low and high temperature ranges", *Proc. Combust. Inst.* 33, 201-208 (2011).
6. C.K. Westbrook, C.V. Naik, O. Herbinet, W.J. Pitz, M. Mehl, S.M. Sarathy and H.J. Curran, "Detailed chemical kinetic reaction mechanisms for soy and rapeseed biodiesel fuels", *Combust. Flame* 158 (4) (2011) 742-755.

7. S.M. Sarathy, C. Yeung, C.K. Westbrook, W.J. Pitz, M. Mehl and M.J. Thomson, "An experimental and kinetic modeling study of n-octane and 2-methyl heptane in an opposed-flow diffusion flame", *Combust. Flame* 158 (7) (2011) 1277-1287.
8. Z. Tian, W. J. Pitz, R. Fournet, P.-A. Glaude and F. Battin-Leclerc, "A detailed kinetic modeling study of toluene oxidation in a premixed laminar flame," *Proc. Combust. Inst.*, 33 (1) (2011) 233-241.
9. C. K. Westbrook, W. J. Pitz, S. M. Sarathy and M. Mehl, "Detailed Chemical Kinetic Modeling of Combustion of Biodiesel Fuels from a Wide Variety of Plant and Other Oils," *Proc. Combust. Inst.*, accepted (2012).
10. S.M. Sarathy, S. Vranckx, K. Yasunaga, M. Mehl, P. Oßwald, C. K. Westbrook, W.J. Pitz, K. Kohse-Höinghaus, R.X. Fernandes, H.J Curran, "A comprehensive chemical kinetic combustion model for the four butanol isomers", *Combust. Flame*, 159 (6) (2012) 2028–2055.
11. Scott A. Skeen, Bin Yang, Ahren W. Jasper, William J. Pitz and Nils Hansen, "The Chemical Structure of Low-Pressure Premixed Methylcyclohexane Flames as Benchmarks for the Development of a Predictive Combustion Chemistry Model", *Energy and Fuels*, 25 (12) (2012) 5611–5625.
12. S. M. Sarathy, C. K. Westbrook, M. Mehl, W. J. Pitz, C. Togbe, P. Dagaut, H. Wang, M. A. Oehlschlaeger, U. Niemann, K. Seshadri, P. S. Veloo, C. Ji, F. Egolfopoulos and T. Lu, "Comprehensive chemical kinetic modeling of the oxidation of 2-methylalkanes from C7 to C20," *Combust. Flame* 158 (12) (2011) 2338-2357.
13. W. Wang, Z. Li, M. A. Oehlschlaeger, D. Healy, H. J. Curran, S. M. Sarathy, M. Mehl, W. J. Pitz and C. K. Westbrook, "An experimental and modeling study of the autoignition of 3-methylheptane," *Proc. Combust. Inst.* (2012), accepted.
14. C. Ji, S. M. Sarathy, P. S. Veloo, C. K. Westbrook and F. N. Egolfopoulos, "Effects of fuel branching on the propagation of octane isomers flames," *Combust. Flame* 159 (4) (2012) 1426-1436.
15. S. M. Sarathy, U. Niemann, C. Yeung, R. Gehmlich, C. K. Westbrook, M. Plomer, Z. Luo, M. Mehl, W. J. Pitz, K. Seshadri, M. J. Thomson and T. Lu, "A counterflow diffusion flame study of lightly branched octane isomers," *Proc. Combust. Inst.* (2012), accepted.
16. N. Liu, S. M. Sarathy, C. K. Westbrook and F. N. Egolfopoulos, "Ignition of non-premixed counterflow flames of octane and decane isomers," *Proc. Combust. Inst.* (2012), accepted.
17. D. Darcy, M. Mehl, J. M. Simmie, J. Wurmel, W. K. Metcalfe, W. C. K., W. J. Pitz and H. J. Curran,

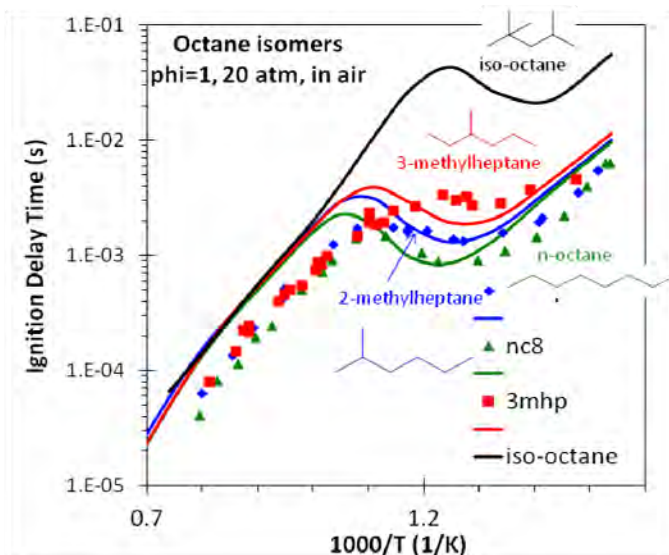


Figure 4: Shock tube ignition delay times of fuel/air mixtures of C8 iso-alkanes. Lines are LLNL models and symbols are experiments at RPI [12].

"An experimental and modeling study of the shock tube ignition of a mixture of n-heptane and n-propylbenzene as a surrogate for a large alkyl benzene," *Proc. Combust. Inst.* (2012), accepted.

18. M. Mehl, W. J. Pitz, S. M. Sarathy, C. K. Westbrook, H. J. Curran, "Modeling the combustion of high molecular weight fuels by a functional group approach", *Int. J. Chem. Kinet.*, 44 (4) (2012) 257-276.
19. M. F. Campbell, D. F. Davidson, R. K. Hanson and C. K. Westbrook, "Ignition delay times of methyl oleate and methyl linoleate behind reflected shock waves," (2012), to be submitted for publication.

INVESTIGATION OF NON-PREMIXED TURBULENT COMBUSTION

Grant: DE-FG02-90ER14128

Stephen B. Pope
Sibley School of Mechanical & Aerospace Engineering
Cornell University
Ithaca, NY 14853
s.b.pope@cornell.edu

1 Scope of the Research Program

The focus of the current work is on the development of computational approaches which allow our detailed knowledge of the chemical kinetics of combustion to be applied to the modeling and simulation of combustion devices. In the past year, the work has been focused on combining strategies for the accurate and efficient implementation of combustion chemistry.

2 Recent Progress

The principal research results from this program are described in the publications listed in Section 4. The following subsections detail the recent progress made in the computationally-efficient parallel implementation of combustion chemistry.

2.1 Efficient Implementation of Combustion Chemistry

Chemical mechanisms of real fuels may involve hundreds or thousands of species and thousands of reactions [1]. Incorporating directly such detailed chemistry in combustion calculations is prohibitive even using distributed parallel computing. The three widely used approaches to reduce the combustion chemistry cost are: (a) *mechanism reduction* to reduce the number of species and reactions involved [2, 3]; (b) *dimension-reduction* to represent chemistry using a reduced number of variables [4, 5]; and (c) *tabulation* to significantly reduce the cost of expensive evaluations of the reaction mappings involving ODE integrations [6].

In this regard, the main thrust in our research group has been on developing a combined dimension-reduction and tabulation approach to enable the use of detailed chemistry in combustion calculations. We have developed a combined reduction-tabulation approach [7] by integrating the Rate-Controlled Constrained Equilibrium (RCCE) [4] dimension reduction method and the *In Situ* Adaptive Tabulation (ISAT) [6] algorithm. In [8, 7] we describe an automated Greedy Algorithm with Local Improvement (GALI) for selecting “good” represented species for representing chemistry using this approach. In [7], we tested this combined ISAT-RCCE-GALI approach with the 31-species GRI Mech 1.2 methane chemistry and the 111-species USC Mech II ethylene chemistry. We showed that this approach provides the same level of accuracy as the detailed chemistry with relatively fewer species (10 for methane and 30 for ethylene) and provides significant speedup (by a factor of 2 for methane and 15 for ethylene) relative to using ISAT alone with the detailed chemistry.

Our recent efforts have been put into extending these methodologies for performing large scale parallel combined Large Eddy-Simulation (LES)/Probability Density Function (PDF) simulations of turbulent combustion as described in the next section.

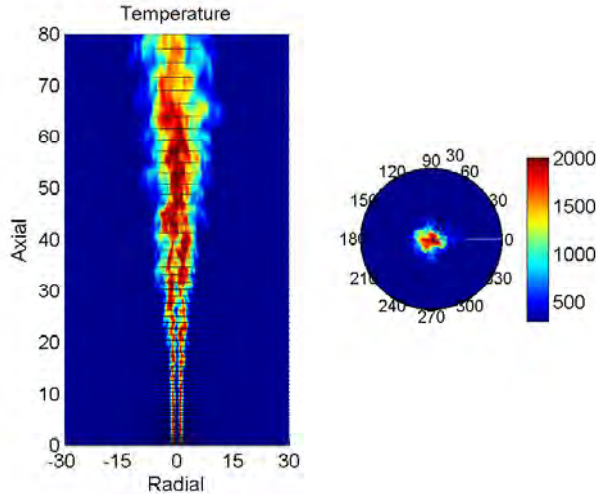


Figure 1: LES/PDF simulation of the Sandia Flame D. Instantaneous temperature distribution in the computational domain.

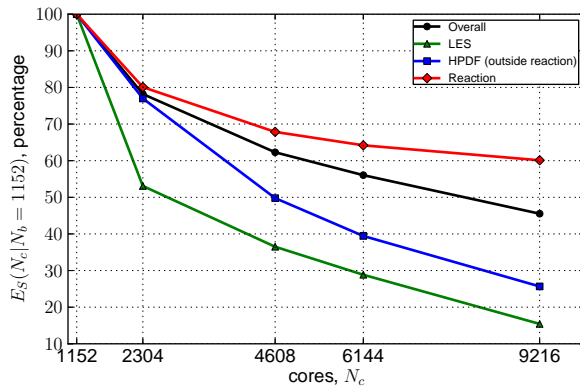


Figure 2: Relative strong scaling efficiency of LES, PDF (outside reaction), Reaction and Overall using the P-URAN strategy with the 38-species mechanism for 1,000 simulation time steps.

2.2 Parallel Implementation of Combustion Chemistry

Modern day LES/PDF simulations are performed using distributed computing on a large number of cores. We have performed simulations on up to 10,000 cores using our in-house LES/HPDF solver.

For performing parallel LES/PDF simulations, the computational domain is split into various sub-domains using domain decomposition, and each sub-domain is assigned to one core. For performing computations using ISAT, each core has its own ISAT table for tabulating chemistry. Since the chemical reactivity may vary significantly over different regions of the computational domain (e.g. regions near the flame front are chemically more reactive than regions in the coflow as seen in Fig.1), one of the main challenges in performing parallel LES/PDF simulations is to balance the chemistry workload among the participating cores to minimize the overall wall clock time required for the simulation.

To this end, we have developed parallel strategies implemented using *x2f_mpi* – a Fortran library for parallel vector-valued function evaluation (used with ISAT in this context) – for the efficient parallel implementation of chemistry [9]. These strategies have been tested for performing full scale LES/PDF simulations of the Sandia Flame D (see Fig.1) using a 16-species methane augmented reduced mechanism and a 38-species C_1 - C_4 skeletal mechanism. Among all the strategies tested, the most promising is the Partitioned Uniform Random (P-URAN) distribution strategy, which is found to yield the lowest wall clock time among all the strategies tested and achieves over 60% relative strong scaling efficiency for reaction on up to 9,216 cores as seen in Fig.2.

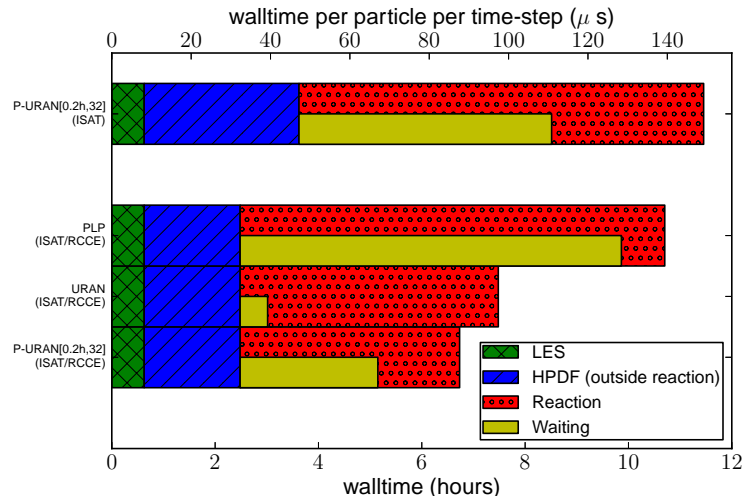


Figure 3: For LES/PDF simulation of Sandia Flame D, wall clock time for 2,000 time steps along with breakdown of time spent in LES, HPDF (outside reaction), Reaction (including $x2f_mpi$ communication) and Waiting (average idle time) using different parallel strategies. Top: using ISAT alone with the 38-species full representation with the P-URAN parallel strategy. Bottom three: using combined ISAT/RCCE with 10 represented species using (i) PLP; (ii) URAN; and (iii) P-URAN parallel strategies.

In [10] we further extend these parallel strategies for use with our combined reduction-tabulation approach using ISAT-RCCE. We demonstrate that the simulation wall clock time can be further reduced (without losing much accuracy) by using our combined ISAT-RCCE approach with the P-URAN strategy. Fig.3 shows that the wall clock time for the Sandia Flame D simulation using the 38-species C_1-C_4 skeletal mechanism with the P-URAN strategy is reduced by more than 40% using the ISAT-RCCE approach with 10 represented species.

3 Future Plans

We are currently working on a more efficient implementation of the RCCE dimension reduction method. In our current implementation of ISAT-RCCE [7], for an unsuccessful retrieve from the ISAT table, the *reaction mapping* (i.e., the species composition at the end of reaction time-step) is computed by integrating a system of n_s -ODEs involving all the n_s -species involved in the detailed mechanism. This implementation becomes computationally expensive for large mechanisms and leads to a large ISAT table *build time* as discussed in [7]. A more efficient implementation involves solving a reduced system of n_r -ODEs directly for the n_r -represented species used to represent the chemistry using the RCCE dimension reduction method. Since typically $n_r \ll n_s$, and the cost of solving a system of n -ODEs scales as $\mathcal{O}(n^3)$, significant cost savings can be achieved by the latter approach.

However, forming a reduced system of n_r -ODEs to obtain accurate reaction mappings is not an easy task. We are considering a formulation based on the work described in [11] using the idea of a Close Parallel Invariant Manifold (CPIM) for implementing RCCE. Our preliminary tests show that we can achieve the same level of accuracy as our current RCCE implementation using this more computationally efficient RCCE/CPIM approach. This implementation will be further tested for performing large scale LES/PDF computations.

4 Publications from DOE Research 2009-2012

1. V. Hiremath, Z. Ren and S.B. Pope (2010) "A Greedy Algorithm for Species Selection in Dimension Reduction of Combustion Chemistry," *Combustion Theory and Modelling*, **14**, 619–652.
2. D.C. Haworth and S.B. Pope (2011) "Transported Probability Density Function and Filtered

Density Function Methods,” in *Turbulent Combustion Modeling: Advances, New Trends and Perspectives*, eds. T. Echehki, E. Mastorakos, Springer.

3. V. Hiremath, Z. Ren and S.B. Pope (2011) “Combined Dimension Reduction and Tabulation Strategy using ISAT-RCCE-GALI for the Efficient Implementation of Combustion Chemistry”, *Combustion and Flame*, **158**, 2113–2127.
4. S.B. Pope (2011) “Simple models of turbulent flows”, *Physics of Fluids* **23**, 011301.
5. Z. Ren, G.M. Goldin, V. Hiremath and S.B. Pope (2011) “Reduced description of reactive flows with tabulated chemistry”, *Combustion Theory and Modelling*, **15**, 827–848.
6. S. Viswanathan, H. Wang and S.B. Pope (2011) “Numerical implementation of mixing and molecular transport in LES/PDF studies of turbulent reacting flows”, *Journal of Computational Physics*, **230** 6916–6957.
7. V. Hiremath, S.R. Lantz, H. Wang and S.B. Pope (2011) “Computationally-Efficient and Scalable Parallel Implementation of Chemistry in Simulations of Turbulent Combustion”, *Combustion and Flame*, (submitted).
8. V. Hiremath, S.R. Lantz, H. Wang and S.B. Pope (2012) “Computationally-Efficient Implementation of Chemistry using Combined Dimension Reduction and Tabulation in Simulations of Turbulent Combustion”, *Proceedings of the Combustion Institute*, **34**, (submitted).

References

- [1] C. K. Westbrook, W. J. Pitz, O. Herbinet, H. J. Curran, E. J. Silke, *Combust. Flame* 156 (2009) 181-199.
- [2] T. Lu, C. K. Law, *Proc. Combust. Inst.* 30 (2005) 1333-1341.
- [3] T. Nagy, T. Turanyi, *Combustion and Flame* 156 (2009) 417-428.
- [4] J.C. Keck, *Prog. Energy Combust. Sci.* 16 (1990) 125-154.
- [5] Z. Ren, S.B. Pope, A. Vladimirovsky, J.M. Guckenheimer, *J. Chem. Phys.* 124 (2006) 114111.
- [6] L. Lu, S.B. Pope, *J. Comput. Phys.* 228 (2009) 361-386.
- [7] V. Hiremath, Z. Ren, S. B. Pope, *Combustion and Flame* 158 (2011) 2113-2127.
- [8] V. Hiremath, Z. Ren, S. B. Pope, *Combustion Theory and Modelling* 14(5) (2010) 619-652.
- [9] V. Hiremath, S. R. Lantz, H. Wang and S. B. Pope (2011), *Combustion and Flame* (submitted)
- [10] V. Hiremath, S. R. Lantz, H. Wang and S. B. Pope (2012), *Proceedings of the Combustion Institute* (submitted)
- [11] Q. Tang and S.B. Pope, *Combustion Theory and Modelling* 8 (2004) 255-279.

OPTICAL PROBES OF ATOMIC AND MOLECULAR DECAY PROCESSES

S.T. Pratt
Building 200, B-125
Argonne National Laboratory
9700 South Cass Avenue
Argonne, Illinois 60439
E-mail: stpratt@anl.gov

PROJECT SCOPE

Molecular photoionization and photodissociation dynamics can provide considerable insight into how energy and angular momentum flow among the electronic, vibrational, and rotational degrees of freedom in isolated, highly energized molecules. This project involves the study of these dynamics in small polyatomic molecules, with an emphasis on understanding the mechanisms of intramolecular energy flow and determining how these mechanisms influence decay rates and product branching ratios. It is also aimed at understanding how internal energy can influence photoionization cross sections and dissociative ionization processes, and at understanding related collision processes such as the dissociative recombination of electrons and ions. The experimental approach combines double-resonance laser techniques, which are used to prepare selected highly excited species, with mass spectrometry, photoion- and photoelectron-imaging, and high-resolution photoelectron spectroscopy, which are used to characterize the decay of the selected species.

RECENT PROGRESS

Photoionization studies and absolute photoionization cross sections

We are continuing to use photoion and photoelectron imaging, vacuum-ultraviolet (vuv), single-photon ionization, and resonant multiphoton ionization to probe the photodissociation dynamics of small polyatomic molecules, and to characterize the photoionization dynamics of combustion-relevant species. One aspect of this work is to determine absolute photoionization cross sections of radicals by photodissociating the appropriate precursor and photoionizing both fragment species. Knowledge of the photoionization cross section of one of the species then allows the determination of the cross section for the other.

In 2010, we constructed a new photoelectron and photoion imaging spectrometer, and performed initial studies by using resonance-enhanced multiphoton ionization. However, because the Rydberg states of many radicals are predissociated, resonant multiphoton ionization is not always effective. We have now modified the apparatus to allow single-photon ionization with tunable vuv light, where the light is generated by using either third-harmonic generation or resonant four-wave mixing in rare gases. Photoelectron imaging with 118 nm light produced by tripling 355 nm light was straightforward. However, resonant four-wave mixing resulted in a huge background of electrons that completely obscures the signal of interest. In particular, the 202 nm light used in difference frequency mixing in Kr created a very intense background. To address this issue, we employed an adjustable, off-axis LiF lens followed by a small aperture to pass the vuv light and block the generating beams from entering the interaction region. This arrangement has proved successful, and provides good photoelectron images with tunable vuv light.

For our first photoelectron imaging experiments with tunable vuv light, we explored the near threshold photoionization of 2-butyne. This molecule displays a very strong and very broad resonance feature peaking about 0.8 eV above the ionization threshold, and with a photoionization cross section about 2.5 times larger than that for the near-threshold photoionization of acetylene, propyne, or even 1-butyne. Calculations by Lucchese (Texas A&M) indicated that this intense feature is produced by an $\ell = 4$, " π " shape resonance. To provide more insight into this mechanism, we have recorded photoelectron images at energies across the resonance and determined the photoelectron energy spectra and the photoelectron angular distributions. Interestingly, neither the photoelectron angular distributions nor the vibrational branching ratios show strong variations across the resonance. However, although the calculations predict the energy of the resonance about 0.4 eV higher than the experiment, if the theoretical photoelectron

angular distribution parameters are shifted by the same amount, they are in excellent agreement with the experimental values. The shift in the resonance energy is consistent with the expected accuracy of the method, and the excellent agreement between the experiment and theory strongly supports the theoretical interpretation of the result. In addition, this explanation supplies a rationale for the lack of this feature in acetylene, propyne, and 1-butyne. The intense $\ell = 4$, π resonance in 2-butyne results from the $\ell = 3$ character of the highest occupied molecular orbital (HOMO), while the HOMOs in the other systems nominally have $\ell = 1$, or 2, reducing the transition probability to an $\ell = 4$ resonance. The results also suggest that larger systems having non-terminal triple bonds may show behavior similar to 2-butyne. If confirmed, this observation could be useful for estimating photoionization cross sections of larger alkynyl radicals. These results are discussed in more detail in Paper 12.

We have also recorded photoelectron images following nonresonant, two-photon ionization of 2-butyne in the same region, as well as images following two-photon resonant, three-photon ionization via low lying Rydberg states. The latter experiments were aimed at characterizing the resonant transition for subsequent two-color studies near the ionization threshold. Although a significant signal was observed, the mass spectrum showed very little parent ion and a large number of different fragment species. The photoelectron images showed that these fragments were produced by ionization of the parent molecule, followed by photodissociation of the $C_4H_6^+$ ion. Unfortunately, the fragmentation was so extensive that it was difficult to map out the resonant structure, and two-color experiments were not performed.

Electric field effects in the imaging of autoionizing states

The electric fields used in photoelectron imaging experiments can affect the decay dynamics of high Rydberg states. Extremely close to threshold, these fields give rise to interesting interference effects of the ejected electrons and have been developed by Bordas, Vrakking, and coworkers as a means to image Rydberg wavefunctions [C. Nicole et al., Phys. Rev. Lett. **85**, 4024 (2000)]. To characterize the effects of electric fields on the imaging of autoionizing states farther from threshold, we studied the electric-field dependence of photoelectron images from autoionizing states of atomic Xe between the $Xe^+ 2P_{3/2}$ ground state threshold and the $2P_{1/2}$ limit. In particular, we have recorded images across the Stark manifold of the $n = 18$ Rydberg states at fields from 50 - 700 V/cm. Although the electric field breaks the cylindrical symmetry required for the standard reconstruction of the three-dimensional distributions, the photoelectron images still provide information on which ℓ components of the Stark states contribute most to the autoionization process, as well as on how the important ℓ components change across the Stark manifold. These results are discussed in more detail in Reference 11.

Dissociative recombination of small polyatomic ions

In collaboration with Christian Jungen, I have continued to work on theoretical models of vibrational autoionization and, in particular, dissociative recombination. In the past year, we made a closer examination of the dissociative recombination of H_3^+ and electrons, in an attempt to understand resonance structure in the experimental cross sections at collision energies below ~ 1 eV. While no convincing assignments of these resonances has emerged to date, their analysis also calls into question some assumptions about the relative rates of predissociation and electron capture. We are currently analyzing previous experimental and theoretical data in an attempt to resolve this issue. We have also performed a more careful fit of the existing theoretical data on the Rydberg states of H_3 to extract both linear and quadratic quantum defect functions, and to assess the role of the quadratic term in the capture process. As expected, this quadratic term is quite small, and although it does provide a direct mechanism for capture involving two vibrational quanta, the contribution of this mechanism to the rate is quite small. This work is discussed in Reference 13.

FUTURE PLANS

We plan on continuing our studies of the photodissociation and photoionization of combustion-relevant radicals by using ion-imaging techniques, vacuum-ultraviolet single-photon ionization, and resonant multiphoton ionization techniques. Following on our photoionization studies on 2-butyne, we are currently performing photoion imaging experiments on its photodissociation at 193 nm. At this wavelength, several fragmentation channels are open, including $CH_3 + C_3H_3$, $2C_2H_3$, and $H + C_4H_5$. Using

single-photon vuv photoionization detection and absolute cross sections from previous studies, we can extract information on the product branching ratios. In addition, by detecting both products in the dissociation to $\text{CH}_3 + \text{C}_3\text{H}_3$, we can provide a consistency check on the values of the absolute photoionization cross sections for these two species. We will continue to study the photodissociation dynamics of other radical precursors and determine absolute photoionization cross sections for the resulting radicals. Potential targets include the phenoxy radical, $\text{C}_6\text{H}_5\text{O}$, which can be produced in conjunction with CH_3 by the photodissociation of anisole, and the vinoxy radical, which can be produced in conjunction with $\text{CH}_2\text{CH}_2\text{OH}$ by the photodissociation of ethylene glycol vinyl ether.

At the suggestion of Marsha Lester, we have initiated an effort to record photoelectron images following the photoionization of OH radicals via the uv-vuv double resonance scheme developed in her group. In this scheme, the uv light excites the $A \leftarrow X$ transition, and vuv light at 118 nm drives transitions from the A state to the region above the lowest ionization threshold. The work in Lester's group has shown that, depending on the rovibrational level of the A state the 118 nm light excites autoionizing levels with large cross sections. Our goal is to use tunable vuv light for the second step, as well as photoelectron imaging, to allow a more thorough characterization of these autoionizing resonances. We have tested out most of the steps for the detection scheme, and we should be able to make our first full attempts at the experiments in the near future. Although we are currently focusing on photodissociation sources of the OH, we are also exploring the possibility of making the radicals by using a discharge source. Both approaches are expected to find considerable utility in future studies of other radicals.

I will continue to collaborate with Christian Jungen on theoretical models of vibrational autoionization and dissociative recombination in polyatomic molecules. In the coming year, we will continue with work on HCO^+ and NH_4^+ , and attempt to resolve some remaining issues with the dissociative recombination of H_3^+ . For the dissociative recombination of NH_4^+ , we have been working on experimental spectroscopic data on the 3p Rydberg states of NH_4 to extract the parameters necessary to predict the autoionization rates (and thus capture rates) at higher principal quantum number. That work will be compared with recent theoretical calculations of the dissociative recombination rates based on quantum chemical calculations on the same states [N. Douguet et al., *J. Phys. B: At. Mol. Opt. Phys.* **45** (2012) 051001]. Our model will also provide the dissociative recombination cross section for ND_4^+ , which will be compared with experimental results. We are currently arranging two potential collaborations with quantum chemists to calculate low-lying potential surfaces for Rydberg and valence states of other systems of interest, such as HCO^+ . Finally, we will also investigate the isotope effect in dissociative recombination. It turns out that our formalism provides a simple expression for the isotope dependence of the cross section that only depends on the ratio of vibrational frequencies of the isotopomers. This feature will provide a benchmark comparison for isotopic recombination rate data. Discrepancies between the experimental data and this model are expected to provide insight both into the nature of the capture process (direct vs. indirect), and into the dissociation mechanism of the electron-ion complex into neutral fragments.

This work was supported by the U.S. Department of Energy, Office of Science, Office of Basic Energy Sciences, Division of Chemical Sciences, Geosciences, and Biological Sciences under contract No. DE-AC02-06CH11357.

DOE-SPONSORED PUBLICATIONS SINCE 2010

1. V. A. Shubert, M. Rednic, and S. T. Pratt
PREDISSOCIATION AND DISSOCIATIVE IONIZATION OF RYDBERG STATES OF Xe_2
AND THE PHOTODISSOCIATION OF Xe_2^+
J. Chem. Phys. **132**, 124108 (2010).
2. N Thiré, R. Cireasa, V. Blanchet, and S. T. Pratt
TIME-RESOLVED PHOTOELECTRON SPECTROSCOPY OF THE $\text{CH}_3\text{I B } ^1\text{E } 6\text{s } [2] \text{ STATE}$
Phys. Chem. Chem. Phys. **12**, 15644-15652 (2010).
3. L. Young, E. P. Kanter, B. Krässig, Y. Li, A. M. March, S. T. Pratt, R. Santra, S. H. Southworth, N. Rohringer, L. F. DiMauro, G. Doumy, C. A. Roedig, N. Berrah, L. Fang, M. Hoener, P. H.

- Bucksbaum, J. P. Cryan, S. Ghimire, J. M. Glowonia, D. A. Reis, J. D. Bozek, C. Bostedt, M. Messerschmidt
 FEMTOSECOND ELECTRONIC DAMAGE BY ULTRAINTENSE X-RAYS
 Nature **466**, 56-61 (2010).
4. V. A. Shubert and S. T. Pratt
 PHOTODISSOCIATION OF ACETALDEHYDE AND THE ABSOLUTE PHOTOIONIZATION CROSS SECTION OF HCO
 J. Phys. Chem. A **114**, 11238 (2010).
 5. M. Hoener, L. Fang, O. Kornilov, O. Gessner, S.T. Pratt, M. Gühr, E.P. Kanter, C. Blaga, C. Bostedt, J.D. Bozek, P.H. Bucksbaum, C. Buth, M. Chen, R. Coffee, J. Cryan, L. DiMauro, M. Glowonia, E. Hosler, E. Kukk, S.R. Leone, B. McFarland, M. Messerschmidt, B. Murphy, V. Petrovic, D. Rolles, and N. Berrah
 ULTRA-INTENSE X-RAY INDUCED IONIZATION, DISSOCIATION, AND FRUSTRATED ABSORPTION IN MOLECULAR NITROGEN
 Phys. Rev. Lett. **104**, 253002 (2010).
 6. L. Fang, M. Hoener, O. Gessner, F. Tarantelli, S.T. Pratt, O. Kornilov, C. Buth, M. Gühr, E. P. Kanter, C. Bostedt, J.D. Bozek, P.H. Bucksbaum, M. Chen, R. Coffee, J. Cryan, J.M. Glowonia, E. Kukk, S. R. Leone, and N. Berrah
 DOUBLE CORE HOLE PRODUCTION IN N₂: BEATING THE AUGER CLOCK
 Phys. Rev. Lett. **105**, 083005 (2010).
 7. Ch. Jungen and S. T. Pratt
 LOW-ENERGY DISSOCIATIVE RECOMBINATION IN SMALL POLYATOMIC MOLECULES
 J. Chem. Phys. **133**, 214302 (2010).
 8. S. T. Pratt and Ch. Jungen
 DISSOCIATIVE RECOMBINATION OF SMALL POLYATOMIC MOLECULES
 J. Phys. Conf. Ser. **300**, 012109 (2011).
 9. V. A. Shubert and S. T. Pratt
 PHOTOELECTRON IMAGING OF SEVERAL 5d AND 6p RYDBERG STATES Xe₂ AND IMPROVING THE Xe₂⁺ I(1/2g) POTENTIAL
 J. Chem. Phys. **134**, 044315 (2011).
 10. N. Thiré, R. Cireasa, D. Staedter, V. Blanchet, and S. T. Pratt
 TIME-RESOLVED PREDISSOCIATION OF THE VIBRATIONLESS LEVEL OF THE B STATE OF CH₃I
 Phys. Chem. Chem. Phys. **13**, 18485-18496 (2011).
 11. V. Alvin Shubert and S. T. Pratt
 PHOTOELECTRON IMAGING OF AUTOIONIZING STATES OF XENON: THE EFFECT OF EXTERNAL ELECTRIC FIELDS
 Phys. Rev. A, **84**, 053413 (2011).
 12. H. Xu, U. Jacovella, B. Ruscic, S. T. Pratt, and R. R. Lucchese
 NEAR-THRESHOLD SHAPE RESONANCE IN THE PHOTOIONIZATION OF 2-BUTYNE
 J. Chem. Phys., in press.
 13. Ch. Jungen, M. Jungen, and S. T. Pratt
 THE JAHN-TELLER EFFECT IN THE 3pe' RYDBERG STATE OF H₃. REVIEW OF EXPERIMENTAL AND AB INITIO DETERMINATIONS
 Philosophical Transactions of the Royal Society of London, in press.

Photoinitiated Reactions of Radicals and Diradicals in Molecular Beams

Hanna Reisler

Department of Chemistry, University of Southern California

Los Angeles, CA 90089-0482

reisler@usc.edu

Program Scope

Open shell species such as radicals and diradicals are central to reactive processes in combustion and environmental chemistry. Our program is concerned with photoinitiated reactions of hydroxyalkyl radicals and carbenes. The goal is to investigate the detailed dynamics of dissociation of free radicals and diradicals for which multiple pathways including molecular rearrangements compete, and compare them with high level calculations. Studies include unimolecular reactions on the ground state as well as photodissociation dynamics on excited Rydberg and valence states that involve multiple potential energy surfaces. The photodissociation of triplet methylene, the prototypical carbene, exhibits several conical intersections and the experiments will be compared with high-level electronic structure calculations. The detailed measurements on simple systems will serve as benchmarks for homologous series.

Recent Progress

Experimental and theoretical studies of the overtone-induced dissociation and isomerization of the hydroxymethyl radical (CH_2OH and CD_2OH)

In order to determine product state distributions in photoinitiated dissociation of combustion-relevant radicals with vibrational resolution and infer mechanisms, the time-of-flight detection in our experimental arrangement was replaced with an imaging arrangement designed specifically to achieve sliced velocity map imaging (SMVI) of H-photofragments with comparable resolution to that obtained by reconstructed velocity map images. The first implementation of the new arrangement was to re-examine the overtone-induced vibrational predissociation of the hydroxymethyl radical with special emphasis on the relative roles of direct dissociation, $\text{CH}_2\text{OH} \rightarrow \text{CH}_2\text{O} + \text{H}$, and dissociation following $\text{CH}_2\text{OH} \leftrightarrow \text{CH}_3\text{O}$ isomerization. In previous work we observed the production of H atoms in CH_2OH and CD_2OH upon excitation to $4\nu_1$ (OH stretch); however, we could not study the predissociation dynamics because the H-photo-fragment time-of-flight detection did not have sufficient resolution to reveal structure in the velocity distribution. As demonstrated below, it is now possible to obtain energy distributions of CH_2O co-fragments by taking sliced images of H^+ . We combined the experimental studies with theoretical investigations, carried out in collaboration with Dr. Eugene Kamarchik, and Professors Anna Krylov and Joel Bowman. The electronic structure calculations gave accurate barrier heights, bond dissociation energies, and vibrational level energies. This allowed us to propose a dissociation mechanism and explore the role of isomerization.

The electronic structure calculations reveal that the barrier heights for $\text{CH}_2\text{OH} \rightarrow \text{CH}_2\text{O} + \text{H}$ and $\text{CH}_2\text{OH} \leftrightarrow \text{CH}_3\text{O}$ are within 400 cm^{-1} of each other and both are close to the examined excitation energy range of $13,600\text{--}13,660 \text{ cm}^{-1}$. The barrier for $\text{CH}_3\text{O} \rightarrow \text{H} + \text{CH}_2\text{O}$ dissociation is lower than the isomerization barrier by $\sim 1700 \text{ cm}^{-1}$ ensuring that CH_2OH isomerization is quickly followed by decomposition. These results are in good agreement with previous calculations.^{1,2} It should be noted, however, that the rates of these two CH_2OH dissociation pathways may depend not only on the barrier heights, but also on the character of the excited vibrational state, and thus may be state-specific.

The observation of predissociation induced by OH stretch overtone excitation is intriguing because here the excited OH stretch is the reaction coordinate, as opposed to other cases of overtone-induced dissociation where the excited bond is not broken in the dissociation and retains its bound character even

above the dissociation threshold. The existence of barriers to CH_2OH dissociation is probably why the OH stretch preserves its character of a bound vibration.

In the present work we have used SVMI to obtain internal energy distributions of CH_2O , CHDO and CD_2O cofragments from images of H^+ and D^+ following overtone induced dissociation of CH_2OH and CD_2OH in the region of $4\nu_1$. Observation of D products from CD_2OH provides direct evidence of isomerization in the $\text{CD}_2\text{OH} \leftrightarrow \text{CHD}_2\text{O}$ system, because direct C-H(D) fission in the radical is not energetically allowed. Analyses of the formaldehyde rovibrational state distributions show that they are qualitatively different for the two decomposition pathways and this allows us to obtain also branching ratios.

Action spectra obtained by monitoring H^+ and D^+ are in agreement with our previous results,³ except that with better sensitivity we are able to observe an additional band in CH_2OH near $13\,660\text{ cm}^{-1}$. The zeroth order $4\nu_1$ state carries most of the oscillator strength for the observed transitions, which are separated by 60 cm^{-1} . However, there is mixing with another close-lying vibrational state due to an accidental near-resonance. The mixing does not occur in CD_2OH . The VCI calculations support this analysis, showing that both bright states found in this region have large contributions from $4\nu_1$ and $3\nu_1 + \nu_2$ basis functions (ν_2 is the antisymmetric CH stretch).

Based on the similarity in the linewidths of the transitions to $4\nu_1$ in CH_2OH and CD_2OH , it was suggested previously that the linewidths were dominated by the dissociation rate.³ We confirm that the bands that are mostly $4\nu_1$ have similar linewidths, but the band at $13\,660\text{ cm}^{-1}$ (large $3\nu_1 + \nu_2$ contribution) has noticeable narrower lines, indicating state-specificity.

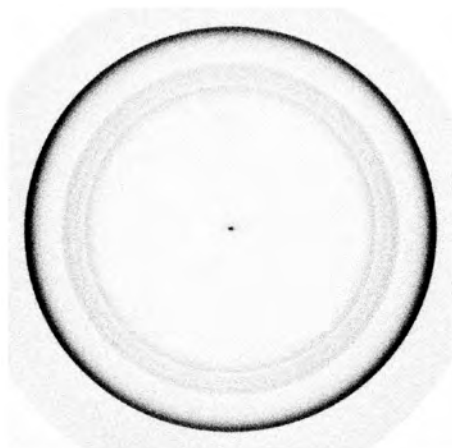


Fig. 1. An H^+ image from CH_2OH obtained by SVMI by exciting $4\nu_1$ at $13\,602\text{ cm}^{-1}$.

Kinetic energy distributions (KEDs) correlated with overtone-induced dissociation were obtained for H and D fragments. An SVMI image is shown in Fig. 1 and the distributions are shown in Fig. 2. The dissociation energy (D_0) of hydroxymethyl and the thresholds of vibrational levels of the formaldehyde cofragment are indicated in the figure.

The most intriguing result of the present study is the observation that H and D products from CD_2OH have very different KEDs (Fig. 2). The detection of D products from overtone-induced dissociation of CD_2OH indicates that in addition to dissociation by OH bond fission, isomerization to methoxy takes place. Using CD_2OH enables us to distinguish between the H atom initially in the OH group (which carries most of the optical excitation) and the D atoms initially attached to the carbon atom, and thus observe the isomerization channel explicitly. Such distinction is impossible for CH_2OH ; nevertheless, analysis of the experimental results shows that isomerization is responsible for a

fraction of H products in both radical isotopologs. The KEDs show that when monitoring D from CD_2OH , there is no CO stretch excitation in formaldehyde, whereas all H-producing reactions lead to a small population ($\sim 3\%$) in this mode. In contrast, methylene group deformation modes (scissors, rock and wag) are significantly excited ($\sim 28\%$ of the total population) in the D-producing reaction [Fig. 2(d)], but show smaller and variable excitations when monitoring H. These observations suggest that direct OH bond fission produces formaldehyde that is predominantly vibrationless or has small CO stretch excitation, but excitation of the deformation modes is associated mainly with the isomerization channel.

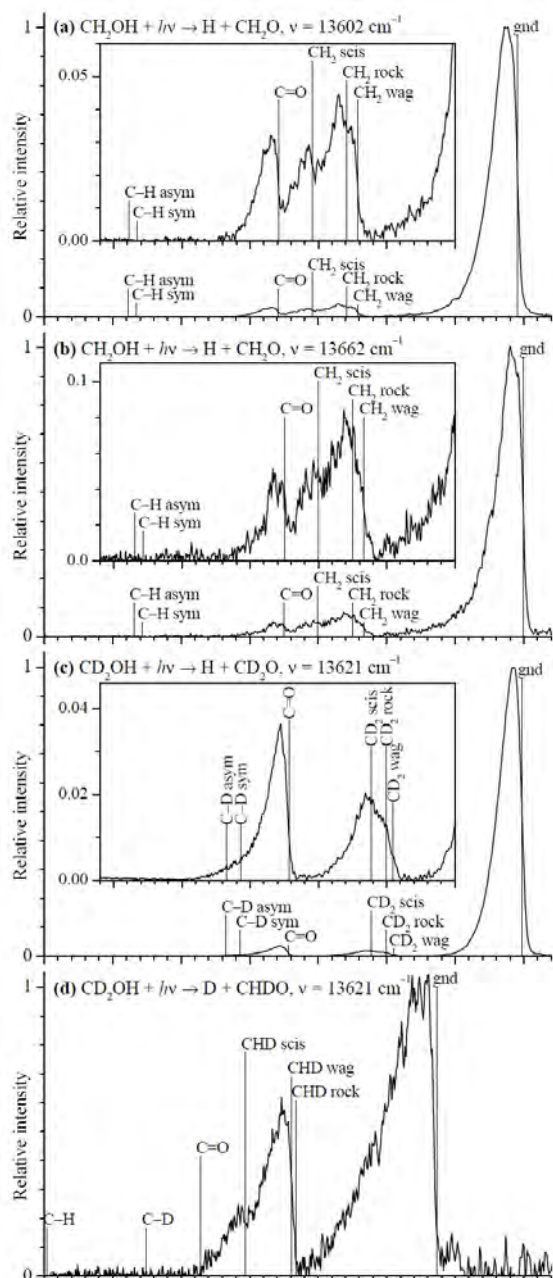


Fig. 2. KED's in the overtone-induced dissociation of CH_2OH (CD_2OH) obtained by SVMF by monitoring H and D photofragments.

times of the vibrationally excited states. No excitation in the CH (CD) stretches was observed in formaldehyde from either reaction.

Global PESs for CH_2OH and CD_2OH were constructed that include the hydroxymethyl and methoxy minima, dissociation products, barriers, and all dissociation channels. Vibrational energies and wave functions were computed by coupled anharmonic vibrational calculations for all fundamentals and for ν_1 overtones up to $\sim 14\,000\text{ cm}^{-1}$, in good agreement with experiment. They show that high OH-stretch overtones are mixed with other modes. The electronic structure calculations show that large torsional motion is required to reach the transition state for OH bond fission from the ground state minimum.

In order to estimate the branching between isomerization and direct dissociation, the experimental vibrational population distributions were analyzed in terms of a simple model with two assumptions: (1) The products observed in each experiment come from two independent dissociation channels; and (2) The distribution for each of the two channels is the same in all experiments, at least in the narrow range ($\sim 100\text{ cm}^{-1}$) used in the present experiments. This simple model reproduces the experimental results well and shows that in CH_2OH dissociation 11–15% of the events proceed by isomerization when the excited level is dominated by $4\nu_1$ [Fig. 2(a)] whereas the corresponding branching for the level dominated by $3\nu_1 + \nu_2$ is larger, 26–30% [Fig. 2(b)]. In dissociation of CD_2OH from a purer $4\nu_1$ level, isomerization accounts for < 13% events [Fig. 2(c)]. It is noteworthy that no excitation of CH (CD) stretch vibrations in the formaldehyde products is observed in either reaction, even though the VCI calculations show that the involved CH_2OH (CD_2OH) excited states contain considerable antisymmetric CH (CD) stretch contributions, and the CD frequencies in CD_2O and CHDO are quite similar to the CO frequencies. Analysis of the data also suggests that the dissociation rate for OH fission depends more strongly on the initially excited level than the isomerization rate, at least for the levels examined in this study.

The calculated global PES shows that the lowest barrier for OH bond fission corresponds to a geometry where the OH group is twisted from the quasiplanar structure of the radical, such that the HOC plane becomes perpendicular to the HCH plane. This geometry reflects the favored approach of an H atom to formaldehyde. The isomerization pathway involves the same OH group torsion, but additionally requires a large change of the HOC angle. Therefore, OH stretch overtone excitation is not an effective way to promote dissociation and is even less effective for isomerization, as reflected in the relatively long life-

Quasiclassical molecular dynamics calculations carried out at energies equivalent to $5\nu_1$ overtone excitation (to avoid the energy region near the barrier) show that the excited molecules, which are trapped between two barriers of fairly similar heights and shapes, live for several picoseconds even at energies $\sim 3000\text{ cm}^{-1}$ above the dissociation barrier. The branching between direct OH bond fission and dissociation via isomerization depends on the mode of vibrational excitation: excitation to pure $5\nu_1$ leads to a larger fraction of direct OH fission than excitation that deposits the energy more democratically among vibrational levels. The computed/experimental dissociation energies are in excellent agreement: $D_0(\text{CH}_2\text{OH} \rightarrow \text{CH}_2\text{O} + \text{H}) = 10\,188/10\,160\text{ cm}^{-1}$, $D_0(\text{CD}_2\text{OH} \rightarrow \text{CD}_2\text{O} + \text{H}) = 10\,167/10\,135\text{ cm}^{-1}$, $D_0(\text{CD}_2\text{OH} \rightarrow \text{CHDO} + \text{D}) = 10\,787/10\,760\text{ cm}^{-1}$.

In summary we have shown that it is possible to distinguish between the two dissociation pathways leading to $\text{H} + \text{CH}_2\text{O}$ by their distinct dynamical signatures in CH_2O . Dissociation proceeding by OH bond fission leads mainly to formaldehyde in the vibrationless state, with some excitation in the CO stretch and yet smaller excitations in the methylene deformation modes (scissors, rock and wag). On the other hand, dissociation following isomerization leads to formaldehyde that is rotationally hotter and has a much larger fraction of the energy deposited in methylene deformations, but not in the CO stretch.

Future Work

Our next goal is to study the photodissociation dynamics of CH_2OH and its isotopologs following excitation to Rydberg states and compare the results with the conical intersection calculations of Yarkony.⁴ Our preliminary SVMI results show direct O-H and C-H bond fission but no isomerization to methoxy. The former leads to formaldehyde with strong excitation in the CO stretch. The latter leads to formation of HCOH in both cis and trans geometries, each with a broad rovibrational state distribution.

References

1. T. P. Marcy, R. R. Díaz, D. Heard, S. R. Leone, L. B. Harding, and S. J. Klippenstein, *J. Phys. Chem. A* **105**, 8361 (2001).
2. S. Saebø, L. Radom, and H. F. Schaefer III, *J. Chem. Phys.* **78**, 845 (1983); N. D. K. Petraco, W. D. Allen, and H. F. Schaefer III, *J. Chem. Phys.* **116**, 10229 (2002);
3. Wei, J., Karpichev, B., and Reisler, H., *J. Chem. Phys.* **125** (2006): 34303.
4. B. C. Hoffman and D. R. Yarkony, *J. Chem. Phys.* **116**:8300-8306 (2002); D. R. Yarkony, *J. Chem. Phys.* **122**:084316, 1-7 (2005).

Publications, 2010-2012

1. B. Karpichev, L. Koziol, K. Diri, H. Reisler and A. I. Krylov, "Electronically excited and ionized states of the $\text{CH}_2\text{CH}_2\text{OH}$ radical: A theoretical study", *J. Chem. Phys.*, **132**, 114308 (2010).
2. L.W. Edwards, M. Ryazanov, H. Reisler and S. J. Klippenstein, "D-atom products in predissociation of $\text{CD}_2\text{CD}_2\text{OH}$ from the 202-215 nm photodissociation of 2-bromoethanol", *J. Phys. Chem. A*, **114** (17), 5453-5461 (2010).
3. E. Kamarchik, L. Koziol, H. Reisler, J. M. Bowman, and A. I. Krylov, "Unexpected roaming pathway leading to water plus vinyl products in $\text{C}_2\text{H}_4\text{OH}$ dissociation." *J. Phys. Chem. Lett.* **1**, 3058-3065 (2010).
4. E. Kamarchik, C. Rodrigo, J.M. Bowman, H. Reisler, and A. I. Krylov, "Overtone-induced dissociation and isomerization dynamics of the hydroxymethyl radical (CH_2OH and CD_2OH). I. A theoretical study", *J. Chem. Phys.* **136**, 084304 (2012).
5. M. Ryazanov, C. Rodrigo and H. Reisler, "Overtone-induced dissociation and isomerization dynamics of the hydroxymethyl radical (CH_2OH and CD_2OH). II. Velocity map imaging studies", *J. Chem. Phys.* **136**, 084305 (2012).

Accurate Calculations and Analyses of Electronic Structure, Molecular Bonding and Potential Energy Surfaces

Klaus Ruedenberg

Ames Laboratory USDOE, Iowa State University, Ames, Iowa, 50011

ruedenberg@iastate.edu

Scope

Theoretical treatments of molecular reactions and their kinetics require accurate potential energy surfaces in non-equilibrium regions of coordinate space. A major challenge is the sufficiently accurate description of the non-relativistic electron correlations in the presence of a multi-configurational dominant zeroth-order component in the electronic wavefunction, as is the case along most reaction paths. A substantial advance towards this goal has been made through the correlation energy extrapolation by intrinsic scaling (CEEIS) method that was recently developed in this group. Combined with the extrapolation to the complete basis limit, it has made it possible to approximate the complete configuration interaction energies within about 0.05 kcal/mol.

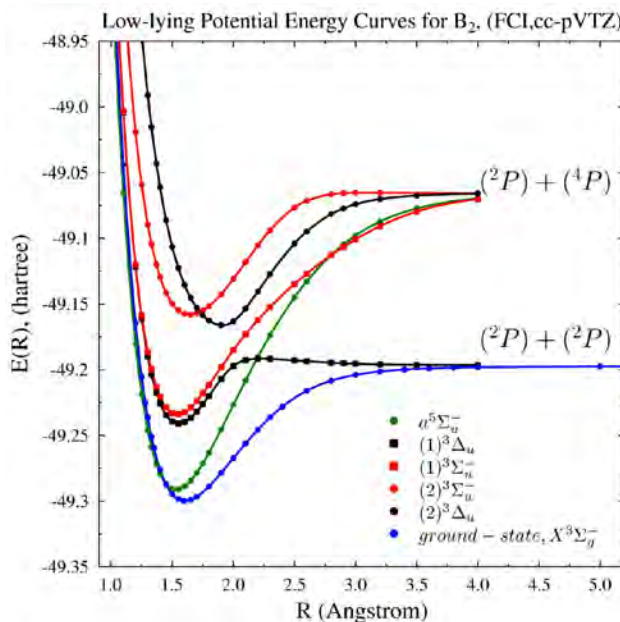
Recent Work

Diatomic potential energy curves have been determined and vibration-rotation spectra have been obtained with near-spectroscopic accuracy ($< 10 \text{ cm}^{-1}$). Information has been generated that has not yet been accessible to experiment. For the ground state of O_2 , the theoretical predictions provided 15% of the full spectrum. For the ground state of F_2 , a competition between quadrupole repulsion and dispersion forces leading to a long range barrier was predicted. Recent work using this method has yielded the complete potential energy curve of the ground state of the electron-deficient diatomic boron molecule and determined all rotational-vibrational levels up to the dissociation limit. Of the 38 vibrational levels found theoretically, only the six levels for $v = 0, 1, 12, 13, 14, 15$ have so far been observed experimentally. For these the average agreement was 5 cm^{-1} .

The CEEIS method has furthermore been generalized so that several states can be determined simultaneously. This has been applied to the ground and four excited states of the boron molecule. The analysis suggests that the electronic transitions to some vibrational levels of the $X^3\Sigma_g^-$ ground state come from the $1^3\Sigma_u^-$ state whereas transitions to other ground state vibrational levels come from the $2^3\Sigma_u^-$ state. This assignment differs from that previously assumed by experimentalists.

Future Work

Using the new CEEIS method the potential energy surface of the lowest two 1A_1 potential energy surfaces of ozone will be calculated. Previous calculations within the full



valence space MCSCF approximation showed that (i) the transition state from the open to the ring structure of the ground state, (ii) the minimum of the excited state and (iii) a quite unexpected conical intersection between these two closed shell singlet states of like symmetry lie within about 0.1 Angstrom of each other. The calculations will determine whether these unusual features are in fact true for the accurate potential energy surfaces.

Publications in 2009, 2010, 2011

A-Priori Identification of Configurational Deadwood.

Laimutis Bytautas and Klaus Ruedenberg
Chem. Phys., 356, 64-75 (2009)

Physical Understanding through Variational Reasoning: Electron Sharing and Covalent Bonding.

K. Ruedenberg and M.W. Schmidt,
J. Phys. Chem., 113, 1954-1968 (2009)

Ab Initio Potential Energy Curve of F₂. IV. Transition from the Covalent to the van der Waals Regime. Competition between Multipolar and Correlation Forces.

L. Bytautas and K. Ruedenberg,
J. Chem. Phys., 130, 204101, 1-14 (2009)

Accurate ab initio potential energy curve of O₂. I. Non-relativistic full CI valence correlation by the CEEIS method.

L. Bytautas and K. Ruedenberg,
J. Chem. Phys. 132, 074109, 1-10 (2010)

Accurate ab initio potential energy curve of O₂. II. Core-valence correlations, relativistic contributions and vibration-rotation spectrum.

L. Bytautas, N. Matsunaga, K. Ruedenberg,
J. Chem. Phys. 132, 074307, 1-15 (2010)

The range of electron correlation between localized molecular orbitals. A full configuration interaction analysis for the NCCN molecule.

L. Bytautas and K. Ruedenberg,
J. Phys. Chem. 114, 8601–8612 (2010)

Electronic structure analysis of the ground state potential energy curve of Be₂.

M.W. Schmidt, J. Ivanic, K. Ruedenberg,
J. Phys. Chem. 114, 8687-8696 (2010)

Analysis of the bonding patterns in the valence isoelectronic series O₃, S₃, SO₂ and OS₂ in terms of oriented quasi-atomic molecular orbitals.

V.A. Glezakou, S.T. Elbert, S. S. Xantheas, K. Ruedenberg,
J. Phys. Chem. 114, 8923–8931 (2010)

Toward a Physical Understanding of Electron-Sharing Two-Center Bonds. II. A Pseudo-Potential Based Approach.

T. Bitter, S.G. Wang, K. Ruedenberg, W.H.E. Schwarz,
Theor. Chem Acc., 127, 237-257 (2010)

Accurate potential energy curve for B₂. Ab initio elucidation of the experimentally elusive ground state rotation-vibration spectrum.

L. Bytautas, N. Matsunaga, G. Scuseria, K. Ruedenberg,
J. Phys. Chem. A., 116, 1717-1729 (2012)

Active Thermochemical Tables – Progress Report

Branko Ruscic

Chemical Sciences and Engineering Division, Argonne National Laboratory,
9700 South Cass Avenue, Argonne, IL 60439
ruscic@anl.gov

Program Scope

The *spiritus movens* of this program is the need to provide the scientific community with accurate and reliable thermochemical information on chemical species that are relevant in combustion, or play prominent roles in the associated post-combustion environmental chemistry, thus contributing to the comprehension of the underlying chemical reactions, and providing the thermochemical base for their quantitative modeling, and/or furnishing reliable benchmark values for development, improvement, and testing of state-of-the-art theoretical approaches. Thermochemistry is one of the essential underpinning scientific blocks that is enabling DOE to successfully interpret, analyze, model, and optimize energy-producing chemical reactions and thus fulfill its mission, and is, as such, a long-term component of the DOE BES research program. The current focus of this program is on bringing substantial innovations to the field of thermochemistry through the development of new tools and methodologies, and utilizing these new approaches to systematically advance the quality and quantity of available thermochemical data relevant to energy-producing processes. In order to accomplish the stated goals, this program has undertaken the development of a novel approach that is centered on the idea of analyzing and optimally utilizing the information content of thermochemically relevant measurements. The aim of these developments is not only to produce *the best currently possible* thermochemical parameters for the targeted chemical species, but also to allow *efficient updates with new knowledge*, properly propagating its consequences through all affected chemical species, as well as to provide *critical tests of new experimental or theoretical data*, and, when possible, to develop *pointers to future determinations that will most efficiently improve the thermochemical knowledge base*. The effort of this program is synergistically coordinated with related experimental and theoretical efforts within the Argonne Chemical Dynamics Group to provide a broad perspective of this area of science.

Recent Progress

Development of Active Thermochemical Tables and the Core (Argonne) Thermochemical Network

Our primary activity over the past year was the continuation of the development and deployment of Active Thermochemical Tables (ATcT). ATcT are a new paradigm of how to develop accurate, reliable, and internally consistent thermochemical quantities for stable, reactive, and transient chemical species by utilizing to the fullest all available experimental measurements as well as state-of-the-art theoretical results. As opposed to traditional sequential thermochemistry, ATcT is based on analyzing and solving the Thermochemical Network (TN). While it must have been quite clear since the dawn of quantitative thermochemistry that the thermodynamical properties of various chemical species are underpinned by numerous intertwined dependencies, which - if correctly determined - must all be simultaneously satisfied by the ‘proper’ thermochemical value, these were historically

considered to be an intractable complication, leading to the adoption of a simplified sequential approach to thermochemistry (A begets B, which begets C, etc). The intractability of simultaneous interdependencies was originally mandated by the (fully excusable) lack of adequate computing analysis tools and the inability to process the necessary amount of information. However, discarding most of the information embedded in the simultaneous interdependences has persisted as the prevailing state of affairs even as both the speed and the bandwidth of information-processing capabilities increased exponentially with time. The quantum leap in the quality and reliability of the thermochemical values resulting from the ATcT approach is rooted in readdressing the original problem by organizing the underlying interdependencies as a Thermochemical Network amenable to explicit mathematical and statistical manipulation that leverage the TN information content to its fullest.

The ATcT effort has two essential fronts: the development of the ATcT software and the development of the underlying Thermochemical Network. On the software front, we have previously reported on a number of additional software tools that we have developed and that enable us to refine the respective partition functions by including various additional corrections that influence the thermochemistry at temperatures relevant in combustion processes (such as, for example, anharmonic effects). During the last year we have extensively tested these new tools by exercising them on various H/O species, which enabled us to identify and perform several additional improvements. In a separate methodological development, we have recently started addressing one of the interesting questions that keeps resurfacing periodically: once an ATcT value is developed from a TN that contains many hundreds of species that are intertwined by (typically) an order of magnitude larger number of determinations, is it possible to look back at the ATcT process and say with some confidence which determination(s) are crucially responsible for the final value? The answer to this question was found by carefully dissecting and analyzing the underlying matrix algebra that leads to the ATcT solution and its uncertainty, and enabled us to provide not only a qualitative, but, in fact, an exact quantitative answer. In retrospect, the solution that we have developed is tantamount to performing a decomposition of the variance attached to each ATcT result, and can be equally applied to decompose the covariances. Furthermore, this can be rather elegantly implemented in ATcT by several relatively simple additional matrix manipulations that are applied after the solution has been found. The ATcT variance decomposition is currently implemented by (yet another) separate post-processing tool. In straightforward cases, our variance decomposition leads directly to the desired answer. We are currently exploring how this approach works in more complicated cases, such as those in which, for example, a substantial portion of the uncertainty essentially originates from the uncertainty of another (i.e. parent) species (and thus the two species are highly correlated).

With respect to the development of the Thermochemical Network, we have continued to implement various improvements for groups of related species that are approaching the 'final' stage. We have concentrated the effort on completing the partition functions of H/O species, and, with the exception of a few stubborn cases (which are quite interesting for the sake of completeness, but otherwise do not appear to be crucial in combustion processes per se), we believe that we have now finalized all species in this group and are ready to provide very accurate thermochemistry for H₂ combustion mechanisms. We are also in the process of addressing the species involved in NO_x formation mechanisms. One species from this group that has so far escaped much attention is NCN. In a collaborative effort (Elke Goos, DLR),

our partners have used the ATcT thermochemistry for all the species involved in prompt NO formation, and demonstrated that the thermochemistry of NCN is crucial in reproducing the experimental targets. We have therefore additionally investigated NCN, and found not only that the existing experimental determinations of its thermochemistry are inconsistent (both mutually and internally), but also that the majority of theoretical computations are incorrect, since the authors missed the fact that their (single reference) results for NCN suffer the consequences of spin contamination. The current ATcT value for this species is similar to the value implied some time ago by the results of multireference methods (L. Harding, ANL). With respect to simple carbon-containing species, we have recently expanded the TN to encompass additional C₃ species (partly in collaboration with R. Sivaramakrishnan and J. V. Michael, ANL). In a parallel collaboration with S. Klippenstein (ANL), we are currently in the process of systematically checking on all chemical species that appear in a hierarchy of chemical mechanisms that describe the combustion of various fuels as the number of carbon atoms successively increases (i.e. H₂, CH₄, C₂H₄, etc.) In a separate effort (collaboration with R. Tranter, ANL), we are currently working on developing the correct thermochemistry of allyl association.

Future Plans

Future plans of this program pivot around further developments and expansive use of Active Thermochemical Tables, providing accurate thermochemistry, and driving targeted theoretical and laboratory experimental investigation of radicals and transient species that are intimately related to combustion processes as well as post-combustion atmospheric processes. A significant part of the effort during forthcoming period will be devoted to continued ‘finalization’ and dissemination of the resulting ATcT thermochemistry. A necessary component of the ‘finalization’ of results for groups of related chemical species consists of testing and analyzing in detail their TN dependencies as well as the accuracy of their partition functions, and, when suggested by such analyses, adding new high-quality results (both virtual, i.e. computational, and actual, i.e. experimental) that will help in coercing their thermochemistry toward convergence to stable, ‘release quality’ values. This iterative process will also result in an expansion of the number of species that belong to the ‘release quality’ category. Another important component in the dissemination of ATcT results is the continuation of the current effort of designing and producing an entirely computer-generated ATcT web site that will be populated by ‘release quality’ results automatically by a suitable post-processing step of ATcT. Besides full automation with archival capability, an additional desideratum for an improved ATcT website is the automatic inclusion of sufficient background information that will document the pedigree for every recommended thermochemical value, providing proper credit to the actual original (experimental and/or theoretical) determination(s) that are responsible for the final ATcT value. Finally, a significant long-term component of future progress in this area will consist of building a second generation of ATcT software. This will be based on a thorough redesign of the current ATcT software, with the aim of making the software not only significantly more streamlined and efficient, but also allowing sufficient flexibility that will enable the adoption and utilization of emerging computing technologies as they become available.

This work is supported by the U.S. Department of Energy, Office of Basic Energy Sciences, Division of Chemical Sciences, Geosciences, and Biosciences, under Contract No. DE-

Publications resulting from DOE sponsored research (2009 – present)

- *Atomization Energies from Coupled-Cluster Calculations Augmented with Explicitly-Correlated Perturbation Theory*, W. Klopper, B. Ruscic, D. P. Tew, F. A. Bischoff, and S. Wolfsegger, *Chem. Phys.* **356**, 14-24 (2009).
- *Is HO₂⁺ a Detectable Interstellar Molecule?*, S. L. Widicus Weaver, D. E. Woon, B. Ruscic, and B. J. McCall, *Astrophys. J.* **697**, 601-609 (2009).
- *Thermal Decomposition of NH₂OH and Subsequent Reactions: Ab Initio Transition State Theory and Reflected Shock Tube Experiments*, S. J. Klippenstein, L. B. Harding, B. Ruscic, R. Sivaramakrishnan, N. K. Srinivasan, M.-C. Su, and J. V. Michael, *J. Phys. Chem. A* **113**, 10241-10259 (2009).
- *Rate Constants for the Thermal Decomposition of Ethanol and Its Bimolecular Reactions with OH and D: Reflected Shock Tube and Theoretical Studies*, R. Sivaramakrishnan, M.-C. Su, J. V. Michael, S. J. Klippenstein, L. B. Harding, and B. Ruscic, *J. Phys. Chem. A* **114**, 9425-9439 (2010).
- *The Heats of Formation of C₆H₅, C₆H₅⁺, and C₆H₅NO by TPEPICO and Active Thermochemical Tables Analysis*, W. R. Stevens, B. Ruscic, and T. Baer, *J. Phys. Chem A* **114**, 13134–13145 (2010).
- *Shock Tube and Theoretical Studies on the Thermal Decomposition of Propane: Evidence for a Roaming Radical Channel*, R. Sivaramakrishnan, M.-C. Su, J. V. Michael, S. J. Klippenstein, L. B. Harding, and B. Ruscic, *J. Phys. Chem. A* **115**, 3366-3379 (2011).
- *Extended Third Millennium Ideal Gas and Condensed Phase Thermochemical Database for Combustion with updates from Active Thermochemical Tables*, E. Goos, A. Burcat and B. Ruscic, *progressive updates of thermochemical polynomials available at <ftp://ftp.technion.ac.il/pub/supported/aetdd/thermodynamics/> (also mirrored at <http://garfield.chem.elte.hu/Burcat/burcat.html>), and available from DLR webpage <http://www.dlr.de/vt/> (2011-2012).*
- *Inhibition of Hydrogen Oxidation by HBr and Br₂*, G. Dixon-Lewis, P. Marshall, B. Ruscic, A. Burcat, E. Goos, A. Cuoci, A. Frassoldati, T. Faravelli, and P. Glarborg, *Combust. Flame* **159**, 528-540 (2012).
- *High-Temperature Rate Constants for H/D + C₂H₆ and C₃H₈*, R. Sivaramakrishnan, J. V. Michael, and B. Ruscic, *Int. J. Chem. Kin.* **44**, 194-205 (2012).
- *Near-threshold shape resonance in the photoionization of 2-butyne*, H. Xu, U. Jacovella, B. Ruscic, S. T. Pratt, and R. R. Lucchese, *J. Chem. Phys.* **136**, 154303/1-10 (2012).
- *Prompt NO formation in flames: The influence of NCN thermochemistry*, E. Goos, C. Sickfeld, F. Mauss, L. Seidel, B. Ruscic, A. Burcat, and T. Zeuch, *Proc. Comb. Inst.*, submitted (2012).

Gas-Phase Molecular Dynamics: High Resolution Spectroscopy and Collision Dynamics of Transient Species

Trevor J. Sears

Department of Chemistry, Brookhaven National Laboratory
Upton, NY 11973-5000

sears@bnl.gov

Program Scope

This research is carried out as part of the Gas-Phase Molecular Dynamics program in the Chemistry Department at Brookhaven National Laboratory. High-resolution spectroscopy, augmented by theoretical and computational methods, is used to investigate the structure, collision dynamics and chemical behavior of intermediates in the elementary gas-phase reactions involved in combustion chemistry. Applications and methods development are equally important experimental components of this work.

I. Recent Progress

A. Spectroscopy with comb-stabilized extended cavity diode lasers

Until very recently, practical limits to accuracy and precision in the measurement of a spectroscopic line were associated with wavelength standards normally used to calibrate spectra. The best measurements using wavelength standards and stabilized cavities reach accuracies of the order of 1 part in 10^8 . Spectroscopy employing frequency-based calibration does not suffer this problem because

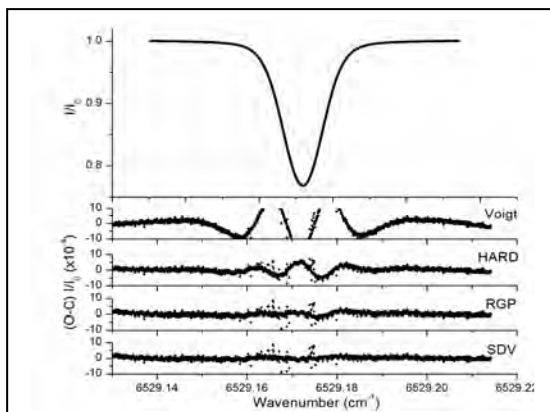


Fig. 1: Transmission spectrum of the acetylene P(11) line at 4 Torr and 150 K and in a 1.085 cm absorption path length. Bottom panels show residuals (O-C) under these conditions resulting from least squares multispectrum fitting of experimental data to the corresponding line shape models.

optical frequencies that are referenced to the Cs atomic clock can routinely provide a few parts in 10^{12} accuracy and precision. Frequency combs provide a convenient method to transfer the microwave standard to optical frequencies, and lasers locked to such a comb can subsequently be used for high precision spectroscopy. This improvement leads to opportunities for dramatic improvements in measurements of both spectral line positions and splittings, and also in line shape determinations. Precisely known spectral line shapes are needed for the determination of species concentrations from remote sensing measurements, for example. In our first experiments, low-power extended cavity diode lasers (ECDLs) have been locked to a commercial frequency comb and used to measure spectral lines of the acetylene $\nu_1 + \nu_3$ band.

The exquisite accuracy of this spectrometer is not only of use for precision measurements of narrow spectral lines, but can be used to improve the measurement of the shapes and widths of broad features.

Figure 1 illustrates some results for a measurement of the P(11) line of the acetylene combination band for a pressure of 4 Torr at 150K. The commonly used Voigt line profile (a convolution of a Gaussian Doppler-broadened line shape with a Lorentz pressure-broadened line shape) cannot reproduce the data at all well. More sophisticated hard or soft collision models that incorporate collisional narrowing are better, but do not reproduce the small asymmetry evident in the measured line shape at higher gas densities. Only the speed-dependent Voigt model was able to fit the data to the experimental precision at all temperatures and for pressures between 3 and nearly 360 Torr. The variations of the speed-dependent Voigt profile line shape parameters with temperature were also characterized, and this model accurately reproduces the observations over their entire range of temperature and pressure. We have continued to measure the effects of foreign gas (nitrogen) pressure broadening and the analysis of these data are in

progress. Our understanding of the properties and behavior of laser frequency comb sources continues to evolve leading to new ideas for their application. Additional work planned in this area is described below. Other frequency comb work at BNL is described in G. Hall's abstract for this meeting.

B. Spectroscopy and photophysics of aromatic species

The sensitivity of vibronic spectral calculations to electronic structure methods and basis sets was explored and compared to accurate relative intensities of the vibrational bands of phenylacetylene. To provide a better measure of vibrational band strengths, the $S_1(A^1B_2) \leftarrow S_0(X^1A_1)$ electronic transition of phenylacetylene was recorded by cavity ringdown absorption spectroscopy in a slit jet sample at energies of up to 2000 cm^{-1} above the band origin. The sample rotational temperature was estimated to be about 30K, but the vibrational temperature was higher, permitting the assignment of many vibrational hot bands. The vibronic structure of the electronic transition was simulated using a combination of time-dependent density functional theory (TD-DFT) electronic structure codes, Franck-Condon integral calculations, and a second order vibronic model developed previously [Johnson P. M., Xu H. F., Sears T. J., *J Chem Phys* **125**, (2006)].

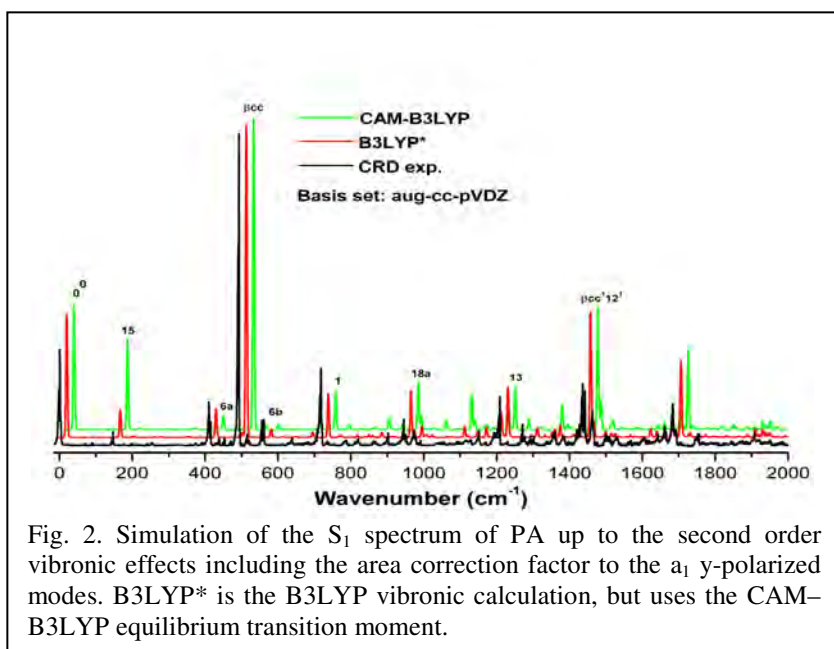


Fig. 2. Simulation of the S_1 spectrum of PA up to the second order vibronic effects including the area correction factor to the a_1 y-polarized modes. B3LYP* is the B3LYP vibronic calculation, but uses the CAM-B3LYP equilibrium transition moment.

using the LRC transition moment combined with the B3LYP vibronic coupling., shown as B3LYP* in figure 2. Enlarging the basis set made very little difference. The cavity ringdown experiment shows that earlier intensities derived from resonance enhanced multi-photon ionization (REMPI) spectra have relative intensity errors; the intensity of strong bands was underestimated in the REMPI spectrum due to saturation effects.

C. Double resonance and sub-Doppler studies of radical spectra and collision dynamics

Rotational energy transfer within and between rotational levels of CN has been studied by saturation recovery and saturation transfer double resonance kinetic spectroscopy, as reported last year. Measurement accuracy has been improved by further stabilizing the Ti:sapphire probe laser to a single frequency He:Ne laser using a stable transfer cavity. In the future, a frequency comb reference will improve this stabilization further. Some of these aspects are discussed in more detail in G. Hall's abstract elsewhere. As a test of the stability of the system, sub-Doppler spectra of metastable N_2 have been recorded. Measured line widths are of the order of 5 MHz, 2-3 times narrower than we measured previously in spectra of CN recorded without the additional He:Ne laser stabilization, and analysis of the spectra will permit an improvement in the determination of the hyperfine interaction in the lowest triplet

excited electronic states of the nitrogen molecule. All future ultra-high resolution spectroscopic and dynamics measurements will benefit from this advance.

II. Future Work

A. Precision spectroscopy and dynamics

During the past year, much effort was devoted to moving our laboratory at BNL to temporary space during the Chemistry Building renovation project. Our laboratory is scheduled to return to the renovated space in fall 2013 and the temporary laboratory will be used until then. Efforts will concentrate on ultra-high resolution spectroscopy of transient species, including triplet C₃ and other radicals and e-EDM measurement candidate PbF in a slit jet expansion, as discussed last year.

First experiments using a fiber amplified, comb-locked ECDL are just beginning at Stony Brook. This source provides approximately 50 mW of comb-stabilized laser power in a single stage of amplification from a few hundred μ W of seed power, making saturation spectroscopy experiments simpler. Improved sub-Doppler spectra of acetylene have already been obtained and a new, more stable, cavity absorption cell is under construction. Changes to the methods used to lock the ECDL to the comb are resulting in beat note widths in the 10 Hz range, 10⁴-10⁵ times better than used in all our previous measurements. Extensive measurements of the temperature-dependent nitrogen foreign gas broadening of C₂H₂ lines have been made and are currently being analyzed. Continuous improvement to the spectrometer is resulting in ever more accurate and precise data as we learn how to best make use of the comb's properties. When the new laboratories are completed, the frequency comb will be moved back to Brookhaven and it will be used to stabilize the Ti:sapphire lasers as well as existing ECDLs.

For now, the newly stabilized Ti:sapphire laser system will also be used for Doppler-resolved dynamics studies of CN radical reactions. Previous work in this direction was complicated by long-term (tens of seconds) drift in the probe laser frequency. This prevented long term signal averaging. However, the new system has an absolute frequency stability of better than 500 kHz for periods of many minutes, and so we can monitor the strength of a sub-Doppler spectroscopic feature during saturation depletion and transfer experiments. These measurements will shed light on such questions as the relative importance of velocity-, alignment-, and polarization-changing collisions of molecular free radicals in chemical systems and provide high precision experimental measurements for comparison to theory.

III. Publications supported by this project since 2010

- Pseudo-continuous resonance-enhanced multiphoton ionization: application to the determination of the hyperfine constants of ²⁰⁸Pb¹⁹F. P. Sivakumar, C. P. McRaven, P. M. Rupasinghe, T. Zh. Yang, N. E. Shafer-Ray, G. E. Hall and T. J. Sears, *Mol. Phys.* **108**, 927-935 (2010).
- Spectroscopic constants of the known electronic states of lead monofluoride, C.P. McRaven, P. Sivakumar, N.E. Shafer-Ray, Gregory E. Hall and Trevor J. Sears, *J. Molec. Spectrosc.* **262**, 89-92 (2010).
- Effect of laser injection seeder on rotationally resolved spectra of benzonitrile, H.-F. Xu, P. M. Johnson and T. J. Sears, *Chin. Phys. Lett.* **27**, 083301(3) (2010).
- Vibronic analysis of the S₁ – S₀ transition of phenyl acetylene using photoelectron imaging and spectral intensities derived from electronic structure calculations, C.-H. Chang, G. Lopez, T. J. Sears and P. M. Johnson, *J. Phys. Chem. A* **114**, 8262-8270 (2010).
- Sub-Doppler spectroscopy of mixed state levels in CH₂, C.-H. Chang, G. E. Hall and T. J. Sears, *J. Chem. Phys.* **133**, 144310(6) (2010).
- The CH₂ $b^1B_1 - \tilde{a}^1A_1$ band origin at 1.20 μ m, C.-H. Chang, J. Xin, T. Latsha, E. Otruba, Z. Wang, G. E. Hall and T. J. Sears, *J. Phys. Chem. A*, **115**, 9440-9446 (2011).
- Transient laser absorption spectroscopy of CH₂ near 780 nm, C.-H. Chang, Z. Wang, G. E. Hall, T. J. Sears and J. Xin, *J. Molec. Spectrosc.* **267**, 50-57 (2011).
- Frequency comb-referenced measurements of self- and nitrogen-broadening in the $\nu_1 + \nu_3$ band of acetylene, C. P. McRaven, M. J. Cich, G. V. Lopez, T. J. Sears, D. Hurtmans and A. W. Mantz, *J. Molec. Spectrosc.* **266**, 43-51 (2011).
- Precision spectroscopy of the ²⁰⁷Pb¹⁹F molecule: implications for measurement of P-odd and T-odd effects, L. D. Alpei, J.-U Grabow, A. N. Petrov, R. Mawhorter, B. Murphy, A. Baum, T. J. Sears, T. Zh. Yang, P. M. Rupasinghe, C. P. McRaven and N. E. Shafer-Ray, *Phys. Rev. A* **83** 040501 (2011).

- Precise characterization of the ground X_1 state of $^{206}\text{Pb}^{19}\text{F}$, $^{207}\text{Pb}^{19}\text{F}$ and $^{208}\text{Pb}^{19}\text{F}$, R. Mawhorter, B. Murphy, A. Baum, T. J. Sears, T. Zh. Yang, P. M. Rupasinghe, C. P. McRaven, N. E. Shafer-Ray, L. D. Alpei and J.-U. Grabow, *Phys. Rev. A* **84** 022508(12) (2011).
- Temperature-dependent pressure broadened line shape measurements of self- and nitrogen-broadening in the $\nu_1 + \nu_3$ band of acetylene, M. J. Cich, C. P. McRaven, G. V. Lopez, T. J. Sears, D. Hurtmans and A. W. Mantz, *Appl. Phys. B*, published on-line, November, 2011 DOI: 10.1007/s00340-011-4829-0.
- What is the best DFT function for vibronic calculations? A comparison of the calculated vibronic structure of the $S_1 - S_0$ transition of phenylacetylene with accurate experimental band intensities, G. V. Lopez, C.-H. Chang, P. M. Johnson, G. E. Hall, T. J. Sears, B. Markiewicz, M. Milan and A. Teslja, *J. Chem. Phys.* (submitted, March 2012).

Theoretical Studies of Potential Energy Surfaces and Computational Methods

Ron Shepard

Chemical Sciences and Engineering Division,
Argonne National Laboratory, Argonne, IL 60439
[email: shepard@tcg.anl.gov]

Program Scope: This project involves the development, implementation, and application of theoretical methods for the calculation and characterization of potential energy surfaces (PES) involving molecular species that occur in hydrocarbon combustion. These potential energy surfaces require an accurate and balanced treatment of reactants, intermediates, and products. This difficult challenge is met with general multiconfiguration self-consistent field (MCSCF) and multireference single- and double-excitation configuration interaction (MR-SDCI) methods. In contrast to the more common single-reference electronic structure methods, this approach is capable of describing accurately molecular systems that are highly distorted away from their equilibrium geometries, including reactant, fragment, and transition-state geometries, and of describing regions of the potential surface that are associated with electronic wave functions of widely varying nature. The MCSCF reference wave functions are designed to be sufficiently flexible to describe qualitatively the changes in the electronic structure over the broad range of molecular geometries of interest. The necessary mixing of ionic, covalent, and Rydberg contributions, along with the appropriate treatment of the different electron-spin components (e.g. closed shell, high-spin open-shell, low-spin open shell, radical, diradical, etc.) of the wave functions are treated correctly at this level. Further treatment of electron correlation effects is included using large-scale multireference CI wave functions, particularly including the single and double excitations relative to the MCSCF reference space. This leads to the most flexible and accurate large-scale MR-SDCI wave functions that have been used to date in global PES studies.

Recent Progress: ELECTRONIC STRUCTURE CODE MAINTENANCE, DEVELOPMENT, AND APPLICATIONS: A major component of this project is the development and maintenance of the COLUMBUS Program System. The COLUMBUS Program System computes MCSCF and MR-SDCI wave functions, MR-ACPF (averaged coupled-pair functional) energies, MR-AQCC (averaged quadratic coupled cluster) energies, spin-orbit CI energies, analytic energy gradients, and nonadiabatic coupling. Geometry optimizations to equilibrium and saddle-point structures can be done automatically for both ground and excited electronic states. The COLUMBUS Program System is maintained and developed collaboratively with several researchers including Isaiah Shavitt (University of Illinois), Russell M. Pitzer (Ohio State University), Thomas Mueller (Jülich Supercomputer Center, Germany), and Hans Lischka (University of Vienna, Austria, and Texas Tech University). The nonadiabatic coupling and geometry optimizations for conical intersections is done in collaboration with David R. Yarkony (Johns Hopkins University). The distributed development effort and software coordination uses an svn repository of source code. The parallel sections of the code are based on the single-program multiple-data (SPMD) programming model with explicit

This work was performed under the auspices of the Office of Basic Energy Sciences, Division of Chemical Sciences, Geosciences, and Biosciences, U.S. Department of Energy, under contract number DE-AC02-06CH11357.

message passing using the portable MPI library, and the portable Global Array Library (distributed from PNNL) is used for data distribution. The COLUMBUS codes incorporate several of the newer language features of F90 and later in order to facilitate future development and maintenance efforts.

REVIEWS OF MULTIREFERENCE METHODS: In the past year we have published three major invited review articles on multireference methods. The first [*WIREs Comput. Mol. Sci.* **1**, 191 (2011)] focuses on the COLUMBUS Program System, particularly on the underlying algorithms and capabilities of the software package. The second [*Advanced Series in Physical Chemistry*, **17** (World Scientific, Singapore, 2011)] is an overview of applications and methodology of nonadiabatic coupling and nonadiabatic direct dynamics using multireference methods. The third [*Chem. Rev.* **112**, 108-181 (2012)] is a general review with 860 references of the MCSCF, MRCI, MR-ACPF, MR-AQCC, and related methods and applications over the past decade.

GRAPHICALLY CONTRACTED FUNCTION METHOD: We have recently developed a novel expansion basis for electronic wave functions [see *Mol. Phys.* **108**, 2717 (2010) and references therein]. In this approach, the wave function is written as a linear combination of *graphically contracted functions* (GCFs), and each GCF in turn is formally equivalent to a linear combination of configuration state functions (CSFs) that comprise an underlying linear expansion space of dimension N_{csf} . The CSF coefficients that define the GCFs are nonlinear functions of a smaller number of variables $N_{\phi} \ll N_{\text{csf}}$. GCF expansions with 10 to 20 basis functions can approach the full-CI PES to within chemical accuracy (1 kcal/mole or better) [*Int. J. Quantum Chem.* **107**, 3203 (2007)]. The method is formulated in terms of spin-eigenfunctions using the Graphical Unitary Group Approach (GUGA) of Shavitt, and consequently it does not suffer from spin contamination or spin instability.

This new method is characterized by several important features. First, open-shell spin-eigenfunctions are included in the wave function expansions. This allows our new method to be used for the chemical reactions that are important to combustion chemistry (e.g. involving radicals and other open-shell electronic states) without introducing artificial spin contamination. Second, no intrinsic restrictions are imposed on the orbital occupations, so the GCFs are not restricted to only geminals or to other preselected molecular fragments, and there are no artificial excitation-level or occupation restrictions with respect to a reference function or reference space; in this sense, the method is more correctly characterized as a multiconfigurational method rather than a multireference method. Third, we use linear combinations of N_{GCF} basis functions rather than a single expansion term. This allows our method to be used for both ground and excited electronic states, the increased wave function flexibility leads to more accurate wave functions, and it will allow the computation of transition moments, nonadiabatic coupling, and other properties that at present can only be computed reliably with MCSCF and MRCI approaches.

In the past year our focus has been on the development and implementation of a *multifacet* generalization of the GCF method. In the previous implementations, a single lower- or upper-walk, recursively contracted, wave function is associated with each node of the Shavitt graph within a GCF basis function; we now term this the *single-facet* GCF approach. With the multifacet approach, each MFGCF basis function has more flexibility than a SFGCF function. This increased flexibility allows accurate wave functions to be

represented with smaller N_{GCF} expansion dimensions. This reduces the N_{GCF}^2 factor in the effort required for Hamiltonian matrix element, reduced density matrix (RDM) elements, and other computational tasks. A general feature of the new method is that arithmetic operations that previously involved scalars are replaced with matrix-vector and matrix-matrix products where the matrix dimensions depend on the number of facets associated with the nodes; f_k^P denotes the number of facets for node k in the GCF $|P\rangle$. Thus the computational effort associated with more flexible wave functions increases with larger f_k values rather than with larger N_{GCF} values alone. The efficient recursive algorithms developed previously for the SFGCF approach carry over in a straightforward way for MFGCF expansions. For the new MFGCF method at present, we have partially or fully implemented the computation of Hamiltonian matrix elements, 1-RDM, 2-RDM [*J. Phys. Chem. A* **110**, 8880 (2006)], spin-Density matrices [*Int. J. Quantum Chem.* **109**, 3552 (2009)], CSF overlaps [*J. Phys. Chem. A* **109**, 11629 (2005)], and Slater determinant overlaps [*J. Comp. Chem.* **30**, 2414 (2009)]. We are also investigating several approaches to the optimization of the nonlinear arc factor parameters with this new wave function parameterization based on analytic gradients with respect to the nonlinear arc factor parameters [*Int. J. Quantum Chem.* **110**, 2938 (2010)]. At present, we have not completed any significant applications with this new expansion basis, but we have succeeded in optimizing some wave functions for a few particular cases. From this limited set of initial calculations we can report that for a given wave function accuracy, the number of facets f_k in the MFGCF basis is usually smaller than the number of basis functions N_{GCF} with the corresponding SFGCF basis. In principle, there is an exponential relationship between these two parameters, $N_{\text{GCF}} \approx (f_k)^{2n}$ where n is the number of molecular orbitals, but we have not yet observed this empirically. We expect to extend the range of applications over the next year as this new implementation matures and as we formulate more robust optimization approaches.

Future Plans: GCF METHOD: Our MFGCF implementation has so far used single-headed Shavitt graphs appropriate for describing individual molecular states with a given number of electrons, with a particular spin state, and that belong to a particular point group irreducible representation (irrep). We will generalize this in several respects. First, we will introduce state averaging over individual irreps and state averaging over multiple irreps. This will allow the nonlinear arc factor parameters to be optimized for several electronic states simultaneously rather than for individual electronic states. For the multiple-irrep case, this will allow the computation of several molecular states with essentially no additional effort over single-irrep calculations. Next, we will employ multiheaded Shavitt graphs in the state-averaging procedure. This will allow the computation of Hamiltonian matrix elements corresponding to states with different numbers of electrons, different spin values, and different irreps simultaneously with only a relatively small increase in effort over the current single-state approach.

The GCF code has now been placed in a development branch of the COLUMBUS svn repository. In this way the code is now available for a wider range of inspection and scrutiny by COLUMBUS developers. We hope to develop a robust implementation and incorporate the GCF method into the standard distribution version of COLUMBUS for even wider use by the broader user community for general chemical applications in the near future.

Publications:

- “An Efficient Recursive Algorithm to Compute Wave Function Optimization Gradients for the Graphically Contracted Function Method”, R. Shepard, G. Gidofalvi and P. D. Hovland, *Int. J. Quantum Chem.* **110**, 2938-2948 (2010).
- “Exploiting Sparsity in the Graphically Contracted Function Configuration Interaction Method,” G. Gidofalvi and R. Shepard, *Mol. Phys.* **108**, 2717-2724 (2010).
- “Excited-State Calculations With the Graphically Contracted Function Method,” G. Gidofalvi and R. Shepard, *50th Sanibel Symposium Program Abstracts*, (2010).
- “A New Algorithm for Computing Optimization Gradients and Orbital-Level Hamiltonian Matrices Within the Graphically Contracted Function Method,” R. Shepard and G. Gidofalvi, *50th Sanibel Symposium Program Abstracts*, (2010).
- “Recent Developments and Applications of the Graphically Contracted Function Method,” R. Shepard and G. Gidofalvi, *Program and Abstracts, Molecular Quantum Mechanics: From Methylene to DNA and Beyond*, 189 (2010).
- “COLUMBUS—A Program System for Advanced Multireference Theory Calculations,” H. Lischka, T. Müller, P. G. Szalay, I. Shavitt, R. M. Pitzer, R. Shepard, *WIREs Comput. Mol. Sci.* **1**, 191 (2011).
- “Computational and Methodological Elements for Nonadiabatic Trajectory Dynamics Simulations of Molecules,” M. Barbatti, R. Shepard, and H. Lischka, in “Conical Intersections: Theory, Computation and Experiment”, W. Domcke, D.R. Yarkony and H. Köppel, Eds., *Advanced Series in Physical Chemistry*, **17** (World Scientific, Singapore, 2011) pp. 415-462.
- “Reduced Density Matrices Within the Graphically Contracted Function Method,” R. L. Shepard, *Abstracts of Papers of the American Chemical Society* **242**, 278-PHYS (2011).
- “Multiconfiguration Self-Consistent Field and Multireference Configuration Interaction Methods and Applications,” P. G. Szalay, T. Mueller, G. Gidofalvi, H. Lischka, R. Shepard, *Chem. Rev.* **112**, 108-181 (2012).
- “The Multifacet Graphically Contracted Function Method: I. Formulation And Implementation”, R. Shepard, G. Gidofalvi, and S. R. Brozell (*manuscript in preparation*).
- “The Multifacet Graphically Contracted Function Method: II. Essential Parameterization Of The Arc Factors”, R. Shepard, G. Gidofalvi, and S. R. Brozell (*manuscript in preparation*).
- “The Multifacet Graphically Contracted Function Method: III. Applications,” G. Gidofalvi, S. R. Brozell, and R. Shepard, (*manuscript in preparation*).

Mechanisms and Models for Combustion Simulations

Raghu Sivaramakrishnan

Chemical Dynamics Group, Chemical Sciences & Engineering Division

Argonne National Laboratory, Argonne, IL 60439

raghu@anl.gov

I. Program Scope

Mechanisms describing the combustion chemistry of even simple fuels can be complex involving a myriad of unimolecular and bimolecular elementary steps. The primary scope of this program is to develop and validate detailed chemical kinetics mechanisms and models for use in simulations for combustion.

The kinetics models will be developed on the basis of a consistent framework incorporating theoretical predictions, experimental measurements, and evaluations of elementary reaction rate coefficients, with feedback loops between them. The detailed models will subsequently be used for simulations of data from reactors, shock-tubes, rapid compression machines, and flames with the aim of validating the mechanistic and kinetic aspects of these models over practical combustion regimes.

II. Recent Progress

A. *The high temperature thermal decomposition mechanism of CH₃CHO*

CH₃CHO thermal decomposition has been a subject of numerous studies over the past 80 years with the essential mechanistic features remaining largely unchanged from the early propositions of Rice and Herzfeld [1]. Initiation through C-C bond fission (R1),



is the only active channel considered in low temperature (<850 K) [2-4] or high temperature (>1000 K) studies [5-7]. However, this well characterized decomposition has merited renewed scrutiny in the combustion and gas phase chemical physics community for two main reasons.

1. This is an intermediate that appears in copious amounts when combusting new generation oxygenated fuels, as such or in blends, with conventional fuels [8].

2. Recent experimental [9,10] and theoretical [11] studies have suggested new mechanistic thermal decomposition pathways not considered in prior literature studies.

The present modeling study in collaboration with S. J. Klippenstein, L. B. Harding and J. V. Michael (Argonne) was necessitated by the observation of a variety of products detected by very sensitive diagnostics in recent high temperature micro-tubular reactor experiments on the thermal decomposition of CH₃CHO and its deuterated analogs [10]. The observations of these products along with the absence of CH₄ prompted the authors of this study [10] to question the validity of the roaming mechanism,



Furthermore Vasiliou et al. [10] suggest that the enol tautomer, C₂H₃OH (vinyl alcohol), is a primary intermediate and that its unimolecular decomposition mechanism is an integral part of the acetaldehyde thermal decomposition mechanism. Our present modeling efforts on acetaldehyde decomposition incorporate a master equation re-analysis of the CH₃CHO potential energy surface [11]. The lowest energy process on this PES is an isomerization of CH₃CHO to C₂H₃OH. However, the subsequent product channels for C₂H₃OH are substantially higher in energy and the only unimolecular process that can be thermally accessed is a re-isomerization to CH₃CHO [11,12]. Theoretical kinetics predictions coupled with our modeling efforts of selected literature experiments [5,6] on CH₃CHO thermal decomposition are in agreement with our earlier experiment and theory based conclusions that the dominant decomposition process in CH₃CHO at high temperatures is C-C bond fission with a minor contribution (~10-20%) from the roaming mechanism. The present modeling efforts also incorporate a master-equation analysis of the H + C₂H₃OH potential energy surface (Figure 1). This bimolecular reaction is the primary mechanism for removal of C₂H₃OH that builds up to minor amounts (~3-4% flux) at the higher temperatures in the recent

micro-tubular reactant experiments [10] that use large initial concentrations of CH_3CHO . The unique combination of sensitive diagnostics, high temperatures and relatively short residence times (100-200 μs) in the micro-tubular reactor is the main reason for the observation of this heretofore unobserved minor intermediate in CH_3CHO decomposition. A master equation analysis of the PES in Fig. 1 predicts a variety of product channels (prompt and abstraction pathways) active at 0.1 atm and high temperatures (Figure 2). Simulations with our model indicate a rich spectrum of products that can be produced at typical conditions (0.1 atm, 1700 K and 100-200 μs) attained in the micro-tubular reactor (Figure 3). The major products observed are due to the major bond fission reaction (R1) with minor contributions from the roaming mechanism, reaction (R2). The modeling results indicate that the observation of ketene in this reactor [10] is primarily due to vinoxy decomposition, with the two sources for vinoxy being $\text{H} + \text{CH}_3\text{CHO}$ (90%) and $\text{H} + \text{CH}_2\text{CHOH}$ (10%). Interestingly, the intriguing observations of H_2O (an intermediate not observed in CH_3CHO thermal decomposition to date and a primary cause for invoking the kinetically insignificant H_2O elimination channel from CH_2CHOH in [10]) is due to the formation of OH (from $\text{H} + \text{CH}_2\text{CHOH} \rightarrow \text{C}_2\text{H}_4 + \text{OH}$, Figures 1 & 2) that instantaneously reacts with the excess reactant, CH_3CHO . C_2H_2 formation is primarily due to the cascading sequence of reactions that lead from $\text{C}_2\text{H}_4 \rightarrow \text{C}_2\text{H}_3 \rightarrow \text{C}_2\text{H}_2$ with the source for C_2H_4 being $\text{CH}_3 + \text{CH}_3 \rightarrow \text{C}_2\text{H}_4 + 2\text{H}$. A minor channel for C_2H_2 formation is the abstraction reaction of H with CH_2CHOH (Figures 1 & 2). In summary, our simulations indicate that the observation of ketene, water and acetylene and their deuterated analogs in the micro-tubular reactor are primarily due to bimolecular reactions of CH_3CHO and $\text{C}_2\text{H}_3\text{OH}$ with H-atoms and OH radicals and have no bearing on the unimolecular decomposition mechanism of CH_3CHO . The model was also used to simulate a typical H-ARAS experiment from Ref. 9 (Figure 4). The simulations indicate that in this dilute system, bimolecular reactions are suppressed and the observed products are entirely consistent with prior conclusions [9,11] that the unimolecular decomposition mechanism of CH_3CHO involves only reactions (R1) and (R2).

B. Thermal decomposition and abstraction reactions of small methylesters

In collaboration with J. V. Michael (Argonne) we have initiated a joint experiment/theory study on the thermal decompositions of small methyl esters, methyl formate (MF) and methyl acetate (MA), and their abstractions by H and CH_3 [13,14]. A master equation analysis was performed with a potential energy surface calculated at the CCSD(T)/cc-pv ∞Z //B3LYP/6-311++G(d,p) level of theory for all thermal decomposition processes in MF and MA. The theoretical predictions were found to be in good agreement with the present experimentally derived rate constants for the bond fissions. TST calculations using CCSD(T)/cc-pv ∞Z //MP2/aug-cc-pvtz energies and molecular properties for the H-atom abstraction reactions also are in good agreement with the experimentally measured rate constants and branching ratios using a combination of H-atom and D-atom ARAS.

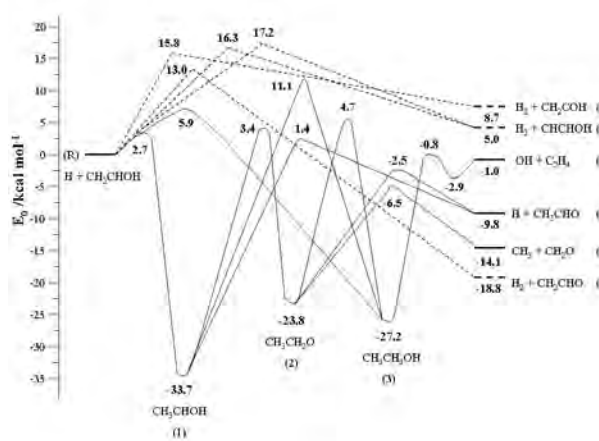


Figure 1: $\text{H} + \text{CH}_2\text{CHOH}$ potential energy surface. Solid lines – Adapted from Senosiain et al. [15], dashed lines – p. w., CCSD(T)/CBS//QCISD/6-311++G(d,p)

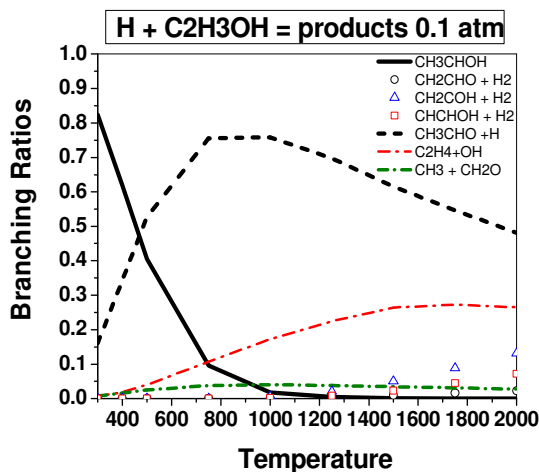


Figure 2: Product branching ratios from master equation calculations. Solid line – stabilization, dashed lines – addition-eliminations, symbols – abstractions.

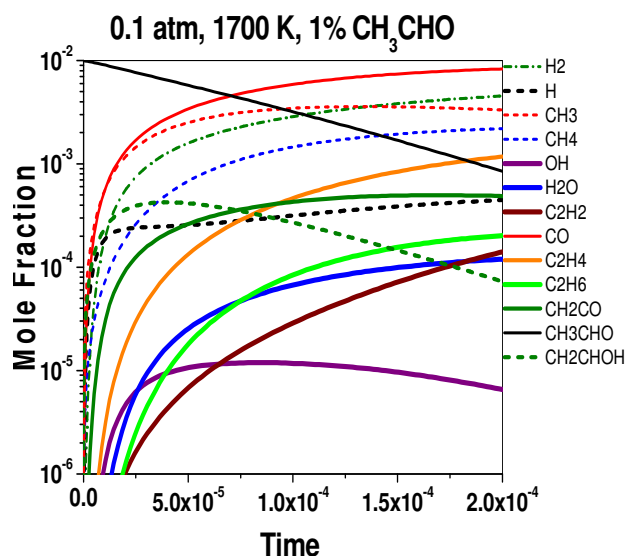


Figure 3: Predicted species profiles from the micro-tubular reactor [10] using the model for CH_3CHO pyrolysis from the present study.

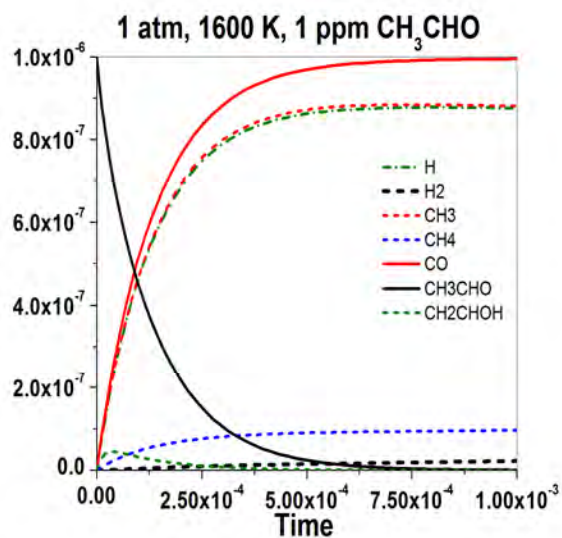


Figure 4: Predicted species profiles in a typical H-ARAS experiment [9] using the present model.

C. Developing detailed and reduced chemical kinetics models for biodiesel engine simulations

In collaboration with Michael Davis (Argonne), Sibendu Som and Douglas Longman (Engines & Emissions group at Argonne) and T. F. Lu (Univ. of Connecticut) we have initiated an engine modeling study of biodiesel surrogates [16]. A detailed chemical kinetic model for a 1st generation biodiesel surrogate (a blend of methyl butanoate and n-heptane) was developed. Graph based methods (DRG) were utilized to reduce the size of this model to enable realistic 3-D engine simulations. The engine simulations show reasonable agreement with available biodiesel engine data.

III. Future work

We plan to complete our small alcohol ($\text{C}_1\text{-C}_2$) combustion modeling and theoretical studies and use this experience to focus on developing models in a systematic approach for selected $\text{C}_3\text{-C}_4$ alcohols. We also propose to characterize theoretically H-atom abstractions by OH from small methylesters in a systematic manner. Consequently we propose to initiate a collaborative effort with Joe Michael (experiments) to characterize the reactions of OH with four small methylesters (methyl formate, methyl acetate, methyl propionate, and methyl butanoate). The elementary kinetics studies on the simple methyl esters are now being incorporated in a detailed chemical kinetic modeling study of small methyl esters. We propose to continue our modeling efforts on small aromatics such as toluene and xylenes.

IV. References

- 1 F. O. Rice, K.F. Herzfeld, J. Amer. Chem. Soc. **1934**, 56, 284.
2. K. J. Laidler, M. T. H. Liu, Proc. Roy. Soc. Lond. A **1967**, 297, 365.
3. M. T. H. Liu, K. J. Laidler, Can. J. Chem. **1968**, 46, 479.
4. I. Bardi, F. Marta, Acta. Phys. Chem. **1973**, 19, 227.
5. K. S. Gupte, J. H. Kiefer, R. S. Tranter, S. J. Klippenstein, L. B. Harding, Proc. Combust. Inst. **2007**, 31, 167 and references within.
6. T. Bentz, F. Striebel, M. Olzmann, J. Phys. Chem. A **2008**, 112, 6120-6124.
7. K. Yasunaga, S. Kubo, H. Hoshikawa, T. Kamesawa, Y. Hidaka, Y. Int. J. Chem. Kinet. **2008**, 40, 73.
8. K. Kohse-Höinghaus, P. Obwald, T. A. Cool, T. Kasper, N. Hansen, F. Qi, C. K. Westbrook, P. R. Westmoreland, Angew. Chem. Int. Ed. **2010**, 49, 3572.
9. R. Sivaramakrishnan, J. V. Michael, S. J. Klippenstein, J. Phys. Chem. A **2010**, 114, 755.

10. A. Vasiliou, K. M. Piech, X. Zhang, M. R. Nimlos, M. Ahmed, A. Golan, O. Kostko, D. L. Osborn, J. W. Daily, J. F. Stanton, G. B. Ellison, *J. Chem. Phys.* **2011**, 135, 014306.
11. L. B. Harding, Y. Georgievskii, S. J. Klippenstein, *J. Phys. Chem. A* **2010**, 114, 765.
12. J.-X. Shao, C.-M. Gong, X.-Y. Li, J. Li, *Theor Chem. Acc.* **2011**, 128, 341.
13. S. L. Peukert, R. Sivaramakrishnan, M.-C. Su, and J. V. Michael, *Comb. and Flame*, In Press, **2012**.
14. S. L. Peukert, R. Sivaramakrishnan, M.-C. Su, and J. V. Michael, *Proc. Combust. Inst.*, in review.
15. J. P. Senosiain, S. J. Klippenstein, J. A. Miller, *J. Phys. Chem. A* **2006**, 110, 6960.
16. R. Sivaramakrishnan, W. Liu, M. J. Davis, S. Som, D. E. Longman, T. F. Lu, *Proc. Combust. Inst.*, in review.

V. Journal articles supported by this project 2010-2012

1. R. Sivaramakrishnan, J. V. Michael and S. J. Klippenstein, "The direct observation of roaming radicals in the thermal decomposition of acetaldehyde," *J. Phys. Chem. A* **114**, 755-764 (2010).
2. R. Sivaramakrishnan, M.-C. Su, J. V. Michael, S. J. Klippenstein, L. B. Harding, and B. Ruscic, "Rate constants for the thermal decomposition of ethanol and its bimolecular reactions with OH and D: Reflected shock tube and theoretical studies" *J. Phys. Chem. A* **114**, 9425-9439 (2010).
3. R. Sivaramakrishnan, M.-C. Su, and J. V. Michael, "H- and D-atom formation from the pyrolysis of C₆H₅CH₂Br and C₆H₅CD₂Br: Implications for high-temperature benzyl decomposition," *Proc. Combust. Inst.* **33**, 243-250 (2011).
4. R. Sivaramakrishnan and J. V. Michael, "Pyrolysis of C₆D₅CH₃: Rate constants and branching ratios in the high temperature thermal decomposition of toluene," *Proc. Combust. Inst.* **33**, 225-232 (2011).
5. R. Sivaramakrishnan, J. V. Michael, A. F. Wagner, R. Dawes, A. W. Jasper, L. B. Harding, Y. Georgievskii and S. J. Klippenstein, "Roaming radicals in the thermal decomposition of dimethyl ether: Experiment and theory," *Combust. and Flame* **158**, 618-632 (2011).
6. S. L. Peukert, R. Sivaramakrishnan, M.-C. Su, and J. V. Michael, "Experiment and theory on methylformate and methylacetate kinetics at high temperatures: Rate constants for H-atom abstraction and thermal decomposition, ASAP article, *Comb. And Flame*, 2012. <http://dx.doi.org/10.1016/j.combustflame.2012.03.007>
7. S. L. Peukert, R. Sivaramakrishnan, M.-C. Su, and J. V. Michael, "High temperature rate constants for H/D + methylformate and methylacetate," In Review, *Proc. Combust. Inst.* 34, 2012.
8. R. Sivaramakrishnan, W. Liu, M. J. Davis, S. Som, D. E. Longman, and T. F. Lu, "Development of a reduced biodiesel surrogate model for compression ignition engine modeling," In Review, *Proc. Combust. Inst.* 34, 2012.
9. R. Sivaramakrishnan, J. V. Michael, L. B. Harding and S. J. Klippenstein, "Revisiting the thermal Decomposition mechanism of CH₃CHO", In Preparation, *J. Phys. Chem. A*, 2012.

Other Publications supported by this project 2010-2012

1. R. Sivaramakrishnan, D. Y. Zhou, R. T. Skodje and M. J. Davis, "A comprehensive mechanism for ethanol combustion" Paper 3A03, 7th National Technical Meeting of the Combustion Institute, Atlanta, GA, Mar 20-23, 2011.
2. R. Sivaramakrishnan and J. V. Michael, "The thermal decomposition of o-xylyl radicals," Paper 2B03, 7th National Technical Meeting of the Combustion Institute, Atlanta, GA, Mar 20-23, 2011.
3. R. Sivaramakrishnan, W. Liu, M. J. Davis, S. Som, D. E. Longman, "A high-temperature model for methylbutanoate combustion," Fall Technical Meeting of Eastern States Section of the Combustion Institute, Storrs, CT, Oct 09-12, 2011.
4. R. Sivaramakrishnan, W. Liu, M. J. Davis, S. Som, D. E. Longman, "Development of a Reduced Biodiesel Surrogate Model for Compression Ignition Engine Modeling", Spring Technical Meeting of the Central States Section of the Combustion Institute, Dayton, OH, Apr 22-24, 2012.

COMPUTATIONAL AND EXPERIMENTAL STUDY OF LAMINAR FLAMES

M. D. Smooke and M. B. Long
Department of Mechanical Engineering
Yale University
New Haven, CT 06520
mitchell.smooke@yale.edu

Program Scope

Our research has centered on an investigation of the effects of complex chemistry and detailed transport on the structure and extinction of hydrocarbon flames in coflowing axisymmetric configurations. We have pursued both computational and experimental aspects of the research in parallel. The computational work has focused on the application of accurate and efficient numerical methods for the solution of the boundary value problems describing the various reacting systems. Detailed experimental measurements were performed on axisymmetric coflow flames using two-dimensional imaging techniques. Spontaneous Raman scattering and laser-induced fluorescence were used to measure the temperature, and major and minor species profiles. Laser-induced incandescence (LII) has been used to measure soot volume fractions and particle sizes. A new approach to optical pyrometry has been developed to measure temperatures where the other techniques fail due to the presence of soot. Our goal has been to obtain a more fundamental understanding of the important fluid dynamic and chemical interactions in these flames so that this information can be used effectively in combustion modeling.

Recent Progress

JP8 Coflow Surrogate Flame Structure

The structure of jet-fuel coflow flames has been investigated by concurrent use of numerical simulations and laser diagnostic measurements. Three different surrogate formulations were considered. Numerical simulations were performed by a parallel, implicit, Newton-based algorithm, and on-the-fly chemistry reduction was used to decrease the computational time. Experimental values for temperature, CO₂, H₂O, and O₂ were collected by Rayleigh and Raman scattering. Fuel molecules were qualitatively tracked measuring CH-stretch Raman emission.

The application of Rayleigh and Raman laser diagnostic techniques to jet-fuel flames is somewhat problematic. For Rayleigh temperature measurements, one needs to account for the presence of species-dependent cross sections. Numerical simulations were used for this purpose but an artificial broadening of the flame front was observed. Simultaneously, the presence of very low levels of soot in the flame core artificially depresses the measured temperature at the tip of the flame.

Raman mole fraction measurements are also difficult because of the intense laser-induced fluorescence signal generated by aromatic molecules in the fuel. To overcome this interference, a polarized/depolarized subtraction was used and a novel filtering technique was developed that interpolates the experimental data with simulated Raman spectra. The combined use of our post-processing technique with the polarized/depolarized subtraction proved very efficient at rejecting the undesired fluorescence signal from the measurement. High quality measurements were obtained through this approach.

Noticeably, it was found that temperature measurements based on the Raman signal from nitrogen are more accurate than the temperature obtained using the Rayleigh scattering signal. This is due to the presence of large differences in species cross-sections in the Rayleigh measurements, which can be corrected but induce an artificial smearing of the temperature distribution. This is a peculiar feature of kerosene and heavy hydrocarbon flames in general, for which the cross section of the fuel molecules can be orders of magnitude higher than the oxidizer.

For all flames considered, the temperature and mole fraction distributions were well predicted by the chemical mechanism. The general flame structure, as defined by the temperature map and the Raman measurements for O_2 is correctly predicted by the numerical simulations. Furthermore, the signal from the fuel molecules correctly identifies the pyrolysis region at the base of the flame.

The experiments for carbon dioxide and water are less accurate because of fluorescence interference and low signal, however, the obtained mole fraction maps seem to be in good agreement with the simulations. These results demonstrate the possibility of using laser diagnostics and numerical simulations as a valid investigation tool to study JP-8 combustion in multidimensional configurations.

Time-Varying Flames

The extension of a low order implicit solver to model time-dependent chemically reacting flows is hindered by the presence of large artificial diffusion, in particular from the first-order upwind discretizations of the convective terms in the governing equations. As in the steady-state problem, this can be reduced through grid refinement. In a time-evolving flow, however, node clustering must be adjusted dynamically to follow the movement of flow structures such as vortices. Otherwise, during some stages of the computations, important flow nonuniformities may penetrate regions of the domain having insufficient grid resolution and experience a significant amount of artificial diffusion, thus spuriously altering the flow dynamics. As an alternative approach, high order discretization schemes with negligible numerical diffusion can be used for flame computations.

We are applying high order compact spatial discretizations in a fully implicit framework that avoid these problems, and offer many advantages over other current approaches to solving reacting flow problems. Compact schemes are well suited to the simulation of time-dependent flows with complicated structures due to their excellent resolution characteristics [3,4]. Their integration into an efficient Newton-based flame code is an extremely challenging problem requiring research in modern iterative linear algebra solvers and preconditioning, novel storage/retrieval methodologies, fast Jacobian matrix algorithms, and domain decomposition methods. The necessity of implementing all these numerical techniques on message-passing parallel architectures only compounds the difficulty. However, efficiency arguments indicate that the use of compact spatial discretizations with implicit time stepping may be able to reduce overall computation times dramatically compared to other numerical methods commonly employed in detailed-chemistry combustion simulations [5].

Soot Measurements in a Series of Elevated Pressure Flames

Experimental investigations of laminar coflow methane-air diffusion flames were extended to assess the influence of moderate changes in pressure up to 2.5 atm. The burner consists of a central fuel jet (4 mm inner diameter, 0.38 mm wall thickness) surrounded by coflowing air (50 mm diameter). The inlet velocity profile of both fuel and coflow was plug flow and was fixed at 35 cm/s, which means that the mass flow rate was increased with pressure accordingly. The burner and ignition system were housed inside a 44.2 liter pressure chamber. The elevated

pressures were stabilized by a servo valve using closed-loop control. Three quartz windows on the chamber provided optical access to the flame. A digital single lens reflex camera (Nikon D90) was used to acquire sooty flame color images through a BG-7 glass filter. By calibration of the detector's spectral response, the soot luminosity images can be used to obtain the soot temperature [6]. An absolute light intensity calibration by using a S-type thermocouple further allows determination of soot volume fraction [7].

Measurements were taken for 80% CH₄/ 20% N₂ and 100% CH₄ flames with varying pressures from 1.2 atm to 2.4 atm with an increment of 0.2 atm. Figure 1 shows the soot temperature (left) and volume fraction (right) for 80% CH₄ flames (top) and 100% CH₄ flames (bottom). The quantitative results from this exploration will be used to guide further studies both computationally and experimentally.

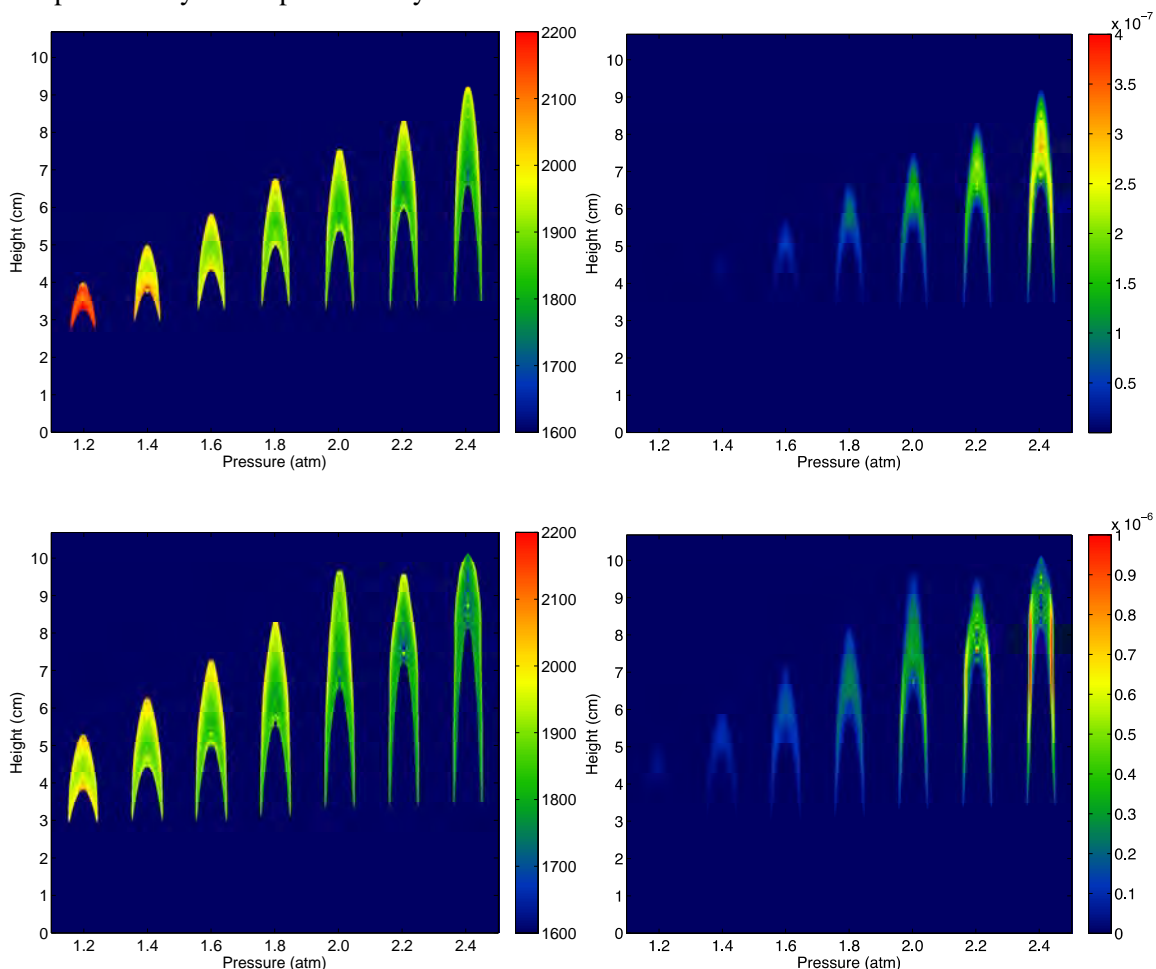


Figure 1. Soot temperature (left) and volume fractions (right) for 80% CH₄ flames (top) and 100% CH₄ flames (bottom), for a range of pressure levels (1.2, 1.4, 1.6, 1.8, 2.0, 2.2 and 2.4 atm). The temperature scale is in K.

Future Plans

During the next year we will continue our study of time varying flames with the goal of fully implementing higher order compact-based methods. We plan to study both sooting and nonsooting hydrocarbon flames. Experimentally, we plan to add minor species measurements (*OH*, *CH* and *NO*) with laser-induced fluorescence to complete the characterization of species in

these time-varying flames. Further, we will perform phase-resolved PIV measurements of the velocity profiles within the flames and, using the same techniques that we have developed for the steady sooting flames, we will perform phase-averaged measurements to characterize the soot in the time-varying flames. We will also continue our studies of coflow flames at higher pressures.

References

1. L. Tosatto, B. A. V. Bennett and M. D. Smooke, "Parallelization Strategies for an Implicit Newton-based Reactive Flow Solver," *Combust. Theory Model.*, **15**, (2011).
2. L. Liang, J. G. Stevens, and J. T. Farrell, *Proc. Combust. Inst.*, **32**, (2009).
3. S.K. Lele, "Compact Finite Difference Schemes with Spectral-Like Resolution," *J. Comput. Phys.*, **103**, (1992).
4. R.V. Wilson, A.O. Demuren, and M. Carpenter, "Higher-Order Compact Schemes for Numerical Simulation of Incompressible Flows, Part II: Applications," *Numer. Heat Transfer, Part B*, **39**, (2001).
5. M. Noskov, Ph.D. Thesis, Yale University, 2004.
6. P. B. Kuhn, B. Ma, B. C. Connelly, M. D. Smooke, and M. B. Long, *Proc. Combust. Inst.* **33**, (2011).
7. B. Ma and M.B. Long, *Proc. Combust. Inst.* submitted (2012).

DOE Sponsored Publications since 2010

1. M. Sanchez-Sanz, B. A. V. Bennett, M. D. Smooke and A. Linan, "Influence of Strouhal Number on Pulsating Methane/Air Coflow Jet Diffusion Flames," **14**, *Comb. Theory and Modelling*, (2010).
2. R. B. Dobbins and M. D. Smooke, "A Fully Implicit Compact Finite Difference Method for the Numerical Solution of Unsteady Laminar Flames," *Flow, Turb. and Comb.*, **85**, (2010).
3. B. C. Connelly, N. B. Long, M. D. Smooke, R. J. Hall, and M. B. Colket, "Computational and Experimental Investigation of Soot and NO in Coflow Diffusion Flames," in *Combustion Generated Fine Carbonaceous Particles*, Edited by H. Bockhorn, et al., KIT Scientific Publishing, Karlsruhe, (2010)
4. B. Coriton, M. D. Smooke and A. Gomez, "Effect of the Composition of the Hot Product Stream in the Quasi-Steady Extinction of Strained Premixed Flames," *Comb. and Flame*, **157**, (2010).
5. P. B. Kuhn, B. Ma, B. C. Connelly, M. D. Smooke, and M. B. Long, "Soot and Thin-filament Pyrometry Using a Color Digital Camera," *Proceedings of the Combustion Institute*, **33**, 2011.
6. B. Coriton, J. H. Frank, A. G. Hsu, M. D. Smooke and A. Gomez, "Effect of Quenching of the Oxidation Layer in Highly Turbulent Counterflow Premixed Flames," *Proceedings of the Combustion Institute*, **33**, 2011.
7. L. Tosatto, B. A. V. Bennett and M. D. Smooke, "Parallelization Strategies for an Implicit Newton-based Reactive Flow Solver," *Comb. Theory and Modelling*, **15**, (2011).
8. L. Tosatto, T. Lu, B. A. V. Bennett and M. D. Smooke, "A Flux-Based Directed Relation Graph Method for the Adaptive On-the-Fly Reduction of Chemical Mechanisms," *Comb. and Flame*, **158**, (2011).
9. J. D. Herdman, B. C. Connelly, M. D. Smooke, M. B. Long, and J. H. Miller, "A Comparison of Raman Signatures and Laser-Induced Incandescence with Direct Numerical Simulation of Soot Growth in Non-Premixed Ethylene/Air Flames," *Carbon*, **49**, (2011).
10. M. B. Colket, S. P. Zeppieri, M. D. Smooke and W. W. Kim, "Laminar Flame Speeds, Flammability Limits, and Flame/Reaction Zone Thicknesses for a Surrogate Kerosene Fuel at Engine Operating Conditions," AIAA Paper 2011.

Quantum Chemistry of Radicals and Reactive Intermediates

John F. Stanton
Institute for Theoretical Chemistry
University of Texas
Austin, TX 78712

Scope of Research

My research group works in the area of theoretical chemical physics, especially on the properties and chemistry of organic radicals and other reactive intermediates. This research follows a number of paths, including first-principles calculations of bond energies and other thermochemical information (as well as development of methodology for such calculations), methods for the simulation and analysis of molecular spectroscopy, especially those relevant to experiments that can be used to glean thermochemical information, and the development of *ab initio* methods needed for the accurate treatment of transient organic molecules.

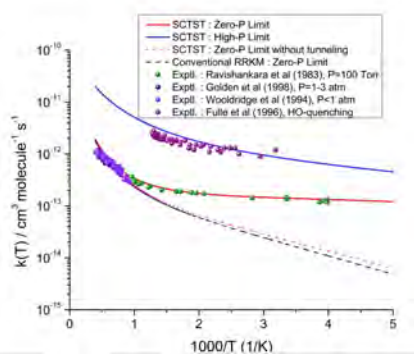
Summary of Selected Recent Accomplishments

We have begun to extend of our HEAT protocol¹ for computational thermochemistry to the study of transition states, something that was part of our most recent renewal proposal. To summarize, the HEAT protocol is a strategy for the computation of molecular energies (both adiabatic electronic energies and zero-point corrections) that is designed to be as accurate as possible, and to involve – apart from basis set extrapolation methods – no “empirical” corrections or assumptions. A number of calibration studies established HEAT to be accurate to within 1 kJ mol⁻¹ (*ca.* 80 cm⁻¹) in the calculation of enthalpies of formation for molecules containing four and fewer atoms (a necessary restriction in the scope of applicability of the method at the time of the studies); more recent work has suggested that a high level of accuracy is maintained for larger molecules that are now accessible due to advances in both algorithmic development and available computational resources. In thermochemistry, the quantities of interest are well-defined quantum mechanically, but the relevant quantity in reaction dynamics – the activation energy – is not similarly well-defined and therefore not amenable to comparable calibration studies. However, for those cases in which the electronic structure of the activated complex is similarly “complicated” to those molecules in the calibration set, a similar level of accuracy can be expected for the corresponding electronic energies and zero-point corrections. We have now applied HEAT to three different reaction systems: the abstraction of a hydrogen atom from H₂ by the hydroxyl radical; the abstraction of a hydrogen atom in methane by chlorine atoms, and the reaction of OH with CO to form CO₂ and hydrogen atoms. The latter reaction, in particular, is extremely important in combustion, and is largely responsible for the generation of heat in many relatively low-temperature combustion processes. For all reactions, the calculated rates are in very good agreement with experimental data, which attests

¹A. Tajti *et al.* *J. Chem. Phys.* 121, 11599 (2004).

to both the accuracy of the quantum chemistry part – HEAT – and the dynamical treatment (see below).

We have continued our work on the applications of semiclassical transition state theory (SCTST) to chemical reactions and the algorithmic improvement of SCTST. SCTST is a method that was conceived of some time ago² and provides rate constants that incorporate effects of both quantum-mechanical tunneling and reaction path curvature. However, unlike formally exact quantum calculations that require extensive information about the potential energy surface, efficient realizations of SCTST can be formulated which use only local information (derivatives through fourth-order in displacement) in regions of the potential surface around the transition state. With advances in quantum chemical methodology – particularly the calculation of analytic derivatives of the potential surface – the ability of SCTST to calculate reaction rates for *real* reactive systems was first realized some time ago³, but only recently has the quantum chemistry become available to make truly accurate calibration of SCTST feasible. A particularly striking application of SCTST, just recently been carried out by my group and others, is to calculate the rate of reaction for $\text{OH} + \text{CO} \rightarrow \text{CO}_2 + \text{H}$. While a number of quite accurate potential energy surfaces exist for this system (and to which, by consequence, our HEAT surfaces offer only slight improvement), calculations of the rate by classical TST and quasiclassical trajectory methods have severely underestimated the observed rate constant at lower temperatures. By contrast, SCTST calculations of the rate are in striking agreement with experiment over the entire range of temperatures at which they have been measured⁴. From this work, we are able to persuasively argue that nearly 90% of the reactive flux under atmospheric conditions occurs *via* tunneling: a finding that is entirely consistent with the quite recent experimental work of Continetti and coworkers⁵.



Rates of the reaction $\text{OH} + \text{CO} \rightarrow \text{HOCO}$, calculated at the low- and high-temperature limits, along with available experimental data. The upper, high-pressure data points come from a quenching study, and the assumption that all quenching comes from chemical reaction (which provides an upper limit to the rate constant). The low-pressure data represent experimentally determined rate constants. Note that the SCTST calculation is in excellent agreement with the experimental data here at all temperatures, and that tunneling (suppressed in the two calculations denoted with dashed lines) makes a substantial contribution to the rate at all temperatures below 1000 K.

With regard to algorithmic development of SCTST, we have worked out a Monte Carlo importance sampling integration method that speeds up calculation of canonical (thermal) rate constants by as much as *five orders of magnitude* relative to previous methods⁶, showing that SCTST can be used to calculate rate constants in just a few seconds of cpu time for systems as large as malonaldehyde (where on the order of 10^9 states have non-negligible reaction probabilities). Also, the scaling of the algorithm – it goes roughly as $n \ln n$ – suggests that SCTST is now applicable (provided the relevant potential is available) for systems with dozens, and even hundreds, of atoms.

²W.H. Miller *Faraday Transactions* 62, 40 (1977).

³M.J. Cohen, N.C. Handy, R. Hernandez and W.H. Miller *Chem. Phys. Lett.* 192, 407 (1992).

⁴L.T. Nguyen, R. Weston, J.R. Barker and J.F. Stanton, submitted to *J. Phys. Chem. Lett.*

⁵C.L. Johnson and R.E. Continetti *J. Phys. Chem. Lett.* 1, 1895 (2010).

⁶C.M. Miller and J.F. Stanton, manuscript in preparation.

In the area of computational thermochemistry, we are working with W.D. Allen (Georgia) on an initiative by which we aim to establish - by high-level HEAT and focal-point calculations - the enthalpies of formation of a group of compounds that serve as a basis set of sorts for a paradigm of computational thermochemistry using what are called hypohomodesmotic reactions⁷. This work, which is described in somewhat greater detail in last year's report, will ultimately provide the foundation for a theoretical thermochemistry that should be able to calculate accurate (*ca.* 1 kcal mol⁻¹) enthalpies of formation for quite large hydrocarbons, simply on the basis of relatively low-level (and therefore cheap) quantum chemical calculations. However, there is a price to be paid on the road to this goal: extremely accurate enthalpies of formation are needed for the aforementioned set of hydrocarbons, which have five and fewer carbon atoms. This set of molecules ranges in size from methane to neopentane, and provides formidable challenges to the levels of *ab initio* theory that are needed to compute highly accurate enthalpies of formation using methods such as HEAT and the focal-point method. In the last year, significant progress has been made towards this goal. Full HEAT energies are now available for all of these molecules apart from neopentane and isobutane, where the most expensive and challenging computational building blocks of a HEAT energy are still in process. Along the way, some of the largest correlated calculations in the history of quantum chemistry have been carried out. This work should be completed and submitted for publication before the 2013 meeting, at which time some numerical results of this work will be communicated.

An additional project that has recently been completed is an experimental-theoretical collaboration on the excited states of propdienylidene (:C=C=CH₂), carried out in collaboration with the Neumark group at Berkeley, Osborn at Sandia, and a number of other groups that are not part of the combustion program⁸. The electronic states of :C=C=CH₂ were studied with photodetachment spectroscopy, and the very complicated spectroscopic signatures of these states were assigned and analyzed, a process that was sometimes assisted by simulations that we have carried out using model Hamiltonians that go beyond the Born-Oppenheimer approximation. Such calculations have been a central theme of our research, as well as that of D.R. Yarkony - also a member of the combustion program - for many years now, and also build upon high-level quantum chemistry calculations. As a result of this large-scale collaboration, a significant amount of knowledge has been gained about five of the electronically excited states of this molecule, as well as an improved characterization of its ground state using the relatively high-resolution SEVI technique in the Neumark laboratory.

Ongoing Research and Future Plans

We have recently begun a committed effort to develop an efficient implementation of "quadruple excitations", which are needed to make quantum chemical methods using coupled-cluster theory more accurate than the very popular CCSD(T) approach. My extremely capable student, Devin Matthews, is the recipient of a DOE computational science graduate fellowship (CSGF), and has been working on both theory (spin adaptation of the CCSDTQ equations, which is a formidable theoretical problem that he has recently completed) and high-level programming efforts. Last summer, Devin did a DOE-CSGF fellowship with the computational science division at Argonne National Laboratory, and this project has now developed into a fairly major collaboration involving my group, ANL, Los Alamos National Laboratory, and UC Berkeley. A decade from now, it is my firm belief that CCSDTQ - more probably its CCSDT(Q) approximation - will be to quantum

⁷S.E. Wheeler, K.N. Houk, P.R. Schleyer and W.D. Allen *J. Amer. Chem. Soc.* 131, 2547 (2009).

⁸J.F. Stanton and fifteen co-authors *J. Chem. Phys.*, in press.

chemistry what CCSD(T) is now: the method of choice for very high accuracy calculations when a single-reference approach is appropriate (and often even when the state of interest has fairly significant multireference character). These quadruple excitations have been proven to be absolutely essential for very high-accuracy thermochemical calculations, and this work should pay significant dividends in this area, further helping out by providing missing data to Ruscic's ATcT endeavor⁹.

References supported by DE-FG02-07ER15884 (2011-)

J.M. Beames, M.I. Lester, C. Murray, M.E. Varner and J.F. Stanton "Analysis of the HOOO Torsional Potential" *J. Chem. Phys.* 134, 044304 (2011).

X. Zeng, H. Beckers, H. Willner and J.F. Stanton "Elusive Diazirinone" *Angew. Chem.* 50, 1 (2011).

T.L. Nguyen, J.F. Stanton and J.R. Barker "A Practical Implementation of Semi-Classical Transition State Theory for Polyatomics" *Chem. Phys. Lett.* 499, 9 (2011).

K. Klein, E. Garand, T. Ichino, D.M. Neumark, J. Gauss and J.F. Stanton "Quantitative Vibronic Coupling Calculations: The Formyloxyl Radical" *Theo. Chem. Acc.* 129, 527 (2011).

J.F. Stanton "Quantitative Vibronic Coupling Calculations. "The Visible Spectrum of Propadienyldiene" *Trans. Farad. Soc.* 150, 331 (2011).

J.H. Baraban, A.R. Beck, A.H. Steeves, J.F. Stanton and R.W. Field "Reduced Dimension DVR Study of cis-trans Isomerization in the S₁ State of C₂H₂" *J. Chem. Phys.* 134, 044304 (2011).

J. Vazquez, M.E. Harding, J.F. Stanton and J. Gauss "Vibrational Energy Levels via Finite-Basis Calculations Using a Quasi-Analytic Form of the Kinetic Energy" *J. Chem. Theo. Comput.* 7, 1428 (2011).

A. Vasilou, K. Piech, X. Zhang, M.R. Nimlos, M. Ahmed, A. Golan, O. Kostko, D.L. Osborn, J.F. Stanton and G.B. Ellison "The Products of the Thermal Decomposition of CH₃CHO" *J. Chem. Phys.* 135, 014306 (2011).

C.J. Johnson, B.L.J. Poad, M.E. Harding, J.F. Stanton and R.E. Continetti "The Electron Affinities, Well Depths, and Vibrational Spectroscopy of Cis- and Trans-HOCO" *J. Amer. Chem. Soc. (Comm)* 133, 19606 (2011).

⁹B. Ruscic *et al.* *J. Phys. Chem.* 108, 9979 (2004).

Universal and State-Resolved Imaging Studies of Chemical Dynamics

Arthur G. Suits
Department of Chemistry, Wayne State University
5101 Cass Ave
Detroit, MI 48202
asuits@chem.wayne.edu

I. Program Scope

The focus of this program is on combining universal ion imaging probes providing global insight, with high-resolution state-resolved probes providing quantum mechanical detail, to develop a molecular-level understanding of chemical phenomena. Particular emphasis is placed upon elementary reactions important in understanding and predicting combustion chemistry. This research is conducted using state-of-the-art molecular beam machines, photodissociation, reactive scattering, and vacuum ultraviolet lasers in conjunction with ion imaging techniques. An ongoing parallel effort is made to develop new tools and experimental methods with which to achieve these goals.

II. Recent Progress

In the past year we have moved our laboratory into a new, state-of-the-art facility as the Chemistry Department here has undergone a total renovation. One of the key goals in configuring the new laboratory has been to deliver almost any laser beam to any beam machine. We believe we have achieved an optimal configuration, and our crossed-beam studies are soon to profit from this greatly as described below.

Systematic studies of polyatomic reaction dynamics. We continue our systematic studies of crossed-beam DC slice imaging of hydrocarbon reactions. Previously we have investigated Cl + pentane isomers, in which we saw surprisingly little variation of the differential cross sections with target isomer. We believe this is because our collision energies are relatively high, reducing our sensitivity to these effects. We have difficulty going to low collision energies because of background problems, but we have plans to overcome this as described in Future Work. We also studied a series of Cl + alkene reactions, in which we saw evidence both for addition/ elimination and direct H abstraction from the alkyl side chain. Abstraction of an allylic H atom is strongly exoergic owing to the formation of the resonantly stabilized radical product, so this is the energetically preferred path. The addition channel (1) produces a chloroalkyl radical and is barrierless and exoergic ($-20 \text{ kcal mol}^{-1}$). The products of addition-elimination (2) and direct abstraction (3) mechanisms are identical on the basis of chemical formula, but formation of distinct product isomers for these two pathways is clearly possible, and we documented this on the basis of the coupled translational energy and angular distributions that come naturally from crossed-beam sliced imaging data.

As mentioned last year, we reported the first crossed-beam imaging study directly probing primary vs. secondary H abstraction in the reaction of Cl with butane-1,1,1,4,4,4- d_6 . The H- and D-atom abstraction channels were studied over a range of collision energies: 10.4 kcal/mol and 12.9 kcal/mol; 5.2 kcal/mol to 12.8 kcal/mol, respectively, using crossed molecular beam dc slice ion imaging techniques. These two channels manifest distinct dynamics principally in the translational energy distributions, while the angular distributions are remarkably similar. The reduced translational energy distribution for the primary abstraction showed marked variation with collision energy in the backward direction, while the secondary abstraction showed this variation in the forward direction. At the collision energies studied, no strong correlation between abstraction site and differential cross

section was seen, perhaps accounting for inconsistent conclusions on this point arising from more indirect approaches over the years. Background issues again prevented us from going to lower collision energies where larger effects might be apparent, and this is a direction we will pursue in the future.

The final Cl atom series we have investigated is Cl + butanol isomers, which has been accepted for presentation at Faraday 157, "Reaction Dynamics in Gases, Liquids and at Interfaces." Butanol is now prominent among the possible renewable biofuels. We have studied oxidation of a variety of butanol isomers under single collision conditions using chlorine atom as the oxidizing agent to gain insight into the energetics and dynamics of these reactions. The interaction of chlorine atom radicals with butanol isomers: n-butanol, iso-butanol, sec-butanol, and tert-butanol have been studied by crossed-beam dc slice ion imaging with VUV radical detection. After background subtraction and density-to-flux correction of the raw images, translational energy distribution and product angular distributions were generated. At "low" collision energy, ~5 kcal/mol, the hydroxyalkyl products are backscattered with respect to the alcohol beam and the scattering shifts strongly to the forward direction as the collision energy is increased. The translational energy distributions are reminiscent of that of Cl + pentane reactions we studied earlier, *i.e.* a sharp forward peak ~80% of the collision energy appears at the high collision energy. Isomer-specificity was minimal at these energies, reminiscent of the pentane study. These reactions, too, will profit from a reinvestigation at very low

The Roaming Saga Continues. In addition to an invitation for a Perspective for JPC-Letters, interest in roaming continues to grow dramatically. Joel Bowman and I were invited to contribute a *Physics Today* article on the subject, and C&E News recently had an extensive feature on the subject in which many Combustion PI's were interviewed. As we develop the new universal tools described below, and a TEA-CO₂ laser that is due to arrive any day, we will expand our studies of roaming along many lines described in Future Plans.

New approaches to universal detection using a strong-field femtosecond laser. We are now developing an approach, termed "Strong Field Slice Imaging" (SFSI) using strong-field non-resonant ionization as a probe strategy. As described last year, we can implement this in a raster fashion to avoid hitting the molecular beam (and producing lots of background ions). On the other hand, for many species the parent molecules have ionization energies much higher than the radical products. In this case we can turn down the laser power and dissociate and probe directly in the beam using counterpropagating lasers. As part of moving the lab we are reconfiguring that apparatus to achieve UHV operation to minimize any background interference. The other advantage of detecting radical products is that the initial ions they produce are closed-shell, so typically have no low-lying electronic states. It is widely recognized that such low-lying electronic states present in the initial cation in strong field ionization operate as the stepping stones leading to fragmentation. We thus benefit from minimal ion fragmentation in this approach (for the right molecules, that is).

Much of this thinking led us to the notion of isomer-specific-probing using the strong field non-resonant laser, which is described in some detail in the Future Plans below.

III. Selected Future Plans

Isomer-specific detection and imaging via "semi-soft" ionization by power-tuning a non-resonant femtosecond laser: demonstration and selected applications. The use of "soft" vacuum ultraviolet photoionization to achieve "universal" but selective detection of reaction products and photofragments began at the Chemical Dynamics Beamline at the Advanced Light Source in the mid-

nineties. However, it was with the recognition that the full shape of the photoionization efficiency (PIE) curves, rather than simply the nominal ionization onset, could be used to identify complex mixtures of isomers in flame studies and kinetics experiments that the power of this approach became clear. This approach has since been widely exploited both at the ALS and at and at the National Synchrotron Radiation Laboratory in Hefei, China. The origin of the characteristic shapes of these PIE curves was less important than that they be consistent and relatively insensitive to internal energy in the products. Traditional universal ionization techniques relying on electron impact ionization generates extensive fragmentation, and cannot so readily be adapted to these approaches. The use of fixed low energy electron impact has been used, however, to achieve some selectivity in product detection in limited instances. But as yet this has not been widely exploited. At the same time, some effort has been made to use shaping of femtosecond laser pulses to achieve isomer-specific identification, although this approach has not seen wide use.

Non-resonant ionization by relatively high peak power femtosecond lasers has clear parallels to tunable VUV photoionization, in that the power needed to induce ionization closely tracks the ionization energy of the subject molecule. Tuning the power of a nonresonant femtosecond pulse, without changing any other characteristics, is quite like tuning the ionizing photon energy, both through the ionization onset and beyond. This is because the photons come sufficiently quickly that they are not registered as distinct entities by virtue of the uncertainty principle. One significant difference is that some molecules undergo significant fragmentation upon ionization in the laser field, while others do not. For short pulses, this has been convincingly attributed to the presence of resonances in the cation that are overlapped by the femtosecond laser wavelength (in all that is considered here this will be the titanium-sapphire fundamental, ~780-820nm). Fortunately, this implies that for detection of radicals, for which the cations are closed-shell, little fragmentation will be the general rule.

In any case, in the presence of modest fragmentation, or double ionization, or no fragmentation at all, these observations suggest that, as has been demonstrated to great effect in the kinetics and flame studies at the ALS and Hefei, the use of photoionization efficiency curves, (now plotted against femtosecond laser power rather than photon energy: “fs-PIE”) or energy-dependent mass spectra can be used as “basis functions” to identify the isomer composition of reaction products in a variety of experiments in a manner entirely analogous to that employed in the synchrotron studies. In fact we will often go beyond this and simply use the TOF spectra at several energies as vectors whose coefficients determine their contribution to the mixture under investigation.

State-resolved and universal crossed-beam DC slice imaging. We have plans to continue exploring a range of systems using our crossed-beam sliced imaging approach. We have increased the radical beam intensity another four-fold, so our background problems should be greatly reduced. Then we can go to lower collision energy and revisit a number of systems mentioned above. Most importantly, we now have two reliable high-power deep UV laser systems so we will be able to do fully state-selective detection using our two-color reduced Doppler (TCRD) probe of the HCl product of these reactions. We were successful with state-resolved HCl detection for the Cl+ethane reaction using a single laser source in the past. With the TCRD probe, we will have twice the power and Doppler-free, so we expect unprecedented sensitivity for rotationally state-selected probing. Aside from our ethylene work, only a single paper from Kopin Liu’s laboratory has achieved this. We expect it to be routine for us in the months to come. We also plan to extend the state-resolved TCRD imaging to study radical-radical reactions. Our first target will be the O+CH₃ reaction, a fascinating system that showed a novel H₂ elimination pathway which anticipated the roaming dynamics seen in formaldehyde.³ For this system we can use TCRD REMPI detection of H₂ and CO products. We will prepare the O atoms photolytically, and the methyl radicals using flash pyrolysis.

Chemical activation and roaming reactions. We have plans to use CH and CH₂ radicals to implement a “chemical activation” investigation of roaming systems. These radicals can insert directly into bonds, forming highly energetic ground state systems at a well-defined total energy. This is ideal for probing roaming reactions quite generally. We will employ both universal and state-resolved detection, and complement these studies using a TEA-CO₂ laser and the CP-mm approach described in the following paragraph.

Chirped-pulse mm-wave detection in uniform supersonic flows. In collaboration with Bob Field, we are developing a unique and powerful new instrument that will combine two uniquely well-matched, emerging technologies: chirped-pulse Fourier-transform micro/mm-wave spectroscopy developed by Brooks Pate and pulsed uniform supersonic flows as developed by Rowe et al. This combination promises a nearly *universal detection method that can deliver isomer and conformer specific, quantitative detection and spectroscopic characterization* of unstable reaction products and intermediates, product vibrational distributions, and molecular excited states. The proposed technique will be suitable for application in diverse fields including fundamental studies in spectroscopy and reaction dynamics, kinetics, and combustion. The instrument is being developed with NSF funds, but DOE related work will certainly be one of the principal applications of the machine.

V. DOE Publications 2010-present

A. D. Estillore, L. M. Visger, and A. G. Suits, “Imaging the dynamics of chlorine atom reactions with alkenes,” *J. Chem. Phys.* **133**, 7 (2010).

M. P. Grubb, M. L. Warter, A. G. Suits, S. W. North, “Evidence of roaming dynamics and multiple channels for molecular elimination in NO₃ photolysis,” *J. Phys. Chem. Lett.* **1**, 2455 (2010).

A. D. Estillore, L. Visger and A. G. Suits, “Crossed-beam DC slice imaging of chlorine atom reactions with pentane isomers,” *J. Chem. Phys.* **132** 164313 (2010).

A. D. Estillore, L. M. Visger-Kiefer, T. A. Ghani, A. G. Suits, "Dynamics of H and D abstraction in the reaction of Cl atom with butane-1,1,1,4,4,4-d₆," *Phys. Chem. Chem. Phys.*
DOI:10.1039/c1cp20137a (2011).

N. Herath and A. G. Suits, "Roaming radical reactions," *J. Phys. Chem. Lett.*, **2** 642 (2011).

J.M. Bowman and A. G. Suits, “Roaming reactions: The Third Way,” *Phys. Today*, **64** 33 (2011).

A. M. Estillore, L. M. Visger-Kiefer and A. G. Suits, “Reaction dynamics of Cl + butanol isomers by crossed-beam sliced ion imaging,” *Faraday Discussion 157 (accepted)*.

Elementary Reaction Kinetics of Combustion Species

Craig A. Taatjes

Combustion Research Facility, Mail Stop 9055, Sandia National Laboratories,

Livermore, CA 94551-0969

cataatj@sandia.gov

SCOPE OF THE PROGRAM

This program aims to develop new methods for studying chemical kinetics and to apply these methods to the investigation of fundamental chemistry relevant to combustion science. One central goal is to perform accurate measurements of the rates at which important free radicals react with each other and with stable molecules. Another goal is to characterize complex reactions that occur via multiple potential wells by investigating the formation of products. Increasingly, these investigations are moving towards simultaneous time-resolved detection of multiple species in well-characterized photolytically-initiated reaction systems where multiple consecutive and competing reactions may occur. Understanding the reactions in as much detail as possible under accessible experimental conditions increases the confidence with which modelers can treat the inevitable extrapolation to the conditions of real-world devices. Another area of research is the investigation and application of new detection methods for precise and accurate kinetics measurements. Absorption-based techniques and mass-spectrometric methods have been emphasized, because many radicals critical to combustion are not amenable to fluorescence detection.

An important part of our strategy, especially for complex reaction systems, is using experimental data to test and refine detailed calculations (working in close cooperation with Stephen Klippenstein at Argonne and Ahren Jasper and Judit Zádor at Sandia), where the theory offers insight into the interpretation of experimental results and guides new measurements that will probe key aspects of potential energy surfaces. This methodology has been applied in our investigations of the reactions of alkyl radicals with O₂, where the combination of rigorous theory and validation by detailed experiments has made great strides toward a general quantitative model for alkyl oxidation. The focus of our laboratory is shifting to include investigations of the reactions of oxygenated molecules relevant to biofuel combustion as well as studies of the effects of unsaturation on the chemistry leading to autoignition.

RECENT PROGRESS

We continue to apply frequency-modulation and direct absorption spectroscopy to measurements of product formation in reactions of alkyl radicals with O₂ and kinetics of unsaturated hydrocarbon radicals. In addition, the multiplexed photoionization mass spectrometric reactor at the Advanced Light Source (ALS), an experimental effort led by David Osborn (see his abstract), has become a major part of our investigations of low-temperature hydrocarbon oxidation chemistry. Several highlights of the recent work are described briefly below.

Low-temperature oxidation chemistry of butanol isomers. Butanol isomers are promising next-generation biofuels. Their use in internal combustion applications, especially those that rely on low-temperature autoignition, requires an understanding of their low-temperature combustion chemistry. Whereas the high-temperature oxidation chemistry of all four butanol isomers has been the subject of substantial experimental and theoretical efforts, their low-temperature oxidation chemistry remains underexplored. We carried out an experimental study on the fundamental low-temperature oxidation chemistry of two butanol isomers, *tert*-butanol and isobutanol, in low-pressure (4 – 5.1 Torr) experiments at 550 and 700 K. We used pulsed-photolytic chlorine atom initiation to generate hydroxyalkyl radicals derived from *tert*-butanol and isobutanol, and probed the chemistry of these radicals in the presence of an excess of O₂ by multiplexed time-resolved tunable synchrotron photoionization mass spectrometry. Isomer-resolved yields of stable products were determined. We find that the reaction of α -hydroxyisobutyl with O₂ is predominantly linked to chain-terminating formation of HO₂. The “Waddington mechanism,”^{1, 2} in which a β -hydroxyalkylperoxy radical transfers the hydroxyl H atom to the peroxy radical site before dissociating into two carbonyl compounds and OH, is the main product channel in the reactions of O₂ with β -hydroxyalkyl radicals derived from both *tert*-butanol and isobutanol. Direct HO₂ elimination is not possible in the reaction of hydroxytertbutyl + O₂ because of the absence of a beta C-H bond; this channel is available in the β -hydroxyisobutyl + O₂ reaction, but we find that it is strongly suppressed. The temperature dependence of the main products from 550 K to 700 K can be qualitatively explained by an increasing role of hydroxybutyl decomposition at 700 K.

Chemistry of carbonyl oxides. Carbonyl oxides (often known as “Criegee intermediates” after Rudolf Criegee) are principally produced as intermediates in ozonolysis, and are hence important intermediates in tropospheric hydrocarbon oxidation. Calculations suggest that they may also be products of QOOH + O₂ reactions.³ The carbonyl oxides are singlet biradicals, and their reactivity is of considerable fundamental interest. However, they have been difficult to detect and study in the gas phase, before our detection of CH₂OO by photoionization mass spectrometry several years ago.⁴ With collaborators Carl Percival (Manchester) and Dudley Shallcross (Bristol) we have recently succeeded in producing sufficient quantities of CH₂OO (formaldehyde oxide), via the reaction of CH₂I with O₂, to measure kinetics of its reactions with several species. Upper limits were extracted for reaction rate coefficients with NO and H₂O. The CH₂OO reactions with SO₂ and NO₂ proved unexpectedly rapid and imply a substantially greater role of carbonyl oxides in models of tropospheric sulfate and nitrate chemistry than previously assumed. We have also measured reactions of CH₂OO with carbonyl compounds, which are thought to proceed by 1,3 cycloaddition, and have observed the products of the reactions.

Mechanism of OH-initiated oxidation of cyclohexene. Our earlier synchrotron photoionization mass spectrometry experiments⁵ suggested a prominent ring-opening channel in the OH-initiated oxidation of cyclohexene, based on comparison of product photoionization spectra with calculated spectra of possible isomers. We have re-examined the OH + cyclohexene reaction, measuring the isomeric products of OH-initiated oxidation of partially and fully deuterated cyclohexene. In particular, the directly measured photoionization spectrum of 2-cyclohexen-1-ol differs substantially from the

previously calculated Franck-Condon envelope, and the product spectrum can be fit with no contribution from ring-opening. Measurements of H₂O₂ photolysis in the presence of C₆D₁₀ establish that the addition-elimination product incorporates the hydrogen atom from the hydroxyl radical reactant and loses a hydrogen (a D atom in this case) from the ring. Investigation of OH + cyclohexene-4,4,5,5-*d*₄ confirms this result and allows mass discrimination of different abstraction pathways. Products of 2-hydroxycyclohexyl-*d*₁₀ reaction with O₂ are observed upon adding a large excess of O₂ to the OH + C₆D₁₀ system. Surprisingly, no hexanedial, the “Waddington mechanism” product (see discussion of butanol oxidation above), could be detected. If no hexanedial is formed, this would be in remarkable contrast to our investigations of alcohol oxidation systems, for which the Waddington mechanism is prominent.

Chemistry of QOOH radicals. In collaboration with Judit Zádor, and as detailed in her abstract, we have succeeded in experimentally characterizing decomposition of a QOOH radical, 2-hydroperoxy-2-methylpropan-1-yl, (CH₃)₂C(CH₂)OOH. This radical is conveniently produced by Cl atom reaction with *t*-butylhydroperoxide, as described in my abstract last year. Measurements of OH radical formation by time-resolved infrared absorption were modeled to extract absolute rate coefficients for the unimolecular dissociation, and the dependence of the product signals on O₂ concentration could then be used to derive an absolute rate coefficient for reaction with O₂.

FUTURE DIRECTIONS

We will continue to expand our exceptionally productive collaboration with David Osborn, using the photoionization mass spectrometry machine at the Advanced Light Source. The effects of unsaturation and oxygenation on low-temperature oxidation chemistry will be further explored. The null result for Waddington product in cyclohexene oxidation will be explored to determine whether cyclic compounds, for which the participating groups remain on the same molecule, display different propensity for product formation (or whether there are simply difficulties in detecting hexanedial). Both OH-initiated alkene oxidation measurements and studies of alcohol oxidation will be employed. Measurements of elementary oxidation reactions of representative biofuel molecules in the temperature region 500 K – 800 K will continue, with a continuing goal of developing a more general understanding of the ignition chemistry of alternative fuels. We have begun to measure the fundamental chemistry of some esters and will extend those efforts in the near future.

The study of QOOH reactions will continue the longstanding quest to directly detect QOOH. One key difficulty has been simply making a high enough concentration of QOOH, and the reactions of Cl with alkyl hydroperoxides offer a path to overcome this difficulty. Reactions of QOOH with molecular oxygen remain the most important unmapped area in autoignition chemistry. As advanced theoretical kinetics develops rigorous predictions for these reactions, experiment must be able to detect products of these reactions for validation of theory.

References

- [1] D. J. M. Ray, A. Redfearn and D. J. Waddington, *J. Chem. Soc., Perkin Trans. 2*, 1973, 540-543.
- [2] D. J. M. Ray and D. J. Waddington, *Combust. Flame*, 1973, **20**, 327-334.

- [3] A. Andersen and E. A. Carter, *J. Phys. Chem. A*, 2003, **107**, 9463-9478.
- [4] C. A. Taatjes, G. Meloni, T. M. Selby, A. J. Trevitt, D. L. Osborn, C. J. Percival and D. E. Shallcross, *J. Am. Chem. Soc.*, 2008, **130**, 11883-11885.
- [5] G. Meloni, T. M. Selby, D. L. Osborn and C. A. Taatjes, *J. Phys. Chem. A*, 2008, **112**, 13444-13451.

Publications acknowledging BES support, 2010 –

1. John Savee, Satchin Soorkia, Oliver Welz, Talitha Selby, Craig Taatjes, and David Osborn, "Absolute Photoionization Cross-Section of the Propargyl Radical," *J. Chem. Phys.* **136**, 134307 (2012).
2. Fabien Goulay, Adam J. Trevitt, John D. Savee, Jordy Bouwman, David L. Osborn, Craig A. Taatjes, Kevin R. Wilson, and Stephen R. Leone, "Product detection of the CH radical reaction with acetaldehyde," *J. Phys. Chem. A* in press, doi:10.1021/jp2113126 (A. R. Ravishankara festschrift) (2012).
3. Craig A. Taatjes, Oliver Welz, Arkke J. Eskola, John D. Savee, David L. Osborn, Edmond P.F. Lee, John M. Dyke, Daniel W. K. Mok, Dudley E. Shallcross, and Carl J. Percival, "Direct Measurement of Criegee Intermediate (CH₂OO) Reactions with Acetone, Acetaldehyde, and Hexafluoroacetone," *Phys. Chem. Chem. Phys.* in press, doi:10.1039/C2CP40294G (2012).
4. Oliver Welz, John D. Savee, David L. Osborn, Subith S. Vasu, Carl J. Percival, Dudley E. Shallcross, and Craig A. Taatjes, "Direct Kinetic Measurements of Criegee Intermediate (CH₂OO) Formed by Reaction of CH₂I with O₂," *Science*, 335, 204–207 doi:10.1126/science.1213229 (2012).
5. Fabien Goulay, Satchin Soorkia, Giovanni Meloni, David L. Osborn, Craig A. Taatjes, and Stephen R. Leone, "Detection of pentatetraene by reaction of the ethynyl radical (C₂H) with allene (CH₂=C=CH₂) at room temperature," *Phys. Chem. Chem. Phys.* **13**, 20820-20827 doi:10.1039/C1CP22609F (2011).
6. Adam J. Trevitt, Satchin Soorkia, John D. Savee, Talitha M. Selby, David L. Osborn, Craig A. Taatjes, and Stephen R. Leone, "Revisiting the Branching Fractions of the CN + C₃H₆ Reaction Using Synchrotron Photoionization Mass Spectrometry: Evidence for the 3-Cyanopropene Product," *J. Phys. Chem. A* **115**, 13467–13473 doi:10.1021/jp208496r (2011).
7. Judit Zádor, Craig A. Taatjes, Ravi X. Fernandes, "Kinetics of Elementary Reactions in Low-Temperature Autoignition Chemistry," *Prog. Energy Combust. Sci.* **37**, 371-421 doi:10.1016/j.pecs.2010.06.006 (2011).
8. Haifeng Huang, Daniel J. Merthe, Judit Zádor, Leonard E. Jusinski, and Craig A. Taatjes, "New experiments and validated master-equation modeling for OH production in propyl + O₂ reactions," *Proc. Combust. Inst.* **33**, 293–299 doi:10.1016/j.proci.2010.06.039 (2011).
9. Satchin Soorkia, Craig A. Taatjes, David L. Osborn, Talitha M. Selby, Adam J. Trevitt, Kevin R. Wilson and Stephen R. Leone, "Direct detection of pyridine formation by the reaction of CH (CD) with pyrrole: a ring expansion reaction," *Phys. Chem. Chem. Phys.* **12**, 8750–8758 doi:10.1039/c002135k (2010).
10. Satchin Soorkia, Adam J. Trevitt, Talitha M. Selby, David L. Osborn, Craig A. Taatjes, Kevin R. Wilson and Stephen R. Leone, "Reaction of the C₂H radical with 1-butyne (C₄H₆): Low temperature kinetics and isomer-specific product detection," *J. Phys. Chem. A* **114**, 3340–3354 (Benoît Soep festschrift) doi:10.1021/jp911132r (2010).
11. Craig A. Taatjes, David L. Osborn, Talitha M. Selby, Giovanni Meloni, Adam J. Trevitt, Evgeny Epifanovsky, Anna Krylov, Baptiste Sirjean, Enoch Dames, Hai Wang, "Products of the Benzene + O (³P) Reaction," *J. Phys. Chem. A* **114**, 3355–3370 (Benoît Soep festschrift) doi:10.1021/jp91114145 (2010).
12. Adam J. Trevitt, Fabien Goulay, Craig A. Taatjes, David L. Osborn and Stephen R. Leone, "Reactions of the CN Radical with Benzene and Toluene: Product Detection and Low Temperature Kinetics," *J. Phys. Chem. A* **114**, 1749–1755 doi:10.1021/jp909633a (2010).
13. Erin E. Greenwald, Buddhadeb Ghosh, Katie C. Anderson, Kristin S. Dooley, Peng Zou, Talitha Selby, David L. Osborn, Giovanni Meloni, Craig A. Taatjes, Fabien Goulay, and Simon W. North, "Isomer-Selective Study of the OH Initiated Oxidation of Isoprene in the presence of O₂ and NO: I. The Minor Inner OH-Addition Channel," *J. Phys. Chem. A* **114**, 904–912 doi:10.1021/jp908543a (2010).

Elementary Reactions of PAH Formation

Robert S. Tranter

Chemical Sciences and Engineering Division, Argonne National Laboratory

Argonne, IL-60439

tranter@anl.gov

I. Program Scope

This program is focused on the experimental determination of kinetic and mechanistic parameters of elementary reactions, in particular those involved in the formation and destruction of the building blocks for aromatic species. Recently, the program has also encompassed the study of ethers and cyclic species and their dissociation products that are representative of oxygenated intermediates in combustion mechanisms. In addition, thermal sources of radicals are investigated and characterized for use in more complex reaction systems where secondary chemistry can be significant. The approach involves a diaphragmless shock tube (DFST) equipped with laser schlieren (LS) and a time-of-flight mass spectrometer (TOF-MS) and low pressure, fast flow, reactor equipped with a quadrupole MS. The combination of these techniques permits a wide range of reaction temperatures and pressures to be accessed.

II. Recent Progress

Decomposition and recombination of resonantly stabilized radicals are important in the formation of polyaromatic hydrocarbons, PAH. A prior study of phenyl radical recombinationⁱ indicated that reactions of *o*-benzyne radicals in PAH formation are important and this notion is supported by recent work from Brezinsky and co-workers.ⁱⁱ Consequently, dissociation and recombination of *o*-benzyne has been studied in the DFST. As part of an ongoing investigation of resonantly stabilized radicals reactions of allyl radicals have also been studied in the last year with attention focused on the recombination reaction.

In previous LS studies of the pyrolysis of dimethyl ether, DME,ⁱⁱⁱ the simulated density gradients were found to be sensitive to the reaction between methyl radicals and DME. Consequently, an experiment was devised to study this reaction in the DFST by LS and represents the first attempt to measure a rate coefficient for a radical/molecule reaction by LS where the radical is created by thermal dissociation of a precursor and then allowed to react with a reagent other than the precursor.

Finally, in the last year a number of advances have been made with the experimental equipment. The interface between the DFST and TOF-MS has been completely replaced and the original R. M. Jordan reflectron TOF-MS replaced with a modified CTF5B reflectron from Kaesdorf. The new interface has much improved gas flow and pumping in the section between the nozzle in the end of the shock tube and the skimmer at the entrance to the TOF-MS ion source. The Kaesdorf TOF-MS has about a factor of 2 better mass resolution than the Jordan and due to the compact design results in short flight times allowing masses up to about 230 amu to be observed in a 6.7 μ s period. The net results of the changes are simplified operation and maintenance of the DFST/TOF-MS and improved mass spectra that should permit more accurate determination of rate coefficients and product identification. Progress has been made with the flow reactor and the first experiments to test its capabilities are beginning.

A. Self-reaction of allyl radicals

Similar to propargyl radicals allyl radicals, C₃H₅, are resonantly stabilized and can reach high concentrations in flames and are important in formation of PAHs. Dissociation of allyl radicals has been studied by Fernandes et al.^{iv} (1125-1570K) in reflected shock waves and when dissociation of allyl is slow it will be in competition with recombination, reaction (1a). Georgievskii et al.^v and Matsugi et al.^{vi} have calculated k_{∞} for reaction (1a) that are in good agreement and compare favorably with low temperature experiments. Matsugi et al. also estimated the pressure dependence of k_{1a} however, there are no experimental studies of allyl recombination in the high temperature fall-off region encompassed by

these estimates. DFST/LS experiments are generally an excellent method for studying these types of reaction and determining pressure dependencies.

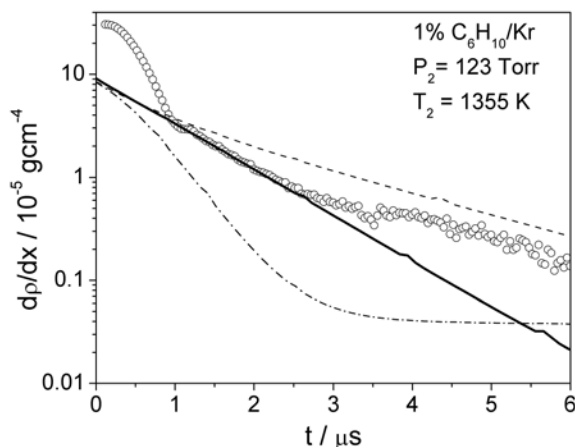
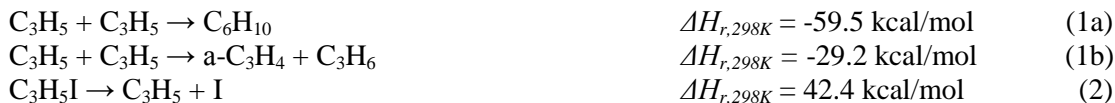


Figure 1 Density gradient from a LS experiment with 1% C₆H₁₀/Kr. Circles are experimental data. Lines represent simulations with only reaction (1a). The broken lines show the effect of varying S_{298} for C₆H₁₀ from the preferred value, solid line. Dash line: $S_{298} + 0.5 \text{ cal mol}^{-1}\text{K}^{-1}$; Dot-dash line: $S_{298} - 0.5 \text{ cal mol}^{-1}\text{K}^{-1}$.

by internal rotations. Consequently, initial estimates were obtained from group additivity and refined iteratively. A final value of $S_{298} = 89.4 \text{ cal mol}^{-1}\text{K}^{-1}$ for 1,5-hexadiene was obtained which is $0.2 \text{ cal mol}^{-1}\text{K}^{-1}$ lower than a recent calculation by Ruscic^{viii} and about $0.15 \text{ cal mol}^{-1}\text{K}^{-1}$ higher than CBS/QB3 results from Matsugi et al.^{vi}

LS experiments on dissociation of allyl iodide and allyl recombination (900-1500 K; 30, 60, 120 Torr) are not sensitive to the equilibrium constant k_{1a}/k_{-1a} and provide an independent measure of k_{1a} . From the initial density gradients k_2 were obtained and show strong fall off and k_{1a} were obtained through

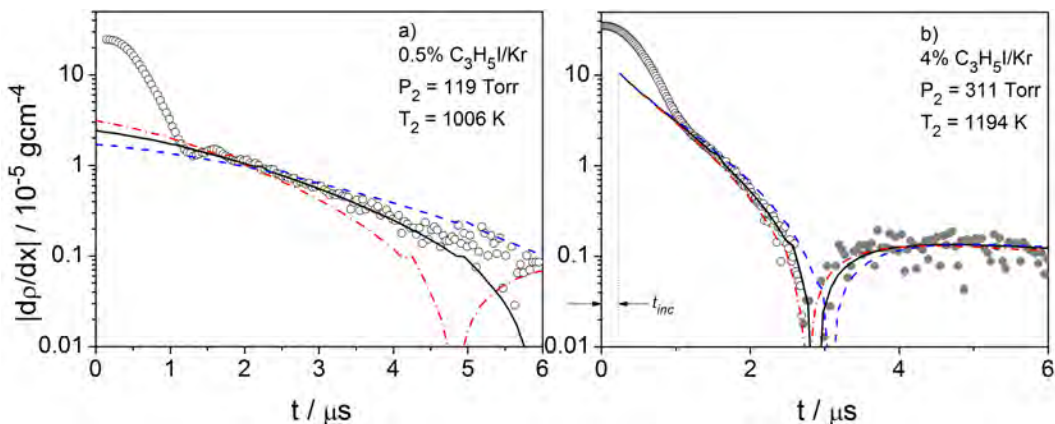


Figure 2: Semi-log plots of density gradients from LS experiments with C₃H₅I/Kr. Note the small incubation delay, t_{inc} , introduced in (b). Absolute values are plotted with open symbols, +ve, closed symbols, -ve. Lines simulations: Bold solid, final, (a) :Dash line $(k_2) \times 0.7$; Dot-dash line $(k_2) \times 1.3$. (b), (c), and (d) Dash line $(k_{1a} + k_{1b}) \times 0.7$; Dot dash line $(k_{1a} + k_{1b}) \times 1.3$.

Two sets of DFST/LS experiments have been conducted to measure k_{1a} using 1,5-hexadiene, C₆H₁₀, and C₃H₅I as precursors for allyl radicals. C₆H₁₀ dissociates by (-1a) and allyl iodide dissociates by cleavage of the weak C-I bond (2) with <1% eliminating HI. Once formed the allyl radicals are expected to recombine to give 1,5-hexadiene, although a small fraction, <3%, disproportionate,^{vii} (1b) to allene and propene.

DFST/LS experiments with 1,5-hexadiene were conducted over 1100-1700 K and nominal pressures of 10, 57 and 124 Torr. At low temperatures the LS density gradient profiles can be simulated very well with a single reversible reaction because reaction (1b) and dissociation of C₃H₅ are negligible. The simulation results are very sensitive to the equilibrium constant k_{1a}/k_{-1a} , and therefore the entropies of C₆H₁₀ and C₃H₅. The entropy of 1,5-hexadiene is somewhat challenging to calculate accurately from *ab-initio* methods because of the large number of rotamers produced

simulation of the complete density gradient profiles. Some example profile and simulations are shown in Fig. 2. Rate coefficients obtained from the experiments with C_6H_{10} and C_3H_5I for reaction (1a) are internally consistent and show greater fall off than predicted by Matsugi et al.^{vi} but are very well reproduced by a Gorin model RRKM calculation which treated the hindrance parameter, η , and $\langle\Delta E_{down}\rangle$ as adjustable parameters yielding: $\eta = 1 - .0006 T^{-0.45}$, and $\langle\Delta E_{down}\rangle = 1050 \text{ cm}^{-1}$ with $E_0 = 59.5 \text{ kcal/mol}$. The extrapolated high pressure limit rate coefficient is in excellent agreement with those of Georgievskii et al.^v and Matsugi et al.^{vi} although the $\langle\Delta E_{down}\rangle$ is somewhat higher than normally found.

B. Dissociation of *o*-benzyne

Previous work on the self-reaction of phenyl radicals revealed that disproportionation reactions of phenyl will generate significant amounts of *o/m/p*-benzynes and suggest that the role of *o*-benzyne radicals may be much more important in the formation of PAH and soot than previously thought. The only high

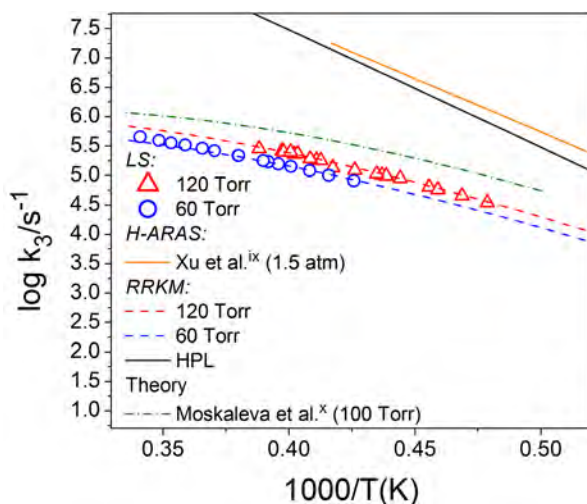


Figure 3 First order rate coefficients from LS experiments for $o\text{-}C_6H_4 \rightarrow C_4H_2 + C_2H_2$. RRKM: $E_0 = 89.3 \text{ kcal/mol}$, $\langle\Delta E_{down}\rangle = 880 \text{ cm}^{-1}$, molecular parameters from Zhang et al.^{xiv}

temperature kinetic study of *o*-benzyne dissociation is a reflected shock H-ARAS one by Xu et al.^{ix} who found that *o*-benzyne dissociates mainly by a retro-Diels Alder reaction to diacetylene and acetylene but that this is in competition with elimination of an H-atom which becomes increasingly dominant as temperature increases and accounts for up to 25% consumption of *o*-benzyne. Pyrolysis of C_6H_5F has been used in DFST/LS/TOF-MS experiments as a thermal source of *o*-benzyne radicals. As reported previously fluorobenzene primarily dissociates by HF elimination to give *o*-benzyne directly although a small fraction eliminates an H-atom to give the C_6H_4F radical which subsequently eliminates HF ultimately leading to triacetylene (C_6H_2) and an H atom. Simulation of the LS experiments allowed rate coefficients for dissociation of *o*-benzyne to be determined and branching between the retro-Diels Alder and H-loss channels to be estimated. Rate coefficients for the retro-Diels Alder channel are shown in Fig. 3 along with the results of an RRKM calculation, the results from Xu et al.^{ix} and theoretical calculations by Moskaleva et al.^x The LS experiments also show good agreement with the results of Xu et al. for both the magnitude and temperature dependence of the branching ratio between dissociation of *o*-benzyne by the retro-Diels Alder and H-loss channels.

C. $CH_3 + CH_3OCH_3$

The reaction between methyl radicals and DME has been proposed to be a key reaction in autoignition of DME.^{xi} However, Zhao et al.^{xi} found it necessary to increase k_3 by about a factor of 3.5 compared to earlier estimates that were determined from modeling flow reactor experiments on the pyrolysis and oxidation of DME.^{xii}



To obtain a more direct measure of the k_3 LS experiments with reagent mixtures containing 0.5% or 1% diacetyl and 10% DME dilute in krypton were performed over 1160-1630K and 60, 120 and 240 Torr. Dissociation of diacetyl has previously been studied in the DFST^{xiii} and here essentially acts as a clean, well-characterized source of CH_3 radicals. Pyrolysis of DME has also previously been studied in this apparatus and over most of the range of the current work dissociation of DME is negligible. Consequently, CH_3 radicals were generated in the presence of a large excess of DME and from simulation of the LS profiles the rate of reaction between them was determined. The rate coefficients are in good

agreement with the lower values of Curran et al. and about a factor of 3 lower than the more recent estimates of Zhao et al.

III. Future Work

The DFST studies of pyrolysis and self-reaction of *o*-benzyl radicals are ongoing. Currently, LS experiments have been performed with F/Cl/Br/I-benzenes. TOF-MS studies with iodobenzene and fluorobenzene have yielded mechanistic information about the dissociation mechanisms of the precursors and dissociation/self-reaction of phenyl and *o*-benzyl radicals. These studies will be supplemented with DFST/TOF-MS investigations of bromobenzene and chlorobenzene which generate both phenyl and *o*-benzyl radicals directly from the precursor. Additional experiments are planned to study reactions of phenyl and *o*-benzyl radicals with small molecules such as C₂H₂ and CH₃. Investigations of the mechanisms and kinetics of high temperature dissociation of cyclic molecules are ongoing with particular emphasis on five membered rings and methylated furans. In the flow reactor we intend to examine reactions between resonantly stabilized radicals and molecules and if possible examine the products of allyl radicals and H-atoms.

IV. References

- i. Tranter R. S., Klippenstein S. J., Harding L. B., Giri B. R., Yang X., Kiefer J. H. *J. Phys. Chem. A* **2010**, *114*, 8240
- ii. Comandini A., Malewicki T., Brezinsky K., *J. Phys. Chem. A*, **2012**, *116*, 2409. Comandini A., Brezinsky K., *J. Phys. Chem. A*, **2012**, *116*, 1183.
- iii. Tranter R. S., Lynch P. T., Yang X., *Proc. Combust. Inst.*, **2012** Submitted.
- iv. Fernandes R, Giri B, Hippler H, Kachiani C, Striebel F., *J. Phys. Chem. A*, **2005**, *109*, 1063.
- v. Georgievskii Y, Miller J, Klippenstein S., *Phys. Chem. Chem. Phys.*, **2007**, *9*, 4259.
- vi. Matsugi A, Suma K, Miyoshi A., *J. Phys. Chem. A*, **2011**, *115*, 7610.
- vii. Selby T, Meloni G, Goulay F, Leone S, Fahr A, Taatjes C, Osborn D. L., *J. Phys. Chem. A*, **2008**, *112*, 9366.
- viii. Ruscic B. Private communication, **2012**
- ix. Xu, C.; Braun-Unkhoff, M.; Naumann, C.; Frank, P. *Proc. Combust. Inst.* **2007**, *31*, 231.
- x. Moskaleva, L., Madden, L., Lin, M., *Phys. Chem. Chem. Phys.*, **1999**, *1*, 3967.
- xi. Zhao Z., Chaos M. Kazakov A., Dryer F. L., *Int. J. Chem. Kinet.*, **40**, 1-18, 2008
- xii. Fischer S. L., Dryer F. L., Curran H. J., *Int. J. Chem. Kinet.*, **2000**, *32*, 713. Curran H. J., Fischer S. L., Dryer F. L., *Int. J. Chem. Kinet.* **2000**, *32*, 741.
- xiii. Yang X., Jasper A. W., Kiefer J. H. Tranter R. S., *J. Phys. Chem. A*, **2009**, *113*, 8318.
- xiv. Zhang, X.; Maccaroni, A. T.; Nimlos, M. R.; Kato, S.; Bierbaum, V. M.; Ellison, G. B.; Ruscic, B.; Simmonett, A. C.; Allen, W. D.; Schaefer, H. F.; III *J. Chem. Phys.* **2007**, *126* (4), 044312-044320

V. Publications and submitted journal articles supported by this project 2010-2012

1. Yang X., Kiefer J. H., Tranter R. S. 'Thermal dissociation of ethylene glycol vinyl ether' *Phys. Chem. Chem. Phys.* **13**, 21288-21300 (2011)
2. Yang X., Tranter R. S. 'High temperature dissociation of ethyl radicals and ethyl iodide' *Int. J. Chem. Kinet.* DOI 10.1002/kin.20601
3. Tranter R. S., Yang X., Kiefer, J. H. 'Dissociation of C₃H₃I and rates for recombination of C₃H₃ high temperatures' *Proc. Combust. Inst.*, **2011**, *33*, 259.
4. Yang X., Jasper A. W., Giri B. R., Kiefer J. H. Tranter R. S. 'A shock tube and theoretical study on the pyrolysis of 1,4-dioxane' *Phys. Chem. Chem. Phys.*, **2010**, *13*, 3686.
5. Tranter R. S., Klippenstein S. K., Harding L. B., Giri B. R., Yang X., Kiefer J. H., "An experimental and theoretical investigation of the self-reaction of phenyl radicals" *J. Phys. Chem. A*, March **2010**, *114*, 8240.

Variational Transition State Theory

Donald G. Truhlar

Department of Chemistry, University of Minnesota
207 Pleasant Street SE, Minneapolis, Minnesota 55455
truhlar@umn.edu

Program scope

This project involves the development of variational transition state theory (VTST) [Garrett and Truhlar 2005] including optimized multidimensional tunneling (OMT) contributions and its application to gas-phase reactions with a special emphasis on developing reaction rate theory in directions that are important for applications to combustion. The further development of VTST/OMT as a useful tool for combustion kinetics also involves (i) developing and applying new methods of electronic structure calculations for the input potential energy surface, which is typically an implicit surface defined by a level of electronic structure theory, (ii) methods to interface reaction-path and reaction-swath dynamics calculations with electronic structure theory, and (iii) methods to treat vibrational anharmonicity and vibration-rotation coupling. The project also involves the development and implementation of practical techniques and software for applying the theory to various classes of reactions and transition states and applications to specific reactions, with special emphasis on combustion reactions and reactions that provide good test cases for methods needed to study combustion reactions.

The application of VTST to gas-phase reactions is carried out by direct dynamics [Truhlar and Gordon 1990, Truhlar 1995], and it involves electronic structure calculations of potential energy surfaces and the use of these surfaces to calculate generalized free energies of activation and multidimensional tunneling probabilities. A key emphasis is the interface of electronic structure calculations with dynamics algorithms as achieved in the POLYRATE computer program and its various RATE interfaces to electronic structure packages. The methods employed in POLYRATE are described in a review article [Fernandez-Ramos 2007].

Recent progress

The atomistic simulation of reactions of complex molecules, such as those involved in combustion, requires one to treat anharmonic, coupled torsions in both reactants and transition states, along with the accompanying torsional anharmonicity, and to consider reaction along more than one reaction path. In the past year, our major accomplishments are the development of an internal coordinate method for including multiple structures and torsional anharmonicity of torsions coupled to each other and to overall rotation and for including multiple reaction paths in reaction rate calculations that include both variationally optimized transition states and multidimensional tunneling. These methods have been incorporated in a computer code called MSTor that is now available to the community at no charge in an international program library and on our Web site. We have applied the method to calculate thermochemical quantities for many molecules and radicals and to calculate reaction rates of combustion reactions. Examples are given in the references below.

Software distribution

We have developed several software packages for applying variational transition state theory with optimized multidimensional tunneling coefficients to chemical reactions. The URL

of our software distribution site is comp.chem.umn.edu/Truhlar. The license requests that we fulfilled during the period Jan. 1, 2010–Apr. 17, 2011 for software packages developed under DOE support is as follows:

	<i>Total</i>	<i>academic</i>	<i>government//DoD/non-profit/industry</i>
POLYRATE	334	299	35
GAUSSRATE	188	173	15
ABCRATE	22	18	4
GAMESSPLUSRATE	18	13	5
NWCHEMRATE	16	13	3
5 other RATE programs	30	24	6

The total number of requests fulfilled for all RATE programs since 1995 is 2356.

Future plans

The general objective of this project is to develop and employ improved methods for calculating the rate constants of gas-phase chemical reactions. Our current plans are as follows:

- (1) First, we aim to make the combination of MSTor with POLYRATE more user friendly.
- (2) Second, we aim to improve the interface of rate theory with electronic structure methods, especially to develop improved utilize multi-configuration wave function methods and improved density functionals for to calculate potential energy surfaces for systems with high multireference character. We are especially interested in developing methods applicable to radicals, reactive intermediates, and complex and unsaturated organic molecules, as required for modeling combustion of real fuels, fuel additives, and their combustion-generated intermediates.
- (3) Third, we plan to calculate benchmark converged partition functions for molecules with multiple torsions and to use them to test approximation schemes.
- (4) Fourth, we propose to continue the development, documentation, and distribution of software for carrying out calculations based on the methods developed in this project.
- (5) We plan to add pressure-dependent modeling capability to POLYRATE. This will involve improved algorithms for microcanonical rate constants and an interface to a master equation program.
- (6) Finally, we plan to continue calculate rate constants for specific applications that are important in combustion.

References Cited

- [Garrett and Truhlar 2005] "Variational Transition State Theory," B. C. Garrett and D. G. Truhlar, in *Theory and Applications of Computational Chemistry: The First Forty Years*, edited by C. E. Dykstra, G. Frenking, K. Kim, and G. Scuseria (Elsevier, Amsterdam, 2005), pp. 67-87.
- [Fernandez-Ramos 2007] "Variational Transition State Theory with Multidimensional Tunneling," A. Fernandez-Ramos, B. A. Ellingson, B. C. Garrett, and D. G. Truhlar, in *Reviews in Computational Chemistry*, Vol. 23, edited by K. B. Lipkowitz and T. R. Cundari (Wiley-VCH, Hoboken, NJ, 2007), pp. 125-232.
- [Truhlar and Gordon 1990] "From Force Fields to Dynamics: Classical and Quantal Paths," D. G. Truhlar and M. S. Gordon, *Science* **249**, 491–498 (1990).

[Truhlar 1995] “Direct Dynamics Method for The Calculation of Reaction Rates,” D. G. Truhlar, in *The Reaction Path in Chemistry: Current Approaches and Perspectives*, edited by D. Heidrich (Kluwer, Dordrecht, 1995), pp. 229–255. [Understanding Chem. React. **16**, 229–255 (1995).]

Publications supported by this grant, 2010-present

1. “Least-Action Tunneling Transmission Coefficient for Polyatomic Reactions,” R. Meana-Pañeda, D. G. Truhlar, and A. Fernández-Ramos, *Journal of Chemical Theory and Computation* **6**, 6-17 (2010). dx.doi.org/10.1021/ct900420e
2. “Efficient Diffuse Basis Sets for Density Functional Theory,” E. Papajak and D. G. Truhlar, *Journal of Chemical Theory and Computation* **6**, 597-601 (2010). dx.doi.org/10.1021/ct900566x. (Letter)
3. “Kinetics of Hydrogen-Transfer Isomerizations of Butoxyl Radicals,” J. Zheng and D. G. Truhlar, *Physical Chemistry Chemical Physics* **12**, 7782-7793 (2010). dx.doi.org/10.1039/b927504e.
4. “Communication: Energetics of Reaction Pathways for Reactions of Ethenol with the Hydroxyl Radical: The Importance of Internal Hydrogen Bonding at the Transition State,” O. Tishchenko, S. Ilieva, and D. G. Truhlar, *Journal of Chemical Physics* **133**, 021102/1-4 (2010). dx.doi.org/10.1063/1.3455996
5. “Direct Dynamics Implementation of the Least-Action Tunneling Transmission Coefficient. Application to the CH₄/CD₃H/CD₄+CF₃ Abstraction Reactions,” R. Meana-Pañeda, D. G. Truhlar, and A. Fernández-Ramos, *Journal of Chemical Theory and Computation* **6**, 3015-3025 (2010). dx.doi.org/10.1021/ct100285a
6. “Minimally Augmented Karlsruhe Basis Sets,” J. Zheng, X. Xu, and D. G. Truhlar, *Theoretical Chemistry Accounts* **128**, 295-305 (2011). dx.doi.org/10.1007/s00214-010-0846-z
7. “Convergent Partially Augmented Basis Sets for Post-Hartree-Fock Calculations of Molecular Properties and Reaction Barrier Heights,” E. Papajak and D. G. Truhlar, *Journal of Chemical Theory and Computation* **7**, 10-18 (2011). dx.doi.org/10.1021/ct1005533
8. “Kinetic Isotope Effects for the Reactions of Muonic Helium and Muonium with H₂,” D. G. Fleming, D. J. Arseneau, O. Sukhorukov, J. H. Brewer, S. L. Mielke, G. C. Schatz, B. C. Garrett, K. A. Peterson, and D. G. Truhlar, *Science* **331**, 448-450 (2011). dx.doi.org/10.1126/science.1199421
9. “Computational Study of the Reactions of Methanol with the Hydroperoxyl and Methyl Radicals. Part I: Accurate Thermochemistry and Barrier Heights,” I. M. Alecu and D. G. Truhlar, *Journal of Physical Chemistry A* **115**, 2811–2829 (2011). dx.doi.org/10.1021/jp110024
10. “High-Level Direct-Dynamics Variational Transition State Theory Calculations Including Multidimensional Tunneling of the Thermal Rate Constants, Branching Ratios, and Kinetic Isotope Effects of the Hydrogen Abstraction Reactions from Methanol by Atomic Hydrogen,” R. Meana-Pañeda, D. G. Truhlar and A. Fernández-Ramos, *Journal of Chemical Physics* **134**, 094302/1-14. dx.doi.org/10.1063/1.3555763
11. “Practical Methods for Including Torsional Anharmonicity in Thermochemical Calculations of Complex Molecules: The Internal-Coordinate Multi-Structural Approximation,” J. Zheng, T. Yu, E. Papajak, I. M. Alecu, S. L. Mielke, and D. G. Truhlar, *Physical Chemistry Chemical Physics* **13**, 10885-10907 (2011). dx.doi.org/10.1039/C0CP02644A

12. "How Well Can Modern Density Functionals Predict Transition State Bond Distances?" X. Xu, I. M. Alecu, and D. G. Truhlar, *Journal of Chemical Theory and Computation* **7**, 1667-1676 (2011). [dx.doi.org/10.1021/ct2001057](https://doi.org/10.1021/ct2001057).
13. Multi-Structural Variational Transition State Theory. Kinetics of the 1,4-Hydrogen Shift Isomerization of the Pentyl Radical with Torsional Anharmonicity," T. Yu, J. Zheng, and D. G. Truhlar, *Chemical Science* **2**, 2199-2213 (2011). [dx.doi.org/10.1039/C1SC00225B](https://doi.org/10.1039/C1SC00225B)
14. "Thermodynamics of C–H Bond Dissociation in Hexane and Isohexane Yielding Seven Isomeric Hexyl Radicals," J. Zheng, T. Yu, and D. G. Truhlar, *Physical Chemistry Chemical Physics* **13**, 19318-19324 (2011). [dx.doi.org/10.1039/C1CP21829H](https://doi.org/10.1039/C1CP21829H)
15. "Statistical Thermodynamics of the Isomerization Reaction Between n-Heptane and Isoheptane," T. Yu, J. Zheng, and D. G. Truhlar, *Physical Chemistry Chemical Physics* **14**, 482-494 (2011). [dx.doi.org/10.1039/c1cp22578b](https://doi.org/10.1039/c1cp22578b).
16. "Kinetics of the Reaction of the Heaviest Hydrogen Atom with H₂, the $^4\text{He}\mu + \text{H}_2 \rightarrow ^4\text{He}\mu\text{H} + \text{H}$ reaction: Experiments, Accurate Quantal Calculations, and Variational Transition State Theory, Including Kinetic Isotope Effects for a Factor of 36.1 in Isotopic Mass," D. G. Fleming, D. J. Arseneau, O. Sukhorukov, J. H. Brewer, S. L. Mielke, D. G. Truhlar, George C. Schatz, B. C. Garrett, and K. A. Peterson, *Journal of Chemical Physics* **135**, 184310/1–18 (2011). [dx.doi.org/10.1063/1.3657440](https://doi.org/10.1063/1.3657440)
17. "Computational Study of the Reactions of Methanol with the Hydroperoxyl and Methyl Radicals. 2. Accurate Thermal Rate Constants," I. M. Alecu, and D. G. Truhlar, *Journal of Physical Chemistry A* **115**, 14599-14611 (2011). [dx.doi.org/10.1021/jp209029p](https://doi.org/10.1021/jp209029p)
18. "Multipath Variational Transition State Theory. Rate Constant of the 1,4-Hydrogen Shift Isomerization of the 2-Cyclohexylethyl Radical," T. Yu, J. Zheng, and D. G. Truhlar, *Journal of Physical Chemistry A* **116**, 297-308 (2012). [dx.doi.org/10.1021/jp209146b](https://doi.org/10.1021/jp209146b)
19. "Multi-Structural Variational Transition State Theory: Kinetics of the 1,5-Hydrogen Shift Isomerization of 1-Butoxyl Radical Including All Structures and Torsional Anharmonicity," X. Xu, E. Papajak, J. Zheng, and D. G. Truhlar, *Physical Chemistry Chemical Physics* **14**, 4204-4216 (2012). [dx.doi.org/10.1039/c2cp23692c](https://doi.org/10.1039/c2cp23692c).
20. "Multi-path Variational Transition State Theory for Chemical Reaction Rates of Complex Polyatomic Species: Ethanol + OH Reactions," J. Zheng and D. G. Truhlar, *Faraday Discussions* **157** (2012), accepted manuscript online at [dx.doi.org/10.1039/C2FD20012K](https://doi.org/10.1039/C2FD20012K). [Accepted on Feb. 29, 2012 and passed to Editorial Production department with a production reference number of C2FD20012K]
21. "MSTor: A program for calculating partition functions, free energies, enthalpies, entropies, and heat capacities of complex molecules including torsional anharmonicity," J. Zheng, S. L. Mielke, K. L. Clarkson, and D. G. Truhlar, *Computer Physics Communications*, in press, corrected proof available online on March 15, 2012 as Accepted Article, Article in Press. [dx.doi.org/10.1016/j.cpc.2012.03.007](https://doi.org/10.1016/j.cpc.2012.03.007)
Article's reference number is COMPHY 4697. Proofs returned March 22, 2012.
22. "A Product Branching Ratio Controlled by Vibrational Adiabaticity and Variational Effects: Kinetics of the H + trans-N₂H₂ Reactions," J. Zheng, R. J. Rocha, M. Pelegrini, L. F. A. Ferrão, E. F. V. Carvalho, O. Roberto-Neto, F. B. C. Machado, and D. G. Truhlar, *Journal of Chemical Physics*, accepted March 16, 2012. Manuscript Number: A11.12.0014.

SISGR: Developing a predictive model for the chemical composition of soot nanoparticles: Integrating Model and Experiment

Lead PI: A. Violi
University of Michigan
Ann Arbor, MI
avioli@umich.edu

Co-PI's: N. Hansen, H. Michelsen
Combustion Research Facility - Sandia National Laboratories

Co:PI: K. Wilson
Lawrence Berkeley National Laboratory
Berkeley

I. Program Scope

Mechanisms of soot formation have been studied for quite some time, and there is a general consensus that polycyclic aromatic hydrocarbons (PAH) are key intermediates: their growth leads to nucleation of particles and the latter continue to add mass via surface growth. Even though we are now able to predict the rate of soot formation to some degree of accuracy due to the development of detailed soot models, key uncertainties remain. Particularly, the mechanisms of soot nucleation and mass growth remain phenomenological.

The research program described here focuses on the development of predictive models for nanoparticle formation from combustion sources. An important part of this project is to study the nucleation process. The kinetics of nucleation control the number of nascent particles and the coagulation of these particles determine the evolution of particle number density. Various pathways have been proposed for the formation of first soot nuclei and in several landmark papers key kinetic and thermodynamic arguments were made that established the central role of condensed PAH.

In this work, we use atomistic simulations to investigate the chemical and physical phenomena related to the formation of PAH dimers, their nucleation, and further growth into nanoparticles.

This project is developed in collaboration with the research group composed by Dr. Michelsen and Dr. Hansen at Sandia National Laboratories and Wilson at Lawrence Berkeley National Laboratory to develop the next generation of soot models, which allow the prediction of chemical compositions of nanoparticles produced in flames of different fuels.

II. Recent Progress

The majority of work on soot formation has been driven by the need of developing predictive models for soot formation and oxidation arising from principles of kinetics and thermodynamics. Various pathways have been proposed for the formation of first soot nuclei [1-11] and in several landmark papers key kinetic and thermodynamic arguments were made that established the central role of condensed PAH. The majority of numerical studies performed with detailed models of soot formation invoke irreversible dimerization of pyrene molecules as initial nucleation step for the condensed phase [12-16]. The choice of pyrene dimerization for initiating particle nucleation was motivated by the great thermodynamic stability of this molecule [17]. The purpose of this study is to determine the thermodynamic driving forces for the formation of PAH dimers using Molecular Dynamics (MD) simulations.

Our recent work has focused on determining the free energy of interactions of various hydrocarbons using atomistic models.

The MD results discard the hypothesis of dimerization of small peri-condensed aromatics in flame conditions, and suggest the importance of aromatics with saturated and unsaturated chains as monomers that can lead to the formation of stable dimers. The presence of aliphatic chains favor proximity of molecules that can react or collide with other species, suggesting a more complex scenario for soot nucleation than the simple stacking of small-sized PAH.

The Helmholtz free energies of dimerization of several PAHs were computed employing molecular dynamics simulations coupled with the well-tempered Metadynamics algorithm [19]. Metadynamics is a technique used to improve the sampling of a system and reconstruct the free energy landscape. The algorithm assumes that the system can be described by a few collective variables, which discern the states (initial, final and intermediates) of the system, as well as the slow events that are relevant to the process of interest.

The following procedure was adopted to study the systems of PAH: for each pair of molecules a canonical simulation was performed for 1 ns at the target temperature (either 500 K or 1000 K). For the interaction potential, the parameters introduced by Herdmann and Miller [6] for the non-bonded potential of the aromatic rings and the all atom version of the Optimized Potentials for Liquid Simulations (OPLS-AA) force field [20] for all the other parameters were employed.

Figure 1 shows the pool of molecules considered in this study.

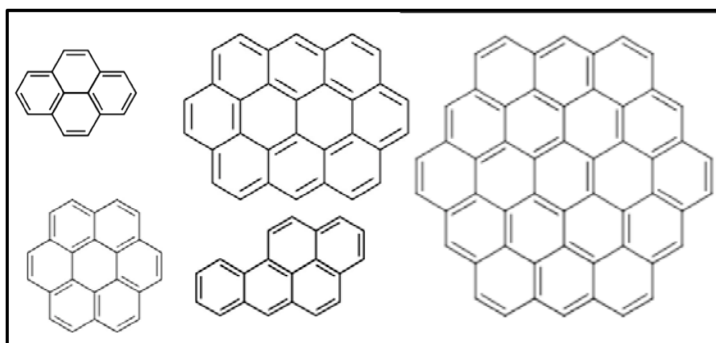


Figure 1. Pool of molecules analyzed in this study

Figure 2 reports the computed free energies of dimerization of different pairs of PAHs as function of the distance of their centers of mass at 500 K and 1000 K.

At low temperature (Fig. 2a) the free energy profiles show that the formation of dimer is preferred over the existence of free monomers for all the systems investigated. However, the minimum of the curve for pyrene molecules is shallow and the energy needed for a dimer to dissociate back to monomers is close to the average thermal energy, $k_B T$. These findings are consistent with the experimental evidence that all these substances have a boiling or melting point above 500 K. At 1000 K (Fig. 2b) only ovalene and circumcoronene give stable dimers, once the error bar of the free energy (~ 0.6 kJ/mol) and the average thermal energy (~ 8.3 kJ/mol) are taken into account.

From these results we deduce that while the number of aromatic rings in the monomer increases the

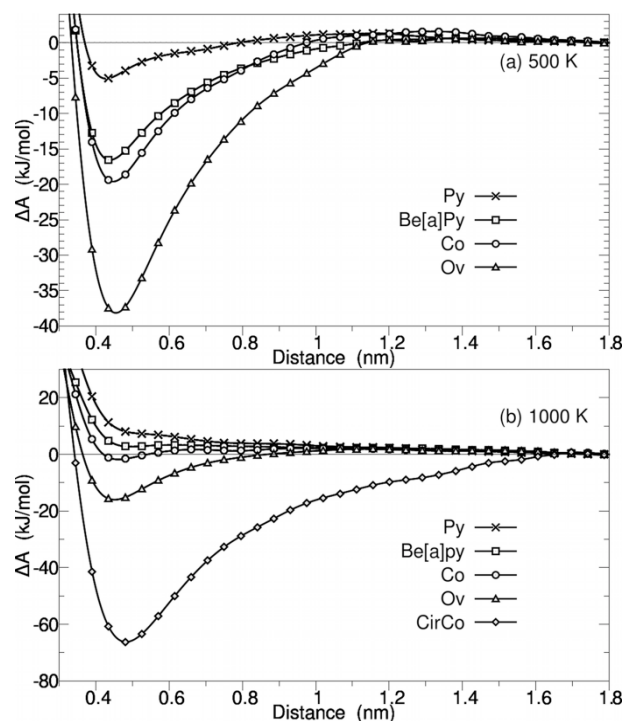


Figure 2. Free energy of the dimerization of different PAHs as a function of the distance between their center of mass at (a) 500 K and (b) 1000 K.

stability of the corresponding dimer, this effect is not linear and this phenomenon is strongly affected by the temperature and the molecular symmetry of the monomer. In particular, benzo[a]pyrene (5 rings, molar mass 252.3 g/mol), which has a stability similar to coronene (7 rings, molar mass 300.35 g/mol) at 500 K, at 1000 K shows a behavior that is intermediate between coronene and pyrene (4 rings, mass 202.25 g/mol). While more extensive studies are needed, this result suggests that the understanding of the dimerization process goes beyond the simple dependency on mass or number of aromatic rings, which are commonly used in the literature.

Since pyrene and its dimerization at high temperatures have been the focus of several recent works, it is worth noting that at 1000 K the dimerization of pyrene it is not favored with a difference of ~ 1.5 kBT between the free monomer (1.8 nm) and the dimer (0.42 nm). To further investigate this issue, we looked at the formation of a pyrene trimer, computing the free energy of the addition of a monomer to a pyrene dimer.

The results show that the trimerization has negative change in free energy at 500 K and a positive value at 1000 K. At low temperature the trimer (distance equal to 0.6 nm) is about 5 kJ/mol more stable the configuration where the dimer and the monomer are dissociated. This energy difference is slightly less than the stabilization energy of the dimer as compared to the free monomers. The location of the minimum at 0.6 nm in Fig. 3 is relative to the distance between the center of mass of the dimer and the monomer. However, if we analyze the relative frequency of the minimum distance between the monomer and either one of the pyrene molecules that compose the dimer (see Fig. 3 inset), we note that the most likely configuration is located at ~ 0.42 nm as it was reported in Fig. 2a.

The picture that emerges from these data indicates that at equilibrium at 1000 K, dimers and trimers of pyrene are present but in very limited quantity. For example, using the computed values of free energy, we determined the equilibrium constant of dimerization of pyrene, and estimated that in these conditions the ratio between pyrene monomers and dimers is about 35, which increases to about 2000 for the monomer trimer ratio.

III. Future Work

Future work will aim at developing a model for the nucleation of nanoparticles that include a physical growth mechanism together with a kinetic process. The uniqueness of the approach will make it possible to determine mass distributions as well as information on the chemical compositions of nanoparticles.

The model will be guided and validated by experimental data. Co-PI's and responsible for the experimental portions of this project are Dr. Michelsen and Dr. Hansen (Sandia) and Dr. Wilson (Lawrence Berkeley National Laboratory). During the report period, a counter-flow diffusion burner system has been set-up and tested successfully. These counter-flow flame systems will be used to study the formation of PAH's and small soot particles. The chemical structure of the counter-low flames and the chemical composition of nanoparticles will be investigated using the flame-sampling mass spectrometer and the aerosol mass spectrometer, both installed on beamline 9.0.2 at the ALS.

IV. References

- [1] Homann KH.. *Angewandte Chemie-International Edition*. **1998**, 37(18), 2435.
- [2] D'Anna A. *Proceedings of the Combustion Institute*. **2009**, 32, 593.
- [3] Frenklach M, Wang H. **1991**, 23(1), 1559.
- [4] Miller JH. *Symposium (International) on Combustion*. **1991**, 23(1), :91.
- [5] Herdman JD, Miller JH. *Journal of Physical Chemistry A*. **2008**, 112(28), 6249.
- [6] Richter H, Benish TG, Mazyar OA, Green WH, Howard JB. *Proceedings of the Combustion Institute*. **2000**, 28, 2609.
- [7] Apicella B, Ciajolo A, Suelves I, Morgan TJ, Herod AA, Kandiyoti R. *Combustion Science and Technology*. **2002**, 174(11-2), 345.
- [8] Chung SH, Violi A. *Journal of Chemical Physics*, **2011**,132.
- [9] Chung SH, Violi A. *Carbon*. **2007**, 45(12), 2400.
- [10] Izvekov S, Violi A. *Journal of Chemical Theory and Computation*, **2006** May;2(3):504-12.
- [11] Violi A, Izvekov S. *Proceedings of the Combustion Institute*. **2007** 2007;31:529-37.
- [12] Kazakov A, Wang H, Frenklach M. *Combustion and Flame*, **1995**, 100(1-2):111-20.
- [13] Appel J, Bockhorn H, Frenklach M. *Combustion and Flame*, **2000** Apr;121(1-2):122-36.
- [14] Marquardt M, Mauss F, Jungfleisch B, Suntz R, Bockhorn H. *Twenty-Sixth Symposium on Combustion* **1996**:2343-50.
- [15] Bai XS, Balthasar M, Mauss F, Fuchs L. *Twenty-Seventh Symposium* **1998**:1623-30.
- [16] Davis SG, Wang H, Brezinsky K, Law CK. *Twenty-Sixth Symposium* **1996**:1025-33.
- [17] Schuetz CA, Frenklach M. *Proceedings of the Combustion Institute*. **2002**;29:2307-14.
- [18] Wang H. *Proceedings of the Combustion Institute*. **2011**, 33, 41.
- [19] Barducci A, Bussi G, Parrinello M. *Physical Review Letters*. **2008**, 100(2), 020603.
- [20] Jorgensen WL, Maxwell DS, Tirado-Rives J. *J. American Chemical Society*. **1996**, 118(45), 11225.

V. Publications and submitted journal articles supported by this project

1. S.H. Chung, A. Violi "Nucleation of Fullerenes as a Model for Examining the Formation of Soot", *The Journal of Chemical Physics*, 132(17): 174502 (2010).
2. S.H. Chung, A. Violi, Peri-condensed aromatics with aliphatic chains as key intermediates for the nucleation of aromatic hydrocarbons" *Proceedings of the Combustion Institute* 33(1), 693-700, (2011).
3. S. A. Skeen, B. Yang, H. A. Michelsen, J. A. Miller, A. Violi, N. Hansen, "Studies of Laminar Opposed-Flow Diffusion Flames of Acetylene at Low Pressures with Photoionization Mass Spectrometry", *Proc. Combust. Inst.*, accepted for presentation (2012).
4. P. Elvati, A. Violi, "Thermodynamic of PAH clustering for soot nucleation ", *Proc. Combust. Inst.*, accepted for presentation (2012).

PRESSURE DEPENDENCE OF COMBUSTION REACTIONS: QUANTUM INELASTIC DYNAMICS ON AUTOMATICALLY GENERATED POTENTIAL ENERGY SURFACES

Albert Wagner
Chemical Sciences and Engineering Division
Argonne National Laboratory
9700 South Cass Avenue
Argonne, IL 60439
Email: wagner@anl.gov

PROJECT SCOPE

This is a new research program aimed both at developing improved ways to automatically construct a reliable potential energy surface (PES) and at using such surfaces to carry out inelastic quantum dynamics studies on pressure effects.

Of particular interest for ab initio PES construction are inelastic processes that control the pressure dependence in elementary combustion reactions. Theoretical efforts in this area have traditionally involved classical trajectories on semi-empirical PESs. However, there have always been fundamental issues about classical trajectories for inelastic scattering, such as the binning problem, resonance effects, and the separation of elastic and inelastic cross sections. In the context of pressure effects, zero point energy issues compromise classical descriptions of inelastic processes of chemically activated molecules right at the energy threshold of bond breaking processes, such as elimination and isomerization, where competition between inelastic and reactive processes is most important in determining kinetic outcomes. This program will use automatically generated PESs with approximate quantum dynamics on parallel computers to determine the limits of quantum effects and the reliability of classical trajectories for rate constant pressure dependence.

The application of automatic PES generation to inelastic scattering problems is appropriate. Inelastic scattering at energies below reaction thresholds may avoid or ameliorate the challenges of describing severe electronic rearrangements that accompany bond-breaking/bond-forming processes. This should lead to more feasible electronic structure approaches with the global reliability needed for automatic PES generation. Furthermore, unlike reactive processes whose kinetics are often governed by restricted portions of the PES like reaction paths, inelastic processes typically need a global PES. Successful automatic generation of PESs for inelastic scattering could make pressure-effect combustion studies more routine whether quantum or classical techniques are used.

RECENT PROGRESS

PES generation methods that can be made automatic share two essential features: they are *interpolative* and they possess a *local error estimator*. Interpolative means that the PES generated goes exactly through the available ab initio information. A local error estimator means that at any geometry, a useful estimate of the fitting error can be constructed. Automatic PES generation is then straightforward: (1) a fit to an initial set of ab initio data subsequently allows the local error estimator to find the geometry of

maximal fitting error, (2) new electronic structure calculations are that geometry are incorporated into a new fit with now no fitting error where formerly the fitting error was maximal; and (3) the error estimator locates a new geometry of maximal error and the process is repeated until a desired accuracy is achieved. Among several methods with these characteristics, this program will initially select the interpolative moving least squares (IMLS) method with a local error estimator based on contending basis sets. This method can fit energies alone or energies in combination with spatial derivatives of various orders. In Fig. 1, the automatic convergence properties of IMLS PESs are illustrated by our results on four chemical systems.^{1,2,3}

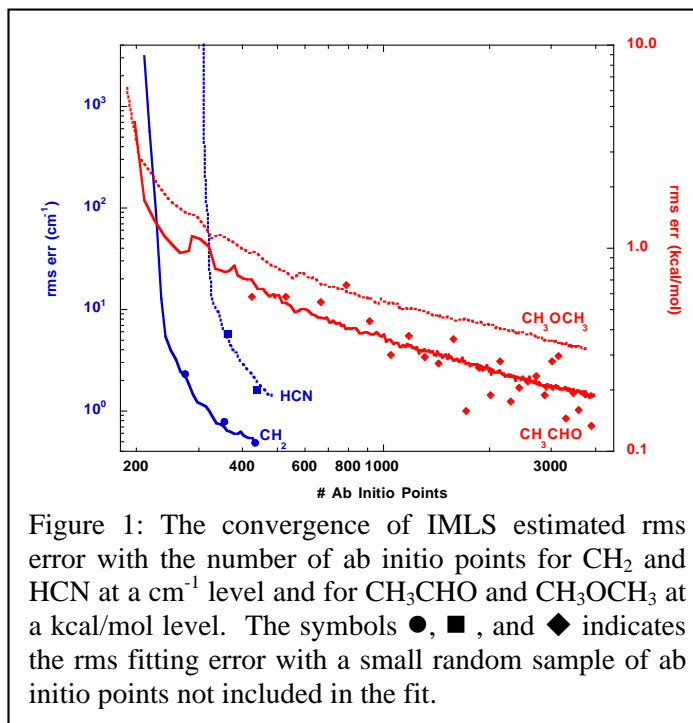


Figure 1: The convergence of IMLS estimated rms error with the number of ab initio points for CH_2 and HCN at a cm^{-1} level and for CH_3CHO and CH_3OCH_3 at a kcal/mol level. The symbols \bullet , \blacksquare , and \blacklozenge indicates the rms fitting error with a small random sample of ab initio points not included in the fit.

In a collaboration with Richard Dawes (Missouri University of Science and Technology) in the lead, we have produced two additional IMLS PESs. One is a 6D reduced dimensionality propane PES to complete a triplet of R- CH_3 surfaces (see the red curves in Fig. 1) for studies of the roaming mechanism in thermal dissociation.³ As in the dimethylether study,² this PES is being used to determine the branching ratio for roaming processes.

Of greater relevance to pressure dependence studies is the development of a ground state $^2A''$ HO_2 PES indicated in Fig. 2. This PES was generated⁴ with MRCI+Q calculations using complete basis set (CBS) extrapolation and 18-reference-states with dynamic weighting.⁵ Starting with a 200 point seed grid, ~1600 points total were required to converge the fitting error to $\sim 1 \text{ cm}^{-1}$. The agreement with experiment of calculated

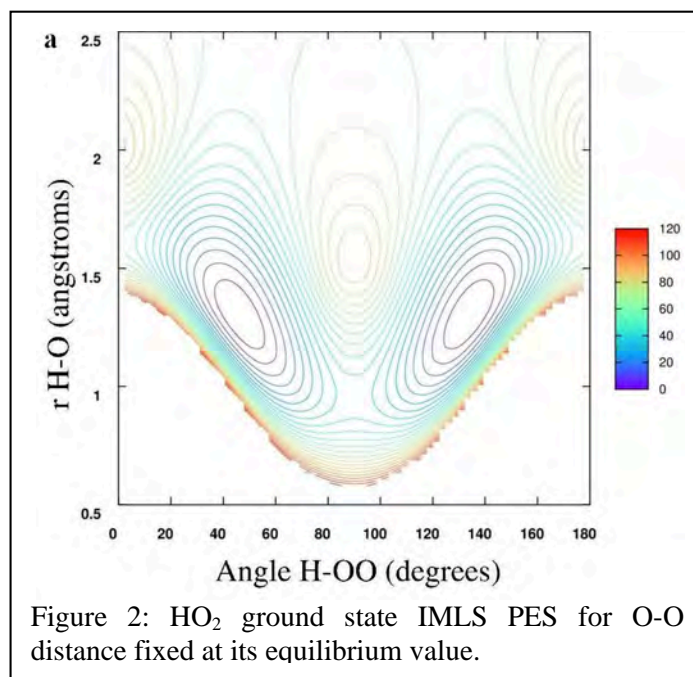


Figure 2: HO_2 ground state IMLS PES for O-O distance fixed at its equilibrium value.

spectroscopic information on this PES is superior to any other PES. In collaboration with Don Thompson (U. Missouri), trajectory studies are under way comparing IVR and isomerization characteristics of this PES relative to other PESs for this system.

In collaboration with the Dawes group, H. Guo (U. New Mexico), and others, we are in the process of developing a third IMLS PES, that being a high quality HOCO PES to compliment recent PESs developed by Guo and Bowman⁶ spurred by the tunneling results of the Continetti group.⁷ POLYRATE studies of the unimolecular decay of HOCO to H+CO₂ are in progress.

The extension of IMLS methods to more complicated species would benefit from an inexpensive zeroth order PES that would allow IMLS methods to be applied to the smaller and hopefully smoother *difference* of ab initio calculations from the zeroth order PES. In collaboration with the Thompson group, we are exploring the AIREBO scheme,⁸ originally developed for condensed phases of hydrocarbons, as a zeroth order PES. Our test case is C₂H₅, the simplest hydrocarbon radical with both dissociation and isomerization saddle points that are comparable in energy.

As illustrated in Fig. 3a, in its native state, the AIREBO PES has, among other issues, too high dissociation and saddle point energies and too spatially constricted a well region. However, AIREBO is largely constructed of pairwise additive terms whose adjustment can produce a modified AIREBO PES in Fig. 3b that agrees in dissociation energy and in saddle point energy, location, and frequency with CBS-QB3 calculations. Trajectory studies of unimolecular decays on the modified AIREBO PES are underway for comparison to experimental results from photo-excitation experiments.

FUTURE PLANS

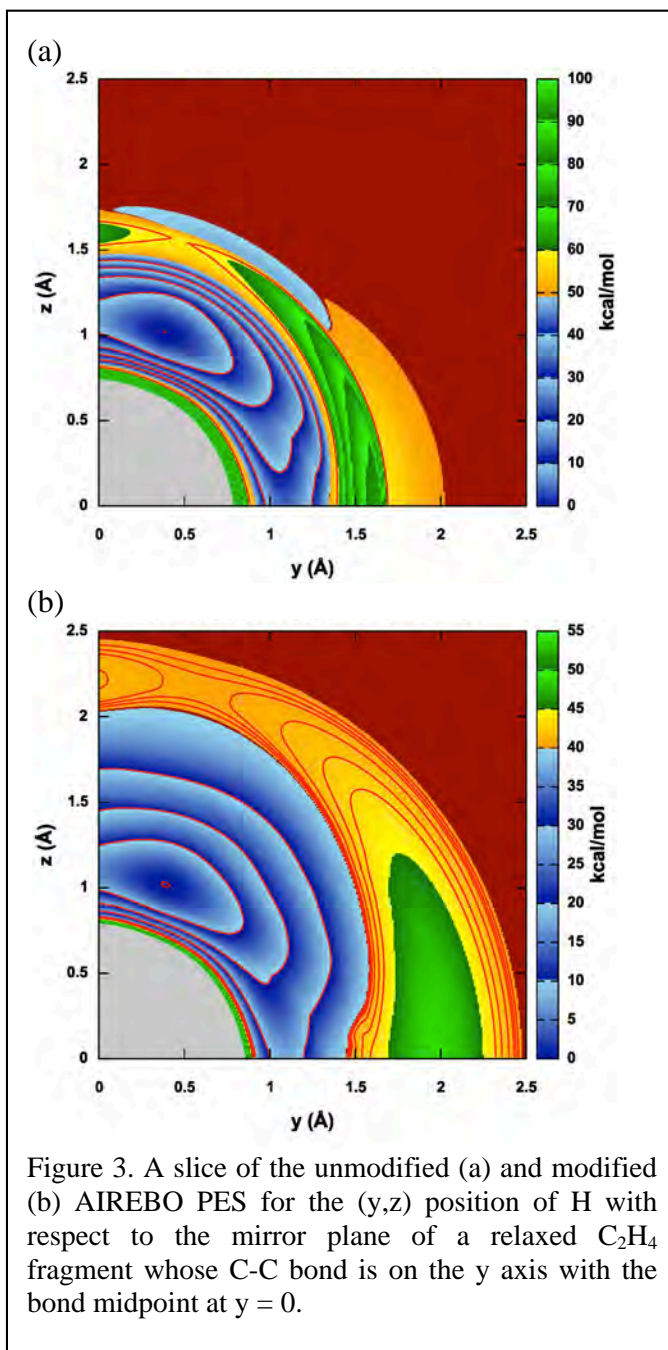


Figure 3. A slice of the unmodified (a) and modified (b) AIREBO PES for the (y,z) position of H with respect to the mirror plane of a relaxed C₂H₄ fragment whose C-C bond is on the y axis with the bond midpoint at y = 0.

In the development of PESs, the IMLS HO₂ and HOCO PES will be extended to include rare gas and other colliders. Since IMLS operates on ab initio information over an irregular array of geometries, spatial and/or compositional extensions of a PES are straightforward. For the C₂H₅ work, M05 DFT calculations will be compared to the modified AIREBO PES to test its usefulness and as a zeroth order PES.

The second aspect of this program is the application of quantum dynamics calculations of the inelastic properties of chemically activated molecular complexes. Such studies can address the effects of zero point energy and the details of mode specificity. In initiating this work, I have the parallelized four atom time dependent quantum dynamics codes⁹ of S. Gray (Argonne). I intend to modify these codes for the infinite order sudden (IOS) approximations to make the calculations more tractable. Essentially all past quantum treatments of pressure effects in combustion reactions used this approximation and it should apply because typically rotations are significantly slower than vibrational inelastic processes. Time-dependent quantum dynamics is a natural framework for this problem because the initial wavepacket can be constructed with a collider component possessing a thermal translational energy profile and with a chemically activated molecular component with filtered eigenstates in a specific energy grain. In this application, the goal is to filter the eigenstates only sufficiently to distinguish one energy grain from another. This incomplete filtering will make the calculations more practical and also more applicable to Master Equation modeling.

-
- ¹ R. Dawes, A. F. Wagner, and D. L. Thompson, *J. Phys. Chem. A* **113**, 4709 (2009).
 - ² R. Sivaramakrishnan, J. V. Michael, A. F. Wagner, R. Dawes, A. W. Jasper, L. B. Harding, Y. Georgievskii, and S. J. Klippenstein, *Comb. Flame* **158**, 618 (2011).
 - ³ In an extension of the collaboration of Ref. 2, R. Dawes has completed IMLS PESs on both CH₃CHO seen in Fig. 1 and CH₃C₂H₅.
 - ⁴ A. Li, D. Xie, R. Dawes, A. W. Jasper, J. Ma, and H. Guo, *J. Chem. Phys.* **133**, 144306 (2010).
 - ⁵ R. Dawes A. W. Jasper, T. C. Richmond, C. Mukarakate, S. H. Kable, and S. A. Reid, *J. Phys. Chem. Lett.* **1**, 641 (2010).
 - ⁶ J. Li, Y. Wang, B. Jiang, J. Ma, R. Dawes, D. Xie, J. M. Bowman, and H. Guo, *J. Chem. Phys.* **136**, 041103 (2012).
 - ⁷ C. J. Johnson, B. L. J. Poad, B. B. Shen and R. E. Continetti, *J. Chem. Phys.* **134**, 171106 (2011).
 - ⁸ A. Liu and S. J. Stuart, *J. Comp. Chem.* **29**, 601 (2008).
 - ⁹ E.M. Goldfield and S.K. Gray, *J. Chem. Phys.* **117**, 1604 (2002); J. Mayneris, M. Gonzalez, and S. K. Gray, *Comp. Phys. Comm.* **179**, 741 (2008).

DOE-SPONSORED PUBLICATIONS SINCE 2010

R. Sivaramakrishnan, J. V. Michael, A. F. Wagner, R. Dawes, A. W. Jasper, L. B. Harding, Y. Georgievskii, and S. J. Klippenstein
ROAMING RADICALS IN THE THERMAL DECOMPOSITION OF DIMETHYL
ETHER: EXPERIMENT AND THEORY
Comb. Flame **158**, 618 (2011).

Ultrafast Structural Dynamics in Combustion Relevant Model Systems

Peter M. Weber
Department of Chemistry
Brown University, Providence, Rhode Island 02912
Peter_Weber@brown.edu

I. Program Scope

We have found that Rydberg electron binding energies are quite useful measures that relay a molecular ion core's geometrical structure. One can understand the structure sensitivity of the Rydberg electron by realizing that its orbit is defined by the charge distribution of all components of the ion core molecule. In the experiment we measure the electron binding energy, i.e. the energy difference between the electron in the Rydberg state and the electron at infinite distance. If the ion core changes its structure then the Rydberg electron has to adjust its energy. This provides us with a handle to observe, in real time, the structural dynamics of molecules.

Several features make this spectroscopy uniquely applicable. For one, the Rydberg electron is very large, and therefore encompasses the entire molecule. Secondly, the ionization does not change vibrational quantum numbers, so that even complicated and large molecules provide comparably well-resolved spectra. Important also is that any vibrational excitation is not seen in the spectrum. This has the interesting consequence that the spectra are blind toward internal, vibrational energy. For the study of chemical dynamics, where the molecules are invariably very energetic, this is a tremendously advantageous feature. It implies that, as a tool to probe the time-dependent structural dynamics of chemically interesting molecules, Rydberg spectroscopy may well be better suited than diffraction techniques. At present, we can interpret the Rydberg spectra only qualitatively, but anticipating that in the future one may be able to calculate Rydberg binding energy spectra, the technology may indeed be developed into a structure determination method.

We implement Rydberg ionization spectroscopy using a time-resolved pump-probe multi-photon ionization/photoelectron scheme in which a first laser pulse excites the molecule to a Rydberg state, and a probe pulse ionizes the molecule. A time-of-flight detector measures the kinetic energy spectrum of the photoelectrons. The photoelectron spectrum directly provides the binding energy of the electron, and thereby reveals the molecule's time-dependent structural fingerprint. The time resolution of the measurement is given by the duration of the laser pulses, which in our experiment is on the order of 100 fs. To measure structural dynamics in Rydberg-excited states we delay the ionization photon from the pump photon. To measure the structural dynamics in ground or excited valence states we induce the dynamics using a near UV laser pulse, and use a multi-photon ionization scheme via the Rydberg states as a probe process.

II. Recent Progress

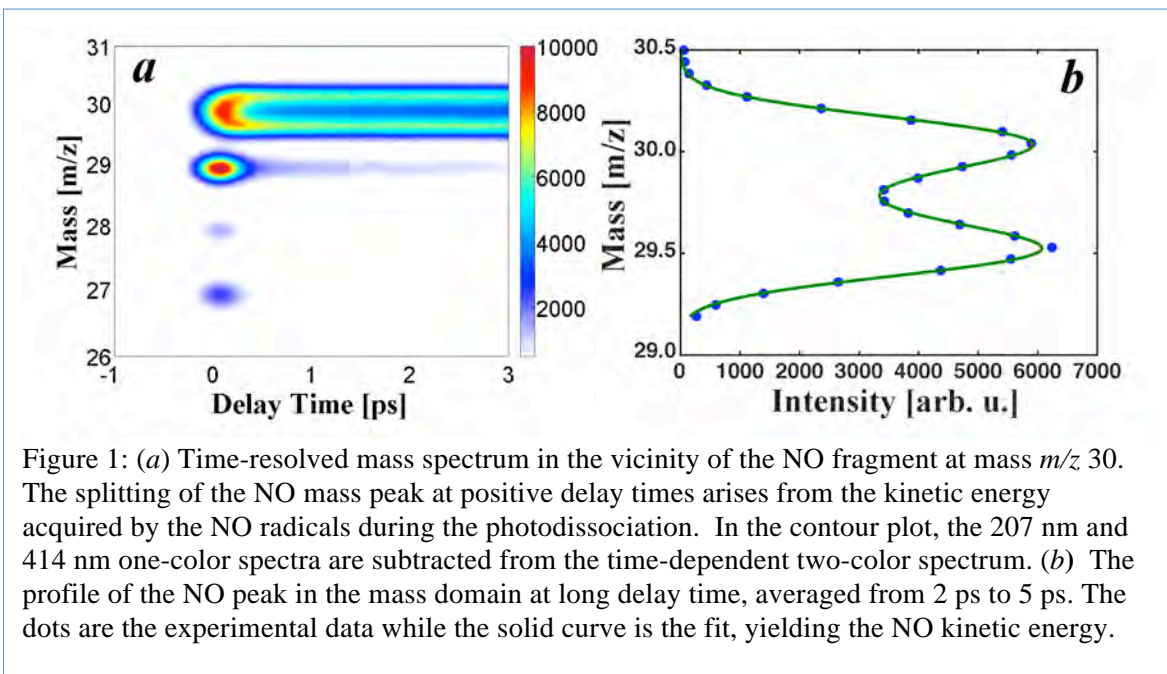
During the past year, we studied the dependence of electronic curve crossing dynamics on the nature of the initially excited electronic state [4], the structural dynamics of molecular clusters [3], the ultrafast dissociation dynamics of amyl nitrite [2], and the isomerization of a highly energetic, strained system [1]. The last two are illustrated here:

Electronic curve crossing dynamics: faster than a direct dissociation!

The homolytic, photochemical bond cleavage of alkyl nitrites, RONO, to form two radicals, RO· and NO·, has been a model system for a long time. It is well known that when excited by near UV radiation, the dissociation occurs on a femtoseconds time scale and on the S_1 surface. In our experiments, we have excited amyl nitrite ($C_5H_{11}ONO$) at wavelengths of the S_2 absorption, at 266 nm and at 207 nm. The ejection of the NO radical is observed using time-delayed probe pulses and mass spectrometry as well as photoelectron spectroscopy. Figure 1 shows the time dependence of the NO radical fragment upon excitation of amyl nitrite by a 207 nm pulse and ionization of NO by a delayed 414 nm pulse. The splitting, which arises from the kinetic energy of the NO fragment, can be well modeled and yields the kinetic energy of the fragments.

Combining evidence from the kinetic energy, the one-color photoelectron spectra and the time-resolved two-color photoelectron spectra, we concluded that even though the NO is excited at wavelengths of the electronic transition to S_2 , the dissociation does not proceed on the S_2 surface. Instead, the molecule internally converts to the S_1 surface, evidently on a time scale faster than the dissociation on the repulsive S_2 surface!

While our studies on amyl nitrite are quite conclusive, it remains to be seen how general this phenomenon is. Going forward, we plan to study amyl nitrite over a broader wavelength range, as well as other nitrites.



Structural Dynamics in energetic systems: the isomerization of quadricyclane to norbornadiene

The quadricyclane – norbornadiene system is an important model for the isomerization dynamics between highly strained molecules. Using time-resolved photoionization from Rydberg states, we observe the time-dependent structural dynamics and the time-evolving structural dispersion even while the molecule is crossing electronic surfaces. Excitation at 207 nm prepares quadricyclane in the 3p state, which quickly decays to the lower 3s state and isomerizes to norbornadiene. We observe the formation

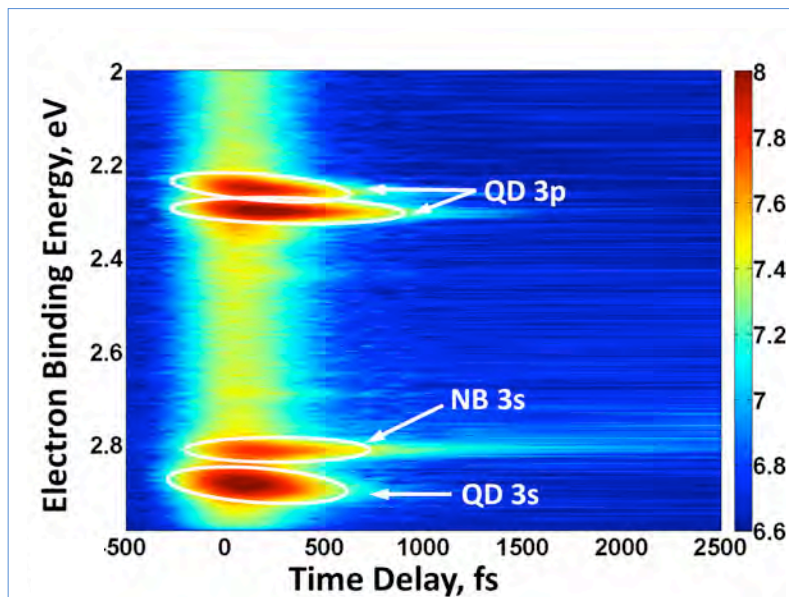


Figure 2: Photoelectron binding energy spectra obtained upon two-color photoionization of quadricyclane with 208 nm pump pulses and 416 nm probe pulses. The one-color contributions to the spectra are subtracted. The initial excitation prepares quadricyclane (QD) in 3p, but it relaxes quickly to the 3s, before converting to norbornadiene.

and evolution of the vibrational wavepacket on the Rydberg surface and the internal conversion from the 3p Rydberg states to the 3s state. In that state, quadricyclane isomerizes to norbornadiene with a time constant of $\tau_2=136(45)$ fs. The lifetime of the 3p Rydberg state in quadricyclane is $\tau_1=320(31)$, and the lifetime of the 3s Rydberg state in norbornadiene is $\tau_3=394(32)$. The energy of the quadricyclane Rydberg levels depends on time (figure 2), revealing a structural adjustment even while the molecule is reacting. A careful analysis of the peaks also shows that the width changes with time, suggesting that the wavepacket spreads as the molecule relaxes its structure on the Rydberg surface.

III. Future Plans

Ongoing work continues to take advantage of the power inherent in the Rydberg ionization spectroscopy. We continue to explore model systems that are relevant to combustion and that test the limits of applicability. This includes systems that exhibit conformeric motions and molecular clusters. Systems in the former category include cyclic diamines, such as morpholine, where we already have observed interesting temporal dynamics that relate to structural motions. In the latter category are clusters of large molecules, in particular tetramethyl ethyl diamine, where we continue to learn interesting aspects of the cluster dynamics.

In collaboration with theorists, we attempt to calculate the Rydberg electron binding energies from two vantage points. First, we use model systems to gain insights into the physical parameters that determine the binding energies in large molecules. Secondly, we work toward calculating Rydberg electron binding energies using ab initio methods.

IV. Publications resulting from DOE sponsored research (2009 - 2012)

1. “Ultrafast structural and isomerization dynamics in the Rydberg-excited Quadricyclane – Norbornadiene System,” Fedor Rudakov and Peter M. Weber, *The Journal of Chemical Physics*, 136, 1343031 - 7 (2012).
2. “The Far-UV Photochemical Bond Cleavage of n-Amyl Nitrite: Bypassing a Repulsive Surface” M. P. Minitti, Y. Zhang, M. Rosenberg, R. Y. Brogaard, S. Deb, T. I. Sølling and P. M. Weber; *J. Phys. Chem. A* **2012**, 116, 810 – 819.
3. “Structural Dynamics and Energy Flow in Rydberg-Excited Clusters of N,N-Dimethylisopropylamine,” S. Deb, M. P. Minitti, and P. M. Weber, *The Journal of Chemical Physics* 135, 044319 (2011). See also *Virtual Journal of Ultrafast Science*, August 2011.
4. “Ultrafast Dynamics of 1,3-Cyclohexadiene in Highly Excited States,” Christine C. Bühler, Michael P. Minitti, Sanghamitra Deb, Jie Bao, Peter M. Weber, *Journal of Atomic, Molecular, and Optical Physics*, Vol. 2011, Article ID 637593, 6 pages, **2011**. doi:10.1155/2011/637593.
5. “Structural Dynamics in Floppy Systems: Ultrafast Conformer Motions in Rydberg-Excited Triethylamine,” Brian Bayes, Sanghamitra Deb, Michael P. Minitti and Peter M. Weber, *J. Phys. Chem. A*. *J. Phys. Chem. A* **2011**, 115, 1804–1809.
6. “Dissociative energy flow, vibrational energy redistribution and conformeric structural dynamics in bifunctional amine model systems,” Joseph C. Bush, Michael P. Minitti and Peter M. Weber, *J. Phys. Chem. A* **2010**, 114, 11078–11084.
7. “The Ultrafast Pathway of Photon-Induced Electrocyclic Ring Opening Reactions: The case of 1,3-cyclohexadiene” Sanghamitra Deb and Peter M. Weber, *Annu. Rev. Phys. Chem.* **2011**. 62, 19–39.
8. “Electron Diffraction with Bound Electrons: the Structure Sensitivity of Rydberg Fingerprint Spectroscopy” Xiao Liang, Michael G. Levy, Sanghamitra Deb, Joseph D. Geiser, Richard M. Stratt, and Peter M. Weber, *Journal of Molecular Structure* 978 (2010), pp. 250-256.
9. “Probing the Lifetimes of Internally Excited Amyl Nitrite Cations” Martin Rosenberg, Michael P. Minitti, Nerijus Rusteika, Christer Z. Bisgaard, Sanghamitra Deb, Peter M. Weber, Theis I. Sølling, *J. Phys. Chem. A* **2010**, 114, 7021–7025.
10. “Ultrafast Formation of an Intramolecular Cation-Pi Bond,” Joseph C. Bush, Michael P. Minitti and Peter M. Weber. *Journal of Photochemistry and Photobiology A: Chemistry* 213 **2010**, 70–72.
11. “Ultrafast Curve Crossing Dynamics through Conical Intersections in Methylated Cyclopentadienes,” Fedor Rudakov and Peter M. Weber, *J. Phys. Chem. A*, **2010**, 114 (13), pp 4501–4506.
12. “Ground State Recovery and Molecular Structure upon Ultrafast Transition through Conical Intersections in Cyclic Dienes,” Fedor Rudakov and Peter M. Weber, *Chemical Physics Letters* 470, **2009** 187-190.
13. “Excited-state ions in femtosecond time-resolved mass spectrometry: An investigation of highly excited chloroamines”, R. Y. Brogaard, N. Rusteika and T. I. Sølling, F. M. Rudakov and P. M. Weber, *J. Phys. Chem. A*, **2009**, 113 (1), pp 40–43.

Detailed Studies of Hydrocarbon Radicals: C₂H Dissociation Dynamics

Curt Wittig
Department of Chemistry
University of Southern California
Los Angeles, CA 90089-1062
wittig@usc.edu

Program Scope

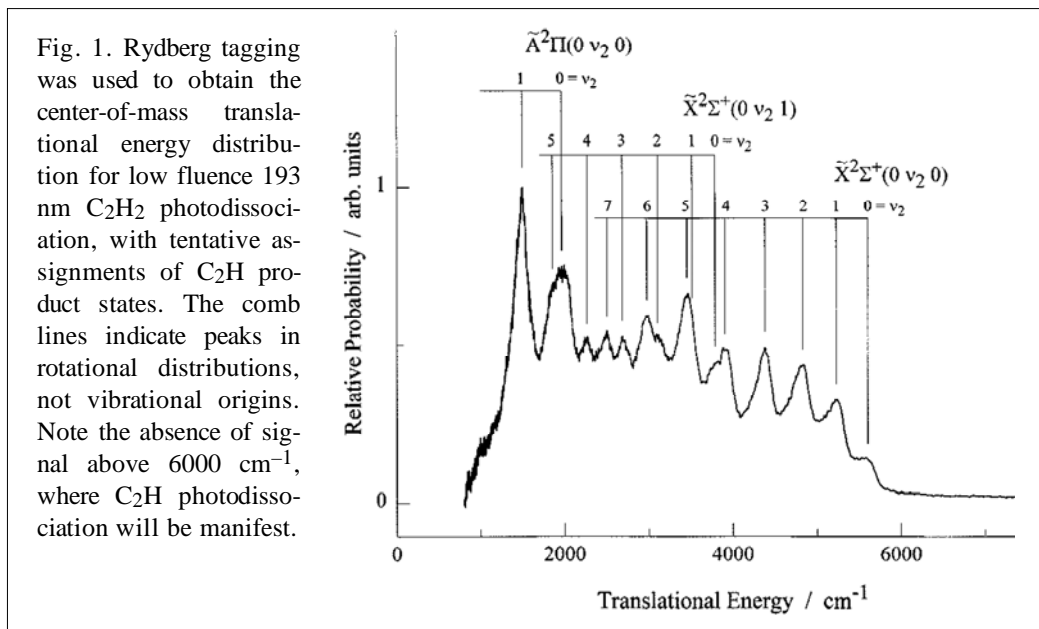
This program examines C₂H excited state properties and dynamics throughout the energy range that begins at dissociation threshold, D₀(C₂-H), and extends as far above D₀ as possible. The central role played by this species in hydrocarbon chemistry cannot be overstated. It is also an excellent prototype for examining important properties and phenomena: electronic states; curve crossings and associated nonadiabatic transitions; intramolecular and dissociation dynamics; and so on. It is small enough to provide experimental parent and product state resolution, and it is tractable at a high level of theory — electronic structure and quantum mechanical nuclear dynamics, including nonadiabatic couplings. It is an example of systems in which more than two conical-type intersections need to be taken into account simultaneously.

In last year's abstract, preliminary results using soft ionization were presented. It was shown that the C₂H photoproduct from C₂H₂ photodissociation could be isolated in our time-of-flight mass spectrometer (TOFMS) by turning down the electron energy to the extent that, for all practical purposes, no C₂H⁺ daughter ions derived from electron impact ionization of C₂H₂. The abstract focused on this, with a few comments at the end regarding the theoretical component, which addressed the popular and ubiquitous issues of conical intersection and geometric phase.

Experimental Studies

This past year it was hoped that under high fluence conditions photodissociation could be detected through C₂H₂⁺ depletion and/or C₂H⁺ appearance. The latter is potentially more sensitive because the C₂H⁺ signal that is present without C₂H₂ photodissociation can be almost eliminated. In other words, conditions can be arranged such that there is no C₂H⁺ background. The system was tested with H₂S and large depletion signals were observed. However, C₂H⁺ was not observed, despite C₂H₂ clearly being dissociated.

This is likely due to a large difference in absorption cross-sections: $\sigma_{\text{C}_2\text{H}}^{193} \gg \sigma_{\text{C}_2\text{H}_2}^{193}$. Thus we are proceeding to the Rydberg tagging experiments with a team of two graduate students and a postdoc. The idea is to start by examining the regime where the center-of-mass (c.m.) translational energy is in excess of 6000 cm⁻¹, *i.e.*, there is no signal due to C₂H₂ + *hν* → C₂H + H (Fig. 1). Given the large difference in bond strengths between C₂H₂ and C₂H (131.6 versus 116 kcal mol⁻¹, respectively) plus the internal energy of the nascent C₂H, the photodissociation of C₂H will almost certainly result in significant signal at $E_{\text{c.m.}} > 6000 \text{ cm}^{-1}$, *i.e.*, that will be easily detected (Fig. 1).



These measurements will enable an estimate to be made of $\sigma_{\text{C}_2\text{H}_2}^{193}$ for expansion-cooled C₂H₂, which we believe (on the basis of the experiments to date) will turn out to be smaller than its room temperature counterpart. Likewise, relative cross-sections, *i.e.*, $\sigma_{\text{C}_2\text{H}}^{193}$ versus $\sigma_{\text{C}_2\text{H}_2}^{193}$, will be determined. Importantly, by using CF₃C₂H as a C₂H precursor, it should be possible to minimize the amount of H-atom signal that derives from parent. At this point, the respective contributions of the CF₃C₂ + H versus CF₃ + C₂H channels are unknown. However, CF₃C₂H is known to be a good photolytic source of C₂H, so there is no doubt that CF₃ + C₂H is a major channel. Hopefully it is dominant. Its extent of participation will be established quantitatively through comparison of H-atom signals from CF₃C₂H and C₂H₂ (or C₂D₂). In addition, we will carry out photolysis experiments using the high repetition rate (up to 200 kHz) TOFMS apparatus that was used for the earlier C₂H₂⁺ and C₂H⁺ studies reported last year.

Coming back to the C₂H₂ experiments, with sufficiently high S/N, HRTOF spectra due to photodissociation of C₂H₂ are determined with good precision. The S/N indicated in Fig. 1 can be improved by a factor of several without requiring significant changes. The spectra obtained using high fluence will contain a substantial contribution from C₂H photodissociation. However, it should be possible to subtract the C₂H contribution to get an (admittedly rough) idea of the portion of the C₂H → C₂ + H contribution that lies at *E*_{c.m.} values below 6000 cm⁻¹. Let's call this phase one, *i.e.*, a warm-up experiment. Next, CF₃C₂H will be used as a C₂H precursor. Two complete machines are dedicated 100% to the above studies: the Rydberg tagging apparatus, and the 200 kHz TOFMS apparatus. This comprises 2/3 of the entire laboratory.

Theory

An invited (International Year of Chemistry Perspectives) article for Phys. Chem. Chem. Phys. was prepared between early Summer and mid-Fall, and it is now in print. Our experimental studies have been, and continue to be, involved with crossings and near crossings of potential surfaces, with accompanying non-adiabaticity and geometric phases. The article addresses these issues from a perspective enlisted infrequently in chemical physics, namely, gauge field theory. A lot of credit goes to Don Truhlar and C. Alden Mead, whose seminal papers of the late 1970's opened doors into

this area. The gauge field theory approach embeds these issues in a broad and sophisticated theoretical framework. In so doing, it is hoped that readers will acquire deep understanding of the relevant phenomena, and perhaps apply the ideas even outside the realm of Born-Oppenheimer, *e.g.*, high versus low frequency vibrations. The article is not short (24 double-column journal pages), and it required a lot of effort. It is the culmination of several years of work on my part.

The relationship between the Born-Oppenheimer adiabatic approximation and the standard model of particle physics is uncanny. The issue of geometric phase connects these in a way that is compelling. Specifically, geometric phases can only appear in systems in which parts act externally with respect to one another. A completely isolated system cannot manifest a geometric phase. In electrodynamics, charged particles interact with something exterior, *i.e.*, the electromagnetic field, and geometric (Aharonov-Bohm) phase accrues. In molecules, the nuclear and electron degrees of freedom each perceive the other as external, as long as non-adiabatic couplings are minimal. Likewise, geometric phase accrues. A brief summary is given below.

Gauge field theory and Born-Oppenheimer

Vladimir Fock and Hermann Weyl introduced gauge field theory in electrodynamics. It yields the gauge field, particle-field couplings, and Aharonov-Bohm phase, while Yang-Mills theory, the cornerstone of the standard model of physics, is a template for non-Abelian gauge symmetries. Electronic structure theory, including non-adiabaticity, is a non-Abelian gauge field theory with matrix-valued covariant derivative. Because the wave function of an isolated molecule must be single-valued, products of nuclear and electron functions such as $\chi_n\psi_n$ cannot undergo local phase transformation on \mathbf{R} , where \mathbf{R} denotes nuclear degrees of freedom.

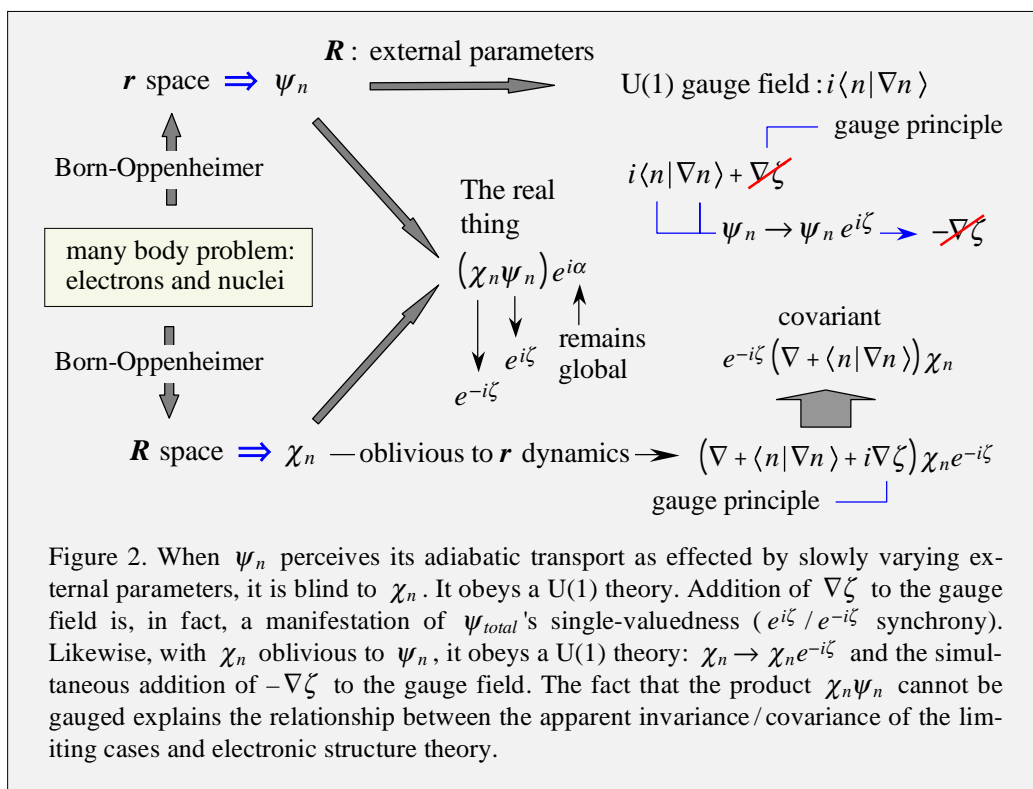


Figure 2. When ψ_n perceives its adiabatic transport as effected by slowly varying external parameters, it is blind to χ_n . It obeys a U(1) theory. Addition of $\nabla \zeta$ to the gauge field is, in fact, a manifestation of ψ_{total} 's single-valuedness ($e^{i\zeta} / e^{-i\zeta}$ synchrony). Likewise, with χ_n oblivious to ψ_n , it obeys a U(1) theory: $\chi_n \rightarrow \chi_n e^{-i\zeta}$ and the simultaneous addition of $-\nabla \zeta$ to the gauge field. The fact that the product $\chi_n \psi_n$ cannot be gauged explains the relationship between the apparent invariance/covariance of the limiting cases and electronic structure theory.

On the other hand, the synchronous transformations: $\psi_n \rightarrow \psi_n e^{i\zeta(\mathbf{R})}$ and $\chi_n \rightarrow \chi_n e^{-i\zeta(\mathbf{R})}$, preserve single-valuedness and enable wave functions in each subspace to undergo phase transformation on \mathbf{R} . Thus, each subspace is compatible with a U(1) (unitary group of dimension one) gauge field theory. The central object is Berry's adiabatic connection $i\langle n|\nabla n\rangle$, which serves as a communication link between the two subsystems. It was shown that additions to the connection according to the gauge principle are manifestations of the synchronous nature of the ψ_n and χ_n phase transformations.

This is the situation well away from an intersection, though an intersection must exist if there is to be a geometric phase. Turning to the conical intersection point, the largest gauge group applicable in the immediate vicinity of a two-state intersection is U(2), which factors to $U(1) \times SU(2)$. Gauging SU(2) yields three fields, whereas U(1) is not gauged, as the result cannot be brought into registry with electronic structure theory, and there are other problems. Loss of SU(2) symmetry as the energy gap between adiabats increases yields the inter-related U(1) symmetries of the upper and lower adiabats, with spinor character imprinted in the vicinity of the degeneracy. A flow chart is given in Fig. 2.

In the near future, the theory part will proceed in parallel with the experiments. It will be applied to vibrational relaxation in complex environments. The experiments will continue to focus on C₂H₂ and C₂H systems, enlisting the complete resources of the Rydberg tagging apparatus and the molecular beam / TOFMS systems, and the efforts of two graduate students and one postdoc.

Publication last year listing DOE support

1. C. Wittig, *Geometric phase and gauge connection in polyatomic molecules*, Phys. Chem. Chem. Phys. **14**, 6402-6425 (2012). This is an International Year of Chemistry Perspective Article. The work was funded through grants from NSF and DOE. Specifically, the DOE portion focused on the conical intersection aspect, which is germane to the dynamics of potential energy surfaces, including non-adiabatic transitions. The NSF support addressed the larger issue of the relationship of the adiabatic approximation to the standard model of physics.

Experimental Ignition Studies of Oxygenated Hydrocarbons

Margaret S. Wooldridge

Departments of Mechanical and Aerospace Engineering, University of Michigan

Ann Arbor, MI 48109-2121

mswool@umich.edu

I. Program Scope

The chemical physics of oxygenated fuels is an area which, until recently, has seen little scrutiny from the fundamental combustion science community. The chemistry of oxygenates presents an exciting area to apply our learning from hydrocarbons and adapt our methods to develop a similar level of predictive capabilities for elementary reaction theory and combustion reaction mechanisms. This research program uses ignition studies to investigate combustion and flame chemistry from the initiation and fuel oxidation phase to the heat release phase of combustion. Ignition delay time data provide valuable information on fuel reactivity for a range of state conditions, and speciation data provide direct insight into the dominant reaction pathways. The University of Michigan (UM) rapid compression facility (RCF) is used to create the temperature and pressure conditions of interest for the ignition studies. UM RCF studies focus on intermediate temperatures (600 – 1200 K) and high pressures (1-25 atm) where there are high uncertainties in the combustion chemistries.

During the past year, we completed ignition and speciation studies of the unsaturated ester methyl3hexenoate. We have also complete ignition and speciation studies of n-heptane to provide a hydrocarbon baseline for comparison with our oxygenate data. Ignition delay time data were acquired using the UM RCF for methyl3hexenoate over a range of temperatures. Mass sampling and gas chromatography were applied to quantify the stable intermediates present during ignition for methyl3hexenoate and n-heptane.

II. Recent Progress

The long test times of the UM RCF allow application of rapid gas sampling methods to simultaneously measure a large number of stable species during ignition experiments. Details on the dimensions, components and performance characterization of the UM RCF can be found in Donovan *et al.* [1]. Previous UM RCF studies have considered iso-octane ignition [2] and radical growth during iso-octane ignition [3], H₂/CO ignition [4], particle nucleation [5], and C₅ ester ignition [6]. Previous gas sampling studies on iso-octane can be found in He *et al.* [7] and on methyl butanoate in Walton *et al.* [8].

Since these earlier studies, the UM RCF gas sampling system has been modified to allow multiple sampling events to occur within one ignition experiment, and the trapped residual volume in the gas sampling system has been reduced to improve the accuracy of the species measurements. In the 2011 progress report, the results of ignition and speciation studies of n-butanol were reported. The results of the n-butanol study are summarized in Karwat *et al.* [9].

This progress report presents a brief summary of the methyl3hexenoate studies. Biodiesel fuels consist predominantly of unsaturated esters. Westbrook and Pitz biodiesel fuel models have shown that the C=C double bonds in biodiesel fuels provide the keys to understanding biodiesel autoignition. Methyl3hexenoate was selected for ignition studies using the UM RCF since it is an unsaturated methyl ester with a centrally located C=C double bond and for the convenience of the relatively high vapor pressure.

A. Ignition and speciation studies of methyl3hexenoate

We recently completed speciation studies of methyl3hexenoate to complement the ignition delay time data reported last year. Measurements of intermediate species were made using discrete sampling events applied to a series of ignition experiments each targeting the same end-of-compression conditions. Details on the high-speed gas sampling system and the gas chromatography analysis are provided in Karwat *et al.* [9].

A summary of the ignition delay time data for all the methyl3hexenoate experiments, including the speciation studies, is provided in Figure. 1. Experimental conditions were held at a fixed equivalence ratio of $\phi = 0.3$ and a fixed inert gas to oxygen ratio of 3.76. Pressures were targeted for 10.5 atm and the data range from 9.5-11.5 atm, while the temperatures span 884-1085 K. The speciation data (solid star symbols in Figure 1) are in excellent agreement with the other ignition data confirming the gas sampling does not perturb the ignition behavior. (Recall, the transparent end-wall is used for high speed imaging during ignition delay time experiments and the end wall is replaced with the gas sampling system for speciation experiments.)

The methyl3hexenoate data are compared with previous ignition data for other esters and iso-octane in Figure 1. Methyl3hexenoate ignites more rapidly than methyl butanoate consistent with expectations as the experiments were not conducted in the low temperature regime where the methyl3hexenoate allylic sites would retard ignition. The results show clearly that the methyl3hexenoate experiments are in the higher temperature regime where it is common for olefinic fuels (e.g. propene or ethene) to ignite faster than saturated fuels such as propane or ethane.

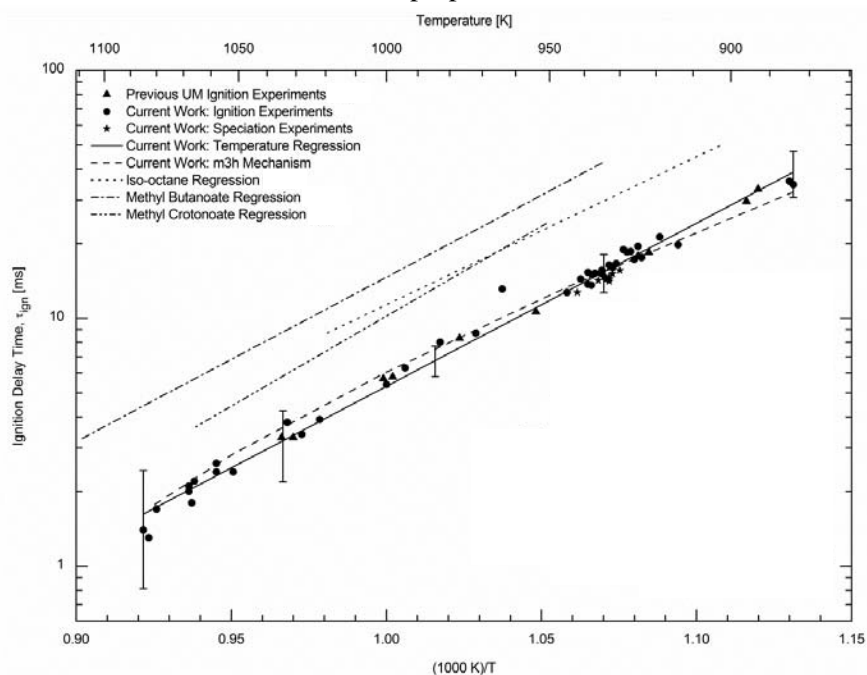


Figure 1. Results for experimentally measured methylhexenoate ignition delay time. The methylhexenoate data were acquired at conditions of $P = 10.5$ atm, $\phi = 0.3$ and $\chi(O_2) = 20.9\%$. The solid line is a linear regression to the experimental data for methylhexenoate. Linear regressions of experimental data for iso-octane (dashed line), methyl butanoate (dotted line), and methyl crotonoate (dashed-dotted line) are from the studies Walton et al. [10] for iso-octane, Walton et al. [8] for methyl butanoate, and Walton et al. [11] for methyl crotonoate.

Led by Dr. Charles Westbrook, a reaction mechanism was developed to represent methyl3hexenoate ignition. The mechanism was based on the mechanism of Herbinet et al. [2] for methyl 5-decenoate. The key features of the mechanism were the portions describing the effects of the C=C double bond in methyl3hexenoate. The results of the new reaction mechanism are compared with the experimental data in Figure 1 as the dashed line.

Figure 2 presents the stable intermediates measured during ignition, where the horizontal error bars represent the total sample time or half of the trigger pulse width (± 0.75 ms). The vertical error bars represent the uncertainty in the species concentration. The model predictions using the methyl3hexenoate reaction mechanism are included in Figure 2, where the initial conditions were the average of the sampling experiments: $P_{\text{eff}} = 10.3$ atm, $T_{\text{eff}} = 934$ K, $\phi = 0.29$, $\chi(O_2) = 20.9\%$, and inert: $O_2 = 3.76$. The

agreement between the experimental data and the model predictions is generally quite good, typically within a factor of two. Some key observations include that the model predicts the peak for the alkanes and the oxygenates later than is observed experimentally, and the experimental data are typically higher than the model predictions at early times during the ignition period. However, the model only predicts trace amounts of n-butyraldehyde, less than 18 ppb, which does not agree with the experimental results. Additionally, acetylene mole fractions of over 1500 ppm were predicted by the model which is significantly higher than the upper limit determined experimentally of less than 10 ppm.

The speciation results underscore the importance of new studies of unsaturated methyl esters. The first few reactions for fuels with one or more C=C double bonds are not much different from those of saturated fuels, but eventually smaller fragment species are produced with one or more double bonds, and current modeling capabilities are comparably much less developed for such species. Examples of such species are C₃H₄, C₄H₆, C₅H₈, as well as the many polyunsaturated radical species that can be produced. These unsaturated species have multiple isomeric forms, often resonantly related, and most have yet received very little kinetic analysis. Without prior guidance about how to deal with these species, it is often difficult to identify the specific products from their reactions. In the methyl3hexenoate mechanism, it is clear that too many of these reactions have been assumed to produce acetylene or vinyl radicals, and the large overestimate of acetylene, relative to the experimentally measured value, is evidence that this portion of the mechanism needs further attention. Results derived from further small molecule studies will benefit future mechanisms for large biodiesel fuels.

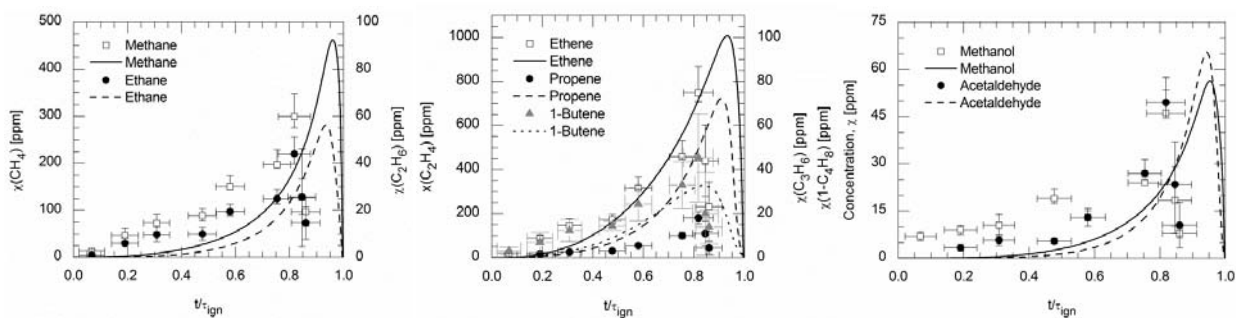


Figure 2. Alkane (left), alkene (middle) and oxygenate (right) mole fraction time histories during methyl3hexenoate ignition. Average conditions for the sampling experiments were $P = 10.3$ atm, $T = 934$ K, $\phi = 0.29$, $\chi(\text{O}_2) = 20.9\%$, inert: $\text{O}_2 = 3.76$.

B. Ignition and speciation studies of n-heptane

N-heptane remains an important reference compound for ignition studies. Speciation experiments of n-heptane have recently been conducted to provide a baseline at comparable conditions to the oxygenate data. Figure 3 presents an example of a pressure time history of a sampling experiment of n-heptane ignition. The pressure data show the distinct two-stage behavior anticipated for these conditions. We are currently analyzing the GC data and comparing the results with reaction mechanisms proposed for n-heptane.

Future Work

Our future work includes ignition and speciation studies of additional esters, particularly the unsaturated C7 ester methyl hexanoate to

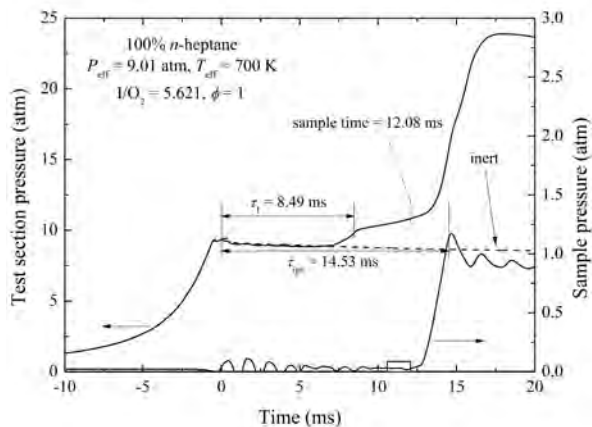


Figure 3. Pressure time history of gas-sampling experiment of n-heptane ignition. The times of first and second stage ignition are noted in the figure.

complement the methyl3hexenoate studies. We will continue to work with Dr. Westbrook to develop a more accurate understanding of the intermediates formed during ignition of saturated and unsaturated methyl esters. We also hope to partner with Dr. Craig Taatjes of Sandia National Laboratories to expand the experimental data on ester chemistry to conditions not achievable using the UM RCF. We will also complete the speciation study of n-heptane to provide a quantitative basis for comparing with the oxygenate speciation data.

III. References

1. Donovan, M.T., He, X., Zigler, B.T., Palmer, T.R., Wooldridge, M.S., Atreya, A. (2004) "Demonstration of a Free-Piston Rapid Compression Facility for the Study of High Temperature Combustion Phenomena" *Combust. Flame* **137** 351.
2. He, X., Donovan, M.T., Zigler, B.T., Palmer, T.R., Walton, S.M., Wooldridge, M.S., Atreya, A., (2005) "An Experimental and Modeling Study of Iso-octane Ignition Delay Times under Homogeneous Charge Compression Ignition Conditions," *Combust. Flame* **142** 266.
3. He, X., Zigler, B.T., Walton, S.M., Wooldridge, M.S., Atreya, A., (2006) "A Rapid Compression Facility Study of OH Time Histories During Iso-octane Ignition," *Combust. Flame* **145** 552.
4. Walton, S.M., He, X., Zigler, B.T., Wooldridge, M.S., (2007) "An Experimental Investigation of the Ignition Properties of Hydrogen and Carbon Monoxide Mixtures for Syngas Turbine Applications," *Proc. Combust. Inst.* **31** 3147.
5. Donovan, M.T., He, X., Zigler, B.T., Palmer, T.R., Walton, S.M., Wooldridge, M. S., (2005) "Experimental Investigation of Silane Combustion and Particle Nucleation Using a Rapid Compression Facility," *Combust. Flame* **141** 360.
6. Walton, S. M., Wooldridge, M. S., and Westbrook, C. K., (2009) "An Experimental Investigation of Structural Effects on the Auto-Ignition Properties of Two C5 Esters" *Proc. Combust. Inst.* **32** 255.
7. He, X., Walton, S.M., Zigler, B.T., Wooldridge, M.S., Atreya, A., (2007) "An Experimental Investigation of the Intermediates of Iso-octane During Ignition," *Int. J. Chem. Kinet.* **39** 498.
8. Walton, S.M., Karwat, D.M., Teini, P.D., Gorny, A., and Wooldridge, M.S., (2011) "Speciation Studies of Methyl Butanoate Ignition," *Fuel* **90** 1796.
9. D. M. A. Karwat, S. W. Wagnon, P. D. Teini, M. S. Wooldridge, *J. Phys. Chem. A* **115** (2011) 4909-4921.
10. Walton, S. M., He, X., Zigler, B. T., Wooldridge, M. S., and Atreya, A., (2007) "An Experimental Investigation of Iso-octane Ignition Phenomena," *Combustion and Flame*, **150**, pp. 246-262.
11. S.M. Walton, Ph.D. Dissertation, 2008, *Experimental Investigation of the Auto-Ignition Characteristics of Oxygenated Reference Fuel Compounds*, University of Michigan.

IV. Publications supported by this project 2008-2012

1. Karwat, D. M. A., Wagnon, S., Teini, P. D., Wooldridge, M. S., (2011) "On the chemical kinetics of n-butanol: ignition and speciation studies," *Journal of Physical Chemistry A*, **115**, pp. 4909-4921.
2. Wagnon, S. W., Karwat, D. M. A., and Wooldridge, M. S., "On the ignition chemistry of methyl trans-3-hexenoate," Central States Meeting of the Combustion Institute, Dayton, Ohio, April 2012.
3. Walton, S. M., Karwat, D. M., Teini, P. D., Gorny, A., and Wooldridge, M. S., (2011) "Speciation Studies of Methyl Butanoate Ignition," *Fuel*, **90**, pp. 1796-1804.
4. Wagnon, S., Karwat, D. M. A., Wooldridge, M. S., "Chemical Kinetics of an Unsaturated Ester: Methyl Trans-3-hexenoate," 7th U.S. National Combustion Meeting, Atlanta, Georgia, March 2011.
5. Karwat, D. M. A., Wagnon, S., Teini, P. D., Wooldridge, M. S., "N-butanol ignition and speciation studies," 7th U.S. National Combustion Meeting, Atlanta, Georgia, March 2011.
6. Karwat, D. M. A., Wagnon, S., Lai, J. Y. W., Wooldridge, M. S., Westbrook, C. K. "An Experimental and Computational Investigation of n-Dodecane Ignition and Chemical Kinetics," AIAA Conference, Orlando, Florida, January 2011.

THEORETICAL STUDIES OF THE REACTIONS AND SPECTROSCOPY OF RADICAL SPECIES RELEVANT
TO COMBUSTION REACTIONS AND DIAGNOSTICS

DAVID R. YARKONY

DEPARTMENT OF CHEMISTRY, JOHNS HOPKINS UNIVERSITY, BALTIMORE, MD 21218

yarkony@jhu.edu

I. Overview

A. Photoionization/Photodetachment Spectra

We continued our work on anion photoelectron and photoionization spectra that describe states of a residual molecule (the species left after the electron is removed) that are strongly coupled by conical intersections. As part of a continuing study of alkoxide photoelectron spectra, we have finished the determination of the coupled electronic potential energy surfaces needed for simulation of the hydroxymethoxide anion photoelectron spectrum. We are currently investigating the photoionization spectrum propyne, where the combined effects of the Jahn-Teller and spin-orbit interactions require clarification. We have also completed a work which provides the formal underpinning for a computational determination of anion photodetachment and photoionization cross sections and angular distributions. Implementation of this approach is in progress.

B. Nonadiabatic Dynamics

Using our algorithm for representing adiabatic potential energy surfaces coupled by conical intersections in processes involving bond breaking,¹⁻³ we are developing an accurate representation of the $1,2,3^2A$ potential energy surfaces of H_3O needed to describe the electronic quenching $OH(A^2\Sigma^+) + H_2 \rightarrow H_2O + H_2$ or $OH(A^2\Pi) + H_2$. In this regard we have surveyed, for the first time, the non coplanar portion of the crossing seams and investigated the possible role of a fourth electronic state in certain high symmetry regions of nuclear coordinate space.

In a related investigation we have teamed with Marsha Lester at the University of Pennsylvania in a combined experimental and computational study of the quenching reaction, $OH(A^2\Sigma^+) + CO \rightarrow CO_2 + H$, $OH(A^2\Pi) + CO$ or $HCO + O(^3P)$.

II. Work Completed

A. Electronic Structure of Hydroxymethoxide.⁴

Hydroxymethoxy can be viewed as a derivative of Jahn-Teller molecule methoxy with a hydrogen replaced by an OH group. Hence one might expect

conical intersections to play a role in the electronic structure of the low-lying states of this molecule and perhaps contribute to its photoelectron spectrum. Indeed a recent, high quality theoretical study of the low-lying electronic states of hydroxymethoxy found the minimum of the excited \tilde{A} state to be only 3142 cm^{-1} above the ground state minimum.⁵ However, that theoretical study explicitly avoided the issue of the nonadiabatic interactions due to conical intersection seams in its simulation of the hydroxymethoxide photoelectron spectrum which has yet to be measured experimentally.

In a work currently being prepared for submission,⁴ we addressed this deficiency, studying the nonadiabatic interactions between the two states in question. Fig. 1 below, clearly demonstrates the need for considering such interactions, reporting a portion of the seam of conical intersection as a function of the HOCO torsion angle

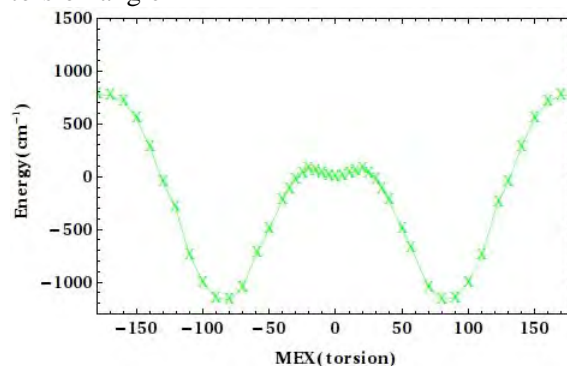


Figure 1: Energy in cm^{-1} relative to that of the minimum energy C_s crossing of the $1,2^2A$ states of hydroxymethoxy.

We find minimum energy crossing point shown in Fig. 1 to be 3100 cm^{-1} above the ground state minimum, putting it only $\sim 400\text{ cm}^{-1}$ above the \tilde{A} state minimum. The g - h plane of the minimum energy crossing point, is shown below. Note that the hydroxyl hydrogen is not involved in the g or h vectors.

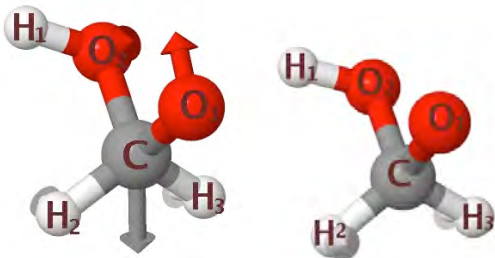


Figure 2: **g** and **h** vectors for minimum energy conical intersection of hydroxymethoxy.

We have used the *ab initio* energies, energy gradients and derivative couplings determined in this study to construct a coupled diabatic state representation, \mathbf{H}^d , of the two adiabatic states in question of sufficient accuracy to be used for simulating the photodetachment spectrum. The representation was obtained using polynomials through 6th order, using the higher order polynomial technology we recently developed for constructing \mathbf{H}^d for bound molecules.⁶ From Fig. 1 it is seen that the periodic dependence of the crossing energy on the torsional coordinate will preclude a uniformly accurate representation of the data in that figure. However over its domain of definition \mathbf{H}^d reliably reproduces the *ab initio* data from which it is derived. Fig. 3 illustrates the quality of the constructed representation over its domain of definition, comparing the derivative coupling obtained from the fit with those obtained from the *ab initio* calculations. In this plot exact agreement is represented by points along the 45° line. The excellent agreement for the large derivative couplings over 6 orders of magnitude is evident. Errors in the smaller values of the derivative couplings evident in Fig. 3 are expected since our representation does not describe the small removable part.

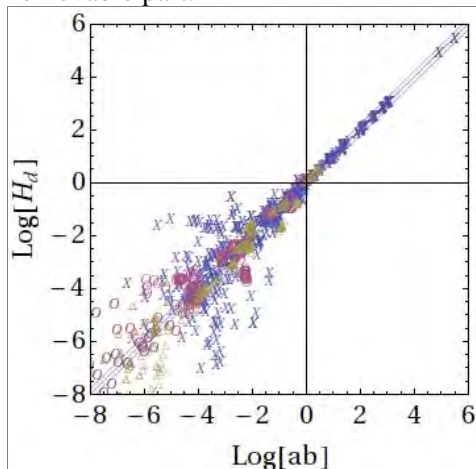


Figure 3. Scatter plot of derivative coupling obtained from the fit (H^d) vs that obtained from *ab initio* calculations.

This H^d will be used as the basis for a simulation of the hydroxymethoxy electron photodetachment spectrum in a future work.

B. Cross Sections for Photoelectron Spectra⁷

When simulating a photoelectron spectrum where the residual molecule has nondegenerate electronic states strongly coupled by conical intersections, a first principles simulation of the spectrum requires the transition moments to the individual diabatic electronic states. The determination of these transition moments is a complex problem in electron scattering and is routinely ignored in current simulations. In our work, see also Ref. ⁸, the transition moments (assumed geometry independent) are estimated by comparing the simulated and measured photoelectron spectra. This approach is not predictive.

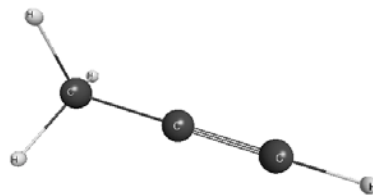
We have formulated a computational approach for determining the partial differential cross sections for both anion photodetachment and photoionization using a Lippmann-Schwinger equation approach.⁷ In this description the scattering orbital, which depends on the vibronic state of the target, is *not* orthogonal to the target electrons, but is geometry independent. Our approach takes approximate account of the antisymmetrizer,

As part of our DoE funded research the proposed approach will be implemented.

III. Work in Progress

A. Propyne Photoionization spectrum⁹

$\text{CH}_3\text{C}\equiv\text{CH}$ is an important intermediate in combustion chemistry being known to participate in the formation of polycyclic aromatic hydrocarbons.¹⁰



Propyne has a C_{3v} ground state equilibrium geometry and the ground state electronic wave function transforms as 1A_1 . The ionized species, the propyne cation, has a 2E ground state, which

exhibits a Jahn-Teller distortion. The 2E state is also split by the spin-orbit interaction, producing ${}^2E_{1/2}$ and ${}^2E_{3/2}$ states. Grant and coworkers have recorded and analyzed a nonresonant two-photon pulsed field ionization-photoelectron (PFI-PE) spectrum¹¹ of propyne, $C_3H_4^+(\tilde{X}^2E_{1/2, 3/2}) \leftarrow C_3H_4(\tilde{X}^1A_1)$. They conclude that the spin-orbit (A) constant of this 2E state is the same as that for the acetylene cation $\tilde{X}^2\Pi_{1/2,3/2}$, which is $A = -30.9$ cm^{-1} , Ref. ¹². Using this value of the spin-orbit constant, they report good agreement for their measured rotational profile and a structure very little altered by Jahn-Teller distortion.

More recently Ng and coworkers, have used the IR-VUV-PFI-PE method,^{13,14} to analyze the $C_3H_4^+(\tilde{X}^2E, \nu_1^+) \leftarrow C_3H_4(\tilde{X}^1A_1, \nu_1)$. These authors very carefully compared measured and simulated spectra and find $A = -13.9 \pm 0.2$ cm^{-1} . Their results are not consistent with those of Grant and coworkers in Ref. ¹¹.

Using techniques developed as part of prior DoE funded research¹⁵ we are in the process of determining the photoionization spectrum of propyne including both the effects of the Jahn-Teller and spin-orbit interactions. Analysis of these calculations will enable us to understand the effect of the Jahn-Teller coupling, and vibrational motion, on the spin-orbit interaction in $C_3H_4^+(\tilde{X}^2E)$. We will be particularly interested in the extent to which the Ham reduction effect influences the level splitting.

To date we have determined the key extrema on the ground state potential energy surface and the Jahn-Teller stabilization energy. We are currently calculating the spin-orbit interaction and its geometry dependence.

B. $OH(A^2\Sigma^+) + CO \rightarrow CO_2 + H_2$, $OH(A^2\Pi) + CO$ or $HCO + O(^3P)$

This project is done in collaboration with Professor Marsha Lester of the University of Pennsylvania and her student Julia Lehman.

The nonadiabatic collisional quenching of electronically excited hydroxyl radical has, and continues to be, a matter of considerable interest. For the captioned system, calculations are being carried out in my laboratory by Julia Lehman to gain mechanistic insights into the product distribution. While this project is certainly a work in progress, considerable progress has been made. A previously unknown, extended seam of conical intersection has been mapped out which reaches from the reactant channel to the minimum energy

crossing region, pictured below. This portion of the seam of conical intersection is relevant to the production of $HCO + O(^3P)$, determined by Lehman and Lester to be the principal product of the captioned reaction.

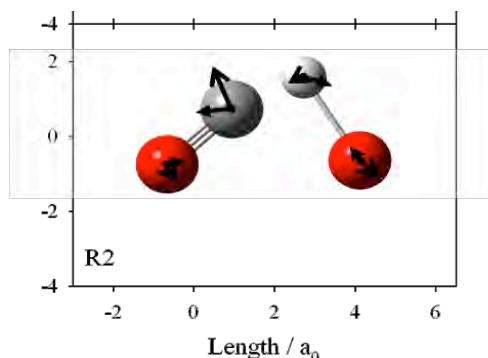


Figure 4: Minimum energy crossing point leading to $HCO+O$. Oxygen = red, carbon= dark grey, H=light grey. g and h vectors shown

C. $OH(A^2\Sigma^+) + H_2 \rightarrow H_2O + H$, $OH(A^2\Pi) + H_2$

As noted in the preamble, as a prelude to constructing a quasi diabatic representation of the three coupled adiabatic states needed to describe the captioned reaction, we have extended the known locus of seams of conical intersection to include nonplanar nuclear configurations.¹⁶ The representation of the nonplanar portion of the seam is essential in the context of full three dimensional dynamics. A portion of the nonplanar seam and its connection to the coplanar C_s seam is shown below.

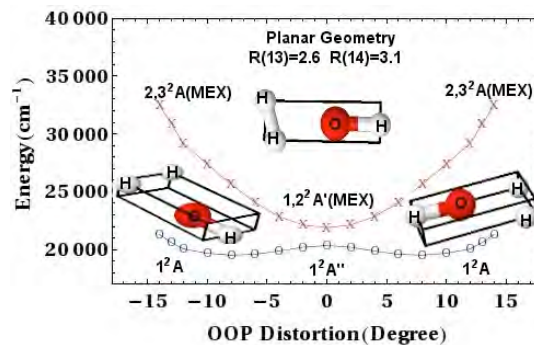


Figure 5. Energy as a function of the out of plane distortion for the $1,2^2A'$ [the $2,3^2A$] seam of conical intersection. Also shown is the energy of the $1^2A''$ [the 1^2A] state.

Literature Cited

- X. Zhu and D. R. Yarkony, *J. Chem. Phys.* **132**, 104101 (15 pages) (2010).
- X. Zhu and D. R. Yarkony, *Molec. Phys.* **108** (19), 2611 (2010).

- ³ X. Zhu and D. R. Yarkony, *J. Chem. Phys.*, submitted for publication (2012).
- ⁴ J. Dillon, N. Kopf, and D. R. Yarkony, *J. Chem. Phys.*, manuscript in preparation (2012).
- ⁵ W. Eisfeld and J. Francisco, *J. Chem. Phys.* **131**, 134313 (2009).
- ⁶ J. J. Dillon, D. R. Yarkony, and M. S. Schuurman, *J. Chem. Phys.* **134**, 044101 (11 pages) (2011).
- ⁷ S. Han and D. R. Yarkony, *Mol. Phys.*, (to appear) (2012).
- ⁸ T. Ichino, A. J. Gianola, W. C. Lineberger, and J. F. Stanton, *J. Chem. Phys.* **125**, 084312 (2006).
- ⁹ Sara Marquez and D. R. Yarkony, work in progress.
- ¹⁰ X. Xing, M.-K. Bahng, B. Reed, C. S. Lam, K.-C. Lau, and C. Y. Ng, *J. Chem. Phys.* **128**, 094311 (2008).
- ¹¹ H. Matsui, Y.-F. Zhu, and E. R. Grant, *Laser Chem.* **16**, 161 (1996).
- ¹² S. T. Pratt, P. M. Dehmer, and J. L. Dehmer, *J. Chem. Phys.* **99**, 6233 (1993).
- ¹³ C. Y. Ng, *J. Electron Spectrosc. Relat. Phenom.* **142**, 179 (2005).
- ¹⁴ H. K. Woo, P. Wang, K. C. LAu, X. Xing, C. Chang, and C. Y. Ng, *J. Chem. Phys.* **119**, 9333 (2003).
- ¹⁵ M. S. Schuurman, D. E. Weinberg, and D. R. Yarkony, *J. Chem. Phys.* **127**, 104309(12 pages) (2007).
- ¹⁶ J. Dillon and D. R. Yarkony, work in progress.

PUBLICATIONS SUPPORTED BY DE-FG02-91ER14189: 2010 – present

1. *On the Role of Conical Intersections and their Local Topography in the Photodissociation of 1-Hydroxyethyl Radical*,
Kousik Samanta and David R. Yarkony, *Chem. Phys.* 378, 110-117 (2010).
2. *A Lippmann – Schwinger Approach for the Determination of Photoionization and Photodetachment Cross Sections Based on a Partial Wave Green’s Function Expansion and Configuration Interaction Wave Functions*.
Seungsuk Han and David R. Yarkony, *Mol. Phys.* (2012) to appear.

GAS-PHASE MOLECULAR DYNAMICS: THEORETICAL STUDIES IN SPECTROSCOPY AND CHEMICAL DYNAMICS

Hua-Gen Yu (hgy@bnl.gov) and James T. Muckerman (muckerma@bnl.gov)
Chemistry Department, Brookhaven National Laboratory, Upton, NY 11973-5000

Program Scope

The main goal of this program is the development and application of computational methods for studying chemical reaction dynamics and molecular spectroscopy in the gas phase. We are interested in developing rigorous quantum dynamics algorithms for small polyatomic systems and in implementing approximate approaches for complex ones. Particular focus is on the dynamics and kinetics of chemical reactions and on the rovibrational spectra of species involved in combustion processes. This research also explores the potential energy surfaces of these systems of interest using state-of-the-art quantum chemistry methods, and extends them to understand some important properties of materials in condensed phases and interstellar medium as well as in combustion environments.

Recent Progress

Infrared and UV-visible spectra of Stone-Wales defected PAHs

We (with Nyman at Göteborg, Sweden) have investigated the infrared (IR) spectra of polycyclic aromatic hydrocarbons (PAHs, also called soot species) containing (5, 7)-member ring defects based on a $C_{48}H_{18}$ model. Calculations are performed using the hybrid B3LYP density functional theory. The results show that the Stone-Wales defect in PAHs can yield a strong IR band at 1448 cm^{-1} and a weak band at 611 cm^{-1} , which may contribute to the UIR (unidentified infrared) bands at $6.9\text{ }\mu\text{m}$ and $16.4\text{ }\mu\text{m}$ observed in the interstellar medium, for instance, see Fig. 1. The charge effect on the IR spectra is discussed. The stability of the ring defected PAHs is also addressed by exploring the minimum energy pathway on the potential energy surface and through their UV-visible spectra, which are computed using a TDDFT method.

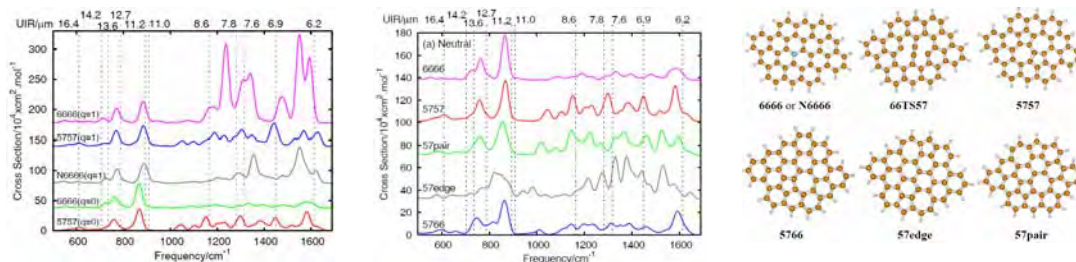


Figure 1. Theoretical IR spectra of some PAHs, and Stone-Wales defected PAHs, their cations, and one N-substituted PANH⁺. Some bands in μm are indicated by dashed lines.

Detailed investigations show that a peak near $6.9\text{ }\mu\text{m}$ may be produced by SW defected PAHs that have both a 5-member ring close to a boundary carbon atom and (6,5,5,6)-member rings in a row with duo hydrogens at the edges. But those large PAHs with a deeply embedded SW defect can not produce a strong band at $6.9\text{ }\mu\text{m}$. In addition, the

SW-defected charged PAHs are less likely to contribute to the 6.9 μm UIR band than 5757.

Raman spectra and structures of boron nitride-carbon sheets

Boron nitride sheet is isoelectronic to graphene sheet but they have dramatically different electronic properties. The mixed BN-C sheets might have band gap engineered applications in electronics and optics. In this work, we (with Han at CFN, BNL) did a combined experimental and theoretical study to understand the structures of carbon units in BN sheets. The theoretical calculations were done using the B3LYP DFT method, based on a circumcoronene-like model. The Raman spectra, structures, and their relative stability are displayed in Fig.2. Results clearly demonstrated that the most stable BN-C sheet is **III** with an armchair linked C-B/N structure. In other words, the armchair linked structure is energetically preferable so that there is relatively large fraction in BN-C sheets, or higher Raman intensities as shown in Fig.2 (a) and (c). Furthermore, Fig. 2(d) shows that the occurrence of embedded C₂ and benzene C₆ units is likely. This finding does support the experimental observations by Krivanek et al. (O.L. Krivanek et al. *Nature* (London) 464 (2010) 571) and Ci et al. (L. Ci et al. *Nature Mater.* 9 (2010) 430). Indeed, the finding of the armchair connection of graphene fragments to BN can be understood by the fact that graphene sheets with armchair edges are metallic. In addition, the weaker C-B and C-N bond strengths relative to C-C are consistent with the redshift of the Raman peak around 1580 cm^{-1} .

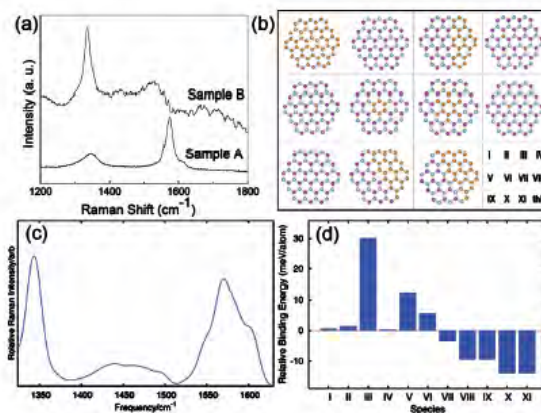


Figure 2. (a) Experimental Raman spectra of BN-C sheets; (b) the C (brown), B (purple), and N (blue) skeletons of circumcoronene-like sheets studied in this work, their labeling map is given in the right-bottom panel; (c) simulated Raman spectrum of the armchair-connected BN-C species (**III**); (d) calculated relative stability of the BN-C sheets among the group in (b).

Quantum dynamics calculations of cold collisions of methylene radicals with S-state atoms in a magnetic field

A rigorous quantum dynamics study has been performed for the low-temperature collisions of polyatomic molecular radicals with $^1\text{S}_0$ atoms in the presence of an external magnetic field using the CCSD(T) *ab initio* and scaled potential energy surfaces. Results are shown in Fig.3. The He-CH₂(X³B₁) interaction potential is weakly isotropic. Quantum scattering calculations show that collision-induced spin relaxation of the prototypical methylene molecule CH₂(X³B₁) and nine other triatomic radicals in cold ^3He gas occurs at a slow rate, demonstrating that cryogenic buffer-gas cooling and magnetic trapping of those molecules is feasible with current technology. The calculations also suggest that it may be possible to create ultracold gases of polyatomic molecules by sympathetic cooling with alkaline-earth atoms in a magnetic trap. This work was done in collaboration with Tscherbul and Dalgarno at Harvard.

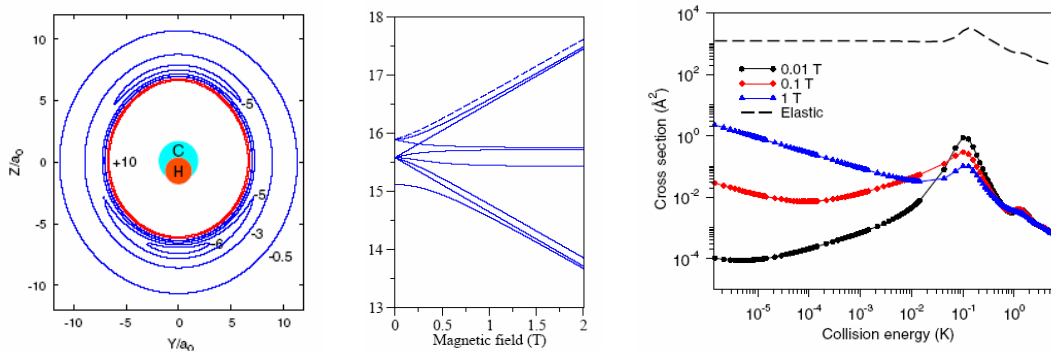


Figure 3. (a) A contour plot of the CCSD(T) potential energy surface for the He-CH₂(X) interactions; (b) The lowest Zeeman energy levels in cm⁻¹ of *p*-CH₂; (c) Cross sections for elastic scattering (dashed line) and spin relaxation in He + CH₂ collisions plotted vs collision energy for different magnetic field strengths.

Future Plans

Kinetics and dynamics study of combustion-related reactions

We will continue to study some important combustion reactions using the direct *ab initio* molecular dynamics program. An interesting direction will focus on the kinetics and dynamics of cyclic, N- and O-containing fuel molecules. The concentration of cyclic compounds in diesels and other future transportation fuels, produced largely from non-traditional sources such as oil shales and sand oils, are much higher than those in current fuels. There are only limited kinetics data on cyclic fuel molecules, yet they are required to design future internal combustion engines using such fuels. A new unique step in the chemistry is the ring-opening processes resulting in, for example cyclopentoxy (cyc-C₅H₉O) radicals discussed by us before. Such radicals may well contribute to enhanced formation of soot without a ring-opening reaction. In this work, we will start this project with the reactions of morpholine (1-oxa-4-aza-cyclohexane, i.e. cyclic -OCH₂CH₂NHCH₂CH₂-) and its derivatives with small radicals such as O₂, HO₂ and OH. Westmoreland et al. have recently demonstrated that morpholine is an ideal compound for modeling those hydrocarbon, oxygenated and N-containing fuels.

Recently, we have investigated the energies, geometries, and vibrational frequencies of the stationary points on the ground-state surfaces of the morpholinyl radicals with oxygen molecule using DFT and CCSD(T) methods. The ring-opening mechanism of morpholinyl radicals was fully explored. In near future, their dynamics will be carried out using the DualOrthGT program, together with variational RRKM theory.

Vibronic spectrum calculations of CH₂ and its interactions with He

In our GPMD group, Sears and Hall have observed rich and complicated rovibronic levels of CH₂ near the C + H₂ and CH + H dissociation limits. They provide a challenge for multiple surface dynamics theory, with relevance to the reactive system as well as CH₂ spectroscopy. We have calculated five low-lying electronic potential energy surfaces of CH₂ using a multireference CI (MRCI) method. The adiabatic surfaces will be transformed into a set of diabatic ones using the quasi-adiabatic approximation of Koppel et al. Full-dimensional quantum dynamics will then be performed on the five

coupled surfaces. The principal interest is in the energy levels and non-adiabatic coupling effects, for detailed comparison with experimental observations. In addition, we have calculated the singlet and triplet potential energy surfaces of the He-CH₂ (X/A) interaction system using the CCSD(T)/aug-cc-pVQZ level of theory. The surfaces will be used for investigating the dynamics of singlet and triplet states of CH₂ in collaboration with Tscherbul at Toronto/Harvard

Non-adiabatic molecular dynamics studies of polyatomic molecular reactions

Electronically excited species such as ¹CH₂ also play an important role in combustion chemistry. However, the studies of their reactivity are rather limited, partially due to the non-adiabatic dynamics effects because those reactions often occur on multiple potential energy surfaces. In this research, we will extend the surface hopping direct *ab initio* molecular dynamics algorithm, developed for the SECH MD studies, to simulate the bimolecular reactions and the photo-dissociation chemistry. The first application would be the photodissociation dynamics of acetone at 193-230 nm. This system has been investigated by Suits et al. using a universal ion imaging technique. The photon excited acetones produce two major types of products: CH₃CO + CH₃ and CO + 2CH₃. The latter products result from poorly understood dissociation mechanisms. Here we will attempt to explore the dissociation pathways of acetone on its three low-lying electronic states.

Publications since 2010

- J.S. Francisco, J.T. Muckerman, and H.-G. Yu, *HOCO radical chemistry*, Acc. Chem. Res. **43**, 1519 (2010).
- W.-Q. Han, Z. Liu and H.-G. Yu, *Synthesis and optical properties of GaN/ZnO solid solution nanocrystals*, App. Phys. Lett. **96**, 183112 (2010).
- T.V. Tscherbul, H.-G. Yu, and A. Dalgarno, *Sympathetic cooling of polyatomic molecules with S-state atoms in a magnetic trap*, Phys. Rev. Lett. **106**, 073201 (2011).
- H.-G. Yu, *An ab initio molecular dynamics study of the roaming mechanism of the H₂ + HOC⁺ reaction*, Physica Scripta **84**, 028104 (2011).
- S.-Y. Du, T. Germann, J. Francisco, K. Peterson, H.-G. Yu, and J. Lyons, *The kinetics study of the S + S₂ → S₃ reaction by the Chaperon mechanism*, J. Chem. Phys. **134**, 154508 (2011).
- H.-G. Yu, *An optimal density functional theory method for GaN and ZnO*, Chem. Phys. Lett. **512**, 231 (2011).
- W.-Q. Han, H.-G. Yu, Z. Liu, *Convert graphene sheets to boron nitride and boron nitride-carbon sheets via a carbon-substitution reaction*, App. Phys. Lett. **98**, 203112 (2011).
- H.-G. Yu and G. Nyman, *The infrared and UV-visible spectra of polycyclic aromatic hydrocarbons containing (5,7)-member ring defects: A theoretical study*, Astrophys. J. **749**, doi:10.1088/0004-637X/749/1/1 (2012).
- P.P Dholabhai and H.-G. Yu, *Exploring the ring opening pathways in the reaction of morpholinyl radicals with oxygen molecule*, J. Phys. Chem. A, (submitted, 2012).
- G. Nyman and H.-G. Yu, *Quantum approaches to polyatomic reaction dynamics*, Int Rev. Phys. Chem. (submitted, 2012).

Chemical Kinetics of Elementary Reactions

Judit Zádor

Combustion Research Facility, Mail Stop 9055, Sandia National Laboratories
Livermore, CA 94551-0969
jzador@sandia.gov

I. PROGRAM SCOPE

My program focuses on the theoretical determination of rate coefficients and branching fractions relevant to combustion chemistry. Specifically, the formation and dissociation of primary radicals derived from various fuel molecules, and the pressure- and temperature-dependent formation and reactions of peroxyalkyl radicals associated with low-temperature autoignition processes are studied. A particular aspect of the program is the close collaboration with experimental groups to minimize the effects of inherent uncertainties in the theoretical methods and also to reveal the parts of our current theoretical models that cause most of these uncertainties. The work involves quantum chemical calculations, application of transition-state theory, solution of the master equation, and modeling of small reaction systems related to the experimental conditions.

II. RECENT PROGRESS

A. Primary radical formation reactions: H-abstraction from fuel molecules

Propanol + OH and butanol + OH In collaboration with Jim Miller, hydrogen-abstraction rate coefficients were calculated for the *n*- and *i*-propanol and *n*-butanol + OH reactions. We found high sensitivity to the level of theory applied. Also, the analysis of the 2D hindering potentials revealed that the strong interaction between the alcoholic and the radical OH groups leads to significant coupling between the rotors. This causes the overestimation of the number and densities of states. We also showed that higher energy conformers with larger entropy (compared to the lowest energy conformer) also contribute significantly to the rate coefficients, therefore, the separable 1-D hindered rotor approximation is not accurate enough for these types of reactions.

Theoretical methods to obtain rate coefficients are essential to fundamental combustion chemistry research, yet the associated uncertainties are greatly unexplored in a systematic manner. In an exploratory work, in collaboration with Habib Najm, we focused on the parametric uncertainties for the hydrogen-atom-abstraction reaction, $\text{CH}_3\text{CH}(\text{OH})\text{CH}_3 + \text{OH} \rightarrow \text{CH}_3\text{C}(\text{OH})\text{CH}_3 + \text{H}_2\text{O}$. The barrier height, one of the lowest vibrational frequencies at the transition state, and the imaginary frequency were identified as the parameters causing the most significant uncertainty in the rate-coefficient calculations. Bayesian inference was employed to determine the joint probability distribution function of these parameters using the experimental data of Dunlop and Tully on isopropanol + OH.¹

We found that although most of the commonly used high-level ab initio calculations result in not more than a factor of two difference in the rate coefficient for this specific reaction in the 293-745 K temperature range, significant uncertainties remain in these types of calculations. We have clearly demonstrated that it is not necessarily true that the lion's share of the uncertainty in the calculated rate coefficient arises solely due to the uncertainties in the barrier height, and the presented methodology provided a transparent way of assessing the various quantum chemical methods.

B. Unimolecular dissociation of primary fuel radicals

Alkene + OH reactions, and the unimolecular dissociation of the hydroxypropyl and propoxy radicals Propene is an important intermediate in many combustion mechanisms and is also a prototype alkene, which exhibits richer combustion chemistry than ethene and yet is simple enough to permit a detailed theoretical analysis. In our previous work¹¹ we investigated the rich chemistry of the propene + OH

reaction by high-level quantum chemical methods coupled to multiwell master equation methodology, which provided excellent agreement with the literature experimental results.

In our more recent work, in collaboration with Craig Taatjes and Matthias Olzmann (Karlsruhe Institute of Technology), we investigated the behavior of this interesting reaction focusing on the ~650-700 K temperature range, where addition to the double bond, backdissociation of the adducts to propene + OH, and H-abstraction interact. We devised a method to decompose the biexponential OH LIF signals to extract the backdissociation and the abstraction rate coefficients directly in this previously unexplored temperature region. We also provided a simplified parameterization of this reaction to be used in combustion modeling. An interesting aspect of the work was the kinetic isotope effect (KIE) of the abstraction reaction. We have shown that the dislocation of the energy maximum along the reaction coordinate relative to the electronic saddle point on the adiabatic potential energy surface (PES) plays the major role in the KIE, and other variational effects are negligible.

We also calculated dissociation rate coefficients based on the propene + OH PES in collaboration with Jim Miller. The C₃H₇O isomers found on this surface correspond to the isomers obtained from propanol by H-abstraction and are inherently important in setting the stage for propanol combustion. All rate coefficients were obtained with internal consistency with particular attention paid to shallow wells. After minor adjustments very good agreement with the experimental results on *i*-propoxy dissociationⁱⁱⁱ was obtained. Several interesting pathways were uncovered, such as the catalytic dehydration, well-skipping reactions, and reactions forming enols. Our work quantitatively described the dissociation pathways from the radicals derived from propanol, which can be used for both the improvement of propanol models as well as to make better predictions for larger alcohols.

In collaboration with Ron Hanson and Jim Miller, the H-abstraction reactions from 1,3-butadiene by OH radical were studied. Below ~1000 K, the formation of *i*-C₄H₅ is more favored; however, above ~1000 K, the differences in the barrier heights become less important, and the fact that there are twice as many hydrogen attached to the terminal carbon atoms than to the nonterminal ones drives the branching ratio in favor of the *n*-C₄H₅ isomer. Adduct formation of course also takes place in this reaction. Our thermodynamic analysis has shown that because of the resonance stabilization of the CH₂CHCHCH₂(OH) adduct it is likely that at the lower end of the experimental temperature range (~1000 K) backdissociation is not instantaneous compared to the addition reaction, therefore, the observed loss of OH is faster than the abstraction rate alone.

C. Low-temperature autoignition chemistry

Alkene + HO₂ reactions It is well known that OH radicals play a central role in combustion, especially at lower temperatures, where it is the main chain carrier and is ultimately responsible for autoignition. HO₂, although a much less reactive radical, weighs in by being produced in much larger quantities. In our study, in collaboration with Stephen Klippenstein and Jim Miller, we have shown that HO₂ + alkene reactions can provide an important pathway in which HO₂ radicals are converted into the more reactive OH ones.

We have investigated seven HO₂ + unsaturated molecule reactions. Despite the belief, it is generally not true that the alkene + HO₂ reaction leads mostly to oxirane and OH. At low temperatures the formation of the alkylperoxy radical is favored due to the lower barrier height, while at higher temperatures the hydroperoxyalkyl and/or oxirane + OH formation is faster because of the looser transition state structure. An important exception is 2-butene, where the QOOH formation is both entropically and energetically favorable. Allylic abstraction is non-negligible from alkenes by HO₂ and competes with the addition reactions. This influences the effect that alkene + HO₂ reactions have on autoignition. The example of vinyl alcohol + HO₂ showed that substituted alkenes produce a completely different chemistry: instead of OH formation, a simple HO₂-assisted isomerization is predicted. Recent mechanisms overpredict the ethenol concentration in flames compared to experimental results.^{iv} This reaction can be one that corrects for that discrepancy. However, the effect has to be tested numerically, because the rate coefficient is small.

Propyl + O₂ and ethyl + O₂ In collaboration with Craig Taatjes we modeled new chlorine-atom initiated propane oxidation experiments using the previously established PES for these reactions.^v The goal of the work was to eliminate previously existing discrepancies between theory and experiment for the OH production. Using a better Cl-atom source and absolute OH-concentration measurements we achieved good agreement between the calculated and measured OH concentrations when the RO₂↔QOOH barrier heights were reduced by 0.25 kcal mol⁻¹. We also showed that these new low-pressure experiments are sensitive to the long-range part of the potential governing rate constants for R+O₂ addition, to the RO₂↔QOOH isomerization and QOOH↔OH + cyclic ether dissociation barriers, and indirectly to the energy transfer processes. In the case of the ethyl + O₂ reaction there is a strong indication that the CH₃CH₂O₂ + HO₂ reaction produces a significant amount of OH radicals above 600 K.

Direct investigation of QOOH radicals The carbon-centered hydroperoxyalkyl radicals (QOOH's) are formed mainly by internal H-abstraction reactions of peroxyalkyl radicals (ROO) and are key players in autoignition. Despite their importance, these ephemeral species have never been studied directly, and especially on the "second O₂ addition" reaction our knowledge is purely theoretical. The biggest difficulty when studying QOOH radicals is their very low steady-state concentration in the R+O₂→ROO→QOOH→P sequence.

In collaboration with Craig Taatjes, we devised a new experimental strategy to make QOOH radicals, which opened up a new avenue to study it and its reactions, and provided yet another rigorous test for theoretical calculations. By abstracting an H-atom from *tert*-butylhydroperoxide by Cl-atoms, the corresponding QOOH radicals were produced directly in high-enough concentration to observe their kinetics. The experimentally obtained rate coefficient for QOOH decomposition required a relatively small energy transfer parameter, which is consistent with the low (~12 kcal mol⁻¹) barrier height. However, this finding raises interesting questions for combustion modeling, where reactions sample both the high and low ranges of the rovibrational population. The rate coefficient for the second O₂ addition also shows a surprising trend when put in context with recently calculated QOOH + O₂ rate coefficients.^{vi} Although the hydroperoxy *tert*-butyl radical was not observed directly because of the poor Franck-Condon factor, in principle we have shown that with this strategy we will most likely achieve that goal.

III. FUTURE WORK

We continue our efforts to calculate more rigorous and accurate kinetic parameters to be used in combustion models. We plan to make progress on reactions involving OH radicals, especially in the context of oxygenated biofuels, where hydrogen-bonding influences the kinetics. We also plan to explore possibilities to efficiently calculate state densities for coupled hindered rotors with multiple important minima in order to improve our results on the *n*-butanol + OH calculations. Also, in collaboration with Leonid Sheps and based on the propene + OH study, we started to study the reactions of the various butene isomers with OH, which can extend our knowledge on butanol chemistry. Another area of recent interest that we plan to contribute to is the oxidation of heterocycles,^{vii} where ring-opening pathways can result in significantly different reactivity compared to acyclic compounds.

The current work on uncertainty is only a first step towards understanding the uncertainty in the currently used models. In the future we would like to consider all of the parameters in a screening procedure to select the most important candidates systematically for the Bayesian inference study. Moreover, it would be important to explore better the inherent correlation of the molecular parameters as obtained from electronic structure calculations, and if possible, use this information both in the forward uncertainty propagation and the inference step. These correlations would be employed in the construction of the joint prior on the parameters. Such correlation will reduce the uncertainty predictions, and also point to weak points in the model more directly.

Building on my current LDRD project, I would like to bring to the program computational capabilities, which would enable the automated exploration of stationary points on potential energy surfaces for at least common reaction types encountered in combustion, and enable systematic studies on larger molecules.

IV. References

- i. Dunlop, J. R.; Tully, F. P., *J. Phys. Chem.* **1993**, *97*, 6457-6464.
- ii. Zádor, J.; Jasper, A. W.; Miller, J. A., *Phys. Chem. Chem. Phys.* **2009**, *11*, 11040-11053.
- iii. Devolder, P.; Fittschen, C.; Frenzel, A.; Hippler, H.; Poskrebyshv, G.; Striebel, F.; Viskolcz, B., *Phys. Chem. Chem. Phys.* **1999**, *1*, 675-681.
- iv. Hansen, N.; Harper, M. R.; Green Jr., W. H., *Phys. Chem. Chem. Phys.* **2011**, *13*, 20262-20274.
- v. DeSain, J. D.; Klippenstein, S. J.; Miller, J. A.; Taatjes, C. A., *J. Phys. Chem. A* **2003**, *107*, 4415-4427.
- vi. Goldsmith, C. F.; Green, W. H.; Klippenstein, S. J., *J. Phys. Chem. A* **2012**, *116*, 3325-3346.
- vii. Roman-Leshkov, Y.; Barrett, C. J.; Liu, Z. Y.; Dumesic, J. A., *Nature* **2007**, *447*, 982-U985.

V. DOE supported publications, 2010-present

1. Zádor, J.; Miller, J. A., Unimolecular dissociation of hydroxypropyl and propoxy radicals. *Proc. Combust. Inst.* **2012**, *accepted*.
2. Prager, J.; Najm, N. H.; Zádor, J., Uncertainty quantification in the ab initio rate-coefficient calculation for the $\text{CH}_3\text{CH}(\text{OH})\text{CH}_3 + \text{OH} \rightarrow \text{CH}_3\text{C}(\text{OH})\text{CH}_3 + \text{H}_2\text{O}$ reaction. *Proc. Combust. Inst.* **2012**, *accepted*.
3. Welz, O.; Zádor, J.; Savee, J. D.; Ng, M. Y.; Meloni, G.; Fernandes, R. X.; Sheps, L.; Simmons, B. A.; Lee, T. S.; Osborn, D. L.; Taatjes, C. A., Low-temperature combustion chemistry of biofuels: pathways in the initial low-temperature (550 K-750 K) oxidation chemistry of isopentanol. *Phys. Chem. Chem. Phys.* **2012**, *14*, 3112-3127.
4. Zádor, J.; Taatjes, C. A.; Fernandes, R. X., Kinetics of elementary reactions in low-temperature autoignition chemistry. *Prog. Energy Comb. Sci.* **2011**, *37*, 371-421.
5. Kappler, C.; Zádor, J.; Welz, O.; Fernandes, R. X.; Olzmann, M.; Taatjes, C. A., Competing channels in the propene + OH reaction: Experiment and validated modeling over a broad temperature and pressure range. *Z. Phys. Chem.* **2011**, *225*, 1271-1293.
6. Zádor, J.; Klippenstein, S. J.; Miller, J. A., Pressure-Dependent OH Yields in Alkene plus HO₂ Reactions: A Theoretical Study. *J. Phys. Chem. A* **2011**, *115*, 10218-10225.
7. Huang, H.; Merthe, D.; Zádor, J.; Jusinski, L. E.; Taatjes, C. A., New experiments and validated master-equation modeling for OH production in propyl + O₂ reactions. *Proc. Combust. Inst.* **2010**, *33*, 293-299.
8. Vasu, S. S.; Zádor, J.; Davidson, D. F.; Hanson, R. K.; Golden, D. M.; Miller, J. A., High-temperature Measurements and a theoretical study of the reaction of OH with 1,3-butadiene. *J. Phys. Chem. A* **2010**, *114*, 8312-8318.

Isomer-specific Spectroscopy and Isomerization in Aromatic Fuels

Timothy S. Zwier

Department of Chemistry, Purdue University, West Lafayette, IN 47907-2084
zwier@purdue.edu

Program Definition and Scope

Under fuel-rich conditions, reactions that lead toward soot formation occur, with aromatic molecules and resonance-stabilized radicals playing key roles as intermediates. A key objective of this research program is to develop and utilize laser-based methods to characterize the spectroscopy and isomerization dynamics of conformational and structural isomers of aromatic derivatives and resonance-stabilized free radicals that play a role in soot formation. We are also characterizing the spectroscopy of model lignin compounds with the goal of providing deeper insight to the chemistry involved in the combustion and pyrolysis of wood and biofuels. Double-resonance laser spectroscopies are being used to record single-conformation IR and UV spectra of the molecules and radicals, including UV-UV hole-burning and resonant ion-dip infrared (RIDIR) schemes(1) (paper 1). Populations of the isomers are determined, where possible, using population transfer(2) or infrared ion-gain spectroscopy (paper 5).

Recent Progress

A. Model lignin compounds and biofuels

Lignin (Figure 1) is an aromatic-rich biopolymer that is second in natural abundance only to cellulose. It encases cellulose, providing an architectural framework for the plant, providing needed resistance to degradation, but also hindering the extraction of biofuels from the plant material. Its complex structure belies the fact that it is composed of only three monomers: *p*-coumaryl alcohol, coniferyl alcohol, and sinapyl alcohol. Enzyme-catalyzed radical polymerization of these monomers leads to a variety of chemical linkages. Given the importance of lignin to biofuel production, and the fundamental role played by its degradation products in the combustion and pyrolysis of wood, we are studying the conformation-specific spectroscopy of model lignin compounds, beginning with the three monolignols (paper 3), and an oxidized form of coniferyl alcohol that has the -O-4 side chain (paper 10).

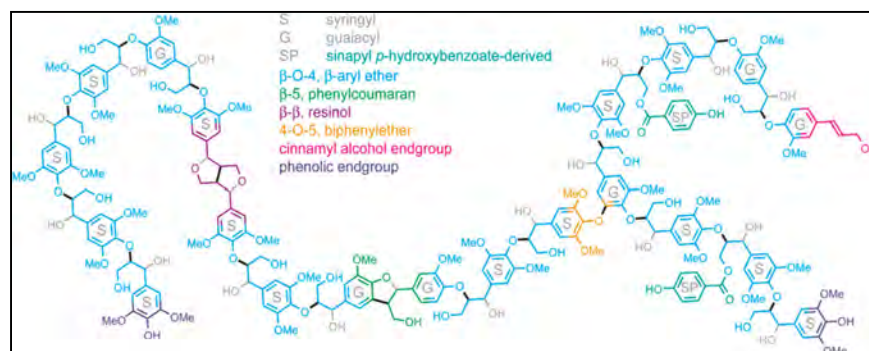


Figure 1: Chemical structure of lignin.(3)

Over the past year, we have moved both towards simpler and more complex lignin models. We were motivated to look at simpler analogs by the desire to understand the photodegradation pathways of this biopolymer. We hope to determine whether there are significant non-radiative pathways available to the excited states that could potentially lead to bond breakage. To that

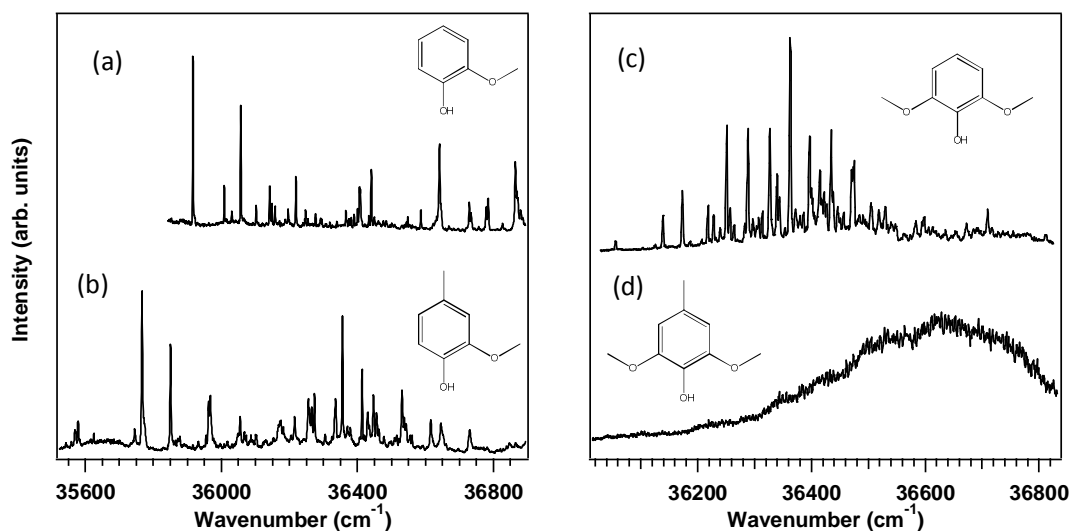
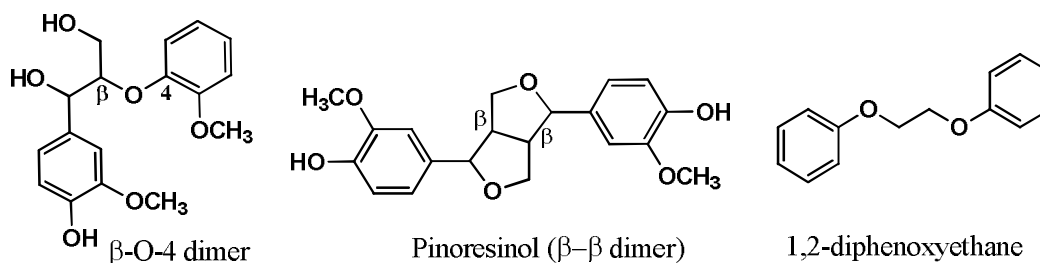


Figure 2: LIF excitation spectra of (a) guaiacol, (b) 4-methyl-guaiacol, (c) 2,6-dimethoxyphenol, and (d) 4-methyl-2,6-dimethoxyphenol.

end, we have studied the vibronic spectroscopy of a series of four methoxyphenols, whose structures are shown as insets in Figure 2. The LIF and R2PI spectra of these molecules were recorded under jet-cooled conditions. While guaiacol and 4-methyl-guaiacol (Fig. 2a,b) show vibronic structure typical of a phenyl derivative, with S_0 - S_1 origin transitions dominating the spectrum, 2,6-dimethoxyphenol (Fig. 2c) displays complicated vibronic structure that reflects a large geometry change upon electronic excitation. Despite the modest additional substitution of a methyl group (to mimic the branches present in a lignin polymer), the spectrum of 4-methyl-2,6-dimethoxyphenol (Fig. 2d) shows no resolved structure, even under jet-cooling. Furthermore, both the latter two molecules show red-shifted broadened emission devoid of resolvable features. Since the 2,6-dimethoxy substitution is characteristic of guaiacyl (G) subunits in lignin (Fig. 1), this characteristic broadening is of potential importance, especially if it leads to characteristic bond cleavage. In collaboration with Lyudmila Slipchenko at Purdue, we are currently carrying out high level excited state calculations to track the potential presence of close-lying excited states that could be responsible for the broadening observed.

We are currently studying the single-conformation IR and UV spectroscopy of two lignin dimers (structures below), in which the monomer units are connected by the -O-4 and - linkages which are both common in lignin (Fig. 1). Somewhat surprisingly, there are only two conformers of the -O-4 dimer and a single conformer in pinosresinol. The UV spectra of these two linkages are readily distinguishable, as are differences in the fragmentation following photoionization, which is completely absent in pinosresinol, but significant in the -O-4 dimer. Single-conformation IR spectra in the OH and CH stretch regions have provided characteristic IR signatures for the two linkages, but is hard to interpret in the latter case.



Since the alkyl CH stretch region will need to play a significant role in structural deductions in larger lignin oligomers, we are interested in developing a deeper understanding of the spectra in this region based on our single-conformation data. The alkyl CH stretch fundamentals are often challenging to assign due to extensive stretch-bend Fermi resonances. In collaboration with Ned Sibert (UW-Madison), we are developing a model of these Fermi resonance interactions, using the simpler aromatic dimers 1,2-diphenylethane and 1,2-diphenoxyethane (structure above) as starting points. The single-conformation spectra of the *anti* and *gauche* conformers of both molecules in the alkyl CH stretch region have been accounted for in exquisite detail, and we are hopeful that a foundation is being laid for application to the lignin linkages. One of the side benefits of using these flexible bichromophores as model systems is that their vibronic spectroscopy is also fascinating, with excitonic splittings of no more than a few inverse centimeters, continuing our on-going investigations(4-7) into the intermingled excited states present in flexible bichromophores (papers 3,4).

B. Resonance-stabilized radicals

We also continue to pursue isomer-specific and conformation-specific spectroscopy of resonance-stabilized radicals. We are nearing completion of a study of *p*-methylbenzyl radical, $C_6H_5-\dot{C}H-CH_3$. The two-color resonant two-photon ionization (2C-R2PI) spectrum of this radical shows extensive methyl internal rotor activity that reflects the change in preferred orientation for the methyl group in ground and excited electronic states. In collaboration with the McCarthy group, we are currently studying the dispersed fluorescence spectra of these internal rotor transitions. There are puzzling aspects of these spectra that point to a potential role for vibronic coupling involving two excited states known to be in close proximity in benzyl radical. Photoionization efficiency scans have been used to determine the IP of this radical with high precision (6.835 eV). RIDIR spectra in the CH stretch region are being analyzed with the model developed by the Nesbitt group for the ethyl radical.(8) We have also carried out RIDIR spectroscopy on the phenylallyl, benzylallenyl,(paper 1) and inden-2-yl-methyl radicals, establishing the method as a general tool for IR characterization of single conformations of radicals.

Future Work

We will complete our studies of the four model lignin chromophores (Fig. 2) and the lignin dimers as neutrals. The *p*-methyl benzyl radical analysis will be completed, and written up for publication. A Chen nozzle will be tested out as an alternative means of creating free radicals for spectroscopic investigation, including lignin-related radicals, following the lead of Ellison and co-workers.(9) Single-conformation alkyl CH stretch spectra of other model compounds will be recorded and analyzed as a means of expanding our modeling of spectra in this region.

Employing a new multi-stage mass spectrometer with a cryo-cooled 22-pole ion trap, we have recently demonstrated its ability to record UV photofragment spectra of ions cooled to temperatures of ~ 10 K. Initial tests of electrospray ionization of lignin oligomers demonstrate adequate ion signals for UV photofragmentation spectroscopy of model lignin compounds and oligomers as ions. Over the coming year, we will begin exploring the UV and conformation-specific IR spectra of these lignin-related ions, probably initially in sodiated form, so as to disturb the electronic structure of the aromatic residues minimally. Our longer-term goal is to see whether wavelength-selective photofragmentation can be used to diagnose sequences of lignin oligomers, using the unique absorption properties of the multiple chromophores present in the oligomers to selectively excite and fragment at different positions along the lignin backbone.

References

1. N. R. Pillsbury, T. S. Zwier, Conformation-Specific Spectroscopy and Excited State Photophysics of 5-Phenyl-1-pentene. *J. Phys. Chem. A* **113**, 118 (Jan, 2009).
2. N. R. Pillsbury, T. S. Zwier, Conformational Isomerization of 5-Phenyl-1-pentene Probed by SEP-Population Transfer Spectroscopy. *J. Phys. Chem. A* **113**, 126 (Jan, 2009).
3. R. Vanholme, B. Demedts, K. Morreel, J. Ralph, W. Boerjan, Lignin Biosynthesis and Structure. *Plant Physiol.* **153**, 895 (Jul, 2010).
4. N. R. Pillsbury, C. W. Muller, W. L. Meerts, D. F. Plusquellic, T. S. Zwier, Conformational Effects on Excitonic Interactions in a Prototypical H-Bonded Bichromophore: Bis(2-hydroxyphenyl)methane. *J. Phys. Chem. A* **113**, 5000 (Apr, 2009).
5. N. R. Pillsbury, C. W. Muller, T. S. Zwier, Conformational Isomerization and Collisional Cooling Dynamics of Bis(2-hydroxyphenyl)methane. *J. Phys. Chem. A* **113**, 5013 (Apr, 2009).
6. N. R. Pillsbury, J. A. Stearns, C. W. Muller, D. F. Plusquellic, T. S. Zwier, State-specific studies of internal mixing in a prototypical flexible bichromophore: Diphenylmethane. *J. Chem. Phys.* **129**, 114301 (Sep, 2008).
7. J. A. Stearns *et al.*, Rotationally resolved studies of S-0 and the exciton coupled S-1/S-2 origin regions of diphenylmethane and the d(12) isotopologue. *J. Chem. Phys.* **129**, (Dec, 2008).
8. T. Haber, A. C. Blair, D. J. Nesbitt, M. D. Schuder, CH stretch/internal rotor dynamics in ethyl radical: High-resolution spectroscopy in the CH₃-stretch manifold. *J. Chem. Phys.* **124**, (Feb 7, 2006).
9. A. M. Scheer, C. Mukarakate, D. J. Robichaud, M. R. Nimlos, G. B. Ellison, Thermal Decomposition Mechanisms of the Methoxyphenols: Formation of Phenol, Cyclopentadienone, Vinylacetylene, and Acetylene. *J. Phys. Chem. A* **115**, 13381 (Nov 24, 2011).

Publications acknowledging DOE support, 2010-present

1. Joshua A. Sebree, Nathan Kidwell, Evan G. Buchanan, Marek Zgierski, and Timothy S. Zwier, "Spectroscopy and Ionization Thresholds of π -Isoelectronic 1-Phenylallyl and Benzylallenyl Resonance Stabilized Radicals", *Chemical Science*, **2**, 1746-1754 (2011).
2. Chirantha P. Rodrigo, William H. James III, and Timothy S. Zwier, "Single-conformation ultraviolet and infrared spectra of jet-cooled monolignols: p-coumaryl alcohol, coniferyl alcohol, and sinapyl alcohol", *J. Am. Chem. Soc.* **133**, 2632-2641 (2011).
3. Chirantha P. Rodrigo, Christian W. Müller, Nathan R. Pillsbury, William H. James III, Timothy S. Zwier, and David F. Plusquellic, "Conformer-specific vibronic spectroscopy and vibronic coupling in a flexible bichromophore: bis-(4-hydroxyphenyl)methane", *J. Chem. Phys.* **134**, 164312 (2011).
4. Shin G. Chou, Chirantha P. Rodrigo, Christian W. Müller, Kevin O. Douglass, Timothy S. Zwier, and David F. Plusquellic, "Rotationally resolved C₂ symmetric conformers of bis-(4-hydroxyphenyl)-methane: Prototypical examples of Excitonic coupling in the S₁ and S₂ Electronic States, *J. Phys. Chem. A* **115**, 9643-9652 (2011).
5. Jacob C. Dean, Deepali Mehta, William H. James III, and Timothy S. Zwier, "Conformation-specific spectroscopy and populations of diastereomers of a model monolignol derivative: Chiral effects in a triol chain", *J. Phys. Chem. A* **115**, 8464-8478 (2011).

Participant List

33rd Annual Combustion Research Meeting Participation List

Last Name	First Name	Organization	Email
Ahmed	Musahid	Lawrence Berkeley National Laboratory	MAhmed@lbl.gov
Alexander	Millard	University of Maryland	mha@umd.edu
Allen	Wesley	University of Georgia	wdallen@uga.edu
Barlow	Robert	Sandia National Laboratories	barlow@sandia.gov
Bellan	Josette	JPL, California Institute of Technology	josette.bellan@jpl.nasa.gov
Blanquart	Guillaume	California Institute of Technology	g.blanquart@caltech.edu
Bowman	Joel	Emory University	jmbowma@emory.edu
Bravaya	Ksenia	University of Southern California	bravaya@usc.edu
Brown	Nancy	Lawrence Berkeley National Laboratory	njbrown@lbl.gov
Bunel	Emilio	Argonne National Laboratory	ebunel@anl.gov
Butler	Laurie	The University of Chicago	L-Butler@uchicago.edu
Casassa	Michael	Basic Energy Sciences, Dept of Energy	michael.casassa@science.doe.gov
Chandler	David	Sandia National Laboratories	gdecast@sandia.gov
Chen	Jacqueline	Sandia National Labs	jhchen@sandia.gov
Continetti	Robert	University of California, San Diego	rcontinetti@ucsd.edu
Crim	Fleming	University of Wisconsin - Madison	fcrim@chem.wisc.edu
Dagdigian	Paul	Johns Hopkins University	pjdagdigian@jhu.edu
Davis	Michael	Argonne National Laboratory	davis@tcg.anl.gov
Davis	H. Floyd	Cornell University	hfd1@cornell.edu
Dibble	Theodore	SUNY-Environmental Science and Forestry	tsdibble@esf.edu
Ervin	Kent M.	University of Nevada, Reno	ervin@unr.edu
Fiechtner	Gregory	DOE/Basic Energy Sciences	gregory.fiechtner@science.doe.gov
Field	Robert	MIT	rwfield@mit.edu
Flynn	George	Columbia University	gwf1@columbia.edu

Frank	Jonathan	Sandia National Laboratories	jhfrank@sandia.gov
Frenklach	Michael	University of California at Berkeley	myf@me.berkeley.edu
Goldsborough	Scott	Argonne National Laboratory	scott.goldsborough@anl.gov
Goncharov	Vasily	Brookhaven National Laboratory	vgoncharov@bnl.gov
Green	William H.	MIT Chemical Engineering	whgreen@mit.edu
Hanson	Ronald	Stanford University	rkhanson@stanford.edu
Hall	Gregory	Brookhaven National Lab	gehall@bnl.gov
Hansen	Nils	Sandia National Laboratories	nhansen@sandia.gov
Harding	Lawrence	Argonne National Laboratory	harding@anl.gov
Harris	Alexander	Brookhaven National Laboratory	alexh@bnl.gov
Hase	William	Texas Tech University	bill.hase@ttu.edu
Head-Gordon	Martin	Lawrence Berkeley National Lab/ UC Berkeley	mhg@cchem.berkeley.edu
Herrmann	Marcus	Arizona State University	marcus.herrmann@asu.edu
Hershberger	John	North Dakota State University	john.hershberger@ndsu.edu
Hirata	So	University of Illinois at Urbana-Champaign	sohirata@illinois.edu
Hoffmann	Mark	University of North Dakota	mhoffmann@chem.und.edu
Jasper	Ahren	Sandia National Laboratories	ajasper@sandia.gov
Kaiser	Ralf	University of Hawaii at Manoa	ralfk@hawaii.edu
Kellman	Michael	University of Oregon	kellman@uoregon.edu
Kirchhoff	William	Retired	william.kirchhoff@post.harvard.edu
Kliewer	Christopher	Sandia National Laboratories	ckliew@sandia.gov
Klippenstein	Stephen	Argonne National Laboratory	sjk@anl.gov
Leone	Stephen	LBNL and UC Berkeley	srl@berkeley.edu
Lester	Marsha	University of Pennsylvania	milester@sas.upenn.edu
Lester, Jr.	William A.	Lawrence Berkeley National Laboratory	walester@lbl.gov
Lighty	JoAnn	University of Utah	jlighty@utah.edu
Long	Marshall	Yale University	marshall.long@yale.edu
Lu	Tianfeng	University of Connecticut	tlu@enr.uconn.edu
Lucht	Robert	Purdue University	lucht@purdue.edu
Macdonald	Robert	Argonne National Laboratory	rgmacdonald@anl.gov

Manley	Dawn	Sandia National Laboratories	mpatter@sandia.gov
Mebel	Alexander	Florida International University	mebela@fiu.edu
Michael	Joe	Argonne National Laboratory	jmichael@anl.gov
Michelsen	Hope	Sandia National Labs	hamiche@sandia.gov
Miller	James	Argonne National Laboratory	jim.miller1946@gmail.com
Miller	Terry	Ohio State University	tamiller@chemistry.ohio-state.edu
Miller	William H.	UC Berkeley, and LBNL	millerwh@berkeley.edu
Mullin	Amy	University of Maryland	mullin@umd.edu
Najm	Habib	Sandia National Laboratories	hnnajm@sandia.gov
Nesbitt	David	JILA/University of Colorado	djn@jila.colorado.edu
Neumark	Daniel	Lawrence Berkeley National Laboratory	dneumark@berkeley.edu
Ng	Cheuk-Yiu	University of California, Davis	cyng@ucdavis.edu
Oefelein	Joseph	Sandia National Laboratories	oefelei@sandia.gov
Osborn	David	Sandia National Laboratories	dlosbor@sandia.gov
Parish	Carol	University of Richmond	cparish@richmond.edu
Parker	James	U.S. Army Research Office	james.k.parker30.civ@mail.mil
Pederson	Mark	U.S. Department of Energy	mark.pederson@science.doe.gov
Perry	David	The University of Akron	dperry@uakron.edu
Piecuch	Piotr	Michigan State University	piecuch@chemistry.msu.edu
Pitz	William	LLNL	pitz1@llnl.gov
Pope	Stephen	Cornell University	s.b.pope@cornell.edu
Pratt	Stephen	Argonne National Laboratory	stpratt@anl.gov
Reisler	Hanna	University of Southern California	reisler@usc.edu
Rothamer	David	University of Wisconsin-Madison	rothamer@wisc.edu
Ruedenberg	Klaus	Ames Laboratory	walkerkm@scl.ameslab.gov
Ruscic	Branko	Argonne National Laboratory	ruscic@anl.gov
Schaefer	Henry	University of Georgia	fri@uga.edu
Sears	Trevor	Brookhaven National Laboratory	sears@bnl.gov
Settersten	Tom	Sandia National Laboratories	tbsette@sandia.gov
Shepard	Ron	Argonne National Laboratory	shepard@tcg.anl.gov

Sheps	Leonid	Sandia National Lab	lsheps@sandia.gov
Sisk	Wade	DOE / BES	wade.sisk@science.doe.gov
Sivaramakrishnan	Raghu	Argonne National Laboratory	raghu@anl.gov
Smooke	Mitchell	Yale University	mitchell.smooke@yale.edu
Som	Sibendu	Argonne National Laboratory	ssom@anl.gov
Stanton	John	University of Texas at Austin	jfstanton@mail.utexas.edu
Suits	Arthur	Wayne State	asuits@chem.wayne.edu
Taatjes	Craig	Sandia National Laboratories	cataatj@sandia.gov
Tranter	Robert	Argonne National Laboratory	tranter@anl.gov
Truhlar	Donald	University of Minnesota	truhlar@umn.edu
Vander Wal	Randy	Penn State University	ruv12@psu.edu
wagner	albert	Argonne National Laboratory	wagner@anl.gov
Weber	Peter	Brown University	Peter_Weber@Brown.edu
Westbrook	Charles	Lawrence Livermore	westbrookck@earthlink.net
Wilson	Kevin	Lawrence Berkeley National Laboratory	krwilson@lbl.gov
Wittig	Curt	U.S.C.	wittig@usc.edu
Wooldridge	Margaret	University of Michigan	mswool@umich.edu
Yarkony	David	Johns Hopkins University	yarkony@jhu.edu
Yu	Hua-Gen	Brookhaven National Laboratory	hgy@bnl.gov
Zádor	Judit	Sandia National Laboratories	jzador@sandia.gov
Zhang	Jingsong	University of California, Riverside	jingsong.zhang@ucr.edu
Zwier	Timothy	Purdue University	zwier@purdue.edu